PHYLOGENY, EVOLUTIONARY HISTORY AND PAN-GENOME DYNAMICS OF *ARMILLARIA*

JIANWEI LIU

DOCTOR OF PHILOSOPHY

IN

BIOLOGICAL SCIENCE

SCHOOL OF SCIENCE

MAE FAH LUANG UNIVERSITY

2025

©COPYRIGHT BY MAE FAH LUANG UNIVERSITY

PHYLOGENY, EVOLUTIONARY HISTORY AND PAN-GENOME DYNAMICS OF *ARMILLARIA*

JIANWEI LIU

THIS DISSERTATION IS A PARTIAL FULFILLMENT OF THE REQUIREMENTS FOR THE DEGREE OF DOCTOR OF PHILOSOPHY IN BIOLOGICAL SCIENCE

SCHOOL OF SCIENCE
MAE FAH LUANG UNIVERSITY
2025
©COPYRIGHT BY MAE FAH LUANG UNIVERSITY

DISSERTATION APPROVAL

MAE FAH LUANG UNIVERSITY

FOR

DOCTOR OF PHILOSOPHY IN BIOLOGICAL SCIENCE

Dissertation Title: Phylogeny, Evolutionary History and Pan-genome Dynamics of *Armillaria*

Author: Jianwei Liu

Examination Committee:

Professor Rui-Lin Zhao, Ph. D.	Chairperson
Chitrabhanu Sharma Bhunjun, Ph. D.	Member
Professor Zhu-Liang Yang, Ph. D.	Member
Adjunct Professor Kevin David Hyde, Ph. D.	Member
Professor Fuqiang Yu, Ph. D.	Member

Advisors:

.....Advisor

(Chitrabhanu Sharma Bhunjun, Ph. D.)

Zhu-Liang Yang .....Co-Advisor

(Professor Zhu-Liang Yang, Ph. D.)

Dean:

.....

(Professor Surat Laphookhieo, Ph. D.)

ACKNOWLEDGEMENTS

After years of field sampling, data analysis, and dissertation writing, I have received invaluable support from numerous institutions and mentors. I would like to express my deepest gratitude to the following individuals and teams:

I would like to extend my heartfelt gratitude to Prof. Kevin D. Hyde for granting me the opportunity to pursue my PhD at Mae Fah Luang University, and to my main advisor, Dr. Chitrabhanu S. Bhunjun, for his steadfast guidance. Your scholarly rigor and exacting standards have been a constant inspiration in the refinement of my research. I am also especially grateful to my co-advisors, Prof. Zhuliang Yang and Prof. Fuqiang Yu. From Prof. Yang's thought-provoking question 5 years ago— "What is the future direction of taxonomy?" —to both professors encouraging me to spend years tackling the "two fungus" challenge in the *Gastrodia elata* industry, you have provided selfless support in funding, experimental design, and manuscript revision. It is thanks to you that I have overcome countless obstacles and journeyed across China, Hungary, and Thailand to advance my research on *Armillaria*.

I also thank Prof. László G. Nagy of the Fungal Genomics & Evolution Lab at the Biological Research Centre, Hungary, for his patient guidance during the partial data analyses. My sincere appreciation goes to Dr. Thatsanee Luangharn and Mr. Kasiphat Limsakul for their mentorship and personal and academic support during my time at Mae Fah Luang University. Special thanks to my external advisor, Dr. Guofu Qin, for his invaluable advice, and to Prof. Xinhua He at Southwest University for his assistance with manuscript revisions. Without your help, I could not have completed my studies.

During sample collection, we thank Dr. Ting Guo from Shanghai Academy of Agricultural Sciences, Dr. Tiezheng Wei and Ms. Zhuo Du at the Beijing Institute of Microbiology; Prof. Zuohong Chen and Prof. Ping Zhang at Hunan Normal University; Prof. Tolgor Bau at Jilin Agricultural University; Dr. Chaoqun Wang, Dr. Ming Zhang, and Dr. Ting Li at the Guangdong Institute of Microbiology; Dr. Menghua Tian, Dr. Peichao Ding, and Dr. Changfei Zhang at the Zhaotong Gastrodia Research Institute; Mr. Zhanling Li and Mr. Shengming Zhang; Prof. Gregory M. Bonito at Michigan State University; associated Prof. Shanping Wan at Yunnan Agricultural University

I extend my heartfelt thanks to colleagues who supported me in daily life and work: Ms. Zhuyue Yan, Ms. Shimei Yang, Mr. Rui Yan, Ms. Jing Song, Ms. Duanyu Qi, Ms. Shaowei Wang, Dr. Wei Liu, Dr. Zhenyan Yang, Dr. Yanliang Wang, Dr. Dong Liu, Dr. Xiaofei Shi, Ms. Chengmo Yang, and Dr. Indunil C. Senanayake. I am especially grateful to Mr. Xin Xu for his invaluable assistance with cultivation experiments, and to Associate Professor Bang Feng at the Kunming Institute of Botany for his timely and generous support. I also thank Yu Yang, Xingjuan Xiao, Jingyi Zhang, Na Wu, Tianye Du, and all my classmates for their help during my research in Thailand. Finally, I owe deep appreciation to the Fungal Genomics & Evolution Lab and BRC Hungary team—Xiaobin Liu, Zhihao Hou, Hongli Wu, Neha Sahu, Bálint Balázs, and Dr. Botond Hegedüs—for their expert guidance during my studies in Hungary.

Finally, I owe my deepest gratitude to my family for their unwavering support, understanding, and love throughout my PhD journey—this work would not have been possible without them. I would also like to acknowledge myself: for enduring solitude, remaining steadfast in my passion, overcoming countless challenges, and embracing creative innovation throughout this demanding doctoral journey.

This research was funded by the Strategic Priority Research Program of the Chinese Academy of Sciences (XDA26050302), the Poverty Alleviation through Science and Technology Project (KFJ FP 201905), the Technology Transfer into Yunnan Project (202003AD150005), the Zhaotong Rural Revitalization Project (2023TMXJZ02), and the Dissertation Writing Grant (7702(6)/334 no.0452) and the Publishing Grant 7702(6)/707 (no.0315) from university.

Jianwei Liu

Dissertation Title	Phylogeny, Evolutionary History and Pan-genome Dynamics of *Armillaria*
Author	Jianwei Liu
Degree	Doctor of Philosophy (Biological Science)
Advisor	Chitrabhanu Sharma Bhunjun, Ph. D.
Co-Advisor	Professor Zhu-Liang Yang, Ph. D.

ABSTRACT

Recent studies have shown that phylogenetic discordance, caused by incomplete lineage sorting, hybridization, introgression, and horizontal gene transfer, is much more common across the tree of life than previously recognized. This widespread discordance makes reconstructing evolutionary relationships particularly challenging. *Armillaria* species are a compelling example, given their complex ecological roles. They function as destructive forest pathogens with significant economic impact, as saprotrophs contributing to wood decomposition and nutrient cycling, and as symbiotic partners of medicinal plants and fungi such as *Gastrodia elata* (Tianma) and *Polyporus umbellatus* (Fuling). These combined roles support an estimated annual market value of ¥14–21 billion. However, several fundamental questions remain unresolved, including the true extent of species diversity, boundaries between species, compatibility with *Gastrodia* under cultivation, and the evolutionary processes driving speciation.

Many studies have revealed that incomplete reproductive isolation between species is common in the genus *Armillaria*. This potential incomplete reproductive isolation may indicate ongoing gene flow, which could be the one factor underlying past difficulties in delineating species boundaries within this fungal genus. Here, focusing on China while including global specimens, we analyzed 600 biparentally inherited nuclear genomes and 605 maternally inherited mitochondrial genomes to establish a robust phylogenetic framework for the genus *Armillaria*. Through comprehensive comparisons of population genetic differentiation metrics, including Weir & Cockerham's F_{ST}, absolute differentiation (dxy), mitochondrial gene relative differentiation (ΦST), we delineated 21 distinct *Armillaria* lineages in China, comprising 6 cryptic novel taxa

(designated as *A. borealis* subsp. *sinoborealis*, *A. griseocapilla*, *A. linzhiensis*, *A. pseudoostoyae*, and *A. tabescens* subsp. *orientala*, *A. violacea* (CBS N) lineage 2-mtDNA), and a comprehensive review of all 73 previously described species was performed. Threshold analysis of population differentiation coefficients demonstrated that, from the nuclear-genomic perspective, an F_{ST}-nDNA value of ≥ 0.09 can serve as a preliminary threshold for delimiting species in *Armillaria*; however, the status of a lineage as a species or subspecies must still be confirmed with biological mating trial statistics and other supporting evidence. For those clades that receive strong support in the mitochondrial phylogeny, one must first verify that they also form independently supported clades in the nuclear phylogeny; only under that condition, when the corresponding mitochondrial divergence metrics reach F_{ST}-mtDNA = 0.37, dxy = 0.04, and ΦST = 0.45, be considered important criteria for species or subspecies delimitation. Meanwhile, a nuclear genomic divergence threshold of approximately 1.052 Ma may serve as a meaningful temporal criterion for species delimitation may serve as empirical criteria for species delimitation within the genus, facilitating the recognition of cryptic novel taxa.

Our results demonstrate strong concordance between phylogenetic and biological species concepts across all 14 recognized taxa. In light of this, we recommend retaining *A. pungentisquamosa* as a valid name, despite its potential synonymy with *A. xiaocaobanensis*, given the global consensus that species delimitation in *Armillaria* should prioritize reproductive compatibility and genomic distinctiveness over nomenclatural priority. Notably, analyses of widespread species complexes uncovered significant maternal-lineage phylogeographic patterns. For example, the Chinese biological species (hereafter abbreviated as CBS) J complex is resolved into five discrete geographic lineages: Xinjiang, China; Central China; the Eastern Himalayas; the Hengduan Mountains; and Southern Tibet based on mitochondrial genome data. Despite these clear mitochondrial breaks, nuclear-genome monophyly and high interfertility support retaining the current taxonomic circumscription without further subdivision. Although we did not delimit species according to these mitochondrial geographic lineages, their well-defined spatial structure provides an ideal framework for future fungal biogeographic (mycobiogeographic) investigations. Building on a clear species delimitation, our

systematic *Armillaria* and *Gastrodia* co-cultivation experiments suggest that, to date, only species in sect. *Gallicae* may be suitable for *Gastrodia elata* cultivation.

Our study also uncovers extensive phylogenetic discordance between nuclear and mitochondrial genomes, as well as between gene trees and the species tree, across the genus *Armillaria*. Phylogenetic-cause analyses indicate that incomplete lineage sorting is the primary driver of phylogenetic incongruence within *Armillaria*, although the roles of hybridization and introgression should not be overlooked. PhyloNet-based network analysis shows that the *Gallicae* section represents a hybrid lineage derived from the *Ostoyarum* section (weight 0.844) and the *Armillaria* section (weight 0.156), while the *A. tibetica* (CBS J) complex originates from a mixture of *A. bruneocystidia* (CBS H) (weight 0.51) and *A. sinapina* subsp. *alpina* (CBS A) + *A. luteopileata* (CBS C) + *A. sinensis* (CBS F) + *A. cepistipes* + *A. sinapina* subsp. *sinapina* (weight 0.49). Divergence time and ancestral range reconstruction analyses revealed that the most recent common ancestor (MRCA) of *Armillaria* originated in the Oligocene from Holarctic-Asia and subsequently underwent a complex history of global dispersal and diversification, with an estimated age of 27.7 Ma based on nuclear genome data and 24.40 Ma based on mitochondrial genome data.

To enable rapid and accurate species identification in *Armillaria*, we developed an integrated, multi-level identification framework combining genomic and computational approaches. First, we constructed two offline-searchable genomic databases (mitochondrial and nuclear) using *skani*, allowing users to perform efficient species classification with locally stored data. Second, we implemented a deep learning-based method that transforms raw genome sequences into visual DNA barcodes by encoding k-mer frequencies, enabling high-throughput pattern recognition for species discrimination. Third, through systematic evaluation of 31 primer pairs targeting 11 candidate genes, including internal primers for the longer loci, we found that almost every gene is suitable as a candidate barcode. Finally, we developed three SSR (simple sequence repeat) fingerprinting systems tailored for strain-level identification, providing breeders, industries, and researchers with robust tools for cultivar authentication, intellectual property protection, and population genetic analyses.

Keywords: DNA Barcording, Gene Flow, New Species, Phylogenetic Discordance, SSR

TABLE OF CONTENTS

CHAPTER	Page
1 INTRODUCTION	**1**
1.1 Background	1
1.2 Objectives	9
1.3 Expected Outcomes	9
1.4 Research Contents	10
2 PHYLOGENETIC RECONSTRUCTION OF *ARMILLARIA*	**12**
2.1 Introduction	12
2.2 Materials and Methods	12
2.3 Results	15
2.4 Conclusions	20
3 GENETIC DIFFERENTIATION AMONG *ARMILLARIA* PHYLOGENETIC LINEAGES	**21**
3.1 Introduction	21
3.2 Methods	21
3.3 Results	23
3.4 Conclusions	35
4 PHYLOGENETIC CONFLICT AND RETICULATE EVOLUTION IN *ARMILLARIA*	**41**
4.1 Introduction	41
4.2 Methods	41
4.3 Results	45
4.4 Conclusions	67
5 DNA BARCODING MARKERS AND SSR MOLECULAR FINGERPRINT RECOGNITION SYSTEM DEVELOPMENT	**69**
5.1 Introduction	69
5.2 Methods	70
5.3 Results	76
5.4 Discussion	93

TABLE OF CONTENTS

CHAPTER	Page
6 DIVERGENCE TIME AND ANCESTRAL RANGE ESTIMATION	**94**
6.1 Introduction	94
6.2 Results	96
6.3 Discussion	108
6.4 Conclusion	111
7 SCREENING *ARMILLARIA* SPECIES FOR OPTIMAL SYMBIOSIS WITH *GASTRODIA ELATA*	**113**
7.1 Introduction	113
7.2 Screening *Armillaria* Species For Optimal Symbiosis with *G. elata*	113
7.3 Results	120
7.4 Conclusion	125
8 TAXONOMY	**128**
8.1 Introduction	128
8.2 Morphological Studies	128
8.3 Conclusion	281
9 OVERALL CONCLUSIONS AND FUTURE PERSPECTIVES	**283**
REFERENCES	**285**
APPENDICES	**301**
APPENDIX A ABSTRACT OF PUBLICATIONS	301
APPENDIX B PATENTS	309
APPENDIX C SUPPLEMENTARY TABLES	312
APPENDIX D SUPPLEMENTARY FIGURES	388
CURRICULUM VITAE	**409**

LIST OF TABLES

Table	Page
1.1 Information of 72 known species in genus *Armillaria*.	6
4.1 Log-Likelihood values for varying numbers of reticulation events	64
5.1 *Armillaria* species used for DNA barcode development and their corresponding BUSCO results	71
5.2 Candidate genes and primer sets with amplification success rates	79
5.3 Candidate genes and corresponding primers sequences	80
5.4 SSR loci and information of repeat type and corresponding primer sequences	82
5.5 Genetic diversity information of different SSR loci	83
5.6 SSR loci and information of repeat type and corresponding primer sequences	86
5.7 Genetic diversity information of different SSR loci	87
5.8 SSR loci and information of repeat type and corresponding primer sequences	90
5.9 SSR loci and information of repeat type and corresponding primer sequences	90
7.1 *Armillaria* strains used for validating cultivability and Cativation results	121
8.1 Comparison of basidiospore length and Q values between the newly measured species	129

LIST OF FIGURES

Figure	Page
1.1 Morphological characteristics of *Armillaria*	2
2.1 Maximum-likelihood (ML) phylogenetic tree of *Armillaria* inferred from 385 orthologues protiens across 600 nuclear genomes	16
2.2 Maximum-Likelihood (ML) phylogenetic tree of genus *Armillaria* constructed from a concatenated dataset of 605 mitochondrial homeblocks	19
3.1 Principal component analysis (PCA) of nuclear genome variation among 473 diploid studied *Armillaria* individuals	24
3.2 Principal component analysis (PCA) of mitochondrial genome variation among 584 studied *Armillaria* individuals	26
3.3 Pairwise Weir & Cockerham's F_{ST} of *Armillaria* based on lineages derived from nuclear phylogenomic analyses	28
3.4 Pairwise Weir & Cockerham's F_{ST} of *Armillaria* based on lineages derived from mitochondrial phylogenomic analyses	29
3.5 Weir & Cockerham's F_{ST} of *Armillaria* based on lineages derived from mitochondrial phylogenomic analyses	31
3.6 Absolute genetic distance (dxy) of *Armillaria* based on lineages derived from mitochondrial phylogenomic analyses	33
3.7 Relative differentiation index (ΦST) of *Armillaria* based on lineages derived from mitochondrial phylogenomic analyses	35
4.1 Phylogenetic tanglegram comparing nuclear and mitochondrial trees	47
4.2 Species tree inferred by ASTRAL from 629 orthologues gene trees	48
4.3 Ten most common topologies and species tree of *Armillaria*	50
4.4 Concordance factor analysis of 629 *Armillaria* orthologous single-copy protein sequences using IQ-TREE 2	52
4.5 Species tree topology of *Armillaria* inferred by CASTER-site	55
4.6 Internode certainty all (ICA) values for the genus *Armillaria*	56

LIST OF FIGURES

Figure	Page
4.7 Quartet Sampling (QS) scores inferred from the 629 orthologous single-copy protein datasets	58
4.8 Coalescent-based species tree reconstructed using ASTRAL	59
4.9 Mean pairwise *D* per species pair	60
4.10 The mean total proportion of introgressed loci per species pair inferred through the QuIBL analysis	61
4.11 SplitsTree phylogenetic network reconstructed using the 385 orthologous proteins in 600 samples in 2.1.1	62
4.12 SplitsTree phylogenetic network reconstructed using the homesblock of mitochondrial genomes generated by ORPA in 605 samples in 2.2.2	63
4.13 Phylogenetic networks inferred by PhyloNet using Maximum pseudo-likelihood under zero to seven reticulation models	64
4.14 Visual result of Phytop on species level of *Armillaria* with default parameters	66
4.15 Visual result of Phytop on section level of *Armillaria* with default parameters	67
5.1 Phylogeny and genomic signature varKodes for 42 species of *Armillaria*	76
5.2 Alleles and allele frequency distribution diagram of 12 SSR loci amplified in 81 *Armillaria gallica* strains	84
5.3 UPGMA tree constructed based on 12 SSR loci from 81 *Armillaria gallica* strains	85
5.4 Alleles and allele frequency distribution diagram of 30 SSR loci amplified in 17 strains of highly parasitic *Armillaria mellea* complex from different sources	88
5.5 UPGMA tree constructed based on 30 SSR sites for 17 strains	89

LIST OF FIGURES

Figure	Page
5.6 Alleles and allele frequency distribution of 13 SSR loci amplified in 39 strains of 12 weakly parasitoid *Armillaria* species	91
5.7 UPGMA tree constructed based on 13 SSR loci for 39 strains of 12 weakly parasitoid *Armillaria* species	92
6.1 Time-calibrated phylogeny inferred from Maximum Likelihood (ML) analysis of 629 single-copy concatenated nuclear protein sequence and one *Guyanagaster* species	97
6.2 Time-calibrated phylogeny inferred from Maximum Likelihood (ML) analysis of mitochondrial homologous gene blocks across 48 *Armillaria* species and one *Guyanagaster* species	98
6.3 Ancestral area reconstruction and divergence time estimation of *Armillaria* using 629 concatenated nuclear single-copy orthologous genes	106
6.4 Ancestral area reconstruction and divergence time estimation of *Armillaria* based on the mitochondrial home blocks dataset	107
7.1 The life cycle of *Gastrodia elata*, from seed germination to reproductive maturity, spans three years in natural conditions	115
7.2 In vitro germination validation system for *Gastrodia elata* seeds co-cultured with *Mycena purpureofusca* mycelium on PDA medium	117
7.3 Validation system for cultivating *Gastrodia elata* Using Indoor *Armillaria* strains	120
7.4 *Armillaria* spp. strains exhibiting cultivation suitability for *Gastrodia elata* in field trials	123
7.5 *Armillaria* spp. strains lacking cultivation suitability for *Gastrodia* elata in field trials	124
7.6 Taxonomic composition of commercial fungal strains analyzed in this study	125

LIST OF FIGURES

Figure	Page
8.1 The basidiospores coordinate plane of *Armillaria* species	131
8.2 Basidiomata and morphological characteristics of *Armillaria borealis* subsp. *Sinoborealis* (HKAS 135492)	136
8.3 Distribution of samples of *Armillaria borealis* subsp. *sinoborealis* used in this study	137
8.4 Basidiomata and morphological characteristics of *Armillaria griseocapilla* (HKAS 132000, holotype)	139
8.5 Distribution of samples of *Armillaria griseocapilla* used in this study	140
8.6 Basidiomata and morphological characteristics of *Armillaria linzhiensis* (HMAS 272515, holotype)	142
8.7 Distribution of samples of *Armillaria linzhiensis* used in this study	143
8.8 Basidiomata and morphological characteristics of *Armillaria melleamericana* subsp. *melleasiana*	146
8.9 Distribution of samples of *Armillaria melleamericana* subsp. *melleasiana* used in this study	147
8.10 Basidiomata and morphological characteristics of *Armillaria melleoasian* subsp. *macrospora*	152
8.11 Distribution of samples of *Armillaria melleoasian* subsp. *macrospora* used in this study	153
8.12 Basidiomata and morphological characteristics of *Armillaria pseudoostoyae* (HKAS 56108, holotype)	156
8.13 Distribution of samples of *Armillaria pseudoostoyae* used in this study	157
8.14 Basidiomata and morphological characteristics of *Armillaria tabescens* subsp. *oriental* (HKAS 91090, holotype)	160
8.15 Distribution of samples of *Armillaria tabescens* subsp. *orientala* used in this study	161
8.16 Basidiomata and morphological characteristics of *Armillaria xiaocaobaensis* (SWFC 12638, holotype)	164

LIST OF FIGURES

Figure	Page
8.17 Basidiomata and morphological characteristics of *A. tibetica* (CBS J) lineage 1-mtDNA	169
8.18 Distribution of samples of *A. tibetica* (CBS J) lineage 1-mtDNA used in this study	170
8.19 Basidiomata and morphological characteristics of *A. tibetica* (CBS J) lineage 2-mtDNA	173
8.20 Distribution of samples of *A. tibetica* (CBS J) lineage 2-mtDNA used in this study	174
8.21 Basidiomata and morphological characteristics of *A. tibetica* (CBS J) lineage 3-mtDNA (herbarium no)	177
8.22 Distribution of samples of *A. tibetica* (CBS J) lineage 3-mtDNA used in this study	178
8.23 Basidiomata and morphological characteristics of *A. tibetica* (CBS J) lineage 4-mtDNA (HKAS 135516)	181
8.24 Distribution of samples of *A. tibetica* (CBS J) lineage 4-mtDNA used in this study	182
8.25 Basidiomata and morphological characteristics of *A. tibetica* (CBS J) lineage 5-mtDNA (HMAS 99623)	184
8.26 Distribution of samples of *A. tibetica* (CBS J) lineage 5-mtDNA used in this study	185
8.27 Basidiomata of *Armillaria algida*	189
8.28 Distribution of samples of *Armillaria algida* used in this study	189
8.29 Basidiomata of *Armillaria amygdalispora*	193
8.30 Distribution of samples of *Armillaria amygdalispora* used in this study	194
8.31 Basidiomata of *Armillaria bruneocystidia*	201
8.32 Distribution of samples of *Armillaria bruneocystidia* used in this study	202
8.33 Distribution of samples of *Armillaria conifericola* used in this study	210

LIST OF FIGURES

Figure	**Page**
8.34 Basidiomata of *Armillaria gallica* subsp. *calidusa*	220
8.35 Distribution of samples of *Armillaria gallica* subsp. *calidusa* used in this study	221
8.36 Basidiomata of *Armillaria gallica* subsp. *gallica*	224
8.37 Basidiomata and morphological characteristics of *Armillaria korhonenii*	233
8.38 Distribution of samples of *Armillaria korhonenii* used in this study	234
8.39 Basidiomata of *Armillaria luteopileata*	240
8.40 Distribution of samples of *Armillaria luteopileata* used in this study	241
8.41 Basidiomata of *Armillaria pelmaspora*	255
8.42 Distribution of samples of *Armillaria pelmaspora* used in this study	255
8.43 Basidiomata of *Armillaria sinapina* subsp. *sinapina*	259
8.44 Distribution of samples of *Armillaria sinapina* subsp. *sinapina* used in this study	259
8.45 Basidiomata of *Armillaria sinensis*	263
8.46 Distribution of samples of *Armillaria sinapina* subsp. *sinapina*	263
8.47 Basidiomata of *Armillaria violacea*	267
8.48 Distribution of samples of *Armillaria violacea* used in this study	268
8.49 Basidiomata of *Armillaria violacea*	277
8.50 Distribution of samples of *Armillaria violacea* used in this study	278

ABBREVIATIONS AND SYMBOLS

com.	combination
diam.	diameter
e.g.	for example
et al.	and others
h	hours
gen.	genus/genera
ibid.	ibidem
min	minute
ml	maximum likelihood support
mm	millimetre
nov.	novum (Latin for new thing)
pp	posterior probabilities
sp.	species
spp.	species (plural)
viz.	that is
vs.	versus
$\bar{x}$	average
°C	degree centigrade
µm	micrometer
µl	microliter
%	percent
CBS	Chinese biological species
NA	Not Available
F_{ST}	Wright's F-statistics/Fixation index
ΦST	Relative differentiation index

CHAPTER 1

INTRODUCTION

1.1 Background

1.1.1 Taxonomy, Morphology, Ecological Significance, and Species Delimitation Challenges in *Armillaria*

Armillaria (Fr.) Staude is one genus of Physalacriaceae (Matheny et al., 2006; Collins et al., 2013), and the type species of this genus is *Armillaria mellea* (Vahl: Fr.) P. Kumm. This genus is characterized by its fruit body with a central stem, mostly fasciculate; cap convex to bell-shaped later expanded to slightly depressed, scaly, dry, somewhat hygrophanous; gills adnate to short decurrently, medium spaced to crowded; stem cylindrical, often with clavate, bulbous or tapering base, smooth or with floccose remnants of a veil, with or without a white to yellow, membranous or cottony ring; rhizomorphs black and conspicuous in some species; smell indistinct; taste mild to bitter (Figure 1.1). The micro characteristics are distinctive with basidiospores deposit white to cream, ellipsoid, smooth, hyaline, without iodine reactions; cheilocystidia small, cylindrical to clavate or branched, often septate; the basidia 4-spored; pileipellis a cutis to a trichoderm; clamps present or absent (Petersen & Vesterholt, 2008).

Species of *Armillaria* have a broad geographic distribution, they can be found on all continents due to their high adaptability to changing environments along geological timeframes (Heinzelmann et al., 2019). The species of this fungus can acquire new food resources by adopting different strategies, and employing the efficient dispersal strategy combining different modes of spread (Heinzelmann et al., 2019). Species of *Armillaria* are of significant economic and ecological importance, with both positive and negative aspects from the view of an anthropocentric point. As serious pathogens of woody plants, they can kill living plants, causing damage to forests with

huge economic losses. As saprotrophs, they are important wood decomposers that contribute to carbon and mineral cycling in forest ecosystems (Petersen & Vesterholt, 2008). In addition, it can act as a symbiont of orchid plants and other fungi, both the Chinese traditional medicinal herb *Gastrodia elata* Blume (Traditional Chinese Medicine Tianma) and the medicinal fungus *Polyporus umbellatus* (Pers.) Fr. (Traditional Chinese Medicine Fuling) needs the help of *Armillaria* to grow. In 2024, China's total output of medicinal *G. elata* is expected to reach 6,823 tons, rising to 7,040 tons by 2025 (https://www.emushroom.net/); at 20–30 RMB /kg for fresh Tianma, this equates to an annual market value of 14–21 billion RMB.



Note a–b Chinese biological species K (CBS K). c Chinese biological species M. d Chinese biological species

Figure 1.1 Morphological characteristics of *Armillaria*

From the past to the present, species definition in *Armillaria* has been challenging, and three operational species concepts were applied to distinguish different taxa, viz. morphological, biological, and phylogenetic species recognition, but

these methods always give conflicting results (Guo et al., 2016; Liang et al., 2021). At present, most of the currently known *Armillaria* species were first described as biological species firstly since Korhonen (1978) and Anderson and Ullrich (1979), which applied mating experiments to identify if there were reproductive barriers. However, biological species recognition has some serious limitations, it is difficult to obtain all single spore strains of known species for different researchers then to identify the somatic compatibility and incompatibility rely on experienced experimenters, sometimes, allopatric species may show incomplete reproductive barriers, at least partially, interfertile (e.g. *A. cepistipes* and *A. sinapina*; Bérubé et al., 1996; Banik & Burdsall, 1998) and mating tests for species identification in single spore strains of known species are paired with diploid strains of unknown species sometimes provide ambiguous results (e.g. Hasegawa et al., 2011; Keča et al., 2015; Heinzelmann et al., 2019). For morphological species recognition, the difference in macro- and micro-characteristics of fruiting bodies of related *Armillaria* species is very small, and sometimes it is difficult to obtain available fruiting bodies in the field. For phylogenetic species recognition, single gene phylogenies sometimes do not truly reflect a species' evolutionary history and relationship because of incomplete lineage sorting, homoplasy, or horizontal gene transfer (Heinzelmann et al., 2019).

To overcome these delimitation challenges, most newly described *Armillaria* taxa employ single or multilocus sequence data, including ribosomal markers (ITS, IGS-1, 28S), protein-coding genes (TEF-1α, β-tubulin, actin-1, gpd, RPB1, RPB2), and lineage-specific loci (h3h, hisps), analyzed via GCPSR, PTP, or BPP frameworks (Anderson & Stasovski, 1992; Antonín et al., 2009; Brazee et al., 2012; Coetzee et al., 2015; Duchesne & Anderson, 1990; Elías-Román et al., 2018; Guo et al., 2016; Hasegawa et al., 2010; Harrington & Wingfield, 1995; Hood & Ramsfield, 2016; Kim et al., 2000, 2006; Koch et al., 2017; Liang et al., 2021; Liu et al., 2024; Maphosa et al., 2006; Mulholland et al., 2012; Peng & Zhao, 2020; Ross-Davis et al., 2012; Tsykun et al., 2013). Up to now, the genus *Armillaria* is currently divided into two subgenera—

Desarmillaria and *Armillaria* (the latter comprising sections *Armillaria*, *Gallicae*, *Korhoneniorum*, *Ostoyarum*) (Qin et al., 2025), and 73 species have been described globally (Table 1.1). In China, 17 species have been reported (Coetzee et al., 2015; Guo et al., 2016; He et al., 1996; Liu et al., 2024; Peng & Zhao, 2020; Qin, 2002, 2007, 2024, 2025) (Table 1.1). Despite substantial progress in characterizing species diversity within *Armillaria*, the speciation history and true phylogenetic relationships, and its relation to *G. elata* cultivation, remain poorly understood.

1.1.2 Reproductive Compatibility and Potential Gene Flow within *Armillaria*

As Samarasinghe et al. (2020) proposed, "Hybridization is increasingly recognized as an important force impacting adaptation and evolution in many lineages of fungi." The expanding availability of genomic data shows that hybridization can spawn novel species, drive adaptive innovation, and even promote pathogenicity: the allopolyploid lager yeast *Saccharomyces pastorianus* (*S. cerevisiae* × *S. eubayanus*) combines fermentative vigor with cryotolerance for industrial brewing (Libkind et al., 2011); the wheat pathogen *Zymoseptoria tritici* harbors ~5 % of its genome as adaptive introgressions from *Neurospora* spp., including ≥ 18 virulence genes (Feurtey et al., 2019); and within Dutch elm disease, *Ophiostoma novo-ulmi* subspp. SSNU and SSAM interbreed extensively and carry 0–8 % introgression from *O. ulmi*, correlating with enhanced virulence and epidemic spread (Hessenauer et al., 2020). Such cases underscore ongoing gene flow: introgression blocks in *Z. tritici* reflect exchanges with other fungi (Feurtey et al., 2019), and powdery mildew *Blumeria graminis* f. sp. *triticale* emerged via repeated hybridization and backcrossing between wheat- and rye-adapted lineages, yielding a lineage with dramatically increased triticale pathogenicity (Menardo et al., 2016). These examples likely represent only the tip of the iceberg, and key questions remain about hybridization's broader role in fungal evolution and biodiversity (Steensels et al., 2021).

Qin et al. (2024, 2025) reported partial interfertility rates among *Armillaria* species pairs—particularly within Chinese biological species (hereafter CBS)—which

provide valuable insights into reproductive compatibility and potential gene flow among these taxa. Here's a breakdown of the findings: The partial interfertility rates among *Armillaria* species pairs (Qin et al., 2024, 2025) demonstrate a broad spectrum of reproductive compatibility, with values ranging from 0.1% to 41.1%. Except for species with complete reproductive isolation, the lowest compatibility was observed between CBS A and CBS B (0.1%), followed by CBS B and CBS C (0.3%), and *A.* cepistipes with CBS H (0.9%). Slightly higher rates were found in CBS A with CBS J (1.4%), CBS A with CBS M (1.4%), and CBS C with CBS M (1.7%). Moderate compatibility (3-5.4%) was recorded for multiple pairs, including CBS H with CBS L (3.4%), *A. calvescens* with CBS C (3.6%), CBS B with CBS L (3.6%), *A. cepistipes* with CBS B (3.7%), CBS B with CBS F (4.3%), CBS L with CBS N (4.8%), and CBS G with *A. mellea* (5.4%). Higher interfertility rates were observed in CBS H with CBS Q (13.1%), CBS C with CBS H (16.0%), CBS G with CBS K (16.6%), CBS O with CBS H (22.2%), with the maximum compatibility occurring between CBS C and CBS O (41.1%). These results collectively illustrate the varying degrees of reproductive isolation among different *Armillaria* lineages (Qin et al., 2024, 2025). *A. ostoyae* × *A. solidipes* hybrids can even produce fertile progeny (Qin et al., 2025). Host-interaction assays show dichotomous taxa (*A. borealis*, *A. mellea*, *A. ostoyae*) are more pathogenic than monopodial rhizomorphic species (*A. cepistipes*, *A. gallica*, *A. nabsnona*) (Morrison et al., 2004), and several lineages (e.g., *A. cepistipes*, *A. nabsnona*, Lineages 2, 3, 6, Nag E) are implicated in *G. elata* associations (Guo et al., 2016). Interspecific hybrid-affinity likely drove the gain/loss of pathogenicity clusters, modulating host infection. Frequent introgression could cause single-gene and genome-wide phylogenies to conflict, complicating evolutionary reconstruction. The genomic era necessitates a comprehensive integration of multi-omics data and diverse analytical methodologies to elucidate speciation processes and address complex evolutionary questions.

Table 1.1 Information on 73 known species in the genus *Armillaria*

Phylogenetic species	Biological species	References	Distributed continents
A. adelpha (Berk.) Sacc.	NA	Saccardo et al., (1882)	Asia
A. affinis (Singer) T.J. Volk & Burds.	NA	Volk and Burdsa (1995)	Caribbean, Central America
A. algida G.F. Qin, J. Zhao, W.M. Qin & Y.C. Dai	CBS O	Qin et al., (2024)	Asia
A. altimontana Brazee, B. Ortiz, Banik & D.L. Lindner	NABS X	Brazee et al., (2012)	North America
A. amygdalispora H.C. Wang, G.F. Qin, J. Zhao & Y.C. Dai	CBS L	Qin et al., (2024)	Asia
A. aotearoa I.A. Hood & T.D. Ramsfield	NA	Hood and Ramsfield (2016)	New Zealand
A. apalosclera (Berk.) A. Chandra & Watling	NA	Chandra and Watling (1982)	Asia
A. appendiculata Peck	NA	Peck (1897)	North America
A. argentina Speg.	NA	Spegazzini (1899)	South America
A. borealis Marxm. & Korhonen	EBS A	Marxmüller (1982)	Europe, “East Asia”
A. bruneocystidia H.C. Wang, G.F. Qin, J. Zhao & Y.C. Dai	CBS H	Qin et al., (2024)	Asia
A. calvescens Bérubé& Dessur.	NABS III	Bérubé and Dessureault (1989)	North America
A. camerunensis (Henn.) Courtec.	NA	Courtecuisse (1995)	Africa
A. cepistipes Velen.	EBS B	Velenovský (1920)	Europe, “North America”
A. conifericola G.F. Qin, J. Zhao, W.M. Qin & Y.C. Dai	CBS D	Qin et al., (2025)	Asia
A. desertorum T. Bau	NA	Hou et al., 2025	Asia
A. dicupella (Berk.) Sacc.	NA	Saccardo et al., (1882)	Asia
A. duplicata (Berk.) Sacc.	NA	Saccardo et al., (1882)	Asia
A. ectypa (Fr.) R.A. Koch & Aime	NA	Lamoure (1965)	Europe
A. fellea (Hongo) Kile & Watling	NA	Kile and Watling (1983)	Australia
A. fumosa Kile & Watling	NA	Kile and Watling (1983)	Australia
A. fuscipes Petch	NA	Petch (1909)	“Africa”, Asia
A. gallica subsp. *calidusa* G.F. Qin, W.M. Qin, J. Zhao, & Y. Yuan	CBS B	Qin et al., (2025)	Asia
A. gallica subsp. *canadensis* G.F. Qin, W.M. Qin, J. Zhao, & Y. Yuan	NABS VII	Qin et al., (2025)	North America
A. gallica subsp. *gallica* G.F. Qin, W.M. Qin, J. Zhao, & Y. Yuan	EBS E	Qin et al., (2025)	Europe

Table 1.1 (continued)

Phylogenetic species	Biological species	References	Distributed continents
A. gemina Bérubé& Dessur.	NABS III	Bérubé and Dessur (1989)	North America
A. granulosoides Zeller	NA	Zeller (1933)	South America
A. griseomellea (Singer) Kile & Watling	NA	Kile and Watling (1983)	"North America", South America
A. heimii Pegler	NA	Pegler (1977)	Africa
A. hinnulea Kile & Watling	NA	Kile and Watling (1983)	Australasia
A. horrens (Berk.) Sacc.	NA	Saccardo et al., (1882)	Asia
A. jezoensis J.Y. Cha & Igararashi	Nag. H	Cha et al., (1994)	Asia
A. korhonenii J.W. Liu, G.F. Qin, J. Chen, F.Q. Yu & Zhu L. Yang	CBS Q	Liu et al., (2024)	Asia
A. laricina (Bolton) Sacc.	NA	Saccardo et al., (1882)	Europe
A. limonea (G. Stev.) Boesew.	NA	Boesewinkel (1977)	Australasia, "South America"
A. luteobubalina Watling & Kile	NA	Podger et al., (1978)	Australasia, "South America"
A. luteopileata G.F. Qin, J. Zhao, W.M. Qin & K. Korhonen	CBS C	Qin et al., (2024)	Asia
A. macrospora Peck	NA	Peck (1900	North America
A. mellea (Vahl) P. Kumm	EBS D	Kummer (1871)	Europe, "East Asia, North America"
A. melleamericana J.W. Liu, W.M. Qin, J. Zhao, G.F. Qin & Y.C. Dai	NABSVI	Qin et al., (2025)	North American
A. melleasiana G.F. Qin, W.M. Qin, J. Zhao & Y.C. Dai	CBS K	Qin et al., (2025)	Asia
A. melleasiana subsp. *nipponica* (Cha & Igarashi) G.F. Qin, J. Zhao, W.M. Qin & Y.C. Dai	CBS G	Qin et al., (2025)	Asia
A. melleorubens (Berk. & M.A. Curtis) Sacc.	NA	Saccardo et al., (1882)	"Europe", North America, "South America"
A. mexicana Elías-Román, Medel, Alv.-Ros., J.W. Hanna, Ross-Davis, Mee S. Kim & N.B. Klopf.	NA	Elías-Román et al., (2018)	Mexico, Central America
A. montagnei (Singer) Herink	NA	Herink (1973)	"Europe", South America
A. multicolor (Berk.) Sacc.	NA	Saccardo et al., (1882)	Asia
A. nabsnona T.J. Volk & Burds.	NABSI X	Volk et al., (1996)	North America
A. nigropunctata (Fr.) Herink	NA	Herink (1973)	Europe
A. novae-zelandiae (G. Stev.) Boesew.	NA	Boesewinkel (1977)	Australia, South America

Table 1.1 (continued)

Phylogenetic species	Biological species	References	Distributed continents
A. omnituens (Berk.) Sacc.	NA	Saccardo et al., (1882)	Asia
A. ostoyae (Romagn.) Herink	EBS C	Herink (1973)	Europe, “East Asia”
A. pallidula Kile & Watling	NA	Kile and Watling (1988)	Australia
A. paulensis Capelari	NA	Qin et al., (2025)	Asia
A. pelmispora G.F. Qin, H.X. Ma, J.W. Liu, J. Zhao & W.M. Qin	NA	Qin et al., (2025)	Asia
A. procera Speg.	NA	Spegazzine (1889)	South America
A. puiggarii Speg.	NA	(Spegazzine (1889)	South America
A. pungentisquamosa G.F. Qin, W.M. Qin, J. Zhao & K. Korhonen	CBS P	Qin et al., (2024)	Asia
A. sinapina subsp. *alpina* G.F. Qin, J. Zhao, Y. Yuan & Y.C. Dai	CBS A	Qin et al., (2025)	Asia
A. sinapina subsp. *sinapina* G.F. Qin, J. Zhao, Y. Yuan & Y.C. Dai	NABS IV–V	Qin et al., (2025)	North American
A. sinensis G.F. Qin, J. Zhao, H.C. Wang, Y. Yuan & Y.C. Dai	CBS F	Qin et al., (2024)	Asia
A. singula J.Y. Cha & Igarashi	Nag. G	Cha et al., (1994)	East Asia, “North America”
A. solidipes Peck	NA	Peck (1900)	“Europe, Asia”, North America
A. sparrei (Singer) Herink	NA	Herink (1973)	“Europe, Asia, North America”, South America
A. tabescens (Scop.) Emel	NA	Emel (1921)	Europe, “Asia, North America”
A. tibetica G.F. Qin, H.C. Wang, J. Zhao, Y. Yuan & Y.C. Dai	CBS J	Qin et al., (2024)	Asia
A. tigrensis (Singer) T.J. Volk & Burds	NA	Volk and Burdsall (1995)	South America
A. umbrinobrunnea (Singer) Pildain & Rajchenb.	NA	Pildain et al., (2010)	South America
A. vara (Berk.) Sacc.	NA	Saccardo et al., (1882)	Asia
A. violacea H.C. Wang, W.M. Qin, G.F. Qin, J. Zhao & Y.C. Dai	CBS N	Qin et al., (2024)	Asia
A. viridiflava (Singer) T.J. Volk & Burds.	NA	Volk & Burdsall (1995)	Europe, “South America”
A. xiaocaobaensis J.H. Peng & C.L. Zhao	NA	Peng & Zhao (2019)	Asia
A. yungensis (Singer) Herink	NA	Herink et al., (1973)	South America

1.2 Objectives

1.2.1 To resolve *Armillaria* species diversity, true phylogenetic relationships, and speciation history by integrating mitochondrial and nuclear genomes with mating-experiment results and morphological observations.

1.2.2 To assess and characterize phylogenomic discordance arising from incomplete lineage sorting, introgression, and dispersal, and relate these patterns to host specificity and biogeographic distribution.

1.2.3 To develop a multi-level identification framework combining graphical barcodes, DNA barcodes, and SSR markers for rapid discrimination of *Armillaria* species and strains.

1.2.4 To screen *Armillaria* species for optimal symbiosis with *Gastrodia elata* through integrated phylogenetic–physiological analyses, thereby informing cultivation practices.

1.3 Expected Outcomes

1.3.1 High-Resolution Species Tree

An integrated phylogeny of *Armillaria* based on mitochondrial and nuclear genomes, corroborated by mating experiments and morphological data, clearly resolve species diversity, boundaries, and speciation history.

1.3.2 Detection and Analysis of the Causes of Phylogenetic Conflict

1.3.2.1 A systematic survey of gene-tree versus species-tree topologies that quantifies conflict at key nodes (e.g., using gene concordance factors, Quartet Sampling, etc.).

1.3.2.2 Preliminary inference of underlying causes, such as incomplete lineage sorting, introgression, or dispersal via D-statistics (ABBA–BABA) and QulBL analyses, etc.

1.3.3 Validated Multi-Level Identification Toolkit

A practical framework combining graphical barcodes, DNA barcode loci, and SSR marker panels, experimentally validated to discriminate all target *Armillaria* species and strains with high accuracy.

1.3.4 Optimized Symbiotic Strain Selection

1.3.4.1 Identification of more *Armillaria* species showing good compatibility and growth-promotion in *Gastrodia elata* pairing assays.

1.3.4.2 Phylogenetic and physiological profiling of these strains to inform and enhance Tianma cultivation practices.

1.4 Research Contents

This thesis comprises nine chapters.

Chapter 1 introduces the morphological characteristics, economic value, and ecological significance of *Armillaria*, while addressing the challenges in species delimitation and recent advances in taxonomic research. It explores the role of hybridization in fungal evolution and biodiversity, as revealed by omics studies, and discusses how widespread interfertility within the genus may facilitate gene flow. The chapter emphasizes the necessity of integrating multi-omics approaches in the genomic era to elucidate the speciation history of *Armillaria*.

Chapter 2 describes the study samples, DNA extraction, library preparation, and sequencing, followed by sequencing data processing, including quality control, nuclear and mitochondrial genome assembly, annotation, gene prediction, and presents the methods and results of phylogenetic analyses based on both nuclear and mitochondrial datasets.

Chapter 3 examines genetic structure and differentiation in *Armillaria* by applying PCA and ancestry assignment and admixture analysis, calculating interspecific F_{ST} (nuclear and mitochondrial), mitochondrial ΦST and dxy, and integrating these benchmarks with Chapter 2's phylogenies to evaluate the need to formally recognize candidate lineages as new species.

Chapter 4 compares conflicts between the nuclear and mitochondrial phylogenies of *Armillaria* and rigorously validates their incongruence using multiple approaches. We employ D-statistics, QuIBL, and reticulate-evolution analyses to dissect the underlying causes of phylogenetic discordance. Our results show that incomplete lineage sorting is the primary driver of phylogenetic discordance within

Armillaria, while hybridization and introgression also contribute measurably to the observed signal.

Chapter 5 offers a concise, systematic overview of our marker-development framework in *Armillaria*, covering three key strategies: the use of neural networks on low-coverage genome data to generate distinctive graphic barcodes; a genome-wide pipeline for mining and validating candidate DNA barcode loci; and the design and testing of SSR markers for high-resolution, strain-level discrimination across the genus.

Chapter 6 leverages mitochondrial and nuclear genome data to pinpoint divergence times across *Armillaria* species and, through molecular-clock calibration, reconstruct their ancestral distribution ranges. By integrating the heterogeneity between mitochondrial and nuclear genomes, this chapter elucidates the connections between *Armillaria* speciation and contemporary plant biogeography and reveals how historical climatic fluctuations have driven shifts in population connectivity and isolation.

Chapter 7 delivers a comprehensive review of research on the two key fungi involved in Tianma (*Gastrodia elata*) cultivation—the germination fungus and the symbiotic *Armillaria* species. It systematically describes the cultivation trials carried out with different *Armillaria* taxa and the development of associated cultivation systems. Finally, in response to current industry demands, the chapter offers strategic recommendations for promoting the sustainable development of the Tianma industry, with an emphasis on the selection and application of high-performance fungal strains and the establishment of intellectual property protection mechanisms for those strains.

Chapter 8 provides formal descriptions of the newly identified species and offers a systematic summary of the morphological characteristics of all known species.

Chapter 9 summarizes the advances made in this study, discusses the current challenges it faces, and outlines the key priorities for future research.

CHAPTER 2

PHYLOGENETIC RECONSTRUCTION OF *ARMILLARIA*

2.1 Introduction

This chapter aims to reconstruct a robust phylogenetic framework for *Armillaria* by integrating biparentally inherited nuclear genomes with maternally inherited mitochondrial genomes. These two genomic compartments often capture different aspects of evolutionary history, where the nuclear loci reflect biparental ancestry and genome-wide divergence, and the mitochondrial genomes preserve uniparental lineage signals. By combining these complementary datasets, this chapter seeks to resolve relationships among major clades, evaluate the coherence of species complexes, and identify potential cryptic diversity within *Armillaria*.

2.2 Materials and Methods

2.2.1 Sampling

Specimens for this study were obtained through field collections and interlibrary loans, while the test strains were sourced from field isolations, commercial purchases, and generous personal donations. We also incorporated publicly available sequencing data from NCBI (https://www.ncbi.nlm.nih.gov) and JGI (https://jgi.doe.gov). In total, we used 625 *Armillaria* research materials (Table C1).

2.2.2 DNA Extraction, Library Preparation, and Sequencing

Illumina libraries were prepared using the Nextera XT DNA Sample Preparation Kit (Illumina Inc., USA). Approximately 100 μg of genomic DNA was sequenced on the Illumina HiSeq 2000 platform. The 150 bp paired-end libraries were prepared to generate approximately 3‑5 GB of raw data.

2.2.3 Sequencing Data Processing

2.2.3.1 Data quality control

Raw second-generation sequencing reads were first assessed for quality with FastQC (http://www.bioinformatics.babraham.ac.uk/projects/fastqc; Andrews, 2010), which provides detailed summary statistics but does not perform filtering or correction (Andrews, 2010). Next, reads were trimmed, filtered, and filtered of adapters using Trimmomatic v0.39 (Bolger et al., 2014) in paired-end mode (ILLUMINACLIP: TruSeq3-PE.fa:2:30:10, LEADING:3, TRAILING:3, SLIDINGWINDOW:4:15, MINLEN:36; detailed workflow at https://www.jianshu.com/p/105c61aec64c). To eliminate PCR and optical duplicates, FastUniq (Xu et al., 2012; http://sourceforge.net/projects/fastuniq/) was employed to rapidly identify and remove paired-end duplicate reads (see http://blog.sina.com.cn/s/blog_938257710102xju6.html for parameters and results). Filtered reads then underwent error correction with Musket (Liu et al., 2013; https://www.plob.org/article/7865.html), correcting erroneous k-mers before assembly.

2.2.3.2 Nuclear and Mitochondrial Genome Assemble, Annotation, and Gene Prediction

Genomes were assembled from the clean reads using SPAdes v3.15.3 with the --careful flag and k-mer sizes 21,33,55,77,99,127 (Bankevich et al., 2012). Then, assembly completeness and gene content were evaluated with BUSCO using the agaricales_odb10 lineage dataset (Simão et al., 2015); the results of assembly quality assessment are shown in Table C2. Finally, nuclear genomes were annotated using BRAKER3 in both reference-guided and ab initio gene prediction modes (Brůna et al., 2023).

The mitochondrial genomes were assembled by GetOrganelle v. 1.7.5 with the default parameters (Jin et al., 2019; the results of assemblies are shown in Table C3) and first annotated automatically using the MFannot tool (Beck & Lang, 2010) (http://megasun.bch.umontreal.ca/cgi-bin/mfannot/mfannotInterface.pl) based on the genetic code 4 (i.e., Mold, Protozoan, and Coelenterate Mitochondrial genetic code). Annotation of rRNA and tRNA genes was checked by using RNAweasel (https://megasun.bch.umontreal.ca/apps/rnaweasel/) (Beck & Lang, 2010) and tRNAscan-

SE 2.0 (http://lowelab.ucsc.edu/tRNAscan-SE/index.html) (Lowe & Chan, 2016), respectively. Sequences longer than 300 bp of hypothetical proteins, including ORFs and LAGLIDADG, GIY-YIG homing endonuclease families, were detected in intergenic regions based on the NCBI Open Reading Frame Finder (https://www.ncbi.nlm.nih.gov/orffinder) (Coordinators, 2017), as well as the product of possible protein sequences, were checked by smart-blast searches against the NCBI non-redundant protein sequence database (Bleasby & Wootton, 1990). For a precise annotation, the intron and exon borders of PCGs were individually verified, starting with aligning gene sequences to cognate allele sequences (acquired via Extract Regions in Geneious Prime) in the previously annotated mitogenomes of Armillaria using the MAFFT (Katoh et al., 2005) program in Geneious Prime 2020.0.3 (BioMatters, Ltd., Auckland, New Zealand).

2.2.3.3 Phylogenetic Relationships between the Species

1. Nuclear dataset

Single-copy nuclear genes identified in the sample with the lowest BUSCO completeness score (HKAS45820: C: 9.9%, S: 9.9%, D: 0%, F: 9.1%, M: 81%) were used as reference. Custom scripts were developed to extract orthologous proteins from the BUSCO results of the remaining 600 samples, yielding a set of 385 protein genes for phylogenetic analysis. Each protein gene was individually aligned using MAFFT v7.407 (Katoh, 2013), and the resulting alignments were concatenated in Geneious Prime 2020.0.3 (Biomatters Ltd., Auckland, New Zealand). Phylogenetic reconstruction was conducted using RAxML v8.2.12 under the PROTGAMMAWAG model, and the tree was rooted with *Guyanagaster necrorhizus*. Node support was assessed using 100 rapid bootstrap replicates.

2. Mitochondrial dataset

Homologous mitochondrial genome blocks across all 605 samples were identified using ORPA (Bi et al., 2024), with CBSK00111 serving as the reference genome. Multiple sequence alignments were generated, and phylogenetic reconstruction was performed using RAxML v8.2.12 (Stamatakis et al., 2014) under

the GTR+GAMMA substitution model. The tree was rooted with *Guyanagaster necrorhizus*. Node support was evaluated using 100 rapid bootstrap replicates to assess the robustness of inferred relationships.

2.3 Results

2.3.1 Phylogenetic Relationships Generated from the Nuclear Dataset

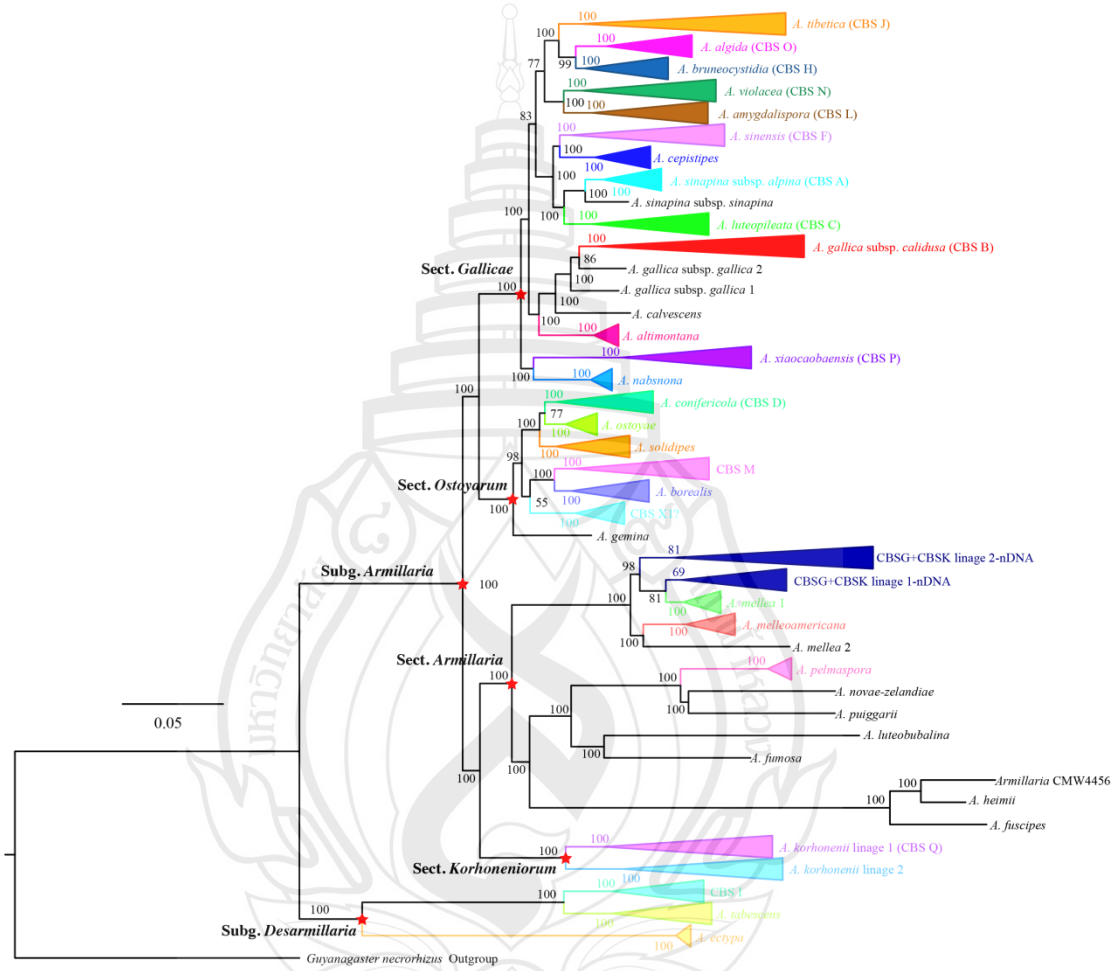
As shown in Figure 2.1 (where branches remain uncollapsed to clearly display species-level relationships; see Figure D1 for details), our phylogenetic analysis of 385 concatenated nuclear orthologues resolved 42 distinct lineages within *Armillaria*. All currently recognized Chinese biological species of *Armillaria* formed distinguish lineages were strongly supported (bootstrap values = 100%), with the exception of the CBSG and CBSK under *mellea* complex which exhibited a mixed and cross distribution pattern across two highly supported lineages (CBSG+CBSK linage 1-nDNA and CBSG+CBSK linage 2-nDNA), Consequently, this analysis resolved a total of 19 evolutionary lineages in China.

Following the latest classification by Qin et al., (2025) at the subgeneric and sectional levels, *Armillaria* is divided into two subgenera:

Subgenus *Desarmillaria*: comprising CBS I, *A. ectypa*, and *A. tabescens*.

Subgenus *Armillaria*, which includes 39 species divided into four sections: (1) Section *Armillaria*: including 13 species, CBSG+CBSK lineage 1-nDNA, CBSG+CBSK lineage 2-nDNA, *A. fumosa*, *A. fuscipes*, *A. heimii*, *A. luteopileata*, *A. mellea*-1, *A. mellea*-2, *A. melleoamericana*, *A. novae-zelandiae*, *A. pelmaspora*, *A. puiggarii*, and *Armillaria* sp. CMW4456; (2) Section *Gallicae*: including 17 species, *A. algida* (CBS O), *A. altimontana*, *A. amygdalispora* (CBS L), *A. bruneocystidia* (CBS H), *A. calvescens*, *A. cepistipes*, *A. gallica* subsp. *calidusa* (CBS B), *A. gallica* subsp. *gallica* 1, *A. gallica* subsp. *gallica* 2, *A. luteopileata* (CBS C), *A. nabsnona*, *A. pungentisquamosa* (CBS P), *A. sinapina* subsp. *alpina* (CBS A), *A. sinapina* subsp.

sinapina, *A. sinensis* (CBS F), *A. tibetica* (CBS J), and *A. violacea* (CBS N). 3) Section *Korhoneniorum*: Contains two lineages—*A. korhonenii* lineage 1 and lineage 2 (CBSQ). 4) Section *Ostoyarum* containing *A. borealis*, *A. conifericola* (CBS D), *A. gemina*, CBS M, *A. ostoyae*, *A. solidipes*, and *Armillaria* sp. 1.



Note Maximum-likelihood (ML) phylogenetic tree of *Armillaria* inferred from 385 orthologous proteins across 600 nuclear genomes, branches are collapsed to illustrate species-level relationships. Bootstrap (BS) values (≥ 70%) derived from the ML analysis are shown above the branches at the nodes. The tree is rooted with *Guyanagaster necrorhizus.*

Figure 2.1 Maximum-likelihood (ML) phylogenetic tree of *Armillaria* inferred from 385 orthologues orthologous proteins across 600 nuclear genomes

2.3.2 Phylogenetic Relationships Generated from the Mitochondrial Dataset

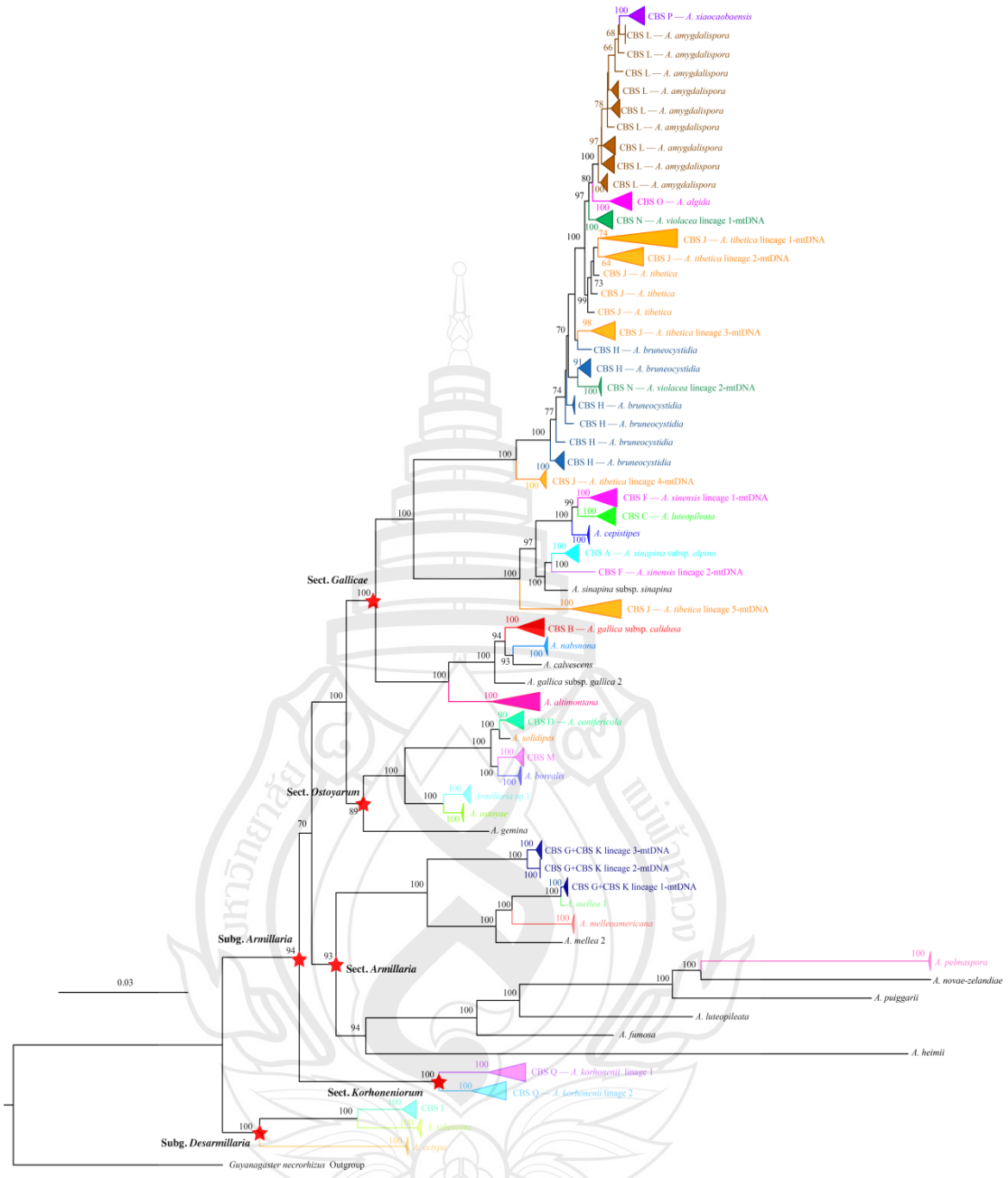
As shown in Figure 2.2 (where branches remain uncollapsed to clearly display species-level relationships; see Figure D2 for details). Phylogenetic analysis of mitochondrial genomes identified 46 main distinct phylogenetic clades within the genus *Armillaria*. The subgenus *Desarmillaria* comprises three phylogenetic species: *A. ectypa*, *A. tabescens*, and CBS I.

The subgenus *Armillaria* encompasses 43 phylogenetic lineages, organized into the following sections: (1) Section *Armillaria*: Contains 12 species, including *A. fumosa*, *A. heimii*, *A. luteopileata*, *A.* mellea 1, *A. mellea* 2, *A. melleoamericana*, *A. novae-zelandiae*, *A. pelmaspora*, *A. puiggarii*, CBS G + CBS K lineage 1-mtDNA, CBS G + CBS K lineage 2-mtDNA, and CBS G + CBS K lineage 3-mtDNA. (2) Section *Gallicae*: encompasses 22 main lineages, including *A. altimontana*, *A. algida* (CBS O), *A. calvescens*, *A. cepistipes*, *A.* gallica *subsp*. *calidusa* (CBS B), *A. gallica* subsp. *gallica* 2, *A. luteopileata* (CBS C), *A. nabsnona*, *A. sinapina* subsp. *alpina* (CBS A), *A. sinapina* subsp. *sinapina*, two distinct lineages of *A. sinensis* (CBS F) (mtDNA lineages 1 and 2), five major geographic clades of *A. tibetica* (CBS J) (mtDNA lineages 1–5), *A. violacea* (CBS N) (mtDNA lineages 1 and 2), and *A. xiaocaobaensis* (CBS P), with *A. amygdalispora* (CBS L) and *A. bruneocystidia* (CBS H) each forming paraphyletic assemblages. (3) Section *Korhoneniorum*: Includes two species, *A. korhonenii* linage 1 (CBS Q) and *A. korhonenii* linage 2. (4) Section *Ostoyarum*: Comprises seven species, including *A. borealis*, *A. conifericola* (CBS D), *A. gemina*, *A. ostoyae*, *A. solidipes*, *Armillaria* sp. 1, and CBS M.

Analysis of the nuclear gene phylogeny recovered 19 well-supported clades from China, 12 of which were also strongly supported by the mitochondrial tree, including *A. algida* (CBS O), *A. conifericola* (CBS D), *A. gallica* subsp. *calidusa* (CBS B), *A. korhonenii* lineages 1 (CBS Q) and 2, *A. luteopileata* (CBS C), *A. pelmaspora*, *A. sinapina* subsp. *alpina* (CBS A), *A. xiaocaobaensis* (CBS P), *Armillaria* sp. 1, and

CBS I and M. The remaining seven clades showed clear conflict: in the mitochondrial phylogeny *A. sinensis* (CBS F) splits into two clades; *A. tibetica* (CBS J) forms five geographically structured subclades (J1–J5); *A. violacea* (CBS N) divides into two lineages; and the nuclear CBS G + CBS K lineages (1-nDNA and 2-nDNA) further subdivide into three mitochondrial clades. Furthermore, *A. amygdalispora* (CBS L) and *A. bruneocystidia* (CBS H) appear paraphyletic in the mitochondrial tree (Figure 2.2).

A closer look at the nuclear phylogeny (Figure D2) confirms that the two mitochondrial clades of *A. sinensis* (labeled as *A. sinensis* (CBS F) lineage 2-mtDNA) and *A. violacea* (labeled as *A. violacea* (CBS N) lineage 2-mtDNA) also form distinct sister clades in the nuclear tree. It highlights the conflicts between the CBS G + CBS K nuclear lineages and their three mitochondrial counterparts, *A. tibetica* (CBS J) subdivides into five geographically structured mitochondrial subclades, including *A. tibetica* (CBS J) lineage 1-mtDNA (samples from central China), *A. tibetica* (CBS J) lineage 2-mtDNA (subalpine Hengduan Mountains of southwest China), *A. tibetica* (CBS J) lineage 3-mtDNA (southern Tibet), *A. tibetica* (CBS J) lineage 4-mtDNA (Xinjiang Province), *A. tibetica* (CBS J) lineage 5-mtDNA (eastern Hengduan Mountains), and the paraphyletic groupings of *A. amygdalispora* and *A. bruneocystidia*.



Note Maximum-Likelihood (ML) phylogenetic tree of genus *Armillaria* constructed from a concatenated dataset of 605 mitochondrial homeblocks. Bootstrap support values (BS ≥ 70%) from the ML analysis are indicated above the branches at corresponding nodes. The tree is rooted with *Guyanagaster necrorhizus*.

Figure 2.2 Maximum-Likelihood (ML) phylogenetic tree of genus *Armillaria* constructed from a concatenated dataset of 605 mitochondrial homeblocks

2.4 Conclusions

In this chapter, we reconstructed the phylogeny of *Armillaria* using both biparentally inherited nuclear genomes and maternally inherited mitochondrial genomes. The nuclear-gene analysis resolved 42 highly supported lineages, while the mitochondrial tree recovered 46 distinct phylogenetic clades. Fourteen of these lineages that originated from China were congruently supported in both nuclear and mitochondrial trees, underscoring their taxonomic stability. Notably, *Armillaria korhonenii* lineage 2, *Armillaria* sp. 1, *A. violacea* (CBS N) lineage 2-mtDNA, and strains CBS I and CBS M emerge as strong candidates for undescribed species (Figure D1 − D2). In contrast, *A. xiaocaobaensis* and *A. pungentisquamosa* are shown to represent a single species (Figure D1 − D2).

At the same time, multiple instances of topological conflict were uncovered (e.g., within the *A. sinensis* and *A. tibetica* complexes, the CBS G+K group, and the paraphyletic arrangements of *A. amygdalispora* and *A. bruneocystidia*).

Overall, our integrative phylogenomic framework provides a robust foundation for delimiting species in the genus *Armillaria*, highlights several putative novel taxa for further taxonomic investigation, and illustrates the importance of combining nuclear and organellar data to disentangle complex evolutionary histories in fungi.

CHAPTER 3

GENETIC DIFFERENTIATION AMONG *ARMILLARIA* PHYLOGENETIC LINEAGES

3.1 Introduction

In this chapter, we applied principal component analysis (PCA) and individual ancestry inference, calculated Weir and Cockerham's F_{ST} for both nuclear and mitochondrial SNPs, and estimated absolute genetic distance (dxy) along with the relative differentiation index (ΦST) for the mitochondrial dataset to characterize genetic differentiation in *Armillaria*. By integrating these population-genetic metrics with the phylogenetic framework established in Chapter 2, we assessed the taxonomic validity of divergent lineages and evaluated whether candidate undescribed groups warrant formal recognition as novel species.

3.2 Methods

3.2.1 SNP Calling and Filtering

Based on the aforementioned quality-controlled sequencing data, this study systematically analyzed genome-wide variations across 584 samples. First, paired-end reads from each sample were aligned to the combined nuclear and mitochondrial reference genome of *Armillaria mellea* (strain CBSK00111) using BWA-MEM software v 0.7.17 (Li, 2013) with critical parameters: multithreaded parallel computing (-t 50) and sequencing metadata embedding (-R '@RG\tID:SAMPLE\tLB:SAMPLE\tSM:SAMPLE\tPL:ILLUMINA'). Sorted BAM files were generated through coordinate sorting (sort -@ 20) using SAMtools v 1.9 (Danecek et al., 2021). Variant calling was performed using DeepVariant v 1.6.1 (Poplin et al., 2018) in the WGS model, with the --haploid_contigs parameter specifically added to optimize mitochondrial SNP detection. Subsequently,

GLNexus v 1.2.7 (Yun et al., 2020) was employed for scalable gVCF merging and joint analysis. BCFtools (v1.10; Danecek et al., 2011) was used to extract SNP data from the integrated dataset, filtering out variants with quality scores below 20. Then, due to our dataset included many haploid strains and experience-based assignments of mono- or dikaryotic status can be unreliable, we implemented an inline Bash workflow to filter nuclear SNPs: we first ran bcftools query -f '[%CHROM\t%POS\t%GT]\n' input.vcf.gz and piped its output into a while read -r chrom pos gt; do…done loop (with set -euo pipefail) that, for each sample, incremented a total[sample] counter for every genotype call and a het [sample] counter when the GT field contained a heterozygous call (i.e., an "x/y" with x≠y). After processing all sites, we iterated over each sample to compute rate = het[sample]/total[sample] (using awk) and excluded any sample for which rate ≤ 0.05 by printing a message such as "Excluding $sample (heterozygosity rate = $rate)". This approach ensures that strains with heterozygosity rates at or below 5%, likely haploid, are removed from downstream analyses; see Table C4 for the final list of diploid samples. Principal component analysis was conducted and visualzed in a 3D scatterplot representing the first three principal components (PC1, PC2, and PC3) using VCF2PCACluster (He et al., 2024). Then the samples were grouped by phylogenetic sections (e.g., sect. *Armillaria*, sect. *Gallicae*) based on prior phylogenomic inferences, and the PCA analysis on phylogenetic sections was conducted in R using ggplot2 and plotly, with species-specific shapes and colors assigned consistently across groups.

3.2.2 Weir & Cockerham's F_{ST} of Nuclear SNPs, Absolute Genetic Distance (dxy) and Relative Differentiation Index (ΦST) of Mitochondrial SNPs

This study builds upon the mitochondrial phylogenetic framework presented in Chapter 2, at the mitochondrial genome level, absolute genetic distance (dxy) and relative differentiation index (ΦST) were calculated in R using the ape package's dist.dna (model="raw", pairwise.deletion=TRUE) (Paradis & Schliep, 2019) and estimated by analysis of molecular variance (AMOVA) in the pegas package (Paradis, 2010). In addition, although Weir & Cockerham's F_{ST} is primarily designed for biallelic nuclear data, it was also computed for mitochondrial SNPs using VCFtools v0.1.16 (Danecek et al., 2011) as a supplementary comparative metric. At the nuclear genome level, Weir & Cockerham's F_{ST} was similarly calculated using VCFtools v0.1.16 to assess overall genetic differentiation among species.

3.3 Results

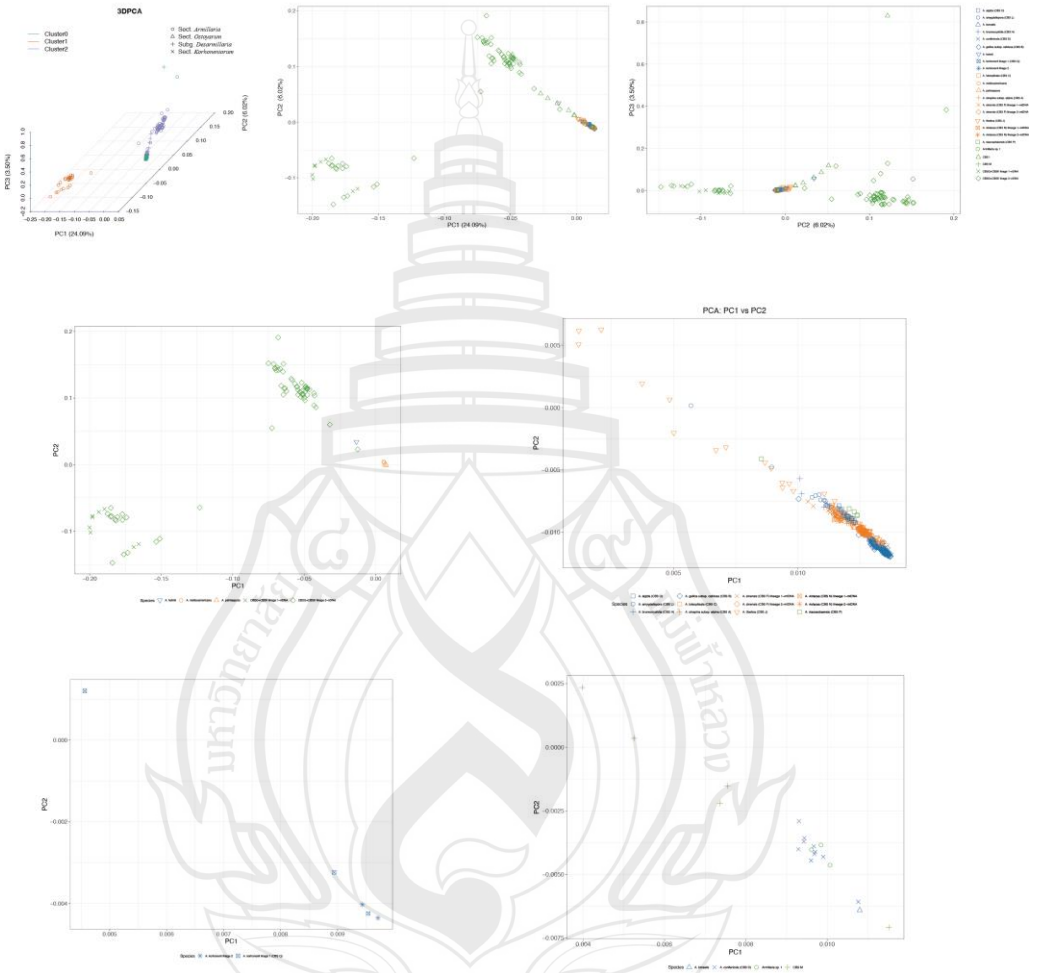
3.3.1 PCA Analysis of Nuclear and Mitochondrial SNPs

3.3.1.1 Nuclear SNP analysis

For nuclear SNP data, we conducted PCA on the genetic covariance matrix of all 473 individuals using 6356916 biallelic sites. The first three principal components (PC1, PC2, and PC3) explained 24.09 %, 6.02 %, and 3.50 % of the total genetic variation, respectively (Figure 3.1a). This analysis demonstrated a considerable level of genetic differentiation within the genus Armillaria, although species within the four sections (sect. *Armillaria, Gallicae, Korhoneniorum,* and *Ostoyarum*) did not each form distinct clusters. The species in sect. *Armillaria* and subg. *Desarmillaria* showed the greatest separation, whereas those in sect. *Gallicae*, sect. *Korhoneniorum*, and sect. *Ostoyarum* grouped more closely together. Panels (b) and (c) of Figure 3.1 (PC1 vs. PC2 and PC2 vs. PC3) provide a finer resolution of these patterns: aside from four lineages—CBSG + CBSK lineage 1 (nDNA), CBSG + CBSK lineage 2 (nDNA), CBS I, and *A. heimii*, all other species almost overlap within a single broader cluster.

To highlight genetic differentiation within each section, we performed section-specific PCA (PC1 vs. PC2), shown in Panels d to g of Figure 3.1. Panel d illustrates clustering within sect. *Armillaria*: *A. heimii*, *A. melleoamericana*, *A. pelmaspora*, and the CBSG + CBSK lineage 1 (nDNA) each form well-defined clusters. In contrast, CBSG + CBSK lineage 2 (nDNA) splits into two primary clusters—one relatively distinct, and the other intermixed with CBSG + CBSK lineage 1 (nDNA); Panel e depicts clustering within sect. *Gallicae*: *A. tibetica* (CBS J) forms the most dispersed cluster, while the remaining species largely overlap yet still resolve into relatively distinct groupings, such as *A. algida* (CBS O), *A. amygdalispora* (CBS L), *A. gallica* subsp. *calidusa* (CBS B), *A. luteopileata* (CBS C), *A. sinensis* (CBS F) lineage 1−mtDNA, *A. violacea* (CBS N) lineage 1−mtDNA, and *A. xiaocaobaensis* (CBS P); Panel f depicts clustering within sect. *Korhoneniorum*: due to limited sample size, clustering patterns for *A. korhonenii* lineage 2

and *A. korhonenii* lineage 1 (CBS Q) could not be resolved; Panel g depicts clustering within sect. *Ostoyarum*: CBS M forms a distinct cluster, *A. conifericola* (CBS D) and *Armillaria* sp. 1 are intermixed, yet each centers around its own cluster; *A. borealis*, represented by a single sample, lies distant from CBS M's main cluster.



Note a Three-dimensional visualization showing genetic differentiation along the first to three principal components (PC1, PC2, PC3) for all individuals. b PC1 vs PC2 for all individuals. c PC2 vs PC3 for all individuals. Subsequent panels illustrate genetic structure within taxonomic subdivisions: d sect. *Armillaria* (PC1 vs PC2). e sect. *Gallicae* (PC1 vs PC2); f sect. *Korhoneniorum* (PC1 vs PC2); g sect. *Ostoyarum* (PC1 vs PC2).

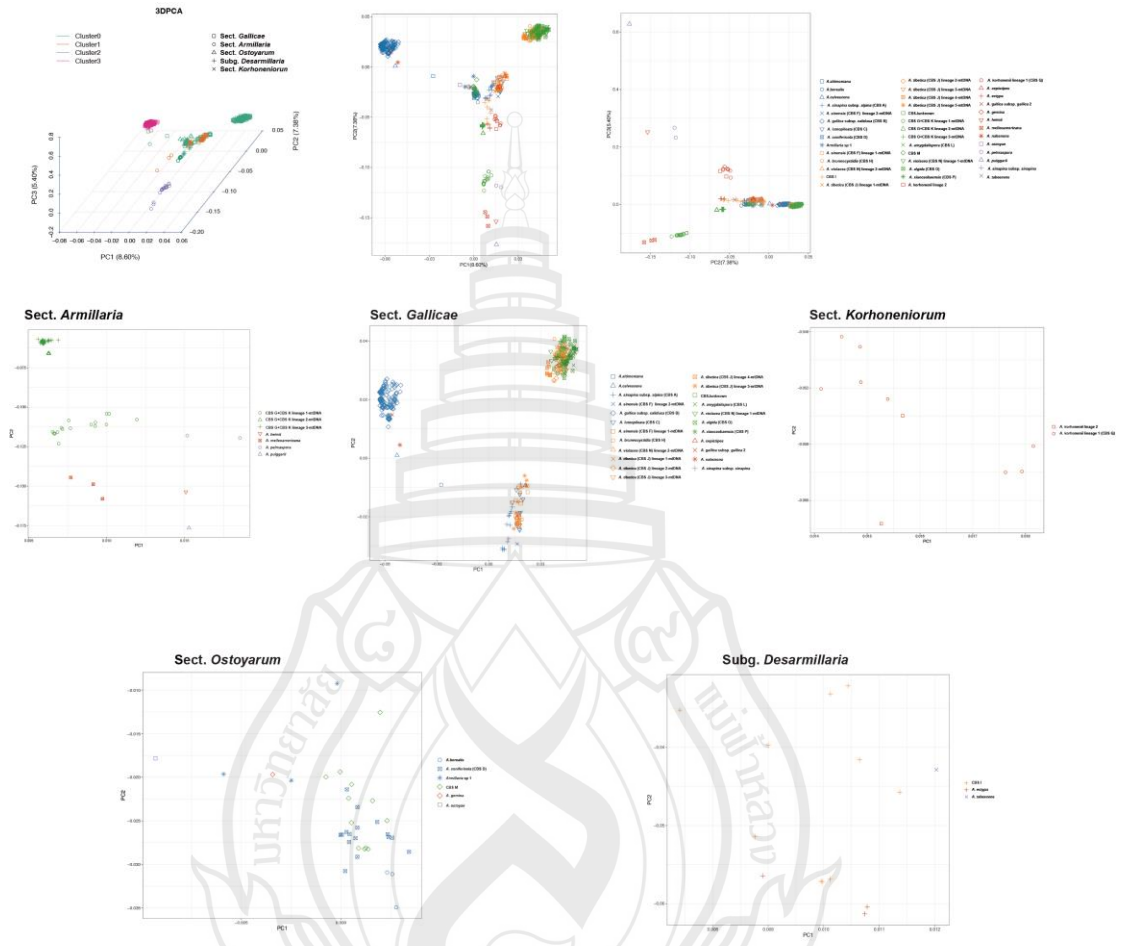
Figure 3.1 Principal component analysis (PCA) of nuclear genome variation among 473 studied *Armillaria* individuals

3.3.1.2 Mitochondrial SNP analysis

For mitochondrial SNP data, we conducted PCA on the genetic covariance matrix of all 584 individuals using 21217 haploid sites (including all haploid samples). The first three principal components (PC1, PC2, and PC3) explained 8.60%, 7.38%, and 5.40% of the total genetic variation, respectively (Figure 3.2a). This analysis demonstrated a considerable level of genetic differentiation within the genus *Armillaria*, sect. *Armillaria, Korhoneniorum,* and *Ostoyarum* of subg. *Armillaria* and subg. *Desarmillaria* each forms distinct clusters; meanwhile, the species of sect. *Gallicae* resolved into three separate clusters. Panels (b) and (c) of Figure 3.2 (PC1 vs. PC2 and PC2 vs. PC3) provide a finer resolution of these patterns: samples are distributed in a Y-shaped configuration (PC1 vs. PC2). Several taxa form well-defined clusters—for example, *A. altimontana, A. calvescens, A. gallica* subsp. *calidusa* (CBS B), *A. melleoamericana, A. nabsnona, A. puiggarii, A. heimii*, CBS G + CBS K lineage 1 (mtDNA), *A. pelmaspora,* CBS G + CBS K lineage 2 (mtDNA), and CBS G + CBS K lineage 3 (mtDNA). Although the remaining species overlap, they nonetheless appear to form discrete lattice-like subclusters within the broader distribution.

The section-specific PCA (PC1 vs. PC2) shown in Figure 3.2's Panels d–h reveals clear intra-section differentiation. In sect. *Armillaria* (Panel d), seven lineages—*A. heimii, A. melleoamericana, A. pelmaspora, A. puiggarii*, CBS G + CBS K lineage 1-mtDNA, CBS G + CBS K lineage 2-mtDNA, and CBS G + CBS K lineage 3-mtDNA—form distinct clusters, indicating distinct differentiation within the section. Within sect. *Gallicae* (Panel e), all taxa resolve into three major clusters consistent with Chapter 2's phylogeny (Figure 2.2): the leftmost cluster contains *A. altimontana, A. calvescens, A. gallica* subsp. *calidusa* (CBS B), *A. gallica* subsp. *gallica* 2, and *A. nabsnona*; the lower cluster includes *A. cepistipes, A. luteopileata* (CBS C), *A. sinapina* subsp. *alpina* (CBS A), *A. sinapina* subsp. *sinapina, A. sinensis* lineages 1 and 2 (CBS F), and *A. tibetica* lineage 5 (CBS J); and the upper-right cluster comprises *A. algida* (CBS O), *A. amygdalispora* (CBS L), *A. bruneocystidia* (CBS H), *A. violacea* lineages 1 and 2 (CBS N), *A. xiaocaobaensis* (CBS P), and *A. tibetica* lineages 1–4 (CBS J). sect. *Korhoneniorum* (Panel f) shows no clear clustering, likely due to limited *A. korhonenii* lineage 2 samples. In sect. *Ostoyarum* (Panel g), *A. borealis, A. gemina, A. ostoyae,* and *Armillaria* sp. 1 each form separate clusters, while *A. conifericola* (CBS D) and CBS M

overlap. Finally, Subg. *Desarmillaria* (Panel h) exhibits a broad distribution of CBS I, a lower-region grouping of *A. ectypa*, and a right-side position for the single *A. tabescens* sample.



Note a Three-dimensional visualization showing genetic differentiation along the first to three principal components (PC1, PC2, PC3) for all individuals. b PC1 vs PC2 for all individuals. c PC2 vs PC3 for all individuals. Subsequent panels illustrate genetic structure within taxonomic subdivisions: d sect. *Armillaria* (PC1 vs PC2). e sect. *Gallicae* (PC1 vs PC2); f sect. *Korhoneniorum* (PC1 vs PC2); g sect. *Ostoyarum* (PC1 vs PC2). h Subg. *Desarmillaria.*

Figure 3.2 Principal component analysis (PCA) of mitochondrial genome variation among 584 studied *Armillaria* individuals

3.3.2 Weir & Cockerham's F_{ST} of Nuclear SNPs and Mitochondrial SNPs, Absolute Genetic Distance (dxy) and Relative Differentiation Index (ΦST) of Mitochondrial SNPs

3.3.2.1 Weir & Cockerham's F_{ST} of nuclear SNPs

As shown in Figure 3.3, among all formally described *Armillaria* species, genetic differentiation ranges from moderate to extremely high, with the lowest F_{ST} value of 0.09 observed between *A. bruneocystidia* (CBS H) and *A. tibetica* (CBS J), and the highest reaching 0.84 between *A. heimii* and *A. xiaocaobaensis*. Several potential new lineages discussed in Chapter 2 also exhibit moderate differentiation from their closely related species: F_{ST} = 0.23 between *Armillaria korhonenii* lineage 2 and lineage 1 (CBS Q); F_{ST} = 0.22 between *Armillaria* sp. 1 and CBS M; F_{ST} = 0.18 between *A. violacea* CBS N lineage 2-mtDNA and lineage 1-mtDNA; and F_{ST} = 0.10 between *A. sinensis* (CBS F) lineage 1-mtDNA and lineage 2-mtDNA. These moderate differentiation levels support their recognition as distinct taxonomic units. In contrast, CBS G + CBS K lineage 1-nDNA versus lineage 2-nDNA shows an F_{ST} of only 0.03, indicating almost no genetic differentiation and insufficient basis for classification as separate species. Due to a lack of data, CBS I and CBS M require further evaluation.

As shown in Figure 3.4, to assess nuclear-genome differentiation among sample groups that appear undifferentiated in the nuclear phylogeny but form multiple independent clades in the mitochondrial tree, we first clustered our nuclear SNP data by mitochondrial lineage and then calculated pairwise F_{ST}. Within the five *A. tibetica* (CBS J) mtDNA lineages (lineages 1–5), only lineage 4 versus the other four lineages exhibited moderate differentiation (F_{ST} = 0.10–0.14), whereas all other pairwise comparisons yielded very low F_{ST} values (0.00–0.05).

Similarly, among the three CBS G + CBS K mtDNA lineages (lineages 1–3), only lineage 1 versus lineage 2 showed substantial genetic differentiation (F_{ST} = 0.17), while lineage 1 vs 3 and lineage 2 vs 3 yielded F_{ST} values of only 0.06 and 0.09, respectively.

Mitochondrial signals indeed reflect historical fragmentation of maternal lineages, but this differentiation has not been maintained in the recombining nuclear genome. When nuclear samples are grouped by mitochondrial clade, the relatively high F_{ST} (≈0.17) primarily may reflect the Wahlund effect (an artefactual differentiation due to stratified sampling) rather than genuine, long-term nuclear isolation among the three groups. In contrast, the overall nuclear-genome analysis reveals a strong mixing signal (F_{ST} = 0.03), and this low level of differentiation provides the key evidence for assessing current population structure and species boundaries.

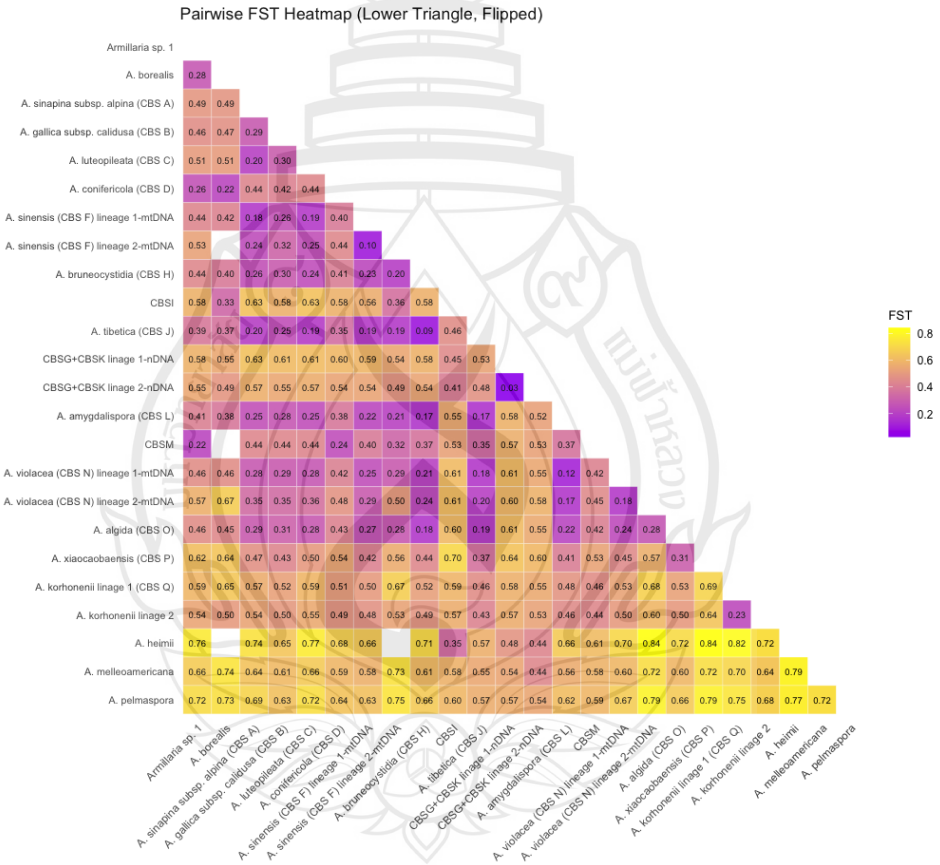


Figure 3.3 Pairwise Weir & Cockerham's F_{ST} of *Armillaria* based on lineages derived from nuclear phylogenomic analyses

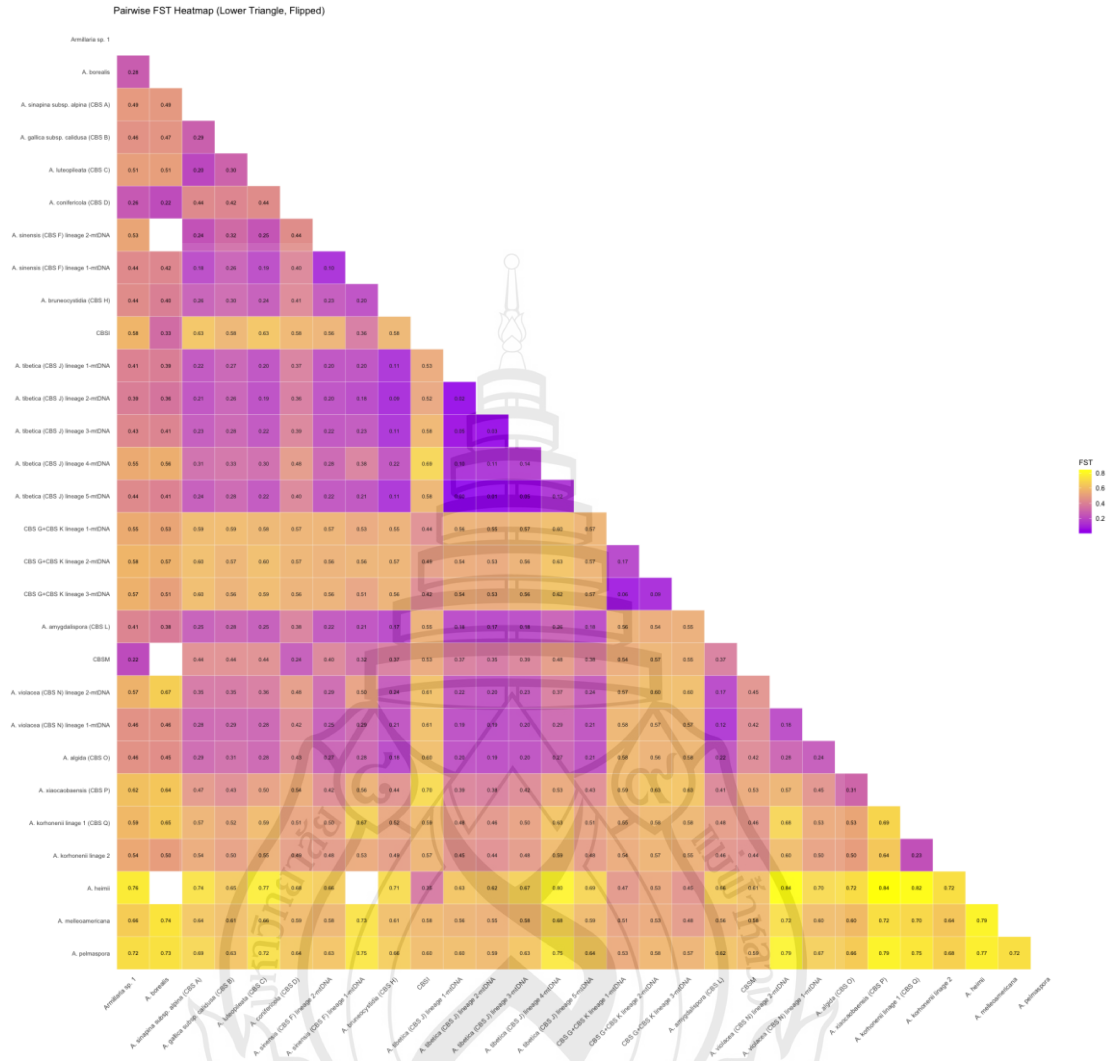


Figure 3.4 Pairwise Weir & Cockerham's F_{ST} of *Armillaria* based on lineages derived from mitochondrial phylogenomic analyses

3.3.2.2 Weir & Cockerham's F_{ST} of mitochondrial SNPs

As shown in Figure 3.5, we first examined those formally described species that each form a single, well-supported clade in both nuclear and mitochondrial phylogenies and whose close relatives are not missing in the heatmap—namely *A. altimontana*, *A. algida* (CBS O), *A. calvescens*, *A. cepistipes*, *A. conifericola* (CBS D), *A. ectypa*, *A. gemina*, *A. heimii*, *A. luteopileata* (CBS C), *A. melleoamerica*, *A. nabsnona*,

A. ostoyae, *A. pelmaspora*, *A. puiggarii*, and *A. xiaocaobaensis* (CBS P). Pairwise F_{ST} values among these species range from 0.37 to 1.00.

At the subspecies level, F_{ST} between *A. sinapina* subsp. *alpina* (CBS A) and *A.* subsp. *sinapina*, and between *A. gallica* subsp. *calidusa* (CBS B) and *A.* subsp. *gallica*, falls between 0.36 and 0.53. The putative new lineages discussed in Chapter 2 exhibit the following F_{ST} values against their closest described relatives: *Armillaria korhonenii* lineage 2 vs. lineage 1 (CBS Q): 0.55; *A. violacea* (CBS N) lineage 2 mtDNA vs. lineage 1 mtDNA: 0.38; *Armillaria* sp. 1 vs. *A. ostoyae*: 0.48; *A. sinensis* (CBS F) lineage 1 mtDNA vs. lineage 2 mtDNA: 0.59; CBS I vs. *A. tabescens*: 0.53; CBS M vs. *A. conifericola* (CBS D): 0.62; Within *A. tibetica* (CBS J), five mitochondrial lineages show F_{ST} values of 0.33–0.78. Lineage 5 is most differentiated from the other four (F_{ST} = 0.73–0.78), followed by lineage 4 (F_{ST} = 0.53–0.78), whereas lineages 1–3 exhibit weaker differentiation (F_{ST} = 0.33–0.39). Finally, the three nuclear lineages of CBS G + CBS K display extremely high F_{ST} values of 0.83–0.95, indicating very deep genetic divergence.

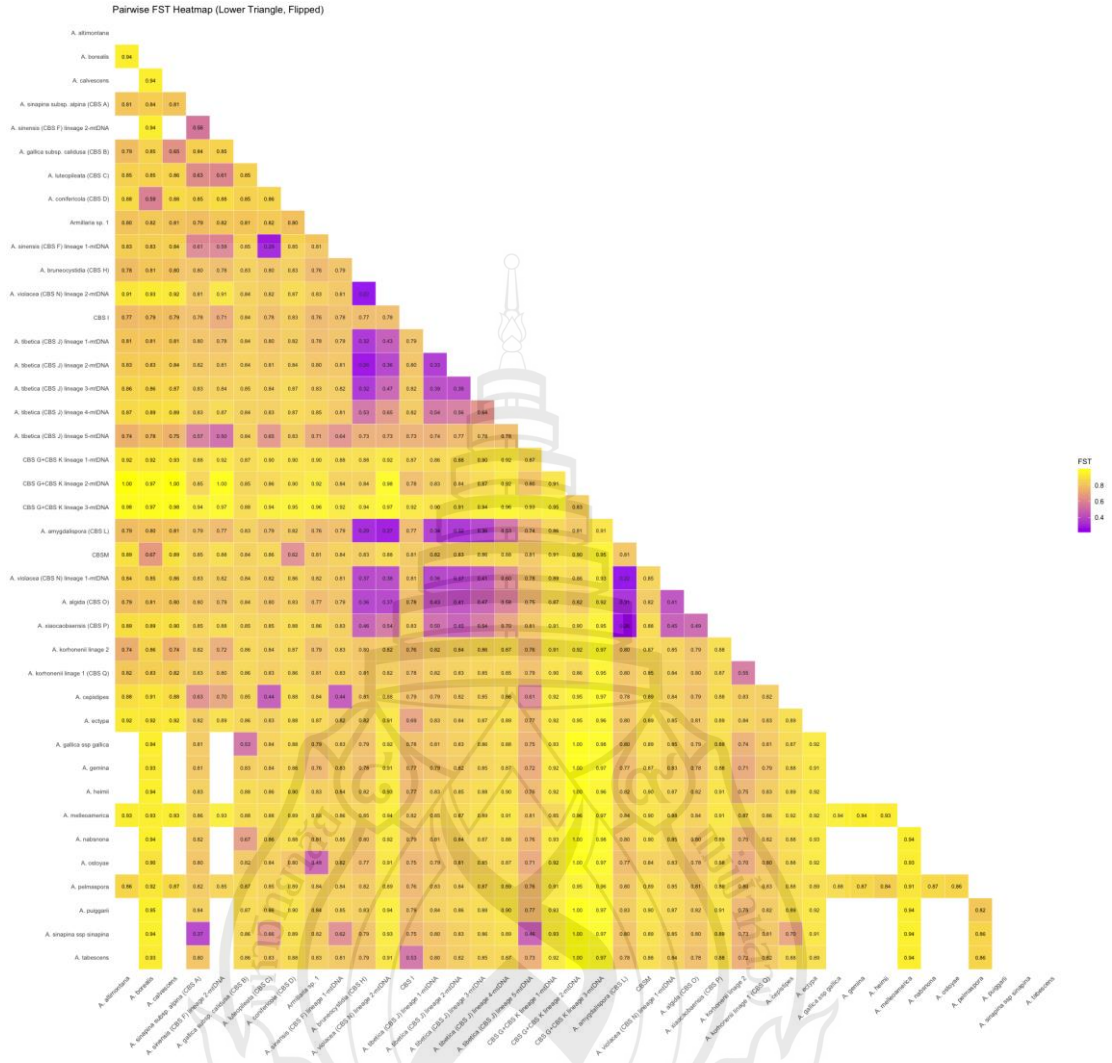


Figure 3.5 Weir & Cockerham's F_{ST} of *Armillaria* based on lineages derived from mitochondrial phylogenomic analyses

3.3.2.3 Weir & Cockerham's F_{ST} of mitochondrial SNPs

We examined those formally described species that each form a single, well-supported lineage in both nuclear and mitochondrial phylogenies and whose close relatives are not missing in the heatmap as 3.3.2.2. Absolute genetic distance dxy among these species ranges from 0.04 to 0.23. As shown in Figure 3.6, at the subspecies level, dxy values between *A. sinapina* subsp. *alpina* (CBS A) and *A. sinapina* subsp.

sinapina, as well as between *A. gallica* subsp. *calidusa* (CBS B) and *A. gallica* subsp. *gallica*, fall between 0.04 and 0.05, indicating relatively shallow differentiation.

The putative new lineages identified in Chapter 2 exhibit the following dxy values when compared with their closest described relatives: the two lineages of *Armillaria korhonenii* (lineage 2 vs. lineage 1) differ by 0.09; the two mitochondrial lineages of *A. violacea* (CBS N) differ by 0.04; *Armillaria* sp. 1 vs. *A. ostoyae* show a distance of 0.05; the two mitochondrial lineages of *A. sinensis* (CBS F) differ by 0.07; CBS I vs. *A. tabescens* by 0.07; and CBS M vs. *A. borealis* by 0.05. Within *A. tibetica* (CBS J), five main mitochondrial lineages span dxy values of 0.04–0.14: lineage 5 is most divergent (0.14), followed by lineage 4 (0.06), while lineages 1–3 show weaker divergence (0.04). Finally, the three nuclear lineages represented by CBS G + CBS K display extremely deep divergence (dxy = 0.02–0.14), supporting their status as distinct evolutionary units.

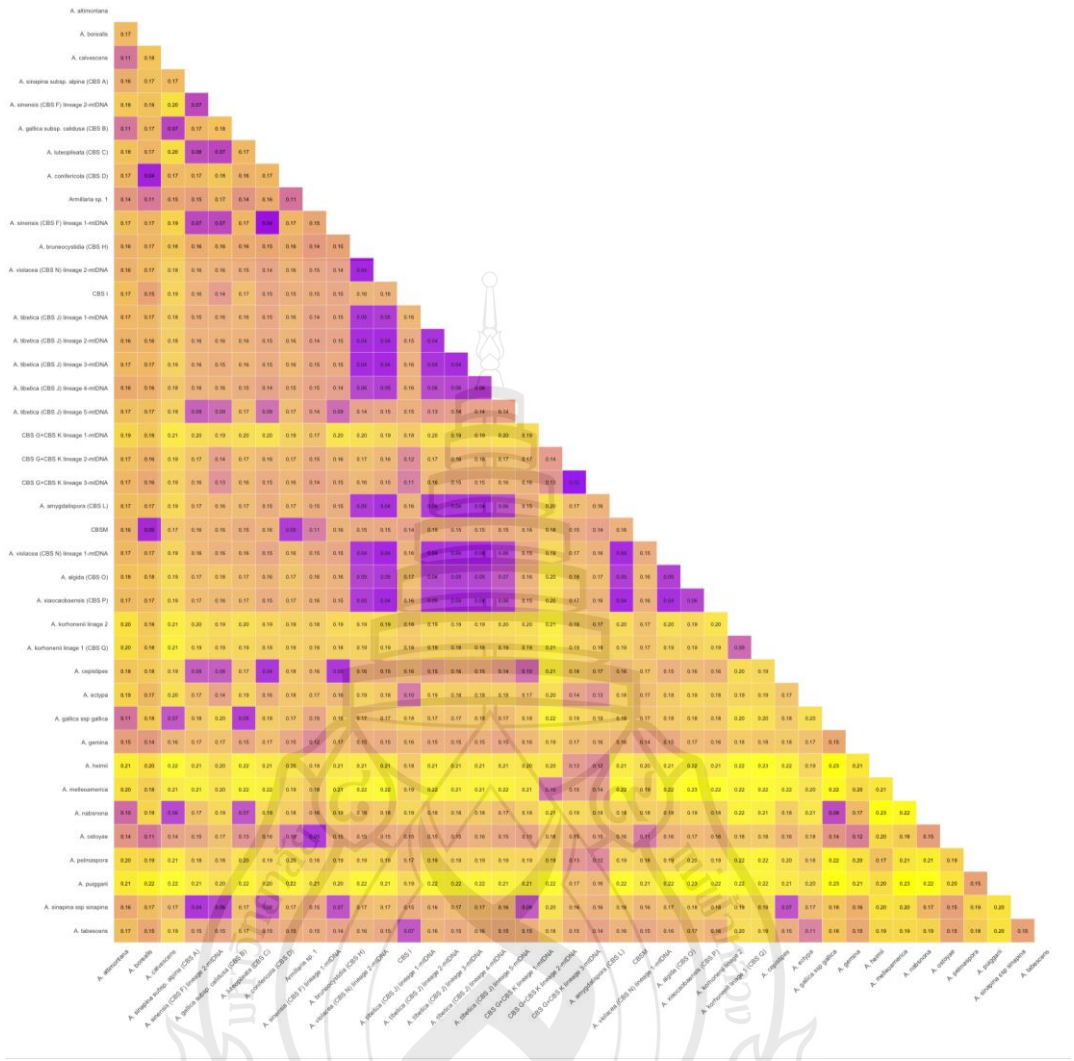


Figure 3.6 Absolute genetic distance (dxy) of *Armillaria* based on lineages derived from mitochondrial phylogenomic analyses

3.3.2.4 Relative differentiation index (ΦST) of mitochondrial SNPs

As in as 3.3.2.2 and 3.3.2.3, we compared the ΦST of formally described species that each form a single, well-supported lineage in both nuclear and mitochondrial phylogenies. As shown in Figure 3.7, the relative differentiation index ΦST among these species ranges from 0.45 to 1.0. At the subspecies level, ΦST values between *A. sinapina* subsp. *alpina* (CBS A) and *A. sinapina* subsp. *sinapina*, as well as between *A. gallica* subsp. *calidusa* (CBS B) and *A. gallica* subsp. *gallica*, fall between 0.57 and 0.77.

The putative new lineages identified in Chapter 2 exhibit the following ΦST values when compared with their closest described relatives: the two lineages of *Armillaria korhonenii* (lineage 2 vs. lineage 1) differ by 0.81; the two mitochondrial lineages of *A. violacea* (CBS N) differ by 0.59; *Armillaria* sp. 1 vs. *A. ostoyae* show a distance of 0.68; the two mitochondrial lineages of *A. sinensis* (CBS F) differ by 0.85; CBS I vs. *A. tabescens* by 0.80; and CBS M vs. A. borealis by 0.90. Within *A. tibetica* (CBS J), five main mitochondrial lineages span ΦST values of 0.56–0.96: lineage 5 is most divergent (0.94–0.96), followed by lineage 4 (0.78–0.88), while lineages 1–3 show weaker divergence (0.56–0.61). Finally, the three nuclear lineages represented by CBS G + CBS K display extremely deep divergence (ΦST = 0.97–1), supporting their status as distinct evolutionary units.

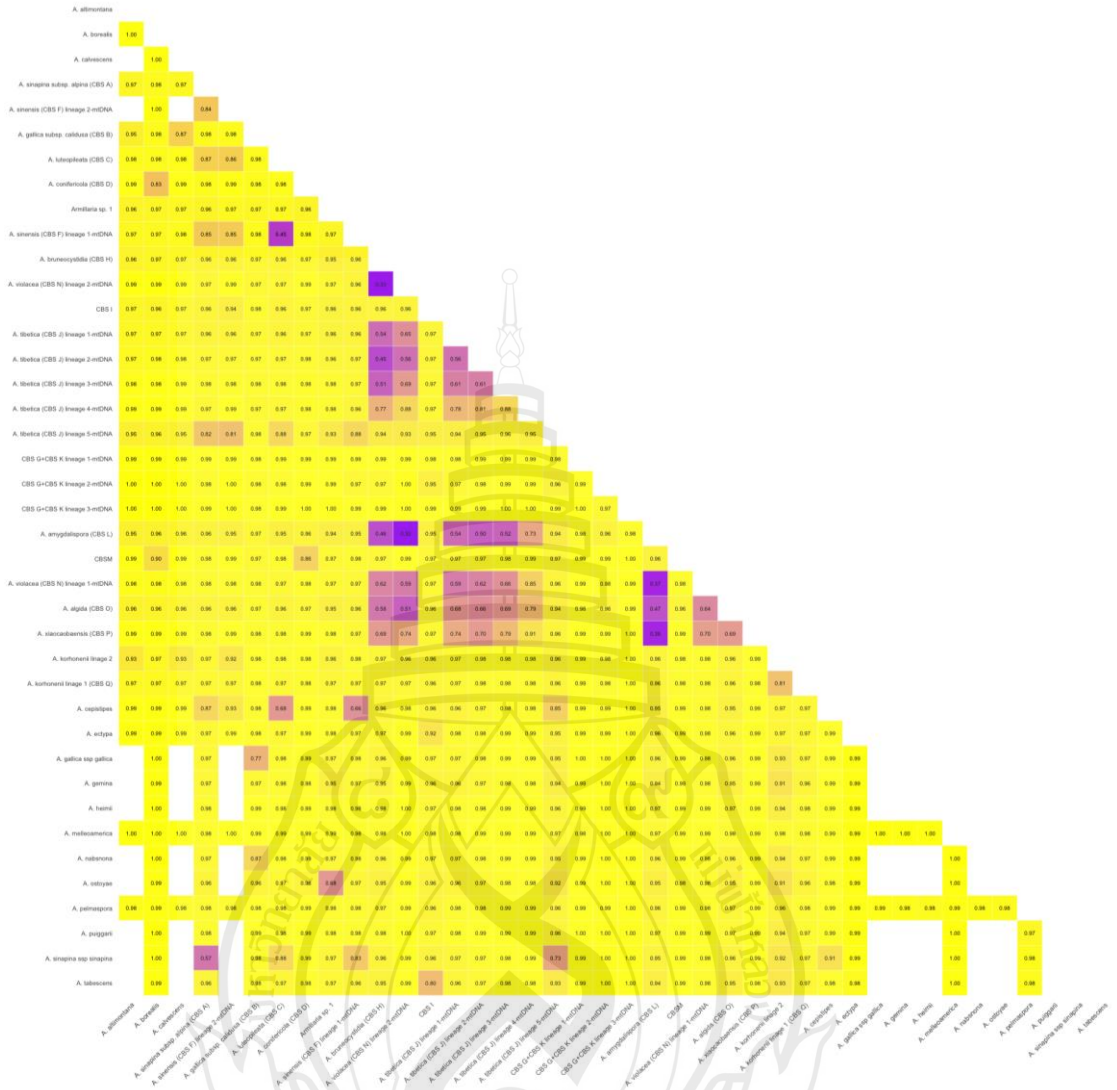


Figure 3.7 Relative differentiation index (ΦST) of *Armillaria* based on lineages derived from mitochondrial phylogenomic analyses

3.4 Conclusions

Integrating the results of PCA, nuclear genome differentiation (Weir & Cockerham's F_{ST}), and mitochondrial divergence metrics (F_{ST}, dxy, ΦST), and in light of the phylogenetic findings presented in Chapter 2, we propose that the following lineages should be recognized as distinct taxonomic units: CBSI, CBSM, *Armillaria korhonenii* lineage 2, *Armillaria* sp.1, *A. sinensis* (CBSF) lineage 2-mtDNA, and *A. violacea* (CBSN)

lineage 2-mtDNA. The CBSG + CBSK lineage 1-nDNA and lineage 2-nDNA, each of which harbors both homothallic (self-compatible) and heterothallic (outcrossing) mating types. Clearly, delimiting species solely within this species complex by mating system is impractical in the genomic era. Instead, we propose renaming this "super-complex" according to its phylogenomic structure: treating the two subclades as subspecies rather than a whole species. Within each subspecies, we further recognize two "reproductive biotypes" (homothallic vs. heterothallic groups) to reflect their differing breeding systems while preserving genomic coherence.

The details are as follows:

We compared the Asian lineage (CBS I) to *Armillaria tabescens* sensu stricto and found clear evidence of subspecific differentiation. Nuclear genomes exhibit a tip-to-tip distance of 10.35% (Figure 2.1), and mitochondrial genomes 2.68% (Figure 2.2). Although nuclear F_{ST} could not be calculated (monomorphic loci), mitochondrial F_{ST} is 0.53, dxy is 0.07, and ΦST reaches 0.80, indicating substantial cytoplasmic divergence. In both PCA analyses, CBS I consistently forms a distinct, non-admixed cluster. Biologically, crosses between this Asian lineage and North-temperate *A. tabescens* strains show 100% inter-fertility and no sterility, supporting subspecific—but not whole species—status (Qin et al. 2007). Accordingly, in Chapter 8 we describe this lineage as *Armillaria tabescens* subsp. *orientala*, reflecting its unique genomic signature and East Asian distribution.

We similarly evaluated the Chinese lineage CBS M against *Armillaria borealis*. Nuclear tip-to-tip distance is 6.8% (Figure 2.1), and mitochondrial distance is 1.0% (Figure 2.2). While nuclear F_{ST} is not computable due to low polymorphism, mitochondrial F_{ST} is 0.67, dxy is 0.11, and ΦST reaches 0.90—values indicative of strong cytoplasmic divergence. In PCA analysis, CBS M forms a discrete, non-admixed cluster separate from other *A. borealis* samples. Crosses with typical *A. borealis* strains yield 64.4% inter-fertility (Qin et al., 2007), reflecting partial reproductive isolation consistent with subspecific rank. Given its distinctive genomic signature and distribution in China, we designate this lineage as *Armillaria borealis* subsp. *sinoborealis* in Chapter 8.

The two *Armillaria korhonenii* lineages are diverged both genomically and geographically. Lineage 2 versus Lineage 1 shows a nuclear tip-to-tip distance of 14.13% (Figure 2.1) and a mitochondrial distance of 3.10% (Figure 2.2). Genome-wide differentiation is substantial F_{ST} = 0.23, and mitochondrial markers also display high divergence F_{ST} = 0.55, dxy = 0.09, ΦST = 0.81, indicating limited gene flow. The PCA analysis recovers them as separate, non-admixed clusters. Geographically, the two lineages occupy opposite sides of the Ailao-Honghe watershed, suggesting historical vicariance. Although mating interaction data are unavailable, the pronounced genomic differentiation combined with consistent morphological differences (notably cap coloration) justify recognizing Lineage 2 as a new species. In Chapter 8, we formally describe it as *Armillaria griseocapilla*, reflecting its distinctive gray-capped morphology.

The putative species *Armillaria* sp. 1 is clearly distinct from *A. conifericola* across multiple genomic and population-genetic axes. Nuclear genomes exhibit a tip-to-tip distance of 9.28% (Figure 2.1) and mitochondrial genomes 4.07% (Figure 2.2). Genome-wide nuclear differentiation is high, F_{ST} = 0.26, and mitochondrial divergence is even more pronounced, F_{ST} = 0.80; dxy = 0.11; ΦST = 0.96, indicative of deep cytoplasmic isolation. In PCA analysis, *Armillaria* sp. 1 consistently forms a separate, non-admixed cluster. Although mating compatibility data are unavailable, the magnitude of genomic differentiation—nuclear F_{ST}—supports recognition at least at the species level. Given its endemic distribution in Asia and its phylogenomic distinctiveness, we designate this lineage in Chapter 8 as *Armillaria pseudoostoyae*.

The two mitochondrial lineages of *Armillaria sinensis* (CBS F)—lineage 2-mtDNA versus lineage 1-mtDNA—are genomically distinguishable and geographically segregated. Nuclear tip-to-tip distance between them is 6.32% (Figure 2.1), and mitochondrial distance is 2.94% (Figure 2.2). Nuclear F_{ST} = 0.10 indicates moderate genomic differentiation, while mitochondrial F_{ST} = 0.59, dxy = 0.11, and ΦST = 0.82 reflect substantial cytoplasmic divergence. In PCA analysis, these two lineages form stable, non-admixed clusters. Although mating compatibility data are unavailable, their consistent genomic separation

supports species-level recognition. Accordingly, in Chapter 8 we designate lineage 2 as *Armillaria* sp. PXL; due to a lack of available specimens, no further formal description is provided.

The two lineages of *Armillaria violacea* (CBS N) are clearly differentiated genomically and form distinct clusters in PCA analysis. Nuclear tip-to-tip distance between lineage 2-mtDNA and lineage 1-mtDNA is 7.19% (Figure 2.1), with mitochondrial divergence of 1.6% (Figure 2.2). Genome-wide differentiation is moderate F_{ST} = 0.18, and mitochondrial values F_{ST} = 0.38; dxy = 0.04; ΦST = 0.59) further underscore their separation. Although mating-compatibility data are lacking, the consistent genomic partitioning and geographic distinctness warrant recognition as a separate taxonomic unit. Accordingly, a formal description under the name *Armillaria linzhiensis* is provided in Chapter 8.

The two nuclear subclades—CBS G + CBS K lineage 1-nDNA and CBS G + CBS K lineage 2-nDNA—nested within the mixed major clade of homothallic CBS G and heterothallic CBS K exhibit a tip-to-tip distance of 12.15% but an overall F_{ST} of only 0.03, reflecting deep pairwise divergence despite virtually no population structure. Mitochondrial metrics were omitted because their clustering conflicts with the nuclear phylogeny. As CBS G and CBS K strains are intermixed across both subclades, inter-fertility and inter-sterility were not assessed. Previous taxonomic treatments based solely on mating system (homothallism vs. heterothallism) lack phylogenetic support—neither type forms a monophyletic group—and are impractical in the genomic era. Therefore, in Chapter 8, we recognize these lineages as subspecies—*Armillaria melleasiana* subsp. *melleasiana* (CBS G + CBS K lineage 1-nDNA) and subsp. *macrospora* (CBS G + CBS K lineage 2-nDNA)—each further subdivided into homothallic and heterothallic groups, thereby reconciling phylogenomic structure with reproductive biology.

The analyses in this chapter demonstrate that mitochondrial genomes within *Armillaria* exhibit much higher levels of divergence than nuclear genomes. However, when

defining species boundaries, overall nuclear-genome differentiation should take priority, with mitochondrial divergence serving as a supplementary criterion. For delineating species versus subspecies, a nuclear-genome F_{ST} reaching a threshold of 0.09 may be used as a standard reference for *Armillaria*. Mitochondrial metrics (F_{ST}, dxy, ΦST) should be applied with caution and only when the species' distribution patterns and genetic history are well understood. Specifically, if a lineage has experienced limited ecological differentiation and no evidence of population admixture, mitochondrial capture, bottlenecks, or geographic isolation, then reaching a threshold of 0.37, 0.04, 0.45 in mitochondrial F_{ST}, dxy, and ΦST may justify recognizing distinct evolutionary units. Conversely, lineages affected by these processes are often unsuitable for species delimitation based solely on mitochondrial divergence, because mitochondria are maternally inherited and have an effective population size approximately one-quarter that of the nuclear genome, which accelerates genetic drift. Moreover, mitochondrial genes frequently undergo strong selection—such as for energy-metabolism functions influenced by temperature, nutrients, oxygen levels, or host physiology—and hybridization or mitochondrial capture events can create discordance between nuclear and mitochondrial signals.

Our mitochondrial divergence analyses reveal that certain super-complexes with broad geographic ranges and diverse ecological niches exhibit intraspecific mitochondrial divergence that far exceeds interspecific levels. For example, the mitochondrial differentiation of CBS G + CBS K lineage 1–3 and *A. tibetica* (CBS J) lineage 1–5 corresponds closely to geographic branches, the former corresponds to samples across China (lineage 1,3) and Motuo (lineage 2), the later corresponds to central China (lineage 1), Hengduan Mountains (lineage 2), southern Tibet (lineage 3), Xinjiang province (lineage 4), and eastern Hengduan (lineage 5). Similarly, the distributions of *A. korhonenii* lineages 1 (CBS Q) and lineage 2 precisely follow the biogeographic split on either side of the Ailao and Red River valleys, underscoring the utility of mitochondrial data in fungal biogeography.

In comparison to geographic isolation alone, our results suggest that elevation and temperature gradients may exert a stronger influence on mitochondrial divergence. Multiple intercontinental species pairs—such as *A. sinapina* subsp. *alpina* (Asia) vs. *A. sinapina* subsp. *sinapina* (North America); *A. gallica* subsp. *calidusa* (Asia) vs. *A. gallica* subsp. *gallica* (Europe) vs. *A. gallica* subsp. *canadensis* (North America); *A. borealis* (Europe) vs. CBS M (Asia); and *A. ostoyae* (Europe) vs. *A. conifericola* (CBS D) (Asia)—show much lower mitochondrial divergence than the intraspecific differentiation observed in the CBS G + CBS K lineage 1–3 and *A. tibetica* lineage 1–5 super-complexes, despite experiencing far greater geographic separation. This pattern indicates that climatic factors associated with elevation and temperature may play a more critical role than continental barriers in shaping mitochondrial genetic structure.

CHAPTER 4

PHYLOGENETIC CONFLICT AND RETICULATE EVOLUTION IN *ARMILLARIA*

4.1 Introduction

The phylogenetic analyses in Chapter 2 revealed potential conflict between the nuclear and mitochondrial genomes of *Armillaria* (Figure 4.1–4.2), indicating the existence of underlying nuclear–mitochondrial phylogenetic conflict. Such conflict may result from processes such as incomplete lineage sorting, introgression, or historical hybridization. So, this chapter investigates the extent and origins of these potential conflicts by analyzing genome-scale gene-tree discordance and evaluating evidence for reticulate evolutionary processes that may have shaped the diversification of *Armillaria*.

4.2 Methods

4.2.1 Comparative Analysis of Nuclear and Mitochondrial Phylogenetic Conflict

We first screened samples that possessed both nuclear and mitochondrial genomes from all nuclear and mitochondrial genome data. Samples with BUSCO nuclear genome completeness scores below 50% were subsequently filtered out, resulting in the final selection of 545 samples. Using the orthologous proteins identified in the sample with the lowest BUSCO score (SJ182: C:50.10%, S:37.70%, M:12.40%, F:14.30%, M:35.60%) as reference genomes, we developed custom scripts to extract homologous orthologous from BUSCO assessment results of other samples. Homologous orthologous with sequence counts below two-thirds of the total sample

size (363) in individual orthologous protein matrices were further filtered, leaving 1,386 genes for phylogenetic analysis. These gene matrices were aligned with MAFFT v7.407 (Katoh, 2013), trimmed with Trimal v1.4. rev22 (-gt 0.9), and concatenated using Geneious Prime 2020.0.3 (BioMatters, Ltd., Auckland, New Zealand).

For mitochondrial genome phylogeny, homologous mitochondrial genome blocks across all 545 samples were obtained using ORPA (Bi et al., 2024) with CBSK00111 as the reference genome. Both mitochondrial and nuclear gene phylogenies were reconstructed using RAxML v.8.2.12 (Stamatakis et al., 2014) under the PROTGAMMAWAG model, and their tanglegram tree was generated using R scripts.

4.2.2 Detecting Incongruence

Measures of Branch Support

4.2.2.1 Coalescent-Based Species Tree Inference

We selected one representative sample from each *Armillaria* lineage—plus the outgroup *Guyanagaster necrorhizus*—based on the highest BUSCO-estimated protein-gene completeness, yielding 50 taxa in total (Table C5). These proteomes were processed with OrthoFinder v2.5.4 (Emms & Kelly, 2015) to recover 629 single-copy gene families, which were each aligned using MAFFT v7.407 (Katoh, 2013) under default settings. For every alignment, we inferred a maximum-likelihood tree in RAxML v8.2.12 (Stamatakis et al., 2014) with the PROTGAMMAWAG model. Finally, the resulting 629 gene trees were analyzed in ASTRAL v5.7.3 (Mirarab et al., 2014; Rabiee et al., 2019) to reconstruct the species tree under the multispecies coalescent framework and to calculate gene-tree topology frequencies as described below.

4.2.2.2 Gene-Tree Topology Frequency Statistics

To obtain a clearer picture of phylogenetic topology conflicts across a broader set of single-copy genes and to avoid the statistical challenges posed by low per-locus species-level resolution, we also narrowed our phylogenetic topology

analyses to the subgenus and section levels. Specifically, We chose one representative from each clade—subgenus *Desarmillaria* (*A. tabescens* subsp. *tabescens* CBAS213), and within subgenus *Armillaria*: section *Armillaria* (*Armillaria mellea* DSM3731), section *Gallicae* (*A. gallica* subsp. *gallica* 21-2), section *Korhoneniorum* (*Armillaria korhonenii* DWS01), and section *Ostroyarum* (*Armillaria ostoyae* C189), with *Guyanagaster necrorhizus* (MCA3950) as the outgroup, OrthoFinder then recovered 4,857 single-copy genes from these species, aligned each with MAFFT v7.407 (Katoh, 2013) using default settings, and inferred maximum-likelihood trees for every alignment in RAxML v8.2.12 (Stamatakis et al., 2014) under the PROTGAMMAWAG model.. Finally, topology frequency analyses at the species, subgenus, and section levels were all performed using PhyBin v0.1.2 (Newton & Newton, 2013).

4.2.3 Gene Support Frequencies and Concordance Factors

We employed IQ-TREE v. 2.2.2 (Minh et al., 2020) to calculate both the Gene Concordance Factor (gCF) and Site Concordance Factor (sCF) using the aligned matrix of 629 single-copy genes obtained from 4.2.2.1 as the input dataset.

4.2.4 Internode Certainty

Internode Certainty (IC) was then calculated on this reference tree using PhyParts v0.0.1 (Smith et al., 2015) with a support threshold of 70 (-s 70). The reference topology here is the ML tree inferred from the concatenated alignment of the 629 single-copy genes described in 4.2.2.1, and the exact concatenated matrix was supplied as the input dataset. To portray conflicting versus concordant gene-tree signal at each node, we overlaid pie-chart summaries generated by the Python script phypartspiecharts.py (source code: https://github.com/mossmatters/MJPythonNote-books /blob/master/phypartspiecharts.py)—onto the reference tree, and finally polished and annotated the figure in Adobe Illustrator.

4.2.5 Quartet Sampling (QS) Test

We utilized Quartet Sampling v. 1.3.1 (--data-type amino) (James et al., 2018) to calculate Quartet Concordance (QC), Quartet Differential (QD), and Quartet

Informativeness (QI) using the species tree generated from the concatenated matrix of 629 single-copy genes and the original data matrix obtained from 4.2.2.1.

4.2.6 Polytomy Test

We used ASTRAL v5.7.8 (Zhang et al., 2018) to perform a polytomy test on the 629 single-copy gene trees generated as described in 4.2.2.1.

4.2.7 D-Statistics

Dsuite v0.5 r58 (Malinsky et al., 2021) was employed to compute Patterson's D statistic and f4 ratio for detecting potential introgression signals among lineages; only the filtered diploid sample data in 3.2.1 of Chapter 3 was used for the next analysis.

4.2.8 QuIBL Analysis

To further assess phylogenetic discordance and potential hybridization history, QuIBL (Edelman et al., 2019) was employed to quantify the relative contributions of incomplete lineage sorting (ILS) and introgression. The analysis was conducted based on the matrix of 629 single-copy gene trees obtained from 4.2.2.1.

4.2.9 Phylogenetic Networks Inference

We first constructed phylogenetic networks in SplitsTree v6.1.10 (Huson & Bryant, 2024) using the original sequence matrices of mitochondrial homologous blocks and nuclear orthologue genes generated in 2.1.3.3 of Chapter 2.

We then inferred reticulate evolutionary relationships in *Armillaria* with the maximum pseudo-likelihood (MPL) method in PhyloNet v3.8.2 (Wen et al., 2018), based on 3,469 single-copy genes present in at least two-thirds (≥ 33) of the 50 taxa (including the outgroup) defined in 4.1.2.1 of Chapter 4: families were classified with a custom script, aligned and gene trees inferred using the parameters and methods from that section, and a reticulate network reconstructed allowing zero to seven hybridization events.

4.3 Results

4.3.1 Comparative Analysis of Nuclear vs. Mitochondrial Phylogenetic Conflict

This study presents a tanglegram (Figure 4.1) comparing mitochondrial and nuclear phylogenies in *Armillaria*. At the subgeneric level, both subg. *Desarmillaria* and subg. *Armillaria* are recovered as monophyletic in each tree; however, within subg. *Armillaria* a clear sectional conflict emerges. In the mitochondrial phylogeny, sect. *Ostoyarum* and sect. *Gallicae* form a strongly supported sister clade (BS = 99), which is sister to sect. *Armillaria* (BS = 80); these three together are sister to sect. *Korhoneniorum* (BS = 91). By contrast, the nuclear topology resolves sect. *Armillaria* and sect. *Korhoneniorum* is a well-supported sister pair (BS = 100), which is sister to the *Ostoyarum* + *Gallicae* clade (BS = 100).

At the species level, the three taxa in the subgenus *Desarmillaria* exhibit fully concordant topologies in both mitochondrial and nuclear trees (Figure 4.1). In contrast, subg. *Armillaria* maintains sectional monophyly (*Armillaria*, *Gallicae*, *Korhoneniorum*, *Ostoyarum*) but exhibits pronounced intergenomic phylogenetic topology conflicts at multiple nodes in species-level relationships within those sections (Figure 4.1).

In Section *Armillaria*, the primary topology conflict involves *A. fumosa* and *A. luteobubalina*, which are paraphyletic in the mitochondrial tree (BS = 100) but monophyletic in the nuclear tree (BS = 100). The other species—*A. heimii*, *A. novaezelandiae*, *A. pelmaspora*, and *A. puiggarii*—show no significant conflict. Although minor topological variations occur within the different phylogenetic species of the global *A. mellea* supercomplex, these are not considered true phylogenetic conflicts.

In the mitochondrial phylogeny, *A. gemina* is sister to a clade that splits into two subclades: one uniting *A. conifericola* (CBSD) with *A. solidipes* (BS = 89) as sister to the CBS M + *A. borealis* pair (BS = 100), and the other comprising *A. ostoyae* and *Armillaria* sp. 1 (BS = 100). In the nuclear phylogeny, *A. gemina* is sister to a clade in which *Armillaria* sp. 1 is sister to two deeply diverging subclades: one uniting CBS M with *A. borealis*, and

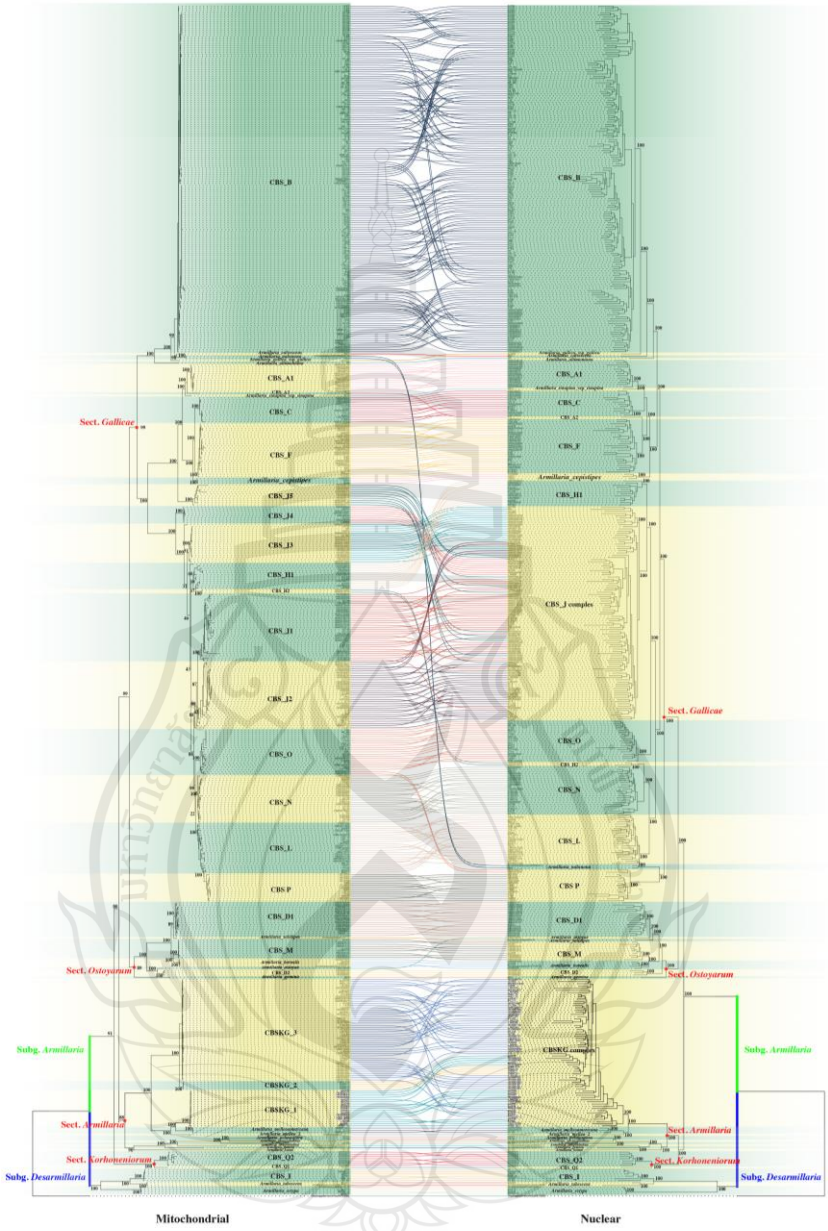
the other grouping *A. solidipes* with a *A. conifericola* (CBS D) + *A. ostoyae* clade (BS = 100).

Section *Gallicae* demonstrated the most extensive phylogenomic conflict: (1) Mitochondrial clade I: *A. gallica* subsp. *calidusa* (CBS B), *A. calvescens*, *A. nabsnona*, *A. gallica* ssp. *gallica*, and *A. altimontana* formed a strongly supported cluster (BS = 100). (2) Mitochondrial clade II: subdivided into subclade IIa (*A. sinapina* subsp. *alpina* (CBS A), *A. sinensis* (CBS F) lineage 2-mtDNA, *A. sinapina* subsp. *sinapina*, *A. luteopileata* (CBS C), *A. sinensis* (CBS F) lineage 1-mtDNA, *A. cepistipes*, *A. tibetica* (CBS J) lineage 5-mtDNA, and subclade IIb (*A. tibetica* (CBS J) lineage 4-mtDNA, *A. tibetica* (CBS J) lineage 3-mtDNA, *A. bruneocystidia* (CBS H), *A. violacea* (CBS N) lineage 2-mtDNA, *A. tibetica* (CBS J) lineage 1-mtDNA, *A. tibetica* (CBS J) lineage 2-mtDNA, *A. algida* (CBS O), *A. violacea* (CBS N) lineage 1-mtDNA, *A. amygdalispora* (CBS L), *A. xiaocaobaensis* (CBS P).

The nuclear tree revealed drastic topological shifts: *A. nabsnona* diverged from mitochondrial-associated taxa in clade I; subclade IIa members (excluding *A. tibetica* (CBS J) lineage 5-mtDNA) regrouped with altered internal relationships; subclade IIb split into two paraphyletic groups—(1) *A. xiaocaobaensis* (CBS P) + *A. nabsnona* and (2) *A. amygdalispora* (CBS L)/*A. violacea* (CBS N)/*A. sinapina* subsp. *alpina* (CBS A), *A. bruneocystidia* (CBS H)/*A. violacea* (CBS N) lineage 2-mtDNA/*A. algida* (CBS O)+ the *A. tibetica* (CBS J). Crucially, two *A. algida* (CBS O) specimens (grouped in mitochondrial subclade IIb) unexpectedly clustered with *A. xiaocaobaensis* (CBS P) and *A. nabsnona* in the nuclear tree (Figure 4.1).

Phylogenetic conflict can stem from both biological and analytical sources. Biological drivers include incomplete lineage sorting, horizontal gene transfer, hybridization, introgression and recombination, and natural selection, whereas analytical (technical) factors encompass stochastic errors, systematic biases, and data-treatment artefacts (Steenwyk et al., 2023). Although our analyses reveal pronounced topological discordance across multiple clades, determining whether these conflicts reflect genuine

phylogenetic incongruence within *Armillaria* requires further validation—especially by ruling out artefacts introduced by technical factors.



Note Phylogenetic tanglegram comparing nuclear and mitochondrial trees of 50 taxa: mitochondrial homologous blocks (left) and a concatenated alignment of 1,386 homologous orthologues (right). Colored lines link samples of the same species across the two dendrograms.

Figure 4.1 Phylogenetic tanglegram comparing nuclear and mitochondrial trees

4.3.2 Detecting Incongruence

4.3.2.1 Coalescent-Based Species Tree Inference

Coalescent-based analysis of 629 single-copy gene trees recovered the same, highly supported species topology as our RAxML concatenated analysis (Figure 4.2; Figure D3), with an ASTRAL quartet score of 76.3%, and two internal nodes, one within sect. *Armillaria* and one within the sect. *Gallicae* exhibited lower support values of 0.46 and 0.51, respectively. This suggests that the incongruence between the mitochondrial and nuclear phylogenies is real and not simply due to phylogenetic error using concatenated data sets (Wang & Hahn, 2018).

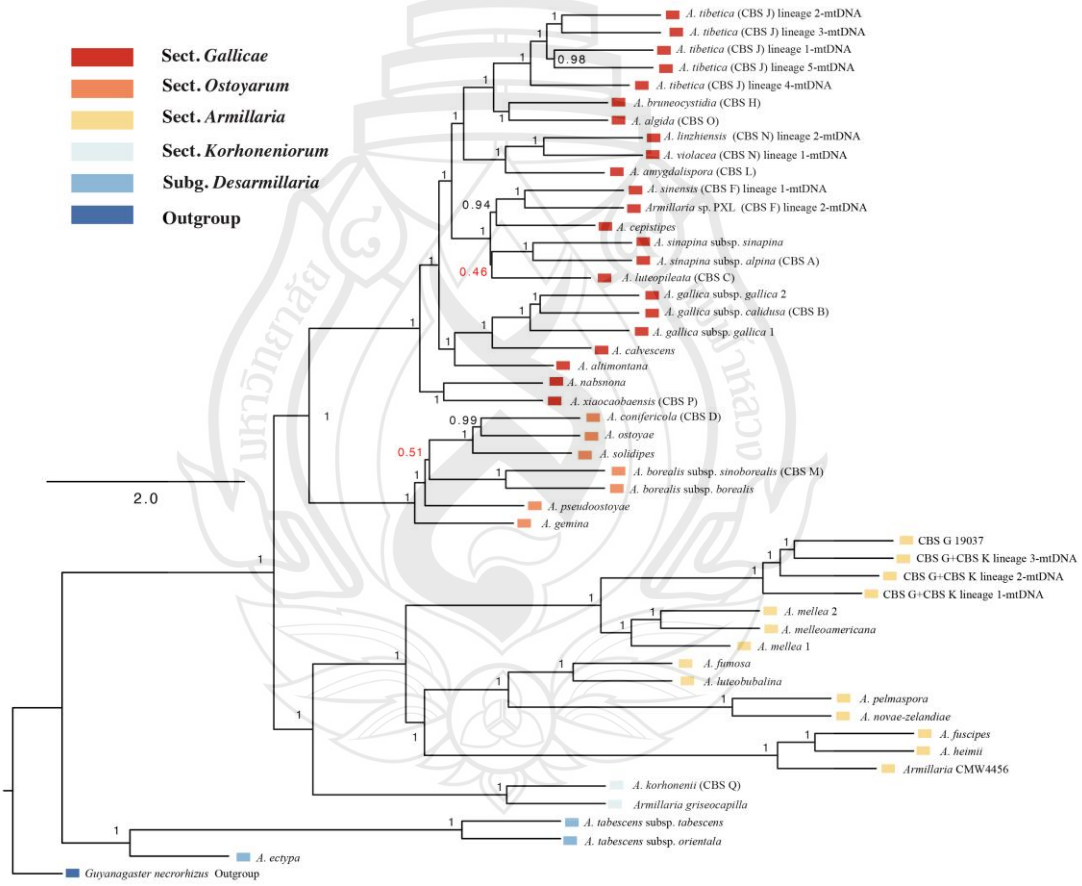
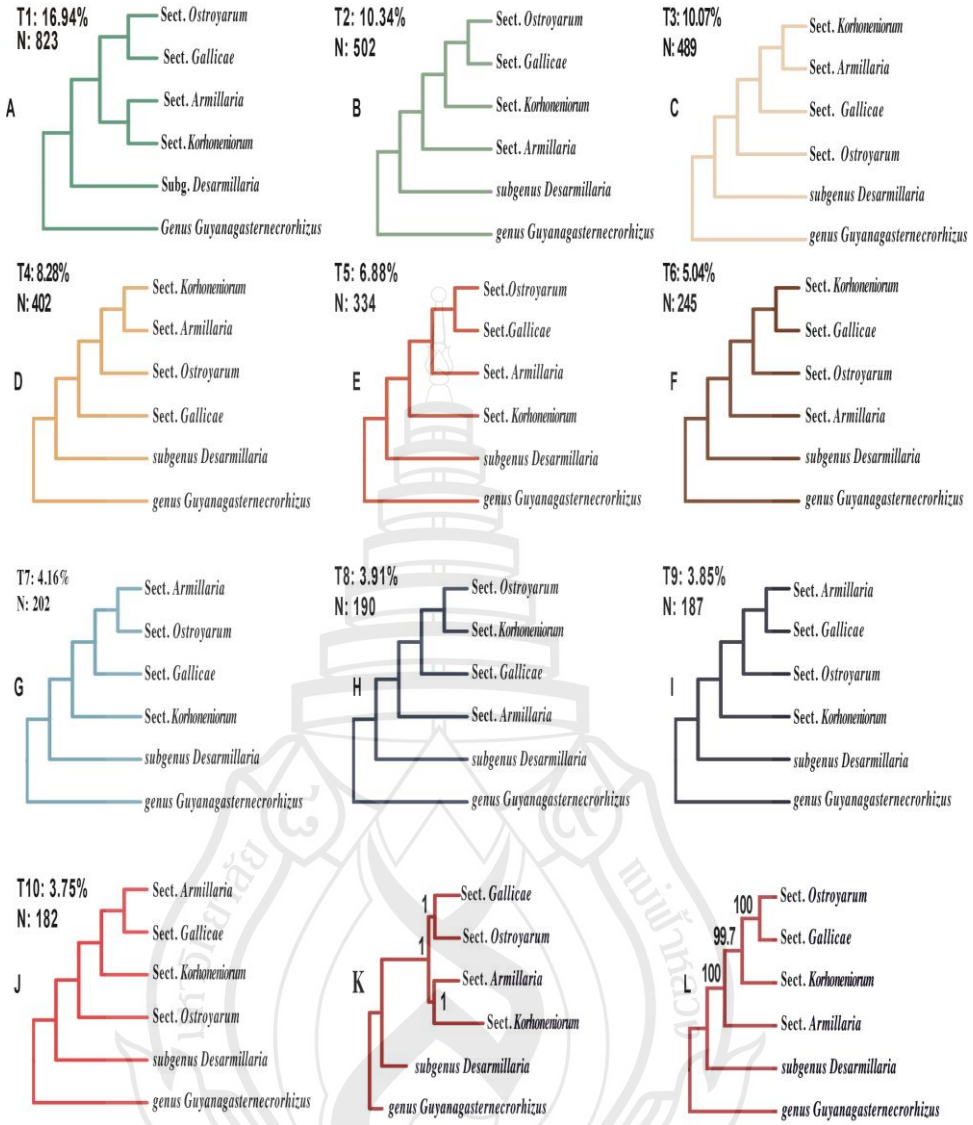


Figure 4.2 Species tree inferred by ASTRAL from 629 single-copy gene trees

4.3.2.2 Gene-Tree Topology Frequencies

PhyBin analysis revealed that each of the 629 gene trees had a unique topology, which likely reflects weak nodal support and the limited resolving power of individual loci in *Armillaria*. Including multiple conspecifics and subspecific lineages further increased the diversity of gene-tree shapes and made species-level topology counts impractical. Accordingly, we selected the nine gene trees with the highest overall node-support for display (Figure D4). Even among these best-supported trees, species-level relationships remain highly variable, underscoring the pervasive topological incongruence across the genus.

At subgenus and section levels, as shown in Figure 4.3, the ten most frequent topologies (A–J) together accounted for 16.94%, 10.34%, 10.07%, 8.28%, 6.88%, 5.04%, 4.16%, 3.91%, 3.85%, and 3.75% of all observed trees—corresponding to 823, 502, 489, 402, 334, 245, 202, 190, 187, and 182 supporting gene trees, respectively.



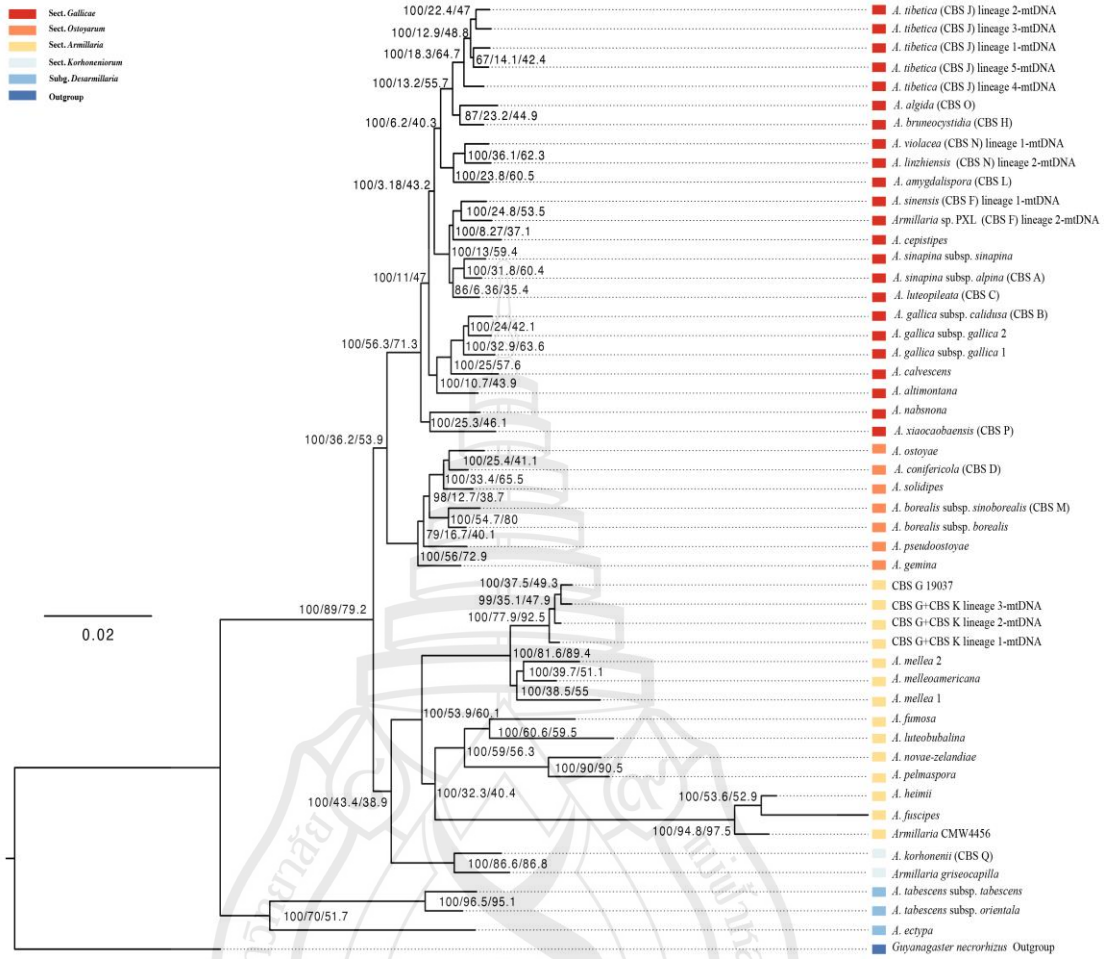
Note Ten most common topologies and species tree of *Armillaria* reconstructed from 4857 single-copy gene alignments at the subgenus and section levels. (A-G) The ten most frequently observed intergroup phylogenetic topologies. T-values indicate the percentage of gene trees supporting each specific topology among the 4857 single-gene trees, while N-values represent the absolute number of gene trees supporting each topology. (K-L) Species trees were constructed using coalescent-based methods, with K generated using ASTRAL and L constructed using CASTER.

Figure 4.3 Ten most common topologies and species tree of *Armillaria*

4.3.3 Concordance Factor

The concordance factors analysis results are shown in Figure 4.4. Most nodes exhibited robust bootstrap support (>90%), indicating strong phylogenetic signal across loci. However, notable discrepancies were observed in gene concordance factor (gCF) and site concordance factor (sCF) metrics: gCF values spanned 35.4%–97.5%, many nodes were below 50%, suggesting moderate to high consistency in gene tree topologies, sCF values ranged from 3.18% to 96.5%, reflecting substantial heterogeneity in site-level phylogenetic signal, especially in subgenus *Armillaria*.

The combination of strong bootstrap support and low gCF/sCF values suggests that, although the concatenated tree yields highly supported branches, substantial gene tree and site-level discordance persists. This discordance likely reflects incomplete lineage sorting, gene flow, or rapid diversification, all of which can obscure locus-specific resolution. Importantly, as our dataset includes only genes present in all taxa, the low concordance factors cannot be attributed to missing data, but instead point to either a weak phylogenetic signal or genuine evolutionary conflict.



Note Concordance factor analysis of 629 *Armillaria* single-copy gene proteins using IQ-TREE 2. Branch labels display bootstrap support values, gene concordance factors (gCF), and site concordance factors (sCF) in the format: bootstrap/gCF/sCF.

Figure 4.4 Concordance factor analysis of 629 *Armillaria* single-copy gene protein sequences using IQ-TREE 2

4.3.4 Internode Certainty

In this study, we conducted a concordance analysis of the species tree topology using a bootstrap support threshold of 70%. The results revealed significant variation in support for phylogenetic relationships across taxonomic ranks (Figure 4.5).

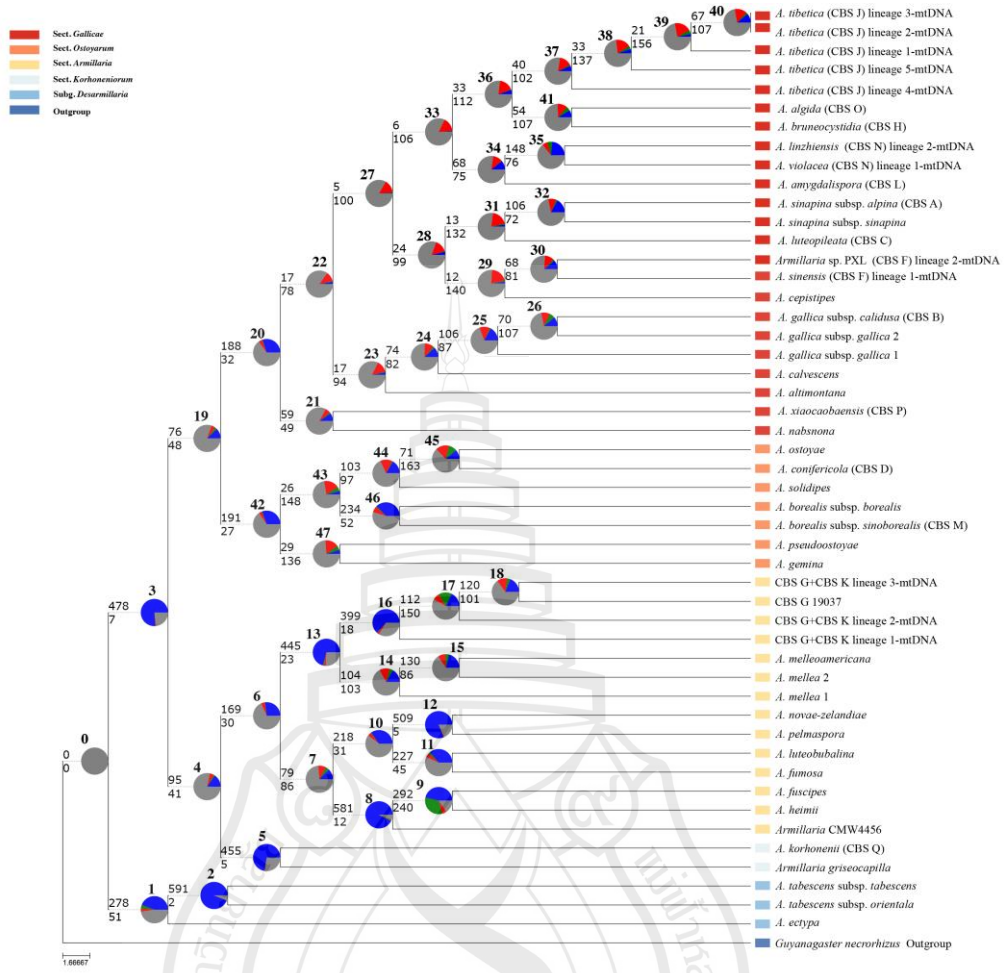
At the subgenus level, the phylogenetic relationship of subg. *Desarmillaria* was supported by 288 out of 629 gene trees (45.79% support), while 51 gene trees (8.10%) exhibited conflicting topologies. In contrast, subg. *Armillaria* received support from 478 gene trees (76.00%), with only 7 gene trees (1.11%) showing conflicting topologies; the remaining gene trees did not provide sufficient phylogenetic information.

At the section level, sect. *Korhoneniorum* demonstrated high phylogenetic stability, supported by 455 gene trees (72.34% support) and with only 5 gene trees (0.79%) displaying conflicting topologies. sect. *Armillaria* was supported by 169 gene trees (26.87% support) but had 30 conflicting gene trees (4.77%). sect. *Ostoyarum* received support from 191 gene trees (30.37%) and 27 conflicting gene trees (4.29%), while sect. *Gallicae* was supported by 76 gene trees (12.08% support) but had 48 conflicting gene trees (7.63%). Additionally, the sister group relationship between sect. *Korhoneniorum* and sect. *Armillaria* was supported by 91 gene trees (14.47% support) but conflicted with 41 gene trees (6.52%). Similarly, the sister group relationship between sect. *Ostoyarum* and sect. *Gallicae* was supported by 76 gene trees (12.08% support) but conflicted with 48 gene trees (7.63%).

At the species level, the phylogenetic relationships among the three species within the subgenus *Desarmillaria* received relatively high support, particularly the relationship between *A. tabescens* subsp. *orientala* and *A. tabescens* subsp. *tabescens*. Within sect. *Korhoneniorum*, the relationship between *A. korhonenii* (CBS Q) and *A. griseocapilla* was supported by 455 gene trees (72.34%), in sect. *Armillaria*, the clade comprising *Armillaria* CMW4456 and *Armillaria heimii* + *Armillaria fuscipes* received strong support, while the relationship between *A. pelmaspora* and *A. novaezelandiae* was supported by 509 gene trees (80.92% support). However, in sect. *Ostoyarum* and sect. *Gallicae*, the phylogenetic relationships of most terminal species lacked sufficient support (supported by < 50% of gene trees).

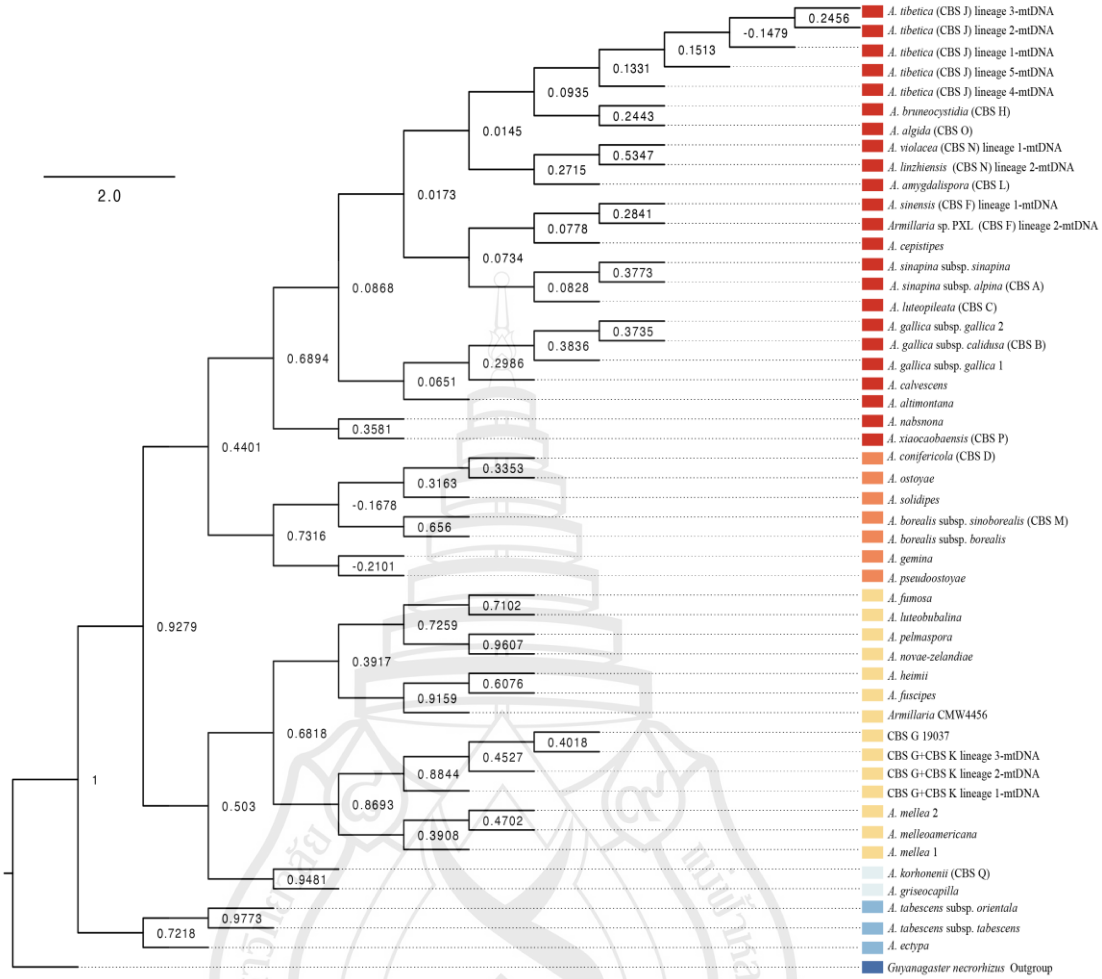
In summary, at the subgenus level, subg. *Armillaria* received higher support (76.00%) compared to subg. *Desarmillaria* (45.79%). At the section level, sect. *Korhoneniorum* exhibited the strongest support (72.34%), while sect. *Ostoyarum* (30.37%), sect. *Gallicae* (12.08%), and sect. *Armillaria* (26.87%) showed relatively weaker support. At the species level, the relationships between *Armillaria* CMW4456 and *A. heimii* + *A. fuscipes*, *A. pelmaspora* and *A. novaezelandiae*, *A. korhonenii* (CBS Q) and *A. griseocapilla*, and the CBSKG complex received robust support.

The Internode Certainty All (ICA) statistics are presented in Figure 4.6. At the subgenus level, subg. *Desarmillaria* had an ICA value of 0.72, while subg. *Armillaria* showed a higher ICA value of 0.93. At the section level, sect. *Korhoneniorum* had the highest ICA value (0.95), followed by sect. *Armillaria* (0.68), sect. *Ostoyarum* (0.73), and sect. *Gallicae* (0.69). At the species level, ICA values ranged widely from -0.21 (Negative values may be due to insufficient phylogenetic signal) to 0.98. These findings indicate that nearly all internal nodes in the *Armillaria* phylogenetic tree exhibit discordance between gene tree topologies and the species tree, reflecting significant conflicts between gene trees and the species tree.



Note Species tree topology of *Armillaria* inferred by CASTER-site based on the 629 single-copy protein datasets, integrating gene-tree concordance and conflict patterns within *Armillaria* from PhyParts analysis. For each branch, the top number indicates the number of homologs concordant with the species tree at that node, and the bottom number indicates the number of homologs in conflict with that clade in the species tree. Pie charts indicate the proportion of gene trees categorized as follows: Blue: Supporting the depicted topology; Green: Conflicting with the depicted topology (most common conflicting bipartition); Red: Conflicting with the depicted topology (all other supported conflicting bipartitions); Gray: No support for conflicting bipartitions.

Figure 4.5 Species tree topology of *Armillaria* inferred by CASTER-site



Note ICA values are shown below each branch.

Figure 4.6 Internode certainty all (ICA) values for the genus *Armillaria*

4.3.5 Quartet Sampling (QS) Test

The Quartet Sampling (QS) phylogenomic concordance analysis (Figure 4.6) revealed that, during sensitivity testing with progressively stringent log-likelihood thresholds (i.e., the --lnlike parameter increased from 2 to 5 and 10), the quartet concordance (QC), quartet differential (QD), and quartet informativeness (QI) indices showed that most internal nodes among species of the *Armillaria* genus received full support concordance (QC/QD/QI = 1/NA/1). Examples include nodes 1, 2, 3, 5, 6, 7, 9, 10, 12, 14, 16, 17, 18, 19, 20, 23, 24, 26, 27, 28, 29, 30, 31, 32, 34, 36, 38, 40, 41, 44, 45, and 47, indicating complete phylogenetic concordance at these positions.

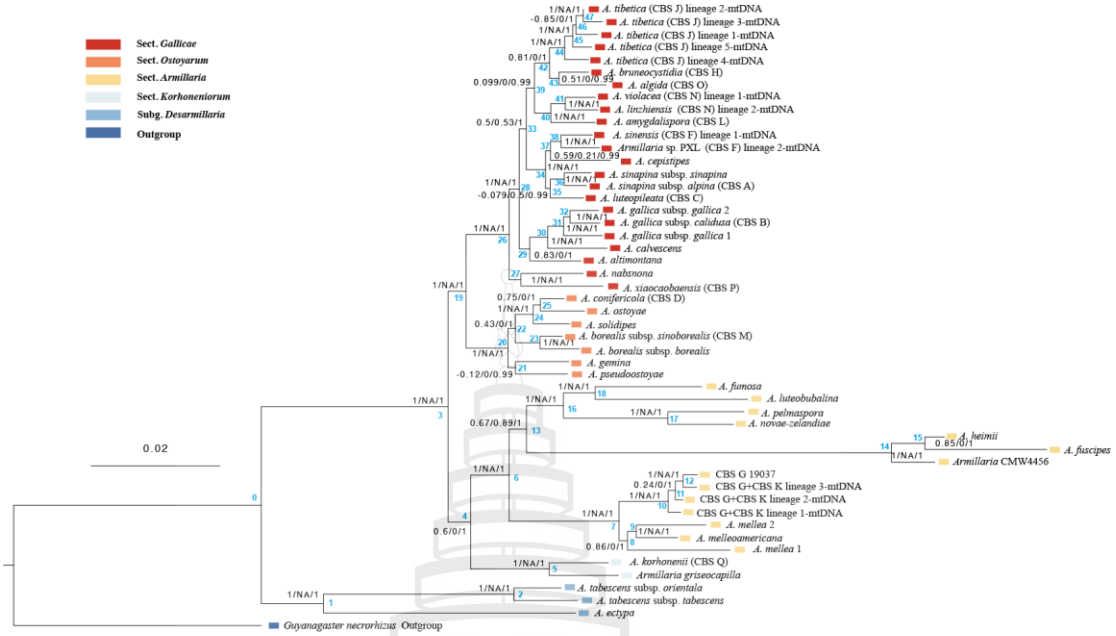
Several nodes showed strong support concordance, such as node 13 (QC/QD/QI = 0.67/0.89/1) and node 33 (QC/QD/QI = 0.5/0.53/1). While node 13 had a QD value close to 0.89, suggesting balanced frequencies among discordant topologies (i.e., no skew), node 33 had a QD of 0.53, indicating moderate discordance skew, which may reflect potential phylogenetic incongruence.

Numerous nodes exhibited strong support concordance with discordant skew, such as node 4 (0.6/0/1), 8 (0.86/0/1), 15 (0.85/0/1), 25 (0.75/0/1), 29 (0.83/0/1), 37 (0.59/0.21/0.99), 43 (0.51/0/0.99), and 42 (0.81/0/1). These results suggest the possible presence of supported secondary evolutionary histories, indicating phylogenetic discordance.

Cases of weak support with discordant skew were also observed, such as node 22 (0.43/0/1) and node 39 (0.099/0/0.99), further indicating potential secondary histories or complex evolutionary signals.

Finally, counter-support was identified at nodes 21 (–0.12/0/0.99) and 35 (–0.079/0.5/0.99), where a strong majority of quartets support one of the discordant alternative topologies, clearly suggesting phylogenetic conflict.

In summary, while most nodes within *Armillaria* exhibit strong or full phylogenetic concordance, a subset of nodes displays evidence of secondary evolutionary histories or topological conflict, underscoring the real and detectable presence of phylogenetic incongruence within the genus.



Note Node labels display the QS scores, including values for Quartet Concordance (QC), Quartet Differential (QD), and Quartet Informativeness (QI), along with node numbers.

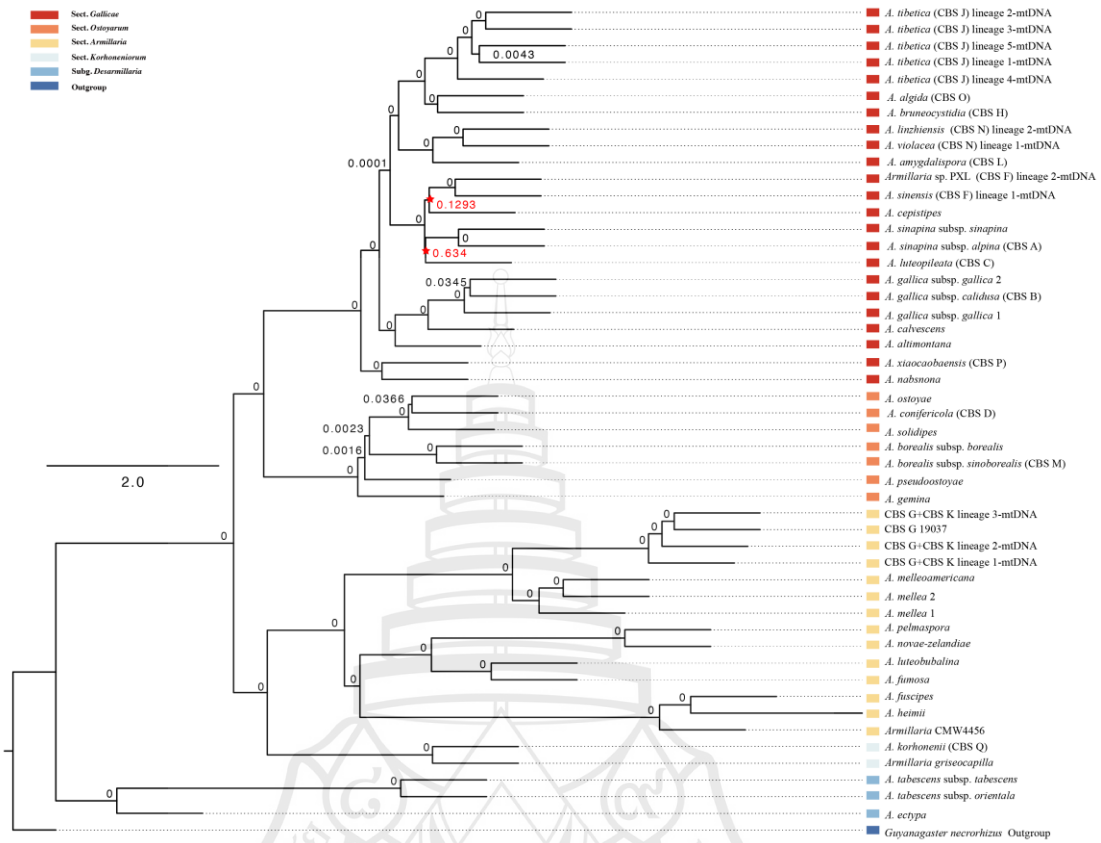
Figure 4.7 Quartet Sampling (QS) scores inferred from the 629 orthologous single-copy protein datasets

4.3.6 Polytomy Test

Phylogenetic analysis failed to reject the null hypothesis of polytomy ($p > 0.05$), indicating unresolved evolutionary relationships at two critical nodes (Figure 4.8):

1. Node 1: *Armillaria cepistipes* clustered with *A. sinensis* (CBS F) lineage 1-mtDNA + *Armillaria* sp. PXL (CBS F) lineage 2-mtDNA ($p = 0.1293$);

2. Node 2: *A. luteopileata* (CBS C) + *A. sinapina* subsp. *alpina* (CBS A) grouped with *A. sinapina* subsp. *sinapina* (0.634). These potential multifurcations may reflect rapid radiation events or incomplete lineage sorting during speciation processes.



Note Coalescent-based species tree reconstructed using ASTRAL, with p-values from the polytomy test displayed above branches. Red stars indicate nodes where the null hypothesis of a polytomy ($p > 0.05$) could not be rejected.

Figure 4.8 Coalescent-based species tree reconstructed using ASTRAL

4.3.7 D-Statistics

In this analysis, six species pairs were excluded from evaluation because they represent sister taxa in our dataset—*Armillaria borealis* subsp. *borealis* and *A. borealis* subsp. *sinoborealis* (CBS M); *A. sinensis* (CBS F) lineage 1-mtDNA and lineage 2-mtDNA; *A. bruneocystidia* (CBS H) and *A. algida* (CBS O); A. *melleasiana* subsp. *macrospora* and subsp. *melleasiana*; *A. violacea* (CBS N) lineage 1-mtDNA and *A. linzhiensis* (CBS N) lineage 2-mtDNA; and *A. korhonenii* lineage 1 (CBS Q) and lineage 2. Because these sister-taxon pairs are exceedingly similar at the genomic level, they were excluded from statistical testing.

Our analysis revealed that D is significant in 3.8% of triplets (3,853 out of 101,270, as assessed by Z-scores), so we calculated the mean absolute D for each species pair from those triplets showing significant values. These mean |D| values ranged from 0.02 to 0.39 (Figure 4.9). Notably, the species pairs with evidence of gene flow overlap with many of the nodes previously identified as phylogenetically incongruent, suggesting that historical gene exchange may have contributed to the observed discordance.

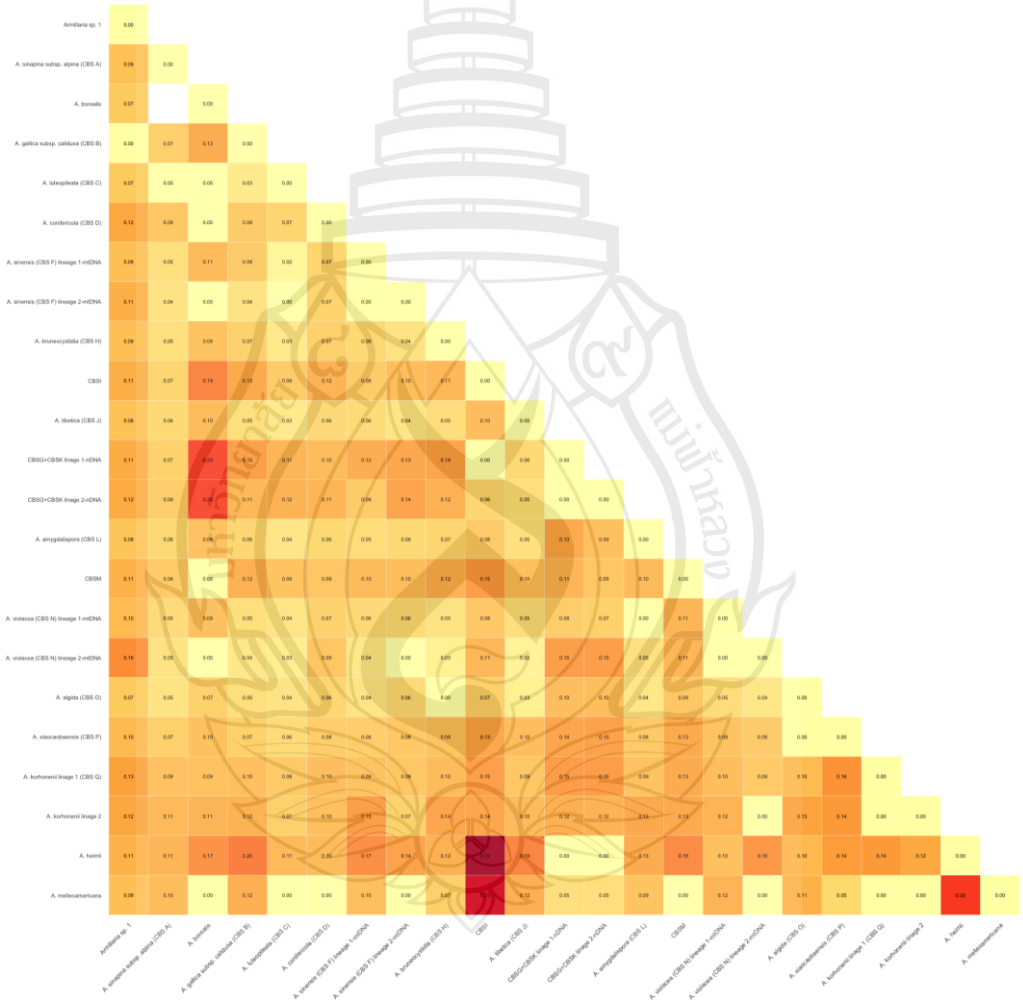


Figure 4.9 Mean pairwise *D* per species pair

4.3.8 QuIBL Analysis

Only 12.7% of the tested triplets showed very strong statistical support for an introgression model (ΔBIC > 10), indicating that introgression is limited to a small subset of species relationships. Nevertheless, these few relationships involve a substantial portion of the genome, with 23.3% of all loci appearing to be introgressed in the supported triplets—reflecting extensive gene flow within those specific lineages. As shown in Figure 4.10, however, almost all species pairs exhibit some degree of introgression, with estimated proportions ranging from 0.08 to 0.49, except for *A. ectypa*, which shows no detectable introgression with any other species. These results suggest that post-speciation introgression, though not ubiquitous, is a non-negligible contributor to phylogenetic discordance among *Armillaria* species.

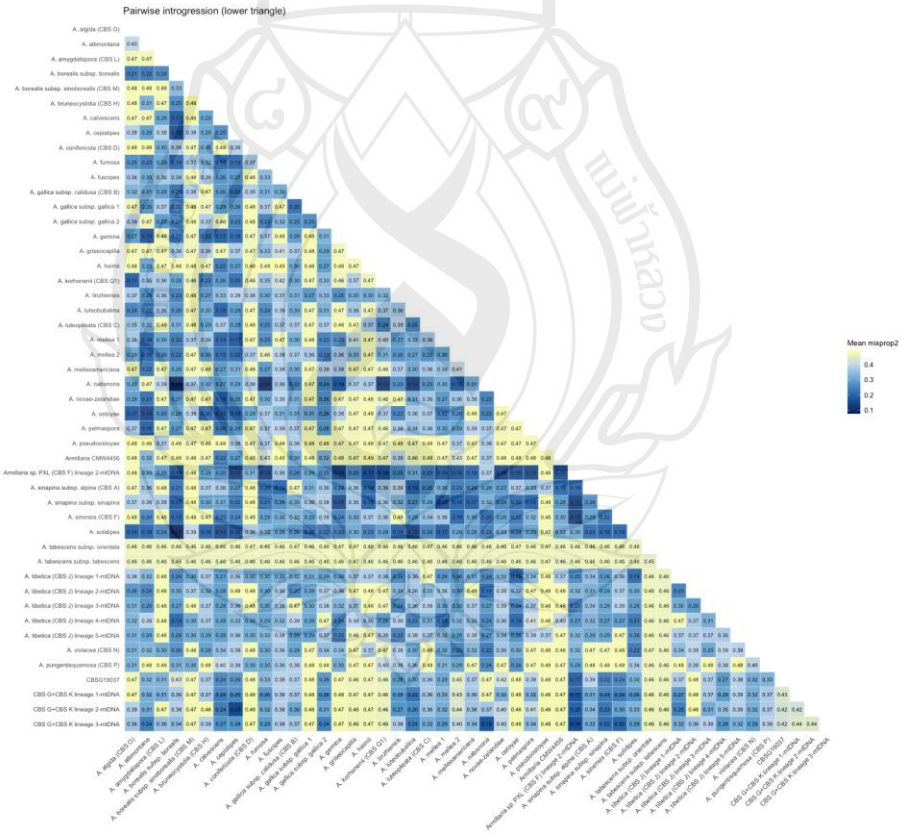
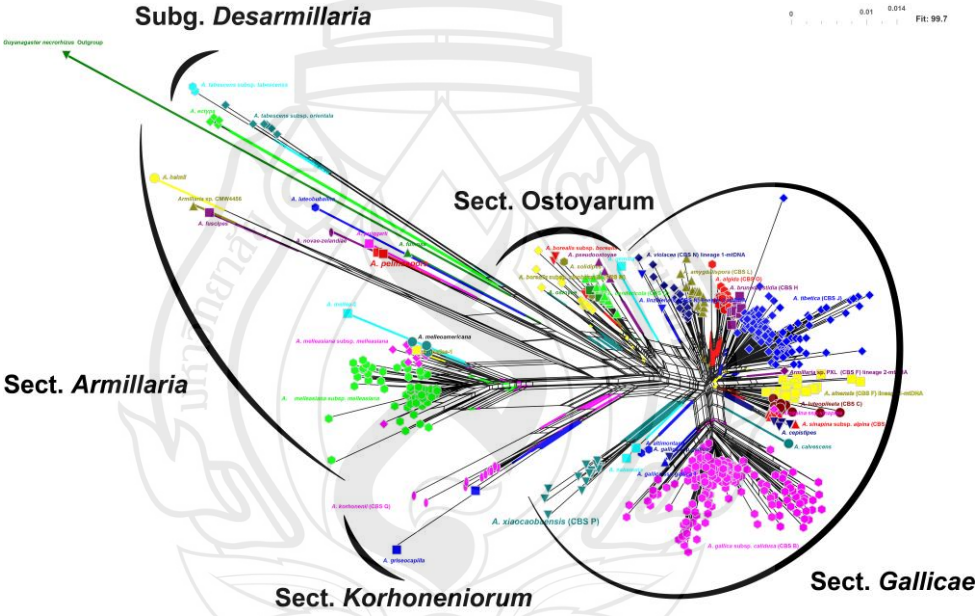


Figure 4.10 The mean total proportion of introgressed loci per species pair inferred through the QuIBL analysis

4.3.9 SplitsTree Network

The SplitsTree analyses (Figures 4.11 and 4.12) recovered the same major clades as the ML trees based on nuclear (Section 2.2.1) and mitochondrial (Section 2.2.2) datasets in Chapter 2. However, whether nuclear or mitochondrial data were used, relationships among lineages within and between certain clades remain complex, as reflected by numerous reticulation branches. In the SplitsTree network for the nuclear dataset (Figure 4.11), sect. *Gallicae*, sect. *Ostoyarum*, and sect. *Armillaria* each displays multiple box-like structures—clear evidence of conflicting phylogenetic signals. The mitochondrial network (Figure 4.12) is somewhat simpler overall, but even here several subclades within sect. *Gallicae* exhibit intricate branching patterns.



Note SplitsTree phylogenetic network reconstructed using the 385 orthologous proteins in 600 samples in 2.1.1. The strains cluster in the subg. *Desarmillaria* and four sections of subg. *Armillaria*.

Figure 4.11 SplitsTree phylogenetic network reconstructed using the 385 orthologous proteins in 600 samples in 2.1.1

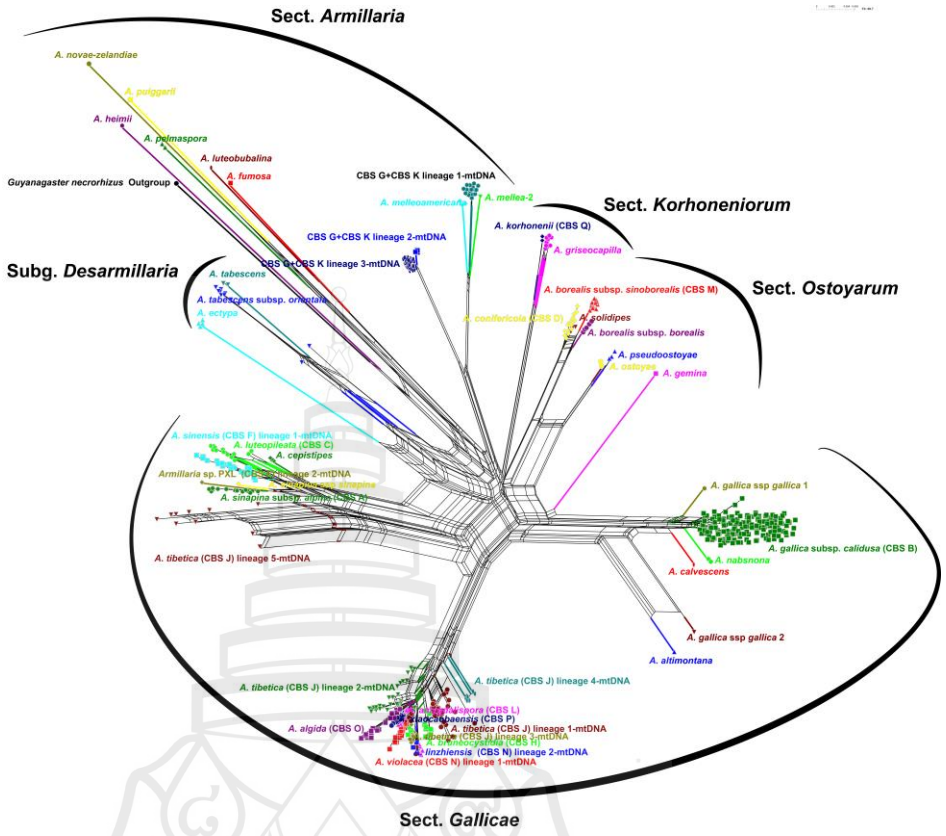


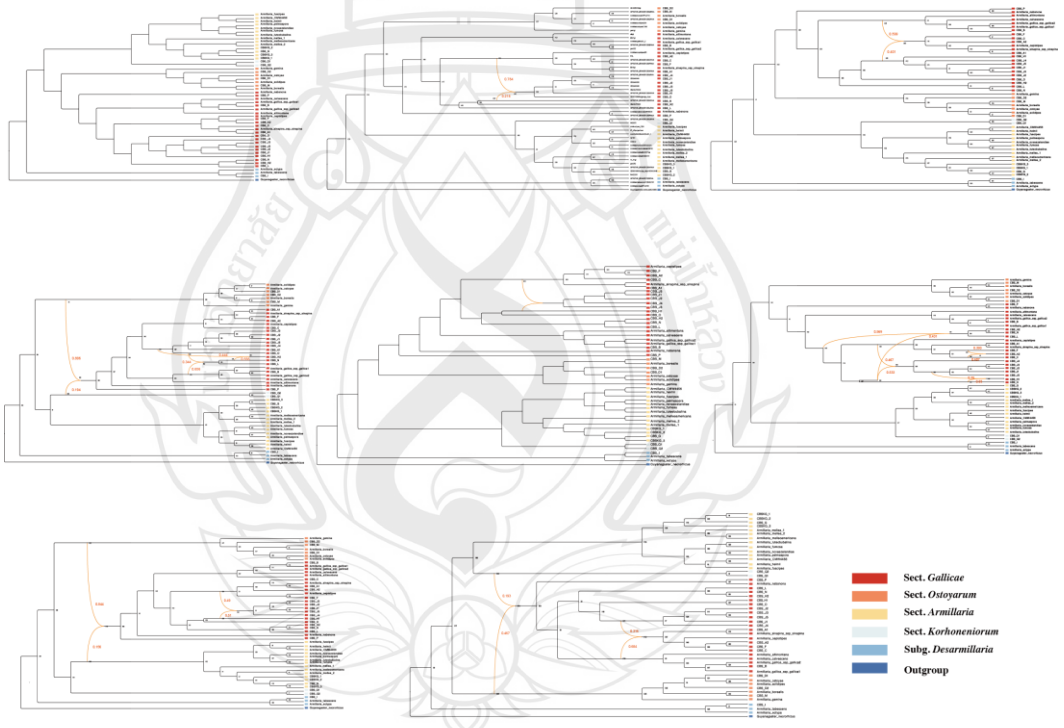
Figure 4.12 SplitsTree phylogenetic network reconstructed using the homesblock of mitochondrial genomes generated by ORPA in 605 samples in 2.2.2

4.3.10 PhyloNet

We evaluated models with 0–7 reticulation events (Table 4.1) and found that log-likelihood improved steadily from -3.69996×10^7 (0 events) to -3.69366×10^7 (6 events), then declined slightly to -3.69712×10^7 at 7 events—indicating the six-event network fits best. Using both the elbow method and minimum AIC, we inferred two major hybridization events: (1) between sect. *Armillaria* and sect. *Ostoyarum*, with an inheritance probability of 0.156 from sect. *Armillaria* and 0.844 from sect. *Ostoyarum*, giving rise to sect. *Gallicae*; and (2) between *A. bruneocystidia* and a lineage composed (in alphabetical order) of *A. cepistipes*, *A. luteopileata*, *A. sinensis*, *A. sinapina* subsp. *alpina*, *A. sinapina* subsp. *sinapina*, and *Armillaria* sp. PXL, with 51% of the genome inherited from *A. bruneocystidia* and 49% from that lineage, produces the *A. tibetica* complex.

Table 4.1 Log-likelihood values for varying numbers of reticulation events

Reticulation events	The log-likelihood values
0	-3.69996167561583E7
1	-3.7003349172600344E7
2	-3.700234569777389E7
3	-3.697127698720209E7
4	-3.699134843717706E7
5	-3.699177772955772E7
6	-3.693664355858423E7
7	-3.697117124637973E7



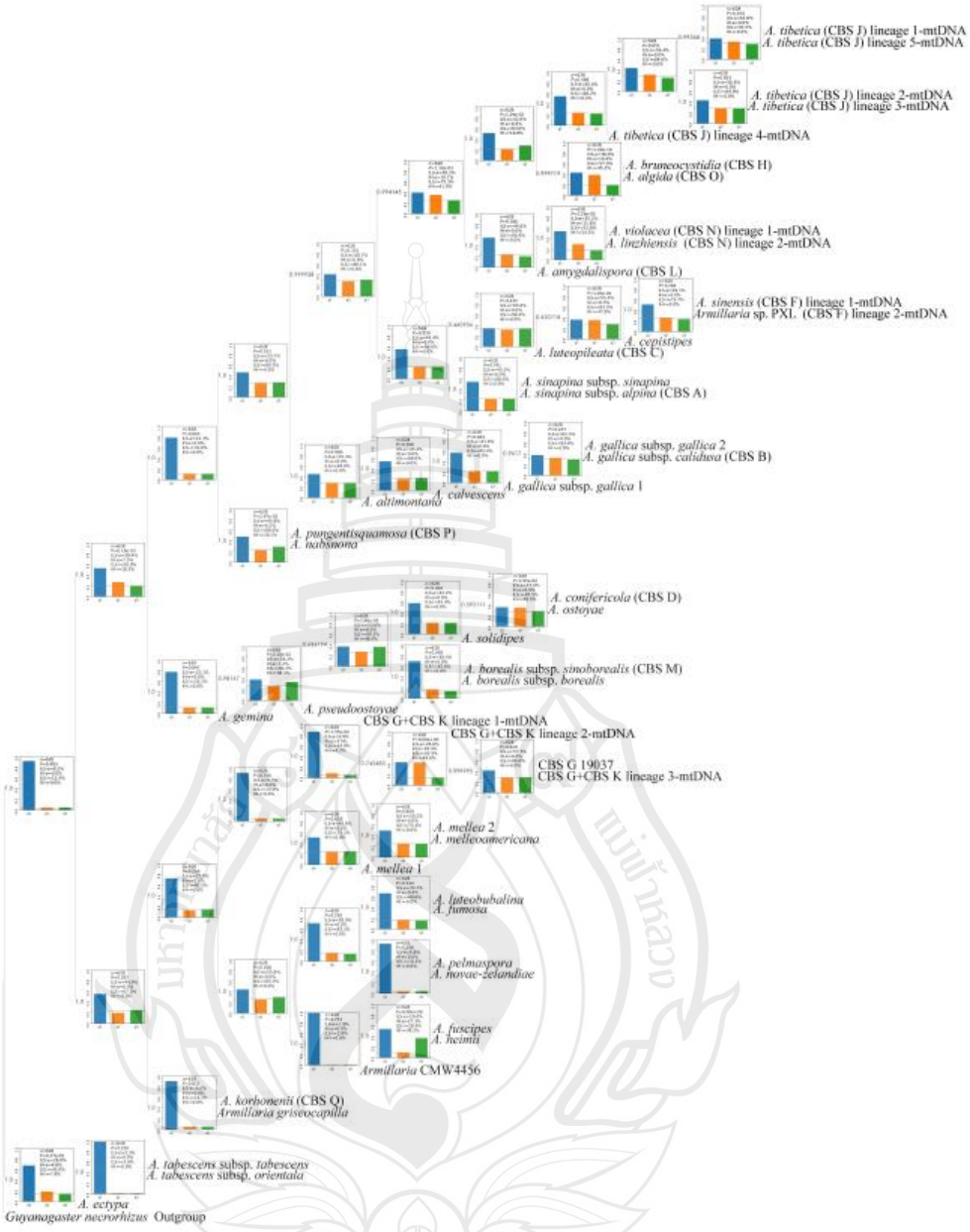
Note Blue branches indicate lineages involved in reticulated histories, and numerical values are the inheritance probabilities for each reticulation. The figure was constructed in Dendroscope and modified in Adobe Illustrator. A. B. C. D. E. F. G. represent the assumed number of hybridizations from 0 to 7.

Figure 4.13 Phylogenetic networks inferred by PhyloNet using Maximum pseudo-likelihood under zero to seven reticulation models

4.3.11 Visualizing and Recognizing Signals of Incomplete Lineage Sorting and Hybridization

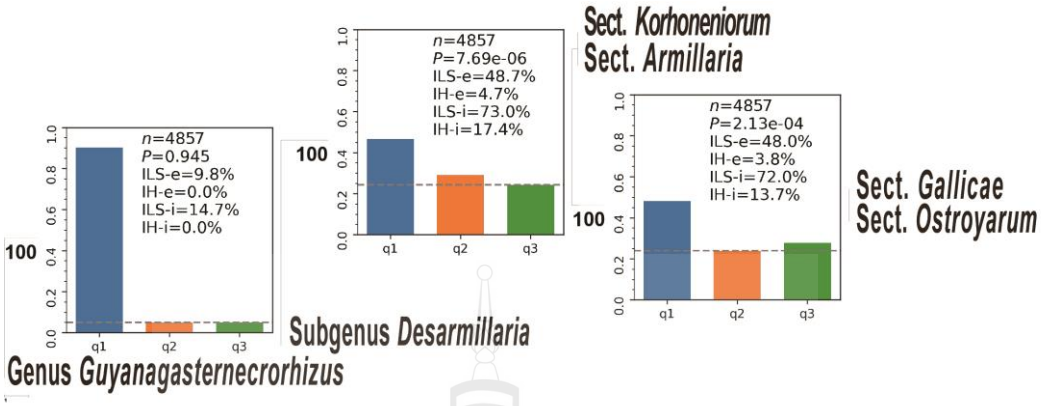
As shown in Figure 4.14, at the species level, topological incongruence among most nodes was primarily attributable to incomplete lineage sorting (ILS). The ILS-i values ranged from 2.4 % to 98.4 %, whereas 33 of the 47 nodes exhibited IH-i values of 0 %, indicating that ILS was the dominant source of discordance across the majority of species. In contrast, even among the 14 nodes with non-zero IH-i values, the IH-i ranged from 4.2 % to 49.6 % across certain species pairs, but these signals were comparatively weak and did not play a dominant role relative to ILS.

At the section level (Figure 4.15), analyses based on a larger dataset of 4,857 gene trees revealed a pattern consistent with that observed at the species level: incomplete lineage sorting (ILS) remained the predominant cause of phylogenetic conflict across the genus *Armillaria*, whereas hybridization/introgression made a secondary but measurable contribution. No phylogenetic discordance attributable to introgression was detected between the outgroup *Guyanagaster necrorhizus* and the subgenera *Desarmillaria* and *Armillaria*. Among *Desarmillaria* and the sections within subgenus *Armillaria*, ILS accounted for 73.0 % of the observed conflict, while IH contributed 17.4 %. Within subgenus *Armillaria*, ILS remained dominant (72.0 %), with IH explaining 13.7 % of the discordance.



Note N represents the number of gene trees, P is the p-value of the $\chi 2$ test to check whether the number of topologies q2 and q3 are equal, ILS-i and IH-i represent the calculated ILS index and IH index, respectively, and ILS-e and IH-e represent the proportion of gene tree topological incongruence that can be explained by the ILS and IH, respectively.

Figure 4.14 Visual result of Phytop on the species level of *Armillaria* with default parameters



Note Visual result of Phytop on the section level of *Armillaria* with default parameters. n represents the number of gene trees, P is the p-value of the $\chi 2$ test to check whether the number of topologies q2 and q3 are equal, ILS-i and IH-i represent the calculated ILS index and IH index, respectively, and ILS-e and IH-e represent the proportion of gene tree topological incongruence that can be explained by the ILS and IH, respectively.

Figure 4.15 Visual result of Phytop on the section level of *Armillaria* with default parameters

4.4 Conclusions

In this chapter, we revealed widespread phylogenetic conflicts within the genus *Armillaria*, both between nuclear and mitochondrial genomes and between gene trees and the species tree. Causative analyses indicate that incomplete lineage sorting (ILS) is the primary factor underlying these topological incongruences, while introgression also plays an important role. This may represent one of the earliest comprehensive efforts to elucidate the evolutionary relationships of macrofungi through an integrative framework that combines phylogenomic discordance detection with causal inference analyses. The above findings help explain why previous phylogenetic studies based on single or a few loci have been unable to accurately resolve the species diversity and evolutionary relationships within *Armillaria*. Across both animals and plants, an

increasing number of studies have demonstrated that ILS, hybridization, and introgression play crucial roles in the process of speciation (Cervantes et al., 2023, Feng et al., 2022, Lopes et al., 2023, Meleshko et al., 2021, Zhang et al., 2023). The same pattern holds true for fungi (Feurtey et al., 2019, Hessenauer et al., 2020, Libkind et al., 2011, Steensels et al., 2021). Accordingly, future phylogenetic studies of fungi should incorporate comprehensive genomic datasets to reconstruct species relationships and delimit species boundaries, while explicitly accounting for the effects of ILS, gene flow, and other biological processes. Phylogenetic analyses should not only focus on inferring phylogenetic relationships but also aim to interpret the biological causes underlying phylogenetic conflicts. After all, species are products of evolution, and strictly bifurcating relationships often represent idealized models, whereas reticulate evolution may more accurately reflect the true evolutionary history of life in many groups.

CHAPTER 5

DNA BARCODING MARKERS AND SSR MOLECULAR FINGERPRINT RECOGNITION SYSTEM DEVELOPMENT

5.1 Introduction

Traditional DNA barcoding markers, such as ribosomal DNA (nrDNA) and several proteins gene sequences, often fail to achieve precise species identification due to insufficient genetic variation or the limited universality of selected genomic loci across the tree of life. In recent years, a method for estimating interspecies genetic distances based on unassembled genome skims has been developed, significantly improving species identification rates (Coissac et al., 2016). For instance, the Skmer tool enables direct estimation of genomic distances from low coverage sequencing reads (genome skims) without requiring assembly or alignment steps (Sarmashghi et al., 2019). Additionally, DNA graphic barcoding technology, which leverages K-mer frequency variation, has emerged as a promising approach. This method trains convolutional neural networks to identify species from graphical representations of genomic data and uses the trained models to query new samples, as demonstrated by tools like varKoder (de Medeiros et al., 2025). Furthermore, de Medeiros et al. (2025) introduced four curated datasets specifically designed for benchmarking molecular identification tools using low-coverage genomes. These datasets provide researchers with a reliable, standardized resource to evaluate the accuracy, efficiency, and robustness of their tools in a consistent and reproducible manner.

Despite the significant potential of these tools in advancing novel barcode development, their application at the species level, particularly within the field of mycology, has not yet been extensively validated. This study aims to develop graphic

barcodes based on K-mer frequency variation within the genus *Armillaria* using whole-genome short-read data. We will assess the feasibility and identification accuracy of this method for fungal species recognition and construct the corresponding graphic barcodes.

Although Qin et al. (2025) recently published eight nuclear loci (Table C6) and primer sets for *Armillaria*, single-locus approaches still struggle to resolve closely related species. By contrast, our genome-wide strategy seeks efficient markers capable of distinguishing most *Armillaria* taxa with a single assay.

To further enable strain discrimination and population-genetic analyses, we also developed a comprehensive SSR fingerprinting system for *Armillaria*. Employing three distinct discovery pipelines, we mined simple sequence repeats across the entire genus to generate robust, multilocus molecular fingerprints.

5.2 Methods

5.2.1 Development of K-mer Frequency–Based DNA Barcodes

We initially organized all clean Illumina short-read data into species-specific folders, adhering to the folder input format as exemplified on the GitHub page: https://github.com/brunoasm/varKoder/blob/main/docs/image.md. A total of 584 datasets were included in this analysis; the used samples are the same with 3.3.1.2 in Chapter 2. subsequently, we employed the varKoder image (cgr) for generating varKode images by using varKoder v1.1.0 (de Medeiros et al., 2024). To evaluate the species identification accuracy of the trained models, we partitioned the generated image data into three training and validation sets, excluding species represented by only one sample. For the validation sets, we selected 1 to 3 samples per species, depending on the total number of available samples. The validation sets were then tested against the models generated from the training sets using the varKoder query module. Finally, we compiled all generated images to train a comprehensive model (Model architecture:

hf-hub:brunoasm/vit_large_patch32_224.NCBI_SRA), which is made available for download.

5.2.2 Development of Nuclear Gene DNA Barcodes in the Genus *Armillaria*

5.2.2.1 Collection and Preprocessing of Genomic Data

We selected samples with a completeness score greater than 90% in the BUSCO evaluation for the development of candidate DNA barcodes. A total of 36 species' genomic data met the above criteria. Detailed species information can be found in Table 5.1.

Table 5.1 *Armillaria* species used for DNA barcode development and their corresponding BUSCO results

Species	BUSCO results				
	C	S	M	F	M
A. altimontana	97.80%	97.00%	0.80%	0.20%	2.00%
A. borealis	95.30%	94.70%	0.60%	0.60%	4.10%
A. calvescens	97.90%	97.10%	0.80%	0.20%	1.90%
A. cepistipe	97.50%	96.60%	0.90%	0.20%	2.30%
A. fumosa CBS122221	98.60%	97.30%	1.30%	0.70%	0.70%
A. gallica 21-2	98.80%	97.30%	1.50%	0.70%	0.50%
A. gallica subsp. *gallica*	97.70%	96.90%	0.80%	0.30%	2.00%
A. gemina	97.90%	97.30%	0.60%	0.30%	1.80%
A. luteobubalina	97.80%	93.10%	4.70%	1.00%	1.20%
A. mellea	97.90%	97.30%	0.60%	0.20%	1.90%
A. melleoamericana	98.00%	97.30%	0.70%	0.30%	1.70%
A. nabsnona CMW6904	98.90%	98.10%	0.80%	0.50%	0.60%
A. novae-zelandiae	97.10%	94.80%	2.30%	1.30%	1.60%
A. ostoyae	96.10%	95.40%	0.70%	1.90%	2.00%
A. puiggarii	94.40%	93.80%	0.60%	0.80%	4.80%
A. sinapina subsp. *sinapina*	98.00%	97.10%	0.90%	0.30%	1.70%
A. solidipes	98.70%	97.90%	0.80%	0.90%	0.40%
Armillaria CMW4456	97.90%	96.50%	1.40%	0.50%	1.60%
CBSA	97.80%	97.00%	0.80%	0.20%	2.00%
CBSB	97.60%	96.80%	0.80%	0.40%	2.00%

Table 5.1 (continued)

Species	BUSCO results				
	C	**S**	**M**	**F**	**M**
CBSC	97.80%	96.70%	1.10%	0.30%	1.90%
CBSD	96.80%	96.00%	0.80%	0.40%	2.80%
CBSF	97.60%	96.70%	0.90%	0.40%	2.00%
CBSH	96.70%	96.00%	0.70%	0.40%	2.90%
CBSH1	91.60%	90.90%	0.70%	0.90%	7.50%
CBSI	97.30%	96.50%	0.80%	0.30%	2.40%
CBSJ2	96.90%	96.10%	0.80%	0.50%	2.60%
CBSJ04043	96.60%	95.80%	0.80%	0.50%	2.90%
CBSJ3	97.10%	94.40%	2.70%	0.50%	2.40%
CBSK+G 3	97.10%	96.40%	0.70%	0.50%	2.40%
CBSK+G 2	95.70%	95.00%	0.70%	0.50%	3.80%
CBSL	98.00%	97.20%	0.80%	0.30%	1.70%
CBSN	97.80%	97.10%	0.70%	0.20%	2.00%
CBSO	96.40%	95.60%	0.80%	0.60%	3.00%
CBSP	97.60%	97.10%	0.50%	0.30%	2.10%
CBSQ2	98.00%	97.30%	0.70%	0.20%	1.80%

5.2.2.2 Screening of Candidate Genes

We initially identified 3,941 single-copy genes from 36 Armillaria species using OrthoFinder v. 2.5.4 (Emms & Kelly, 2015). These single-copy genes were subsequently aligned using MAFFT v7.407 (Katoh, 2013). Considering that candidate genes should neither be too short nor too long, sequences shorter than 150 amino acids (aa) or longer than 700 aa were filtered out. Following this step, a total of 3,889 genes were retained for further analysis.

5.2.2.3 Evaluation of Single-Gene Identification Capability

We initially constructed a phylogenetic tree using RAxML v. 8.2.12 (Stamatakis et al., 2014) based on the aligned single-copy gene matrix. Subsequently, nodes with support values below 50 were collapsed using PhyKIT v1.12.0 (Jacob et al.,

2021). After statistically analyzing the node support values, the top 250 trees with the highest number of supported nodes were manually inspected, resulting in 28 gene trees that effectively distinguished most species. Next, we identified the protein-coding genes corresponding to these 28 gene trees and extracted their nucleotide sequences from the *A. sinapina* subsp. *alpina* (CBS A) genome annotation file.

Using GetOrganelle v1.7.7.1 (Jin et al., 2020), we retrieved the corresponding gene sequences from the sequenced population genomes of Chinese *Armillaria* species, with the *A. sinapina* subsp. *alpina* genome nucleotide sequences as the reference. These sequences were aligned and used to construct phylogenetic trees following the same methods described above. We further evaluated the species identification capabilities of these candidate genes in population samples. Ultimately, 11 genes were selected for primer design and development, as they effectively clustered samples of the same species while distinguishing between different species.

5.2.2.4 Determination of Optimal Gene Loci

Using the multi-species matrix of the 11 genes obtained in the previous step, we designed primers in Geneious Prime. For longer genes, intermediate primers were designed. Among the numerous primers generated, we selected those located in conserved regions of the population data for validation.

5.2.3 Development of a Molecular Fingerprinting System for *Armillaria* Species Identification

These three strategies collectively provide a comprehensive SSR molecular fingerprinting system for the *Armillaria* genus, enabling accurate strain identification and population genetic analysis.

The molecular marker development process is as follows: (1) First, SSR loci in the target population genome were detected using CandiSSR software (Xia et al., 2016), and primers were developed within a 200 bp range upstream and downstream of these loci. Primer development conditions were set to default values in the software. (2) The designed primers were first arranged in ascending order based on missing rates,

retaining primers with a missing rate of 0. Then, they were arranged in descending order based on standard deviation, and the top 40-60 primers were tested on strains of the development population. (3) SSR data were calculated for various genetic diversity indices of SSR loci and populations using GenAlEx version 6.501 (https://biology-assets.anu.edu.au/GenAlEx/), PowerMarker V3.25 software (Liu & Muse, 2005), and POPGENE32 Version 1.32. (4) Ultimately, SSR loci with an average polymorphic information content (PIC) greater than 0.25, with good numbers of alleles (Na), Shannon diversity index (I), average observed heterozygosity (Ho), and expected heterozygosity (He) were obtained.

5.2.3.1 Development of an SSR molecular fingerprinting system for *A. gallica* subsp. *calidusa* (CBS B):

This species is one of the most widely used in the market. The SSR system was developed based on population genomics, and the detailed process is outlined in the patent titled "Polymorphic Microsatellite Molecular Markers of *Armillaria gallica* and Their Primers and Applications" (Patent No. ZL 2023 1 0299314.5). For more information, refer to the patent documentation: CN116426677B.

5.2.3.2 Development of an SSR molecular fingerprinting system for the strongly parasitic *Armillaria mellea* complex (*A. melleasiana* subsp. *melleasiana* and *A. melleasiana* subsp. *macrospora*)

This system was developed based on the findings of Guo et al., (2016), which highlighted the strong parasitic nature of these species. The development process is detailed in the patent titled "Universal Polymorphic Microsatellite Molecular Markers of Two Highly Parasitic *Armillaria* Species and Their Primers and Applications" (Patent No. ZL 2023 1 0299313.0). Further details can be found in the patent documentation: CN116790783B.

5.2.3.3 Development of an SSR molecular fingerprinting system for weakly parasitic *Armillaria* clades

This system targets twelve biological species (CBSA, CBSB, CBSC, CBSD, CBSF, CBSH, CBSJ, CBSL, CBSM, CBSN, CBSO, and CBSP) identified by Guo et al. (2016) as relatively weakly parasitic. The development process is detailed in the patent titled "Universal Polymorphic Microsatellite Molecular Markers of Twelve Weakly Parasitic *Armillaria* Species and Their Primers and Applications" (Patent No. ZL 2023 1 0299315.X). For more information, refer to the patent documentation: ZL 2023 1 0299315.X. However, it was ultimately confirmed that “CBSD and CBSM” are obligate parasites. This set of molecular fingerprints can still be used to identify strains of sect. *Gallicae* and sect. *Ostoyarum*.

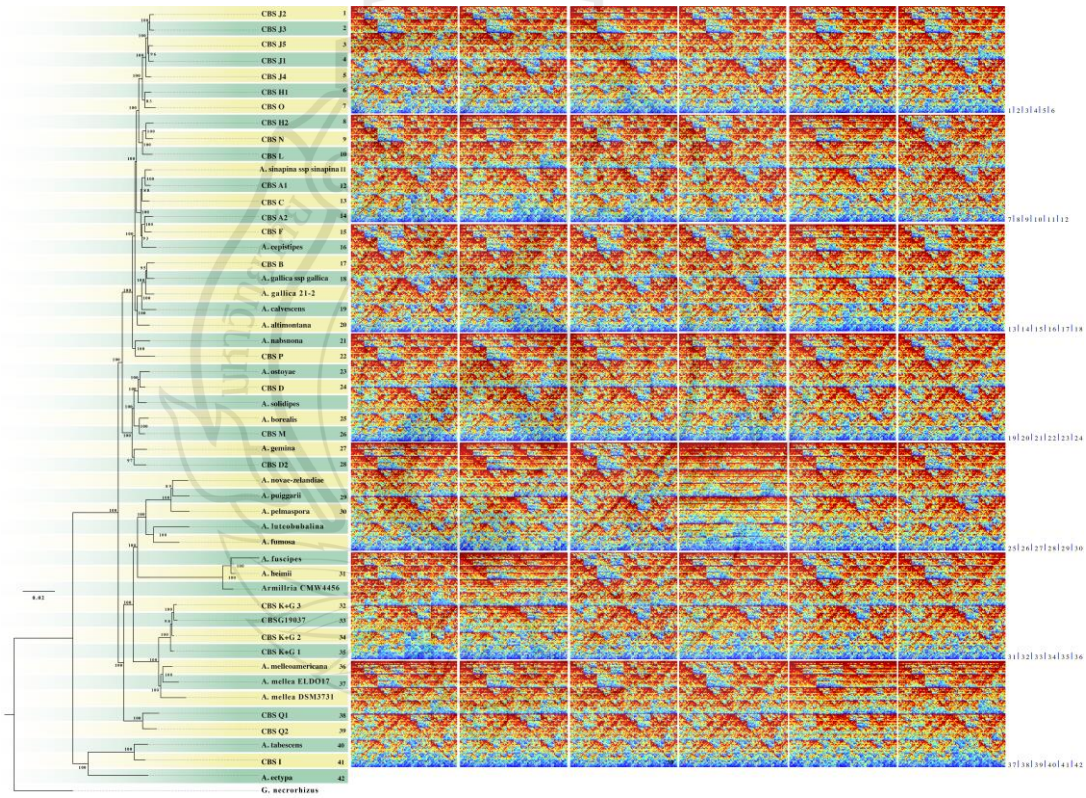
5.2.4 Construction of Offline Databases for Nuclear and Mitochondrial Genomes

We created offline ANI databases for all available *Armillaria* nuclear and mitochondrial genomes using skani v0.2.2 (Shaw & Yu, 2023). By sketching the full complement of nuclear and mitochondrial assemblies into separate databases, we provided users with a seamless platform for rapid genome-to-database comparisons and queries. skani’s approximate mapping approach not only delivers reliable ANI and aligned fraction estimates—even for incomplete or medium-quality metagenome-assembled genomes—but also enables quick searches of large genome collections on a single CPU with modest memory requirements. This setup allows researchers to easily compare new assemblies against the *Armillaria* reference set in just seconds, facilitating efficient identification, clustering, and exploration of genomic relationships.

5.3 Results

5.3.1 Development of K-mer Frequency–Based DNA Barcodes

All 584 samples utilized for training successfully generated images. Subsequently, we examined the Varkoder Low Quality Flag for these images, finding that all samples had the flag set to False (as detailed in Table C7). This indicates that varKoder can produce genome-based images effectively, even in the presence of suboptimal input data quality. To provide a more intuitive representation of the differences between varKoder images across species, we have illustrated these variations in Figure 5.1.



Note Phylogeny and genomic signature varKodes for 42 species of *Armillaria*. The images are natively grayscale but have been mapped to a rainbow color scale to enhance contrast and improve visual clarity. Number of post-cleanings base pairs to make an image.

Figure 5.1 Phylogeny and genomic signature varKodes for 42 species of *Armillaria*

5.3.1.1 Species identification rate and results

In this study, three validation sets comprising a total of 201 samples from 29 species were employed. Among these, 175 samples from 29 species were successfully and accurately identified to their corresponding species (see Table C8), yielding an overall identification accuracy of 87.06%, which indicates the high reliability of the identification method. However, 25 samples failed to be accurately identified to the species level. These samples were primarily distributed among the following groups: CBSA1, CBSD1, CBSI, CBSJ1, CBSJ2, CBSJ3, CBSJ4, CBSJ5, CBSKG1, CBSKG2, CBSKG3, CBSM, CBSO, CBSP, CBSQ1, and EBSB. The reasons for the failed identifications can be attributed to two main factors: (1) the input graphical barcodes failed to generate valid results, and (2) the samples were matched to closely related species complexes within the phylogenetic relationships (see Supplementary Table 5.3 for details). Specifically, among the 7 CBSA1 samples, 6 were accurately identified as CBSA1, while 1 was misidentified as CBSC. Of the 9 CBSD1 samples, 8 were accurately identified as CBSD1, and 1 failed to be identified due to the absence of a valid result. Similarly, for CBSI, most samples were accurately identified, with 1 failing due to the lack of a valid result. For CBSJ1, CBSJ2, CBSJ3, CBSJ4, and CBSJ5, the majority of samples were accurately identified, while the failed identifications were primarily due to the absence of results or internal cross-matching. The CBSKG1, CBSKG2, and CBSKG3 groups exhibited similar patterns, with some samples failing due to the absence of results or cross-identification, though all belonged to the species complex clade of CBSK and CBSG. Among the 9 CBSM samples, 2 were incorrectly matched to CBSD1 due to the absence of valid results. Of the 9 CBSO samples, 2 were incorrectly matched to CBSP for the same reason. Among the 9 CBSP samples, 1 was incorrectly matched to CBSM. All CBSQ1 samples were identified as CBSQ2. Additionally, 1 EBSB sample was simultaneously identified as CBSC and EBSB. In summary, the validation results demonstrate that the method employed in this study exhibits high accuracy and reliability for most samples. However, the failed identifications were primarily concentrated in species complexes with close phylogenetic relationships or

due to technical issues in generating valid results. Overall, this set of barcoding methods is suitable for species-level identification. Future research could focus on optimizing the graphical barcode generation and matching algorithms to enhance the identification accuracy of complex groups.

5.3.1.2 A Benchmark *Armillaria* K-mer Graphical Barcode Database

Based on the k-mer graphical barcodes generated from 584 *Armillaria* samples, we successfully constructed a barcode model, which has been saved as *Armillaria*_model.pkl. This model integrates comprehensive species information and enables efficient and accurate identification and analysis of *Armillaria* groups, providing critical technical support for related research. Utilizing this model, users can rapidly compare the k-mer graphical barcodes of unknown samples against the reference database based on second-generation genomic data, achieving precise species identification. Additionally, the model serves as a reliable data foundation for studies on the phylogenetics, biodiversity conservation, and ecological functions of *Armillaria*. We anticipate that this model will be widely adopted in research and practical applications within the *Armillaria*-related fields and will further advance the development of barcode technology for fungal taxonomy.

5.3.2 Development of Nuclear Gene DNA Barcodes in the Genus *Armillaria*

These primers were synthesized by Tsingke Biotechnology Co., Ltd. (Beijing, China) and tested against Chinese *Armillaria* species. The experimental results, as shown in Table 5.2, indicate that nearly all primers successfully amplified the corresponding gene sequences for most species. In the initial round of testing, CBSI, CBSKG, CBSJ5, CBSM, and *A. pelmaspora* failed to amplify with most primers (see Supplementary Figure 5.2). To rule out the possibility of DNA quality issues, we selected additional samples from these five species for re-amplification. The results showed that, except for CBSI and CBSM, the other three species were successfully amplified to varying degrees. Since CBSI and CBSM can be identified using conventional universal ITS and TEF sequences, we did not optimize primers specifically for these two species. Based on the detection results, the primers listed in the table are sufficient for identifying most species. Additionally, we have updated the

corresponding reference sequences in NCBI, enabling other researchers to select appropriate primers for species identification as needed.

Table 5.2 Candidate genes and primer sets with amplification success rates (Success Rate = Number of Species Successfully Amplified/Total Species Tested)

Forward Primers	Reverse Primers	Amplification Length (bp)	Amplification Success Rate	Annealing Temperature (°C)
OG0003339-400F	OG0003339-1260R	861	15/19	58
OG0003339-1241F	OG0003339-2044R	804	15/19	58
OG0003339-400F	OG0003339-2044R	1645	14/19	58
OG0003743-877F	OG0003743-2525R	1649	12/19	58
OG0003743-2506F	OG0003743-4483R	1978	11/19	58
OG0003743-4464F	OG0003743-6143R	1680	15/19	58
OG0003806-993F	OG0003806-2670R	1678	17/19	58
OG0003806-2651F	OG0003806-3956R	1306	16/19	59
OG0003855-835F	OG0003855-2064R	1230	15/19	58
OG0003855-2045F	OG0003855-3911R	1867	13/19	56
OG0004269-1210F	OG0004269-2801R	1592	17/19	60
OG0004269-2782F	OG0004269-4383R	1602	15/19	58
OG0004596-1162F	OG0004596-2191R	1030	15/19	60
OG0004596-2172F	OG0004596-3379R	1208	14/19	59
OG0004596-1162F	OG0004596-3379R	2218	14/19	59
OG0005440-2886F	OG0005440-4097R	1212	18/19	58
OG0005440-4078F	OG0005440-4662R	585	17/19	57
OG0005440-2886F	OG0005440-4662R	1777	16/19	57
OG0005634-1074F	OG0005634-2412R	1339	15/19	58
OG0005634-2393F	OG0005634-3536R	1144	17/19	57
OG0005634-1074F	OG0005634-3536R	2463	15/19	58
OG0006242-1017F	OG0006242-2498R	1482	17/19	57
OG0006242-2479F	OG0006242-3905R	1427	15/19	58
OG0006242-3886F	OG0006242-5498R	1613	14/19	58
OG0006242-5479F	OG0006242-7097R	1619	15/19	58
OG0006242-7078F	OG0006242-8402R	1325	17/19	57
OG0007328-1045F	OG0007328-2442R	1398	17/19	59
OG0007328-2423F	OG0007328-4046R	1624	15/19	60
OG0007328-4027F	OG0007328-6192R	2166	14/19	59
OG0008605-1038F	OG0008605-2397R	1360	14/19	57
OG0008605-2378F	OG0008605-3767R	1390	14/19	58

Table 5.3 Candidate genes and corresponding primers sequences

Primer names	Sequences
OG0003339-400F	TCTCGAAAAAGGACACGGCA
OG0003339-1260R	CCACTCGTCTTAGCTGCCAA
OG0003339-1241F	TTGGCAGCTAAGACGAGTGG
OG0003339-2044R	CTCGTGATGGGCCTGTCATT
OG0003743-877F	AGAGGGCGGGATTTGTCAAG
OG0003743-2525R	GTGAACGACCTCACTGCAGA
OG0003743-2506F	TCTGCAGTGAGGTCGTTCAC
OG0003743-4483R	AGCGCTTGAACGAGACAAGA
OG0003743-4464F	TCTTGTCTCGTTCAAGCGCT
OG0003743-6143R	GGAGGGATTGAGGGGAGTCT
OG0003806-993F	GCCTCCATCGTGCTCAACAT
OG0003806-2670R	GCTAGCGGAGGTGGAAGTTT
OG0003806-2651F	AAACTTCCACCTCCGCTAGC
OG0003806-3956R	CGTCGTAGAAGAGAAAGCAGC
OG0003855-835F	GGGAGAGGGAGAGGAGACAG
OG0003855-2064R	AGTTGGATGCTTCTTCCCGG
OG0003855-2045F	CCGGGAAGAAGCATCCAACT
OG0003855-3911R	AATGTGGTGGGTGGTGGTAG
OG0004269-1210F	CGCGTCGAGGATCCTCTG
OG0004269-2801R	ATTCGCAGCCTCTTCAGCTT
OG0004269-2782F	AAGCTGAAGAGGCTGCGAAT
OG0004269-4383R	AGCCATTAAACTGACAACGGG
OG0004596-1162F	CTCAGGCTGGATGCAAGGAG
OG0004596-2191R	ACGTATTCTAAGCCGGCGAG
OG0004596-2172F	CTCGCCGGCTTAGAATACGT
OG0004596-3379R	TGACGATGCAGAACTAGCAGA
OG0005440-2886F	GACTCGTCCCGCTTCTCAAC
OG0005440-4097R	CCTCTTCACTTGCTCGTGGT
OG0005440-4078F	ACCACGAGCAAGTGAAGAGG
OG0005440-4662R	GGGAGCAACGACAGGATACA
OG0005634-1074F	TCTCCCAGATGCATTATCGCT
OG0005634-2412R	CAACTTCAGCACCAGCAACC

Table 5.3 (continued)

Primer names	Sequences
OG0005634-2393F	GGTTGCTGGTGCTGAAGTTG
OG0005634-3536R	GTCTTCTTACCTCCTGCCACC
OG0006242-1017F	CCCACGTGATACCTCGAACC
OG0006242-2498R	CGCGTAAGGTTGGCACAAAA
OG0006242-2479F	TTTTGTGCCAACCTTACGCG
OG0006242-3905R	TCGCAAGCCCGATATCCTTC
OG0006242-3886F	GAAGGATATCGGGCTTGCGA
OG0006242-5498R	GACGTCCGCTAAATCAACGC
OG0006242-5479F	GCGTTGATTTAGCGGACGTC
OG0006242-7097R	TCAGTGGAAAGTCGTGGACG
OG0006242-7078F	CGTCCACGACTTTCCACTGA
OG0006242-8402R	TGTTCCGGTATGTGAATGCCA
OG0007328-1045F	CTAGTCTGCCACCTTCACCG
OG0007328-2442R	CATCCCGCTCATTTCGCAAG
OG0007328-2423F	CTTGCGAAATGAGCGGGATG
OG0007328-4046R	AGACTCGGCTAGCTCTTCCA
OG0007328-4027F	TGGAAGAGCTAGCCGAGTCT
OG0007328-6192R	TTAGATGGTGGCAGTGCTGG
OG0008605-1038F	ACAATGCCCCAGTGTTCCTT
OG0008605-2397R	TGCTTGTATTCAGGCTGGCA
OG0008605-2378F	TGCCAGCCTGAATACAAGCA
OG0008605-3767R	CCTTTCCCTCGACCTGCATT

5.3.3 Development of a Molecular Fingerprinting System for *Armillaria* Species Identification

5.3.3.1 Development of an SSR molecular fingerprinting system for *A. gallica* subsp. *calidusa* (CBSB)

Among the 60 evaluated primers, 12 SSR loci showed high polymorphism in *Armillaria gallica* samples (Table 5.5). The 12 SSR loci had a number of alleles (Na) ranging from 4 to 10 in the 81 strains, with an average of 5.833. The average Shannon

diversity index (I) was 1.297, the average observed heterozygosity (Ho) was 0.542, the average expected heterozygosity (He) was 0.455, and the average polymorphism information content (PIC) was 0.675. The corresponding repeat types and forward and reverse primers are shown in Table 5.4, and the alleles and allele frequencies are illustrated in Figure 5.2. These 12 SSR loci were able to distinguish and classify all 81 *Armillaria gallica* samples, as shown in Figure 5.3. The strains at the base and top of the UPGMA tree mainly originated from the strain market, with many strains clustering into a single branch, indicating that these strains have a consistent genetic background and possibly the same source. In contrast, the strains in the middle of the UPGMA tree mainly originated from wild environments, forming distinct branches that differentiate from each other.

Table 5.4 SSR loci and information on repeat type and corresponding primer sequences

Loci	Repeat type	Forward primer sequence	Reverse primer sequence
CBSBSSR120	AT	TCGGGAAGCCATTTGGTCAA	GGACAGAACGGTGTTGTTGC
CBSBSSR198	CAA	CTCAGATGGTCCAGCAGCAG	CCTCTCCCAAACCCACAACA
CBSBSSR208	CAC	ACATCGACCTCGTCTCAGGA	AAACATAAGGCGACGGAGCA
CBSBSSR273	CGA	GTCATGGTGGCAGGAACAGA	AGCCTGTCGAGGTATACGGT
CBSBSSR353	CTG	GTCAGTCGCAGGAGGTATCG	CTCACCTTTCTGCGGGAAGT
CBSBSSR364	CTTC	GGATCCACAGCGAAGTCGAT	AGAGTGGTGTGCATCCAAGG
CBSBSSR431	GAG	TGGCTTTGGGACCAGATGTC	CTTGGTCAGCGATCTCCTGT
CBSBSSR468	GCA	ACAAACGAGCACCGAAAAGC	TAGTGTCGTCATCGCCATCG
CBSBSSR495	GGCA	CATCGATGCACAGACTTGCG	CCTGTAGCTCTGCTCCATCG
CBSBSSR620	TCA	CAACCACGGAAGCACACAAG	TCGGAGGTGACGAAAAGGAC
CBSBSSR648	TCG	ACAAACGAGCACCGAAAAGC	TAGTGTCGTCATCGCCATCG
CBSBSSR723	TGG	GGGGTCTGGTAAGGGTGGTA	GTACCAGGTCCCAGTTCACG

Table 5.5 Genetic diversity information of different SSR loci

Loci	Na	I	Ho	He	PIC
CBSBSSR120	4	1.141	0.407	0.668	0.597
CBSBSSR198	5	0.969	0.519	0.536	0.471
CBSBSSR208	7	1.158	0.802	0.626	0.562
CBSBSSR273	6	1.508	0.728	0.763	0.722
CBSBSSR353	10	1.690	0.864	0.791	0.758
CBSBSSR364	6	1.301	0.704	0.677	0.619
CBSBSSR431	4	1.225	0.370	0.673	0.616
CBSBSSR468	5	1.292	0.333	0.657	0.617
CBSBSSR495	7	1.482	0.407	0.706	0.668
CBSBSSR620	4	1.336	0.519	0.725	0.675
CBSBSSR648	5	0.904	0.114	0.513	0.438
CBSBSSR723	7	1.556	0.741	0.768	0.729
Mean	5.833	1.297	0.542	0.675	0.623

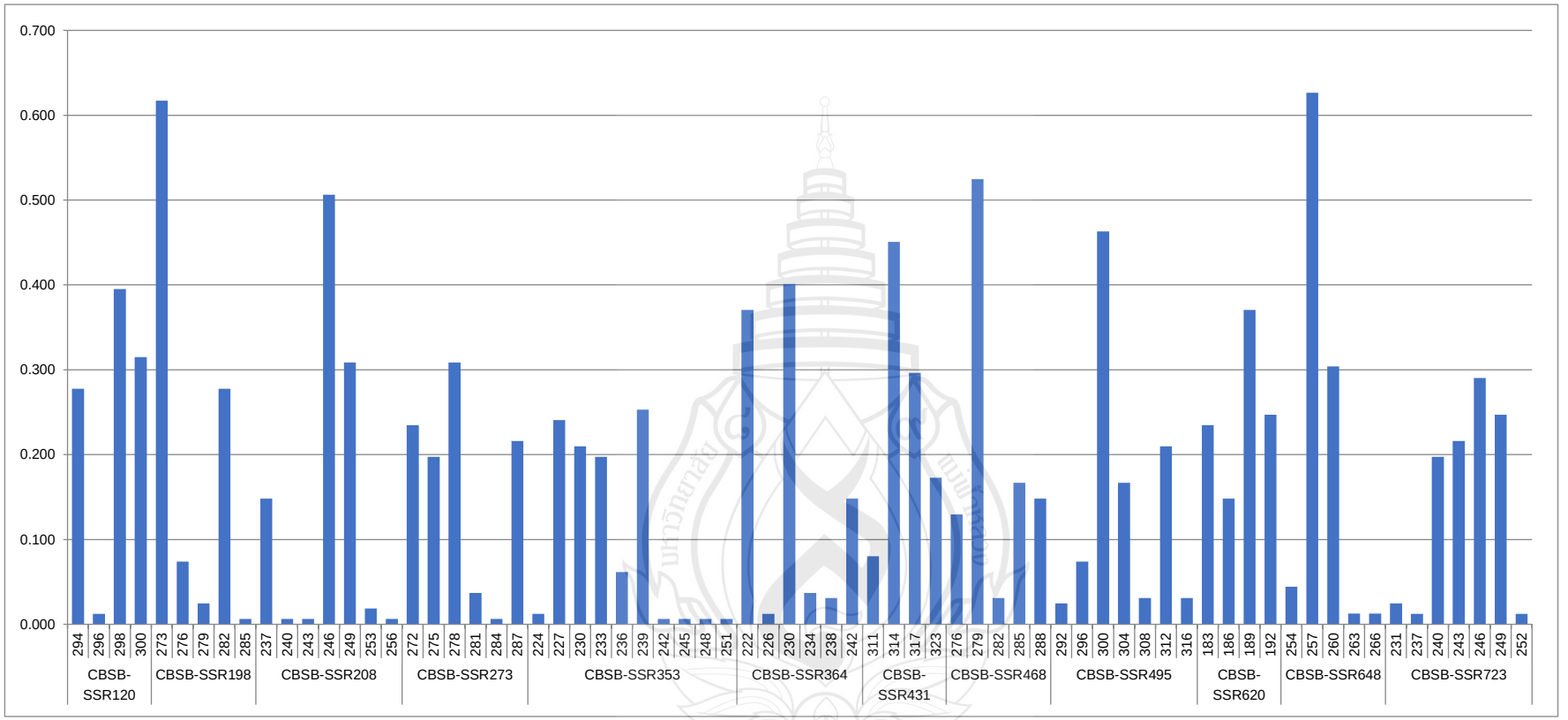


Figure 5.2 Alleles and allele frequency distribution diagram of 12 SSR loci amplified in 81 *Armillaria gallica* strains

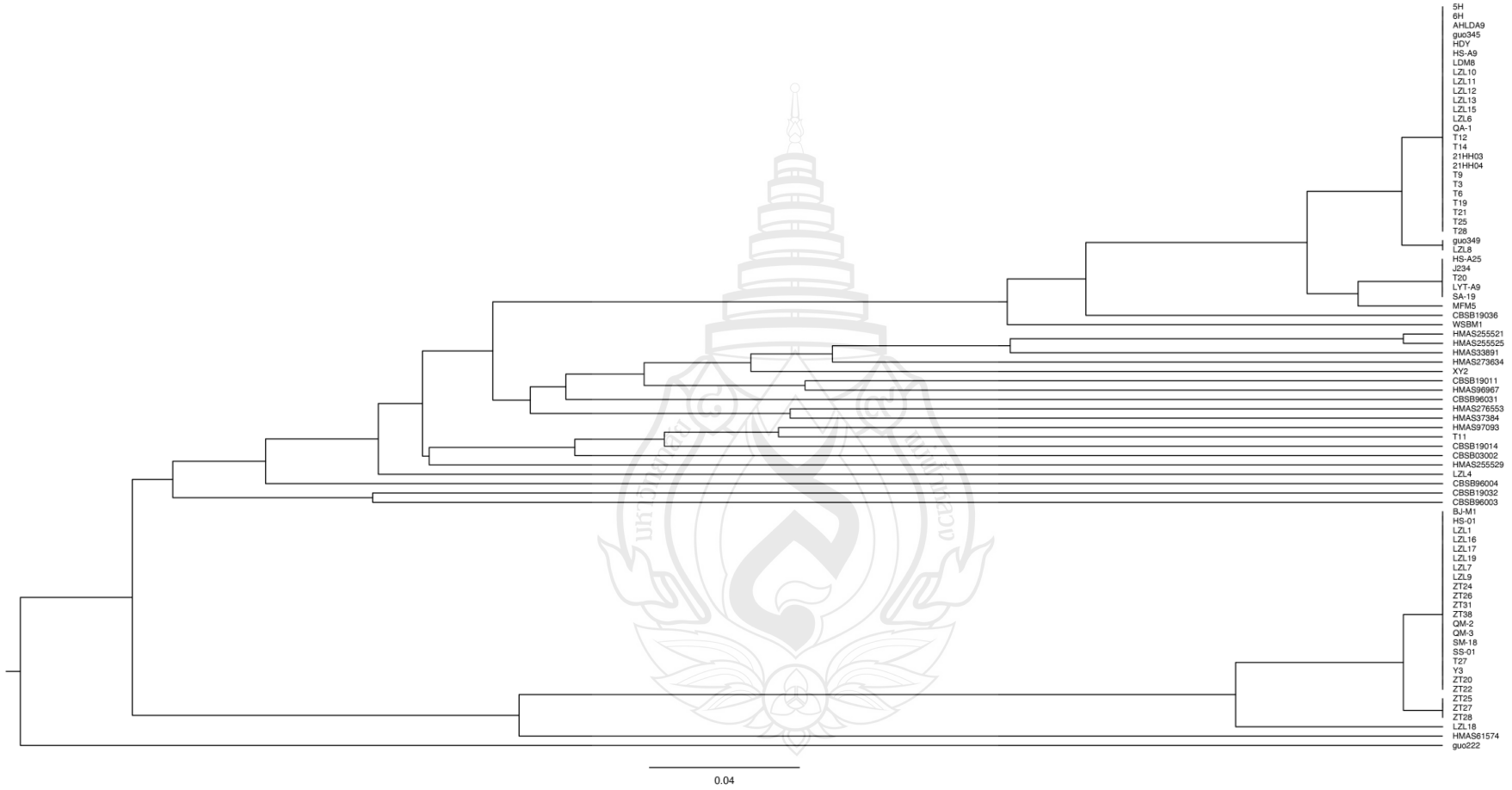


Figure 5.3 UPGMA tree constructed based on 12 SSR loci from 81 *Armillaria gallica* strains

5.3.3.2 Development of an SSR molecular fingerprinting system for the strongly parasitic *Armillaria mellea* complex (CBSK and CBSG)

Among the 40 evaluated primers, 30 SSR loci showed high polymorphism in the strongly parasitic *Armillaria mellea* complex (Table 5.7). The number of alleles (Na) at 30 SSR loci in 17 samples ranged from 2 to 9, with an average of 4.63. The average Shannon diversity index (I) was 1.10, the average observed heterozygosity (Ho) was 0.45, the average expected heterozygosity (He) was 0.56, and the average polymorphism information content (PIC) was 0.57. The 30 SSR loci exhibited high polymorphism in the samples. The corresponding repeat types and forward and reverse primers are shown in Table 5.6, and the alleles and allele frequencies are depicted in Figure 5.4. As shown in Figure 5.5, the developed 30 SSR loci can distinguish all 17 highly parasitic *Armillaria* strains.

Table 5.6 SSR loci and information of repeat type and corresponding primer sequences

Loci	Repeat type	Forward primer sequence	Reverse primer sequence
QJSSSR26	ACC	CGTTTGGACCTTCTCAGCCT	AAACTTGGCCGCTTTGAACG
QJSSSR41	ACG	GAATAGAGCGCGATGGGTGA	CGACTCGGAGCTTGCAATTG
QJSSSR111	CA	TCTCTCAAACGCTATCACCGT	TGTGTGGAAACAAGGCTGGT
QJSSSR114	CA	TCGACATCATCTCTCTCAAATGCT	TGTGTGGAAACAAGGCTGGT
QJSSSR116	CA	TCTCTCAAACGCTATCACCGT	TGTGTGGAAACAAGGCTGGT
QJSSSR135	CAC	CCGTGCCAAGGGAAGGTTAT	TAAGTCGGAGCCGCAAAGTT
QJSSSR137	CAG	GACGACGAGCAACGACTTTG	GGAGGAGCTGGACAATAGCG
QJSSSR141	CAG	AGAACCCATCGCAGTGGATG	CTGAGAGGGCGGAGGAAATC
QJSSSR145	CAG	GTTGTAACGCAGCCTTCGTC	GTTGCTGTTGCTGCTGTTGA
QJSSSR159	CCA	TTCACTCGTTCCTCCGAAGC	CCTGGTGCAGATGGAATGGT
QJSSSR178	CGA	CCGAGTACACCGTCCACATC	GCTGGCATAGGTCTCCCATC
QJSSSR219	CTG	GTCAGTCGCAGGAGGTATCG	CTCACCTTTCTGCGGGAAGT
QJSSSR224	CTT	CTGAGCCGGTGGTTTTACCT	CTCAGCAAGTGCAGCAACAG
QJSSSR252	GA	TTGTCGACCTCCGTGAACTG	AGGCCCATGCTACATGTACG
QJSSSR267	GAC	CGCCATGGAGGTGCTTAAGA	ATAGTTCCGTCGTGGGCTCA
QJSSSR282	GAC	AAAGCCGCGGTGATCCATTA	CCGCTCATGAATCTGGACGA
QJSSSR305	GAG	AGTTCCTCCGACATCCGAGA	CGGAGCCGTCTTCTTGTTCT
QJSSSR311	GAT	TGCGGGTCGAATAGATGTCG	GGCAACCTACGACTCAGTCC

Table 5.6 (continued)

Loci	Repeat type	Forward primer sequence	Reverse primer sequence
QJSSSR336	GCT	GATTGCGATCGGGGTTGTTG	CCCAGGTCAACCCGGTTTTA
QJSSSR376	GGT	ATACGACGAATCCGGAACCG	CCGGCAATAATGTCCGAACC
QJSSSR380	GT	TGAAGGCCGCGTATCTATGG	CCCCTCCATCATCACACTCG
QJSSSR394	GTC	CATCAACGTCCCAGTCGTCA	AGAACGACCTCTACCGCTCT
QJSSSR401	GTC	GTCCTTCCGGTTCAGCTTGA	CAAGAAGAAACCGCCCGTTG
QJSSSR490	TCG	TTCTTCGTCTGGCTCCCAAC	GGTATCTACGGTGGCGTACG
QJSSSR501	TG	CGAGAAGGGGTATTGGTGGT	TCTTGGAACCACCCACACAC
QJSSSR503	TG	CGAGAAGGGGTATTGGTGGT	ACCCACACACACACACACTT
QJSSSR511	TGA	CAGCAGTTCTTGGCCCTAGT	TCCACTCAAAGCTCCGTTCC
QJSSSR513	TGC	GCTACTTTGACCCACCTGCT	TTATCCAGCTCCTCCGGGAA
QJSSSR517	TGC	CAAACAAGCCCAGCCCATTC	ACTCAGGGAAGCGGTAGTCT
QJSSSR520	TGG	CTATCGTCGCGAGCGTGATA	TGGATCTCGCCGAATCATGG

Table 5.7 Genetic diversity information of different SSR loci

Loci	Na	Ne	I	Ho	He	PIC
QJSSSR26	4.00	2.79	1.17	0.41	0.64	0.42
QJSSSR41	4.00	2.21	0.91	0.29	0.55	0.80
QJSSSR111	5.00	3.34	1.36	0.47	0.70	0.52
QJSSSR114	6.00	2.90	1.35	0.41	0.66	0.44
QJSSSR116	5.00	3.30	1.34	0.59	0.70	0.69
QJSSSR135	4.00	1.97	0.85	0.29	0.49	0.55
QJSSSR137	5.00	2.13	0.97	0.18	0.53	0.69
QJSSSR141	4.00	2.64	1.10	0.65	0.62	0.72
QJSSSR145	6.00	4.28	1.61	0.65	0.77	0.59
QJSSSR159	6.00	3.69	1.52	0.73	0.73	0.64
QJSSSR178	9.00	5.61	1.90	0.71	0.82	0.82
QJSSSR219	4.00	3.38	1.29	0.76	0.70	0.27
QJSSSR224	3.00	1.44	0.59	0.35	0.31	0.62
QJSSSR252	2.00	1.33	0.42	0.06	0.25	0.45
QJSSSR267	3.00	2.12	0.81	0.59	0.53	0.74
QJSSSR282	4.00	1.88	0.91	0.47	0.47	0.46
QJSSSR305	5.00	2.99	1.29	0.59	0.67	0.62
QJSSSR311	6.00	3.96	1.56	0.53	0.75	0.75
QJSSSR336	6.00	3.68	1.50	0.81	0.73	0.34
QJSSSR376	4.00	2.30	1.07	0.35	0.57	0.65

Table 5.7 (continued)

Loci	Na	Ne	I	Ho	He	PIC
QJSSSR380	2.00	1.49	0.51	0.18	0.33	0.65
QJSSSR394	3.00	1.68	0.67	0.18	0.40	0.42
QJSSSR401	5.00	3.26	1.32	0.56	0.69	0.71
QJSSSR490	3.00	1.20	0.35	0.18	0.16	0.58
QJSSSR501	7.00	4.50	1.69	0.67	0.78	0.37
QJSSSR503	3.00	1.13	0.26	0.06	0.11	0.58
QJSSSR511	5.00	2.71	1.26	0.76	0.63	0.28
QJSSSR513	5.00	1.66	0.83	0.24	0.40	0.69
QJSSSR517	8.00	6.15	1.93	0.53	0.84	0.28
QJSSSR520	3.00	1.44	0.58	0.35	0.30	0.65
Mean	4.63	2.77	1.10	0.45	0.56	0.57

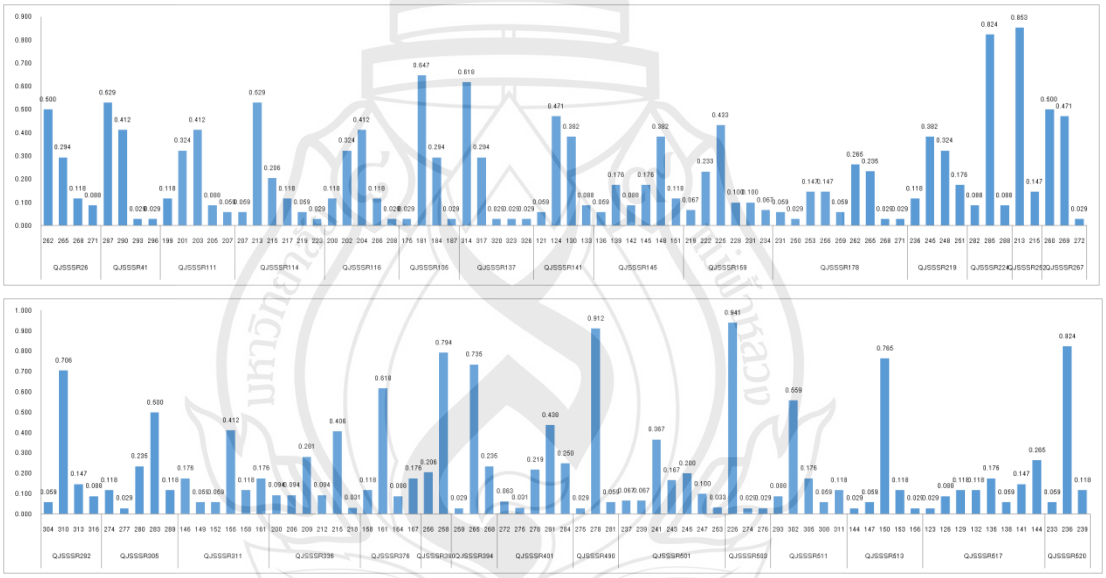


Figure 5.4 Alleles and allele frequency distribution diagram of 30 SSR loci amplified in 17 strains of highly parasitic *Armillaria mellea* complex from different sources

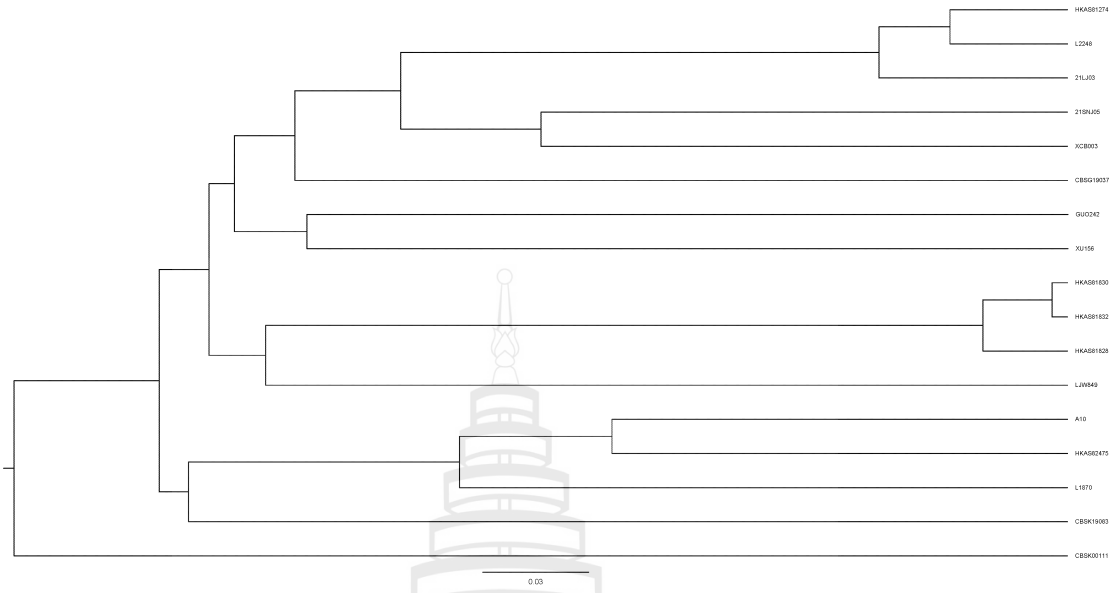


Figure 5.5 UPGMA tree constructed based on 30 SSR sites for 17 strains

5.3.3.3 Development of an SSR molecular fingerprinting system for weakly parasitic *Armillaria* clades

Among the 40 evaluated primers, 13 SSR loci showed high polymorphism in twelve weakly parasitic *Armillaria* species (Table 5.9). The observed number of alleles (Na) at 13 SSR loci in 39 samples of the weakly parasitic branch ranged from 4 to 9, with an average of 6.23. The average Shannon diversity index (I) was 1.18, the average observed heterozygosity (Ho) was 0.17, and the average expected heterozygosity (He) was 0.62. The average polymorphism information content (PIC) was 0.58. The 13 universal SSR loci showed high polymorphism across all weakly parasitic *Armillaria* samples. The corresponding Repeat type and forward and reverse primers are shown in Table 5.8, and Allele and Allele Frequencies are shown in Figure 5.6. As shown in Figure 5.7, the 13 universal SSR loci were able to distinguish all 39 strains of weakly parasitic *Armillaria*.

Table 5.8 SSR loci and information on repeat type and corresponding primer sequences

Loci	Repeat type	Forward primer sequence	Reverse primer sequence
RJSSSR7	ACC	AGGACCATAGACCGTCGACA	GAACCGGACATTGGGTGGTA
RJSSSR9	ACC	GCGTGACGTCACAAAGTCTC	TGACCTCGCTCTCTTCCTCA
RJSSSR13	ACC	AGTCGACGCCAAAAGGGAAT	TTGAGGAGAGGACGGGAGAG
RJSSSR107	CG	AGCGAAACCCGTCAATGACT	GGGGCTTCTTGGTTCGTGTA
RJSSSR147	CG	CGGTTATCGAGACGGCTCTC	GGTGCGTTCTGGATGGTGTA
RJSSSR189	GAC	ACTTGTACGCAGTGGACTCG	CCGACGTGAGGTACAGATCG
RJSSSR213	GATG	GGCGAATACTAGTGGGCGAA	GCAAGCTCGATCGGATGTCT
RJSSSR226	GCC	CGTGGTGGTCATCGTCGTAT	TTTCGCTTGGGATGCTAGCA
RJSSSR245	GGT	AGGGAAGCTCCGGTAAAAGC	ACGTACCTCGGACCATCGTA
RJSSSR275	TA	TGCCGGACCTATTGCACAAA	CCCTCCCAATTTACGCTGGT
RJSSSR290	TC	CGAGGGTTTGATGGACACGA	GCAACCCAGTAGACGACACA
RJSSSR326	TCG	AACACGGTCGAGATGCAGAG	TGCCTTCCACATGCATCACT
RJSSSR376	TTG	CCTCTCCCAAACCCACAACA	CTCAGATGGTCCAGCAGCAG

Table 5.9 SSR loci and information on repeat type and corresponding primer sequences

Loci	Na	Ne	I	Ho	He	PIC
RJSSSR7	8.00	2.16	1.18	0.15	0.54	0.51
RJSSSR9	5.00	3.92	1.48	0.10	0.74	0.71
RJSSSR13	4.00	2.37	1.06	0.12	0.58	0.52
RJSSSR107	6.00	1.84	0.87	0.08	0.46	0.41
RJSSSR147	9.00	4.99	1.77	0.24	0.80	0.77
RJSSSR189	6.00	2.98	1.29	0.02	0.66	0.61
RJSSSR213	6.00	3.16	1.42	0.07	0.68	0.65
RJSSSR226	6.00	1.69	0.88	0.15	0.41	0.39
RJSSSR245	6.00	3.10	1.33	0.17	0.68	0.63
RJSSSR275	7.00	4.35	1.67	0.07	0.77	0.74
RJSSSR290	6.00	3.88	1.53	0.32	0.74	0.71
RJSSSR326	4.00	1.93	0.92	0.07	0.48	0.45
RJSSSR376	8.00	2.25	1.18	0.17	0.56	0.52
Mean	6.23	2.97	1.28	0.13	0.62	0.58

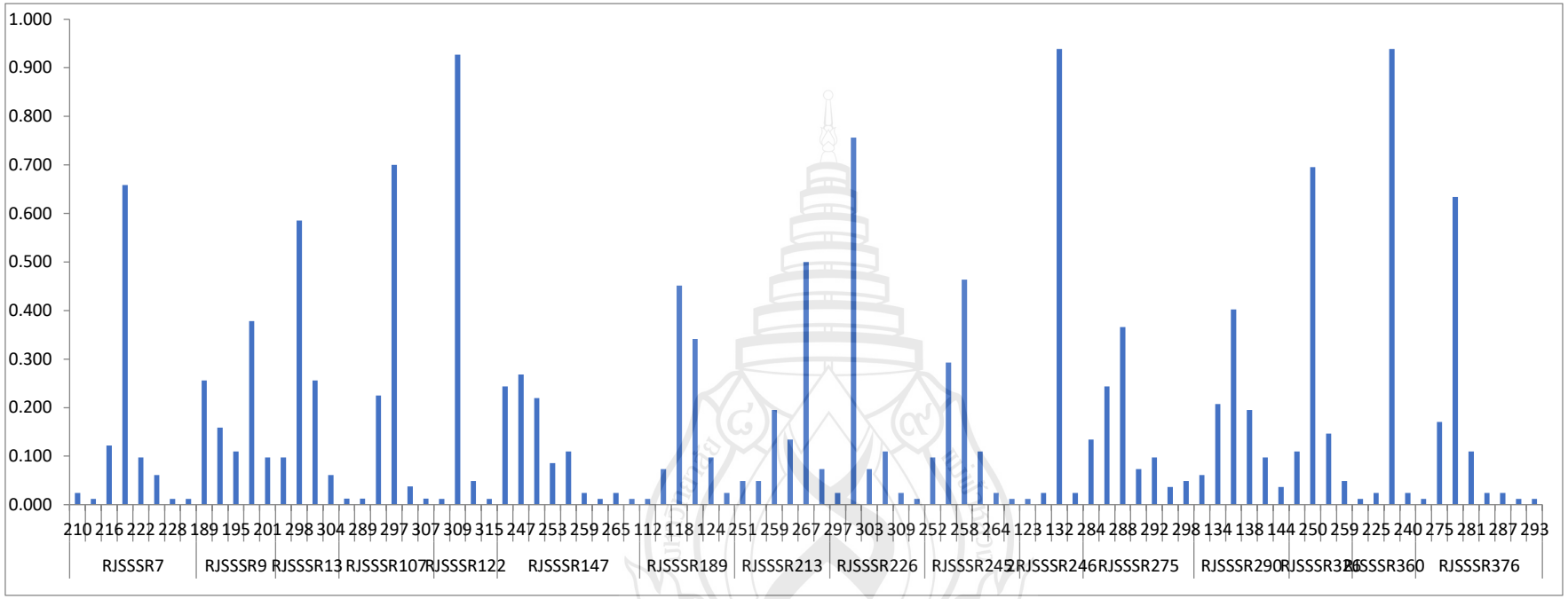


Figure 5.6 Alleles and allele frequency distribution of 13 SSR loci amplified in 39 strains of 12 weakly parasitoid *Armillaria* species

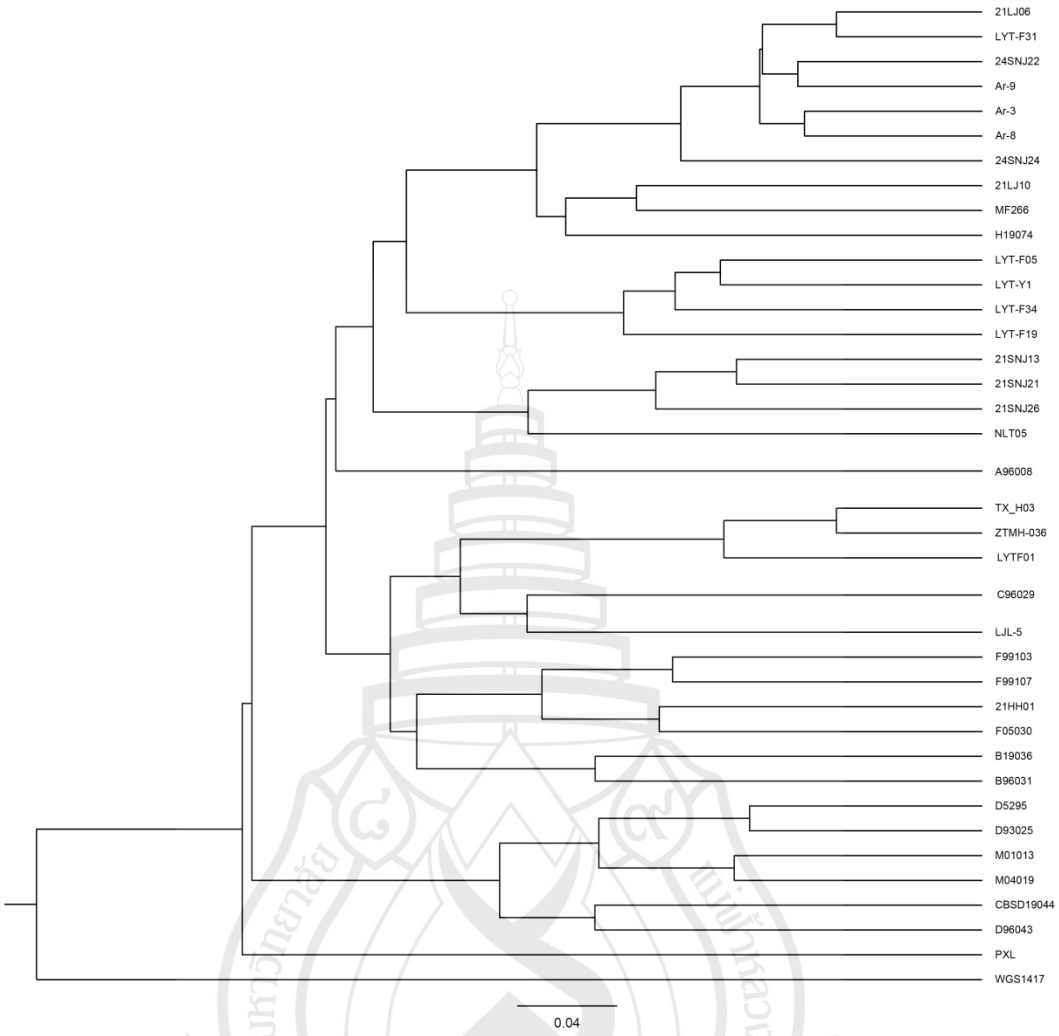


Figure 5.7 UPGMA tree constructed based on 13 SSR loci for 39 strains of 12 weakly parasitoid *Armillaria* species

5.3.4 Construction of Offline Databases for Nuclear and Mitochondrial Genomes

All 600 nuclear-genome assemblies and 605 mitochondrial-genome assemblies were successfully sketched into two *Armillaria*-specific databases using skani v 0.2.2.

5.4 Discussion

Accurate identification of *Armillaria* species and strains has long been challenging. In this study, we developed an integrative framework that unifies multiple complementary approaches. The deep-learning-based image barcoding module achieved an overall identification accuracy of 87.06%, representing the first attempt at species-level recognition in macrofungi. Likewise, the curated nuclear and mitochondrial genome databases enable rapid, within-second species identification, marking the first implementation of a genome-based instant diagnostic system for macrofungal taxa. At the genus level, we evaluated 3,889 single-copy genes to assess their phylogenetic performance, and at the population level, we examined their intraspecific stability, ultimately designing 13 candidate DNA barcodes and corresponding universal primers, which further complement those reported by Qin et al. (2024). In addition, a high-resolution SSR marker system was established, allowing comprehensive discrimination of strains across all *Armillaria* sections. In practice, once a sample is obtained, users can apply our integrative framework through several complementary routes. Raw sequencing reads (FASTQ), or assembled sequences (FASTA), can first be converted into genomic image encodings representing the relative frequencies of different k-mers by creating varKodes or rfCGRs with varKoder.py image, which are then queried against our trained image database using varKoder.py query to obtain species-level identification. Alternatively, assembled nuclear or mitochondrial genomes can be directly compared against our curated reference databases using Skani, which calculates average nucleotide identity (ANI) and aligned fraction (AF) for DNA sequences (contigs/MAGs/genomes), with species-level similarity typically defined by ANI ≥ ~80%. For molecular verification, any of the 13 candidate DNA barcodes and corresponding universal primers developed in this study can be PCR-amplified and sequenced for BLAST or phylogenetic identification. Finally, after species determination, the corresponding SSR fingerprinting system allows high-resolution strain-level discrimination across all *Armillaria* sections. Together, these modules form an end-to-end integrative diagnostic framework that enables accurate, hierarchical, and reproducible identification from the genome to the strain level in genus *Armillaria*.

CHAPTER 6

DIVERGENCE TIME AND ANCESTRAL RANGE ESTIMATION

6.1 Introduction

This chapter aims to establish a temporal and spatial framework for the evolution of *Armillaria* by integrating divergence time estimation with ancestral area reconstruction. Although previous studies have proposed general timelines and geographic origins for the genus, uncertainties remain due to limited genomic sampling and inconsistent phylogenetic placements. Building on the nuclear and mitochondrial phylogenies inferred in the preceding chapters, we use fossil-calibrated molecular clocks and model-based biogeographic analyses to clarify when major lineages originated, how they diversified, and what historical processes shaped their intercontinental distributions.

6.1.1 Nuclear and Mitochondrial Divergence Time Estimation of the Genus *Armillaria*

We estimated divergence times using MCMCTree from the PAML package v4.10.7 (Yang, 2007). Initial substitution rate estimation was performed separately for 629 single-copy concatenated nuclear protein sequences and homologous block matrices from 49 mitochondrial genomes using ORPA (Bi et al., 2024) using *codeml* and *baseml*, respectively. Substitution rate is per time unit (mitochondrial: 0.070266 ± 0.002955; nuclear: 0.169983 substitutions/site/unit time) was used to set the rgene_gamma prior (mitochondrial: 1 5.88; nuclear: 1 8.33) for subsequent analyses. The approximate-likelihood method in MCMCTree was implemented following a two-step procedure. First, with usedata = 3, mcmctree will prepare three temporary files for each locus and then invoke *baseml* (nucleotide sequences) or *codeml* (amino acid sequences) to calculate the MLEs of branch lengths and the Hessian matrix on the unrooted trees without the clock. The output file out.BV from usedata = 3 then were renamed to in.BV. With usedata = 2, mcmctree will read the MLEs and Hessian matrix

from in.BV and apply the approximate method for calculating the likelihood in the MCMC on the RAxML rooted tree with with fossil calibrations. Fossil calibrations were applied at the root node, constraining the Armillarioid lineage (the ancestral node of *Guyanagaster* and *Armillaria*) to 29 Ma (He et al., 2024). The MCMC analysis included a burn-in of 400,000 generations followed by sampling every 10 generations until 500,000 samples were collected. Two independent runs with different random seeds were performed to ensure reproducibility. Convergence was assessed using Tracer v1.7.1, with all parameters showing effective sample sizes (ESS) > 200, indicating sufficient sampling. Geological time periods on the length axis refer to the International Chronostratigraphic Chart (2024/12 edition).

6.1.2 Ancestral Range Reconstruction Using Biparental Nuclear and Maternal Mitochondrial Genomes

To reconstruct the ancestral distribution ranges of *Armillaria* and its lineages, we performed biogeographic analyses using RASP (Yu et al., 2015) on both nuclear and maternal mitochondrial genomes. The concatenated alignment of 629 single-copy orthologous proteins and homologous block matrices from 49 mitochondrial genomes was used to infer the consensus and posterior tree sets using the parallel version of MrBayes v3.2.7a (Ronquist et al., 2012) on a Linux system. Based on the latest global floristic regionalization framework (Liu et al., 2023), we delineated eleven biogeographic regions: African (A), Australian (B), Neotropical (C), Novozealandic (D), Indo-Malaysian (H), Chile-Patagonian (I), and Saharo-Arabian (J), along with three subregions of the Holarctic: Holarctic-Asia (E), Holarctic-Europe (F), and Holarctic-North America (G). Refered to Koch et al., (2017), to estimate the ancestral range of the armillarioid clade and lineages within, we used Dispersal-Extinction-Cladogenesis (DEC) analysis in the package Lagrange and implemented in the program RASP. Each taxon in our data set was assigned to areas based on its current known range. In the scenario we tested, movement between any area at any time was unconstrained. Under this model, all areas are treated as equally probable ancestral ranges. This model was tested under three area constraints.

6.2 Results

6.2.1 Nuclear and Mitochondrial Divergence Time Estimation of the Genus *Armillaria*

The divergence time to the most recent common ancestor (tMRCA) of the armillarioid clade was estimated at 29 million years ago by He et al. (2024), based on an analysis of 1,764 single-copy orthologous genes from 487 species representing 127 families, 47 orders, 14 classes, and four subphyla across Basidiomycota. Molecular dating analyses based on the nuclear and mitochondrial genomes (Figure 6.1 and Figure 6.2) indicate that the tMRCA of subgenus *Desarmillaria* represents the earliest diverging lineage within the genus *Armillaria*, followed by the diversification of ring-bearing species in subgenus *Armillaria*. The tMRCA of subgenus *Armillaria* was 21.6 million years based on the nuclear genome and 13.1 million years based on the mitochondrial genome, both occurring in the Miocene. For subgenus *Armillaria*, the divergence time was estimated at 27.7 million years based on the nuclear genome and 24.4 million years based on the mitochondrial genome, both in the Oligocene. Meanwhile, substantial discrepancies were observed in the divergence times of the four sections within *Armillaria* between the nuclear and mitochondrial genomes. In sect. *Korhoneniorum*, the nuclear-based divergence time was 14.9 million years (Miocene), whereas the mitochondrial estimate was 3.3 million years (Pliocene). In sect. *Gallicae*, divergence times were 19.9 million years (nuclear) and 22.3 million years (mitochondrial), both in the Miocene. For sect. *Ostoyarum*, the estimates were 21.2 million years (nuclear) and 18.5 million years (mitochondrial), also in the Miocene. In sect. *Armillaria*, divergence times were 18.9 million years (nuclear) and 17.8 million years (mitochondrial), again both in the Miocene.

At the species level, divergence time estimates based on both nuclear and mitochondrial genomes indicate that most species diverged during the Miocene, while a few species completed their divergence during the Pliocene and Pleistocene.

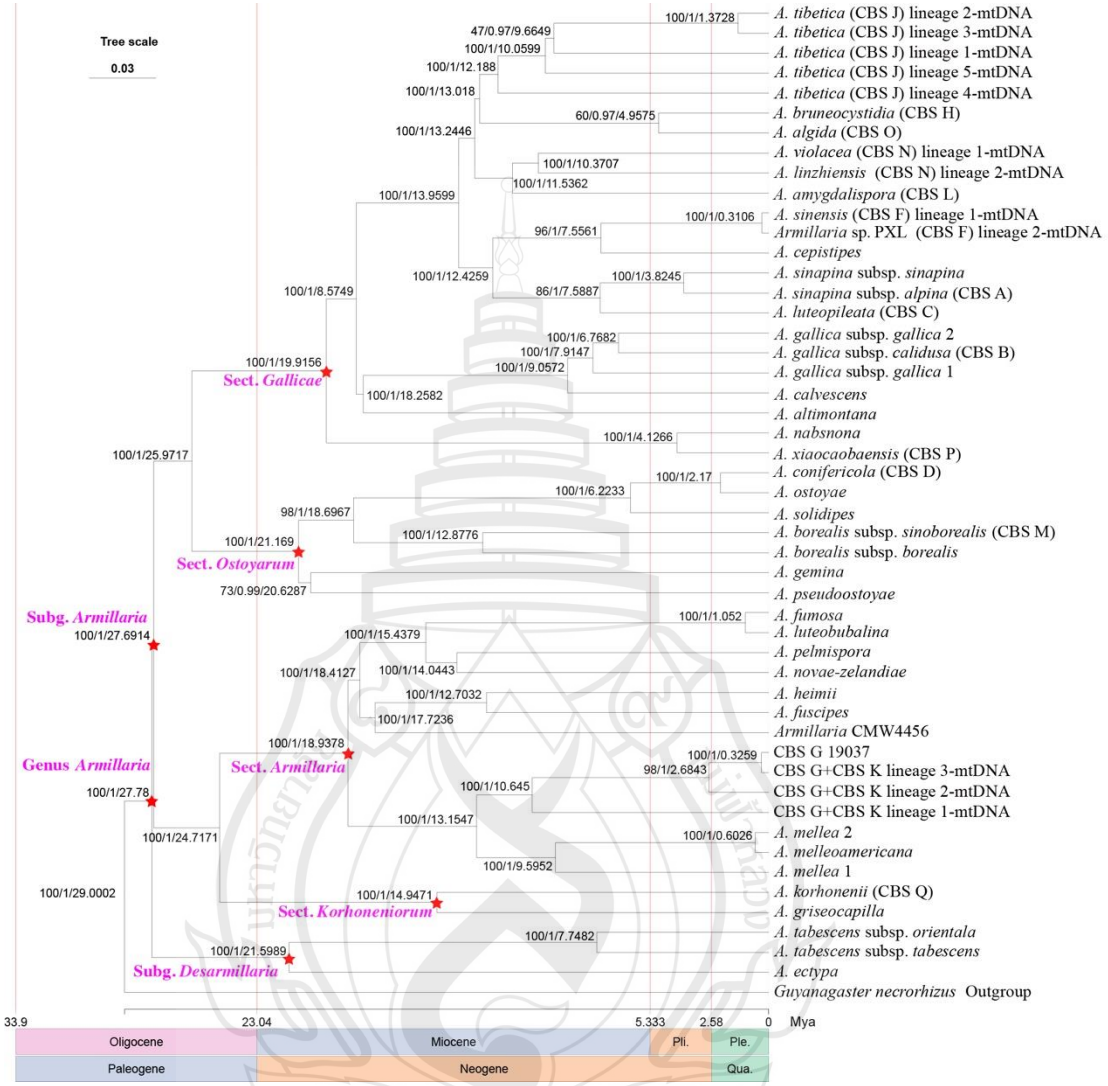


Figure 6.1 Time-calibrated phylogeny inferred from Maximum Likelihood (ML) analysis of 629 single-copy concatenated nuclear protein sequences and one *Guyanagaster* species

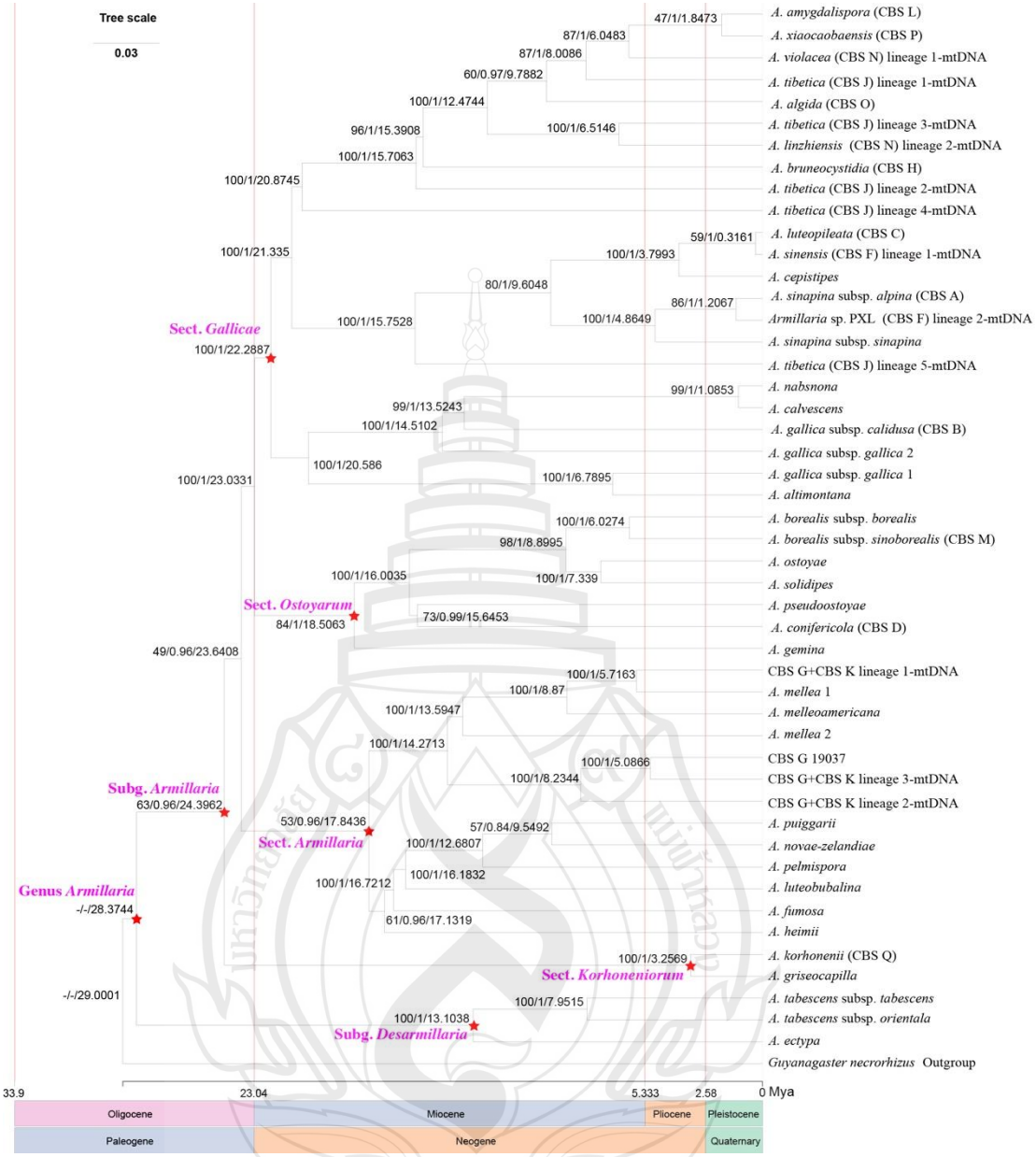


Figure 6.2 Time-calibrated phylogeny inferred from Maximum Likelihood (ML) analysis of mitochondrial homologous gene blocks across 48 *Armillaria* species and one *Guyanagaster* species

6.2.2 Ancestral Range Reconstruction Using Biparental Nuclear and Maternal Mitochondrial Genomes

Ancestral area reconstruction based on the S-DEC model suggests that the Holarctic-Asia is the most probable ancestral range for the genus *Armillaria* (Figures 6.3 and 6.4), followed by subsequent dispersal into other regions. Results from S-DEC analyses

based on both nuclear and mitochondrial genomes also indicate that *Armillaria* has undergone a complex biogeographic history, involving at least 28 dispersal and 15 vicariance events in the nuclear dataset, and 31 dispersal and 15 vicariance events in the mitochondrial dataset. Both analyses support Holarctic Asia as the most likely ancestral area of *Armillaria*. The high species diversity in Asia, with 20 currently recognized phylogenetic species, further supports the view that this region represents the primary center of diversification for the genus.

Overall, both mitochondrial and nuclear genome-based S-DEC analyses consistently indicate that the annulate and exannulate lineages of the genus *Armillaria* originated in Holarctic-Asia. Subsequently, the exannulate lineages primarily dispersed across the Northern Hemisphere, including Holarctic-Asia, Holarctic-Europe, and Holarctic-North America, and underwent multiple diversification events. In contrast, the annulate lineages exhibited a broader geographic dispersal pattern, spreading to multiple regions worldwide and experiencing independent diversification both in their region of origin and in newly colonized areas.

Based on the S-DEC analysis of nuclear genome data, the common ancestor of the genus *Armillaria* is inferred to have originated in Holarctic-Asia (region E) around 27.78 Ma (NODE98). This ancestral lineage subsequently underwent successive dispersal events, expanding first into Holarctic-Europe (region F) and then into Holarctic-North America (region G), eventually forming a lineage broadly distributed across regions E, F, and G. NODE98 marks the point at which the ancestral lineage, following its expansion into Holarctic-Europe and Holarctic-North America, experienced its first geographically structured divergence: one descendant lineage remained in Holarctic-Asia (E), while the other became widely distributed across the entire Holarctic region (regions E, F, and G). This ancestral lineage later gave rise to two major evolutionary clades, corresponding to the exannulate lineage (NODE97) and the annulate lineage (NODE95).

For the exannulate clade, corresponding to subgenus *Desarmillaria*, the common ancestor is inferred to have been broadly distributed across the Holarctic region (regions E, F, and G) around 21.6 Ma (NODE97). At this node, one lineage underwent range contraction and became restricted to Holarctic-Europe (region F), while the other retained its widespread distribution across the Holarctic region (EFG →EFG^F→F|EFG). The lineage restricted to region F evolved into the extant species *Armillaria ectypa*, whereas the

lineage maintaining a broad distribution underwent further divergence around 7.75 Ma due to geographic isolation, giving rise to two geographically distinct lineages distributed in Holarctic-Europe and Holarctic-North America (regions F and G), and in Holarctic-Asia (region E), respectively, corresponding to the modern species *A. tabescens*.

Compared to the relatively simple dispersal and divergence history of the exannulate subgenus *Desarmillaria*, species in the annulate subgenus *Armillaria* have undergone a more complex and dynamic evolutionary process, with section *Armillaria* being particularly notable. In contrast, sections *Korhoneniorum*, *Gallicae*, and *Ostoyarum* exhibit distributions primarily confined to the Northern Hemisphere, reflecting relatively stable geographic patterns.

The common ancestor of subgenus *Armillaria* is inferred to have originated in Holarctic-Asia (region E) around 27.69 Ma (NODE95). No geographic dispersal or vicariance events occurred at this node, and lineage divergence remained entirely restricted to the Asian region. Subsequently, one lineage of this subgenus continued evolving within Holarctic-Asia (E), leading to the formation of the common ancestor of sections *Armillaria* and *Korhoneniorum* around 24.71 Ma (NODE94). Meanwhile, another lineage, also originating from Holarctic-Asia (E), underwent two consecutive dispersal events toward Holarctic-North America (region G) around 25.97 Ma (NODE79), following the pathway E → E^E^G → EG^E^G → EG|EG. This lineage ultimately established a broad distribution across Holarctic-Asia and Holarctic-North America (regions E and G), and underwent divergence at NODE79, giving rise to the common ancestor of sections *Gallicae* and *Ostoyarum*.

Subsequently, one lineage from the common ancestor of sections *Armillaria* and *Korhoneniorum* underwent further divergence within Holarctic-Asia (region E) (E → E^E → E|E), and around 14.94 Ma (NODE93) gave rise to two representative species of section *Korhoneniorum*. Over more than ten million years of evolution, this lineage remained restricted to Holarctic-Asia (E), without experiencing significant geographic dispersal or vicariance events, thereby exhibiting a high degree of geographic conservatism and ecological stability. Nevertheless, the present-day distribution of these two species shows a north–south divergence pattern demarcated by the Ailao Mountains–Red River region, suggesting that this area may have acted as an important ecological barrier driving in situ lineage differentiation, even in the absence of pronounced geological events.

In contrast, another lineage (NODE92, approximately 18.93 Ma) underwent two consecutive dispersal events (E → E^E → AEF^E → AEF|E), expanding southwestward from Holarctic-Asia (E) into Africa (region A) and subsequently into Holarctic-Europe (region F). This resulted in the establishment of a lineage broadly distributed across Africa, Holarctic-Europe, and Holarctic-Asia (regions A, F, and E), which then underwent geographic divergence at this node, with one descendant lineage remaining in Asia, and the other broadly distributed across all three regions.

Subsequently, this AEF-distributed lineage experienced a vicariance event at NODE91 (13.15 Ma) (AEF → F | AE), giving rise to two geographically structured clades: one restricted to Holarctic-Europe (F), and the other retained in Africa and Holarctic-Asia (regions A and E). The lineage that had remained in Holarctic-Asia (E) following earlier divergence later underwent a large-scale expansion (E → ABCE), extending its distribution into Africa (A), Australia (region B), and the Neotropical region (C), thus forming an ancestral lineage with a broad range covering regions A, B, C, and E. Based on this distribution, a subsequent vicariance event (ABCE → A | BCE) led to the formation of two geographically distinct clades: one restricted to Africa (A), and the other distributed across Asia, Oceania, and South America (regions B, C, and E), as inferred at NODE85 (18.41 Ma).

Following this, the lineage distributed in Holarctic-Europe (F) at NODE91 underwent further westward expansion into Holarctic-North America (region G), following the trajectory F → F^F → FG^F → F | FG. This resulted in the formation of two geographically defined clades at NODE90 (9.59 Ma): one remained confined to Europe, while the other became broadly distributed across Europe and North America (regions F and G). Simultaneously, the lineage distributed in Africa and Holarctic-Asia (regions A and E) experienced a clear geographic split (AE → A | E), resulting in two regionally restricted clades: one confined to Africa (A) and the other to Asia (E).

In addition, the lineage that remained in Holarctic-Asia (region E) following NODE92 underwent a large-scale geographic expansion in subsequent evolutionary stages (E → ABCE), successfully extending its range into Africa (region A), Australia (region B), and the Neotropical region (C), thereby forming an ancestral lineage broadly distributed across both the tropical Old and New Worlds. This widespread lineage subsequently experienced a geographic vicariance event (ABCE → A | BCE), resulting in the divergence

of two clades: one restricted to Africa (A), and the other distributed across Asia, Oceania, and South America (regions B, C, and E).

The lineage originating and remaining in Africa (A) later gave rise to Armillaria CMW4456 and underwent further geographic expansion (A → A^A → AH^A → A | AH). This clade first expanded into the Indo-Malaysian region (H), forming an ancestral lineage broadly distributed across Africa and the Indo-Malaysian region. Subsequently, a vicariance event within the Africa–Indo-Malaysian range (AH) led to the formation of two geographically distinct clades: one restricted to Africa (A) and the other distributed across both Africa and Indo-Malaysian regions (AH).

Meanwhile, the clade distributed across Australia, the Neotropical region, and Holarctic-Asia (BCE) also experienced multiple episodes of regional divergence. First, after expanding into Australia, the lineage underwent a vicariance event (BCE → BCE^B → BCE | B), leading to the formation of one lineage still broadly distributed across BCE and another restricted to Australia (B). Second, the lineage confined to region B further expanded into the Neotropical region (C) (B → B^B → BC^B → B | BC), ultimately resulting in two geographically distinct clades. Third, another BCE-distributed lineage experienced an even broader expansion into the Novozealandic region (D) (BCE → BCDE), followed by a vicariance event (BCDE → BCD | E), which led to the formation of two separate clades distributed in regions BCD and E, respectively.

This series of geographic dispersal and vicariance events has driven repeated parallel diversification of *Armillaria* lineages in tropical and Southern Hemisphere regions, revealing a strong trend toward regionalized phylogenetic structuring.

Compared to other lineages, species within sections *Gallicae* and *Ostoyarum* have experienced frequent dispersal and vicariance events across various regions of the Northern Hemisphere, resulting in complex distribution patterns and phylogenetic structures. In the shallower nodes of their phylogenetic tree (e.g., NODE51–NODE59), lineages consistently underwent diversification within Holarctic-Asia (region E), following event paths such as E → E^E → E|E, without substantial geographic changes. This pattern reflects a high degree of geographic conservatism.

However, in some nodes (e.g., NODE60–NODE79), the evolutionary history of these lineages began to involve multiple inter-regional dispersal and isolation events. For instance, NODE61 indicates a further expansion from Holarctic-Asia and Holarctic-North

America (EG) into Holarctic-Europe (F), followed by geographic isolation (EG → EFG → FG | E). Both NODE66 and NODE73 document vicariance events between Holarctic-Europe (F) and Holarctic-Asia (E) (EF → E | F or F | E), suggesting repeated episodes of geographic fragmentation and lineage divergence between western and eastern Eurasia. NODE74 shows evidence of a secondary expansion toward Holarctic-North America (G) (EF → EF^F → EFG^F → FG | EF), reflecting the multiple episodes of geographic expansion into region G by this clade.

Furthermore, multiple nodes reveal lineage differentiation within a wide geographic range (e.g., EG → EG^G → EFG^G → G | EFG, NODE69), indicating that certain species diverged not through regional isolation but through partitioned evolution following extensive dispersal. Overall, the phylogenetic diversification of sections *Gallicae* and *Ostoyarum* has been jointly driven by inter-regional dispersal and local vicariance across the Holarctic regions, highlighting the complex biogeographic history of temperate areas in the Northern Hemisphere.

The S-DEC analysis based on mitochondrial genome data suggests that the most recent common ancestor of *Armillaria* originated in Holarctic-Asia (region E) around 28.37 Ma (NODE96). This lineage subsequently expanded to Holarctic-Europe (region F) and Holarctic-North America (region G), ultimately forming an ancestral lineage broadly distributed across regions E, F, and G. NODE96 represents the first spatially structured divergence following dispersal across the Holarctic region, with one lineage remaining confined to Holarctic-Asia (E), while the other maintained a widespread presence across all three regions (EFG). This ancestral lineage further split into two major evolutionary branches: the exannulate lineage (NODE95) and the annulate lineage (NODE93). This result is consistent with inferences based on nuclear genome data, indicating a high level of congruence between the two datasets in reconstructing the early geographic origin and lineage diversification of *Armillaria*.

For the exannulate subgenus *Desarmillaria*, its most recent common ancestor around 13.10 Ma (NODE95) was widely distributed across the Holarctic region (EFG). At this node, one lineage contracted and became restricted to Holarctic-Europe (region F), while the other retained its broad distribution across regions E, F, and G (EFG → EFG^F → F | EFG). The lineage confined to region F gave rise to the extant species *Armillaria ectypa*. In contrast, the widespread lineage underwent further divergence around 7.95 Ma

due to geographic isolation, resulting in two geographically structured lineages distributed in Holarctic-Europe and Holarctic-North America (regions F and G), and in Holarctic-Asia (region E), corresponding to modern *A. tabescens*.

Species within the annulate subgenus *Armillaria* underwent a more complex and dynamic evolutionary process, most notably in section *Armillaria*. In contrast, sections *Korhoneniorum*, *Gallicae*, and *Ostoyarum* remained largely confined to the Northern Hemisphere, displaying relatively stable distribution patterns. The common ancestor of subgenus *Armillaria* is inferred to have originated in Holarctic-Asia (region E) around 24.39 Ma (NODE93), where no dispersal or vicariance events occurred, and lineage diversification remained restricted to Asia. One lineage continued evolving within Holarctic-Asia (E), and around 3.25 Ma (NODE92) gave rise to the common ancestor of section *Korhoneniorum*. Meanwhile, another lineage originating from Holarctic-Asia (E) underwent two consecutive dispersal events toward Holarctic-Europe and Holarctic-North America (regions F and G) around 23.64 Ma (NODE91), forming the common ancestor of sections *Armillaria*, *Gallicae*, and *Ostoyarum*.

The Holarctic-Asia (E) lineage diverging at NODE91 underwent a sequence of dispersal events (E → E^E → EFG^E → E | EFG), eventually giving rise to the common ancestor of section *Armillaria* around 17.84 Ma (NODE90). The two daughter lineages from this node followed distinct evolutionary trajectories: one remained restricted to Asia (E), while the other became widespread across the Holarctic region (EFG).

The lineage retained in region E later expanded and experienced a vicariance event at NODE89 (ca. 17.13 Ma) (E → ABE → A | BE), giving rise to *A. heimii* in Africa (A). The lineage distributed across BE subsequently expanded (BE → BE^B → BCE^B → B | BCE), forming *A. fumosa* in Australia (region B, NODE88, ca. 16.72 Ma). This BCE lineage underwent further divergence (BCE → BCE^B^C → BC | BCE), resulting in *A. luteobubalina* in regions B and C (NODE87, ca. 16.18 Ma). The lineage retained in BCE split at NODE86 (ca. 12.68 Ma) into lineages in regions BC and E, with *A. pelmispora* arising in Asia and the BC lineage continuing to expand (BC → BC^C → BCD^C → C | BCD), eventually giving rise to *A. puiggarii* in the Neotropical region (C) and the widespread species *A. novae-zelandiae* in regions B, C, and D (NODE85, ca. 9.54 Ma).

Simultaneously, the other lineage derived from NODE90 and distributed across regions E, F, and G, experienced complex geographic expansion and isolation. A vicariance

event occurred at NODE83 (ca. 8.23 Ma) (EFG → AEFG → E | AFG), giving rise to the common ancestor of CBS G and CBS K in Asia (E). The AFG-distributed lineage subsequently expanded into Holarctic-Europe (F), where it gave rise to *A. mellea* 2 at NODE81 (ca. 13.59 Ma) (AFG → AFG^F → F | AFG). This lineage later expanded into Holarctic-North America (G), forming *A. melleoamericana* at NODE80 (ca. 8.87 Ma) (AFG → G | AF). The residual lineage in the Africa–Europe region (AF) eventually underwent isolation at NODE79 (ca. 5.71 Ma) (AF → A | F), resulting in CBS G + CBS K lineage 1-mtDNA in Africa and *A. mellea* 1 in Europe.

Within the Holarctic region (EFG), the lineages of sections *Gallicae* and *Ostoyarum* exhibit highly dynamic patterns of geographic dispersal and isolation, leading to complex regional migration routes and phylogenetic restructuring. Multiple nodes (NODE50–NODE58) show strong geographic conservatism, with lineages remaining confined to Holarctic-Asia (region E) and undergoing divergence without substantial geographic expansion (E → E^E → E | E). Starting from NODE60, frequent dispersal events occurred among regions E, F, and G (e.g., E → E^E → EF^E → EF | E; EF → EF^E → EFG^E → EF | EG; EFG → EFG^F^G → FG | EFG; EFG → EFG^E^F → EFG | EF), contributing to range expansion and overlapping distributions. These were followed by a series of geographic isolation events (e.g., EG → G | E; EF → F | E; EFG → E | FG; FG → G | F), driving independent lineage evolution within each region and leading to clades restricted to regions F or G, as well as others broadly distributed across EF, EG, or FG. These patterns highlight a complex and fine-scale model of phylogenetic diversification within the Holarctic region.

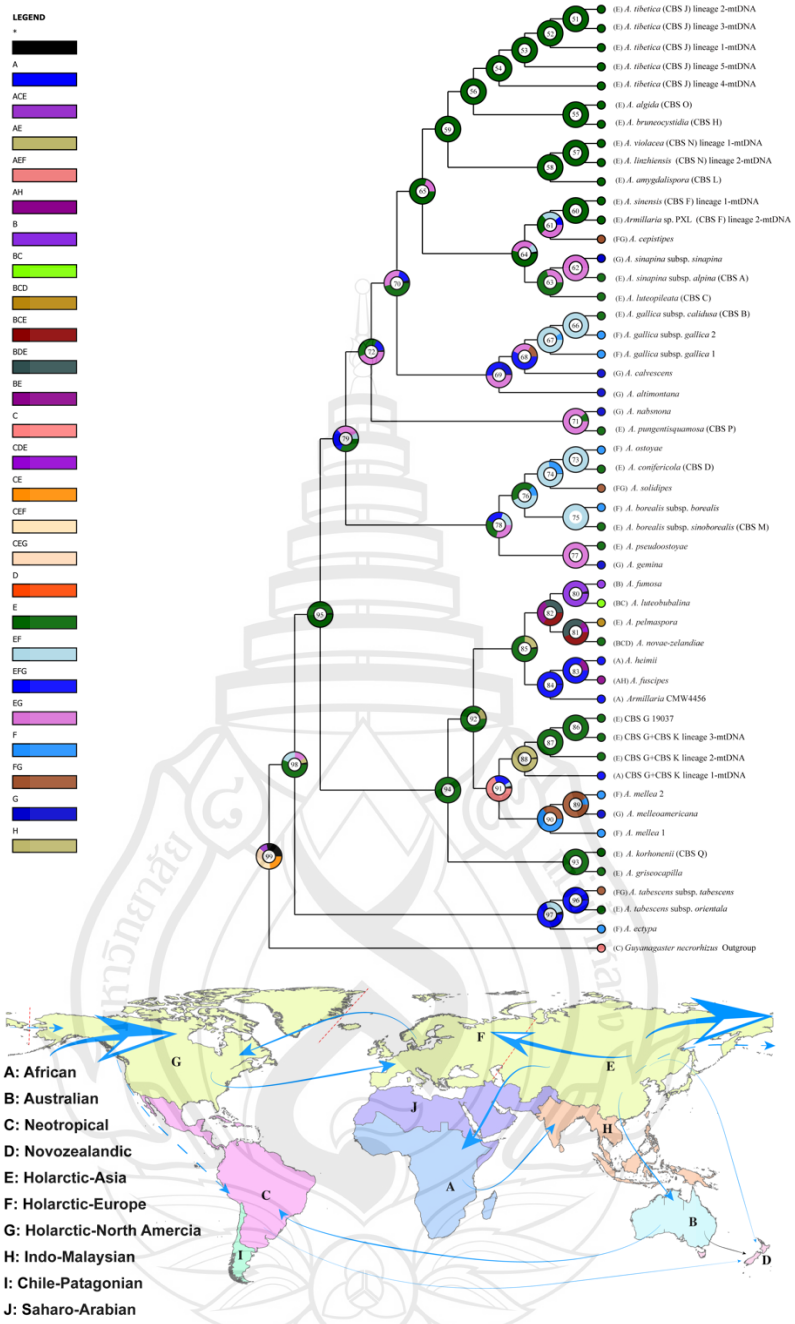


Figure 6.3 Ancestral area reconstruction and divergence time estimation of *Armillaria* using 629 concatenated nuclear single-copy orthologous genes

Figure 6.3 a. The pie chart in each node indicates the possible ancestral distributions inferred from dispersal-extinction-cladogenesis (DEC) analysis. b. Possible dispersal routes of *Armillaria*. Geographic origins of specimens are indicated by colored boxes to the left of taxon names, following the floristic realms of Liu et al.

(2023): red = African, blue = Australian, brown = Novozealandic, lime green = Indo-Malesian, purple = Neotropical, turquoise = Chile-Patagonian, gray = Holarctic, orange = Saharo-Arabian. Geologic epochs are labeled above the time scale. Node numbers correspond to lineages detailed in Table 6.2, and gray-blue bars represent 95% highest posterior density (HPD) intervals (values provided in Table 6.2).

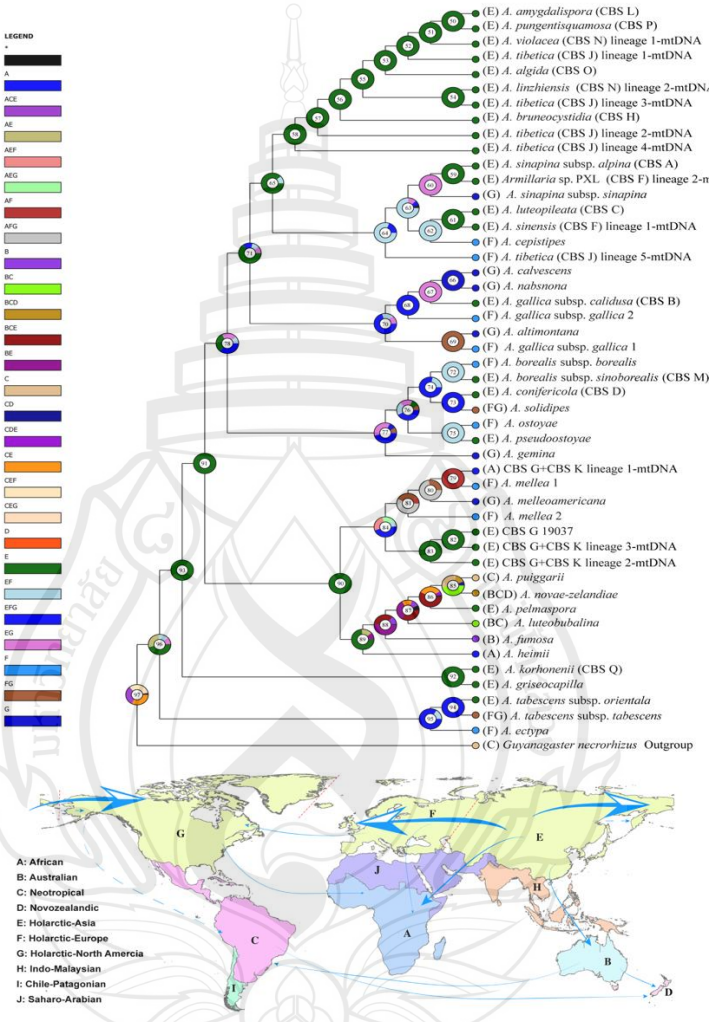


Figure 6.4 Ancestral area reconstruction and divergence time estimation of *Armillaria* based on the mitochondrial home blocks dataset

Figure 6.4 Ancestral area reconstruction and divergence time estimation of *Armillaria* based on the mitochondrial home blocks dataset. a. The pie chart in each node indicates the possible ancestral distributions inferred from dispersal-extinction-cladogenesis (DEC) analysis. b. Possible dispersal routes of *Armillaria*. Geographic

origins of specimens are indicated by colored boxes to the left of taxon names, following the floristic realms of Liu et al. (2023): red = African, blue = Australian, brown = Novozealandic, lime green = Indo-Malesian, purple = Neotropical, turquoise = Chile-Patagonian, gray = Holarctic, orange = Saharo-Arabian. Geologic epochs are labeled above the time scale. Node numbers correspond to lineages detailed in Table 6.1, and gray-blue bars represent 95% highest posterior density (HPD) intervals (values provided in Table 6.1). The lower-left inset map illustrates the proposed historical dispersal pattern.

6.3 Discussion

According to Qin et al. (2025), the genus *Armillaria* can be classified into two subgenera: the annulate subgenus *Armillaria* and the exannulate subgenus *Desarmillaria*. Consistent with the findings of Koch et al. (2017) and Qin et al. (2025), subgenus *Desarmillaria* occupies the basal position in the phylogenetic tree of the genus, suggesting that it may represent an evolutionarily ancestral lineage. Divergence-time analyses indicate that the most recent common ancestor (MRCA) of *Armillaria* originated in the Oligocene, with estimated ages of 27.78 Ma based on nuclear genome data and 24.40 Ma based on mitochondrial genome data. These estimates are slightly younger than those proposed by Koch et al. (2017) and Qin et al. (2025), who inferred an Eocene origin (24.47–59.07 Ma), likely due to differences in fossil calibration schemes.

Within subgenus *Armillaria*, the divergence times and order of section-level splits inferred from nuclear and mitochondrial genomes differ markedly. Nuclear genome data suggest that Sect. *Korhoneniorum* and Sect. *Armillaria* represents the earliest divergent lineages (MRCA at 24.71 Ma), followed by the Northern Hemisphere-distributed Sect. *Ostoyarum* (MRCA at 25.97 Ma) and Sect. *Gallicae* (MRCA at 19.91 Ma). In contrast, mitochondrial genome analysis indicates Sect. *Korhoneniorum* diverged first (MRCA at 24.39 Ma), followed sequentially by Sect. *Armillaria* (MRCA at 23.64 Ma), Sect. *Ostoyarum* (MRCA at 23.03 Ma), and Sect. *Gallicae* (MRCA at 22.28 Ma).

Koch et al. (2017) proposed that diversification of *Armillaria* (corresponding to subgenus *Armillaria* in our study) began on the Eurasian continent approximately 33–41.8 Ma (late Eocene to early Oligocene), during a period of global climatic transition from warm, ice-free conditions to glacial climates. The MRCA of *Armillaria* likely inhabited tropical environments that were later replaced by pronounced cooling, increased seasonality, and a significant reduction in tropical rainforest extent, while deciduous vegetation began to expand. Our divergence time estimates suggest that the diversification of subgenus *Armillaria* occurred primarily in the Oligocene, slightly after this major climatic turning point. We hypothesize that this lineage, characterized by annulate fruiting bodies, adapted to temperate seasonal climates, and co-expanded with woody hosts into cooler and drier environments, continuing to diversify and radiate throughout the Oligocene and subsequent epochs. Our results indicate that most extant species of *Armillaria* diverged during the Miocene, with only a few lineages undergoing further speciation in the Pliocene and Pleistocene.

The expansion of *Armillaria* into Africa (region A) likely occurred during two key periods. Nuclear genome analyses reveal two independent migration events: one at approximately 18.41 Ma (NODE85: E → ABCE → A | BCE), and another around 10.64 Ma (NODE88: EFG → AEFG → E | AFG), both representing southward dispersals of Eurasian or broadly Holarctic lineages into Africa. Mitochondrial genome-based divergence estimates support similar scenarios: one migration occurred around 17.13 Ma (NODE89: E → ABE → A | BE), in which a lineage originally distributed in Eurasia (E) expanded into Africa (A), followed by vicariance; another event around 14.27 Ma (NODE84: EFG → AEFG → E | AFG) reflects dispersal from the Holarctic (EFG) into Africa, followed by geographic isolation. These results suggest that African Armillaria diversity did not arise from a single colonization event but rather from multiple independent inputs from Eurasian lineages.

Koch et al. (2017) suggested that Africa and Eurasia were separated by a shallow marine barrier during the Paleogene to early Miocene, which acted as a major constraint on biotic exchange until it receded in the early Miocene (~19–12 Ma), allowing direct faunal and floral connections. Their molecular clock analyses further inferred that the diversification of extant African *Armillaria* species began around 15 Ma, which broadly corresponds to the Miocene migration events identified in our study.

Notably, the phylogenetic analyses of Koch et al. (2017) resolved African *Armillaria* species as a monophyletic group and proposed that they represent the earliest divergent clade within *Armillaria* sensu stricto. However, our divergence time reconstructions based on both nuclear and mitochondrial genomes do not support this conclusion. In both nuclear and mitochondrial datasets, the East Asian species *A. korhonenii* (Liu et al. 2024) occupies the earliest-diverging position within subgenus *Armillaria*, suggesting that Holarctic-Asia, rather than Africa, is more likely to represent the center of origin for this group. The African lineage likely arrived during the middle Miocene via dispersal from Holarctic-Asia, followed by rapid diversification under geographic isolation and local environmental selection.

Previous studies have proposed that the earliest divergence of *Armillaria* in temperate regions of the Southern Hemisphere (e.g., Australia, New Zealand, South America) occurred around 19 Ma (Koch et al., 2017). They hypothesized that this lineage may have dispersed alongside its host plants from Eurasia to Australasia during the early Miocene. During this period, the collision of the Southeast Asian continental shelf with the New Guinea–Australian margin (~25 Ma onward) caused ecosystem instability and created numerous ecological vacancies, greatly increasing the colonization success of exotic plants and their associated fungal pathogens, including *Armillaria* (Crisp et al., 2011). Our findings refine and support this dispersal model. Ancestral area reconstruction based on nuclear genome data indicates that around 18.41 Ma (NODE85), a lineage originating in Eurasia (E) dispersed into the ABCE region and, through subsequent vicariance, gave rise to separate African (A) and BCE (including the Southern Hemisphere) lineages. Mitochondrial genome analysis similarly suggests a migration event from E to ABE around 17.13 Ma (NODE89), followed by further lineage expansion (NODE88: BE → BE^B → BCE^B → B | BCE) that resulted in the formation of the Australian (B) clade. This was followed by sequential expansions and isolations across the Southern Hemisphere (e.g., BCE → BCE^B^C → BC | BCE; BCE → E | BC; BC → BC^C → BCD^C → C | BCD), eventually establishing *Armillaria* lineages in South America (region C) and New Zealand (region D).

In summary, our divergence time estimates are slightly younger than those proposed by Koch et al. (2017), but they more clearly elucidate the stepwise southward

expansion of *Armillaria* from Eurasia into the Southern Hemisphere. These results support a model of intercontinental dispersal via host association, with colonization and subsequent radiation facilitated by ecological opportunities following Miocene climate perturbations and biogeographic rearrangements.

Our ancestral-area reconstructions further suggest that many *Armillaria* species and subspecies were historically widely distributed across the Holarctic regions (E, F, and G) or confined to combinations thereof. Divergence time analyses based on both nuclear and mitochondrial genomes indicate that these dispersal and differentiation events predominantly occurred during the Miocene and later. This period was characterized by substantial global geological and climatic changes, including the formation of land bridges, alternating glacial and interglacial cycles, and the expansion of temperate climatic zones. Such environmental dynamics likely provided new ecological opportunities for cross-regional movement and adaptation, promoting frequent dispersal and phylogenetic diversification of *Armillaria* across the Northern Hemisphere.

Finally, our study reveals that only sect. *Gallicae* currently exhibits strong symbiotic affinity with cultivated *Gastrodia elata*. This section is inferred to have originated around 19.91 Ma in the nuclear genome analysis and around 22.28 Ma in the mitochondrial genome analysis, both during the early Miocene. In contrast, other sections of *Armillaria* exhibit stronger parasitic tendencies and are generally unsuitable for symbiosis with *G. elata*. This specificity may reflect a long-term co-adaptive relationship between Sect. *Gallicae* and certain host plant root systems, leading to the evolution of more benign, or even mutualistic interactions and greater compatibility with artificial cultivation systems of *G. elata*.

6.4 Conclusion

Divergence time analyses based on both nuclear and mitochondrial genomes indicate that the most recent common ancestor (MRCA) of *Armillaria* originated in Holarctic Asia during the Oligocene, approximately 27—24 Ma, which is slightly younger than previous estimates by Koch et al. (2017) and Qin et al. (2025). The basal placement

of *Desarmillaria* suggests that it represents an evolutionarily ancestral lineage. Within subgenus *Armillaria*, the two genomic datasets reveal discordant divergence orders among sections, reflecting distinct evolutionary trajectories between biparentally inherited nuclear and maternally inherited mitochondrial genomes. The diversification of *Armillaria* likely began during the major climatic transition from the warm Eocene to the cooler Oligocene, when temperate deciduous forests expanded across Eurasia (Zachos et al., 2001; Utescher & Mosbrugger, 2007; Pound & Salzmann, 2017). Adaptation to increasingly seasonal climates and co-expansion with woody hosts probably facilitated the early radiation of lineages characterized by annulate fruiting bodies (Koch et al., 2017; Qin et al., 2025). Our analyses further indicate that most extant *Armillaria* species diversified during the Miocene (23.04—5.33 Ma), coinciding with intensified global cooling and progressive geographic fragmentation across Eurasia (Jia et al., 2018; Shi et al., 2013; Palcu et al., 2021). These isolation events, driven by mountain uplift, aridification, and the retreat of forest corridors, likely promoted allopatric speciation within temperate forest ecosystems. Contrary to Koch et al. (2017), who proposed an African origin of genus *Armillaria*, our results support Holarctic Asia as the primary evolutionary center, with African lineages derived from mid-Miocene dispersal and subsequent in situ diversification. Following this southward expansion, additional intercontinental dispersal and regional isolation events during the late Miocene to Pliocene further shaped the present biogeographic structure of the genus. Ancestral area reconstruction also suggests a southward expansion from Eurasia to the Southern Hemisphere around 18–17 Ma, giving rise to the Australian, South American, and New Zealand clades. Finally, recurrent dispersal and vicariance across Holarctic regions from the Miocene to the Pleistocene were likely driven by intermittent land-bridge connections and glacial-interglacial climatic oscillations, collectively shaping the present-day biogeographic diversity of *Armillaria*.

CHAPTER 7

SCREENING *ARMILLARIA* SPECIES FOR OPTIMAL SYMBIOSIS WITH *GASTRODIA ELATA*

7.1 Introduction

This chapter focuses on identifying *Armillaria* species suitable for the cultivation of *Gastrodia elata* by integrating current knowledge of its tripartite symbiotic system—*Mycena*-dominated seed germination, *Armillaria*-dependent tuber development, and reserve-driven reproduction. Although numerous studies have documented the diversity of germination-promoting fungi and the variable symbiotic compatibility among *Armillaria* lineages, practical screening of cultivation strains has largely relied on slow and environmentally variable field trials. To address this limitation, we establish a sterile, laboratory-based germination and symbiosis evaluation system that enables rapid assessment of fungal compatibility. By combining updated taxonomic insights, controlled co-cultivation experiments, and large-scale strain surveys, this chapter aims to clarify which *Armillaria* species exhibit stable and effective symbiotic interactions with *G. elata* and to provide a framework for strain selection and industrial application.

7.2 Screening *Armillaria* Species for Optimal Symbiosis with *Gastrodia elata*

This chapter reviews recent advances in the two key groups of symbiotic fungi associated with each stage of the *Gastrodia elata* life cycle: first, the germination-promoting roles of *Mycena* spp. during seed germination and protocorm development; and second, the latest findings on *Armillaria* spp. in tuber nutrition supply and compatibility screening. It also introduces, for the first time, an indoor sterile germination and symbiosis evaluation system, uses co-cultivation trials to validate

several *Armillaria* strains suitable for *G. elata* cultivation, and finally offers systematic recommendations for industrial development and the selection of new fungal cultivars.

7.2.1 Life Cycle of *Gastrodia elata*

As shown in Figure 7.1, the life cycle of *Gastrodia elata* spans three years to complete its progression from seed germination to flowering and fruiting, relying entirely on mycoheterotrophic interactions throughout. In April of the first year, seeds are co-cultured with germination-promoting fungi (e.g., *Mycena* spp.) and subsequently transferred to cultivation bags containing live wood segments and *Armillaria* spp. From November of the first year to March of the second year, the developmental stages sequentially progress through: protocorm formation → differentiation of the protocorm foot → development of the primary corm → juvenile tuber → immature tuber (commonly termed “Baitouma”). In early spring of the second year, the immature tuber is transplanted to an *Armillaria*-colonized substrate, where it acquires carbon sources via fungal mycelial bridges, ultimately forming a mature tuber ("Jianma") by late October. During April to June of the third year, the Jianma consumes stored nutrients to produce a flowering scape (50–100 cm tall), followed by capsule maturation in July to August, releasing tens of thousands of dust-like seeds. This completes its unique life cycle characterized by “germination dependent on germination fungi → vegetative growth reliant on Armillaria → reproductive growth fueled by stored reserves.” (Xu, 1993; Zhou et al., 1987)

Notably, laboratory studies reveal that *G. elata* seeds can germinate on *Mycena*-free media (e.g., ½MS or oat agar), but protocorm foot development stalls without *Armillaria*-mediated carbon supply. Intriguingly, this symbiosis exhibits environmental contingency: under stressors such as flooding, *Armillaria* spp. may shift from mutualist to necrotroph, consuming the tuber entirely. This dynamic interaction—oscillating between resource exchange and antagonism—highlights the ecological plasticity of *G. elata*'s tripartite life strategy: germination dependent on germination fungi, vegetative growth fueled by *Armillaria*, and reproduction sustained by stored reserves.

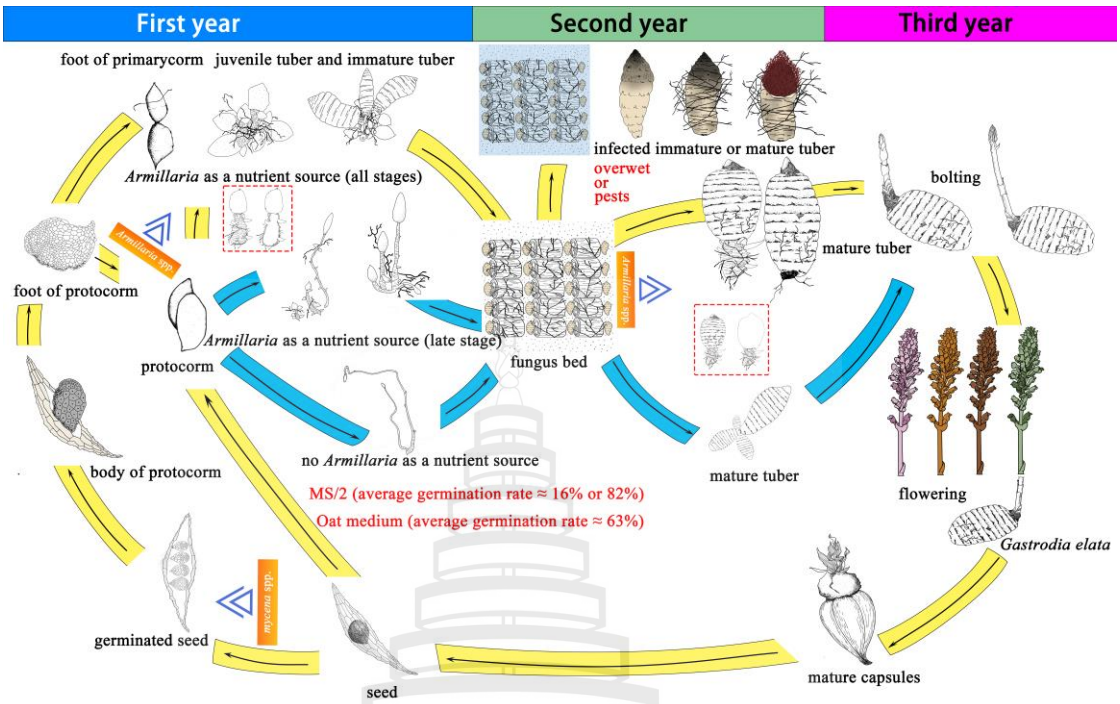


Figure 7.1 The life cycle of *Gastrodia elata*, from seed germination to reproductive maturity, spans three years in natural conditions

7.2.2 Research Progress on Fungal Species Diversity Associated with Seed Germination in *Gastrodia elata*

Since Xu and Guo (1989) first isolated and validated the germination-promoting function of *Mycena osmundicola* from protocorms of *Gastrodia elata*, researchers have progressively uncovered the diversity of germination-enhancing species within the genus *Mycena*. Fan and Guo (1996) isolated *M. orchidicola* from orchid mycorrhizae in the tropical forests of Xishuangbanna, Yunnan Province. Guo et al. (1999) identified *M. dendrobii* based on wild *Dendrobium moniliforme* from Yunnan Province. Guo et al. (1997) discovered *M. anoectochila* through symbiotic tissues of *Anoectochilus roxburghii* in Xishuangbanna, Yunnan. Tang and Tu (2020) further confirmed the germination-promoting capabilities of *M. citrinomarginata* and *M. purpureofusca* using *Mycena* strains from northeastern China. Kitahara et al. (2022) found *Mycena* cf. *abramsii* from Japan. Liu et al. (2022, 2025) systematically characterized the germination-enhancing activities of *M. subpiligera*, *M. abramsii*, *M. adnexa*, *M. filopes*, *M. galericulata*, *M. haematopus*, *M. maculata*, and *M. pura* in subtropical regions of China, expanding the number of validated species within this genus to 15.

In addition to *Mycena* species with germination-promoting activity on *Gastrodia elata*, taxa such as *Cubamyces lactineus* (Wang et al., 2006), *Epulorhiza* spp. (Fan et al., 1998), and members of the family Marasmiaceae (Kitahara et al. 2022), the genera *Atheniella*, *Favolaschia*, *Panellus*, and *Roridomyces* (Liu et al., 2025), have also been confirmed to exhibit germination-enhancing properties. Notably, these fungi commonly display bioluminescence, and whether their germination-promoting mechanisms are functionally associated with luminescent gene clusters remains a subject requiring in-depth exploration.

7.2.3 Establishment of *Gastrodia elata* Seed Germination System

To establish a sterile germination system for sustainable acquisition of *G. elata* seedlings, this study optimized a co-culture system with *Mycena purpureofusca* (Figure 7.2). The detailed protocol is as follows:

7.2.3.1 Activation of Germination Fungus

Inoculate *Mycena purpureofusca* onto PDA medium and incubate at 25°C for 1–2 weeks until stable colony morphology is achieved, forming uniform colonies with diameters of 3–5 cm.

7.2.3.2 Preparation of Fungus-Loaded Substrate

Select intact leaves of Fagaceae plants, rinse under running water to remove surface impurities, and cut into 2 × 2 cm squares. Sterilize via autoclaving (121°C, 0.12 MPa for 30 min), then transfer to a clean bench.

7.2.3.3 Mycelial Colonization Induction

Under sterile conditions, place sterilized leaves (abaxial side down) onto the fungal colony. Maintain at 25°C for 5–7 days until both leaf surfaces are fully colonized by mycelium.

7.2.3.4 Assembly of Co-Culture System

Position colonized leaves (abaxial side up) on the surface of 1.6% water-agar medium (16 g agar, 1000 mL distilled water, pH unadjusted). Uniformly distribute *Gastrodia elata* seeds around the leaf periphery (1–2 cm range) using a sterile brush.

7.2.3.5 Germination Environment Control

Seal culture dishes with parafilm and incubate in darkness at 24±1°C. Monitor protocorm formation periodically and developmental progress via microscopic observation.

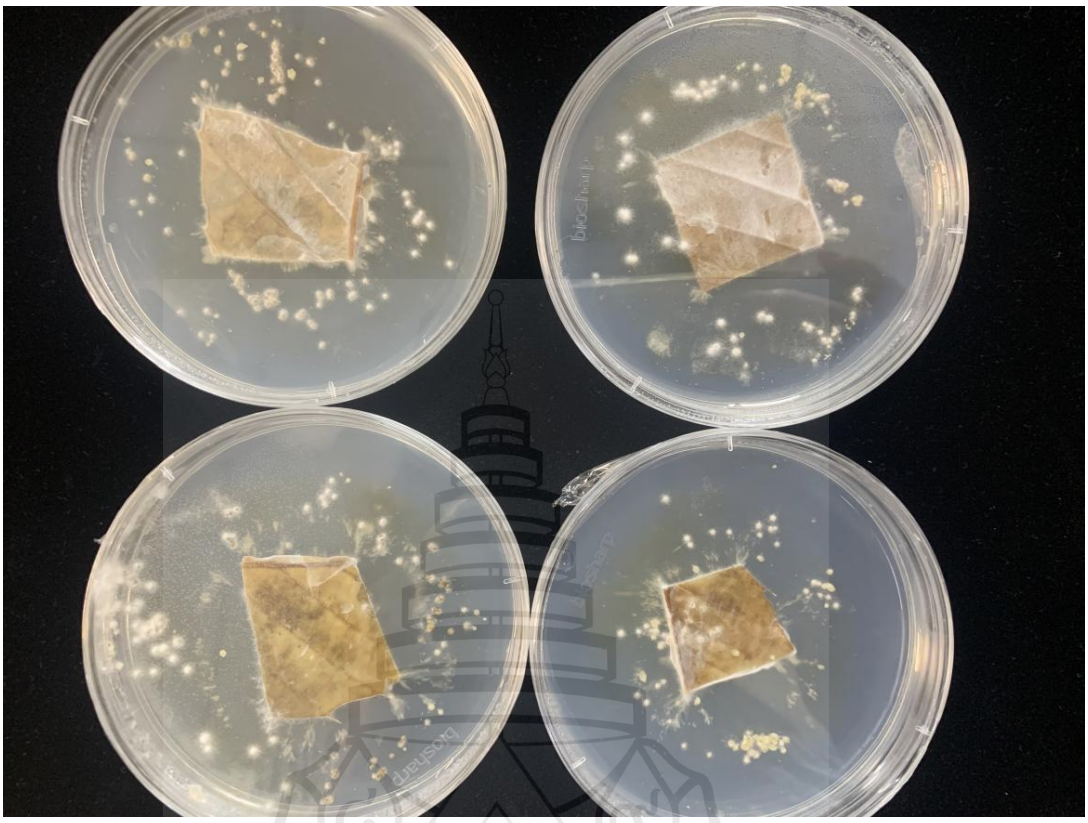


Figure 7.2 In vitro germination validation system for *Gastrodia elata* seeds co-cultured with *Mycena purpureofusca* mycelium on PDA medium

7.2.4 Research Progress on the Species Diversity of *Armillaria* Symbiotic with *Gastrodia elata*

Numerous studies have investigated the symbiotic relationship between *Gastrodia elata* and *Armillaria* species. Cha and Igarashi (1995) conducted a study in Japan, utilizing mating compatibility tests to analyze 22 *Armillaria* isolates obtained from *G. elata* tubers. Their results revealed the following species distribution: *A. gallica* dominated at 45.5%, followed by *A. singula* (22.7%), *A. fezoensis* (13.6%), and *A. sinapina* (13.6%). Notably, *A. ostoyae* was detected in only one isolate (4.5%). According to observations by Mohammed et al. (1994), *A. ostoyae* exhibits excessive aggressiveness, potentially hindering stable symbiotic associations with orchids. Therefore, except for *A. ostoyae*, the remaining species are likely capable of forming symbiotic relationships with *Gastrodia elata*.

As reported by Zhao and Zhao (2007), the CBS F strain exhibits dense rhizomorphs with moderate growth speed, which facilitates the propagation of seed-

derived rice-sized Tianma tubers; however, *Armillaria ostoyae* and *A. mellea* exhibit potent infectivity and are recognized as pathogenic fungi affecting multiple tree species. Qin et al. (1999) identified *A. tabescens* as a pathogenic fungus targeting fruit trees in North China. Guo et al. (2016) proposed that *A. cepistipes*, *A. nabsnona*, Lineage 2, Lineage 3, Lineage 6, and Lineage Nag. E might be linked to Tianma in China. However, our findings reveal that *A. nabsnona* is not distributed in China, *A. nabsnona* and Lineage Nag. E described in Guo et al. (2016) should be classified under the CBSP in our study, while Lineage 2 belongs to the CBSO, Lineage 3 belongs to the CBSL, and Lineage 6 belongs to the CBSB. Wang et al. (2020) conducted a systematic identification of 19 commercial *Armillaria* strains from 9 provinces in China. The results revealed that 16 strains (84.2%) belonged to the CBS B, while the remaining 3 strains were classified as CBS F, CBS A, and *A. mellea*, respectively; Furthermore, the study screened four wild *Armillaria* strains from the Western Region of Hubei Province with potential cultivation value: 16022 (CBS N), 16032 (CBS O), 17021 (CBS F), and 18001 (*A. mellea*); Their cultivation trials in Hubei Province demonstrated that CBS F and CBS N strains exhibited superior efficacy in *Gastrodia elata* (Tianma) symbiosis systems.

In summary, *A. gallica*, *A. sinapina*, *A. singula*, *A. fezoensis*, *A. cepistipes*, CBS B, CBS F, CBS P, CBS O, CBS L, and CBS N should exhibit symbiotic compatibility, whereas *A. ostoyae*, the *A. mellea* complex, and *A. tabescens* demonstrate strong parasitic characteristics and may not be suitable for *Gastrodia elata* cultivation.

7.2.5 Establishment of *Armillria-Gastrodia* Symbiotic Strain Evaluation System

Traditional screening of *Armillaria* spp. strains relies on field cultivation trials, which suffer from long cycles and observational challenges. Based on the previously established sterile germination system for *Gastrodia elata* (Figure 7.2), this study developed a rapid laboratory-scale evaluation protocol for strain cultivation efficiency. The optimized workflow is as follows:

7.2.5.1 Strain Propagation

Inoculate *Armillaria* spp. strains onto PDA plates and incubated at 24 °C until mycelia cover two-thirds of the plate area (1–2 weeks) to prepare primary inoculum. Select mycelial blocks (5 mm diameter) from the growing frontier and

transfer to 250 mL Erlenmeyer flasks containing 100 mL malt-yeast agar (MYA) medium. Incubate at 24°C with shaking at 120 rpm for several weeks to obtain secondary liquid inoculum.

7.2.5.2 Substrate Preparation

The culture substrate consists of Fagaceae sawdust (50%), branch segments (3–5 cm, 12.5%), and PDA medium (37.5%). After soaking sawdust and branches for 12 h and draining, mix the components proportionally and fill bottles (400 g/bottle). Apply fractional sterilization: autoclave at 121°C for 90 min, repeat twice at 24 h intervals to ensure complete sterilization.

7.2.5.3 Inoculation and Cultivation

Inoculate cooled substrate with secondary inoculum at a ratio of 1:3 (v/w). Incubate inoculated bottles in a growth chamber at 24±1°C and 65±5% RH for several weeks until mycelia fully colonize the substrate surface.

7.2.5.4 Symbiotic System Assembly

Inoculate *G. elata* protocorms (50–100 per bottle) onto mycelium-colonized substrate surfaces. Place 2–3 sterile, moist cotton balls on the substrate surface to maintain microenvironment humidity. Continue co-cultivation under identical conditions, recording weekly protocorm biomass growth and rhizomorph formation.



Figure 7.3 Validation system for cultivating *Gastrodia elata* using indoor *Armillaria* strains

7.3 Results

7.3.1 *Armillaria-Gastrodia elata* Symbiotic Interaction Experimental Results

Although preliminary investigations in Section 1.3 explored the suitability of various *Armillaria* species for *Gastrodia elata* cultivation, these studies were limited by: (1) potential inaccuracies in species identification relying on limited genetic markers, and (2) incomplete taxonomic coverage of experimental strains of known species. To address these limitations, we conducted a systematic *Armillaria-G. elata* symbiotic interaction cultivation experiments at species-level resolution, see Table 7.1 for strain details.

As shown in Table 7.1, cultivation results were classified into three categories: (1) sparse protocorm development (<less protocorms/unit), (2) undetectable protocorms, and (3) abundant protocorm proliferation. The first two phenotypes may result from fungal hyperparasitism or impaired hyphal viability, and require validation with extended fungal isolates. In contrast, the third phenotype demonstrates fungal strains suitable for *Gastrodia elata* cultivation. Our cultivation experimental results indicate that six species (CBSB, CBSC, CBSF, CBSH, CBSL, and CBSO) can be utilized for *Gastrodia elata* cultivation (Figure 7.3 and Figure 7.4), while the applicability of the remaining species requires further verification. Interestingly, certain strains within the *Armillaria mellea* species complex, traditionally considered highly parasitic, were observed to produce sparse protocorms during cultivation (Figure 7.5), albeit in limited quantities. This suggests that the supposedly strongly parasitic *Armillaria* species may potentially promote *Gastrodia* tuber growth under specific developmental stages or conditions. However, the natural environmental context in which this symbiotic relationship transitions to parasitism, and the precise stage at which this reversal occurs, remain subjects for future investigation.

Table 7.1 *Armillaria* strains used for validating cultivability and cativation results

Strain number	Biological species	Cativation results
19041*19042	*A. cepisticeps*	sparse protocorm development
19041	*A. cepistipes*	undetectable protocorms
guo216	*A. ectypa*	sparse protocorm development
96016*96008	CBSA	undetectable protocorms
guo345	CBSB	abundant protocorm proliferation
SJ18	CBSB	sparse protocorm development
21024*96038	CBSC	abundant protocorm proliferation
21024	CBSC	sparse protocorm development
21019	CBSC	abundant protocorm proliferation
21043	CBSD	undetectable protocorms
21049*19020	CBSF	abundant protocorm proliferation
22KM01	CBSG	sparse protocorm development
19037/1	CBSG	sparse protocorm development
0006*00123	CBSH	undetectable protocorms

Table 7.1 (continued)

Strain number	Biological species	Cativation results
21LJ05	CBSH	abundant protocorm proliferation
21SNJ24	CBSJ	sparse protocorm development
Ar-8	CBSJ	sparse protocorm development
19083*19105	CBSK	sparse protocorm development
00111*19052	CBSK	undetectable protocorms
21LJ11	CBSK	sparse protocorm development
ZTMH-036	CBSL	abundant protocorm proliferation
17003*17017	CBSL	abundant protocorm proliferation
guo82	CBSL	undetectable protocorms
guo278	CBSL	abundant protocorm proliferation
05020*05021	CBSM	undetectable protocorms
19017*02066	CBSN	undetectable protocorms
19080*19095	CBSO	sparse protocorm development
BD4H	CBSO	abundant protocorm proliferation
LYT*CB003	CBSP	undetectable protocorms



Note a CBSB (SJ18). b CBSC (21019). c,d CBSF (21049*19020). e CBSH (21LJ05). f CBSJ (Ar-8). g CBSO (BD4H)

Figure 7.4 *Armillaria* spp. strains exhibiting cultivation suitability for *Gastrodia elata* in field trials



Note a CBSD (21043). b CBSKG1 (19083*19105). c CBSKG3 (CBSG19037). d CBSKG1 (22KM01).

Figure 7.5 *Armillaria* spp. strains lacking cultivation suitability for *Gastrodia elata* in field trials

7.3.2 Identification of Commercial *Armillaria* Strains

To clarify the genetic composition of current commercial *Armillaria* strains, we systematically collected 129 cultivated strains from major *Gastrodia elata*-producing regions in China. Based on taxonomic findings described in Chapter 2 and 8, these strains were classified into 10 species, with the following composition: CBSB (94 strains, 73%), CBSO (15 strains, 12%), CBSP (4 strains, 3%), CBSF (3 strains, 2%), CBSJ1 (3 strains, 2%), CBSKG3 (2 strains, 1.5%), and four additional species (CBSA2, CBSC, CBSL, CBSN) each represented by 1 strain (collectively 4%). The CBSB strain emerged as the dominant species, followed by CBSO, together accounting for 85% of all strains (Figure 7.6). Notably, CBSB strains were detected in all sampled production areas, indicating their broad cultivation adaptability.

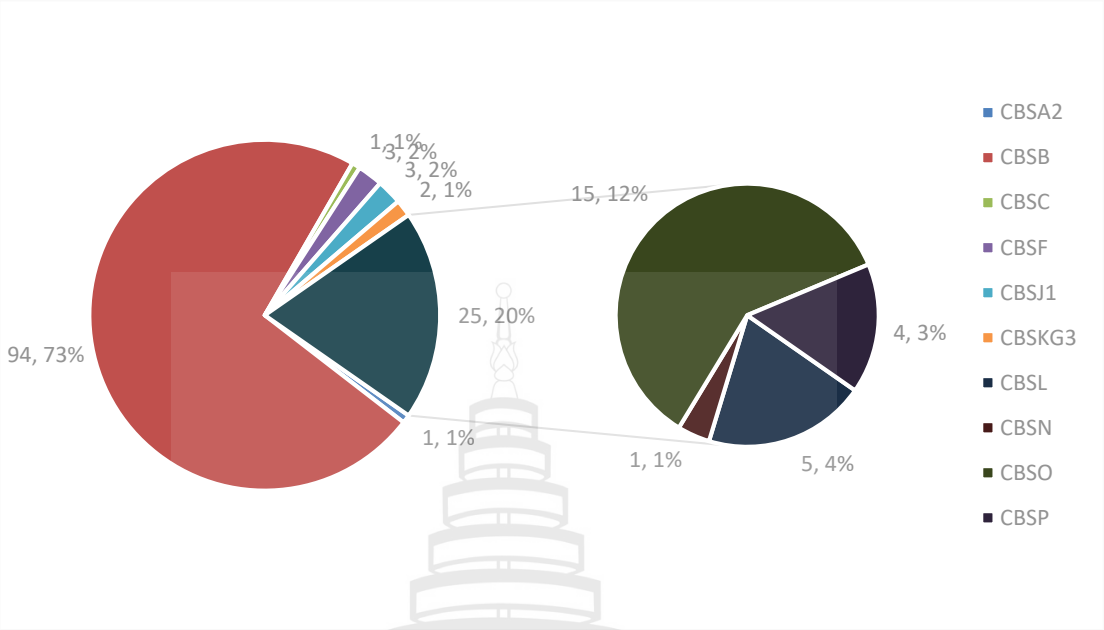


Figure 7.6 Taxonomic composition of commercial fungal strains analyzed in this study. Pie chart illustrates the species-level proportional distribution

7.4 Conclusion

In recent years, research on *Gastrodia elata* symbiotic fungi has achieved breakthrough progress in two critical stages: seed germination and nutrient supply. During the seed germination phase, studies have revealed the diversity characteristics of fungal communities dominated by the *Mycena* genus. Globally, 15 *Mycena* species, as well as non-*Mycena* taxa such as *Cubamyces lactineus* and *Roridomyces* spp., have been identified with significant germination-promoting activity.

In the symbiotic nutrient supply stage, systematic screening of *Armillaria* species demonstrates that members of the sect. *Gallicae* clade, such as *A. gallica* and strain CBS F, exhibits excellent symbiotic compatibility. In contrast, the *A. ostoyae* and *A. mellea* complexes have been confirmed as unsuitable for production due to their strong parasitic traits. Based on multigene phylogenetic analysis, we propose a correlation model between taxonomic units and parasitic intensity: species within sect. *Gallicae* likely universally possess weak parasitic characteristics and are recommended as preferred cultivation strains. Conversely, taxa in subg. *Desarmillaria*, sect. *Armillaria*, and sect. *Ostoyarum* should be

banned from cultivation due to its high pathogenicity. The parasitic features of sect. *Korhoneniorum* species require further validation through infection experiments.

To address critical bottlenecks constraining the high-quality development of the *Gastrodia elata* industry, the following systematic optimization strategies are proposed:

1. Establishing a Molecular Identification System for Fungal Strains and Strictly Banning Strongly Parasitic Taxa

A DNA barcoding-based identification protocol, such as those developed by Qin et al. (2025) or in this study, should be implemented at the upstream stage of fungal strain production to clarify taxonomic classifications through phylogenetic analysis. Production strains should prioritize weakly parasitic species within the sect. *Gallicae* clade (e.g., *A*. *gallica*, CBS F), while strictly prohibiting the use of highly pathogenic taxa under subg. *Desarmillaria* and sect. *Ostoyarum* and sect. *Armillaria*.

2. Constructing an Ecoregion-Adapted Fungal Germplasm Resource Bank

Based on the geographic distribution characteristics of *Armillaria* species, an "Optimized Native Strain Selection" project is recommended: Northeast China production zones should focus on native strains like CBSC and CBSF; Central China regions should promote subtropical dominant species such as CBSL, CBSN, and CBSP; and for widespread strain complexes like CBSB and CBSJ, subspecies resource libraries categorized by distinct ecotypes should be established. By integrating ecological factors (e.g., altitude, vegetation types) via GIS technology, a strain-site compatibility matrix can be developed to achieve precise allocation of fungal resources.

3. Developing a Developmental Stage-Specific Fungal Strain Screening System

As reported by Zhao and Zhao (2007), the CBS F strain exhibits dense rhizomorphs with moderate growth rates, facilitating the propagation of seed-derived rice-sized Tianma tubers. During *Gastrodia-Armillaria* interactions, distinct fungal traits may be required at different developmental stages. For the early tuber formation phase, high rhizomorph density is critical to ensure rapid symbiotic contact between minute tubers and fungal hyphae, thereby improving yield. In contrast, during the immature tuber cultivation stage, fewer rhizomorphs are sufficient for nutrient acquisition, reducing the need for densely branched strains.

4. Coordinated Tianma Germplasm-Strain Compatibility and Regionalized

Cultivation Strategies

Symbiotic interactions between *Gastrodia* variants and *Armillaria* may exhibit germplasm specificity. Guo et al. (2016) demonstrated that brown Tianma (*G. elata* f. *glauca*) and red Tianma (*G. elata* f. *elata*) preferentially associate with distinct *Armillaria* taxa. If future studies confirm this specificity, precision cultivation guided by the "suitable strain for suitable Tianma" principle must be implemented.

5. Integrated Hybrid Strain Development via Multi-Technological Approaches

Maintaining the genetic stability of *Armillaria* strains is crucial for overcoming yield and quality limitations. To address strain degeneration, hybrid breeding should be employed for genetic improvement. By establishing cross-fertility-based hybridization systems, high-activity strains with cultivation adaptability can be selected for directional crosses. Zhao et al. (2007) successfully enhanced mycelial vigor through hybridization between Eurasian *A. gallica* and North American relatives, validating the feasibility of transcontinental germplasm integration for trait enhancement.

6. Genetic Stability Maintenance Technology System

For high-quality strains obtained through domestication, selective breeding, or mutagenesis, ultra-low-temperature liquid nitrogen storage (-196°C) ensures long-term genetic stability. For hybrid strains, a dual preservation strategy is proposed: Monosporic parental strains (aerial white hyphae) with low growth rates and high genetic stability should be cryopreserved as a “genetic seed bank,” while compatible monosporic strains (verified A/B mating types) fused into rhizomorphs (yellow brown to black crustose structures) can be regenerated via in vitro fusion as needed. This “parental cryopreservation—on-demand fusion regeneration” system minimizes rhizomorph degeneration risks during subculturing while ensuring genetic fidelity and functional consistency.

7. Intellectual Property Protection and Quality Traceability System

China’s *Armillaria* strain protection and traceability systems still face challenges, including weak intellectual property awareness, unauthorized propagation of rebranded strains, and market flooding with unverified “variants,” leading to frequent cultivation failures often attributed to poor fungal quality, yet growers lack recourse. Implementing SSR molecular fingerprinting systems developed in this study will resolve these issues through precise strain authentication, legal protection of proprietary germplasm, and quality traceability.

CHAPTER 8

TAXONOMY

8.1 Introduction

This chapter describes the newly recognized *Armillaria* lineages and sublineages inferred from phylogenetic analyses, genetic differentiation patterns, and morphological observations. It further reviews and organizes early species descriptions written in Latin or other non-English languages in the historical literature to enhance understanding of species diversity and morphological traits within the genus.

8.2 Morphological Studies

Dried specimens were meticulously hand-sectioned and mounted in 5% KOH, and then stained with Congo red to enhance visualization. Observations were carried out using a Leica DM2500 compound microscope (Germany). Basidiospore dimensions and morphology were analyzed by measuring at least 30 basidiospores per collection, with sizes and shapes recorded and photographed with a Nikon camera fitted with a Leica DM2500 compound microscope.

Color descriptions followed the standard codes established by Kornerup and Wanscher (1981). Basidiospore sizes were expressed as (a–) b – c (–d), where b – c represented at least 90% of the measured values, and a and d indicated the extremes. The length-to-width ratio (Q) of basidiospores in the inside view was calculated, with the mean value (Qm) presented as Qm ± standard deviation.

Morphological terminology and descriptive terms adhered to the guidelines outlined by Vellinga & Noordeloos (2001) to ensure clarity and consistency. Spore shapes were classified according to Bas (1969): Globose: Q = 1.0–1.05, Subglobose: Q = 1.05–1.15, Broadly ellipsoid: Q = 1.15–1.3, Ellipsoid: Q = 1.3–1.6, Elongate: Q = 1.6–1.8, Cylindrical: Q = 2.0–3.0, and Bacilliform: Q > 3.0.

To represent spore size variation, 10% of measurements from each end of the range were excluded and reported in parentheses. Refer to Qin et al. (2024), Q refers to the range of length-to-width ratios, while Qm ± SD represents the mean and standard deviation of Q. Similarly, Lm ± EL refers to the mean range of the basidiospores lengths of the species with 95% statistical support. Qm ± EL refers to the mean range of the basidiospores Q value of the species with 95% statistical support, respectively.

Table 8.1 Comparison of basidiospore length and Q values between the newly measured species

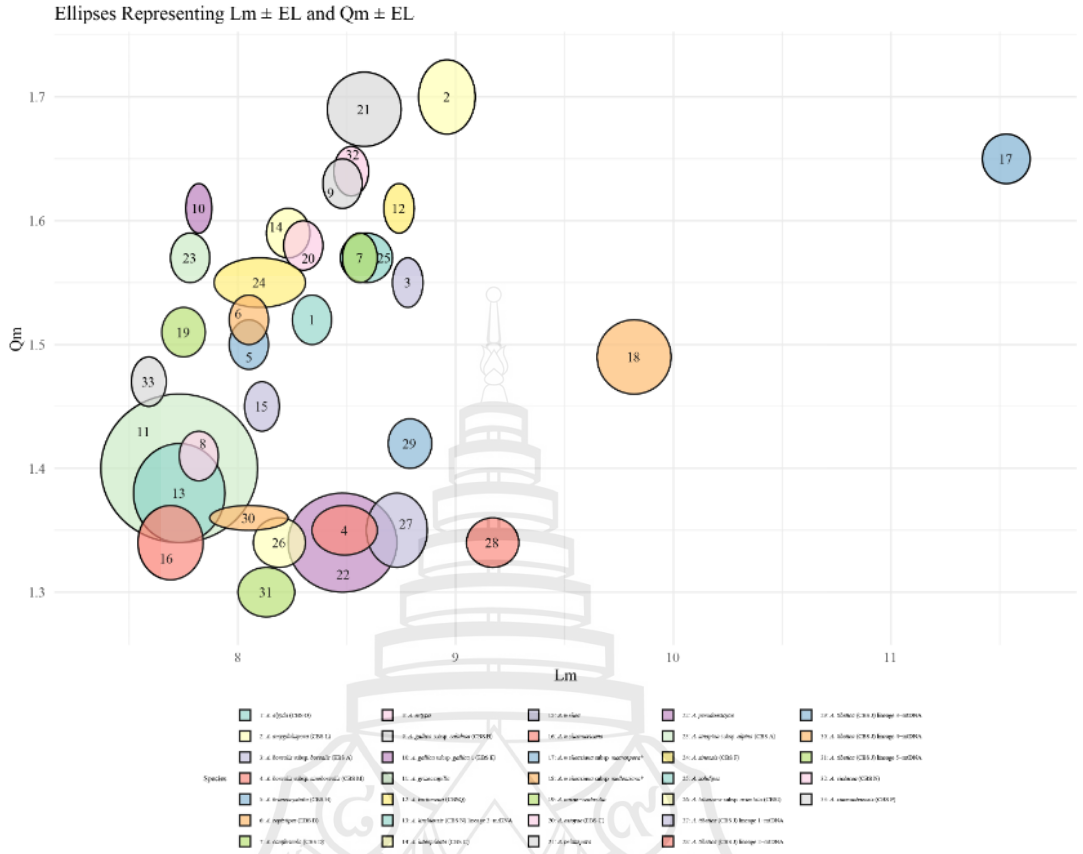
Species	L_m±SD	L_m±EL	Q_m±SD	Q_m±EL	N	n
A. algida (CBS O)	8.34±0.80	8.34±0.09	1.52±0.14	1.52±0.02	10	331
A. amygdalispora (CBS L)	8.96±0.74	8.96±0.13	1.70±0.19	1.70±0.03	4	120
A. borealis subsp. *borealis* (EBS A)	8.78±0.74	8.78±0.07	1.55±0.16	1.55±0.02	13	390
***A. borealis* subsp.** *sinoborealis* **(CBS M)**	8.49±0.82	8.49±0.15	1.35±0.13	1.35±0.02	4	120
A. bruneocystidia (CBS H)	8.05±0.68	8.05±0.09	1.50±0.14	1.50±0.02	10	235
A. cepistipes (EBS B)	8.05±0.82	8.05±0.09	1.52±0.17	1.52±0.02	8	291
A. conifericola (CBS D)	8.56±0.76	8.56±0.08	1.57±0.16	1.57±0.02	12	365
A. ectypa	7.82±0.60	7.82±0.09	1.41±0.12	1.41±0.02	3	182
A. gallica subsp. *calidusa* (CBS B)	8.48±0.80	8.48±0.09	1.63±0.16	1.63±0.02	12	285
A. gallica subsp. *gallica* 1 (EBS E)	7.82±0.57	7.82±0.06	1.61±0.15	1.61±0.02	6	307
A. griseocapilla	7.73±0.99	7.73±0.36	1.40±0.17	1.40±0.06	2	30
***A. korhonenii* (CBSQ)**	8.74±0.83	8.74±0.07	1.61±0.21	1.61±0.02	13	490
***A. linzhiensis* (CBS N) lineage 2-mtDNA**	7.73±0.84	7.73±0.21	1.38±0.16	1.38±0.04	3	63
A. luteopileata (CBS C)	**8.23±0.86**	**8.23±0.10**	**1.59±0.15**	**1.59±0.02**	8	314
A. mellea	8.11±0.53	8.11±0.08	1.45±0.16	1.45±0.02	3	183
A. melleamericana	7.69±0.54	7.69±0.15	1.34±0.10	1.34±0.03	1	51
A. melleasiana* subsp. *macrospora	9.53±1.21	9.53±0.11	1.65±0.22	1.65±0.02	10	429
A. melleasiana* subsp. *melleasiana	9.82±0.99	9.82±0.17	1.49±0.17	1.49±0.03	4	131
A. novae-zealandia	7.75±0.65	7.75±0.10	1.51±0.13	1.51±0.02	2	154
A. ostoyae (EBS C)	8.30±0.64	8.30±0.09	1.58±0.15	1.58±0.02	4	188
A. pelmispora	8.58±1.26	8.58±0.17	1.69±0.24	1.69±0.03	2	221
A. pseudoostoyae	8.48±0.69	8.48±0.25	1.34±0.11	1.34±0.04	1	30
A. sinapina subsp. *alpina* (CBS A)	7.78±0.70	7.78±0.09	1.57±0.15	1.57±0.02	9	243
A. sinensis (CBS F)	8.10±1.98	8.10±0.21	1.55±0.23	1.55±0.02	14	332
A. solidipes	8.59±0.74	8.59±0.12	1.57±0.14	1.57±0.02	3	150

Table 8.1 (continued)

Species	L_m±SD	L_m±EL	Q_m±SD	Q_m±EL	N	n
***A. tabescens* subsp. *orientala* (CBS I)**	8.19±0.70	8.19±0.12	1.34±0.12	1.34±0.02	4	143
***A. tibetica* (CBS J) lineage 1-mtDNA**	8.73±0.83	8.73±0.14	1.35±0.16	1.35±0.03	4	153
***A. tibetica* (CBS J) lineage 2-mtDNA**	9.17±0.77	9.17±0.12	1.34±0.16	1.34±0.02	5	162
***A. tibetica* (CBS J) lineage 3-mtDNA**	8.79±0.64	8.79±0.10	1.42±0.13	1.42±0.02	4	144
***A. tibetica* (CBS J) lineage 4-mtDNA**	8.05±0.85	8.05±0.18	1.36±0.07	1.36±0.01	3	90
***A. tibetica* (CBS J) lineage 5-mtDNA**	8.13±0.72	8.13±0.13	1.30±0.12	1.30±0.02	3	114
A. violacea (CBS N)	8.52±0.62	8.52±0.08	1.64±0.14	1.64±0.02	7	210
A. pungentisquamosa (CBS P)	7.59±0.68	7.59±0.08	1.47±0.14	1.47±0.02	9	300

Source reported by Qin et al. (2024)

Note Several mitochondrial maternal geographical lineages of *A. tibetica* are also included. SD, standard deviation; EL, error limit; N, number of measured specimens; n, number of measured basidiospores. Newly measured lineages are shown in bold.



Note The ellipses were determined by Lm±EL and Qm±EL

Figure 8.1 The basidiospores coordinate plane of *Armillaria* species

Armillaria borealis* subsp. *borealis (Marxm. & Korhonen) J.W. Liu, F.Q. Yu & Zhu L. Yang, ***comb. nov.***

Biological species: Europe Biological Species A (EBS A)

This species was originally described by Marxmüller in 1982 from Germany, Europe, Northern Hemisphere (Marxmüller, 1982).

Basidiomata are loosely grouped and rather slender. **Pileus** (1.8)2.8—5.0 cm before expanding, initially convex to almost campanulate, then becoming plano-convex. It is very hygrophanous, with colors ranging from yellow-brown or cinnamon-buff at first, often with a distinct olivaceous honey-colored tinge towards the disk. Upon expansion, it turns ivory white to dirty buff to pale cinnamon. When dry, the pileus becomes pinkish cream, except at the very margin, where the original color is retained or only slightly paler. The disk is faintly bay or purplish chestnut to chestnut, often obscured by small, suberect (0.25 mm), olivaceous-black to dark brown, ephemeral

floccules. These floccules are concentrically arranged, reflexed, and smaller towards the margin, becoming appressed with age, eventually appearing as reddish-brown or purple-bay smudges. **Margin** is smooth, minutely striate, incurved at first, and covered with white floccose fragments from the inner veil, bruising slightly pinkish or cinnamon-colored. **Stipe** 5.5—6.5 × 6—7 µm (1.2 cm at the base), cylindrical in the center, slightly thickened upwards towards the gills, and somewhat bulbous or clavate, almost smooth, whitish to pale pink at the striate apex, fibrillose-floccose above the ring, and pale cinnamon-buff or pinkish buff downwards, with an "indumentum" of white silky threads and yellow floccose scales with dark brown centers distributed downwards in irregular ring-like zones. The base has ochraceous or olive-yellow fibrils attached to the substrate. The color intensifies with age and handling, and the stipe becomes hollow in overmature basidiomata. The annulus is distinct, double, ochraceous, white to cream-colored, with a whorl of pale-yellow scales marked by dark brown (umber to snuff-brown) floccules, such that the yellow tinge is only clearly seen at the junction of the stipe and veil. It is paler where attached to the pileus margin and ornamented with only a few small brown floccules. **Lamellae** are subdecurrent to adnate, white, only slightly tinged pinkish at first, but bruising pinkish cream or becoming unevenly pink with age. The context is white in the pileus, except for the cortex, which is pinkish or yellowish buff, similar to the stipe cortex and base. It is slightly pinkish above the gills and fluffy-fleshy. The taste is mild or very slightly astringent, becoming unpleasant after a long time (> 2 minutes), while the smell is pleasant and sweetish (Gregory & Watling, 1985).

Basidiospores are white in mass, broadly ellipsoid to elongate-ellipsoid, (6.4)6.8—8(9.2) × 4.4—5.7 µm, rarely reaching 11 × 5 µm, smooth, hyaline, non-amyloid, with slightly thickened walls, and at maturity, they develop a very slight honey-colored tinge. **Basidia** are 4-spored, hyaline or slightly honey-colored in water and alkaline solutions, elongate-clavate, 24—30 × 6—7 µm. They are intermixed with 1—4-spored crassobasidia, which are entirely thick-walled or only thickened at the apex, yellowish honey-colored, with a silvery aspect, 21—30 × 4—6.5 µm, excluding sterigmata, which may be up to 3 µm long. **Pleurocystidia** are absent or replaced by thick-walled basidioles (possibly undeveloped crassobasidia). **Cheilocystidia** are thin-

walled, hardly differentiated, 13.8－22 × 4.5－8 µm, variable in shape, smooth or sometimes with a few flecks of amorphous material, hyaline or faintly tinged honey-colored in water and alkaline solutions, forming an irregular edge to the lamella. **Pileal squamules** is a cutis of repent, hyaline to honey-yellow, thin-walled, narrow hyphae, 2.5－4 µm broad, seated on a pseudoparenchyma-like subpellis of shorter, more ellipsoid cells, 2－4 µm broad, covered in cones of shortened, brown clavate or "sausage" to "torpedo"-shaped end-cells forming scales, many collapsing, 5－6 µm broad. The pileus trama consists of hyaline cells, 2－5 µm broad, showing no obvious alignment (Gregory & Watling, 1985).

Ecology/Substrate/Host: Found on standing living and dead trunks of both coniferous and deciduous trees.

Distribution: Distributed in Europe.

Average nuclear Weir & Cockerham's F_{ST} vs. the closest species (*A. borealis* subsp. *sinoborealis*): 0.13.

Average mitochondrial dxy vs. the closest species (*A. conifericola*): 0.04.

Average mitochondrial ΦST vs. the closest species (*A. conifericola*): 0.83.

Notes: According to Qin et al. (2007), the mating compatibility rate between Chinese (CBS M) and European (EBS A) populations of *Armillaria borealis* was 64.4 %. This relatively high mating compatibility indicates that they belonged to the same biological species. In the present study, samples from the two continents formed two well-supported continent lineages (MLBS = 100; phylogenomic trees, Figures 2.1-2.2). The nuclear Weir & Cockerham's F_{ST} between these two lineages was 0.13, representing a moderate level of genetic differentiation. Therefore, we recognize *A. borealis* as comprising two subspecies, with the European lineage corresponding to *A. borealis* subsp. *borealis* and the Asian lineage to *A. borealis* subsp. *sinoborealis*.

Armillaria borealis* subsp. *sinoborealis J.W. Liu, F.Q. Yu & Zhu L. Yang, ***sp. nov.,*** Figures 8.2－8.3

Biological species: Chinese biological species M (CBSM)

Etymology: The epithet sinoborealis combines Sino- ("China") with borealis.

Holotype: **CHINA**, **Hubei**, Shennongjia, Dajiu Lake, 31.4810°N, 109.9935°E, collected by Jianawei Liu (**holotype**, HKAS 135492).

Basidiomata tricholomatoid, small to large, solitary, scattered, or clustered. pileus 2－6 cm in diameter, initially nearly hemispherical, gradually expanding to convex or slightly depressed at the center. The surface is densely covered with conical or fibrous scales, white to grayish-white when young, becoming concentrated at the center upon maturation. The color varies from white, grayish-white, to pale brown. **Margin** is smooth, with inconspicuous grooves, and often bears remnants of a white cottony veil. **Lamellae** are decurrent, nearly white when young, turning dingy white to pale brown with age, moderately spaced, unequal in length, with smooth edges. **Stipe** 5－12 cm long, 0.4－1.5 cm in diameter, nearly cylindrical, slightly tapering upward, and solid. The upper surface of the stipe above the annulus is white, yellowish-white to pale brown, nearly smooth, while the lower part toward the base transitions to white, grayish-white, or pale brown, with the surface covered in white, erect scales. **Annulus** present, superior, white, relatively thick when young, slightly shrinking with maturity, with brown blotches or banded areas on its surface.

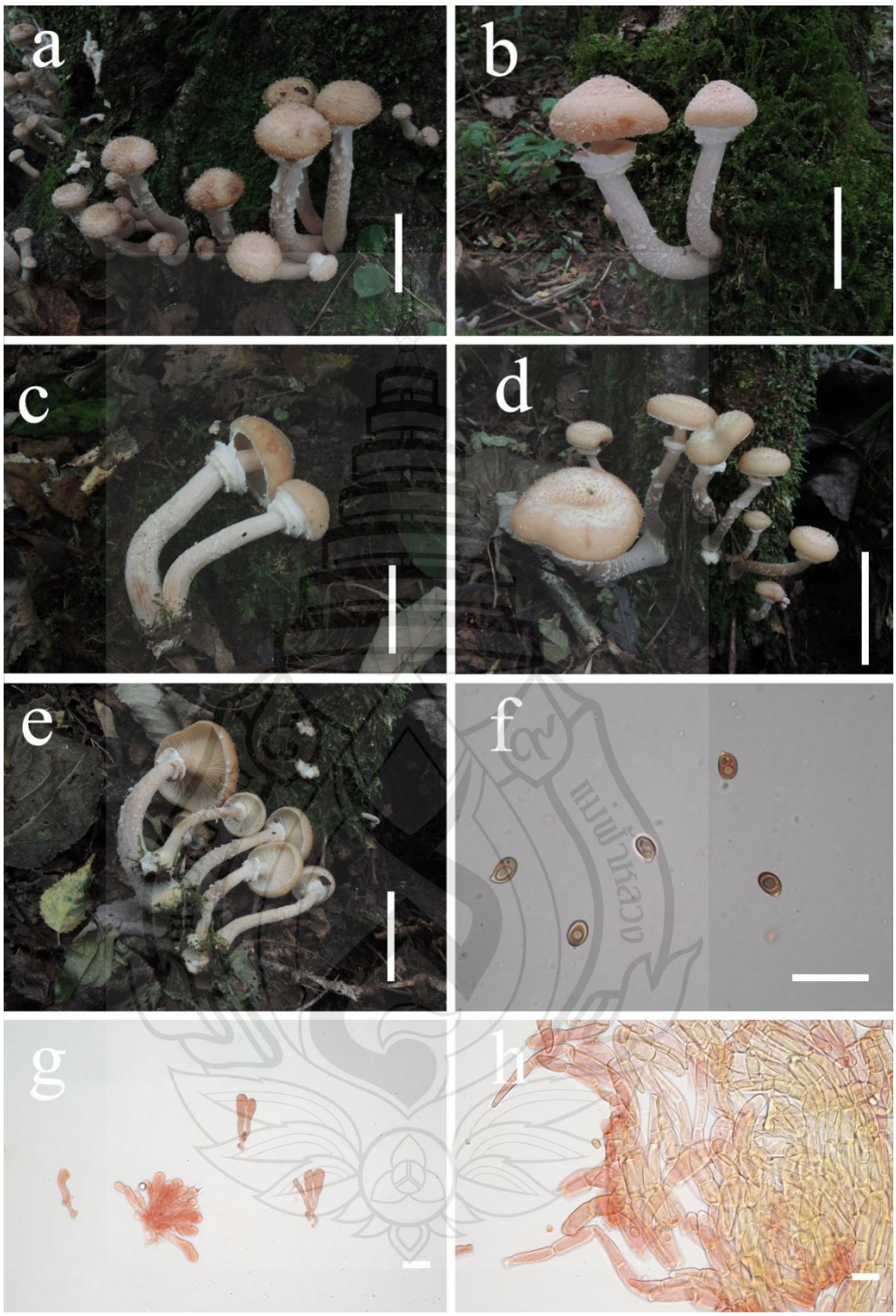
Basidiospores: [120/4/4] (6.28)7.19－9.86(10.06) × (4.51)5.08－7.51(7.73) μm, (Q = (1.12)1.14－1.58(1.73), Qm = 1.35 ± 0.13), subglobose, broadly ellipsoid to ellipsoid, inamyloid. **Basidia** 30－35 × 8－10 μm, clavate, 2 or 4 spored, often with a basal clamp connection; sterigmata 4－5 μm long. **Pileal squamules surface** consist of nearly longitudinally palisaded elliptical cells (17－59 × 9－20 μm), containing brown to yellowish-brown intracellular pigments. The terminal cells (18－33 × 4－11 μm) are spindle-shaped and mostly slender.

Ecology/Substrate/Host: Clustered on rotten wood of Fagaceous plants in subtropical evergreen broad-leaved forests.

Distribution: Distributed across central China.

Additional material examined: **CHINA**, **Hubei**, Shennongjia, Dajiu Lake, 31.4809°N, 109.9930°E, HKAS 135493; Shennongjia Forest Region, Jiuhuping, 31.5000°N, 110.3333°E, CBSM01012 (strain); Shennongjia Forest Region, Jiuhuping, 31.5000°N, 110.3333°E, CBSM01013 (strain); Shennongjia Forest Region, Jiuhuping, 31.5000°N, 110.3333°E, CBSM01019 (strain). Shennongjia Forest Region, Jiuhuping, 31.5062°N, 110.3502°E, HKAS 86617 (specimen), Shennongjia Forest Region, Dajiuhu Scenic Spot, Dajiuhu Town, 31.4810°N, 109.9936°E, SNJ20 (strain). **Shaanxi**,

Baoji City, Mei County, Taibai Mountain, 34.1166°N, 107.8833°E, CBSM04019 (strain); Baoji City, Mei County, Taibai Mountain, Honghegu, 34.1000°N, 107.7333°E, CBSM05020 (strain); Baoji City, Mei County, Taibai Mountain, Honghegu, 34.1000°N, 107.7333°E, CBSM05021 (strain). **Gansu**, Longnan City, Kang County, Laozhuang, 33.0333°N, 105.6000°E, HMAS 131062; Longnan City, Wen County, 32.9440°N, 104.6834°E, HMAS 63163.



Note a–e Basidiomata. f Basidiospores. g Basidia. h Hyphae of pileal squamules. Scale bars: a–e = 1 cm, f–h = 20 µm.

Figure 8.2 Basidiomata and morphological characteristics of *Armillaria borealis* subsp. *sinoborealis* (HKAS 135492)

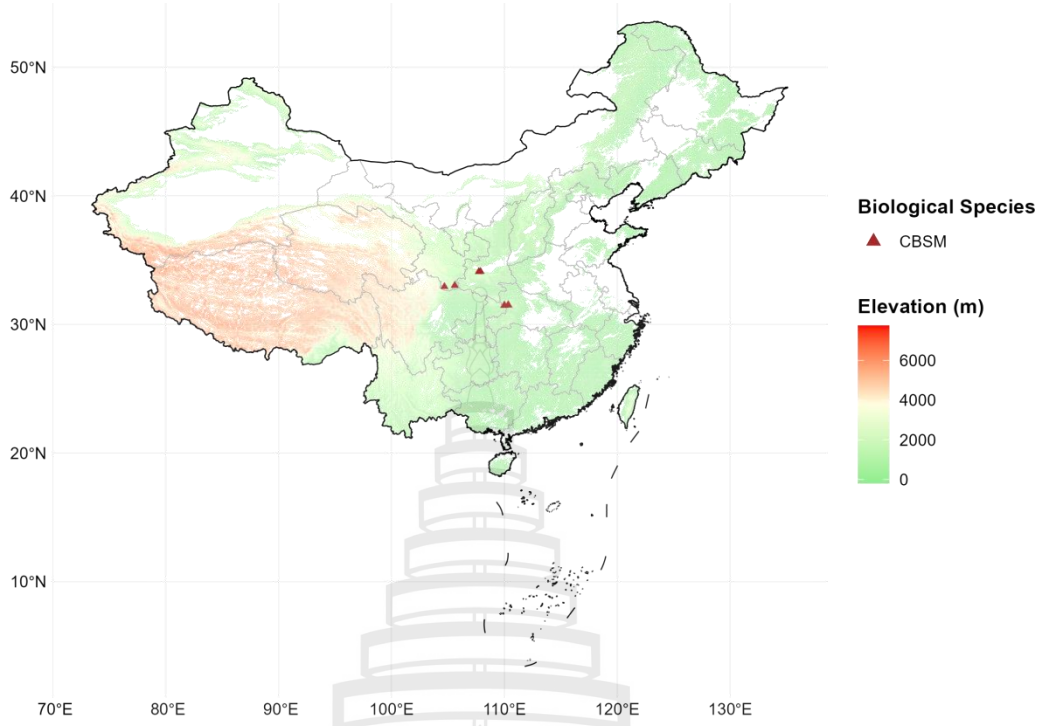


Figure 8.3 Distribution of samples of *Armillaria borealis* subsp. *sinoborealis* used in this study

Average nuclear Weir & Cockerham's F_{ST} vs. the closest species (*A. borealis* subsp. *borealis*): 0.13.

Average mitochondrial dxy vs. the closest species (*A. ostoyae*): 0.11.

Average mitochondrial ΦST vs. the closest species (*A. conifericola*): 0.86.

Notes: *Armillaria borealis* subsp. *sinoborealis* shows moderate genetic differentiation from its close relatives, with a nuclear F_{ST} of 0.13 compared to the closest species, *A. borealis* subsp. *borealis*, a mitochondrial dxy of 0.11 against the closest species *A. ostoyae*, and an average mitochondrial ΦST of 0.86 with the closest species *A. conifericola*. Morphologically, its basidiospores 7.19—9.86 × 5.08—7.51 μm, which are larger than those of *A. borealis* subsp. *borealis* (5.5—6.5 × 6—7 μm). In terms of distribution, *A. borealis* subsp. *sinoborealis* occurs mainly in Asia, now known to be distributed in China, whereas *A. borealis* subsp. *borealis* is restricted to Europe.

Armillaria griseocapilla J.W. Liu, F.Q. Yu & Zhu L. Yang, ***sp. nov.,*** Figures 8.4－8.5

Biological species: No biological species information available.

Etymology: The specific epithet griseocapilla is derived from the Latin words griseus, meaning "gray," and capillus, meaning "hair" or "hair-like." This name refers to the characteristic gray-colored cap (pileus) of the species.

Holotype: **CHINA**, **Yunnan**, Ailaoshan Subtropical Forest Ecosystem Research Station of the Chinese Academy of Sciences (the Ailaoshan Ecosystem Station), Jingdong Yi Autonomous County, Puér City, 24.5315°N, 101.0279°E, HKAS 132000.

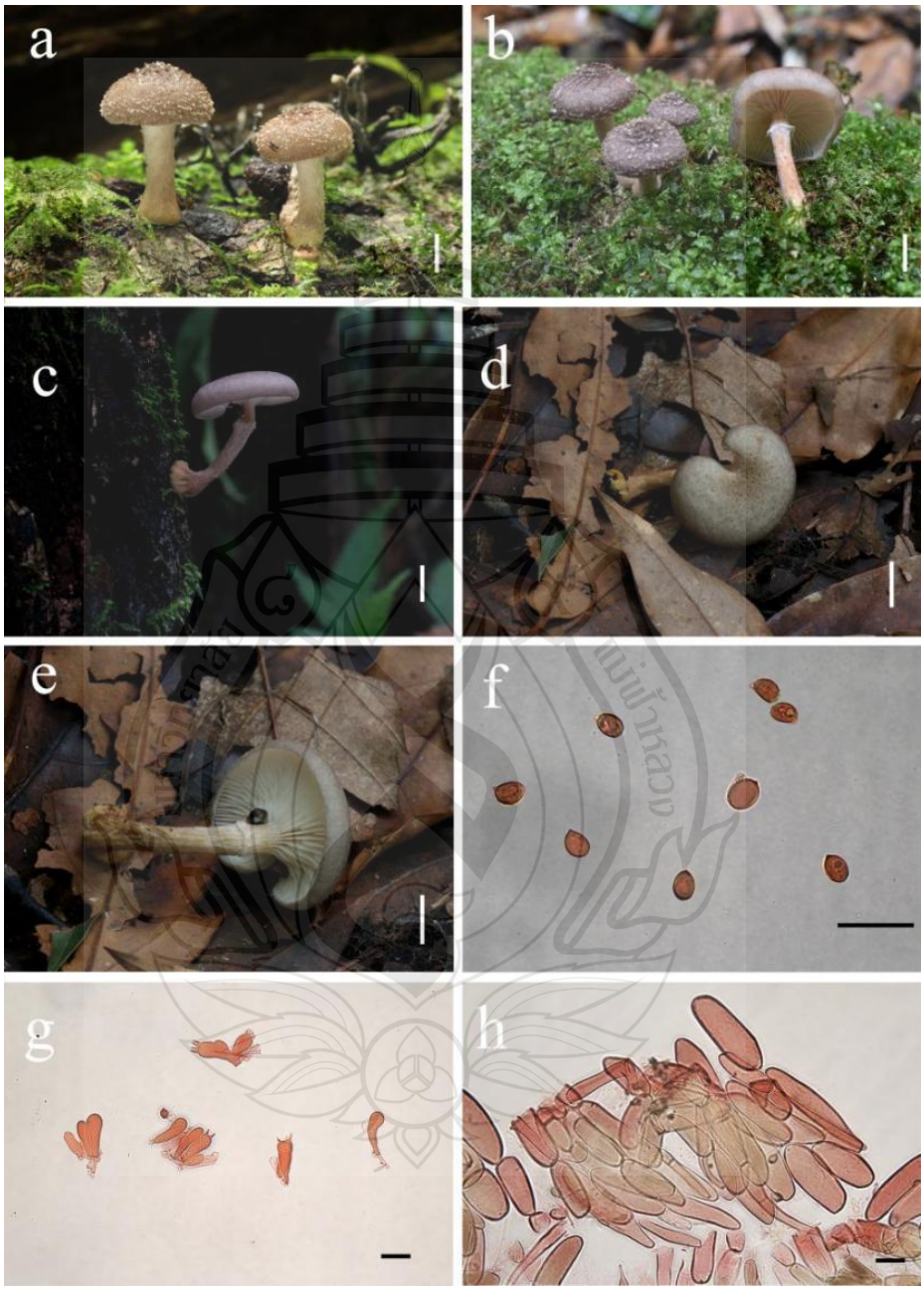
Basidiomata tricholomatoid, small to medium-sized, occurring solitary, scattered, or in clusters. **Pileus** 2－4 cm in diameter, initially nearly hemispherical when young, gradually expanding to plano-convex and eventually flattening out when mature, with an inrolled margin. The cap surface is covered with dense, fibrous, conical scales that range from gray to blackish-gray or dark gray, denser at the center, and with no striations at the margin. **Lamellae** are decurrent, white, relatively sparse, of unequal length, with smooth edges. **Stipe** is 2－3 cm long and 0.3－0.5 cm in diameter, nearly cylindrical, slightly enlarged at the base, and covered with fibrous or cottony white scales. The upper part of the stipe is white to grayish-white, gradually transitioning to pale brown, brown, or dark brown toward the base. **Annulus** present, membranous or cottony in texture, and white in color.

Basidiospores: [30/2/2] (5.84)6.21－9.32(9.74) × (4.43)4.46－7.13(8.05) μm, (Q = (1.07)1.2－1.68(1.92), Qm = 1.40 ± 0.17), broadly ellipsoid, ellipsoid to elongate, inamyloid. **Basidia** 22－36 × 6－8 μm, clavate, 2 or 4 spored, often with a basal clamp connection; sterigmata 4－5 μm long. **Pileal squamules** surface consists of nearly longitudinally palisaded, spindle-shaped to vesicular (50－80 × 13－25 μm), containing brown to yellowish-brown intracellular pigments. The terminal cells (50－60 × 6－10 μm) are spindle-shaped and mostly slender.

Ecology/Substrate/Host: Clustered on rotten wood of fagaceous plants in subtropical evergreen broad-leaved forests.

Distribution: Currently found in the southwestern region of China.

Additional material examined: **CHINA**, **Tibet Autonomous Region**, Zhangmu Valley, Nyalam County, Shigatse City, 27.9886°N, 85.9856°E, HKAS 135519. Yunnan, Baoshan City, Baihualing Ecological Tourism Area, Jiujiezi, 25.297883 °N, 98.775232°E, 2291.2 m, GLG-WGS75.



Note a–e Basidiomata. f Basidiospores. g Basidia. h Hyphae of pileal squamules. Scale bars: a–e = 1 cm, f–h = 20 µm.

Figure 8.4 Basidiomata and morphological characteristics of *Armillaria griseocapilla* (HKAS 132000, holotype)

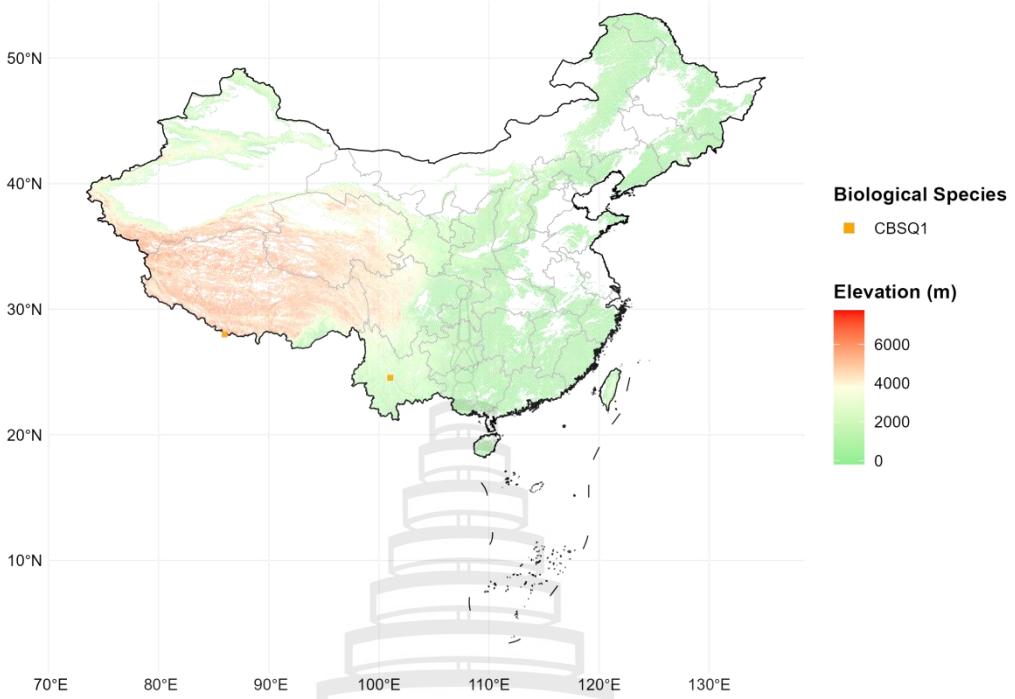


Figure 8.5 Distribution of samples of *Armillaria griseocapilla* used in this study

Average nuclear Weir & Cockerham's F_{ST} vs. the closest species (*A. korhonenii*): 0.24.

Average mitochondrial dxy vs. the closest species (*A. korhonenii*): 0.09.

Average mitochondrial ΦST vs. the closest species (*A. korhonenii*): 0.81.

Notes: *Armillaria griseocapilla* was recovered as phylogenetically close to *A. korhonenii* in both nuclear (MLBS = 100) and mitochondrial (MLBS = 100) phylogenomic trees (Figure 2.1 and Figure 2.2) with strong support. Liu et al. (2024) treated these two taxa as the same species. However, in the present study, with expanded sampling, the specimens previously considered conspecific were consistently resolved as two distinct clades in both nuclear and mitochondrial trees. The level of genetic differentiation was substantial between the two lineages, with a nuclear Weir & Cockerham's F_{ST} of 0.24, a mitochondrial dxy of 0.09, and a mitochondrial ΦST of 0.81. These values support significant divergence, and therefore, despite the absence of mating compatibility data, we recognize the two clades as independent species. Morphologically, *A. griseocapilla* is distinguished by its gray pileus with conspicuously dense, eyelash-like squamules, in contrast to the honey-colored pileus and sparser

squamules of *A. korhonenii*. In terms of distribution, *A. griseocapilla* occurs from the Ailao and Gaoligong Mountains in central Yunnan to southern Tibet, whereas *A. korhonenii* is primarily confined to the Dawei Mountain National Nature Reserve in southern Yunnan.

Armillaria linzhiensis J.W. Liu, F.Q. Yu & Zhu L. Yang, ***sp. nov.,*** Figures 8.6－8.7

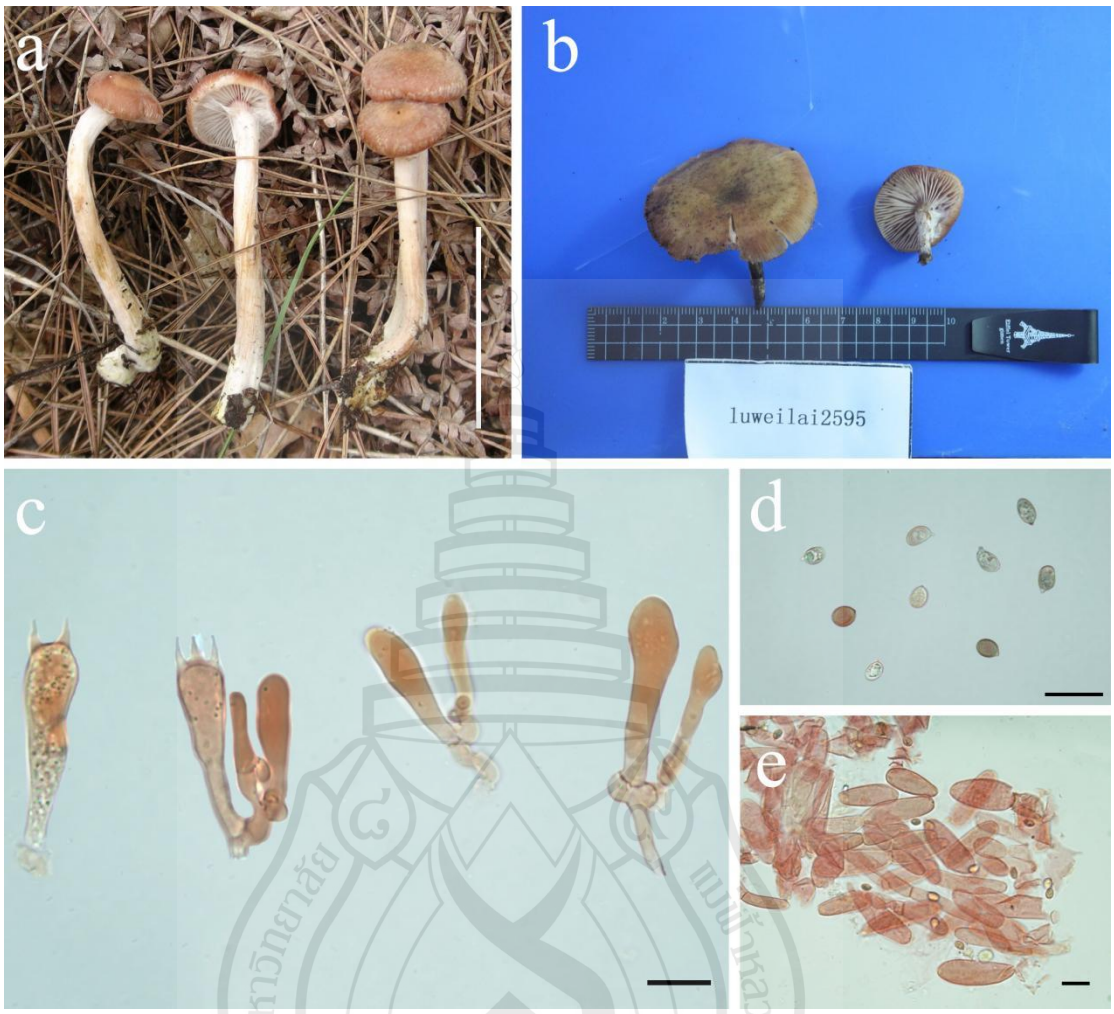
Biological species: No biological species information available.

Etymology: The specific epithet linzhiensis is derived from the name of Linzhi, a region in Tibet, China, where the species was first discovered.

Holotype: **CHINA**, **Tibet Autonomous Region**, Linzhi City, Bayi District, Layue Township, 29.5855°N, 94.4845°E, date, collector, (**holotype**, HMAS 272515).

Basidiomata tricholomatoid, small to medium-sized, solitary or scattered. **Pileus** 2－5 cm in diameter, initially nearly hemispherical to plano-convex, with floccose remnants of the veil at the margin, later becoming broadly expanded. The **Pileus surface** is brown to honey-yellow, densely covered with white to grayish-white fibrous scales, which reduce upon maturity, leaving inverted brown to dark brown scales, the center of the pileus is denser. **Margin** exhibits distinct striations about 0.5－1 cm long. **Lamellae** are nearly adnate, white when young, turning dingy white to pale brown as they mature, relatively sparse, unequal in length, and with smooth edges. **Stipe** is 5－8 cm long and 0.4－0.9 cm in diameter, nearly cylindrical, with a whitish to dingy white surface near the apex, gradually transitioning to grayish-white or blackish-gray toward the base, occasionally tinged with yellow-brown. **Annulus** present, floccose, white.

Basidiospores [63/4/4] 5.7(6.3)－9(10) × 3.97(4.4)－6.65 (7.31) μm, (Q = (1.13) 1.15－(1.65)1.78, Qm = 1.38 ± 0.16), subglobose, broadly ellipsoid, ellipsoid to elongate, inamyloid. **Basidia** 50－80 × 15－24 μm, clavate, 2 or 4 spored, often with a basal clamp connection; sterigmata 10－12 μm long. **Pileal squamules surface** consists of nearly longitudinally palisaded, spindle-shaped to vesicular or elliptical cells (24－55 × 15－24 μm), containing brown to yellowish-brown intracellular pigments.



Note a–b Basidiomata. c Basidiospores. d Basidia. e Hyphae of pileal squamules. Scale bars: a = 5 cm, c–e = 20 µm.

Figure 8.6 Basidiomata and morphological characteristics of *Armillaria linzhiensis* (HMAS 272515, holotype)

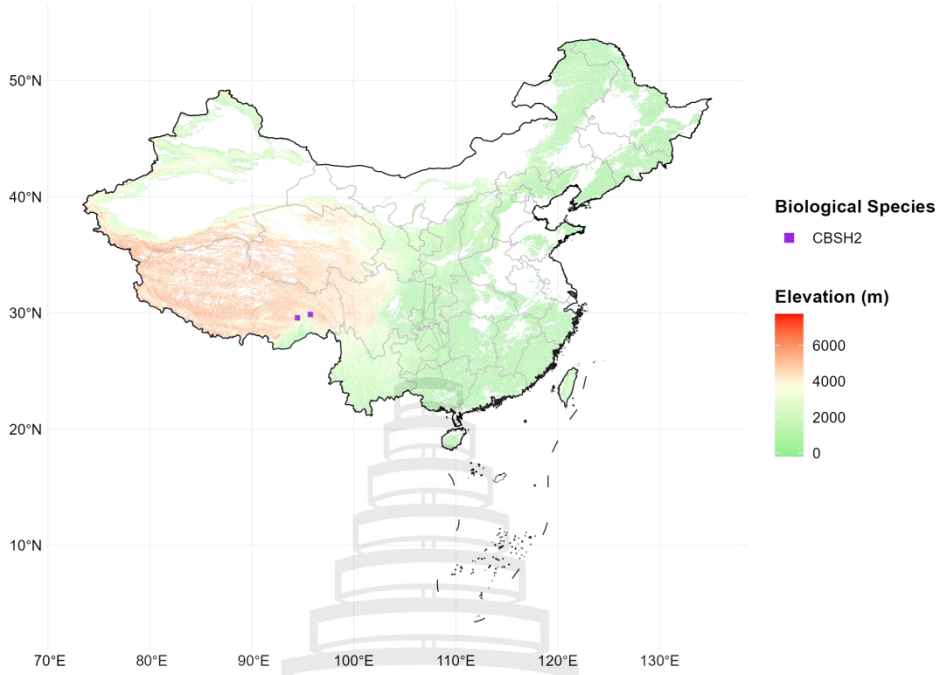


Figure 8.7 Distribution of samples of *Armillaria linzhiensis* used in this study

Ecology/Substrate/Host: Clustered on rotten wood of Fagaceous plants in subtropical evergreen broad-leaved forests.

Distribution: Currently only known from Tibet, China.

Additional material examined: **CHINA**, **Tibet Autonomous Region**, Linzhi City, Bomi County, Songzong Town, Xibu Road, 29.8704°N, 95.7495°E, HMAS 272390.

Average nuclear Weir & Cockerham's F_{ST} vs. the closest species (*A. violacea*): 0.15.

Average mitochondrial dxy vs. the closest species *A. tibetica* (CBS J) lineage 2-mtDNA, *A. tibetica* (CBS J) lineage 3-mtDNA, *A. amygdalispora*, *A. violacea*, *A. pungentisquamosa*: 0.04.

Average mitochondrial ΦST vs. the closest species (*A. amygdalispora*): 0.32.

Notes: *A. linzhiensis* forms a well-supported sister relationship with *A. violacea* in the nuclear phylogeny (MLBS = 100; Figure D1), whereas in the mitochondrial phylogeny, it is recovered as sister to *A. bruneocystidia* with strong support (MLBS = 91; Figure D2). Although mating data are not yet available for this taxon, it shows

moderate to substantial nuclear genomic differentiation (F_{ST} = 0.15) from *A. violacea*, and mitochondrial divergence from its close relatives is also evident (dxy = 0.04; ΦST = 0.32). These results support the recognition of *A. linzhiensis* as an independent species. Morphologically, its basidiospores (5.7－9 × 3.97－6.65 μm) are smaller than those of *A. violacea* (7.5－9.8 × 4.7－6.0 μm). Geographically, *A. linzhiensis* is restricted to Linzhi, Tibet, whereas *A. violacea* occurs in central China.

Armillaria melleasiana* subsp. *melleasiana* (**G.F. Qin, W.M. Qin, J. Zhao & Y.C. Dai) J.W. Liu, F.Q. Yu & Zhu L. Yang, ***sp. nov., Figures 8.8－8.9

Biological species: Chinese biological species G (CBSG) and Chinese biological species K (CBSK).

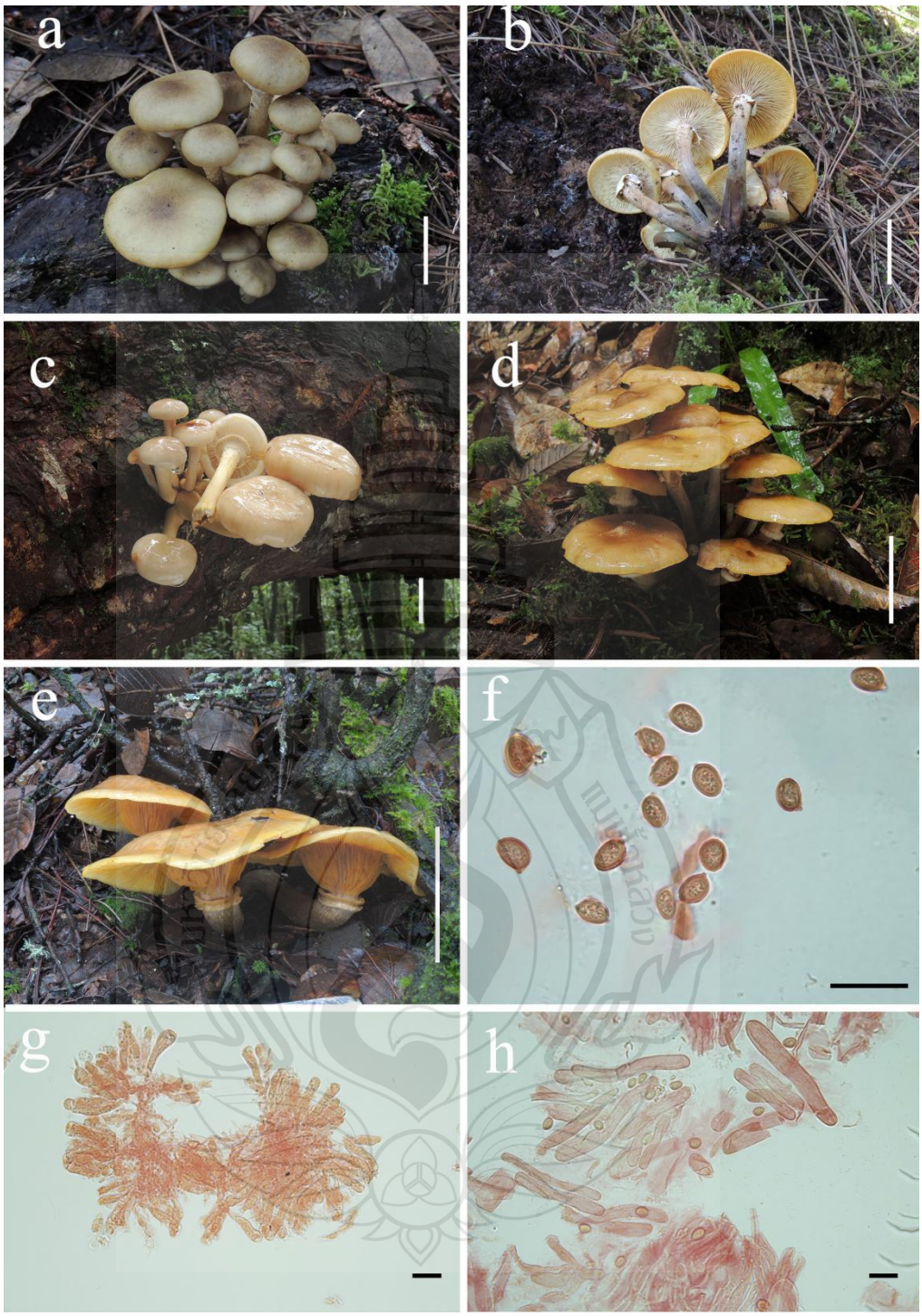
Pileus is 2.5－10 cm in diameter and 0.6－1.4 cm thick, initially subglobose or hemispherical without a mammilla, later becoming plano-convex to applanate or depressed, dry, with a pale yellow to greyish yellow margin and a greyish yellow center when young. As it matures, the margin turns greyish yellow, greyish orange, or brownish orange, while the center becomes pale yellow, pale orange, greyish orange, or brownish orange. Pileal scales are sparse, pale brown, and fibrillose, concentrated at the center when young, becoming smooth or completely denuded with age. **Margin** is entire, usually incurved, with radial striations. **Lamellae** are adnate or decurrent, often with striations extending downward to the annulus, orange-white when young, turning greyish orange when mature, subdistant, with smooth margins. **Stipe** is central, 4－12 cm long, 0.5－2.5 cm in diameter at the apex, cylindrical, equal or slightly thickened at the base, pale yellow to pale brown above the annulus; the middle is greyish yellow to brown, often covered with greyish yellow or yellowish brown suberect tomentose veil remnants and scales. The base is greyish yellow to brown, usually darkening with age. **Annulus** is membranous, rather thick, persistent, pale yellow, golden brown, or yellowish brown, sometimes with yellowish brown merodont scales on the outer margin.

Basidiospores are ivory white in mass, ellipsoid to elongate, lacking a suprahilar depression, (7)7.6－11(12.2) × (4.3)4.9－6.2(6.8) μm, nearly colorless, greenish blue to brownish yellow, smooth, cyanophilous, inamyloid, with a prominent apiculus. **Basidia** are clavate, 22－47 × 5－10 μm, with an upper portion that is

constricted or inconspicuously constricted, simple septate, four-sterigmate, thin- to slightly thick-walled (≤ 0.4 μm), yellowish green to brownish yellow, with pigments gradually dissolving in KOH solutions; crassobasidia are not observed. **Cheilocystidia** are 6－61 × 3－11 μm, poorly differentiated and similar to basidioles, clavate to napiform, carrot-shaped to utriform or broadly subcapitate, simple septate, thin- to slightly thick-walled (≤ 0.4 μm), nearly colorless, greenish blue to brownish yellow, compactly forming a sterile lamella-edge but easily broken and disappearing. Pleurocystidia are absent. **Pileal squamules** are composed of more or less parallel arrays of irregular fusiform, slightly thick-walled (≤ 0.8 μm) hyphae, clampless, greenish blue, grey to brownish yellow, 19－67 × 5－15 μm (Qin et al., 2025).

Ecology/Substrate/Host: The species is found in various habitats, primarily on living or fallen angiosperm and conifer trees, including *Picea likiangensis* (Lijiang Spruce), *Pinus armandi* (Armand Pine), and *Rhododendron*. It is also found on decaying angiosperm wood.

Distribution: Mainly distributed in the southwest and central China.



Note a–e Basidiomata. f Basidiospores. g Basidia. h Hyphae of pileal squamules. Scale bars: a–e = 5cm, f–h = 20 µm.

Figure 8.8 Basidiomata and morphological characteristics of *Armillaria melleasiana* subsp. *melleasiana*

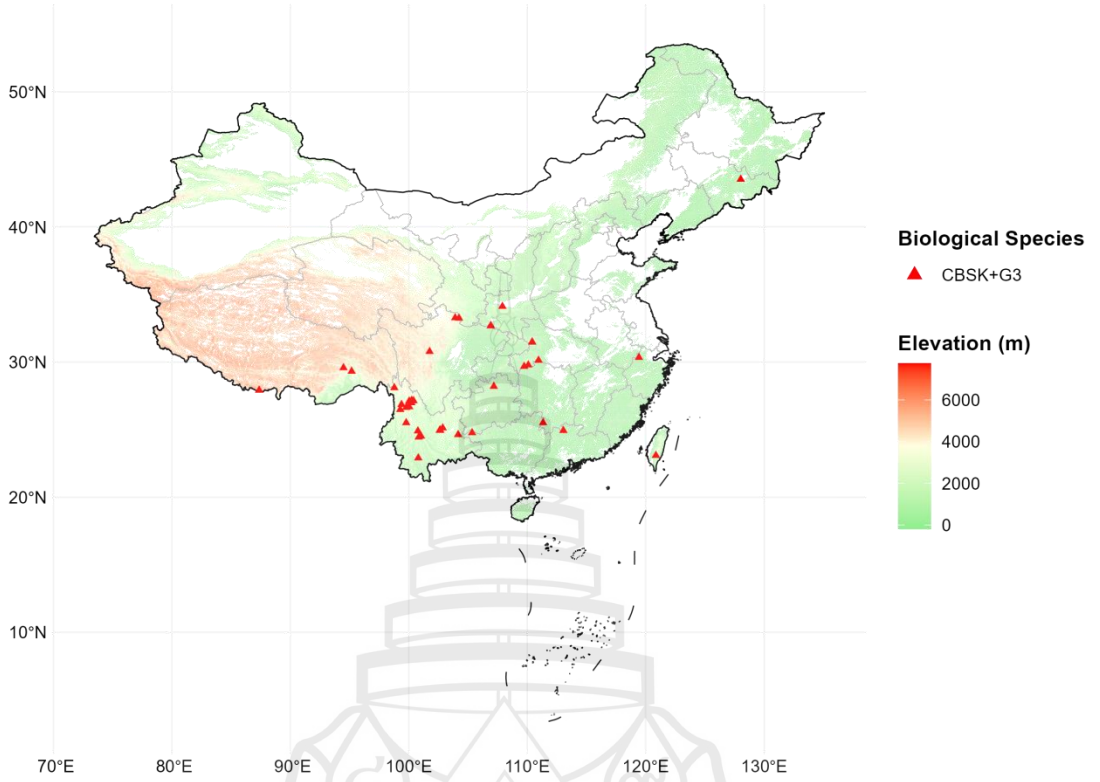


Figure 8.9 Distribution of samples of *Armillaria melleasiana* subsp. *melleasiana* used in this study

Additional material examined: **CHINA**, **Yunnan**, Lijiang Alpine Botanical Garden, Lijiang, 100.1788°E, 27.0043°N, HKAS 135500; Lijiang Alpine Botanical Garden, Lijiang, 100.2255°E, 27.1386°N, HKAS 135504; Lijiang Alpine Botanical Garden, Lijiang, 100.2230°E, 27.1368°N, HKAS 135505; Mushroom Mountain, Shizong County, Qujing City, 104.1572°E, 24.6333°N, 22KM03; Yunshanping, Yulong Naxi Autonomous County, Lijiang City, 100.0333°E, 27.1166°N, CBSK00111; Dasuodao, Yulong Snow Mountain, Yulong Naxi Autonomous County, Lijiang City, 100.2500°E, 27.1500°N, HKAS 86590; Laojun Mountain, Yulong Naxi Autonomous County, Lijiang City, 99.7761°E, 26.6480°N, HKAS 46275; Astronomical Observatory, Yulong Naxi Autonomous County, Lijiang City, 100.0324°E, 26.6929°N, HKAS 57446; Hexi Township, Dayang Village, Lanping Bai Pumi Autonomous County, Nujiang Lisu Autonomous Prefecture, 99.3825°E, 26.8631°N, HKAS 68632; Dadong Township, Gucheng District, Lijiang City,

100.3948°E, 27.1461°N, HKAS 68678; Near X311-152, Lajing Township, Lanping Bai Pumi Autonomous County, Nujiang Lisu Autonomous Prefecture, 99.2744°E, 26.4907°N, HKAS 74997; Next to the horse road next to the ecological station of the Alpine Botanical Garden, Yulong Naxi Autonomous County, Lijiang City, 100.2005°E, 26.9968°N, HKAS 81274; Xishan Scenic Area, Kunming City, 102.6285°E, 24.9646°N, HKAS 81827; Xishan Scenic Area, Kunming City, 102.6285°E, 24.9646°N, HKAS 81828; Xishan Scenic Area, Kunming City, 102.6285°E, 24.9646°N, HKAS 81829; Yeya Lake, Panlong District, Kunming City, 102.8635°E, 25.1267°N, HKAS 82101; Alpine Botanical Garden, Yulong Naxi Autonomous County, Lijiang City, 100.2005°E, 26.9968°N, HKAS 87145; Ailaoshan Nature Reserve, Jingdong Yi Autonomous County, Pu 'er City, 100.8374°E, 24.4529°N, HMAS 253414; From Deqin to Gongshan Kongqueshan Pass in Nujiang Prefecture, 98.7757°E, 28.1061°N; Majie Town, Nanhua County, Chuxiong Yi Autonomous Prefecture, 100.7995°E, 22.9102°N, HKAS 135475; Mahuotang, Wudingshan Township, Nanhua County, Chuxiong Yi Autonomous Prefecture, 100.7661°E, 24.9067°N, HKAS 135476 (specimen). **Hubei**, Zangluping, Muyu Town, Shennongjia, 110.4131°E, 31.4853°N, HKAS 135489; Zangluping, Muyu Town, Shennongjia, 110.4148°E, 31.4870°N, HKAS 135490; Yangzixi, Houhe nature reserve, Wufeng Tujia Autonomous County, Yichang City, 110.9500°E, 30.1333°N, CBSK19052 (strain). **Sichuan**, Donggu Town, Danba County, Ganzi Prefecture, 101.7528°E, 30.7865°N, 221003WSP (strain); Jiuzhaigou County, Aba Tibetan and Qiang Autonomous Prefecture, 103.9115°E, 33.2821°N, HMAS 50995; Jiuzhaigou County, Aba Tibetan and Qiang Autonomous Prefecture, 104.2425°E, 33.2520°N, HMAS 51088; Micangshan National Forest Park, Wuguang Town, Nanjiang County, Bazhong City, 106.9192°E, 32.6919°N, HKAS 135554 (specimen). **Guizhou**, Kuankuoshui Reservoir, Suiyang County, Zunyi City, 107.1754°E, 28.2050°N, HKAS 86592. **Zhejiang**, Tianmushan Nature Reserve, Tianmushan Town, Lin'an District, Hangzhou City, 119.4295°E, 30.3475°N, HKAS 86593 (specimen). **Tibet Autonomous Region**, Chentang Town, Dingjie County, Shigatse City, 87.3643°E, 27.9196°N, FM21-172 (strain); Chentang Town, Dingjie County, Shigatse City, 87.3641°E, 27.9197°N, FM21-173 (strain); Lulang Sedila Mountain Area, Bayi District, Linzhi City, 94.4845°E, 29.5855°N, HMAS 272369; Paimo Road, Motuo

County, Linzhi City, 95.1729°E, 29.3224°N, HKAS 135509. **Hunan**, Badagong Mountain National Nature Reserve, Sangzhi County, Zhangjiajie City, 109.7400°E, 29.6838°N, MHHNU 31945; Jiucailing, Dao County, Yongzhou City, 111.3357°E, 25.5159°N, MHHNU 7419. **Guangdong**, Nanling Xiaohuangshan, Ruyuan Yao Autonomous County, Shaoguan City, 113.0465°E, 24.9372°N, GDGM 76532.

Average nuclear Weir & Cockerham's F_{ST} vs. the closest species (*A. melleasiana* subsp. *melleasiana*): 0.06.

Average mitochondrial dxy vs. the closest species (*A. melleasiana* subsp. *macrospora*): 0.02.

Average mitochondrial ΦST vs. the closest species (*A. melleasiana* subsp. *macrospora*): 0.97.

Notes: In Qin et al. (2025), the biological species CBSK and CBSG were recognized as distinct phylogenetic species. However, the two differ in their mating systems: CBSK is heterothallic, whereas CBSG is homothallic (secondary homothallic). In the phylogenetic tree, these two groups show an intermingled pattern rather than forming two clearly separated lineages. Therefore, Qin et al. (2025) treated them together as *Armillaria melleasiana*, with CBSG assigned as its subspecies *A. melleasiana* subsp. *nipponica*.

In the present study, the CBSK and CBSG complex from China was resolved into two well-defined clades: one forms a sister relationship with the European *A. mellea* and includes samples from Africa, while the other comprises isolates from China, Africa, and North America. Interestingly, both clades contain mixtures of homothallic and heterothallic isolates (Figure D1). By contrast, the mitochondrial phylogeny reveals three distinct clades, which are incongruent with the nuclear topology (Figure D2).

Based on the nuclear phylogenetic relationships, we assign the predominantly heterothallic clade to *A. melleasiana* subsp. *melleasiana*, and establish the clade enriched in homothallic isolates as a new subspecies, *A. melleasiana* subsp. *macrospora*. It should be emphasized that both species harbor isolates of both homothallic and heterothallic types. Morphologically, *A. melleasiana* subsp. *melleasiana* produces smaller basidiospores (7.6－11(12.2) × (4.3)4.9－6.2(6.8) µm),

whereas *A. melleasiana* subsp. *macrospora* has markedly larger basidiospores (9－13 × 5－7 µm).

According to Ota et al. (1998), the Japanese homothallic *A. mellea* is in fact a secondary homothallic species. In young basidia, after meiotic division of the diploid nucleus, four haploid nuclei are produced. These nuclei then fuse in pairs, forming two diploid nuclei that migrate into two developing basidiospores, where they undergo mitotic division. Subsequently, one nucleus from each spore returns to the basidium, leaving a single diploid nucleus in the spore; when nuclear migration does not occur, two nuclei remain within the basidiospore. This demonstrates that reproductive mode is not necessarily serve as an absolute criterion for species delimitation.

Raper and Raper (1966) suggested that secondary homothallic species are often closely related to and derived from heterothallic species. Several cases in fungi illustrate that multiple mating systems can coexist within a single species. For instance, in *Coprinus patouillardii*, different strains exhibit distinct life cycle types, including secondary homothallic strains with two-spored basidia (Eliott, 1994), primary homothallic strains with four-spored basidia (Bayman & Collins, 1989), and heterothallic strains (Eliott, 1994). In *Agaricus bisporus*, the vast majority of basidia produce two basidiospores that develop into fertile mycelia, while a minority produce four basidiospores that give rise to infertile mycelia and exhibit heterothallism (Eliott, 1994). Likewise, *Neurospora tetrasperma* is considered to have evolved from heterothallic ancestors (Corcoran et al., 2012).

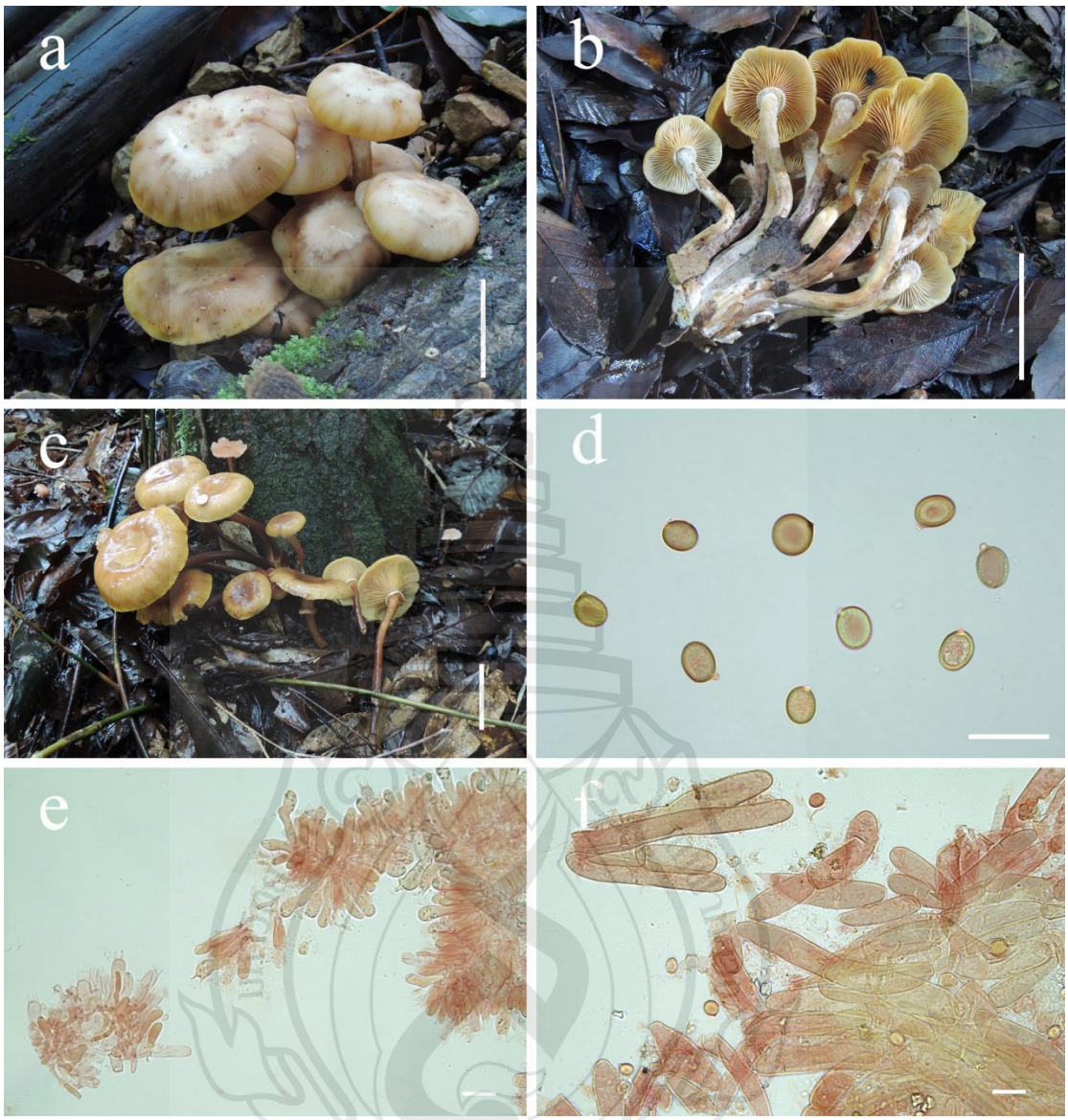
Armillaria melleasiana* subsp. *macrospora J.W. Liu, F.Q. Yu & Zhu L. Yang **subsp. *nov.*,** Figures 8.10－8.11

Basidiocarp is small to medium in size, typically densely clustered on declining trees or dead trunks, rarely solitary. **Pileus** 2.2－9.5 cm in diameter and 1.0－1.6 cm thick, initially subglobose or hemispherical, expanding to convex to applanate, and finally becoming depressed, dry, with a pale yellow, pale orange, or pale-yellow margin and a greyish orange, pale brown, yellow brown, or brown center when young. As it matures, the margin becomes pale orange, greyish orange, or yellowish brown, while the center turns brownish orange, brown, or dark brown. **Pileal scales** are nearly denuded, with fine white fibrils. **Margin** is entire, initially inrolled and then incurved,

with radial striations. **Lamellae** are decurrent, initially yellowish white or orange white, later turning pale yellow to pale brown, subdistant, with smooth margins. The context is yellowish white or orange-white. **Stipe** is central, 6—12 cm long, 0.4—1.5 cm in diameter at the apex, cylindrical, equal or slightly thickened at the base, and longitudinally striped. It is white, orange-white, or pale yellow when young, turning brown with age above the annulus. The middle portion is greyish yellow or pale brown when young, becoming greyish brown to dark brown with age. The base is brownish orange or pale brown when young, darkening to dark brown with age. It is covered with white fibrillose squamules, reminiscent of snakeskin markings. **Annulus** is membranous, rather thick, persistent, and superior, initially white or yellowish white, later turning greyish orange to yellowish brown.

Basidiospores are ivory white in mass, broadly ellipsoid to elongate, lacking a suprahilar depression, (7)9—13(15) × (4)5—7(8) μm. They are initially thin-walled, with mature spores becoming thick-walled (≤ 0.5 μm), nearly colorless, greenish blue to brownish yellow, smooth, cyanophilous, inamyloid, with a prominent apiculus. **Basidia** are clavate, 32—42 × 8—12 μm, with an upper portion that is constricted, simple septate, thin- to thick-walled, four-sterigmate, with sterigmata 2—4.5 μm long at maturity. **Cheilocystidia** are 25—48 × 3—9 μm, poorly differentiated and similar to basidioles, fusiform, napiform to clavate or broadly subcapitate, simple septate, thin- to slightly thick-walled (≤ 0.4 μm). **Pileal squamules** are rare, fusiform, cylindrical to clavate, slightly thick-walled (≤ 0.8 μm) hyphae, 15—50 × 5—12 μm.

Ecology/Substrate/Host: The species is found in various habitats across multiple regions in China, primarily on fallen or living angiosperm and conifer trees, including *Quercus* sp., *Ailanthus altissima Cyclobalanopsis*, *Keteleeria*, and *Pinus densata*. It is also found on decaying angiosperm wood.



Note a–c Basidiomata. d Basidiospores. e Basidia. f Hyphae of pileal squamules. Scale bars: a–c = 5 cm, d–f = 20 µm.

Figure 8.10 Basidiomata and morphological characteristics of *Armillaria melleoasian* subsp. *macrospora*

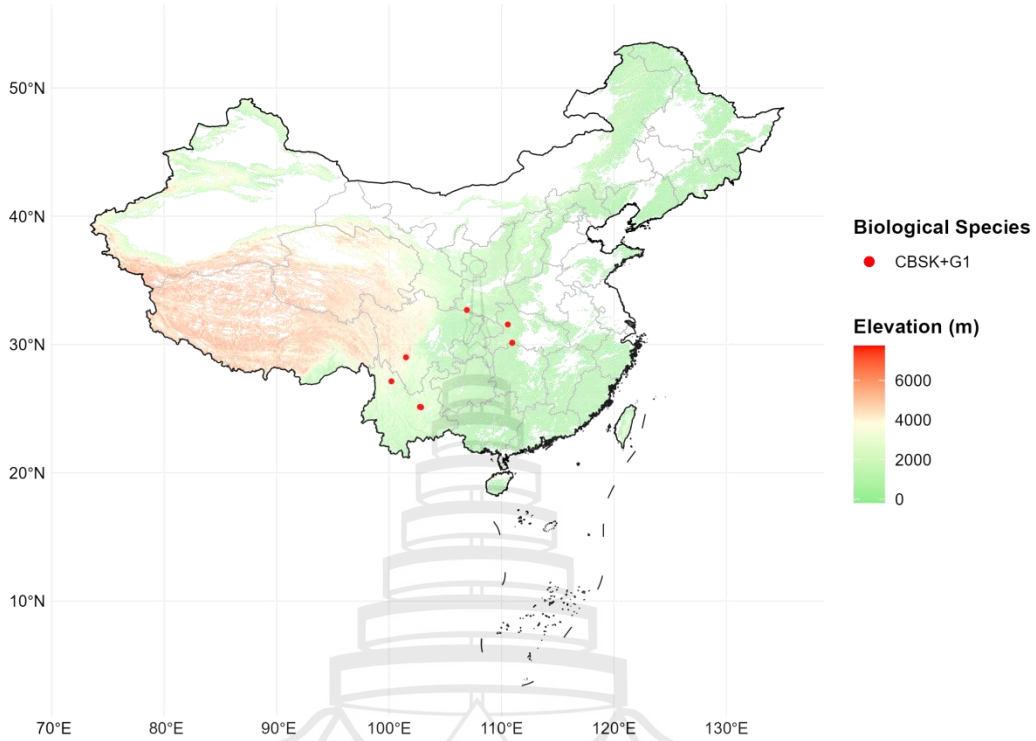


Figure 8.11 Distribution of samples of *Armillaria melleoasian* subsp. *macrospora* used in this study

Distribution: Central and southwest China.

Additional material examined: **CHINA**, **Yunnan**, Shaoxia Village, Kunming, 102.8153°E, 25.1196°N, 22KM01 (strain); Shaoxia Village, Kunming, 102.8162°E, 25.1203°N, HKAS 135514 (specimen); Shaoxia Village, Kunming, 102.8165°E, 25.1212°N, 22KM02 (strain); Inside the Botanical Institute of Kunming City, Panlong District, Kunming City, 102.7427°E, 25.1379°N, HKAS 52389; Jade Dragon Snow Mountain, Yulong Naxi Autonomous County, Lijiang City, 100.2106°E, 27.1294°N, HKAS 68003; Sanjia Village, Shuanglong Township, Panlong District, Kunming City, 102.8492°E, 25.1100°N, HKAS 82475. **Hubei**, Yangzixi, Houhe Nature Reserve, Wufeng Tujia Autonomous County, Yichang City, 110.9500°E, 30.1333°N, CBSK19083 (strain); Yangzixi, Houhe Nature Reserve, Wufeng Tujia Autonomous County, Yichang City, 110.9500°E, 30.1333°N, CBSK19105 (strain); Xujiazhuang, Shennongjia Forest Region, 110.5573°E, 31.5599°N, HKAS 86591. **Sichuan**, about 45 km in the direction of Jiulong County to Mianning County, Ganzi Tibetan Autonomous

Prefecture, 101.5073°E, 29.0003°N, HKAS 49004; Micangshan National Forest Park, Wuguang Town, Nanjiang County, Bazhong City, 106.9156°E, 32.6926°N, HKAS 135553. Japan: Null, Null, HKAS 86588; Null, Null, HKAS 86589. **Africa**, Null, Null, HKAS 86598. **Kenya**, Null, Null, HKAS 86600. **USA**, Moutampa, Null, Null, guo256 (strain).

Average nuclear Weir & Cockerham's F_{ST} vs. the closest species (*A. melleasiana* subsp. *melleasiana*): 0.06.

Average mitochondrial dxy vs. the closest species (*A. melleoamericana*): 0.10.

Average mitochondrial ΦST vs. the closest species (*A. melleoasian* subsp. *macrospora*): 0.97.

Notes: *Armillaria melleasiana* subsp. *macrospora* shows only minor morphological differences from *A. melleasiana* subsp. *melleasiana* and exhibits very low nuclear genetic divergence (F_{ST} = 0.06). Therefore, it is not appropriate to elevate it to the rank of a distinct species, and it is here provisionally treated as a subspecies. According to the phylogenetic analyses conducted in this study, *A. melleasiana* subsp. *macrospora*, *A. melleasiana* subsp. *melleasiana*, the European *A. mellea*, and the North American *A. melleoamericana* together constitute a supercomplex. Notably, each of these independent lineages is often intermixed with samples from other continents, suggesting that the internal phylogenetic relationships of this supercomplex warrant further investigation.

Armillaria pseudoostoyae J.W. Liu, F.Q. Yu & Zhu L. Yang, ***sp. nov.,*** Figures 8.12－8.13

Biological species: No biological species information available.

Etymology: Pseudoostoyae, the specific epithet pseudoostoyae is derived from the Greek prefix pseudo- meaning "false" or "resembling" and the name ostoyae, which refers to the species *Armillaria ostoyae*.

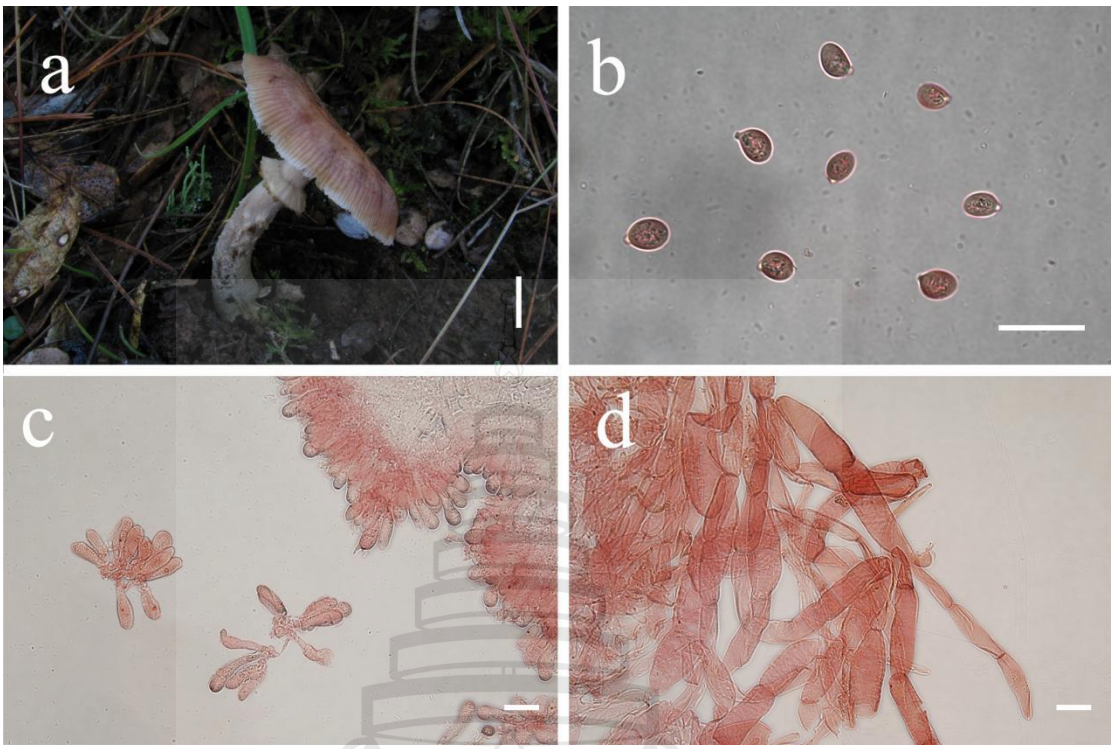
Holotype: **CHINA**, **Yunnan**, Lijiang City, Yulong Naxi Autonomous County, 26.8216°N, 100.2355°E, (**holotype**, HKAS 56108).

Basidiomata tricholomatoid, small to large, occurring singly or scattered. Pileus 4－7 cm in diameter, initially hemispherical in young specimens, later expanding to a plano-convex shape. **Pileus surface** is covered with grayish-white to brownish scales, denser toward the center, with the surface displaying pale brown to honey-yellow hue and partially

purplish-brown areas. **Margin** has distinct striations, 0.5－1 cm wide. **Lamellae** are decurrent, nearly white when young, becoming dingy white to pale brown as they mature, moderately spaced, unequal in length, with smooth edges. **Stipe** is 8－10 cm long and 0.4－1.1 cm in diameter, tapering slightly toward the top and thickening downward. The upper part of the stipe is white to dingy white, gradually transitioning to deep dingy white to blackish-gray at the base, covered with reflexed fibrous scales. **Annulus** present, band-like, membranous, relatively thin, white to grayish-white, with parts slightly tinged with brown.

Basidiospores: [30/1/1] (6.69)7.49－9.63(9.72) × (4.88)4.98－7.6(7.75) μm, (Q = (1.14) 1.15－1.51(1.54), Qm = 8.48±0.69), subglobose, broadly ellipsoid to ellipsoid, inamyloid. **Basidia** 27－35 × 8－10 μm, clavate, 2 or 4 spored, often with a basal clamp connection; sterigmata 4－6 μm long. **Pileal squamules surface** consist of nearly longitudinally palisaded, spindle-shaped or elliptical cells (60－100 × 12－25 μm), containing brown to yellowish-brown intracellular pigments. The terminal cells (30－40 × 12－15 μm) are spindle-shaped, mostly slender.

Ecology/Substrate/Host: clustered on rotten wood of Fagaceous plants in subtropical evergreen broad-leaved forests.



Note a Basidiomata. b Basidiospores. c Basidia. d Hyphae of pileal squamules. Scale bars: a = 5 cm, b–d = 20 µm.

Figure 8.12 Basidiomata and morphological characteristics of *Armillaria pseudoostoyae* (HKAS 56108, holotype)

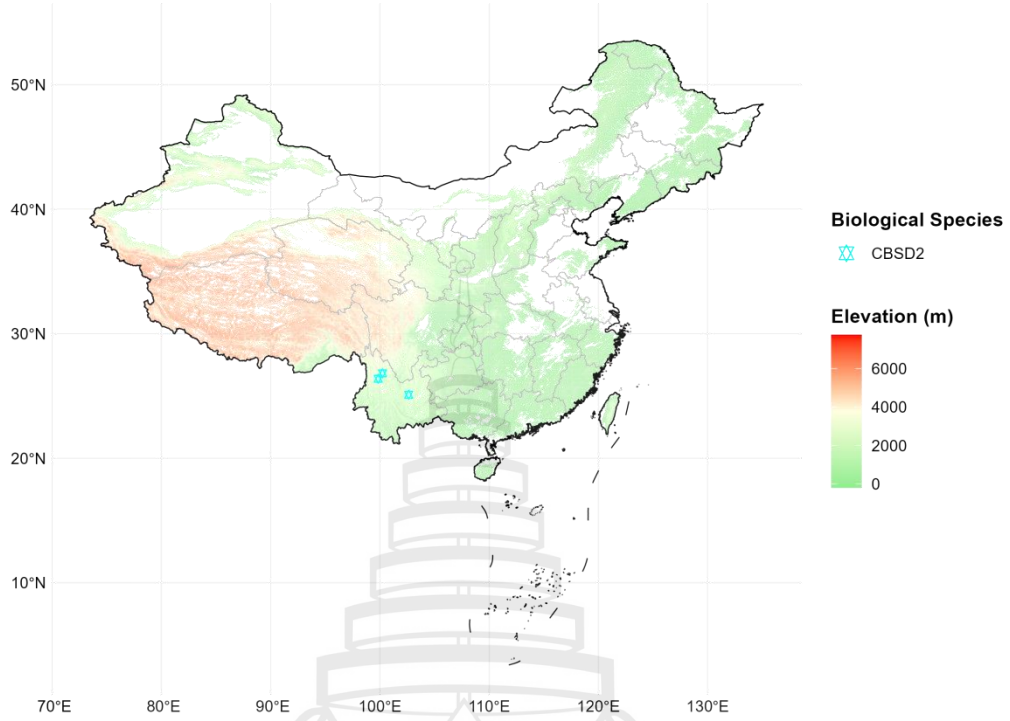


Figure 8.13 Distribution of samples of *Armillaria pseudoostoyae* used in this study

Distribution: Currently known only from Yunnan Province, China.

Additional material examined: **CHINA**, **Yunnan**, Kunming City, Wuhua District, Miaogao Temple, 25.0980°N, 102.6314°E, HKAS 50184; Dali Bai Autonomous Prefecture, Jianchuan County, Shibao Mountain, 26.3929°N, 99.8417°E, HKAS 58853.

Average nuclear Weir & Cockerham's F_{ST} vs. the closest species (*A. conifericola*): 0.24.

Average mitochondrial dxy vs. the closest species (*A. ostoyae*): 0.05.

Average mitochondrial ΦST vs. the closest species (*A. ostoyae*): 0.68.

Notes: In the nuclear species tree, *Armillaria pseudoostoyae* forms a distinct clade together with *A. borealis* subsp. *borealis* and *A. borealis* subsp. *sinoborealis*, with strong support (MLBS = 100; Figure D1). In contrast, in the mitochondrial phylogeny, *A. pseudoostoyae* is resolved as the sister taxon to *A. ostoyae*, also with strong support (MLBS = 100; Figure D1). Genetic differentiation analyses show that *A. pseudoostoyae* exhibits substantial divergence from its closest relatives, with nuclear F_{ST} = 0.24,

mitochondrial dxy = 0.05, and ΦST = 0.68. These results support its recognition as an independent species. Morphologically, *A. pseudoostoyae* is distinguished by its basidiospore size (7.49－9.63 × 4.98－7.6 μm). Geographically, it is currently known only from southwestern China.

Armillaria tabescens* subsp. *orientala J.W. Liu, F.Q. Yu & Zhu L. Yang, ***subsp. nov.,*** Figures 8.14－8.15

Biological species: Chinese biological species I (CBSI).

Etymology: orientala (Lat.), referring to its origin from East Asia.

Holotype: **CHINA**, **Yunnan**, Xishuangbanna Dai Autonomous Prefecture, Mengla County, Wangtianshu Scenic Area, 21.5961°N, 101.5876°E, alt 898 m, LJW282 (**holotype**, KUN-HKAS 91090).

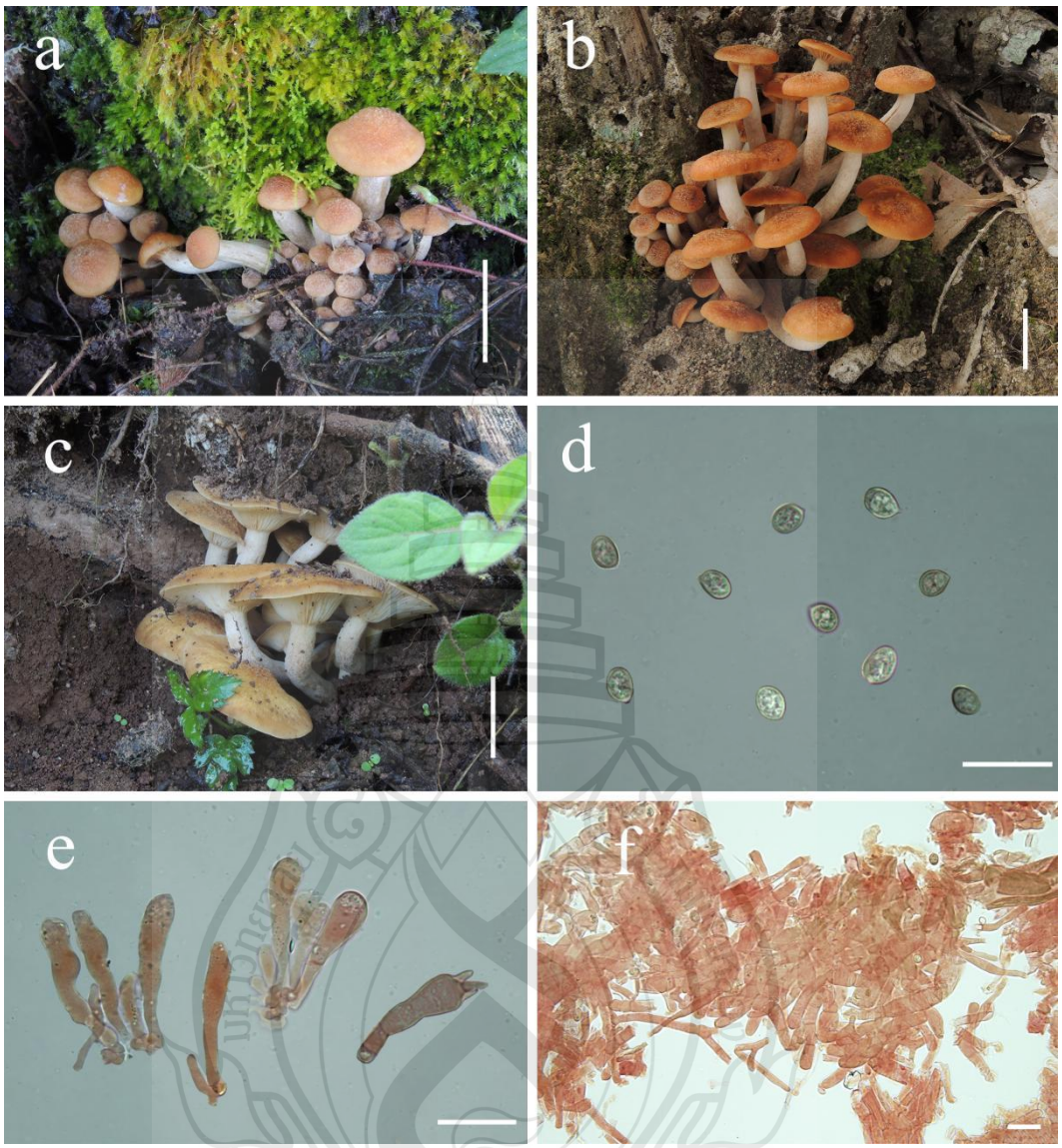
Basidiomata tricholomatoid, pileus is small to large, clustered, 2－8 cm in diameter, initially nearly hemispherical, then gradually expanding to convex or nearly flat, often with a central umbo. The surface of the pileus is covered with grayish-white scales, denser at the center, and varies in color from gray-brown to pale brown and honey yellow. **Lamellae** are nearly adnate, initially almost white, turning dingy white to pale brown at maturity, moderately spaced, unequal in length, with smooth edges. **Stipe** is 5－13 cm long and 0.4－1.1 cm in diameter, nearly cylindrical, solid; the surface of the upper stipe is white, yellowish-white to pale yellow, gradually transitioning to pale brown, brown, or dark brown toward the base. **Annulus** absent.

Basidiospores: [143/4/4] (5.26)7.0－9.5(9.85) × (4.77)5.2－7.3(7.77) μm, (Q = (1.03)1.12－1.54, Qm = 1.34±0.12), subglobose, broadly ellipsoid to ellipsoid, inamyloid. **Basidia** 30－39 × 7－10 μm, clavate, occasionally with thickened walls, usually with four sterigmata **Sterigmata** are 2－5 μm long; the base of the basidia features clamp connections. **Pileal squamules surface** consists of nearly longitudinally palisaded, spindle-shaped to cylinder-shaped cells (14－50 × 5－20 μm).

Ecology/Substrate/Host: clustered on rotten wood of fagaceous plants in subtropical evergreen broad-leaved forests.

Distribution: Widely found across Asian countries, including China, South Korea, and Japan. In China, it is distributed throughout most provinces.

Additional material examined: **CHINA**, **Yunnan**, Puér State, Nuozhadu Dam, 22.6230°N, 100.4397°E, AT (strain); Lincang City, Fengqing County, Xiaowan Township, 24.6761°N, 100.0774°E, HKAS 58683; Dali Bai Autonomous Prefecture, Yongping County, National Highway 320 at 3295 km, 25.5144°N, 99.7759°E, HKAS 58910. Chuxiong Yi Autonomous Prefecture, Nanhua County, Longshan Reservoir, 25.3278°N, 101.2782°E, HKAS 126372. **Beijing**, Haidian District, Beijing Zoo, 39.9333°N, 116.3166°E, CBSI99122 (strain); Xicheng District, Beijing Zoo, 39.420°N, 116.3366°E, HKAS 86603. **Shaanxi**, Ankang City, Zhenping County, Niutoudian Town, Shuijingping Village, 32.1054°N, 109.5726°E, HKAS 80228. **Hunan,** Yizhang County, Tiantai Mountain Scenic Area, Mangshan National Reserve, 24.9490°N, 112.9490°E, MHHNU 8836. **Guizhou**, Qiannan Buyi and Miao Autonomous Prefecture, Longli County, Yangchang Town, 26.2784°N, 107.0469°E, SX_M1 (strain). **South Korea**, **Chungcheongbuk-do**, Cheongju, Chungbuk National University, 36.6286°N, 127.4511°E, NC_042769 (https://www.ncbi.nlm.nih.gov/nuccore/NC_042769).



Note a–c Basidiomata, photos by Jianwei Liu. d Basidiospores. e Basidia. f Hyphae of pileal squamules. Scale bars: a–c = 5 cm, d–f = 20 µm.

Figure 8.14 Basidiomata and morphological characteristics of *Armillaria tabescens* subsp. *orientala* (HKAS 91090, holotype)

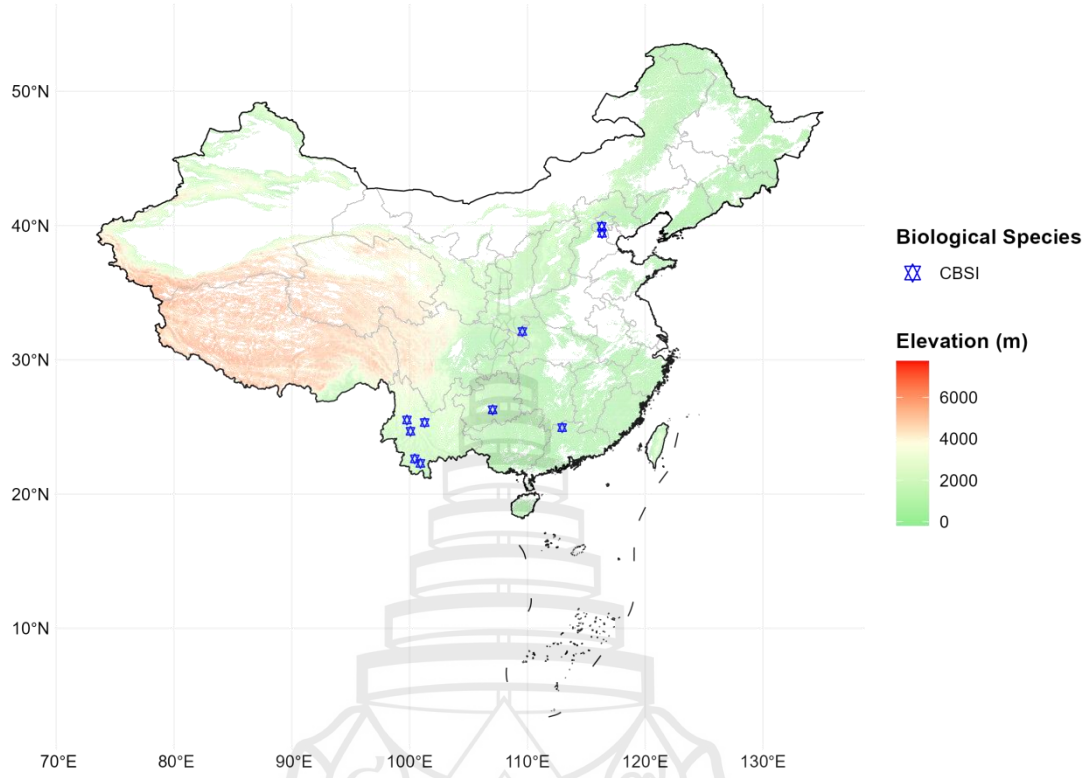


Figure 8.15 Distribution of samples of *Armillaria tabescens* subsp. *orientala* used in this study

Average Weir & Cockerham's F_{ST} of the nuclear genome vs the closest species *A. tabescens* subsp. *tabescens*: No data available.

Average dxy vs the closest species *A. tabescens* subsp. *tabescens* in motichondria: 0.07.

Average ΦST vs the closest species *A. tabescens* subsp. *tabescens* in motichondria: 0.80.

Notes: According to the mating experiments of Qin et al., (2007), *Armillaria tabescens* subsp. *orientala* and *A. tabescens* subsp. *tabescens* are fully mating compatible, representing a single biological species. Phylogenetically, the two lineages form distinct and well-supported clades in both nuclear and mitochondrial gene trees (MLBS = 100; Figure D1－2). Although nuclear genomic differentiation between the two lineages could not be assessed due to limited sampling, mitochondrial analyses revealed a dxy of 0.07 and ΦST of 0.80, indicating a moderate level of genetic

divergence. In addition, the two lineages are geographically separated, occurring in Asia and Europe, respectively. Therefore, we recognize them as two subspecies of *A. tabescens*.

Armillaria tabescens* subsp. *tabescens (Scop.) J.W. Liu, F.Q. Yu & Zhu L. Yang, ***comb. nov.***

Biological species: No biological species information available.

This species was redescribed as a new combination by Koch et al. (2017) from Spain, Europe, and the Northern Hemisphere.

Pilei 3.4—5.2 cm in diameter, transitioning from convex to flattened with age and often featuring a central umbo. **Margin** is inrolled and slightly striate, while the reddish-brown cuticle is adorned with small dark brown scales. **Lamellae** are decurrent, pinkish in color, and have smooth edges. **Stipe** 2.8—7.5 cm in length and 1—5 mm in diameter, is cylindrical, longitudinally striate, and darkens towards the base. The odor is not noticeable (Koch et al., 2017).

Basidiospores are subglobose to ellipsoidal, smooth, hyaline, gutulate, and apiculate, with dimensions of (6.7)7.4—9.2(10.2) × (5.0)5.5—6.8(7.9) µm and a mean Q value of 1.4. **Cystidia are polymorphic** clavate with elongated apices, and (19.0)23.7—47.9(59.5) × (5.0)5.5—9.7(10.0) µm on average. **Basidia** (29.9)39.0—49.0(50.9) × (7.1)7.6—9.3(9.7) µm on average, cylindrical to clavate, tetrasporic, and lack clamp connections. **Pileal squamules** consist of parallel hyphae with fusiform to cylindrical, short, yellowish-brown pigmented terminal hyphae, and lack clamp connections (Koch et al., 2017).

Ecology/Substrate/Host: This species was found on soil over buried wood under *Quercus suber* and *Quercus faginea.*

Distribution: Now known to be distributed in Europe.

New research specimens: **Italy**, **Messina**, guo 262 (strain).

Average nuclear Weir & Cockerham's F_{ST} vs. the closest species: No data available.

Average mitochondrial dxy vs. the closest species (*A. tabescens* subsp. *orientala*): 0.07.

Average mitochondrial ΦST vs. the closest species (*A. tabescens* subsp. *orientala*): 0.80.

Notes: This subspecies corresponds to the European lineage of the *A. tabescens* complex, formally combined by Koch et al. (2017). It is currently known only from Europe, where it typically occurs on soil above buried wood of *Quercus* species. Morphologically, it agrees with descriptions of *A. tabescens* sensu stricto. The phylogenetic analyses consistently separate this lineage from the Asian *A. tabescens* subsp. *orientala*. In light of its morphological stability, European distribution, and phylogenetic distinctness, it is here recognized as a subspecies within *A. tabescens*.

Armillaria xiaocaobaensis J.H. Peng & C.L. Zhao, *Mycotaxon* 135(2): 436 (2019), Figure 8.16

Mycobank: MB 832231

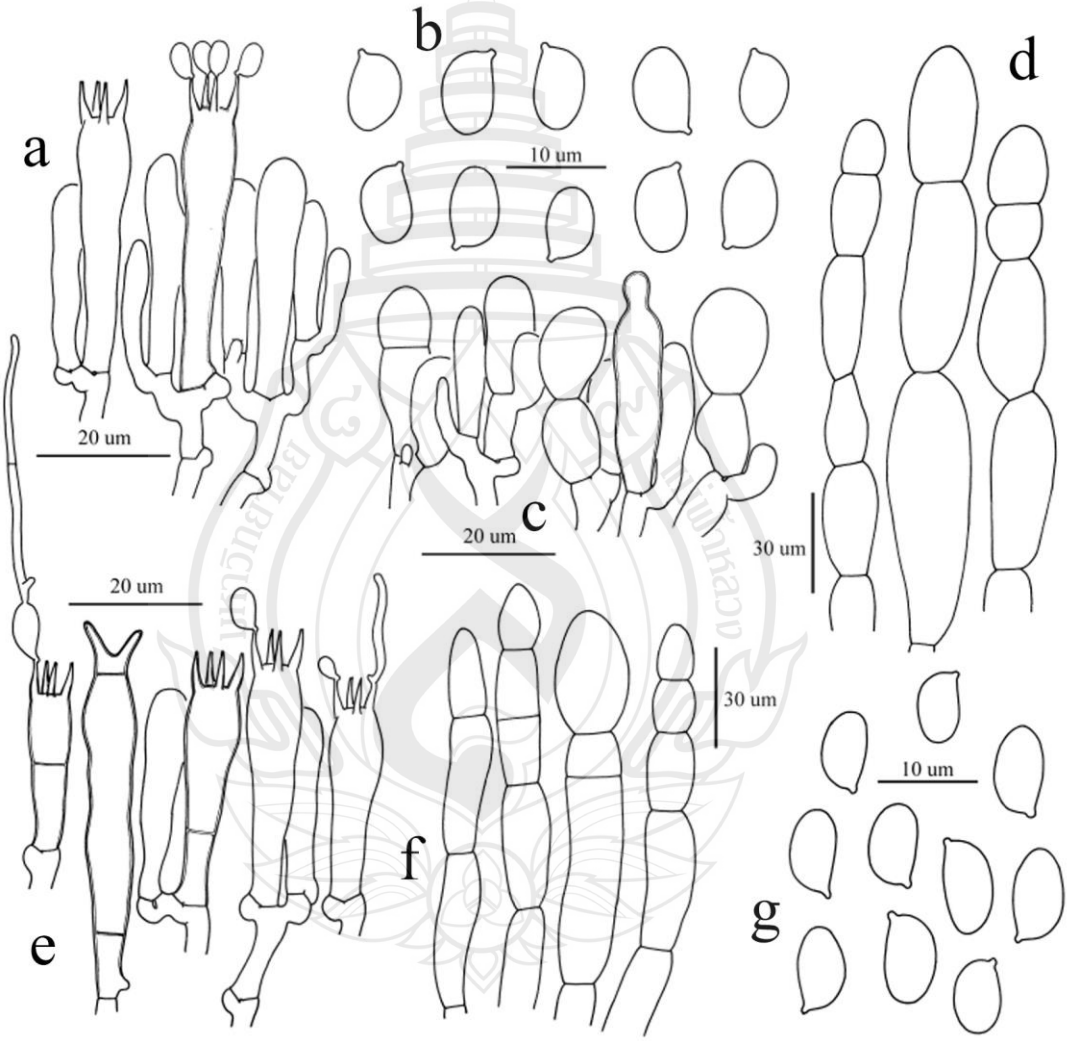
Biological species: No biological species information available.

This species was described from the Northern Hemisphere, Asia, and Southwest China by Peng and Zhao (2020).

Basidiomata are small to large, solitary or clustered, with the lower part of the stipe often fused. Pileus is 3—10 cm, initially nearly hemispherical, and later expanding to nearly plane with a central bump, edges feature radiating striations, which extend about one-third to one-half of the radius. The central part is orange-yellow to reddish-brown, fading to pale yellow to pale brown towards the edges; the center is covered with fine brown to dark brown scales. **Lamellae** are decurrent, initially white and later turning off-white to pale brown when mature, sparse, uneven in length, and smooth at the edges. **Stipe** is 4—12 cm long, 0.5—1.3 cm in diameter, near cylindrical, solid, and often swollen at the base, surface is pale yellow and gradually darkens from pale brown to dark brown toward the base, with a lighter color above the annulus. The annulus is superior, thin, membranous, near white to pale yellow, and often persistent. **Basidiospores** (6.5) 7—9.5 (10.5) × (4)4.5—5.5 (6.5) µm [Q = (1.36) 1.50—1.89 (2.02), Q = 1.65 ± 0.15], ellipsoid to oval or teardrop-shaped, thin-walled to slightly thick-walled, colorless to nearly colorless, smooth, non-starchy, and non-dextrinoid. The spore walls are blue-staining, with small pointed tips. There is no apical pore. **Basidia** (28) 32—50 × 7—9 µm, clavate, thin-walled, occasionally slightly thick-

walled, with 4 sterigmata, sometimes with 1 or 2 sterigmata. **Sterigmata** are 4—5 μm long. The basidium base shows a clamp connection. **Cheilocystidia** are present. **Pleurocystidia** are absent.

Ecology/Substrate/Host: This species can be found on fallen angiosperm trunks, dead stumps of *Betula albosinensis*, fallen trunks of *Fagus* sp., fallen trunks of *Sycopsis sinensis*, dead stumps of *Cerasus pseudocerasus*, rotting fallen trunks of *Salix babylonica*, and rotten wood of *Abies* sp.



Note a, e Hymenium. b, g Basidiospores. c Cheilocystidia. d, f Hyphae of pileal squamules. Drawings by Zhuliang Yang. Scale bars: a–c = 5 cm.

Figure 8.16 Basidiomata and morphological characteristics of *Armillaria xiaocaobaensis* (SWFC 12638, holotype)

Average nuclear Weir & Cockerham's F_{ST} vs. the closest species: No data available.

Average mitochondrial dxy vs. the closest species: No data available.

Average mitochondrial ΦST vs. the closest species: No data available.

Notes: The main characteristics of *A. xiaocaobaensis* include its small to large basidiomata, with the central part of the cap covered by tiny brown to dark brown scales. The annulus is thin, membranous, and persistent, while the base of the basidium exhibits a clamp connection. The basidiospores are elongated to ellipsoidal, and the cystidia at the edge of the basidium are often vesicular. The terminal cells of the cap scales are mostly short and broad.

Based on the molecular phylogenetic analysis conducted by the authors of this study, the biological species "Nag. E" is identified as *A. xiaocaobaensis*. In their original description, Peng and Zhao (2020) noted that *A. xiaocaobaensis* lacked clamp connections. However, the authors of this volume have examined the type specimen SWFC 12638 and another specimen cited in the aforementioned paper, SWFC 12639, and found both to exhibit abundant clamp connections. It is important to note that these two specimens may have been collected at a later stage of maturity, or for other reasons, as many basidia have developed secondary septa. Some basidiospores had already begun germinating while still attached to the basidium, while others started germinating into primary mycelium directly on the small stalks of the basidium, even before forming basidiospores.

Qin et al. (2024) argued that it was procedurally invalid to recognize *Armillaria xiaocaobaensis* as a distinct species solely on the basis of the tef1α gene, without incorporating reproductive isolation as a criterion. Because tef1α sequences lack sufficient resolution to discriminate among closely related nascent species, the mechanism of balancing selection acting on tef1α alleles may result in several species sharing the same evolutionary lineage. Indeed, the IEL analysis in that study demonstrated that multiple *Armillaria* species could share a single tef1α lineage, while a single species could be partitioned into multiple tef1α lineages in the single-gene tree. As a consequence, only 55% of Chinese *Armillaria* isolates could be reliably distinguished at the species level using tef1α sequences.

This study confirmed that *A. xiaocaobaensis* is the same species as *A. pungentisquamosa*. Although the principle of nomenclatural priority would treat *A. pungentisquamosa* (CBSP) as a synonym of *A. xiaocaobanensis*, we do not follow this treatment here. Historically, *Armillaria* has undergone an extremely complex taxonomic treatment until a global consensus was gradually established that species delimitation should primarily rely on the biological species concept. This framework has brought a certain degree of stability to the classification of this difficult genus. Previous studies have shown that, due to the influence of incomplete lineage sorting and other factors, species cannot be reliably identified by single-gene phylogenetic analysis of tef1α without incorporating biological evidence. Therefore, in studies of *Armillaria*, we recommend giving priority to the biologically defined species recognized by the community, supplemented by genome-wide data or, at a minimum, multi-gene phylogenies. In the present study, biological species boundaries are corroborated by genome-scale evidence, which provides strong, independent confirmation of their validity. In contrast, reliance on a single gene or solely on morphological traits tends to revive endless "taxonomic disputes." Indeed, many species described in the past based only on single genes or morphology may actually represent multiple biological species within the same set of specimens. If nomenclatural priority were applied indiscriminately in such circumstances, it is foreseeable that the retrospective reclassification of historical material based on genomic data would inevitably lead to major confusion.

Armillaria tibetica G.F. Qin, Han C. Wang, Jun Zhao, Yuan Yuan & Y.C. Dai, *Mycology* 16(2):801 (2024)

Index Fungorum number: IF 831861

Biological species: Chinese biological species J (CBSJ).

Described from the Northern Hemisphere, Asia, Southwest, Northwest, and Central China by Qin et al. (2024). In this study, this species formed one lineage in the nuclear phylogeny (Figure D1) and five lineages in the mitochondrial phylogenetic analysis (Figure D2), so we studied all five mitochondrial lineages below.

***Armillaria tibetica* (CBS J) lineage 1-mtDNA,** Figures 8.18－8.19

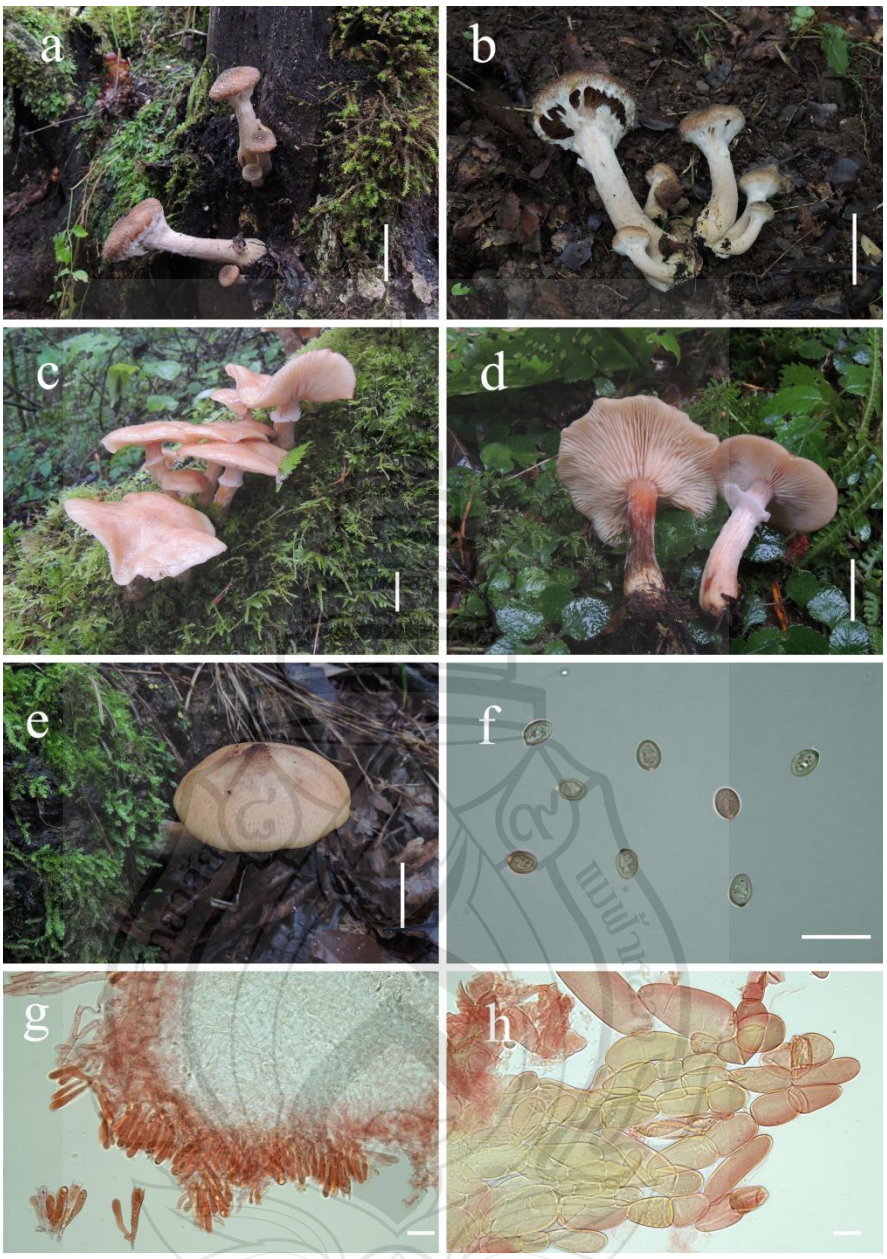
Pilei of the basidiomata are small to large-sized, 2.5－13 cm in diameter and 0.4 － 2.7 cm in thickness. Initially, they are hemispherical-convex to convex, occasionally with a mammilla, and later become plano-convex, applanate, depressed, or undulate, sometimes featuring an umbo. The caps are typically dry, though they can be hygrophanous. In their young stage, the cap margins display colors ranging from greyish orange to brown, while the center is pale brown to dark brown. As they mature, the margins transition to pale orange to violet-brown. The center of mature caps exhibits pale yellow to violet-brown hues. **Pileal surface** is covered with fine-velvety scales that are abundant, white or nearly white, and evenly distributed across the entire cap. These scales are not concentrated towards the center and tend to disappear as the cap matures or after rainfall. The cap margin is entire, usually slightly incurved, strongly striate, and sometimes bears remnants of white velar tissue. **Lamellae** are adnate with a decurrent tooth or sinuate attachment, extending downwards in striped ridges towards the annulus. They are white to orange-white when young, and transition to orange-white to brown when mature, with the presence of lamellulae, and have smooth margins. **Stipe** is central, 2.5－9.8 cm in length and 0.3－2.5 cm in diameter at the apex. It is cylindrical, clavate, or broadened at the base, with longitudinal striations. The stipe coloration varies: above the annulus, it is orange-white to reddish brown; the middle portion is orange-white to violet-brown; and the base is greyish orange to violet-brown. The stipe is covered with white, silky fibrillose velar remnants, which may resemble zigzag markings and tend to disappear when touched. The annulus is arachnoid, thin, ephemeral, and white or nearly white in color (Qin et al., 2024).

Basidiospores are ivory white in mass, ellipsoid in shape, and lack a suprahilar depression (5.31)7.5－10.0(10.83) × (4.04)5.03－7.74(8.53) μm, with a Q ranging from (0.97)1.12－1.64(2.0) and an average Qm of 1.35 ± 0.16. **Basidia** are clavate, 25 －48 × 7－10 μm, with the upper portion constricted or the constriction being inconspicuous with a clamp connection at the base, are four-sterigmate, and are usually thin- to slightly thick-walled, with a yellowish green to brownish yellow coloration. The pigments of the basidia gradually disappear in KOH, and occasionally, thick-walled basidia (≤ 1.5 μm thick) are formed when the lamellae develop abnormally.

Sterigmata 2.0－6.0 μm in length. **Cheilocystidia** 10.5－49 × 4－17 μm and are polymorphic, appearing as clavate, fusiform, cylindrical, elliptical, or ovoid. They have a clamp connection at the base and may feature a papilla or an irregularly branched papilla at the apex. These structures are thin- to slightly thick-walled (≤ 0.5 μm), nearly hyaline, and range in color from greenish blue to brownish yellow. They form a compact, sterile edge on the lamellae that is easily broken and disappears. **Pleurocystidia** (cystidia on the gill faces) are absent. **Pileal squamules** (scales) are composed of parallel, cylindrical, slightly thick-walled (≤ 1.5 μm) hyphae. These hyphae are simple septate (with cross-walls), greenish blue, grey to brownish yellow in color, with 14－110 × 5－22 μm (Qin et al., 2024).

Ecology/Substrate/Host: clustered on rotten wood of Fagaceous plants in subtropical evergreen broad-leaved forests.

Distribution: Distributed in central China.



Note a–e Basidiomata. f Basidiospores. g Basidia. h Hyphae of pileal squamules. Scale bars: a–e = 1 cm, f–h =20 µm.

Figure 8.17 Basidiomata and morphological characteristics of *A. tibetica* (CBS J) lineage 1-mtDNA

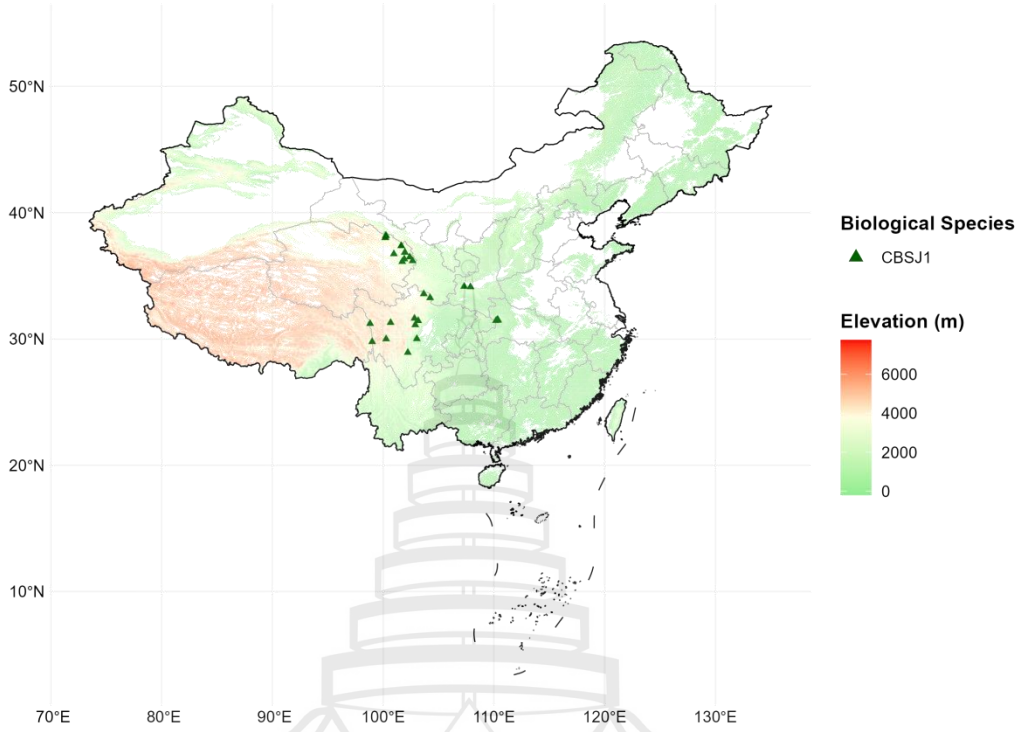


Figure 8.18 Distribution of samples of *A. tibetica* (CBS J) lineage 1-mtDNA used in this study

Additional material examined: **CHINA**, **Hubei**, Shennongjia, Taiziya, 31.4472°N, 110.1931°E, HKAS 135496; Shennongjia, Jinhouling, 31.4762°N, 110.3085°E, HKAS 135497; Shennongjia Mountain, Shennongjia Forest Region, 31.5166°N, 110.3166°E, CBSJ04043 (strain). **Shaanxi**, Baoji City, Mei County, Taibai Mountain, 34.1166°N, 107.8833°E, CBSJ05018 (strain). **Yunnan**, Diqing Tibetan Autonomous Prefecture, Shangri-La County, Shangri-La Grand Canyon, 28.3318°N, 99.4628°E, HKAS 46283 (specimen). **Sichuan**, Liangshan Yi Autonomous Prefecture, Mianning County, Zhile Nature Reserve, 28.9229°N, 102.2294°E, HKAS 48936; Ganzi Tibetan Autonomous Prefecture, Luhuo County, 25 km in the direction of Wenda, 31.2906°N, 100.6760°E, HKAS 49375; Ganzi Tibetan Autonomous Prefecture, Litang County, Junba Village, 29.9942°N, 100.2691°E, HKAS 51007; Ganzi Tibetan Autonomous Prefecture, Baiyu County, 31.2096°N, 98.8240°E, HKAS 51692; Aba Tibetan and Qiang Autonomous Prefecture, Jiuzhaigou County, Dalu Township, 33.5617°N, 103.6710°E, HKAS 89531; Aba Tibetan and Qiang Autonomous

Prefecture, Lixian County, 31.4358°N, 103.1632°E, HMAS 254250; Aba Tibetan and Qiang Autonomous Prefecture, Xiaojin County, Tricholoma matsutake reserve in Heshang Village, 31.1104°N, 102.9019°E, HMAS 274442; Aba Tibetan and Qiang Autonomous Prefecture, Lixian County, Jiabigou, Miyaluo Township, 31.6286°N, 102.8300°E, HMAS 274553; Aba Tibetan and Qiang Autonomous Prefecture, Jiuzhaigou County, Jiu Dao Guai, Shangsi Village, 33.2520°N, 104.2426°E, HMAS 274644; Ya'an City, Yucheng District, Yajiang, 30.0099°N, 103.0415°E, HMAS 50996 (specimen). **Tibet Autonomous Region**, Changdo City, Mangkang County, Zhubalong Township, 29.7757°N, 99.0097°E, HKAS 89629 (specimen). **Qinghai**, Northern Tibetan Autonomous Prefecture, Qilian County, Babao Township, 38.0166°N, 100.2000°E, HMAS 130389; Huzhu Tu Autonomous County, Nanmenxia Township, Haidong City, 36.8500°N, 101.9666°E, HMAS 130603; Northern Tibetan Autonomous Prefecture, Menyuan Hui Autonomous County, Xianmi Farm, 37.3666°N, 101.6333°E, HMAS 132012; Xigou Township, Haidong Citizen and Hui and Tu Autonomous County, Xigou state-owned forest farm, 36.1793°N, 102.6591°E, HMAS 132015; Xining City, Huangyuan County, Halihe, Shiligou, 36.7300°N, 100.9690°E, HMAS 26066; Haidong City, Ledu District, 36.4822°N, 102.4016°E, HMAS 26067; Haidong City, Ping'an District, Sitai Township, Xiaqunsi Forest Park, 36.3236°N, 101.9084°E, HMAS 276211; Huangnan Tibetan Autonomous Prefecture, Jianzha County, Cambra National Forest Park, 36.1168°N, 101.7234°E, HMAS 276224.

***Armillaria tibetica* (CBS J) lineage 2-mtDNA**, Figures 8.20－8.21

Basidiomata tricholomatoid, small to large, solitary, scattered, or clustered. **Pileus** 3－9 cm in diameter, initially nearly hemispherical to convex, and is densely covered with fibrous or conical scales in gray, dark gray to black, which are more concentrated towards the center. **Pileus surface** varies in color from brown, yellow-brown, honey-colored to dirty brown, with conspicuous striations 0.6－1.2 cm wide on the margin when mature. **Lamellae** are nearly adnate, whitish when young, becoming dirty white to pale brown as they mature, relatively sparse, unequal in length, and with smooth edges. **Stipe** is 4－12 cm long and 0.3－1.5 cm in diameter, nearly cylindrical, slightly tapering upward, and solid. The upper stipe surface is white, gradually turning gray-white to brown at the base, with gray-black to black fibrous or floccose scales.

Annulus present, membranous, white, and becomes inconspicuous upon maturation due to shrinkage.

Basidiospores: [160/5/5] (7.3)8.14－10.52(12.16) × (6.36)5.74－7.75 (9.19) μm, (Q = (1.03)1.1－1.63(1.97), Qm = 1.34 ± 6.16), subglobose, broadly ellipsoid, ellipsoid to elongate, inamyloid. **Basidia** 27－32 × 7－10 μm, clavate, 2 or 4 spored, often with basal clamp connections; sterigmata 4－5 μm long. **Pileal squamules surface** consists of nearly longitudinally palisaded, spindle-shaped to elliptical cells (65－85 × 10－20 μm), containing brown to yellowish-brown intracellular pigments.

Ecology/Substrate/Host: Clustered on rotten wood of Fagaceous plants in subtropical evergreen broad-leaved forests.

Distribution: Currently found in the subalpine regions of the Hengduan Mountains, situated in the southwestern part of China.



Note a–e Basidiomata. f Basidiospores. g Basidia. h Hyphae of pileal squamules. Scale bars: a–e = 5 cm, f–h = 20 µm.

Figure 8.19 Basidiomata and morphological characteristics of *A. tibetica* (CBS J) lineage 2-mtDNA

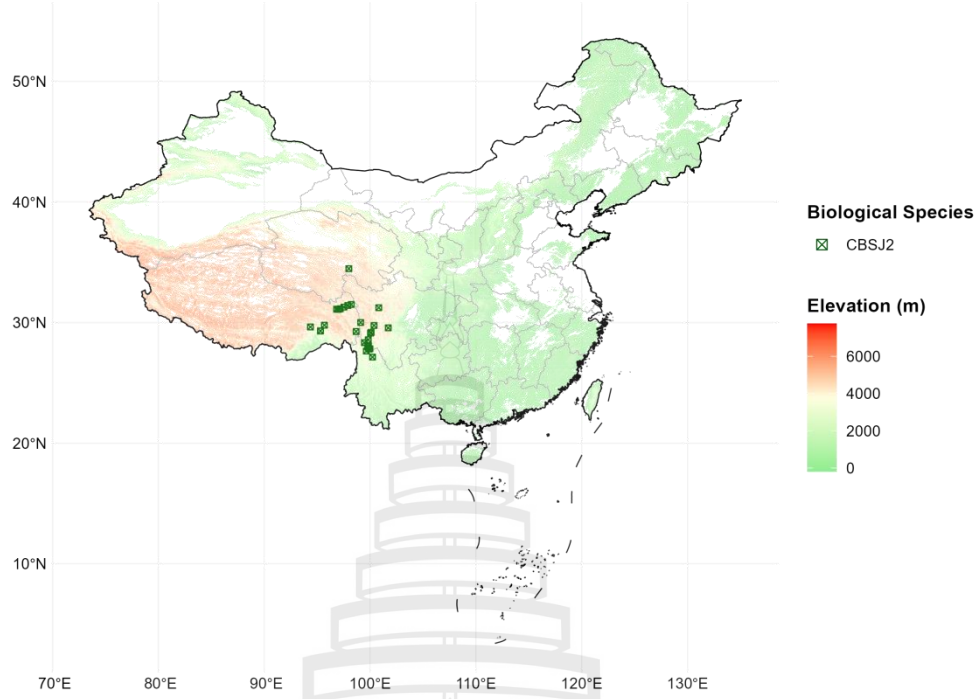


Figure 8.20 Distribution of samples of *A. tibetica* (CBS J) lineage 2-mtDNA used in this study

Additional material examined: **CHINA**, **Tibet Autonomous Region**, Near Qiongka Bridge, Karuo District, Changdu City, 31.1435°N, 97.1682°E, HKAS 45974; Near Jangda County, Changdu City, 31.4991°N, 98.2183°E, HKAS 45609; Mountain near Zhuge Village, Karuo District, Changdu City, 31.0958°N, 96.9998°E, HKAS 45688 ; Near Bini Village, Binda Township, Leiwuqi County, Changdu City, 31.1104°N, 96.8367°E, HKAS 45762; In the mountains near Zhuge Village, Karuo District, Changdu City, 31.0958°N, 96.9998°E, HKAS 45773; On the way from Changdo to Tuoba, Karuo District, Changdu City, 31.1428°N, 97.1704°E, HKAS 45807; On the way from Maodu to Toba, Karuo District, Changdu City, 31.2812°N, 97.5293°E, HKAS 45820; Near 317 road from Qamdo, Tibet to Derge County, Sichuan, 31.4117°N, 97.8966°E; Near Hongla Pass, Mangkang County, Changdu City, 29.2599°N, 98.6802°E, HKAS 82505; Zhagonggou, Milin Town, Linzhi District, 29.7833°N, 95.6833°E, 2105604028 (strain); Bayi District, Linzhi City, 29.6333°N, 94.3666°E, CBSJ04028 (strain); Yadong County, Shigatse City, 27.9196°N, 87.3643°E, FM-X (strain); Motuo County, Linzhi City, 29.3046°N, 95.3189°E, HMAS

272511; Motuo County, Linzhi City, 29.3046°N, 95.3189°E, HMAS 272651. **Sichuan,** Batang County, Ganzi Tibetan Autonomous Prefecture, 30.0053°N, 99.1105°E, HMAS 48351; About 15km from Luoxu to Shambuka Pass, Shiqu County, Ganzi Tibetan Autonomous Prefecture, 34.4662°N, 97.9953°E, HKAS 49197; Near Xinsan Village, Cangdui Township, Daocheng County, Ganzi Tibetan Autonomous Prefecture, 29.1843°N, 100.0987°E, HKAS 51046; Near Jiawa Township, Litang County, Ganzi Tibetan Autonomous Prefecture, 29.7569°N, 100.3765°E, HKAS 93952; Xuehai Village, Renda Township, Luhuo County, Ganzi Tibetan Autonomous Prefecture, 31.2300°N, 100.8213°E, HKAS 93966; WuMing Mountain, Xiangcheng County, Ganzi Tibetan Autonomous Prefecture, 29.1314°N, 100.0426°E, HMAS 51091; Western slope of Gongga Mountain, Kangding City, Ganzi Tibetan Autonomous Prefecture, 29.5613°N, 101.7179°E, HMAS 51095. **Yunnan,** Shangri-La Shudu Lake Tourism Scenic Spot, Diqing Tibetan Autonomous Prefecture, 27.8025°N, 99.9065°E, HKAS 86609; Xuejiping, Geza Township, Shangri-La City, Diqing Tibetan Autonomous Prefecture, 28.0069°N, 99.8239°E, HKAS 135510; Xuejiping, Geza Township, Shangri-La City, Diqing Tibetan Autonomous Prefecture, 28.0069°N, 99.8239°E, HKAS 135511; Xuejiping, Geza Township, Shangri-La City, Diqing Tibetan Autonomous Prefecture, 28.0069°N, 99.8239°E, HKAS 135512; Red Mountain, Gezan Township, Shangri-La County, Diqing Tibetan Autonomous Prefecture, 28.0545°N, 99.7757°E, HKAS 54932; Daxue Mountain, Shangri-La County, Diqing Tibetan Autonomous Prefecture, 28.5731°N, 99.8270°E, HKAS 55489; Geza Township, Shangri-La City, Diqing Tibetan Autonomous Prefecture, 28.0316°N, 99.8437°E, HKAS 135478; Xiaotianchi, Shangri-La City, Diqing Tibetan Autonomous Prefecture, 27.6354°N, 99.6430°E, HKAS 135484; Pudacuo National Park, Shangri-La City, Diqing Tibetan Autonomous Prefecture, 27.8282°N, 99.9818°E, HKAS 135482; Pudacuo National Park, Shangri-La City, Diqing Tibetan Autonomous Prefecture, 27.8289°N, 99.9781°E, HKAS 135483; Lijiang Alpine Botanical Garden, Lijiang, 27.1385°N, 100.2323°E, date, collector, HKAS 135502.

***Armillaria tibetica* (CBS J) lineage 3-mtDNA**, Figures 8.22－8.23

Basidiomata tricholomatoid are small to large, solitary, scattered, or clustered. **Pileus** is 3－11 cm in diameter, convex when young, covered with dense fibrous or conical scales that are gray, gray-black to black, with denser scales in the central region. **Pileus surface** is flesh-colored, pale brown, honey-colored to dark brown, and develops distinct striations of 0.5－1 cm at the margin when mature. **Lamellae** are nearly adnate, whitish when young, becoming dirty white to pale brown when mature, relatively sparse, of unequal lengths, with smooth edges. **Stipe** is 4－8 cm long and 0.3－1.6 cm in diameter, nearly cylindrical, and gradually thickening from top to base. The upper part of the stipe is white, gradually turning brown, gray-black to black toward the base, and is covered with fibrous or floccose scales. **Annulus** present, membranous, white, and becomes inconspicuous as the mushroom matures.

Basidiospores: [144/4/4] 7.13(7.93)－9.87(11) × (4.51)5.1－7.0(7.9) μm, (Q = (1.18)1.22 － 1.65(1.83), Qm = 8.79 ± 0.64), broadly ellipsoid, ellipsoid to elongate, inamyloid. **Basidia** 30－37 × 8－10 μm, clavate, 2 or 4 spored, often with a basal clamp connection; sterigmata 4 － 5 μm long. **Pileal squamules surface** consists of nearly longitudinally palisaded, spindle-shaped to vesicular or elliptical cells (30－90 × 15－30 μm), containing brown to yellowish-brown intracellular pigments. The terminal cells (38 －55 × 8－12 μm) are contracted and spindle-shaped.

Ecology/Substrate/Host: clustered on rotten wood of fagaceous plants in subtropical evergreen broad-leaved forests.



Note a–c Basidiomata. d Basidiospores. e Basidia. f Hyphae of pileal squamules. Scale bars: a–c = 5 cm, d–f = 20 µm.

Figure 8.21 Basidiomata and morphological characteristics of *A. tibetica* (CBS J) lineage 3-mtDNA (herbarium no)

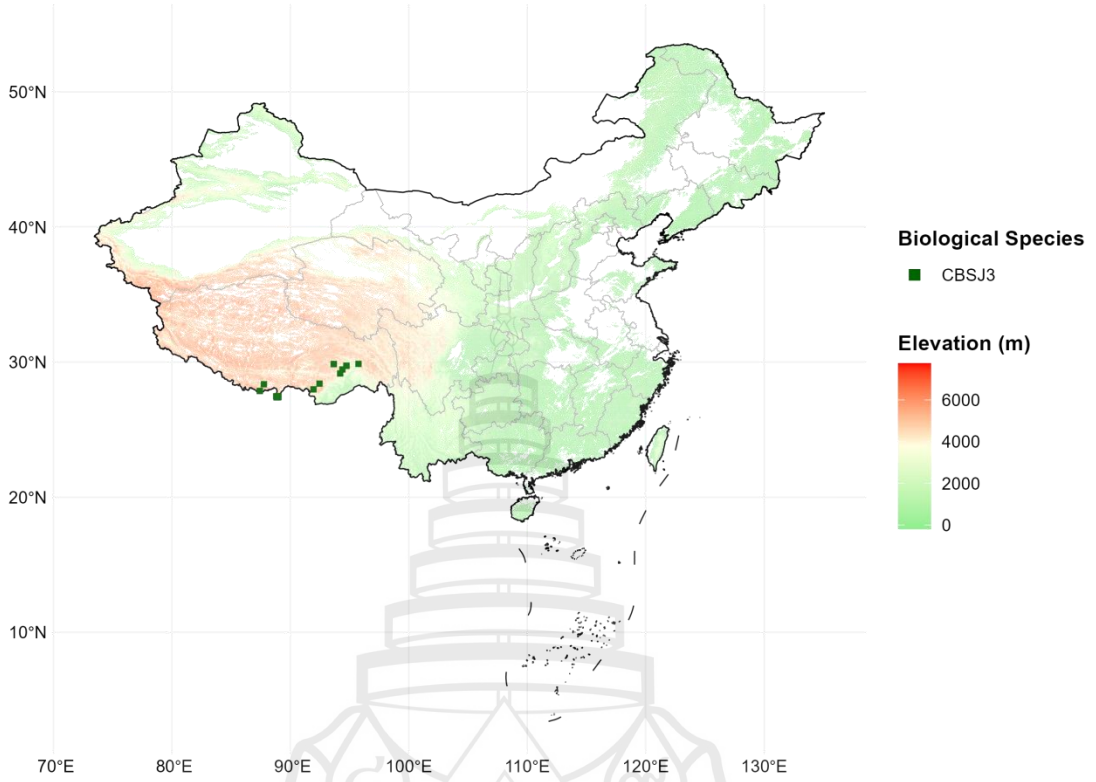


Figure 8.22 Distribution of samples of *A. tibetica* (CBS J) lineage 3-mtDNA used in this study

Distribution: Currently found in Southern Tibet, located in the southwestern region of China.

Additional material examined: **CHINA**, **Tibet Autonomous Region**, Cuona City, Shannan City, 27.9833°N, 91.9500°E, CBSJ04040 (strain); Gongtso Lake, Bayi District, Linzhi County, 29.7419°N, 94.7287°E, HKAS 51258; About 10km from Lulang Township, Bayi District, Linzhi County, 29.7228°N, 94.7339°E, HKAS 57133; Bahe Township, Gongbujiangda County, Linzhi City, 29.8607°N, 93.6652°E, HKAS 89549; Bahe Township, Gongbujiangda County, Linzhi City, 29.8601°N, 93.6652°E, HKAS 90943; Mountain behind Lamaling Monastery, Bujiu Township, Bayi District, Linzhi City, 29.4566°N, 94.3930°E, HKAS 94047; Naidui La Shan Pass, Xiayadong Township, Yadong County, Shigatse City, 27.3941°N, 88.8340°E, HMAS 254378; Chentang Town, Dingjie County, Shigatse City, 27.8629°N, 87.4233°E, HMAS 254476; Dingjie County, Shigatse City, 28.3641°N, 87.7658°E, HMAS 264994; Bomi

County, Linzhi City, 29.8704°N, 95.7495°E, HMAS 272485 ; Chentang Township, Dingjie County, Shigatse City, 27.8629°N, 87.4233°E, HMAS 274066; Nankou Inspection Station, Yadong County, Shigatse City, 27.4860°N, 88.9071°E, HMAS 274072; Xueshadong Township, Longzi County, Shannan City, 28.4074°N, 92.4617°E, HMAS 274889; Nanyigou, Yiluoba Nationality Township, Milin South, Linzhi City, 29.1598°N, 94.2064°E, HMAS 275000; Yadong County, Shigatse City, 27.4707°N, 88.7986°E, HKAS 135521; Yadong County, Shigatse City, 27.3964°N, 88.9673°E, HKAS 135520. Tibet Autonomous Region: Yadong County, Shigatse City, 27.4307°N, 88.9992°E, HKAS 135518.

***Armillaria tibetica* (CBS J) lineage 4-mtDNA**, Figures 8.24—8.25

Basidiomata tricholomatoid, small to large, occurring solitarily, scattered, or in clusters. **Pileus** diameter is 5—12 cm. When young, the cap is nearly hemispherical, gradually expanding to a convex shape. **Pileus surface** is covered with grayish-white to gray-black scales, denser at the center, with a cap surface ranging from grayish-white, pale gray, gray-brown, to dark brown. **Lamellae** are nearly adnate, white when young, turning dingy white to flesh-pink to brown as they mature, relatively sparse, unequal in length, with smooth edges. **Stipe** is 5—10 cm long and 0.8—1.5 cm in diameter, nearly cylindrical, with a swollen base covered in fibrous white scales. The upper part of the stipe is white, gradually transitioning to pale brown, brown, or dark brown towards the base. **Annulus** present, membranous, white, which shrinks easily upon maturity.

Basidiospores: [93/3/3] (6.36)6.6—9.26(9.94) × (4.85)5.23—7.12 (7.95) μm, (Q = (1.05)1.12 — 1.48(1.56), Qm = 1.36 ± 0.07), subglobose, broadly ellipsoid, ellipsoid, inamyloid. **Basidia** 30—45 × 6—10 μm, clavate, 2 or 4 spored, often with a basal clamp connection; sterigmata 4—5 μm long. **Pileal squamules surface** consists of nearly longitudinally palisaded, elliptical cells (60—80 × 5—15 μm), containing brown to yellowish-brown intracellular pigments.

Ecology/Substrate/Host: clustered on rotten wood of fagaceous plants in subtropical evergreen broad-leaved forests.

Distribution: Currently found in Xinjiang, situated in the northwestern part of China.

Additional material examined: CHINA, **Xinjiang Uygur Autonomous Region**, 74th Legion, Zhaosu County, Ilikazak Autonomous Prefecture, 42.6487°N, 80.2326°E, LJW668; Nalati Yangshugou, Xinyuan County, Ilikazak Autonomous Prefecture, 43.2833°N, 84.0166°E, CBSJ02044; Jiangbulake Scenic Spot, Qitai County, Changji Hui Autonomous Prefecture, 44.0200°N, 89.5879°E, HMAS 270241; Tomur Peak in Wensu County, Aksu Prefecture, 41.7738°N, 80.5763°E, HMAS 38334; Tianchi, Fukang City, Changji Hui Autonomous Prefecture, 44.2000°N, 88.0500°E, HMAS 99054; Dongdatang, Shawan County, Tacheng, 43.8540°N, 85.6716°E, HKAS 135474; Qiongkushtai Village, Tekes County, Ili Kazakh Autonomous Prefecture, 42.9122°N, 82.2059°E, MHHNU 10251; Nalati Town, Xinyuan County, Ili Kazakh Autonomous Prefecture, 43.2780°N, 84.2553°E, HKAS 135517; Gongnaisi Forest Farm, Gongnaisi Town, Hejing County, Ili Kazakh Autonomous Prefecture, 43.3008°N, 84.5449°E, HKAS 135516.



Note a–e Basidiomata. f Basidiospores. g Basidia. h Hyphae of pileal squamules. Scale bars: a–e = 5 cm, f–h= 20 µm.

Figure 8.23 Basidiomata and morphological characteristics of *A. tibetica* (CBS J) lineage 4-mtDNA (HKAS 135516)

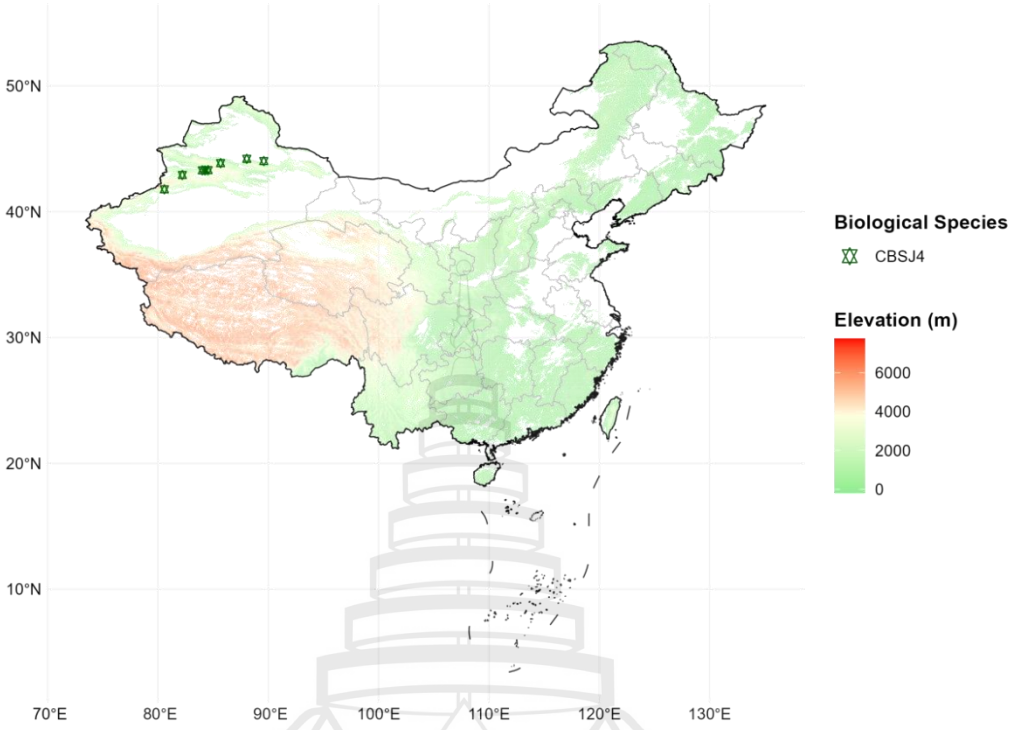


Figure 8.24 Distribution of samples of *A. tibetica* (CBS J) lineage 4-mtDNA used in this study

***A. tibetica* (CBS J) lineage 5-mtDNA**, Figures 8.26—8.27

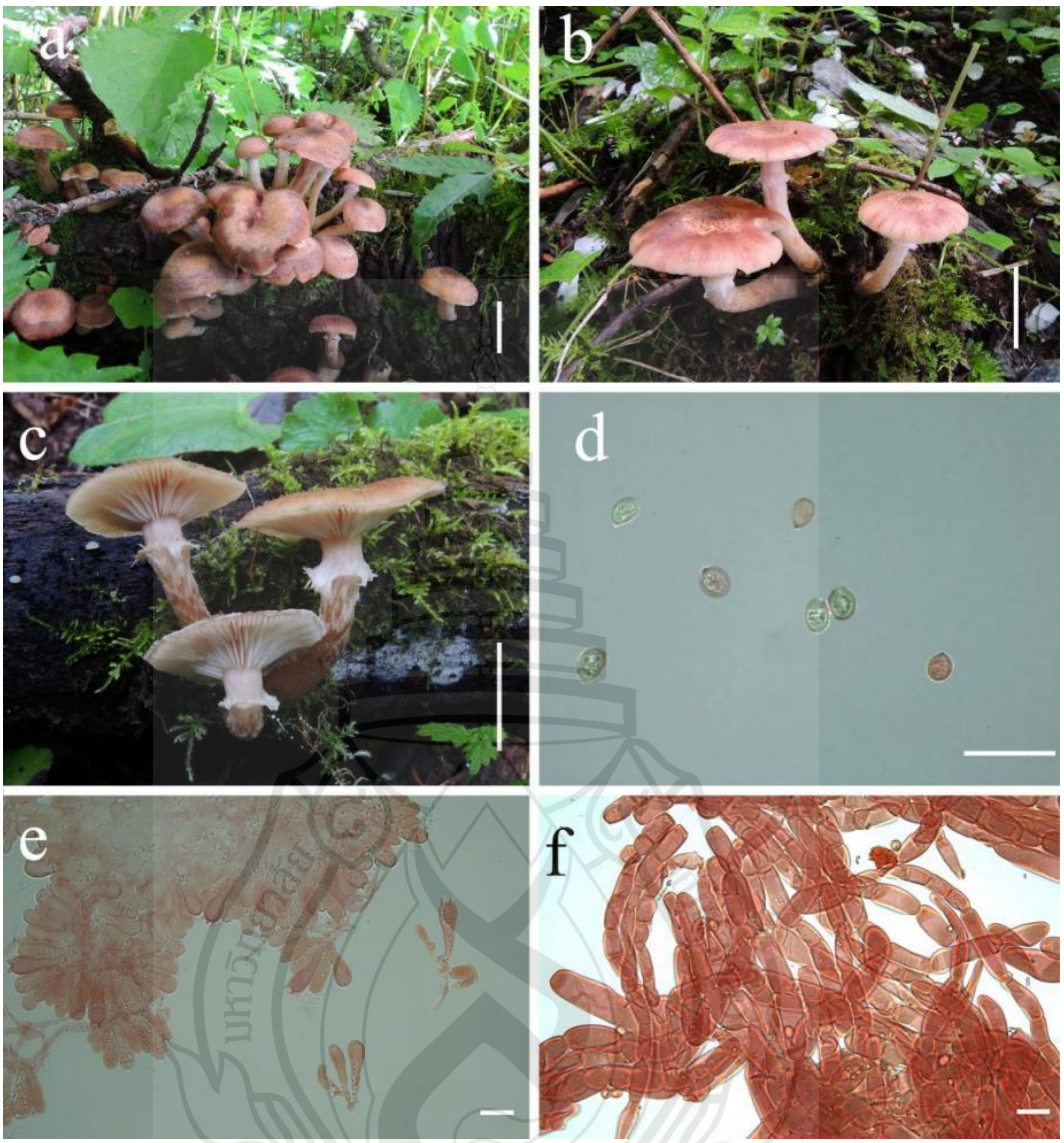
Basidiomata tricholomatoid, small to large, occurring solitary, scattered, or clustered. **Pileus** is 4—13 cm in diameter, initially nearly hemispherical when young, gradually expanding to convex, and finally flattening with maturity. **Pileus surface** is covered with grayish-white, gray, or dark gray scales, denser towards the center, with the cap flesh ranging from brownish to reddish-brown or yellow-brown. Mature caps exhibit distinct striations at the margin, approximately 1 cm wide. **Lamellae** are nearly adnate, whitish when young, turning dirty white to pale brown with age, relatively sparse, of varying lengths, and with smooth edges. **Stipe** is 4—12 cm long and 0.5—1.6 cm in diameter, nearly cylindrical, with a swollen base covered in fibrous or flocculent white scales. The upper part of the stipe is white, gradually transitioning to pale brown, brown, or dark brown towards the base. **Annulus** present, membranous, white.

Basidiospores: [114/3/3] (6.36)7.0－9.42(10.02) × (4.8)5.62－7.25 (7.98) μm, (Q = (1.04)1.1－1.4(1.58), Qm = 1.30 ± 0.12), subglobose, broadly ellipsoid, ellipsoid, inamyloid. **Basidia** 29－38 × 10－14 μm, clavate, 2 or 4 spored, often with a basal clamp connection; sterigmata 4－5 μm long. **Pileal squamules surface** consists of nearly longitudinally palisaded, short cylindrical cells (20 － 50 × 9 － 20 μm), containing brown to yellowish-brown intracellular pigments. The terminal cells (27－35 × 6－9 μm) are contracted and spindle-shaped.

Ecology/Substrate/Host: clustered on rotten wood of fagaceous plants in subtropical evergreen broad-leaved forests.

Distribution: Currently found in the Eastern Hengduan Mountains, situated in the northwestern region of China.

Additional material examined: **CHINA**, **Gansu**, Sidalong Forest Farm, Sunanyuguzu Autonomous County, Zhangye City, 38.4459°N, 99.8983°E, GDGM 83473. **Sichuan**, About 18km from Luoxu to Shambuka Pass, Shiqu County, Ganzi Tibetan Autonomous Prefecture, 34.4662°N, 97.9953°E, HKAS 49177; Daofu County, Ganzi Tibetan Autonomous Prefecture, 30.9734°N, 101.1251°E, HKAS 53619; Zhugencha, Wanglang National Nature Reserve, Pingwu County, Mianyang City, 32.9386°N, 104.0674°E, HKAS 89525; Shuangqiao Goukou, Siguniang Mountain Town, Xiaojin County, Aba Tibetan and Qiang Autonomous Prefecture, 30.9790°N, 102.7718°E, HMAS 254774; Songpan County, Aba Tibetan and Qiang Autonomous Prefecture, 32.5275°N, 103.5934°E, HMAS 268710; Siguniang Mountain, Xiaojin County, Aba Tibetan and Qiang Autonomous Prefecture, 31.1104°N, 102.9019°E, HMAS 274349; Wolong Nature Reserve, Wenchuan County, Aba Tibetan and Qiang Autonomous Prefecture, 31.1403°N, 103.1434°E, HMAS 50997; Baixionggou, Wanglang National Nature Reserve, Pingwu County, Mianyang City, 32.9080°N, 104.1580°E, HKAS 89519. **Qinghai**, Mengda National Nature Reserve, Xunhua Salar Autonomous County, Haidong City, 35.8094°N, 102.6943°E, HMAS 99623.



Note a–c Basidiomata. d Basidiospores. e Basidia. f Hyphae of pileal squamules. Scale bars: a–c = 5 cm, d–f = 20 µm.

Figure 8.25 Basidiomata and morphological characteristics of *A. tibetica* (CBS J) lineage 5-mtDNA (HMAS 99623)

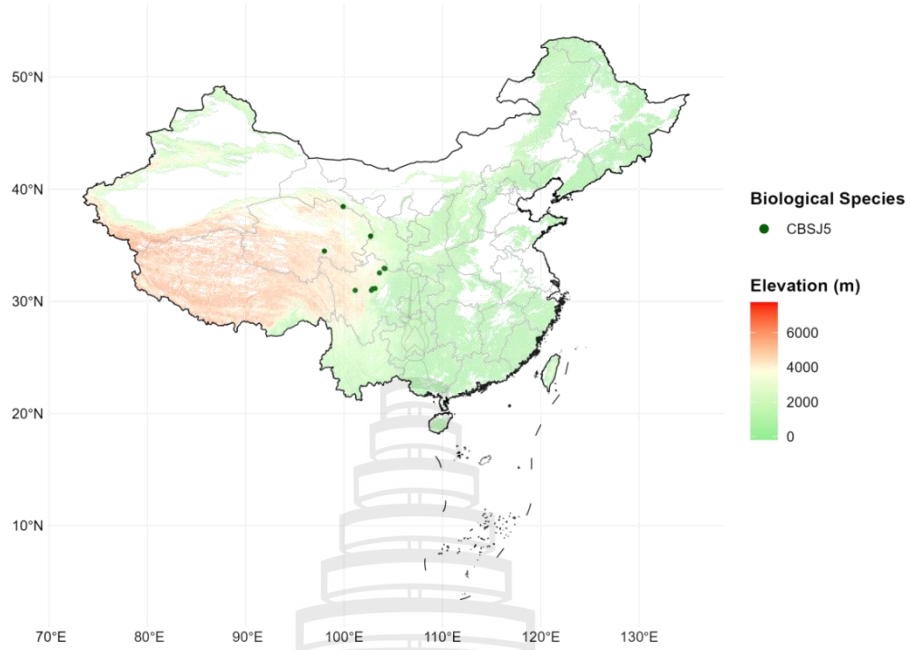


Figure 8.26 Distribution of samples of *A. tibetica* (CBS J) lineage 5-mtDNA used in this study

Notes: *Armillatia tibetica* is one of the most widely distributed species in China, ranging from central to northwestern regions. Although its mitochondrial genome reveals five geographic lineages (Figure D2), all of them cluster into a single independent branch in the nuclear gene species tree (Figure D2). Nuclear genetic differentiation further shows that, apart from the Xinjiang lineage, which exhibits moderate differentiation from the other four lineages (F_{ST} = 0.10—0.14) and distinct spore morphology, the remaining four lineages display only minimal divergence (F_{ST} < 0.05; Figure 3.4), representing intraspecific variation with negligible morphological differences. Considering the complete absence of reproductive isolation among the five geographic lineages and their cohesion as a single nuclear evolutionary lineage, *A. tibetica* is not further subdivided into separate species.

Armillaria adelpha (Berk.) Sacc., *Syll. fung. (Abellini)* 5: 84 (1887)

Index Fungorum number: IF 245622

Biological species: No biological species information available.

This species was described by Saccardo in 1887 from Darjeeling, northeastern India, Asia, and the Northern Hemisphere (Saccardo, 1887).

Basidiomata fleshy, subhemispherical, and deeply umbilicate, with a floccose-squamose center and an arched, striate, and smooth margin. **Pileus** 2.5 cm wide, and is gray in color. **Lamellae** pale, flesh-colored, and long-decurrent. **Stipe** elongated, stuffed, 5 cm or longer, 2 mm thick, reddish-brown, and smooth. **Annulus** remote, spreading, and strict (Saccardo, 1887).

Basidiospores information is currently unavailable. **Cystidia** information is currently unavailable. **Pileal squamules** information currently unavailable (Saccardo, 1887).

Ecology/Substrate/Host: Found on dead wood trunks at elevations of 2100—2400 m (Saccardo, 1887).

Reference mitochondrial genomes: No data available.

Reference nuclear genomes: No data available.

Average nuclear Weir & Cockerham's F_{ST} vs. the closest species: No data available.

Average mitochondrial dxy vs. the closest species: No data available.

Average mitochondrial ΦST vs. the closest species: No data available.

Armillaria affinis (Singer) T.J. Volk & Burds., Syn. Fung. (Oslo) 8: 24 (1995)

Index Fungorum number: IF 434354

Biological species: No biological species information available.

This species was described by Singer in 1989 from Costa Rica, North America, the Northern Hemisphere. This species was reclassified from *Armillariella affinis* (Singer, 1989) to *Armillaria affinis* (Volk & Burdsall, 1995).

Basidiomata in clusters. **Pileus** brown, with minute brown squamules at the center, otherwise nearly smooth, slightly viscid, semi-transparently striate at the middle, smooth or slightly sulcate when dry, convex, obtuse, becoming applanate or slightly depressed at the center, 2.9—3.1 cm in diameter. **Lamellae** pale alutaceous, later pale brownish, often brownish at the edge, crowded, horizontal, decurrent. **Spore prints** creamy white. **Stipe** concolorous with the lamellae above the annulus, brown below, later subfuliginous, superficially white-sericeous, equal, lacking a bulb, rarely slightly attenuated at the apex, 4—4.3 × 0.4 cm, usually 0.3 cm in diameter at the apex,

often forked or doubled near the base. **Annulus** white, thinly membranous, with a lacerate outer margin. **Context of stipe** pale, concolorous with the surface in the cortex of the stipe (Singer, 1989).

Basidiospores (6.5－7.8(－9) × 4.5－5.5(－6) µm, ellipsoid, some ovoid, smooth, walls up to 0.5 µm thick in mature spores, hyaline, a few slightly brownish in KOH, inamyloid. **Basidia** 24－26.8 × 5.5－7.2 µm, lacking basal clamps, hyaline, a few yellowish, thin-walled. **Cystidia** absent, but subhymenial elements occasionally elongated and intercalated among basidia, brown, fusoid, few, e.g., 15 × 2.5 µm. **Cheilocystidia** heteromorphous, numerous, 20－23 × 6－9.5 µm, fusoid, ventricose, or subclavate, hyaline, thin- or firm-walled (Singer, 1989). **Pileal squamules** scarcely or slightly gelatinous, formed of subparallel, clamp-less hyphae, these thin-walled but some ventricose and 7－13 µm wide; above the epicutis (in the squarrulose covering) with ascending fasciculate hyphae, these formed of chains of elongated but relatively short cells, 11－17 µm wide. Pigment in all, intracellular, vacuolar, but in a few cells also intraparietal, even thinly encrusting, cinnamon-colored (Singer, 1989).

Ecology/Substrate/Host: Grows in clusters on dead wood of oak and alder trunks.

Distribution: Found in the tropical montane zone of Central America, Costa Rica.

Reference mitochondrial genomes: No data available.

Reference nuclear genomes: No data available.

Average nuclear Weir & Cockerham's F_{ST} vs. the closest species: No data available.

Average mitochondrial dxy vs. the closest species: No data available.

Average mitochondrial ΦST vs. the closest species: No data available.

Armillaria algida G.F. Qin, Jun Zhao, W.M. Qin & Y.C. Dai, *Mycology* 16(2):786 (2024), Figures 8.28－8.29

Index Fungorum number: IF 836020

Biological species: Chinese Biological Species O (CBSO).

This species was described by Qin et al. in 2024 from the central region to the southwest region of China, Asia, and the Northern Hemisphere.

Basidiomata are small to medium-sized, occurring either solitarily or in compact clusters, with an overall reddish brown to rust-brown coloration adorned with black-brown scales. **Pileus** 1.5—7.0 cm in diameter and 0.4—1.2 cm in thickness, initially convex or hemispherical, later becoming plano-convex to applanate or slightly depressed, occasionally umbonate, and typically dry. In youth, the cap ranges from orange-white to dark brown, maturing to greyish orange or dark brown, with long, stiff, erect hairs at the center and a pale brown to dark brown margin. The center is brown to dark brown, while the margin is entire, incurved, or straight, often displaying striations when mature. **Lamellae** are sinuate or subdecurrent, sometimes with striped ridges extending downward to the annulus. **Stipe** is 3—9 cm long and 0.3—0.7 cm in diameter at the apex, cylindrical, rarely broadening at the base. In young specimens, the area above the annulus is orange-white, pale orange, or greyish orange; the middle portion is greyish orange to greyish brown; and the base is brownish orange, pale brown, or greyish brown. At maturity, the area above the annulus transitions to greyish orange, brownish orange, or pale brown; the middle portion becomes brownish orange, pale brown, or brown; and the base shifts to brownish orange, pale brown, brown, or dark brown. The stipe is covered with white fibrillose veil remnants and sometimes exhibits snake-skin-like markings. **Annulus** is present, arachnoid, thin, ephemeral, and white or nearly white (Qin et al., 2024).

Basidiospores (6.9)7.0—10.0(11.2) × (4.5)4.9—6.5(7.0) μm and are ellipsoid in shape. **Cheilocystidia** 13.0—47.0 × 4.5—11.0 μm are nearly cylindrical and feature a clamp connection at the base. **Pleurocystidia** absent. **Pileal squamules** consist of more or less parallel, cylindrical, thin- to thick-walled (≤ 2 μm) hyphae, which are simple septate and range in color from greenish yellow to brownish yellow, 17.0—127.0 × 5.0—28.0 μm (Qin et al., 2024).

Ecology/Substrate/Host: This species was found on various angiosperm substrates (stumps, fallen wood, rotten wood, and standing dead trees) of *Acer* sp., *Morus alba*, *Pyrus* sp., *Castanopsis sempervirens*, and *Abies* sp.

Distribution: Distributed in southwest and central China.



Note a–c Basidiomata. Scale bars: a–c = 5 cm.

Figure 8.27 Basidiomata of *Armillaria algida*

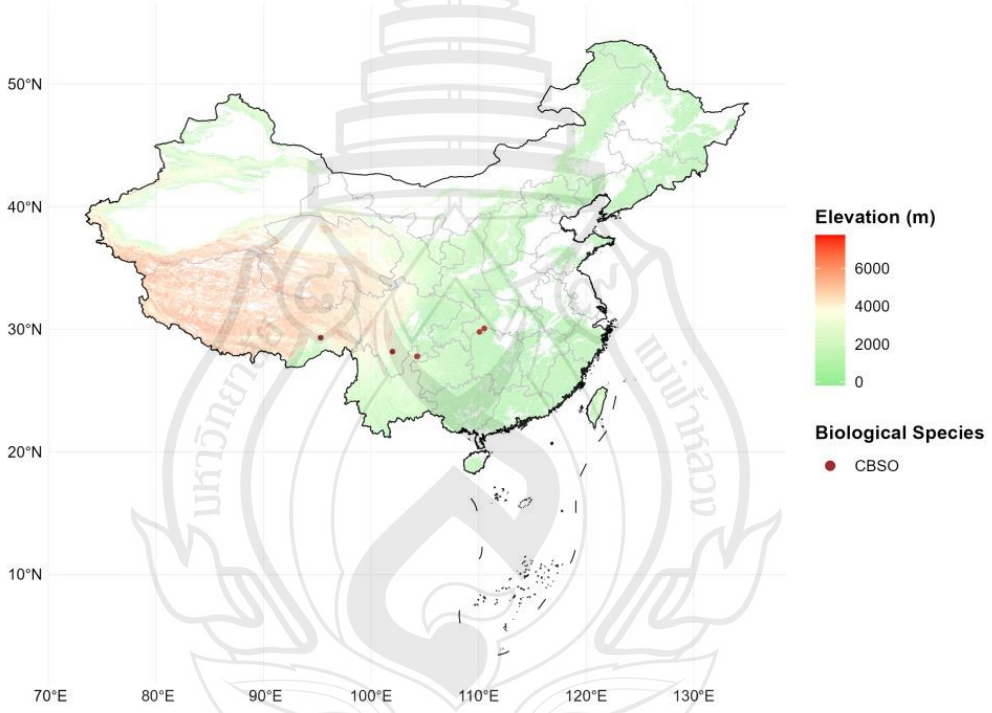


Figure 8.28 Distribution of samples of *Armillaria algida* used in this study

New research specimens: **CHINA**, **Hubei**, Yangzixi, Houhe nature reserve, Wufeng Tujia Autonomous County, Yichang City, 30.0666°N, 110.5333°E, Strain: 19080; Yangzixi, Houhe nature reserve, Wufeng Tujia Autonomous County, Yichang City, 30.0666°N, 110.5333°E, Strain: O19095. **Yunnan**, Mugan Town, Daguan County, Zhaotong City, 28.1687°N, 102.0003°E, Strain: BD4H; Yang Dayong's Fungi Materials, Xiaocaoba, Yiliang County, Zhaotong City, Commercial Strain: guo19; Fungi of

Laomengjia in Longan Village, Yiliang county, Zhaotong City, Commercial Strain: guo37; Daqiao Village, Xiaocaoba Township, Zhaotong City, 27.7782°N, 104.3307°E, HKAS 86554; Xiaocaoba Tianma Trading Market, Xiaocaoba Town, Yiliang county, Zhaotong City, 27.7674°N, 104.2608°E, Strain: LM-1; Yiliang County Tianma Industry Development Center, Yiliang county, Zhaotong City, Commercial Strains: LYT-F05, LYT-F19, LYT-F34; Zhaotong Gastrodia Research Institute, Zhaotong City, Commercial Strains: ZT-M6, ZT-MF, ztmh-1, ztmh-13, ZT15; Yiliang Maofeng Gastrodia elata Industry Development Co., Ltd., Yiliang County, Zhaotong City, Commercial Strain: MF-M6. **Tibet Autonomous Region**, Go to the roadside of Bomi County from Medog County, Linzhi City, 29.3046°N, 95.3189°E, HMAS 253478; Motuo County, Linzhi City, 29.3046°N, 95.3189°E, HMAS 272641. **Hunan**, Badagong Mountain National Nature Reserve, Sangzhi County, Zhangjiajie City, 29.7767°N, 110.0879°E, Specimen: MHHNU 8447. **Shaanxi**, Shaanxi Hanzhong Desheng Seed and Breeding Industry Association, Hanzhong City, Commercial Strain: SM-1.

Average nuclear Weir & Cockerham's F_{ST} vs. the closest species (*A. bruneocystidia*): 0.16.

Average mitochondrial dxy vs. the closest species (*A. bruneocystidia*/*A. linzhiensis*/*A. tibetica* (CBS J) lineage 2-mtDNA/*A. tibetica* (CBS J) lineage 3-mtDNA/*A. amygdalispora*): 0.05.

Average mitochondrial ΦST vs. the closest species (*A. amygdalispora*): 0.47.

Armillaria altimontana B Brazee, B. Ortiz, Banik & D.L. Lindner, *Mycologia* 104(5): 1202 (2012)

Index Fungorum number: IF 563757

Biological species: North America Biological Species X (NABS X).

This species was described by Brazee et al. in 2012 from the United States of America, North America, Northern Hemisphere.

Basidiomata exhibit a tricholomatoid morphology, with the pileus becoming plane in mature specimens and reaching up to 3 cm in diameter in dried samples. **Pileus** is rust brown and adorned with cream-colored scales and short fibrils. **Stipe** 4—7 cm in length, 0.8—0.1 mm in width at the base, and narrows to 0.3—0.5 cm at the apex. **Annulus** is present, appearing cottony and white to cream in color; it is robust and thick in two of the examined specimens but difficult to observe in the third (Brazee et al., 2012).

Basidiospores 7.2—11.7 × 5.4—6.3 μm, broadly elliptical, smooth, guttulate, and hyaline in KOH; nonamyloid. **Basidia** are 34.2—55.8 × 6.3—10 μm, cylindro-clavate, 4-sterigmate, and hyaline in KOH; sterigmata are 2.7—4.5 μm long. Marginal cells among the basidia 24.3—50.4 × 5.4—8.1 μm, clavate to cylindro-clavate, and hyaline in KOH. **Pleurocystidia** are absent. **Pileal squamules** consist of a tangled layer of repent to erect hyphae, 4—18 μm wide, subparallel, and hyaline in KOH. Hyphae of the pileal scales are 6.3—20 μm wide, multiseptate, thin to moderately thick-walled, and hyaline or yellowish in KOH. **Clamp connections** are absent (Brazee et al., 2012).

Ecology/Substrate/Host: This species is typically found on both hardwood and coniferous trees in higher elevation forests, particularly in areas dominated by *Abies* species.

Distribution: Its range includes the Cascade, Great Basin, and Rocky Mountain ranges in western North America, specifically documented in California, British Columbia, Idaho, Oregon, and Washington (Morrison et al., 1985; Hanna et al., 2020; Kim et al., 2023).

Average nuclear Weir & Cockerham's F_{ST} vs. the closest species (*A. tibetica* (CBS J) lineage 2-mtDNA): 0.21.

Average mitochondrial dxy vs. the closest species (*A. nabsnona*): 0.10.

Average mitochondrial ΦST vs. the closest species: No data available.

Armillaria amygdalispora Han C. Wang, G.F. Qin, Jun Zhao & Y.C. Dai, *Mycology* 16(2): 790 (2024), Figures 8.30—8.31

Index Fungorum number: IF 831858

Biological species: Chinese Biological Species L (CBSL).

This species was described by Qin et al. (2024) from southwestern China, Asia, the Northern Hemisphere.

Basidiomata are small to medium-sized, collybioid, and typically grow in imbricate-caespitose clusters on dead trees, often concrescent at the base, though occasionally solitary. **Pileus** 2.6—6.9 cm in diameter and 0.2—0.9 cm in thickness, initially spherical-convex to convex, later becoming plano-convex to applanate, sometimes slightly depressed; they are dry and exhibit colors ranging from brownish orange to pale brown and brown. The margin is entire, usually slightly incurved, and marked with

striations. Pileal scales, colored brown to dark brown, are distributed across the entire surface but are denser and more erect toward the center, becoming more dispersed and flattened toward the margin. **Lamellae** are adnate with a decurrent tooth, white to nearly white when young, maturing to pale red, greyish red, brownish orange, and pale brown. They are subdistant, with lamellulae present, and have smooth margins. **Stipe** is central, measuring 2.5—6 cm in length and 0.4—1 cm in diameter at the apex, clavate or bulbous in shape. Above the annulus, it is orange-white, while the middle portion is brown, and the base is dark brown. The stipe is covered with white fibrillose veil remnants, often resembling snake-skin markings. **Annulus** is cortinate, thin, delicate, usually ephemeral, and white or nearly white in color (Qin et al., 2024).

Basidiospores (7.2)7.8 — 10.2(11.0) × (4.2)4.8 — 6.2(6.3) μm, white in mass, almond-shaped, ellipsoid, inamyloid. **Basidia** are clavate, 8 — 35 × 5.5 — 8 μm. They feature a clamp connection at the base, are 4-sterigmate, and usually thin- to slightly thick-walled, with a yellowish green to brownish yellow coloration. **Sterigmata** 3—5 μm in length. **Cheilocystidia** 20—40 × 4.5—9.5 μm and are polymorphic, appearing clavate, fusiform, cylindrical, elliptical, or ovoid. Pleurocystidia are absent. **Pileal squamules** are composed of parallel, cylindrical, slightly thick-walled (≤ 2.5 μm) hyphae, without clamps at septa, grey to brownish yellow, 20—94 × 4.5—25 μm (Qin et al., 2024).

Ecology/Substrate/Host: This species is found on a variety of substrates and hosts, including: Angiosperm stump (e.g., *Morus alba*, *Pyrus* sp.); Fallen angiosperm wood (e.g., *Pyrus* sp.); Rotten wood (e.g., *Abies* sp.); Fallen trunk of *Acer* sp.; Dead wood of *Castanopsis sempervirens*; Dead angiosperm standing tree.

Distribution: Distributed in central and southwestern China.



Note a–f Basidiomata. Scale bars: a–f = 5 cm.

Figure 8.29 Basidiomata of *Armillaria amygdalispora*

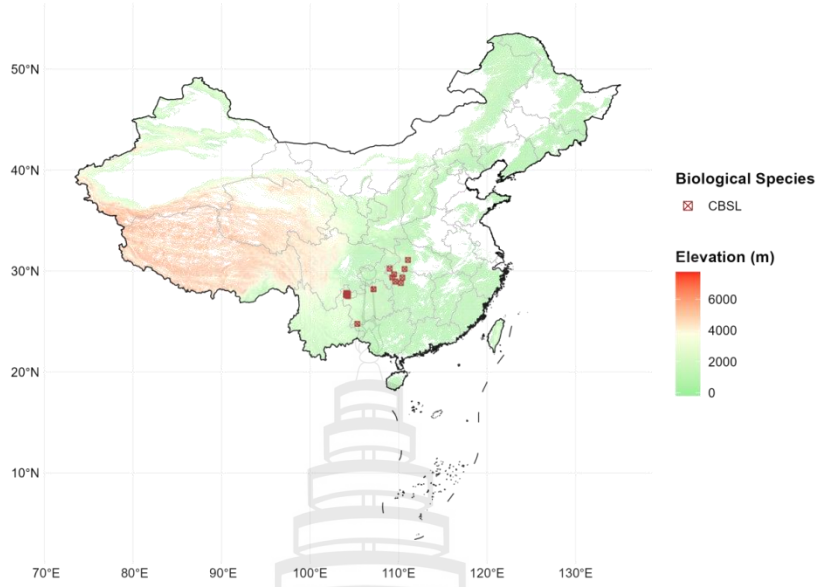


Figure 8.30 Distribution of samples of *Armillaria amygdalispora* used in this study

New research specimens: **CHINA**, **Hubei**, Lushui Town, Laifeng County, Enshi Tujia and Miao Autonomous Prefecture, 29.3666°N, 109.3000°E, CBSL17017 (strain); Liziping Town, Yiling District, Yichang City, 31.1000°N, 111.0666°E, CBSLW17003 (strain); Laifeng County, Enshi Tujia and Miao Autonomous Prefecture, 29.6666°N, 109.5000°E, CBSLW17016 (strain); Yuanbao Town, Lichuan City, Enshi Tujia and Miao Autonomous Prefecture, 30.2333°N, 109.0000°E, CBSLW17039 (strain); Wufeng Tujia Autonomous County, Yichang City, 30.2000°N, 110.6833°E, LW17027 (strain). **Hunan**, Xiaoxi, Yongshun County, Xiangxi Tujia and Miao Autonomous Prefecture, 28.9614°N, 109.6484°E, GDGM 71117; Xiaoxi, Yongshun County, Xiangxi Tujia and Miao Autonomous Prefecture, 28.9614°N, 109.6484°E, HMIGD 71175; Xiaoxi National Nature Reserve, Yongshun County, Xiangxi Tujia and Miao Autonomous Prefecture, 28.8120°N, 110.2693°E, MHHNU 31060; Wulingyuan National Forest Park, Wulingyuan District, Zhangjiajie City, 29.3469°N, 110.4352°E, MHHNU 31772. **Guizhou**, Kuankuoshui Reservoir, Suiyang County, Zunyi City, 28.2050°N, 107.1754°E, HKAS 86613; Kuankuoshui Reservoir, Suiyang County, Zunyi City, 28.2050°N, 107.1754°E, HKAS 86615. **Guangxi Zhuang Autonomous Region**, Longlin Autonomous County, Baise City, 24.7706°N, 105.3438°E, HMAS 22781. **Yunnan**, Haizi Town, Yiliang County, Zhaotong City, 27.5544°N, 104.2598°E,

guo324 (strain); Lianghe Township, Yiliang County, Zhaotong City, HKAS 86548; Lianghe Village, Lianghe Township, Yiliang County, Zhaotong City, 27.8328°N, 104.2081°E, LH-22 (strain); Jiaokui Town, Yiliang County City, Zhaotong City, 27.6254°N, 104.0508°E, KIB5-guo90 (strain); Yiliang County Tianma Industry Development Center, Yiliang County, Zhaotong City, LYT-F01 (commercial strain); Xiaocaoba Town, Yiliang County, Zhaotong City, 27.7388°N, 104.2916°E, LZP-11 (strain); Xiaocaoba Town, Yiliang County, Zhaotong City, 27.7400°N, 104.2916°E, LZP-15 (strain); Zhongming Township, Yiliang County, Zhaotong City, 27.8308°N, 104.0858°E, MW-27 (strain); Lianghe Town, Yiliang County, Zhaotong City, 27.8208°N, 104.1648°E, guo278 (strain); Shulin Yi and Miao Township, Yiliang County, Zhaotong City, 27.5075°N, 104.2966°E, ZG-26 (strain); Zhaotong Gastrodia Research Institute, Zhaotong City, ZTMH-036 (commercial strain), YSLF-1 (commercial strain). Null, TX (strain).

Average nuclear Weir & Cockerham's F_{ST} vs. the closest species (*A. violacea*): 0.11.

Average mitochondrial dxy vs. the closest species (*A. linzhiensis*/*A. tibetica* (CBS J) lineage 2-mtDNA/*A. tibetica* (CBS J) lineage 3-mtDNA/*A. amygdalispora*/*A. violacea*): 0.04.

Average mitochondrial ΦST vs. the closest species (*A. linzhiensis*): 0.32.

Armillaria aotearoa Hood & Ramsfield, *N.Z. Jl For. Sci.* 46(2): 6 (2016)

Index Fungorum number: IF 815529

Biological species: No biological species information available.

This species was described by Hood & Ramsfield in 2016 from New Zealand, Southern Hemisphere, Oceania (Hood and Ramsfield 2016).

Basidiomata pileate, centrally stipitate, caespitose. **Pileus** convex at first, becoming plano-convex, 3.5—6.0 cm in diameter, pinkish brown to brown, moderately smooth, sprinkled more or less evenly (slightly denser at the center) with tiny, dark, granular scales; not striate or with faint striae only at the margin. **Lamellae** adnexed, moderately crowded, pale pink. **Stipe** 3.5—9.0 cm long, with a bulbous base; pale pinkish brown, sometimes with a faint greenish or yellowish tinge; dry, fibrillose, with tiny scattered tufts, becoming hollow; flesh off-white to pale pink. **Annulus** present,

formed by the veil, persistent, dry; lower surface concolorous with the stipe, with dark flecks concentrically arranged (Hood & Ramsfield 2016).

Basidiospores (7)7.5－9.5(10.5) × 5－7(7.5) μm, ellipsoid to ovoid, with a pronounced apiculus, and in some, a prominent vacuole; hyaline, non-amyloid, with smooth walls thin to moderately thick (to 0.8 μm). **Basidia** 31－49 × 5－9.5 μm, 4-spored, clavate-cylindric, without a basal clamp connection; sterigmata up to 6 μm long. **Cystidia** not observed. **Cheilocystidia** not observed. **Pileal squamules** composed of sub-parallel, radially oriented, periclinal hyphae composed of inflated, thin- to occasionally firm-walled cells (16－109 × 8－26 μm), lacking clamp connections. The upper level (60－100 μm deep) is colored brown, with hyphae occasionally projecting slightly above the surface. The lower level is hyaline and merges gradually with the hyphae of the pileus trama beneath (Hood & Ramsfield 2016).

Ecology/Substrate/Host: This species was found on a dead stem of a fallen *Nothofagus* sp.

Distribution: The holotype was collected from the northern Kaimanawa Range, Taupo region, New Zealand, specifically at the lower end of Te Iringa Track, Clements Mill Road.

Reference mitochondrial genomes: No data available.

Reference nuclear genomes: No data available.

Average nuclear Weir & Cockerham's F_{ST} vs. the closest species: No data available.

Average mitochondrial dxy vs. the closest species: No data available.

Average mitochondrial ΦST vs. the closest species: No data available.

Armillaria apalosclera (Berk.) A. Chandra & Watling, *Kavaka* 10: 65 (1982)

Index Fungorum number: IF 115705

Biological species: No biological species information available.

This species was described by Peck (1897) from Darjeeling, India, Asia, Northern Hemisphere.

Pileus 2.75－3 inches broad, umbilicate, depressed, umber, moist, rough with raised pointed scales or warts; margin striate. Very soft, fleshy, and brittle. **Context** soft, tender consistency; odour strong and disagreeable. **Lamellae** decurrent, rather

narrow, pale umber, crenate; interstices venose. **Stipe** 1.5 inches high, 2 lines thick in the centre, ascending, attenuated downwards, solid, firm, darker than the pileus. **Annulus** not mentioned. **Spores** not mentioned.

Ecology/Substrate/Host: On trunks of trees. Darjeeling, 7,000－8,000 feet. June, July. Abundant.

Distribution: India.

Reference mitochondrial genomes: No data available.

Reference nuclear genomes: No data available.

Average nuclear Weir & Cockerham's F_{ST} vs. the closest species: No data available.

Average mitochondrial dxy vs. the closest species: No data available.

Average mitochondrial ΦST vs. the closest species: No data available.

Armillaria appendiculata Peck, Bull. Torrey bot. *Club* 24: 140 (1897)

Index Fungorum number: IF 147016

Biological species: No biological species information available.

This species was described by Peck (1897) from the southeastern United States, North America, and the Northern Hemisphere.

Pileus broadly convex, smooth, whitish, often with a ferruginous or brownish-ferruginous tinge on the disk, 2－4 inches broad. The context is white or whitish. **Lamellae** close, rounded behind, whitish. **Stipe** is 1.5－3.5 inches long and 5－10 lines thick, equal or slightly tapering upward, solid, bulbous, whitish. **Annulus** is either membranous or webby, white, and commonly adhering in fragments to the margin of the pileus.

Basidiospores 0.003 inches long, 0.002 inches broad, subelliptical Peck (1897).

Ecology/Substrate/Host: has no information available.

Distribution: **Auburn**, **Alabama**, southeastern United States.

Reference mitochondrial genomes: No data available.

Reference nuclear genomes: No data available.

Average nuclear Weir & Cockerham's F_{ST} vs. the closest species: No data available.

Average mitochondrial dxy vs. the closest species: No data available.

Average mitochondrial ΦST vs. the closest species: No data available.

Armillaria argentina Speg., Anal. Mus. nac. Hist. nat. B. Aires 6: 99 (1898) [1899]

Index Fungorum number: IF 147333

Biological species: No biological species information available.

This was described by Spegazzini (1898) from the eastern coast of Argentina, South America, Southern Hemisphere.

Pileus 2.5—5.0 cm in diameter, initially globose to hemispherical or subovate, with a blunt and slightly involute margin; later becoming campanulate or hemispherically expanded, with a margin that is not or scarcely revolute. The umbo is obsolete and thick, smooth, and glabrous. In youth, the pileus is pale or yellowish-greenish, with a paler edge. With age, the center becomes pale reddish, while the edge becomes pale greenish. **Lamellae** crowded, somewhat thick, rigid-fragile, and broad, initially entire, first white with a greenish tinge, then becoming dirty reddish and slightly diffluent. The front edge is attenuate-acute, while the back edge is rounded-sinuate and somewhat free. **Stipe** cylindrical, elongated, 3.5—4.0 cm long, 0.3—0.6 cm in diameter, often flexuous-crisped, covered with a thick fibrous cuticle, initially flocculose-filled inside, later becoming almost hollow. It is smooth and glabrous, initially white with a yellowish-greenish tinge in youth, becoming dirty reddish with age. **Annulus** White, initially submembranaceous and entire, later fragmenting and adhering to the margin of the pileus, while the upper part of the stipe becomes squamulose. **Basidiospores** ellipsoid, inequilateral, 4.5—6 μm long, 3—3.5 μm in diameter, smooth, with 1 or 2 large guttules, hyaline.

Ecology/Substrate/Host: Found on humus soil.

Distribution: near La Plata, eastern coast of Argentina.

Reference mitochondrial genomes: No data available.

Reference nuclear genomes: No data available.

Average nuclear Weir & Cockerham's F_{ST} vs. the closest species: No data available.

Average mitochondrial dxy vs. the closest species: No data available.

Average mitochondrial ΦST vs. the closest species: No data available.

Armillaria bruneocystidia Han C. Wang, G.F. Qin, Jun Zhao & Y.C. Dai, *Mycology* 16(2): 792 (2024), Figures 8.32－8.33

Index Fungorum number: IF 831857

Biological species: Chinese Biological Species H (CBSH).

This species was described from China (Northern Hemisphere: Asia: Southwest China) in 2024 by Qin et al. (2024) and is currently known to be distributed in Sichuan and Yunnan provinces, southwestern China, Northern Hemisphere.

Basidiomata small to large-sized, solitary or caespitose or loosely grouped on fallen trunks and woody debris. **Pilei** 1.8－5.4 cm in diameter, 0.5－2.0 cm thick, initially hemispherical-convex to convex, with or without a small pointed umbo, later becoming plano-convex, applanate, or depressed, usually dry, orange-white, pale brown at the margin, pale brown, yellowish brown, brown at the center when young, greyish orange, brownish orange, pale brown, brown, reddish brown at the margin, greyish orange, yellowish brown, pale brown, brown, reddish brown, dark brown at the center when mature, with hairy, brownish grey, yellowish brown, brown, dark brown scales distributed over the entire surface but more concentrated and suberect toward the center, more dispersed and flattened toward the margin, margin entire, usually incurved, usually striate. **Lamellae** adnate with a decurrent tooth or sinuate, usually with striped ridges extending downward to the annulus, white, yellowish white, orange-white, pale orange when young, pale orange, greyish orange, brownish orange, pale brown when mature, subdistant, lamellulae present, margin smooth. **Stipe** central, 2.5－12 cm long, 0.4－1.2 cm in diameter at the apex, cylindrical or clavate, white, orange-white, greyish orange, brownish orange, pale brown to dark brown above the annulus, yellowish white to dark brown in the middle, pale yellow to dark brown at the base, usually covered with nearly white, brownish grey fibrillose veil remnants, sometimes resembling zigzag markings or a white membrane, occasionally the stipe base with pale yellow fine fibers; Annulus present, arachnoid or cortinate, single, thin, usually ephemeral, white or nearly white, sometimes outer margin brown or dark brown (Qin et al., 2024).

Basidiospores (6.0)7.0－9.0(10.0) × (4.0)4.9－6.0(7.0) μm, thin- to thick-walled (≤ 1 μm), ivory white in mass, ellipsoid, lacking a suprahilar depression, nearly hyaline to brownish yellow, smooth, cyanophilous, inamyloid, with a prominent

apiculus. **Basidia** clavate, 14 — 50 × 3 — 16 μm, upper portion constricted or constriction inconspicuous, with a clamp connection at the base, four-sterigmate, thin- to slightly thick-walled, yellowish green to brownish yellow, pigments disappearing gradually in KOH, sometimes brownish yellow crassobasidia (≤ 1.3 μm) forming when the lamellae develop abnormally, sterigmata 2—6 μm. **Cheilocystidia** 14.0—50.0 × 3.0—16.0 μm, polymorphic (fusiform, elliptical, cylindrical, ovoid, clavate), with a clamp connection at the base, usually with a papilla or irregular slender papilla at the apex, thin- to slightly thick-walled (≤ 0.4 μm), occasionally locally thick-walled (0.9 μm), nearly colorless to brownish yellow, forming a compact sterile lamella edge but easily broken and disappearing; pleurocystidia absent. **Pileal squamules** composed of more or less parallel, cylindrical, slightly thick-walled (≤ 0.9 μm) hyphae, simple septate, grey to brownish yellow, 14.0—170.0 × 6.0—38.0 μm (Qin et al., 2024).

Ecology/Substrate/Host: This species is associated with both gymnosperms (e.g., *Cunninghamia*, *Picea*, *Abies*) and angiosperms, primarily growing on dead wood (stumps, fallen trunks, and rotten debris) and occasionally on living trees.

Distribution: It is found in the mountainous regions of southwestern China.



Note a–f Basidiomata. Scale bars: a–d = 5 cm.

Figure 8.31 Basidiomata of *Armillaria bruneocystidia*

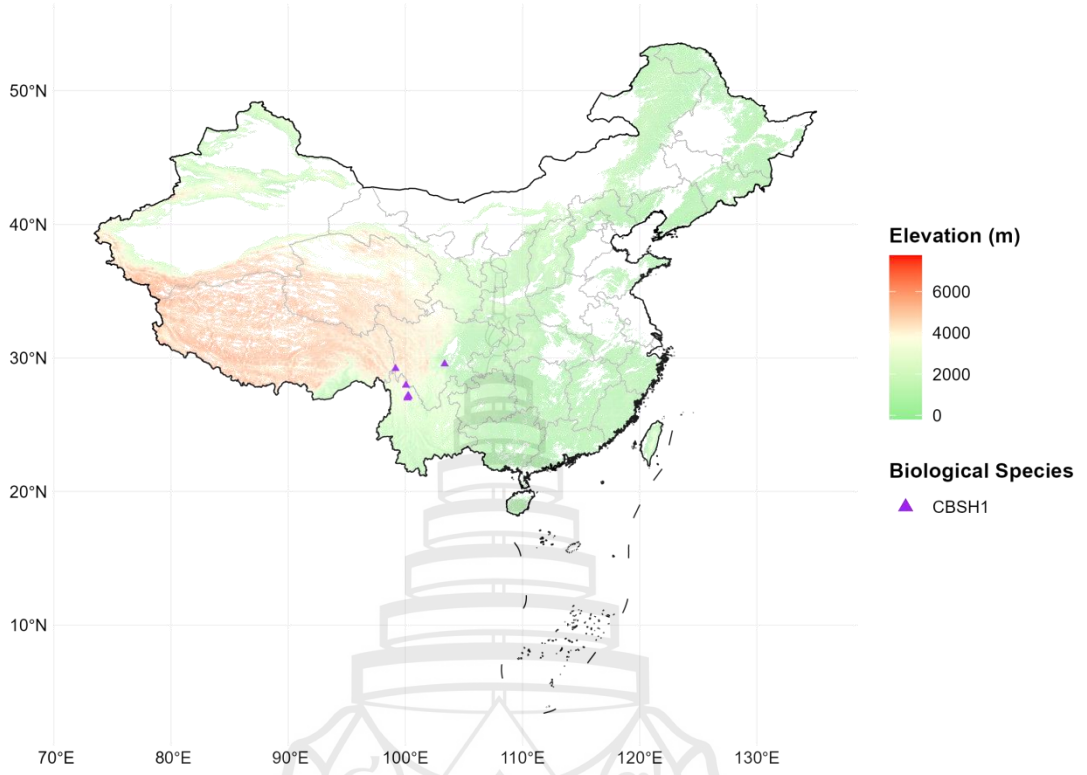


Figure 8.32 Distribution of samples of *Armillaria bruneocystidia* used in this study

New research specimens: **CHINA**, **Yunnan**, Lijiang Alpine Botanical Garden, Lijiang, 27.1385°N, 100.2327°E, HKAS 135501; Lijiang Alpine Botanical Garden, Lijiang, 27.1368°N, 100.2234°E, HKAS 135506; Maoniuiping, Yulong Snow Mountain, Yulong Naxi Autonomous County, Lijiang City, 27.1500°N, 100.2500°E, CBSH00019 (strain); Dasuodao, Yulong Snow Mountain, Yulong Naxi Autonomous County, Lijiang City, 27.1500°N, 100.2500°E, CBSH0006 (strain); Yulong Snow Mountain, Yulong Naxi Autonomous County, Lijiang City, 27.1000°N, 100.2000°E, CBSH99011 (strain); Yulong Snow Mountain, Yulong Naxi Autonomous County, Lijiang City, 27.1000°N, 100.2000°E, CBSH99028 (strain); Lijiang Alpine Botanical Garden, Lijiang City, 27.0043°N, 100.1788°E, HKAS 86601; Jade Dragon Snow Mountain, Yulong Naxi Autonomous County, Lijiang City, 27.1294°N, 100.2106°E, HKAS 48804; Sandaowan, Jade Dragon Snow Mountain, Yulong Naxi Autonomous County, Lijiang City, 27.1646°N, 100.2604°E, HKAS 56216; LuoJi Township, Shangri-La City, Diqing Tibetan Autonomous Prefecture, 27.9596°N, 100.0536°E,

HKAS 135513; Tianshengqiao National Geothermal Park, Shangri-La, Diqing Tibetan Autonomous Prefecture, 27.7948°N, 99.8130°E, CBSH00123 (strain); Dasuodao, Yulong Snow Mountain, Yulong Naxi Autonomous County, 27.1500°N, 100.2500°E, CBSH0003 (strain). **Sichuan**, Chudian, Emei Mountain, Emeishan City, Leshan City, 29.5500°N, 103.3500°E, CBSH19074 (strain); Guyu Township, Batang County, Ganzi Tibetan Autonomous Prefecture, 29.2046°N, 99.1608°E, HMAS 253500.

Average nuclear Weir & Cockerham's F_{ST} vs. the closest species (*A. tibetica* (CBS J) lineage 2-mtDNA): 0.10.

Average mitochondrial dxy vs. the closest species (*A. linzhiensis*/*A. tibetica* (CBS J) lineage 2-mtDNA/*A. tibetica* (CBS J) lineage 3-mtDNA/*A. violacea*): 0.04.

Average mitochondrial ΦST vs. the closest species (*A. linzhiensis*): 0.33.

Armillaria caespitosa (Berk.) Antonín, J.E. Stewart & Medel, in Antonín, Stewart, Medel Ortiz, Kim, Bonello, Tomšovský & Klopfenstein, *Mycologia* 113(4): 781 (2021)

Index Fungorum number: IF 837370

Biological species: No biological species information available.

This species was described by Antonín et al. (2021) from the United States, North America, and the Northern Hemisphere.

Basidiomata are caespitose or frequently gregarious and are lignicolous. **Pileus** 4.0—5.5 cm in width, transitioning from convex to plano-convex as it matures, with a central umbo that becomes depressed with age. It is orbicular in apical view, with a straight, lobed margin and an entire to dentate edge. **Pileus surface** is hygrophanous and zonate, smooth at the margin, and exhibits colors ranging from yellowish brown to reddish white with reddish brown when fresh, to pale brown or brown at the center when dry, pale brown squamules are concentrated mainly at the center and its surrounding area. **Lamellae** are close, decurrent, adnate, and thick, 3—5 mm in width. They are whitish when young, transitioning to reddish gray when fresh, and blond to olive brown or brown to pale brown when dry. The edges are smooth**Lamellulae** are present, arranged in 2—3 series. **Stipe** 4.5—7.5 cm in length and 9—10 mm in width at the apex, tapering to 5 mm at the base. It is central, cylindrical, and hollow, with no annulus. The surface is longitudinally fibrillose to slightly grooved, white with irregular

grayish red tones when fresh, and yellowish white to yellowish gray and fibrillose when dry. Rhizomorphs are frequently absent. The taste and smell of fresh specimens were not observed (Antonín et al., 2021).

Basidiospores (6－)6.5－8.5(－9.5) × (4－)4.5－5.5(－6) μm, with an average size of 7.5 × 4.9 μm and a Q value (length/width ratio) ranging from (1.21－)1.27－1.72, averaging 1.46. They are ellipsoid to broadly ellipsoid, less frequently dacryoid or ovoid, often slightly thick-walled, and appear white to yellowish white in deposit. **Basidia** 22－35 × (6－)7－10 μm, are 4-spored, clavate, and clamped. Basidioles 15－33 × 3－8 μm, are clavate, (sub)cylindrical, or subfusoid, and clamped. Scattered irregularly clavate, subutriform, or capitate cells (20－30 × 5－11 μm) are intermixed with basidia and basidioles in the hymenium or on the edge. **Cheilocystidia** (13－)20－35(－40) × (6－)8－22 μm, are numerous, and form a sterile band. They are (broadly) clavate, (broadly) fusoid, sphaeropedunculate, pyriform, vesiculose, rarely sublageniform, sometimes rostrate, and occasionally 2-celled, often slightly thick-walled. The subhymenium consists of cylindrical, gelatinized, branched, thin-walled hyphae 2－6 μm wide. **Pileal squamules** are a cutis composed of cylindrical or subfusoid, thin- to slightly thick-walled, clampless hyphae 3－9 μm wide, with terminal cells clavate to subcylindrical, up to 12 μm wide. Scales are composed of chains of cylindrical, ellipsoid, barrel-shaped, or (sub)fusoid cells, often short and clampless, mostly slightly thick-walled. **Terminal cells** 15－60 × (6－)8－19(－23) μm, are fusoid, conical, subutriform, subcylindrical, subulate, or subellipsoid, slightly thick-walled, and obtuse, rarely irregular. The stipitipellis (apex) consists of cylindrical, parallel, slightly thick-walled, sometimes slightly gelatinized hyphae 2－7 μm wide, with terminal cells (20－)30－57(－90) × (8－)12－20(－35) μm. These terminal cells are numerous, clavate, fusoid, or subcylindrical, less frequently 2-celled or in short chains, and ± slightly thick-walled (Antonín et al., 2021).

Ecology/Substrate/Host: This species is found in hardwood and mixed woodlands, orchards, and urban areas, typically growing on stumps and buried wood of hardwoods (e.g., *Quercus*, *Acer*, *Prunus*) and less frequently on conifers and palms, with basidiomata mostly occurring from June to November.

Distribution: Distributed in North and Central America.

Average nuclear Weir & Cockerham's F_{ST} vs. the closest species: No data available.

Average mitochondrial dxy vs. the closest species: No data available.

Average mitochondrial ΦST vs. the closest species: No data available.

Armillaria calvescens Bérubé & Dessur., *Mycologia* 81(2): 220 (1989)

Index Fungorum number: IF 136400

Biological species: It belongs to the North American Biological Species III (NABS III) (Bérubé & Dessureault, 1989).

This species was described by Bérubé & Dessureault in 1989 from Canada, North America, the Northern Hemisphere.

Pileus 2－10 cm in diameter, initially globose, becoming convex to plano-convex as it matures, and occasionally featuring a small central bump. **Pileus surface** is dry, finely fibrillose, and often appears almost smooth, with tiny scales sometimes present at the center. The color varies across shades of brown, including caramel, fawn, hazel, raw Sienna, tan, and greyish brown, with darker tones like eye brown occasionally appearing. The universal veil, when present, is golden yellow, covering young basidiocarps and leaving small tufts of fibrils on the cap, which are less common at the center of mature caps. **Margin** is straight, sometimes with faint striations, and matches the cap color or displays shades of hazel or raw Sienna, rarely darker. The flesh is firm, varying from thin to thick, with a white to cream-colored context. **Lamellae** are cream-colored when young, turning pale brown with age. They are sinuate (wavy), subdecurrent to strongly decurrent, and have a thick, closely spaced texture. **Stipe** 4－9 cm in length and 0.5－2 cm in thickness at the apex. It is slightly striate, fibrous, clavate (club-shaped), and often bulbous at the base. **Context** ranges from cream to alabaster, with darker shades like sunburn or hazel. The surface is covered with fine fibers, white, cream, or flesh-colored, often with a golden yellow tint. Bruising may result in a photo brown color. **Annulus** is thin and delicate, submembranaceous, and rarely fibrillous. It often collapses and adheres to the stipe as it matures, displaying colors of white, cream, grey, or brown with a faint golden yellow hue (Bérubé & Dessureault, 1989).

Basidiospores are ivory in mass, broadly elliptical to ovate, and 8.5—10 × 5—7 µm, smooth, apiculate (with a small projection), and non-amyloid. **Basidia** are clavate (club-shaped) and four-spored, with some featuring a clamp connection at the base. Pleurocystidia are absent. **Pileal squamules** consist of three layers: Suprapellis: Irregularly arranged, thin-walled, hyaline, elliptical cells (16—40 × 6—18 µm), with brown pigment uniformly distributed in the cell walls (not in vacuoles). Mediopellis: A tight mosaic of thin-walled, somewhat parallel hyphae (9—44 × 5.1—10 µm), some of which stain blue in toluidine blue. Subpellis: A network of loosely arranged cells, including globular, thin-walled cells (10—30 × 6—14 µm) and long filamentous hyphae (20—70 × 2.5—5 µm), which also stain blue in toluidine blue (Bérubé & Dessureault, 1989).

Ecology/Substrate/Host: grow on dead stumps, healthy roots, and living trees of *Acer saccharum*, forming abundant rhizomorphs beneath loosened bark, and occur singly or in groups of 2—8 from late August to late September.

Distribution: It has been found in New York, Vermont, and Michigan on *A. saccharum* and *F. grandifolia* (Ullrich & Anderson, 1978; Anderson & Ullrich, 1979; Proffer et al., 1987).

Average nuclear Weir & Cockerham's F_{ST} vs. the closest species (*A. tibetica* (CBS J) lineage 2-mtDNA): 0.25.

Average mitochondrial dxy vs. the closest species (*A. nabsnona*): 0.06.

Average mitochondrial ΦST vs. the closest species: No data available.

Armillaria camerunensis (Henn.) Courtec., *African Study Monographs* 16(1): 50 (1995)

Index Fungorum number: IF 412499

Biological species: No biological species information available.

This species was described by Courtecuisse in 1995 from the Congo, Africa, Northern Hemisphere.

Pileus approximately 4 cm in diameter, convex with a depressed disc and a thin, likely wavy or lobate, striate margin. The color is brownish, and the surface appears densely crispate in the exsiccatum, making it difficult to determine whether it was originally squamulose or smooth. Microscopic evidence suggests it was finely

squamulose. **Lamellae** are not very crowded, rather broad, ventricose, and slightly to distinctly decurrent. **Stipe** central, about 4 × 0.4 cm (measured dried), longitudinally striate, and very dark in the exsiccatum (Hennings, 1895; Courtecuisse, 1995).

Basidiospores 6—9 × 4.5—6.5 µm, pale or hyaline, inamyloid, elliptical to subamygdaliform, often stout or subglobose. Basidia 4-spored, 30—35 × 4—9 µm, cylindrical to clavate. Some sclerobasidia with walls up to 1 µm and a slightly yellowish tint were observed. **Cystidia** is not observed, despite multiple mounts; cheilocystidia were not found. Clamp connections are absent. **Pileal squamules are** composed of an interrupted trichodermium with small clusters of semi-erect hyphae. The hyphal elements 40—100 × 12—28 µm, are elongate, elliptical, thick-walled, and yellow-brownish due to smooth, cracked, or encrusting parietal pigmentation. These elements lie on the medio- and subpellis, which consist of hyaline, repent hyphae up to 15—35 µm in diameter (Hennings, 1895; Courtecuisse, 1995).

Ecology/Substrate/Host: No information available.

Distribution: Ngoli Village, Kindu, Maniema, Zaire, Democratic Republic of the Congo (Hennings, 1895; Courtecuisse, 1995).

Average nuclear Weir & Cockerham's F_{ST} vs. the closest species: No data available.

Average mitochondrial dxy vs. the closest species: No data available.

Average mitochondrial ΦST vs. the closest species: No data available.

Armillaria cepistipes Velen. *České Houby (Praze)* 2: 283 (1920)

Index Fungorum number: IF 260244

Biological species: It belongs to Europe Biological Species XI (EBS B).

This species was described by Velenovský in 1920 from the Czech, Europe, Northern Hemisphere. Currently known to be distributed in Czech, Canada, Finland, Italy, USA, Slovakia (Velenovský, 1920; Antonín, 2009; Tsykun, 2013; Keca et al., 2014).

Basidiomata are small, growing singly on twigs or in clusters on fallen trunks and woody debris. **Pileus** 1.5—4 cm in diameter, initially flattened, bell-shaped or conical, later expanding to arched or flattened, thinly fleshy, and pale grayish-green or initially pale grey, becoming pale brown with age. **Pileus surface** is covered with fine,

erect scales or small dark squamules and connected to the stipe by a rich, white cortina. In vitro, the pileus surface is covered with fine, darker-colored hairs, becoming pale brown with darker brown scales when expanded. **Lamellae** are decurrent to subdecurrent, initially white, and turn cream-colored with maturity or remain white. **Stipe** is long or up to 12 cm, 0.2—0.3 cm or 0.35 cm thick, white, and covered with fine scales. It lacks dark squamules but may have sparse tufts of nearly white mycelium. The base is extended and swollen into an elliptical volva or slightly thickened, and the stipe features a cortiniform, nearly white ring. **Basidiospores** 5—9.6 × 4.2—6.3 µm, ovoid, constricted at the base or smooth, elongated, and drop-shaped. **Basidia** 25—40 × 5.5 — 8.5 µm, 4-sterigmate, claviform, with clamp connections at the base. **Cheilocystidia** 15—40 × 8.5 µm, utriform or claviform. **Pileal squamules** composed of cylindrical to fusiform, multiseptate hyphae with hyphal cells 10—70 × 5—25 µm.

Ecology/Substrate/Host: This species is found at elevations ranging from 600 to 1500 m, growing on fallen beech twigs in the humid understory of beech forests or in conifer and broadleaf woods.

Distribution: in the montane and submontane zones of the Alps and Apennines. It occurs in conifer and broadleaf plantations from Liguria east to Tuscany-Emilia and southeast to Calabria.

Average nuclear Weir & Cockerham's F_{ST} vs. the closest species (*A. sinensis*): 0.18.

Average mitochondrial dxy vs. the closest species (*A. luteopileata*): 0.04.

Average mitochondrial ΦST vs. the closest species (*A. sinensis*): 0.66.

Armillaria conifericola G.F. Qin, J. Zhao, W.M. Qin & Y.C. Dai, Figure 8.34

MycoBank: MB 854549

Biological species: Chinese Biological Species D (CBSD).

This species was described by Qin et al. (2024) from northeastern China, Northern Hemisphere.

Basidiocarp small to large in size, solitary to compactly caespitose, generally cinnamon brown with dark brown scales. **Pileus** 3.5—15 cm in diameter, 0.5—2.0 cm thick, initially hemispherical or campanulate, later plano-convex to applanate or slightly depressed, sometimes cupulate or patellate, usually dry, pale orange, brownish

orange, pale brown to brown at the margin, pale brown, brown at the center when young, orange-white to pale brown at the margin, pale brown to dark brown at the center when mature, with brown, dark brown scales distributed over the entire surface but more concentrated and suberect toward the center, more dispersed and flattened toward the margin, margin entire, usually with striations. **Lamellae** adnate or decurrent, sometimes with striae extending downward to the annulus, white to yellowish white when young, orange-white, pale orange, brownish orange when mature, subdistant, margin smooth. **Stipe** central, 3－17 cm long, 0.6－3.5 cm in diameter at the apex, cylindrical or clavate, yellowish white to orange-white above the annulus, greyish yellow, greyish orange in the middle, brown at the base when young, orange-white, pale orange, greyish orange, greyish brown, brownish orange above the annulus, brownish orange, greyish brown, olive brown, pale brown in the middle, olive brown, brown, dark brown at the base when mature, covered with abundant white, pale yellow, reddish yellow tomentose veil remnants and brown to dark brown scales, sometimes with pale yellow fibrils at the base; **Annulus** membranous, rather thick, woolly, persistent, inner veil white or nearly white, outer margin greyish yellow, greyish yellow, dark yellow, greyish orange, brownish orange, pale brown, yellowish brown, brown, dark brown, bordered with brown to dark brown merodont scales, resembling a spiked wheel.

Basidiospores (7)7.5 － 9.8(10.6) × (4.2)4.9 － 6(6.6) µm, white in mass, ellipsoid, lacking a suprahilar depression, thin- to slightly thick-walled (≤ 1 µm), colorless, greenish blue to yellowish honey-colored, smooth, cyanophilous, nonamyloid, with a prominent apiculus. **Basidia** clavate, 31－46 × 7－10.5 µm, unconstricted, with a clamp connection at the base, 4-sterigmate, rarely two-sterigmate, sterigmata 2－7 µm long, usually thin- to slightly thick-walled, yellowish green to brownish yellow, pigments disappearing gradually in KOH solutions, sometimes brownish yellow crassobasidia (≤ 2 µm thick) forming when lamellae develop abnormally. **Cheilocystidia** little differentiated or inconspicuous, subclavate to cylindrical or ampulliform to lageniform, with a long neck and head, 20－45 × 2.5－5 µm, thin-walled. **Pleurocystidia** absent; pileal squamules composed of a more or less parallel array of cylindrical, slightly thick to thick-walled (≤ 2 µm) hyphae,

occasionally locally thick-walled, clampless, greenish blue, grey to brownish yellow, 18—145 × 5—25 µm.

Ecology/Substrate/Host: This species is associated with both gymnosperms (e.g., *Abies nephrolepis*) and angiosperms (e.g., *Betula platyphylla*, *Phellodendron amurense*), and herbaceous plants (e.g., *Equisetum hyemale*). Primarily growing on dead wood (fallen trunks, stumps, wood debris) and occasionally on living trees.

Distribution: It is found in the Changbaishan Nature Reserve (Jilin Province) and Xiaoshi (Liaoning Province), China.

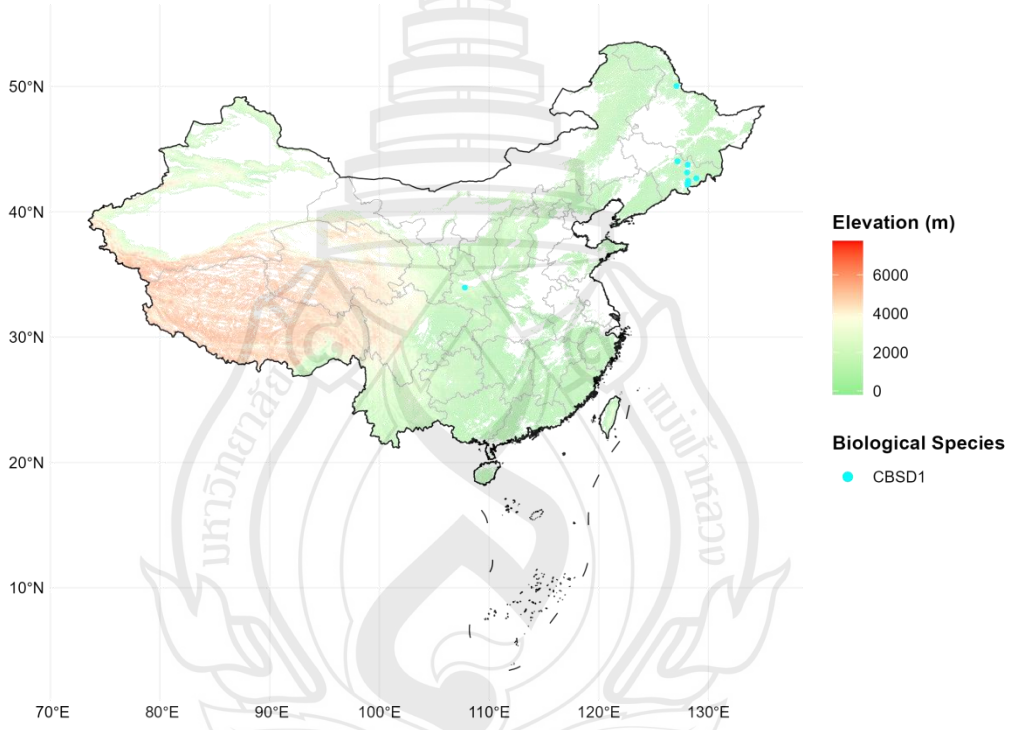


Figure 8.33 Distribution of samples of *Armillaria conifericola* used in this study

New research specimens: **CHINA**, **Jilin**, Heping skiing park, Changbai Mountain, 42.2667°N, 128.1500°E, 21043 (strain); Changbai Mountain Huangsongpu Forest Farm, Antu County, Yanbian Korean Autonomous Prefecture, 42.1299°N, 128.0699°E, CBSD21030 (strain); Emu forest farm, Dunhua city, Yanbian Korean Autonomous Prefecture, 43.7500°N, 128.1166°E, CBSD5193 (strain); Baihe, Changbai Mountain, Antu County, Yanbian Korean Autonomous Prefecture, 42.3000°N, 128.1000°E, CBSD93025 (strain); Qingling Town, Jiaohe City, Jilin City,

44.0307°N, 127.1790°E, HMJAU 25401, 25404, 25478 (specimens); Erdao Baihe Management Station, Yanbian Korean Autonomous Prefecture, 42.4573°N, 128.1439°E, HMJAU 28932, 6143, 7339; Quanshuidong Forestry, Helong City, Yanbian Korean Autonomous Prefecture, 42.6699°N, 128.8870°E, HMJAU 42023, 42034. **Heilongjiang,** Aihui District, Heihe city, 50.0333°N, 127.0833°E, CBSD02171 (strain). **Shaanxi,** Taibai Mountain, Zhouzhi county, Xi'an City, 33.9500°N, 107.7833°E, HMAS 145183.

Average nuclear Weir & Cockerham's F_{ST} vs. the closest species (*A. ostoyae*): 0.11.

Average mitochondrial dxy vs. the closest species (*A. borealis*): 0.04.

Average mitochondrial ΦST vs. the closest species (*A. borealis*): 0.83.

Armillaria dicupella (Berk.) Sacc., *Syll. fung. (Abellini)* 5: 83 (1887)

Index Fungorum number: IF 626698

Biological species: No biological species information available.

This species was described by Saccardo in 1887 from India, Asia, and the Northern Hemisphere. It is known to be distributed in Darjeeling of the northeastern part of India (Saccardo, 1887).

Basidiomata are fleshy. **Pileus** dry, convex, lacquered, with a slightly striated margin, 5 cm in diameter. **Lamellae** are distant, linearly decurrent. **Annulus** is large, convex above, and cup-shaped below. **Basidiospores** are not mentioned. **Cystidia** are not observed (Saccardo 1887).

Ecology/Substrate/Host: This species is found on dead wood at an altitude of 2300 m.

Distribution: Darjeeling, India.

Average nuclear Weir & Cockerham's F_{ST} vs. the closest species: No data available.

Average mitochondrial dxy vs. the closest species: No data available.

Average mitochondrial ΦST vs. the closest species: No data available.

Armillaria desertorum T. Bau, in Hou, Zu & Bau, Phytotaxa 714(3): 217 (2025)

Index Fungorum number: IF 857371

Biological species: No biological species information available.

This species was described by Hou et al. (2025) from China, Asia, the Northern Hemisphere. It is known to be distributed in Inner Mongolia, China (Hou et al., 2025).

Basidiocarp small to medium-sized, 0.5－6.2 cm in pileus diameter, fleshy. **Pileus** initially hemispherical to convex, becoming applanate with age and often slightly depressed at the center. **Pileus surface** is milky white to dark ivory when young, turning light reddish brown with a heather-violet center at maturity. It is smooth or sparsely covered with yellow-brown scaly patches and frequently coated with sand. **Margin** is inrolled when young, later appendiculate and radially cracked; pileus hygrophanous. **Context** white, exuding a sweet, greasy odor. **Lamellae** adnate to decurrent, milky white, moderately to densely spaced (L = 24－48, I = 1－2), 2－6 mm wide, of unequal length, with entire edges. **Stip**e 2.7－7.2 cm long, 0.3－1.5 cm wide, cylindrical and slender, creamy to beige, solid, fleshy, and often longitudinally cracked when dry. **Annulus** superior, white, thick, membranous; the margin first curves upward, then flattens, and finally bends downward. **Rhizomorphs** are dark, compact, and robust (Hou et al., 2025).

Basidiospores (7.6) 8.5－9.1 (10.7) × (6) 6.9－7.5 (9.2) μm, Q = 1.18－1.25 [1.22 ± 0.09, 1.23], ellipsoid, colorless, transparent, smooth, thick-walled, and inamyloid. **Basidia** 34－48 × 7－11 μm, long clavate, usually 4-spored (occasionally 2-spored), sterigmata 3－6.7 μm long, slightly to distinctly thick-walled. **The terminal elements of lamellae** are variable in form; terminal elements of the lamellar edge are fusiform to gourd-shaped, 9.6－32 × 8.1－13 μm, septate, sometimes with short basal branches; also clavate, occasionally constricted at mid-portion, 30－44 × 6.7－8.9 μm, thick-walled, septate, with the apical part (above septum) 6.8－18 × 7.3－9.4 μm. **Pileipellis** is a cutis composed of hyphae 6－22 μm wide; terminal cells are nearly cylindrical, sometimes with blunt finger-like projections at the apex, thin- to slightly thick-walled, hyaline to light brown. **Annular surface hyphae** 4－75 × 6－14 μm, interwoven; terminal cells 17－28 × 6－13 μm, ellipsoid to clavate, sometimes filamentous and irregularly curved.

Ecology/Substrate/Host: Growing buried or partially buried in sandy soil, near the roots of decayed *Caragana korshinskii* and *Populus euphratica*.

Distribution: Currently only known from Inner Mongolia.

Average nuclear Weir & Cockerham's F_{ST} vs. the closest species: No data available.

Average mitochondrial dxy vs. the closest species: No data available.

Average mitochondrial ΦST vs. the closest species: No data available.

Armillaria duplicata (Berk.) Sacc., *Syll. fung. (Abellini)* 5: 83 (1887)

Index Fungorum number: IF 242618

Biological species: No biological species information available.

This species was described by Saccardo in 1887 from India, Asia, and the Northern Hemisphere. It is known to be distributed in the northeastern region of India (Saccardo 1887).

Basidiomata are clustered. **Pileus** flat, dry, and smooth, 5 cm in width, featuring an incurved margin and a grayish surface with reddish-tinged flesh. **Stipe** is elongated, 10 cm long and 0.6 cm thick, brown in color, smooth toward the base, and covered with fibrillose-squamulose structures toward the apex, which is solid and filled. **Lamellae** are narrow, rounded at the back, and decurrent with a tooth-like extension to a double-lined veil. The double veil is deflexed, rose-colored, and shorter on the exterior. The hymenium between the annulus and the broader part of the lamellae is pale red (Saccardo 1887).

Ecology/Substrate/Host: This species grows densely on dead wood at an altitude of 2300 m.

Distribution: Darjeeling, India.

Average nuclear Weir & Cockerham's F_{ST} vs. the closest species: No data available.

Average mitochondrial dxy vs. the closest species: No data available.

Average mitochondrial ΦST vs. the closest species: No data available.

Armillaria ectypa (Fr.) Lamoure, *C. r. hebd. Séanc. Acad. Sci., Paris* 260: 4562 (1965)

Index Fungorum number: IF 326450

Biological species: No biological species information available.

This species was described by Fries in 1821 from Sweden, Europe, the Northern Hemisphere. It is known to be distributed in Austria, China, France, Finland, Japan

(Fries, 1821; Zang, 1996; Ohenoja, 2006; Antonín, 2009; Ota et al., 2011; Guo et al., 2016).

Pileus 2.5—6.0 (up to 10.0) cm in diameter, convex to plano-convex, later explanate, sometimes with a small obtuse umbo or depressed center with age, with a slightly curved or wavy margin, hygrophanous, brown, yellowish brown, or ochraceous brown to pale cream-brown at the margin, with minute dark brown scales at the center, and translucently striated. **Lamellae** decurrent, rather narrow, whitish at first, then pale cream, ochraceous to pinkish. **Stipe** 5.0—10.0 × 0.5—1.1 (up to 1.3) cm, cylindrical to subclavate, slightly thickened at the base, fibrillose, without a ring, of the same color as the pileus. Context thin, white; rhizomorphs absent; spore print whitish or creamish; odor fungoid; taste mild (Stasińska, 2015).

Basidiospores (6.5)7.0—8.5(9.0) × (5.0)5.5—6.5(7.0) µm, broadly ellipsoid to ellipsoid. **Basidia** 30—40 × 7.0—8.0 (up to 9.0) µm, clavate (club-shaped), mostly with 4 sterigmata (Stasińska 2015).

Ecology/Substrate/Host: *Armillaria ectypa* is a saprotrophic fungus that grows on wet ground and peat, often associated with *Sphagnum* moss and herbaceous plants such as *Carex*, *Drosera*, *Eriophorum*, and *Phragmites australis*. It also grows on decaying sedges like *Carex rostrata*. Its habitats include waterlogged areas, active raised bogs, alkaline fens, and *Aapa mires* (Stasińska, 2015).

Distribution: This species is distributed across 14 European countries (Austria, Czech Republic, Denmark, Finland, France, Germany, Great Britain, Netherlands, Russia, Sweden, Switzerland, and Slovakia) and has also been reported in Asia (China, Japan, and Turkey) (Stasińska, 2015).

Average nuclear Weir & Cockerham's F_{ST} vs. the closest species (*A. tabescens* subsp. *orientala*): 0.47.

Average mitochondrial dxy vs. the closest species (*A. tabescens* subsp. *orientala*): 0.10.

Average mitochondrial ΦST vs. the closest species (*A. tabescens* subsp. *orientala*): 0.92.

Armillaria fellea (Hongo) Kile & Watling, *Trans. Br. mycol. Soc.* 81(1): 131 (1983)

Index Fungorum number: IF 108698

Biological species: No biological species information available.

This species was described by Hongo in 1976 from Papua New Guinea, Oceania, Southern Hemisphere (Hongo, 1976; Kile, 1983).

Unable to retrieve available description records.

Average nuclear Weir & Cockerham's F_{ST} vs. the closest species: No data available.

Average mitochondrial dxy vs. the closest species: No data available.

Average mitochondrial ΦST vs. the closest species: No data available.

Armillaria fumosa Kile & Watling, *Trans. Br. mycol. Soc.* 81(1): 129 (1983)

Index Fungorum number: IF 108699

Biological species: No biological species information available.

This species was described by Kile and Watling (1983) from Australia, Oceania, the Southern Hemisphere. It is known to be distributed in Tasmania and Victoria, located to the southeast of the Australia (Kile & Watling, 1983).

Pileus 2.0—12.0 cm in diameter, displaying colors ranging from olivaceous grey to fuscous or drab hazel, often with a yellowish-brown tinge towards the center. Initially convex with a strongly deflexed and revolute margin, it becomes plano-convex as it matures, rarely subumbonate or irregularly depressed. **Pileus surface** is densely covered with minute, dark brown to black fibrillose squamules, which persist at the center. **Stipe** 5.5—13.0 × 0.5—1.4 cm, is typically elongated, broadening towards a clavate base. Above the annulus, it appears very pale pinkish, while below, it transitions from dirty whitish to greyish or dark yellowish brown with age, particularly near the whitish, tomentose base. **Stipe** is fibrillose, cartilaginous, and stuffed, with dark greyish brown flocci when young. The veil is annulate, sometimes appendiculate from the pileus margin, thin, membranous, and usually fugacious, collapsing as darkened remnants on the stipe. Initially white, it may have greyish floccules below. **Lamellae** are decurrent to subdecurrent, moderately crowded, and pliable, ranging from ivory to pale cream, eventually becoming yellowish cream or tinted pale cinnamon with age. The flesh is firm and thick in the pileus, whitish to pallid, becoming more fibrous and

darker towards the base of the stipe. The taste is peppery-astringent, developing within 10—15 seconds, while the smell is not distinct (Kile & Watling, 1983).

Basidiospores are almost white when fresh, darkening to pale cream in herbarium specimens, 6.5—8.5(—9.5) × (4—)4.5—6(—6.5) μm. They are elongate-ellipsoid with a broad apiculus, moderately thick-walled, optically smooth, inamyloid, non-cyanophilic, and guttulate. **Basidia** 35—47.5 × 7.5—9 μm, typically 4-spored (occasionally 2-spored), clavate, hyaline in aqueous solutions, thin-walled, and lack basal clamp connections; crassobasidia are absent. **Pleurocystidia** are absent, while cheilocystidia form a sterile margin, often multicellular, 13—32 × 4—7.5 μm, with end-cells ranging from elongate-cylindric to rounded clavate or occasionally ventricose-rostrate. **Hymenophoral trama** is bilateral, composed of strongly gelatinized, hyaline lateral strata slightly diverging from a compact, subregular mediostratum of hyaline, thin-walled hyphae. **Pileal squamules** is a radially arranged cutis terminating in chains of cells with brown vacuolar pigment, 15—40 × 4—10 μm, ± parallel, ± erect, forming irregular, ascending groups of fibrillose squamules on a layer of compacted, radially arranged hyaline hyphae 2.5—4 μm in diameter; the outer layer is slightly gelatinized. **Stiptopellis** consists of thickened cylindrical cells that give rise to small tufts of caulocystidia or are sparsely covered in differentiated sterile cells; caulocystidia are 30—42.5 × 4—6 μm, highly variable, elongate-flexuous with or without a clavate or subcapitate apex, and similar to those on the lamella margin, occasionally septate, sometimes brownish in aqueous ammoniacal solutions. **Velar hyphae** are hyaline to slightly thick-walled, cylindric, and flexuous (Kile & Watling, 1983).

Ecology/Substrate/Host: Typically occurs in clusters of 5—20 basidiomes on stumps, stem bases, or roots of various host plants, including *Eucalyptus obliqua*, *E. ovata*, *E. amygdalina*, *E. rubida*, *Acacia dealbata*, *A. mearnsi*, and *A. melanoxylon*. It grows in relatively shallow, poorly drained podzolic soils. Most host plants had been damaged or killed by fire, indicating a potential association with post-fire environments (Kile & Watling, 1983).

Distribution: This species is primarily found in south-eastern Australia, particularly in Tasmania and Victoria.

Average nuclear Weir & Cockerham's F_{ST} vs. the closest species: No data available.

Average mitochondrial dxy vs. the closest species: No data available.

Average mitochondrial ΦST vs. the closest species: No data available.

Armillaria fuscipes Petch, *Ann. R. bot. Gdns Peradeniya* 4(5): 299 (1909)

Index Fungorum number: IF 145388

Biological species: No biological species information available.

This species was described by Petch (1909) from Sri Lanka, Asia, Northern Hemisphere. It is known to be distributed in Cameroon, Mpanga, Sri Lanka, and Tanzania (Petch, 1909; Pegler, 1977; Kile & Watling, 1983; Watling, 1992).

Pileus that can reach up to 6 cm in diameter. Initially, the pileus is broadly convex, later becoming flat with a recurved margin. The center features an obtuse umbo surrounded by a depressed zone, sometimes appearing umbilicate. The coloration is brown or yellow-brown at the center, fading to pale brown and then pure white towards the outer edge. The central area is corrugated and covered with small, scattered brown pileal squamules, while the rest of the pileus is smooth. Margin is striate, he flesh is thin, white, and turns brownish when cut. **Stipe** grows up to 10 cm in length, typically starting horizontally at the base and then curving upward. It measures up to 0.9 cm in diameter at the base, tapering to 0.5 cm at the apex, blackish-brown and covered with grayish flocci, becoming lighter and longitudinally fibrillose near the annulus. Above the annulus, it is longitudinally striate and reddish. The stipe is solid, with dark brown outer layers and brownish-white inner tissue. It grows in clusters of six to nine, emerging from a cushion-like mass, with each stipe encircled at the base by a narrow, white, tomentose ring. **Lamellae** are white, fairly crowded, narrow (3—4 mm broad), decurrent, and taper outward. **Annulus**, located near the apex, is dependent, ample, rather thick, and flocculose (Petch, 1909).

Basidiospores are white, oval, or subglobose, smooth, with 6—8 × 5—7 μm. **Basidia** are typical of the genus, producing the basidiospores. **Cystidia** are absent, but cheilocystidia are present, forming a sterile margin on the lamellae (Petch, 1909).

Ecology/Substrate/Host: *Armillaria fuscipes* is found on the roots of *Acacia decurrens*, where it kills the host.

Distribution: This species has been observed in Uda Pussellawa, Ceylon.

Average nuclear Weir & Cockerham's F_{ST} vs. the closest species: No data available.

Average mitochondrial dxy vs. the closest species: No data available.

Average mitochondrial ΦST vs. the closest species: No data available.

Armillaria gallica **subsp.** ***calidusa*** G.F. Qin, W.M. Qin, J. Zhao, & Y. Yuan, Figures 8.35－8.36

MycoBank: MB 854550

Biological species: Chinese Biological Species B (CBSB).

This species was described by Qin et al. (2024) from northeastern and central China, Asia, and the Northern Hemisphere.

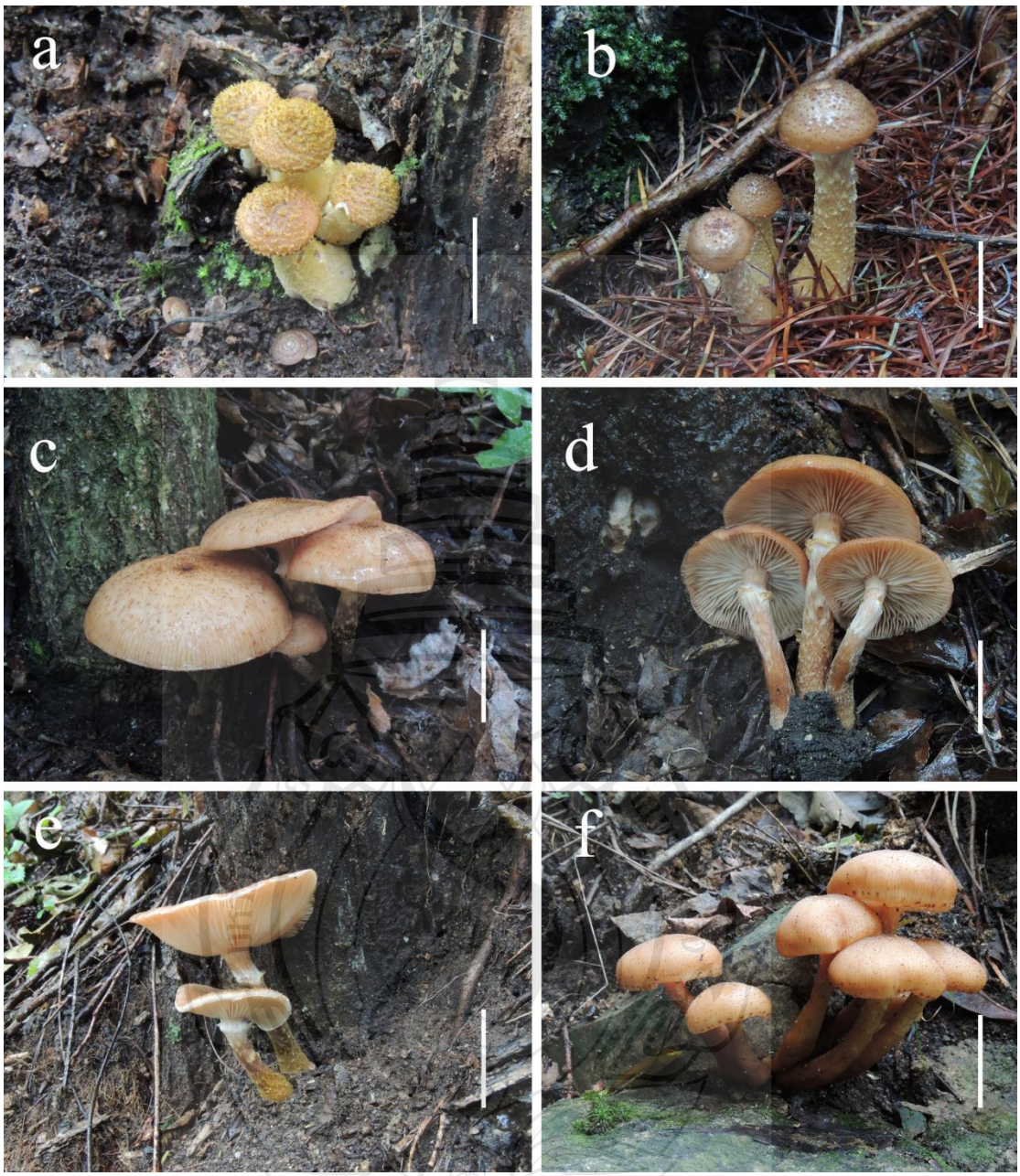
Basidiocarp of this species is small to medium in size and can be found either solitary or clustered, often loosely grouped near trees, shrubs, and woody herbs. **Pileus** 3－12 cm in diameter, starting as hemispherical with or without a mammilla, then becoming plano-convex or applanate with an incurved margin, occasionally retaining a mammilla at the center. **Pileus surface** is usually dry, displaying colors ranging from yellowish grey to brown at the margin, while the center is yellowish grey to dark brown when young. Usually shift to greyish orange to brown at the margin, with the center becoming greyish orange to dark brown when mature. **Pileal squamules** are pale yellow to dark brown, distributed across the cap but more concentrated and suberect toward the center, becoming more dispersed and flattened toward the margin. The margin is straight, entire, usually striate, and sometimes bears white veil remnants. **Lamellae** are decurrent to long-decurrent, with striae extending downward to the annulus. They are white or nearly white when young, turning greyish orange, brownish orange, brown, or dark brown when mature. They are subdistant with smooth margins. **Stipe** is central, 5－13 cm in length and 0.4－2 cm in diameter at the apex. It is cylindrical or clavate, with colors ranging from white, orange-white, orange-grey, and greyish orange above the annulus, to orange-white, orange-grey, greyish orange, and brownish orange in the middle, and greyish orange, brownish orange, pale brown, and brown at the base. The stipe is longitudinally striped and covered with white, grey, or reddish-yellow flocculose veil remnants. **Annulus** is submembranous, thin, single, and

persistent. The inner surface is white, while the outer margin is orange-grey, reddish yellow, brownish grey, or sometimes medium grey to dark grey (Qin et al., 2025).

Basidiospores are ivory white in mass, ellipsoid to elongate, and lack a suprahilar depression. They measure (6.5)7－9.7(11) × (4.2)4.6－5.8(6) μm. They are thin- to thick-walled (≤ 1 μm), colorless, greenish blue to yellowish honey-colored, smooth, cyanophilous, inamyloid, and have a prominent apiculus. **Basidia** are clavate, 31－48 × 7－10 μm, with the upper portion constricted or inconspicuously so. **Clamp connection** present at the base and are four-sterigmate, with sterigmata 2－7 μm (3.52 ± 1.37). Basidia are usually thin- to slightly thick-walled, yellowish green to brownish yellow, with pigments gradually disappearing in KOH solutions. Occasionally, brownish-yellow crassobasidia form when the lamellae develop abnormally. **Cheilocystidia** measure 9－52 × 5－14 μm and are poorly differentiated, appearing fusiform, cylindraceous, napiform, ovate, or clavate. They have a clamp connection at the base and a papilla, or an irregular slender papilla at the apex. They are colorless, thin- to slightly thick-walled (≤ 0.5 μm, occasionally up to 2 μm), and typically form a compact sterile lamella edge, though they are easily broken and may disappear. **Pleurocystidia** are absent. **Pileal squamules** are composed of a more or less parallel array of cylindrical, slightly thick-walled (≤ 3 μm) hyphae, which are clampless and range in color from greenish blue to grey or brownish yellow, 16－143 × 5－22 μm.

Ecology/Substrate/Host: *Armillaria gallica* subsp. *calidusa* was found on a wide range of substrates, including rotten wood of *Quercus mongolica*, *Prunus salicina*, *Corylus* sp., *Tilia amurensis*, *Larix olgensis*, and *Pinus koraiensis*, as well as on living trunks, roots, fallen trunks, and branches of angiosperms such as *Cerasus pseudocerasus* and *Gastrodia elata* cultivation beds, indicating a broad ecological range in forested areas of China (Qin et al., 2025).

Distribution: Distributed in a wide area from southwest and central China to northeast China.



Note a–f Basidiomata. Scale bars: a–f = 5 cm.

Figure 8.34 Basidiomata of *Armillaria gallica* subsp. *calidusa*

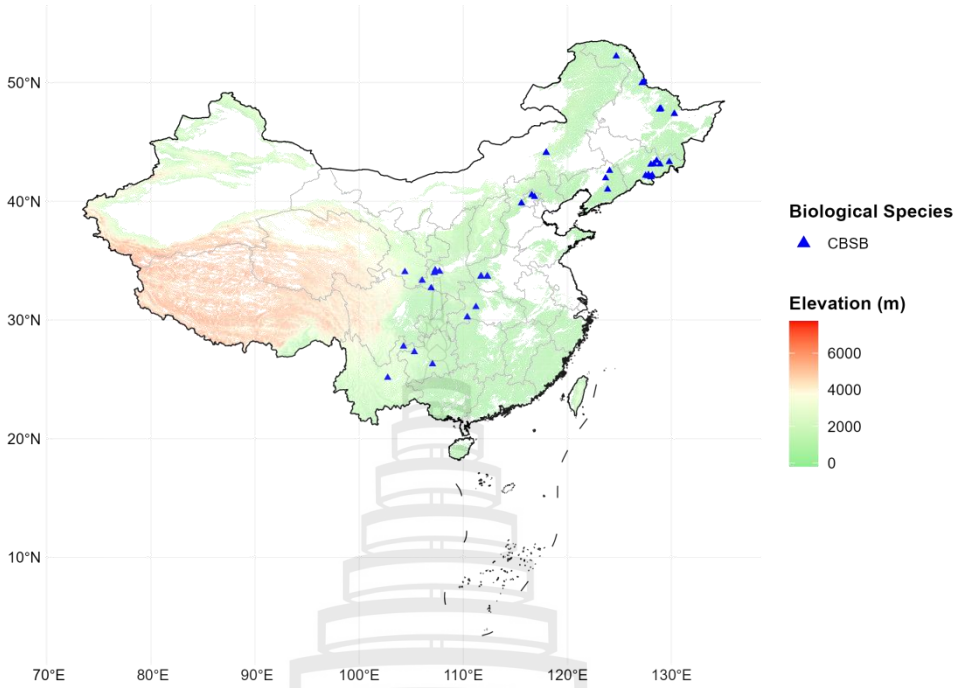


Figure 8.35 Distribution of samples of *Armillaria gallica* subsp. *calidusa* used in this study

Average nuclear Weir & Cockerham's F_{ST} vs. the closest species (*Armillaria gallica* subsp. *gallica*): 0.19.

Average mitochondrial dxy vs. the closest species (*Armillaria gallica* subsp. *gallica*): 0.05.

Average mitochondrial ΦST vs. the closest species (*Armillaria gallica* subsp. *gallica*): 0.77.

Armillaria gallica* subsp. *canadensis G.F. Qin, W.M. Qin, J. Zhao, & Y. Yuan

MycoBank: MB 854551

Biological species: North American Biological Species (NABS VII).

Qin et al. (2025) redefined *Armillaria gallica* from the Northern Hemisphere, North American, as *A. gallica* subsp. *canadensis* and is currently found in USA, Canada and Mexico.

Unable to retrieve available description records.

Average nuclear Weir & Cockerham's F_{ST} vs. the closest species: no data available.

Average mitochondrial dxy vs. the closest species: no data available.

Average mitochondrial ΦST vs. the closest species: no data available.

Armillaria gallica* subsp. *gallica G.F. Qin, W.M. Qin, J. Zhao, & Y. Yuan, Fig. 8.37

MycoBank: MB 854552

Biological species: European Biological Species E (EBS E).

This species was redefined by Qin et al. (2025) from the Northern Hemisphere, Europe, and is currently found in European countries.

Pileus measures 2.5－10.0 cm in diameter, initially broadly conical with a broad obtuse umbo and involute margin when young, later becoming applanate with a low obtuse umbo and inflexed margin. The color ranges from pale or dark brown to pinkish brown, fading to whitish towards the margin when young, and maturing to yellow-ochraceous or brown. The pileus scales are long, fibrillose, densely packed and almost pyramidal at the center, becoming scattered, single, and adpressed to erect towards the margin, dark brown at the center, concolorous with the pileus surface, and yellowish to whitish towards the margin. The margin soon becomes glabrescent, while the center remains scatteredly squamose. **Lamellae** are moderately close, emarginate, and decurrent with a vein. They are whitish initially, turning pale fleshy brown with a concolorous edge. The annulus is fibrillose to thin fibrillose-membranaceous, breaking up star-like, white, often with brown marginal scales and yellowish or brownish velar remnants below. **Stipe** can reach up to 120 × 12 mm, typically cylindrical with a distinctly clavate to (sub)bulbous base (up to 25 mm). It is white to pale fleshy above the annulus and fleshy brown to brown at the base, sometimes with a greyish tinge. Yellow stipe velar remnants are common, scattered, and fibrillose or fibrillose-tomentose. The context has an indistinct or unpleasant camembert smell and an unpleasant astringent taste (Antonín et al., 2009).

Basidiospores measure 7.5－11 (12) × 5.0－6.5 μm. They are often ellipsoid-amygdaloid, mixed with less frequent broadly ellipsoid ones, and can be thin- or thick-walled. **Basidia** are 32－45 × 7.5－9.0 μm, 4-spored, narrowly clavate, and clamped; crassobasidia are present. **Cheilocystidia** 15－25 × 5.0－12 μm, usually regular, less frequently irregular, clavate, subcylindrical, or subfusoid, mostly single, sometimes in

fascicles, 2—3-celled or in chains of cells in the lower part, thin- to slightly thick-walled, and clamped. The pileipellis is a cutis of radially arranged, ± cylindrical, thin- to slightly thick-walled, clampless hyphae with cylindrical, usually irregular to coralloid terminal cells. **Caulocystidia** 20 — 55 × 11 — 23 μm, broadly clavate, vesiculose, fusoid-clavate, and thin- to slightly thick-walled (Antonín et al., 2009). **Pileal squamules** 10—125 (175) × 5.0—25 μm, ellipsoid, subfusoid to cylindrical, slightly thick-walled, hyaline to brownish cells, 0—2-septate; terminal cells 15—130 × 5.0—25 μm, subulate, ellipsoid to cylindrical. Stipe velar hyphae are similar to those of the pileus scales.

Ecology/Substrate/Host: *Armillaria gallica* subsp. *gallica* is found in various habitats, including floodplain forests, wet alder stands, thermophilic oak and hornbeam stands, parks, and secondary plantations, primarily as a saprophyte on decomposing wood, roots, and stumps of broadleaved trees, and less frequently on conifers. It can act as a necrotrophic parasite on weakened trees, causing heart rot, and often co-occurs with other Armillaria species. Its hosts include a wide range of conifers (e.g., *Abies*, *Picea*, *Pinus*) and angiosperms (e.g., *Acer*, *Quercus*, *Populus*), fruiting from September to October (Antonín et al., 2009).

Distribution: Widely distributed in European countries.

Average nuclear Weir & Cockerham's F_{ST} vs. the closest species (*A. gallica* subsp. *calidusa*): 0.19.

Average mitochondrial dxy vs. the closest species (*A. gallica* subsp. *calidusa*): 0.05.

Average mitochondrial ΦST vs. the closest species (*A. gallica* subsp. *calidusa*): 0.77.



Note a–b Basidiomata. Scale bars: a–b = 5 cm.

Figure 8.36 Basidiomata of *Armillaria gallica* subsp. *gallica*

Armillaria gemina Bérubé & Dessur., *Mycologia* 81(2): 217 (1989)

Index Fungorum number: IF 136401

Biological species: North America Biological Species II (NABS II)

This species was described by Bérubé & Dessureault in 1989 from Canada, North America, the Northern Hemisphere. Currently known to be distributed in Quebec, located in the eastern part of Canada, and has been found in the USA (Bérubé & Dessureault, 1989; Tsykun, 2013).

Pileus 2—10 cm in diameter. Initially, it is hemispherical or obtusely parabolic, later becoming convex and eventually flat, sometimes with a small central bump (mammilate). **Pileus surface** is dry and varies in shades of brown, occasionally with hints of titian red but typically darker, resembling agathe. It is covered with distinct scales in dark brown to nearly black tones, more densely packed toward the center. **Margin** starts rolled inward, later turning downward, sometimes showing striations, and is usually the same color as the cap but can be paler, appearing cream, flesh, or hazel. The flesh is firm, 1—2 cm thick near the stipe's apex, and white in color. **Lamellae** are initially white or cream-colored, maturing to greyish orange or cinnamon. They are closely spaced, attached to the stipe (adnate) or slightly running down it (decurrent), and become wavy (sinuate) in mature specimens. They are thicker where they attach to the stipe and thinner toward the cap’s edge. **Stipe** is central, 5—8 cm in length and 0.5—1 cm in diameter at the top. It is club-shaped when young, becoming

more cylindrical with age. The upper part of the stipe, above the annulus, is white, while the lower part darkens to brown or reddish-brown. **Annulus** is thick and membranous, usually white to "alabaster," with a fluffy band at the edge ranging from tan to chestnut. It often breaks, leaving dark, fluffy remnants on the stipe that match the ring's color (Bérubé & Dessureault, 1989).

Basidiospores are ivory in mass, broadly elliptical to ovate, 8.2—10 × 5.2—7 μm, smooth, have a small projection, and are non-amyloid. **Basidia** are club-shaped, produce four spores, and some have a clamp connection. There are no pleurocystidia, but the gill edges are made up of polymorphic sterile cells (Bérubé & Dessureault, 1989).

Ecology/Substrate/Host: The basidiocarps of this species are found from August to late September, typically occurring singly or in large fasciculate groups on dead stumps, dead trees, dead roots, and occasionally healthy trees.

Distribution: Distributed in Canada and the United States in North America.

Average nuclear Weir & Cockerham's F_{ST} vs. the closest species (*A. borealis* subsp. *sinoborealis*): 0.22.

Average mitochondrial dxy vs. the closest species (*A. pseudoostoyae / A. ostoyae*): 0.12.

Average mitochondrial ΦST vs. the closest species: NA.

Armillaria granulosoides Zeller, *Mycologia* 25(5): 377 (1933)

Index Fungorum number: IF 266486

Biological species: No biological species information available

This species was described by Zeller in 1933 from the USA, North America, Northern Hemisphere. Currently known to be distributed in Oregon and Washington located in the northwestern part of the United States (Zeller, 1933).

Pileus measures 2—5 cm in width, starting convex and expanding to a flat shape, often with a depressed center. The surface is covered with squamulose to erect, squarrose scales, ranging in color from pale ochraceous-buff to tawny, sometimes staining nearly russet (drying to pale buff, pale ochraceous-buff, or pale ochraceous-buff). The areas between the scales are creamy or buffy. The flesh is thin and white to creamy in color. **Lamellae** are broad, close but not crowded, and inserted, attaching to the stipe (adnate) or slightly running down it (decurrent). They often break away and

are white to creamy (drying to pale buff), with even edges. **Stipe** is 2—5 cm long and 2—4 mm in diameter. It is rufescent to tawny both above and below, covered with floccose to subfloccose scales that form a slight, fleeting floccose ring. The scales are creamy to tawny in color.

Basidiospores are short ellipsoidal, hyaline, and measure 3—4.5 × 2—3 μm. They often adhere in groups of 2, 3, or 4.

Ecology/Substrate/Host: This species is gregarious and grows in mossy areas at the margins of young Douglas fir (*Pseudotsuga menziesii*) forests, at an elevation of 1300 feet.

Distribution: This species was found on the divide between Wren and Kings Valley in Benton County, Oregon, USA.

Average nuclear Weir & Cockerham's F_{ST} vs. the closest species: No data available.

Average mitochondrial dxy vs. the closest species: No data available.

Average mitochondrial ΦST vs. the closest species: No data available.

Armillaria griseomellea (Singer) Kile & Watling, *Trans. Br. mycol. Soc.* 81(1): 131 (1983)

Index Fungorum number: IF 108700

Biological species: No biological species information available.

Average nuclear Weir & Cockerham's F_{ST} vs. the closest species: No data available.

Average mitochondrial dxy vs. the closest species: No data available.

Average mitochondrial ΦST vs. the closest species: No data available.

Armillaria heimii Pegler, *Kew Bull., Addit. Ser.* 6: 92 (1977)

Mycobank: 308926

Biological species: No biological species information available.

This species was described by Heim (1963) from Madagascar, Africa, the Southern Hemisphere. It is known to be distributed in Madagascar (Heim, 1963).

Pileus 15—25 mm wide, convex, without an umbo, cream-colored at the base, covered with hispid, punctiform scales that remain erect and distant, dark reddish-brown in color, with a long-incurved, striate margin. **Stipe** floccose, ochraceous, white

at the top, thickened at the base, with a dentate, laciniate, whitish, fugacious annulus, initially accompanied by a few caducous scales. **Lamellae** flesh-colored to ivory, subdistant, somewhat thick, and deeply decurrent. Flesh very soft, ivory to white. **Basidiospores** ovoid, smooth, 6.2－8.4 × 5－5.8 µm (Heim, 1963).

Ecology/Substrate/Host: Found on decaying wood in ancient forests.

Distribution: Distributed in Montagne d'Ambre, Madagascar, Africa.

Average nuclear Weir & Cockerham's F_{ST} vs. the closest species (CBSG + CBSK lineage 1-nDNA): 0.40.

Average mitochondrial dxy vs. the closest species (CBSG + CBSK lineage 3-mtDNA): 0.12.

Average mitochondrial ΦST vs. the closest species: No data available.

Armillaria hinnulea Kile & Watling, *Trans. Br. mycol. Soc.* 81(1): 131 (1983)

Index Fungorum number: IF 108701

Biological species: No biological species information available.

This species was described by Kile & Watling in 1983 from Australia, Oceania, and the Southern Hemisphere. It is known to be distributed in Tasmania located to the southeast of Australian, and has been found in New Zealand (Kile & Watling, 1983; Coetzee et al., 2001).

Pileus of this species measures 2.0－8.0 (－10.0) cm in diameter, displaying colors ranging from brown to umber, fawn, or vinaceous-hazel. It is covered with small, obscure brown scales and is initially convex or subumbonate, later becoming plano-concave to slightly depressed with age. **Pileus surface** is tawny and hygrophanous, drying to vinaceous buff, avellaneous, or vinaceous fawn, often darker at the center or forming a darker zone toward the margin. It is squamulosic, particularly at the center, with small persistent 'Cigar Brown' (Ridgway) to fuscous black squamules, and is not viscid or at most subviscid with age. **Margin** is sometimes distinctly striate for up to one-third of the diameter. **Lamellae** are sinuate to subdecurrent, pale vinaceous to flesh-colored, moderately crowded (subconferted), and feature many small gills. **Stipe** 3.0-7.0 (-10.0) × 0.4-0.9 cm, floccose above the annulus, and whitish to ochraceous-brown. It is central, occasionally subcentral when in groups, cartilaginous, cylindrical, and tapers toward a bulbous to sub-bulbous base. The upper third of the stipe is 'Tilleul Buff' to pale 'Vinaceous Fawn', while the lower part is sepia to cigar brown. **Stipe** is

dry, fibrillose, sometimes with yellowish to greyish fibrils, and stuffed. **Veil** is arachnoid, fugacious, and often collapses to form only an annular zone, appearing greyish white or ‘Dresden Brown’ to ‘Old Gold’ (Ridgway) beneath (Kile & Watling, 1983).

Basidiospores measure 6－8.5 (－9) × 3.5－4.6 (－6.5) μm, are non-amyloid, moderately thick-walled, and white in mass. The flesh is ivory-colored in the pileus, sometimes with pinkish tints, and darker in the stipe, particularly toward the base. It has a strong, quickly astringent taste and an indistinct smell. **Basidia** are 21－47 × 5－9 μm, typically 4-spored (occasionally 2-spored), clavate-cylindric, and generally thin-walled, though some crassobasidia are present. They are hyaline or pale honey-colored in aqueous and ammoniacal solutions and lack basal clamp connections. **Pleurocystidia** are absent, while **cheilocystidia** measure 30－46 × 3－9 μm, are variable in shape (mainly cylindrical to cylindro-clavate), and have hyaline end-cells 8－25 μm long. **Pileal squamules** consists of three layers: an irregular suprapellis of hyaline to dark honey-colored, non-encrusted hyphae (3－7.5 μm broad), forming fascicles or solitary, inflated, broadly ellipsoid to clavate cells or chains of cells; a mediopellis that is hyaline and rarely prominent, seated on a subpellis of compacted, short, non-gelatinized cells; and a pileus trama of interwoven, hyaline or slightly colored, anastomosing, cylindric to inflated but rapidly collapsing hyphae, sometimes with latticiferous-like hyphae. The stiptipellis is composed of thickened, cylindrical hyphae, forming a poorly differentiated palisade of clavate to cylindric sterile cells, masked by copious velar material made of hyaline to slightly colored, flexuous, septate hyphae (Kile & Watling, 1983).

Ecology/Substrate/Host: This species is found from mid-February to June, occurring singly or in small groups of two to seven on stumps, standing trees, or fallen logs. Its hosts include *Eucalyptus regnans*, *E. obliqua*, *Nothofagus cunninghamii*, *Atherosperma moschatum*, *Acacia melanoxylon*, and *Pomaderris* sp.

Distribution: Distributed in Australia and New Zealand, Oceania.

Reference mitochondrial genomes: No data available.

Reference nuclear genomes: No data available.

Average nuclear Weir & Cockerham's F_{ST} vs. the closest species: No data available.

Average mitochondrial dxy vs. the closest species: No data available.

Average mitochondrial ΦST vs. the closest species: No data available.

Armillaria horrens (Berk.) Sacc., *Syll. fung. (Abellini)* 5: 82 (1887)

Index Fungorum number: IF 235852

Biological species: No biological species information available.

This species was described by Berkeley in 1850 from the India, Asia, and the Northern Hemisphere. It is currently known to be distributed in West Bengal, the northeastern part of India (Berkeley, 1850).

Pileus is convex, becoming flat, with a slightly wavy (repand) margin, and covered with conical, dark brown warts. It measures 2 inches broad, with arched borders, and is liver-colored, rough with conical dark-brown warts; the flesh is pinkish. **Lamellae** are slightly rounded (subrotund) at the back and extend linearly down the stem (decurrent). **Stipe** is robust, 3 inches or more in height, with a broad annulus (ring) near the top, covered in woolly scales, hollow, and tapering downward (Berkeley, 1850; Saccardo, 1887).

Ecology/Substrate/Host: Clustered on the bark of old trees, etc., at an elevation of 7,500 feet. Collected in June and July.

Distribution: This species is documented to occur in Darjeeling, India.

Average nuclear Weir & Cockerham's F_{ST} vs. the closest species: No data available.

Average mitochondrial dxy vs. the closest species: No data available.

Average mitochondrial ΦST vs. the closest species: No data available.

Armillaria jezoensis J.Y. Cha & Igarashi, *Mycoscience* 35(1): 42 (1994)

Index Fungorum number: IF 580659

Biological species: No biological species information available.

This species was described by Cha et al. (1994) from Japan, Asia, the Northern Hemisphere. It is known to be distributed in Hokkaido, located in the northern part of Japan (Cha et al., 1994).

Pileus measures 4.7－6.8 cm in diameter, initially hemispherical-convex to convex when young, becoming plano-convex to flat with age, sometimes slightly

umbonate, and irregularly undulating toward the margin. **Pileus surface** is dry, typically dark yellowish brown, strong brown, or reddish brown, occasionally reddish brown at the center. It is covered with fine fibers or small scales, dark brown to dusky red at the center, with fibers rarely dispersed toward the margin, transitioning to reddish brown or brownish yellow. **Margin** is inrolled at first, later becoming acute or slightly incurved, striate, and concolorous with the pileus, darkening with age, and attached to a whitish partial veil. The flesh is firm, thin to thick, and white in context. **Lamellae** are white when young, turning reddish brown to pink with age. They are close, sinuate, subdecurrent, and crenate, with a thick texture. **Stipe** is central, 3.9—6.1 cm in length and 0.7—1.1 cm in diameter. It is cylindrical, clavate to subclavate, fibrous, and white at the apex, transitioning to very pale brown or brown toward the base. The stipe is fragile, solid when young, and becomes stuffed with age. **Annulus** is fibrillate, submembranous, thin, and delicate, collapsing and appressed to the stipe later, and white (Cha et al., 1994).

Basidiospores are white in mass, broadly elliptical to ovate, with an apiculus, 6.3—10.3 × 4.8—6.3 μm. They have a smooth surface, are hyaline, and nonamyloid. **Basidia** are clavate, 39.1—44.1 × 6—7.8 μm, with 4 sterigmata and clamped at the base. **Pleurocystidia** are absent. **Pileal squamules:** The suprapellis consists of filamentous, parallel, thin-walled hyphae with cells 24.4—57.5 × 6.9—18.1 μm, featuring a brownish pigmented uppermost layer and septa without clamps. Mediopellis is composed of a tight mosaic of irregular, elliptic to globose, thick-walled hyphae with cells 9.4—54.2 (105) × 6.8—21.3 μm. **Subpellis** is made up of net-like, longitudinal, filamentous, loosely arranged, thin-walled hyphae with cells 27.9—169.2 × 4.2—18.3 μm, partially staining in toluidine blue. **Subhymenial hyphae** are filamentous, binucleate, and sometimes have a clamp. The lamellar trama is bilateral (Cha et al. 1994).

Ecology/Substrate/Host: The basidiomes of this species were collected from mid-September to late October in Hokkaido forests. They grow caespitose (in clusters) to solitary on decaying substrates such as stumps, trunks, and roots. The host range includes broad-leaved trees such as *Quercus mongolica* var. *grosseserrata*, *Ulmus japonica*, and *Prunus sargentii* in mixed and broad-leaved forests. Rhizomorphs are

found beneath the bark of decaying stumps and trunks, with a conspicuous distribution between wood tissues. In both natural habitats and pure culture, rhizomorphs are monopodial and cylindrical. The collection sites range from 10 to 400 meters above sea level.

Distribution: This species is documented to occur in Japan.

Average nuclear Weir & Cockerham's F_{ST} vs. the closest species: No data available.

Average mitochondrial dxy vs. the closest species: No data available.

Average mitochondrial ΦST vs. the closest species): No data available.

Armillaria korhonenii J.W. Liu, G.F. Qin, J. Chen, F.Q. Yu & Zhu L. Yang, *Phytotaxa* 637(2): 158 (2024), Figures 8.38－8.39

Index Fungorum number: IF 850866

Biological species: It belongs to the Chinese Biological Species Q (CBSQ).

This species was described by Liu et al., in 2024 from southwestern China, Asia, and the Northern Hemisphere.

Basidiomata tricholomatoid, small to medium-sized, occurring solitary, scattered, or in clusters. **Pileus** sub-hemispherical, convex to plano-convex when young, and plane to applanate when mature, reaching up to 7 cm in diameter. **Pileus surface** is yellowish orange to honey yellow, densely covered with brown, taupe, or pale reddish brown fibrillose squamules when young, becoming somewhat sparse when mature. **Margin** is incurved, irregular, and adorned with fibrillose squamules derived from the breaking up of the veil, appearing white. **Context** is 0.5－3 mm thick. **Lamellae** decurrent to sub-decurrent, white or cream when young, transitioning to flesh color, slightly yellowish orange, or somewhat yellowish with age. **Stipe** measures 50－90 × 5－9 mm, central, somewhat striate at the apex, fibrous, clavate, and often bulbous. It is honey yellow, brown, dark gray to dark brown, gradually darkening from top to bottom with age. The context is white to whitish. **Annulus** present, cottony to membranous, white to cream when young, and slightly brown to pale brown when mature (Liu et al., 2024).

Basidiospores measure 8－10 × 5－7 μm (Q = 1.33－1.8, Qm = 1.51 ± 0.13), ellipsoid to elongate, colorless, hyaline, smooth, and inamyloid. **Basidia** 25－30 × 7－

10 μm, clavate, 2- or 4-spored, often with a basal clamp connection; sterigmata are 4－5 μm long. **Pileal squamules** consist of sub-parallelly arranged hyphae, 5－20 μm wide, with nearly colorless or yellowish, thin to slightly thick cell walls. **Clamp connections** are common in all parts of the basidioma (Liu et al., 2024).

Ecology/Substrate/Host: Found singly, scattered, or clustered on rotten wood of fagaceous plants in subtropical evergreen broad-leaved forests at elevations of 1858－2529 m.

Distribution: Currently known from southwestern China.



Note a–e Basidiomata. f Basidiospores. g Basidia and Cystidia. h Hyphae of pileal squamules. Scale bars: a–e = 5 cm, f–h = 20 µm.

Figure 8.37 Basidiomata and morphological characteristics of *Armillaria korhonenii*

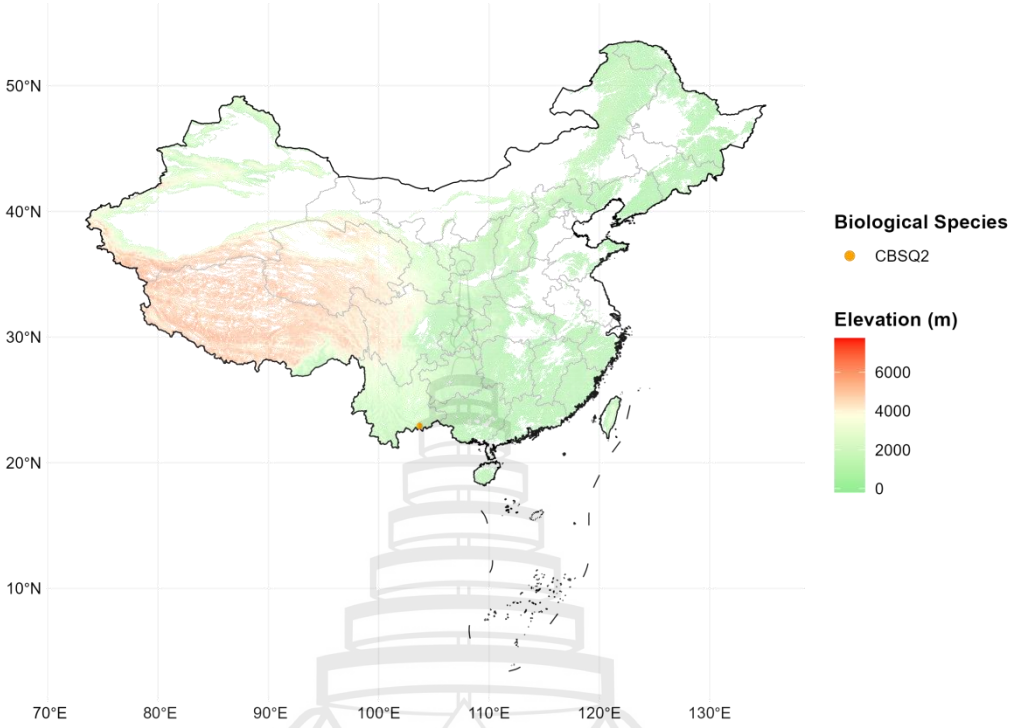


Figure 8.38 Distribution of samples of *Armillaria korhonenii* used in this study

New research specimens: **CHINA**, **Yunnan**, Pingbian County, Daweishan Natural Reserve, 22.9119°N, 103.6994°E, HKAS 126473; Pingbian County, Daweishan Natural Reserve, 22.9204°N, 103.6977°E, HKAS 126466; Pingbian County, Daweishan Natural Reserve, 22.9640°N, 103.7017°E, HKAS 126467; Pingbian County, Daweishan Natural Reserve, 22.9061°N, 103.6977°E, HKAS 126468; Pingbian County, Daweishan Natural Reserve, 22.9076°N, 103.6978°E, HKAS 126469; Pingbian County, Daweishan Natural Reserve, 22.9111°N, 103.7002°E, HKAS 126470; Pingbian County, Daweishan Natural Reserve, 22.9127°N, 103.6995°E, HKAS 126471; Pingbian County, Daweishan Natural Reserve, 22.9134°N, 103.6994°E, HKAS 126472; Near Miaofang Pass, Tianyu Township, Zhen'an Township, Longling County, Baoshan City, 24.4981°N, 98.9673°E, HKAS 95344.

Average nuclear Weir & Cockerham's F_{ST} vs. the closest species (*A. griseomellea*): 0.24.

Average mitochondrial dxy vs. the closest species (*A. griseomellea*): 0.09.

Average mitochondrial ΦST vs. the closest species (*A. griseomellea*): 0.81.

Armillaria laricina (Bolton) Sacc., *Syll. fung. (Abellini)* 5: 81 (1887)

Index Fungorum number: IF 236052

Biological species: No biological species information available.

This species was described by Berk (1887) from Europe, the Northern Hemisphere.

Basidiomata are fleshy, soft, convex, obtuse, and glabrous with a smooth margin. *Lamellae* are adnate, distant, narrow, and white. *Annulus* is apical and floccose. *Stipe* is spongy-solid, thick, and smooth. *Basidiospores* unknown. *Cheilocystidia* not provided. This species can be found single, scattered, or clustered on the trunks of *Larix* species (Larch) in Europe (Saccardo 1887).

Average nuclear Weir & Cockerham's F_{ST} vs. the closest species: No data available.

Average mitochondrial dxy vs. the closest species: No data available.

Average mitochondrial ΦST vs. the closest species: No data available.

Armillaria limonea (G. Stev.) Boesew., *N.Z. Jl agric. Res.* 20: 585 (1977)

Index Fungorum number: IF 308927

Biological species: No biological species information available.

This species was described by Stevenson (1964) from Wellington, New Zealand, Oceania Southern Hemisphere. It is known to be distributed in the North Island, Australasia, and South America (Coetzee et al., 2001, Coetzee et al., 2003).

Pileus measures 8—13 cm in diameter, lemon yellow in color, and is densely covered with dark brown, tufted scales at the center, becoming sparser toward the margin. It is dry, initially convex with a strongly down-rolled margin, and later becomes almost plane with a waved edge. The flesh is firm and white. **Lamellae** are sinuately decurrent, moderately crowded, creamy white when young, and develop a pinkish fawn stain with age. **Stipe** is 10—15 cm long and 1—1.5 cm thick, pale brown above a substantial floccose ring, shading to brown or olive green below. It is velutinate (velvety), sometimes with a few tufted scales, solid, tough, and slightly bulbous at the base (Stevenson, 1964).

Basidiospores are ovoid, 7－8 × 5－6.5 µm, non-amyloid, and moderately thick-walled, with a white spore print (Stevenson, 1964).

Ecology/Substrate/Host: This species is found in dense groups around standing dead *Nothofagus* trees.

Distribution: It is known to be distributed in the North Island, Australasia, and South America.

Average nuclear Weir & Cockerham's F_{ST} vs. the closest species: No data available.

Average mitochondrial dxy vs. the closest species: No data available.

Average mitochondrial ΦST vs. the closest species: No data available.

Armillaria luteobubalina Watling & Kile, *Trans. Br. mycol. Soc.* 71(1): 79 (1978)

Index Fungorum number: IF 308928

Biological species: No biological species information available.

This species was described by Podger in 1978 from Victoria, Oceania, Australia, and the Southern Hemisphere (Podger et al., 1978).

Pileus 4.0－7.0 (up to 10.0) cm in diameter, firm-fleshy but not thick at the margin, initially convex with a strongly inrolled margin, eventually expanding and becoming slightly concave, sometimes with small squamules. It is initially dark brown at the disk, paler towards the margin, soon developing yellowish hues, ranging from lemon-yellow to honey-brown as dark brown squamules disperse. **Squamules** are dense at the disk but sparser towards the margin, dentate at the edge, occasionally striate for 1－5 mm with age, and easily removable along with the "cuticle" by peeling. **Lamellae** are fleshy and pliable, subdecurrent, less frequently distinctly decurrent, sometimes with lines running down the apex of the stipe, white to pallid at first, becoming brownish-cream or pinkish-brown with age, some bifurcating, crowded, with lamellulae of 4－5 lengths, and an even margin. The Flesh is white, woolly to stringy in the stipe, with a lingering, strong, bitter, and acrid taste. **Stipe** is 4.0－10.0 (up to 12.0) cm long and 0.75－1.2 (up to 1.5) cm wide, central, tough but cartilaginous, solid, slightly thickened towards the base, sometimes subbulbous, fibrillose-streaked throughout, pinkish-white at the apex, darkening to brownish and then dark red-brown

to olivaceous brown with age, tinged yellowish below a moderately thick, floccose, persistent ring that may become laciniate with age (Podger et al., 1978).

Basidiospores (5－) 6.5－7.5 (－8) × (4－) 4.5－5.5 (－6) µm, broadly ellipsoid with a distinct broad apiculus, ivory white in mass, becoming cream upon drying, hyaline in water and ammoniacal solutions, non-amyloid, cyanophilic, red in erythrosin in 10 % ammoniacal solution, apparently smooth, moderately to slightly thick-walled. **Basidia** 4-spored (some 2-spored), 20－35 (up to 40) × 5－10 µm, hyaline, thin-walled, lacking basal clamp connections; sterigmata up to 4 µm long. **Pleurocystidia** apparently absent; cheilocystidia variable, predominantly clavate cells forming a sterile margin, interspersed with ventricose cells, some 2-celled, 15－30 × 6－10 µm, hyaline, thin-walled. **Pileal squamules** composed of interwoven, swollen short units forming a cutis with an irregular cubical pattern, overlying an unpigmented subpellis of interwoven, more cylindrical hyphae; mediopellis giving rise to or intimately connected with chains of dark brown, short, elongate ellipsoid, fairly thick-walled cells adhering together in groups to form either appressed or recurved to suberect squamules (Podger et al., 1978).

Ecology/Substrate/Host: Solitary to subcaespitose, found on roots and at the base of stumps of dead or dying *Eucalyptus regnans*.

Distribution: Dumbrell Block, Traralgon, Victoria, Australia.

Average nuclear Weir & Cockerham's F_{ST} vs. the closest species: No data available.

Average mitochondrial dxy vs. the closest species: No data available.

Average mitochondrial ΦST vs. the closest species: No data available.

Armillaria luteopileata G.F. Qin, J. Zhao, W.M. Qin & K. Korhonen, *Mycology* 16(2):793, Figures 8.40－8.41

Index Fungorum number: IF 831855

Biological species: Chinese Biological Species C (CBSC).

This species was described by Qin et al. in 2024 from China, Asia, the Northern Hemisphere.

Basidiomata small to medium-sized, solitary to clustered, caespitose or loosely grouped on fallen trunks and branches, generally golden yellow with brown scales.

Pileus 1.7－7.5 cm in diameter, 0.5－1.5 cm thick, initially hemispherical-convex to convex, then plano-convex to applanate, sometimes slightly depressed; usually dry; brownish yellow to brown at the center when young; pale yellow to brown at the margin, pale yellow to dark brown at the center when mature. Pileal scales fibrillose, yellowish brown, brown, dark brown, distributed over the entire pileal surface but more concentrated and suberect towards the center, more dispersed and flattened towards the margin. **Margin** entire, sometimes slightly incurved, usually striate, sometimes with white velar remnants. **Lamellae** sinuate or decurrent, sometimes with striped ridges down to the annulus, white to yellowish white to orange-grey when mature, subdistant, lamellulae present, margin smooth. **Stipe** central, 3－10 cm long, 0.3－2 cm in diameter at the apex, cylindrical or clavate, white, yellowish-white to brownish orange above the annulus; the middle greyish orange to brown; the base greyish orange to dark brown; densely covered with white, pale yellow, pale yellow flocculose veil remnants, reminiscent of snakeskin markings. **Annulus** membranous or cortinate, persistent or ephemeral, usually a membranous annulus if the outer veil leaves remnants on the margin of the pileus, inner veil white, outer margin pale yellow, reddish yellow, occasionally with yellowish brown scales; sometimes a cortinate annulus when the veils are broken at the junction with the stipe (Qin et al., 2024).

Basidiospores ivory white in mass, ellipsoid, lacking a suprahilar depression, (4.0)7.0－9.8(10.5) × (4.0)4.5－6.0(7.5) μm; thin- to slightly thick-walled (≤ 1 μm), hyaline to brownish yellow, smooth, cyanophilous, inamyloid, with a prominent apiculus. **Basidia** clavate, 10.0－45.0 × 6.0－12.0 μm, upper portion constriction inconspicuous or occasionally constricted, with a clamp connection at the base, four-sterigmate, thin- to slightly thick-walled, yellowish green to brownish yellow. The pigments of the basidia dissolve gradually in KOH; sometimes brownish yellow crassobasidia (≤ 1.5 μm thick) are formed when the lamellae develop abnormally. Sterigmata 1.5－6 μm. **Cheilocystidia** 8－32 × 4.5－13 μm, polymorphic, viz., fusiform, elliptical, cylindrical, ovoid, with a clamp connection at the base, sometimes with a papilla or irregular, slender papilla at the apex; hyaline, thin- to slightly thick-walled (≤ 0.4 μm), forming a compact sterile lamella-edge, but it is easily broken and disappears. **Pleurocystidia** absent. **Pileal squamules** composed of more or less

parallel, cylindrical, slightly thick-walled (≤ 1 μm) hyphae, simple septate, grey to brownish yellow, 12.0－122.0 × 4.0－32.0 μm (Qin et al., 2024).

Ecology/Substrate/Host: The species was found on living or fallen broadleaf and coniferous trees, including *Betula platyphylla* (White Birch), *Picea koraiensis* (Korean Spruce), *Abies nephrolepis* (Sakhalin Fir), *Betula ermanii* (Erman's Birch), *Tilia amurensis* (Amur Linden), and *Ulmus pumila* (Siberian Elm). It was also found on decaying gymnosperm and angiosperm wood (Qin et al., 2024).

Distribution: Distributed in Northeast China.

New study specimens: **CHINA**, **Jilin**, Yuehualin conifers, Changbai Mountain, 128.0500°E, 42.0500°N, 21024 (strain); Baihe fair, Changbai Mountain, Fusong County, Baishan City, 128.0166°E, 42.0500°N, C19004 (strain); Dixiasnelin, Changbai Mountain, Fusong County, Baishan City, 128.0500°E, 42.0500°N, C21019 (strain); Lushuihe town, Changbai Mountain, Fusong County, Baishan City, 127.9833°E, 42.5333°N, CBSB19029 (strain); Dixiasnelin, Changbai Mountain, Antu County, Yanbian Korean Autonomous Prefecture, 128.0666°E, 42.0833°N, CBSC21009 (strain); Baihe, Changbai Mountain, Fusong County, Baishan City, 128.0166°E, 42.0500°N, CBSC96027 (strain); Erdaobaihe, Changbai Mountain, Fusong County, Baishan City, 128.0166°E, 42.0500°N, CBSC96029 (strain); Dixiasnelin, Changbai Mountain, Fusong County, Baishan City, 128.0166°E, 42.0166°N, CBSC96038 (strain). **Heilongjiang**, Daqing Mountain Liangshui Nature Reserve, Yichun City, 128.8923°E, 47.1876°N, HKAS 86578; Fenglin National Nature Reserve, Fenglin County, Yichun City, 129.1958°E, 48.1332°N, HMJAU 24389; Fenglin National Nature Reserve, Fenglin County, Yichun City, 129.1958°E, 48.1332°N, HMJAU 60487. **Inner Mongolia Autonomous Region**, Delbul Forest Farm, Daxinganling, 121.1070°E, 50.9923°N, MHHNU 7783. **Henan**, Xixia Occupy Fungi Industry Co., Ltd., Xixia County, Nanyang City, no coordinates provided, LZL-5 (commercial strain).



Note a–d Basidiomata. Scale bars: a–d = 5 cm.

Figure 8.39 Basidiomata of *Armillaria luteopileata*

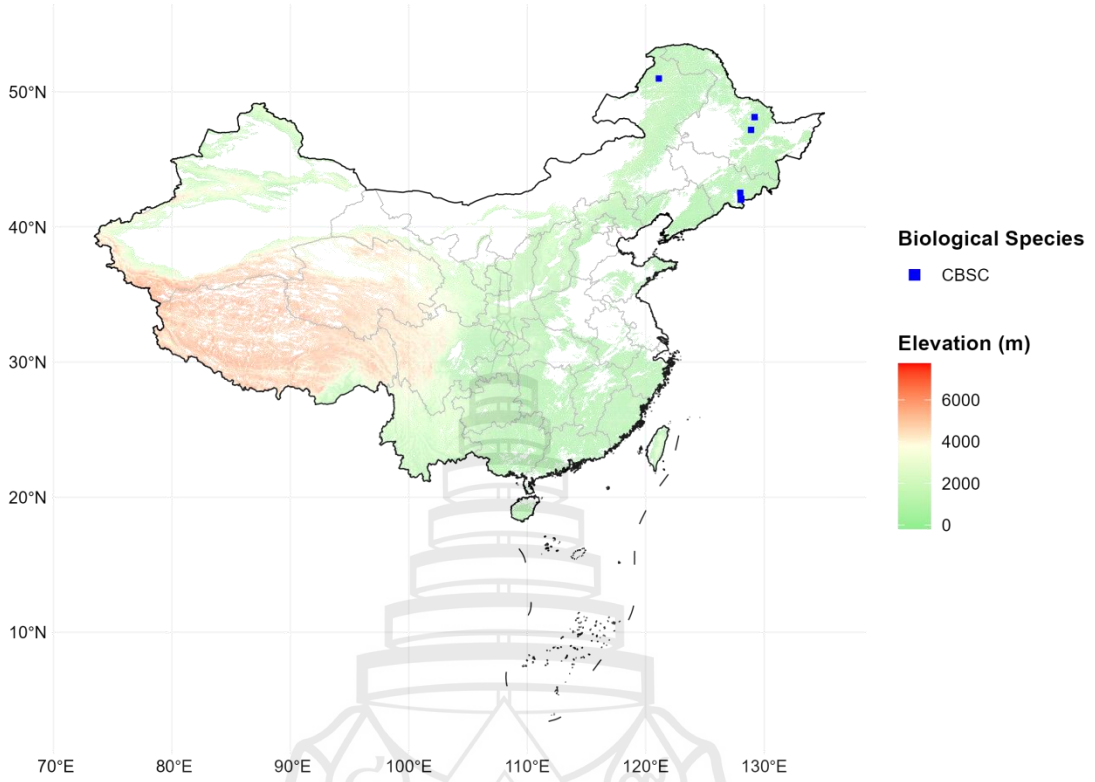


Figure 8.40 Distribution of samples of *Armillaria luteopileata* used in this study

Average nuclear Weir & Cockerham's F_{ST} vs. the closest species (*A. sinapina* subsp. *alpina*/*A. sinensis*): 0.18.

Average mitochondrial dxy vs. the closest species (*A. sinensis*/*A. cepistipes*): 0.04.

Average mitochondrial ΦST vs. the closest species (*A. cepistipes*): 0.68.

Armillaria macrospora Peck, Bull. *Torrey bot. Club* 27(12): 610 (1900)

Index Fungorum number: IF 190323

Biological species: No biological species information available.

This species was described by Peck (1900) from Colorado, North America, the Northern Hemisphere.

Pileus is 5—20 cm in diameter, fleshy, fragile, convex, glabrous, viscid when moist, and shining when dry, white in color with occasional browning at the center; the flesh is white. **Lamellae** are relatively narrow, close, decurrent, and white. **Stipe** is 2.5

—5 cm long and 1.2—2.0 cm thick, short, stout, subequal, white, with a thick, white annulus.

Basidiospores are oblong or subfusiform, 12—15 × 6—8 µm (5.5—8 × 3.5—5 µm, ellipsoid in profile and face view, round in polar view, smooth and hyaline in KOH, thin-walled, walls inamyloid, not dextrinoid, acyanophilic. **Basidia** are 30—33 × 5.5—7 µm, elongate-clavate, 4-sterigmate, lacking cyanophilic bodies. **Hymenial cystidia** are not differentiated. **Lamellar trama** is composed of parallel hyphae, cylindric or often inflated, 2.5—20 µm in diameter. **Subhymenium** is compact and interwoven hyphae, distinct. **Pileal context** consists of interwoven hyphae, 4—15 µm in diameter. **Pileal squamules** an ixolattice (Hesler & Smith, 1979), a loosely interwoven layer (30 — 85 µm thick) of gelatinized hyphae, cylindric or mostly collapsed, 1.5—5 µm in diameter, hyaline in KOH, arising from a compact layer of repent, radially arranged, non-gelatinized hyphae, non-incrusted, cylindric, 3—7 µm in diameter, hyaline in KOH. The **Stipitipellis** below the annulus is a compact layer of repent, parallel hyphae, non-incrusted, cylindric, 4—8 µm in diameter, with a thin interwoven layer of repent gelatinized hyphae, non-incrusted, cylindric, 2—5 µm in diameter, lying over or produced from the layer of compact parallel hyphae. **Veil** is composed of interwoven hyphae, cylindric or inflated, 4—11 µm in diameter, thin-walled and hyaline in KOH. **Clamp connections** are absent.

Ecology/Substrate/Host: The species typically grows singly or in clusters and is found in dense spruce woods.

Distribution: Distributed in Colorado, United States.

Average nuclear Weir & Cockerham's F_{ST} vs. the closest species: No data available.

Average mitochondrial dxy vs. the closest species: No data available.

Average mitochondrial ΦST vs. the closest species: No data available.

Armillaria mellea (Vahl) P. Kumm., *Führ. Pilzk.* (Zerbst): 134 (1871)

Index Fungorum number: IF 190066

Biological species: Europe Biological Species D (EBS D).

This species was described by Kummer (1871) from Europe, the Northern Hemisphere.

Pileus is yellowish-brown or orange-yellow, often with brown spots, and has a wrinkled margin. It is moist and slimy when wet, with abundant hair-like scales that are initially brown or black. **Pileus surface** is typically smooth but can become slightly scaly with age, especially towards the center. The pileus is convex when young, flattening out as it matures, and can reach a considerable size, often growing in clusters (Kummer, 1871).

Ecology/Substrate/Host: Parasitically on a large number of broadleaf trees.

Distribution: Distributed in Europe.

Average nuclear Weir & Cockerham's F_{ST} vs. the closest species: No data available.

Average mitochondrial dxy vs. the closest species: No data available.

Average mitochondrial ΦST vs. the closest species: No data available.

Armillaria melleorubens (Berk. & M.A. Curtis) Sacc., *Syll. fung.* (Abellini) 5: 81 (1887)

Index Fungorum number: IF 184326.

Biological species: No biological species information available.

This species was described by Saccardo (1887) from Cuba, Central America.

Pileus is thin, smooth, striated, and somewhat leathery, 2.5 cm across, with a pale brown color that shades to pink at the edge. **Stipe** is solid, slightly thickened at both ends, powdery, and features an apical ring, standing 4 cm long and 6 mm thick. **Lamellae** are broad, adnate to decurrent, and white with a rosy tint. **Basidiospores** are white and subglobose (Saccardo, 1887).

Ecology/Substrate/Host: This species is found on oaks and in hollow trunks.

Distribution: Now known to be distributed in Cuba and North America.

Average nuclear Weir & Cockerham's F_{ST} vs. the closest species: No data available.

Average mitochondrial dxy vs. the closest species: No data available.

Average mitochondrial ΦST vs. the closest species: No data available.

Armillaria mexicana Elías-Román, Medel, Alv.-Ros., J.W. Hanna, Ross-Davis, Mee-Sook Kim & N.B. Klopf., *Mycologia* 110(2): 352 (2018)

Index Fungorum number: IF 814489

Biological species: No biological species information available.

This species was described by Elías-Román et al. (2018) from Mexico, North America, and the Northern Hemisphere.

Pileus is umbonate, convex, or plane to plane-convex when mature, with the center slightly umbonate to depressed and orbicular in apical view. **Margin** is deflexed to lobed, with an entire to dentate edge and a striate surface. **Pileus surface** is moderate orange-yellow at the center, and pale yellow has fibrillose squamules of moderate brown dispersed toward the margin and is hygrophanous. **Lamellae** are close, decurrent, adnate, thick, with smooth edges, 9 mm deep, and pale yellowish pink to pale yellowish pink. **Lamellulae** are attenuate, concolorous with the lamellae, and have smooth edges. The partial veil has rounded, irregular scales on its underside, pale pink, and falls apart from the stipe to form an annulus. **Stipe** is central, cylindrical, solid, slightly squarrose, with pale greenish-yellow and pale-yellow scales. The stipe color ranges from pale orange under the annulus to pale olive grey, moderate olive brown, and dark grayish reddish brown toward the base in fresh specimens, (39—)74—109 mm long × 5—8 mm wide. The base lacks rhizomorphs. The spore print is white. The taste and odor of fresh samples were not tested. The basidiome is caespitose, gregarious, and rarely solitary when growing in association with Prunus persica roots. **Annulus** is apical, persistent, simple, membranous, slightly striate on the upper surface, peronate, pale orange, and pale yellowish pink, 5—7 mm wide.

Basidiospores are ellipsoidal, smooth under a light microscope but ornamented with a slightly to moderately rugulose surface in a pattern of longitudinal ridges under scanning electron microscopy, hyaline, guttulate, 7—10(—12) × 5—7 µm (mean 8.7±1.2 × 5.9 ± 0.6 µm), thin-walled, and inamyloid. **Basidia** are clavate, with 2—4 sterigmata, hyaline, (32—)36—45 × 8—10 µm (mean 39.6±3.9 × 8.9±0.8 µm), thin-walled, and lack clamp connections at the base. **Sterigmata** are 3.5—4.5 µm long, rarely up to 10 µm (under SEM). **Pileal squamules** consist of parallel hyphae 40—60 µm wide, with hyphae 8—13 µm in diameter, hyaline to slightly yellowish, thin-walled, and without clamp connections.

Subpellis (hypodermium) is 20－30 µm wide, hyaline to slightly yellowish. **Caulocystidia** are scarce, clavate, ventricose, rostrate, hyaline, approximately 30 × 10 µm, and thin-walled. **Cheilocystidia** are cylindrical, clavate to mucronate, some with a long neck, hyaline, 20－40(－46) × (3－)4－7(－11) µm, thin-walled, abundant, and lack clamp connections at the base.

Ecology/Substrate/Host: The species was found in commercial orchards in Coatepec Harinas, State of Mexico, primarily on dead *Prunus persica* and *Quercus* sp. (Oak) trees, as well as on living *Olea europaea* trees. The collection sites are located at elevations of 2200 to 2300 meters above sea level. Specimens were collected in July.

Distribution: Now known to be distributed in Mexico.

Average nuclear Weir & Cockerham's F_{ST} vs. the closest species: No data available.

Average mitochondrial dxy vs. the closest species: No data available.

Average mitochondrial ΦST vs. the closest species: No data available.

Armillaria montagnei (Singer) Herink, *Sympozium o Václavce Obecné Armillaria mellea (Vahl ex Fr.) Kumm.* (Brno): 41 (1973)

Index Fungorum number: IF 134988

Biological species: No biological species information available.

This species was described from Argentina (Southern Hemisphere: South America) by Singer (1956) and is currently known to be distributed in Europe and South America (Herink, 1973).

Average nuclear Weir & Cockerham's F_{ST} vs. the closest species: No data available.

Average mitochondrial dxy vs. the closest species: No data available.

Average mitochondrial ΦST vs. the closest species: No data available.

Armillaria nabsnona T.J. Volk & Burds., in Volk, Burdsall & Banik, *Mycologia* 88(3): 487 (1996)

Index Fungorum number: IF 415561

Biological species: North American biological species ninth (NABS IX).

This species was described by Volk et al. (1996) from Jefferson County, Washington, USA, North America, Northern Hemisphere (Volk et al., 1996).

Pileus is initially convex, becoming plane as it matures, with a diameter of 4—7 cm when fully expanded. **Pileus surface** is smooth and hygrophanous, appearing slimy when wet, and sometimes adorned with short dark fibrils on the disc when young. The disc is "snuff brown," fading to a paler hue toward the margins, often displaying darker, irregular bruise-like areas on or near the surface. **Margin** is slightly incurved, "clay-colored," and translucent, striate to furrowed. **Context** is 0.5—1 mm thick and white. **Lamellae** are adnate to subdecurrent, subdistant, 0.75—1 mm wide, white to cream-colored, darkening with age to pinkish-tan, often developing brownish patches. **Stipe** is 8—10 cm long, 4—5 mm broad at the base, narrowing to 2—3 mm at the apex. The base is "mummy brown," transitioning to a paler "buckthorn brown" or "warm buff" near the annulus. **Stipe** features white cottony patches below the annulus, with a white, fibrous context that "peels" away in parallel strips, a characteristic typical of *Armillaria* species. The partial veil in young specimens is dense and white, cottony until rupture. The annulus initially flares upward but soon becomes ragged as the pileus expands. It may persist as an evanescent cortina but is often washed away, difficult to observe, sometimes completely disappearing upon drying. **Rhizomorphs** are frequently absent; when present, they are thick (1—2 mm broad), black, and branching (Volk et al., 1996).

Basidiospores are white in mass; ovoid to subglobose; (6—)8—10 × 5.5—6.5 µm, smooth, somewhat thick-walled at maturity, hyaline, and negative in Melzer's Reagent. **Basidia** are clavate; 25—35 × 5.5—6 µm, 3—4 µm broad just distal to the clamped basal septum; four-sterigmate; sterigmata 4.5—6 µm long at maturity, 1 µm wide at the base; featuring a clamp connection at the base. A second basidium often forms from the basal clamp connection, and occasionally a third basidium develops from a clamp on the second. This is most evident in young, incompletely expanded basidiomata. **Cystidia** are not observed, but thin (2—3 µm wide) hypha-like cells can occasionally be found among the basidia. **Pileal squamules** is composed of swollen, unbranched, hyaline, terminal cells, 40—60 × 14—16 µm, with an underlying layer of more or less parallel, hyaline hyphae, 7—8 µm wide. The partial veil is composed of

more or less parallel, hyaline hyphae, 4－7 μm in diameter, rarely branching, with frequent simple septa (Volk et al., 1996).

Ecology/Substrate/Host: The species is typically gregarious but not caespitose, forming branched black rhizomorphs or 1 mm-thick pseudosclerotial plates within the wood. Basidiomata have been observed in both the fall (September to November) and the spring (April in Oregon).

Distribution: It is known to be distributed in North America.

Average nuclear Weir & Cockerham's F_{ST} vs. the closest species (*A. tibetica* (CBS J) lineage 1-mtDNA): 0.24.

Average mitochondrial dxy vs. the closest species (*A. calvescens*): 0.06.

Average mitochondrial ΦST vs. the closest species: No data available.

Armillaria nigropunctata Herink, *Sympozium o Václavce Obecné Armillaria mellea (Vahl ex Fr.) Kumm.* (Brno): 44 (1973)

Index Fungorum number: IF 134991

Biological species: No biological species information available.

Unable to retrieve available description records.

Average nuclear Weir & Cockerham's F_{ST} vs. the closest species: No data available.

Average mitochondrial dxy vs. the closest species: No data available.

Average mitochondrial ΦST vs. the closest species: No data available.

Armillaria novae-zelandiae (G. Stev.) Herink, *Sympozium o Václavce Obecné Armillaria mellea (Vahl ex Fr.) Kumm.* (Brno): 43 (1973)

Index Fungorum number: IF 308929

Biological species: No biological species information available.

Described by Stevenson in 1964 from New Zealand, Oceania, the Southern Hemisphere. It is known to be distributed in New Zealand and temperate Australia (Guillaumin, 1992; Kile & Watling, 1983).

Pileus is 3－8 cm in diameter, olivaceous-buff to olivaceous-brown, with minimal dark brown scales scattered toward the center. Initially convex with a strongly deflexed-revolute margin, it later becomes plane to slightly concave. When fresh, the margin is conspicuously striate and moist, darkening when dry. The flesh is cream-white. **Lamellae** are decurrent to nearly sinuate, cream-white when young, later

darkening to fulvous, moderately crowded, with numerous short lamellulae. **Stipe** is 4—7 cm long, 0.4—0.8 cm thick, fulvous above the evanescent annulus, brown to dark purple-brown below, smooth or striate, tough, solid, with swollen and fused bases (Stevenson, 1964).

Basidiospores are 8—9 × 5.5—6.5 µm, non-amyloid, with fairly thick walls; the spore print is white (Stevenson, 1964).

Ecology/Substrate/Host: The species grows on fallen wood or roots in the litter of Nothofagus forests.

Distribution: Now known to be distributed in New Zealand and Australia.

Average nuclear Weir & Cockerham's F_{ST} vs. the closest species: No data available.

Average mitochondrial dxy vs. the closest species: No data available.

Average mitochondrial ΦST vs. the closest species: No data available.

Armillaria omnituens (Berk.) Sacc., *Syll. fung.* (Abellini) 5: 84 (1887)

Index Fungorum number: IF 190438

Biological species: No biological species information available.

This species was described by Berk in 1887 from Darjeeling, India, Asia, Northern Hemisphere, in 1887.

Pileus is 5 cm in diameter, rose-gray in color, umbilicate, thin, and expanded, with a fleshy texture. The center is floccose-verrucose, while the margin is striate and glabrous. **Stipe** is solid, short, dark, and glabrous, over 2 cm in length and reddish-brown in color. **Annulus** is spreading, and the lamellae are pale flesh-colored and decurrent (Berk, 1887).

Ecology/Substrate/Host: This species grows on dead wood at an elevation of 2590 meters.

Distribution: Now known to be distributed in India.

Average nuclear Weir & Cockerham's F_{ST} vs. the closest species: No data available.

Average mitochondrial dxy vs. the closest species: No data available.

Average mitochondrial ΦST vs. the closest species: No data available.

Armillaria ostoyae (Romagn.) Herink, *Sympozium o Václavce Obecné Armillaria mellea (Vahl ex Fr.) Kumm.* (Brno): 42 (1973)

Index Fungorum number: IF 134992

Biological species: Europe Biological Species C (EBS C).

This species was described by Romagnesi et al. (1970) from France, Europe, Northern Hemisphere.

Pileus is 5—10 cm in diameter, broad, hemispherical-campanulate or obtusely parabolic when young, becoming convex and finally plane with age. **Pileus surface** is dry, ranging from pale colors like “orange white” or “caramel brown” to darker shades such as reddish brown, “raw Sienna”, “pale brown”, yellowish brown), “burnt Sienna”, “tan,” or “leather”, and even very dark colors like “eye brown” or “brownish grey”. Distinct scales in shades of dark reddish colors or dark brownish colors are distributed over the surface, more densely toward the center. The margin is inrolled at first, then downturned, sometimes striated, entire, usually concolorous with the cap but sometimes paler, often “cream,” “flesh,” or "camel." The flesh is firm, 1—2 cm thick at the apex of the stipe, with a white context. **Lamellae** are white or “cream” when young, turning greyish orange or “cinnamon” with age, rather close, adnate to slightly decurrent, becoming sinuate in mature specimens, thick at the point of attachment to the stipe but thinner toward the margin. **Stipe** is central, 5—20 cm long, 1.5 cm thick at the apex, clavate when young, becoming more or less equal, fibrous, with a white to “alabaster” context. Bright yellow to greenish yellow mycelial fibers are often present at the base. The stipe is covered with fibers ranging from greyish orange, “pale brown”, “burnt Sienna”, to “hazel”, staining black or sometimes “mahogany red”, and is sometimes deeply striated. **Annulus** is thick, membranous, usually white to “alabaster,” circled with a thick fluffy band at the margin ranging from “tan” to “chestnut”, often broken in many places, leaving the stipe marked and covered with dark fluffy remnants concolorous to the ring (Bérubé & Dessureault, 1988).

Basidiospores are ivory in mass, broadly elliptical to ovate, 5.5—7 × 8—11 µm, smooth, apiculate, and nonamyloid. **Basidia** are clavate, four-spored, some with a clamp connection. Pleurocystidia are absent. The margin of the lamellae is composed of polymorphic sterile cells. **Pileal squamules** consist of three layers: a suprapellis of loose, more or less parallel, thick-walled hyphae (5—20 × 18—55 µm); a mediopellis of tightly arranged, almost regular, very thick-walled cells (4—9 × 9—44 µm), staining

blue in toluidine blue; and a subpellis of loosely arranged, irregular, thin-walled globular cells (9—15 × 25 µm) in a complex network. The subhymenial hyphae are filamentous, unclamped, and binucleate (Bérubé & Dessureault, 1988).

Ecology/Substrate/Host: It is highly pathogenic to a number of commercial softwoods, notably Douglas-fir, true firs, pine trees, and Western Hemlock (Vince, 2015).

Distribution: Distributed in Europe.

Average nuclear Weir & Cockerham's F_{ST} vs. the closest species (*A. conifericola*): 0.11.

Average mitochondrial dxy vs. the closest species (*A. pseudoostoyae*): 0.05.

Average mitochondrial ΦST vs. the closest species (*A. pseudoostoyae*): 0.68.

Armillaria pallidula Kile & Watling, *Trans. Br. mycol. Soc.* 91(2): 307 (1988)

Index Fungorum number: IF 133876

Biological species: No biological species information available.

This species was described by Kile and Watling (1988) from Queensland, Australia, Oceania, Southern Hemisphere.

Pileus is 45—90 mm in diameter, initially campanulate with an inrolled margin, becoming convex to subumbonate and expanding to plano-convex or slightly depressed with age. **Margin** is irregularly revolute and often splits radially as it matures. The color is tawny when young, transitioning to yellowish buff or pale fulvous, darker toward the center, though often becoming concolorous with age. **Pileus surface** is covered with minute fulvous or tawny scales that are irregularly and sparsely distributed initially but disappear with age. The pileus is non-viscid. **Stipe** is 52—64 × 20—24 mm, typically elongate, narrower at the top and enlarging toward the base, which is more or less clavate or bulbous, though in larger basidiomes it may appear more cylindrical, pale overall, particularly below the ring, and is white fibrillose on a buff background when young, flocci are lacking or indistinct, and the stipe is cartilaginous and stuffed. The veil is cortinate, thin, and generally fugacious, usually collapsing into indistinct darkened remnants that adhere to the stipe. It is pallid at first, with darker floccules below. **Lamellae** are subdecurrent to distinctly decurrent in larger basidiomes, anastomosing, fairly crowded, very pliable but relatively thick, pale tawny, somewhat

mottled, with lamellules of 1—2 lengths, sometimes intervened. The flesh is firm and thick in the pileus, pallid, becoming more fibrous in the stipe and darkening downward. Taste and odor are unrecorded.

Basidiospores are cream-colored, darkening to dark cream (crème foncé, Romagnesi, 1967), 4.4—6.3 × 5.6—10 µm (average 5.2—7.1 µm), elongate to broadly ellipsoid, elliptic in side view with a broad prominent apiculus. They are moderately to distinctly thick-walled, hyaline to honey-colored in ammoniacal solutions, cyanophilic in cotton blue, non-amyloid, smooth, lacking surface irregularities and internal wall structures, and lacking a germ pore or apical thinning. **Basidia** are 42.5—55 × 4—5.5 µm, expanding to 8.25—10 µm at the apex, 4-spored (occasionally 2-spored), with sterigmata < 8.5 µm long. They are elongate-clavate, slightly constricted at the lower septum, hyaline to distinctly honey-colored in aqueous ammoniacal solutions and water, intermixed with abundant honey-colored to yellowish, sometimes septate crassobasidia of similar size. **Pleurocystidia**, if present, are not differentiated and resemble elongate crassobasidia or simply abortive basidia. The cheilocystidia form a sterile edge that soon collapses to form an agglutinated zone. They are clavate to cylindric, with an obtuse or slightly tapered (torpedo-shaped) apex, or slightly swollen toward the middle, hyaline or honey-colored, 25—65 × 4—8 µm, thin-walled. **Pileal squamules** is a collapsed radially arranged cutis of two narrow layers, with the suprapellis (when present) consisting of upward-directed hyphae, often reduced to a strongly colored non-gelatinized subpellis seated on the pileus trama of open, floccose, hyaline or pale honey, septate hyphae 7—14 µm broad, compacted upward to give a faint pinkish honey-colored zone in ammoniacal solution. The suprapellis consists of groups of disarticulating hyphae 8—11 µm broad (16—55 µm long), forming islands of erect or upturned short chains of pale tawny orange, smooth cells with slightly more thick-walled and slightly swollen rounded-end cells < 17.5 µm broad. The subpellis is a compacted zone of narrow, hyaline hyphae < 8.5 µm broad, some brick-like, slightly gelatinized toward the base. Caulocystidia are present only at the very apex of the stipe, forming islands of cylindric-clavate, flexuous, thin-walled, smooth, hyaline cells arising as erect or upturned hyphae or as chains similar to those in the pileipellis, though narrower (5—7.5—8 µm broad) and less differentiated toward their apex. They soon

collapse and are masked downward by filamentous hyphae of the velar tissue, often collapsing together to form columns. The inner velar hyphae are 4－8 μm broad, hyaline, thin-walled, flexuous, intertwined, only slightly constricted at septa. The outer velar hyphae are 8－17 μm broad, hyaline, thin-walled, smooth, cylindric, often quite short (>25 μm long), constricted at septa, with end-cells slightly swollen, adhering in parallel groups but ultimately disorganizing to form a tangled web. **Clamp connections** are very rare, sometimes present in the trama. Crystals are frequent throughout the tissues.

Ecology/Substrate/Host: The species grows in subtropical dry coastal lowland sclerophyll eucalypt forests on sandy soils. It is associated with root rot of *Pinus elliottii* and *Pinus caribaea* in plantations that have replaced the native community.

Distribution: Now known to be distributed in Australia.

Average nuclear Weir & Cockerham's F_{ST} vs. the closest species: No data available.

Average mitochondrial dxy vs. the closest species: No data available.

Average mitochondrial ΦST vs. the closest species: No data available.

Armillaria paulensis Capelari, *Mycol. Res.* 112(9): 1125 (2008)

Index Fungorum number: IF 510907

Biological species: No biological species information available.

This species was described by Lima et al. (2008) from Brazil, South America, the Southern Hemisphere.

Pileus is 0.9－9.2 cm in diameter, initially convex, becoming plano-depressed with age, spadiceous-brown to olivaceous-brown, with brown squamules concentrated at the center. **Margin** is dentate to entire, with remnants of the partial veil, and slightly pinkish. The color is brownish beige to olivaceous-brown, darker at the center. **Lamellae** are adnate to somewhat decurrent, pinkish white when immature, becoming distinctly pinkish with age, crowded, with entire margins and lamellulae. **Stipe** is 2.6 －8.5 × 0.2－0.6 cm, central, cylindrical, pinkish beige near the apex and above the annulus, concolorous with the lamellae; dark greyish brown under the annulus, and olivaceous at the base, where it matches the color of the pileus surface. The stipe is longitudinally striate. **Annulus** is well-developed, membranous, persistent to

fugacious, dirty white to cream-colored, with a yellowish to yellow or olivaceous margin. **Spore print** was not observed. The context is white, composed of hyaline, septate, thin-walled hyphae, some inflated, without clamp connections, 14—20 µm in diameter (Lima et al., 2008).

Basidiospores are elongate-ellipsoid, hyaline, slightly thick-walled, without a germ pore, inamyloid, 8.5—10 × 5.5—6 µm. **Basidia** are cylindric, hyaline, thin-walled, 2—4 spored, without clamp connections at the base. Pleurocystidia are absent. The cheilocystidia are clavate, dispersed, hyaline, thin-walled, 31—53 × 7.5—8 µm. The hymenophoral trama is indistinctly bilateral, hyaline, with hyphae hyaline, septate, thin-walled, some inflated, without clamp connections, 6—15 µm in diameter. **Pileal squamules** is undifferentiated, with prostrate hyphae, non-gelatinized, thin-walled, septate, hyaline to brownish hyphae, 6—12 µm in diameter. Rhizomorphs are absent (Lima et al., 2008).

Ecology/Substrate/Host: Gregarious to caespitose, found on logs of an unidentified angiosperm tree within the forest.

Distribution: Now known to be distributed in Brazil.

Average nuclear Weir & Cockerham's F_{ST} vs. the closest species: No data available.

Average mitochondrial dxy vs. the closest species: No data available.

Average mitochondrial ΦST vs. the closest species: No data available.

Armillaria pelmispora G.F. Qin, H.X. Ma, J.W. Liu, J. Zhao & W.M. Qin, Figures 8.42—8.43

MycoBank: MB 854557

Biological species: No biological species information available.

This species was described by Qin et al. (2025) southwestern China, the Northern Hemisphere.

Pileus is 5.0 — 12.0 cm in diameter, 0.5 — 1.5 cm thick, initially convex, becoming plano-convex to depressed with age, and dry. When young, the margin is yellow, and the center is grayish orange. At maturity, the margin becomes grayish orange to brownish orange, while the center turns brownish orange to pale brown. The pileal scales are nearly denuded, with white fine fibrils concentrated at the center. The

margin is entire, incurved or straight, with radial striations. **Lamellae** are adnate to nearly adnate with a decurrent tooth, with striations extending downward to the annulus. Initially pale yellow to dull yellow, they mature to pale yellow, orange white, and pale orange. The lamellae are subdistant, and have smooth margins. **Stipe** is central, 3—9 cm long, 0.4—1.4 cm in diameter at the apex, cylindrical when occurring in fasciculate groups. When young, the stipe is yellowish white above the annulus, dull yellow in the middle, and grayish yellow at the base. At maturity, it becomes yellowish white above the annulus, pale orange in the middle, and brownish orange at the base. The stipe is longitudinally striped and covered with white fibrillose flocks. **Annulus** is membranous, thick, persistent, superior, longitudinally striped, white or nearly white. Rhizomorphs are not observed.

Basidiospores are broadly ellipsoid, ellipsoid, elongate, fusiform, or foot-shaped (nearly 1/5th proportion), (7.0)7.5—11.0(15.0) × (4.0)4.5—5.9(6.0) μm. They lack a suprahilar depression, are slightly thick-walled, colorless to pale yellowish brown, smooth, cyanophilous, and nonamyloid. **Basidia** are clavate, 20—37 × 5.0—9.0 μm, with the upper portion slightly constricted or inconspicuously constricted, simple septate, four-sterigmate (occasionally two-sterigmate), thin-walled, pale yellow to brownish yellow. The pigments of the basidia gradually disappear in KOH solutions. Crassobasidia are not observed. **Cheilocystidia** are 11—38 × 3—10 μm, polymorphic sterile cells, ovate, cylindrical, clavate to utriform to broadly subcapitate, some with a slender, long neck at the apex or forked papilla; usually catenulate-septate, forming chains of cells; simple septate and lacking clamp connections; colorless, thin-walled. Pleurocystidia are absent. **Pileal squamules** are composed of a parallel array of nearly cylindrical, thin-to slightly thick-walled (≤ 1.0 μm) hyphae, clampless, grey to brownish yellow, 16—75 × 8—23 μm.

Ecology/Substrate/Host: Fasciculate to caespitose on fallen trunk or rotten wood.

Distribution: Now known to be distributed in Southwest China.



Note a–d Basidiomata. Scale bars: a–b = 5 cm.

Figure 8.41 Basidiomata of *Armillaria pelmaspora*

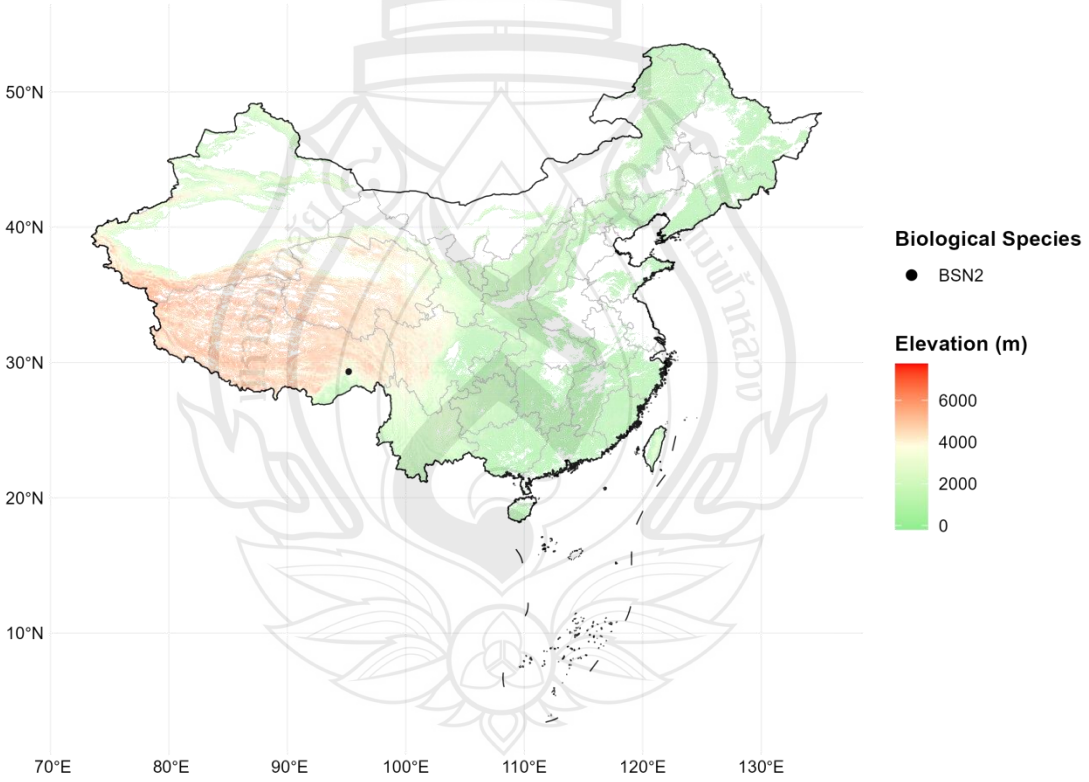


Figure 8.42 Distribution of samples of *Armillaria pelmaspora* used in this study

Additional material examined: CHINA, **Tibet Autonomous Region**, Paimo Road, Motuo County, Linzhi City, 95.1667°E, 29.3000°N, HKAS 135507; Paimo Road, Motuo County, Linzhi City, 95.1834°E, 29.3414°N, HKAS 135508.

Average nuclear Weir & Cockerham's F_{ST} vs. the closest species (*A. puiggarii*): 0.37.

Average mitochondrial dxy vs. the closest species (CBSK+G 3): 0.12.

Average mitochondrial ΦST vs. the closest species: No data available.

Armillaria procera Speg., *Boln Acad. nac. Cienc. Córdoba* 11(4): 385 (1889)

Index Fungorum number: IF 179369

Biological species: No biological species information available.

This species was described by Spegazzini (1889) from Apiahy, Paraguay, South America, Southern Hemisphere.

Pileus is initially ovate or conical, more or less umbonate, later expanding to 3－8 cm, often depressed at the center, densely covered with minute furfuraceous squamules in youth, becoming smoother with age, radially coarsely cracked, with a smooth, striate margin, dark reddish-brown at the center, and pale yellowish-brown at the edges. The flesh is floccose and white, scarcely developed at the center. **Lamellae** are attenuate-acute, adnate to decurrent, with entire edges, pale whitish to white, often with a white powdery coating, moderately crowded, membranous, polymacrious, and 4－5 mm wide. **Stipe** is curved, cylindrical, slightly thickened at both ends (5－7 cm long × 5－8 mm thick), fulvous to reddish-brown or chestnut-colored, paler at the top, adorned with a broad, spreading, thin-membranous ring, often with a crenulate edge, densely covered with minute longitudinal fibrils and furfuraceous particles below, often slightly bulbous-thickened at the base, growing in clusters (Spegazzini 1889).

Basidiospores are ovoid, smooth (8－40 × 6－7 μm), hyaline, and filled with granules.

Ecology/Substrate/Host: It was found on decaying fallen trunks.

Distribution: Now known to be distributed in Paraguay.

Average nuclear Weir & Cockerham's F_{ST} vs. the closest species: No data available.

Average mitochondrial dxy vs. the closest species: No data available.

Average mitochondrial ΦST vs. the closest species: No data available.

Armillaria puiggarii Speg., *Boln Acad. nac. Cienc. Córdoba* 11(4): 384 (1889)

Index Fungorum number: IF 179595

Biological species: No biological species information available.

This species was described by Spegazzini (1889) from Apiahy, Paraguay, South America, Southern Hemisphere.

Pileus honey-colored, smooth, and glabrous; the flesh is white, somewhat succulent, and thin. **Lamellae** moderately crowded, membranous, somewhat thin, attenuate-acute at the front, adnate to sub-sinuate at the back, often with a minute decurrent tooth, white or very pale yellowish-brown, with entire edges. **Stipe** cylindrical, curved, attenuate at the front, obclavate and thickened at the back, with 3－20 stems growing in clusters at the base. The exterior is whitish-yellow, smooth, and glabrous or often notably fibrous-twisted; the interior is white, solid, or almost hollow. **Annulus** white, attached to the upper quarter or fifth of the stem, small, membranous, often quickly disappearing (Spegazzini, 1889).

Basidiospores globose to ovoid, with a minute apiculus at the base (9－10 × 7－8 μm), smooth, without or with granules, hyaline when alive, and very pale yellowish-brown when dry (Spegazzini, 1889).

New study specimens: **Guadeloupr**, **Petit-Bourg**, PPg85-63 (strain).

Average nuclear Weir & Cockerham's F_{ST} vs. the closest species (*A. pelmaspora*): 0.37.

Average mitochondrial dxy vs. the closest species (*A. pelmaspora*): 0.15.

Average mitochondrial ΦST vs. the closest species: NA.

Armillaria pungentisquamosa G.F. Qin, W.M. Qin, J. Zhao & K. Korhonen, *Mycologia* 16(2): 795 (2024), Figures 8.44−8.45

Mycobank: MB 836021

Biological species: It belongs to the Chinese Biological Species P (CBS P).

This species was described by Qin et al. (2024) from China, Asia, and the Northern Hemisphere.

Basidiomata small to medium-sized, solitary, fasciculate, caespitose, or loosely clustered on fallen trunks, stumps, and at the base of living trees. **Pileus** 2－10 cm diam., 0.3－1.5 cm thick; initially convex with a small pointed umbo, later plano-convex to applanate or depressed, usually with mammilla, surface dry. Color ranges from pale to brownish orange and yellowish brown at the margin, becoming light to

dark brown toward the center; young pilei are paler, mature pilei are darker. **Pileal squamules** spiky with stiff, erect hairs, denser and suberect at the center, more dispersed and flattened toward the margin, colored light to dark brown. **Margin** entire, incurved to straight, striate. **Lamellae** sinuate, sometimes subdecurrent or adnate with a decurrent tooth, with ridges extending downward toward the annulus; initially orange-white to pale orange, later yellowish brown to dark brown; subdistant, lamellulae present, edge smooth. **Stipe** central, 2－11 cm long, 0.3－1.2 cm diam. at apex, cylindrical in clusters or broader at base when solitary, longitudinally striate. Color greyish yellow to orange above annulus, brownish orange to dark brown below, base often covered with dense greyish yellow to greenish floccules. **Veil remnants** white to greenish yellow, sometimes forming zigzag markings. **Annulus** submembranous to arachnoid, thin, ephemeral, white to nearly white. **Rhizomorphs** black, thick, cylindrical, monopodially branched (Qin et al., 2024).

Basidia clavate, 18－41 × 6－8.5 μm, sometimes slightly constricted near apex, with basal clamp connections, four-sterigmate, thin-walled, pale yellow to brownish yellow; pigments dissolve in KOH, occasionally forming crassobasidia ≤ 1 μm thick; sterigmata 2－6 μm long. **Basidiospores** ivory white in mass, ellipsoid, lacking suprahilar depression, (6.0)6.5－8.8(9.6) × (4.0)4.5－6.0(6.4) μm; Q = (1.16)1.22－1.79(2.05), Qm = 1.47 ± 0.14; thin- to thick-walled (≤ 1 μm), nearly colorless to pale yellow, smooth, cyanophilous, inamyloid, with prominent apiculus. **Cheilocystidia** 10－80 × 4－11 μm, polymorphic (clavate, fusiform, cylindrical), with basal clamp connections, often bearing irregular or branched papillae at apex; nearly colorless to yellowish brown, thin- to slightly thick-walled (≤ 0.5 μm), forming compact sterile lamellar edges that are fragile and easily lost. **Pleurocystidia** absent. **Pileal squamules** composed of parallel cylindrical hyphae, 15－98 × 5－29 μm, thin- to slightly thick-walled (≤ 1 μm), clampless, brownish yellow (Qin et al., 2024).

Ecology/Substrate/Host: Fruiting bodies occur on a wide range of substrates, including fallen trunks, dead stumps, and rotten roots of both angiosperms and gymnosperms. Recorded hosts comprise *Betula albosinensis*, *Fagus* sp., *Sycopsis sinensis*, *Cerasus pseudocerasus*, *Salix babylonica*, and other broad-leaved trees, as well as rotten wood of *Abies*.

Distribution: Known from several localities in central and western China, including Hubei Province (Hefeng County, Mulinzi Nature Reserve; Wufeng County, Houhe Nature Reserve), Sichuan Province (Meishan, Emei Mountains), Xizang Autonomous Region (Motuo County, Nyingchi), and Yunnan Province.



Note a–d Basidiomata. Scale bars: a–b = 5 cm.

Figure 8.43 Basidiomata of *Armillaria pungentisquamosa*

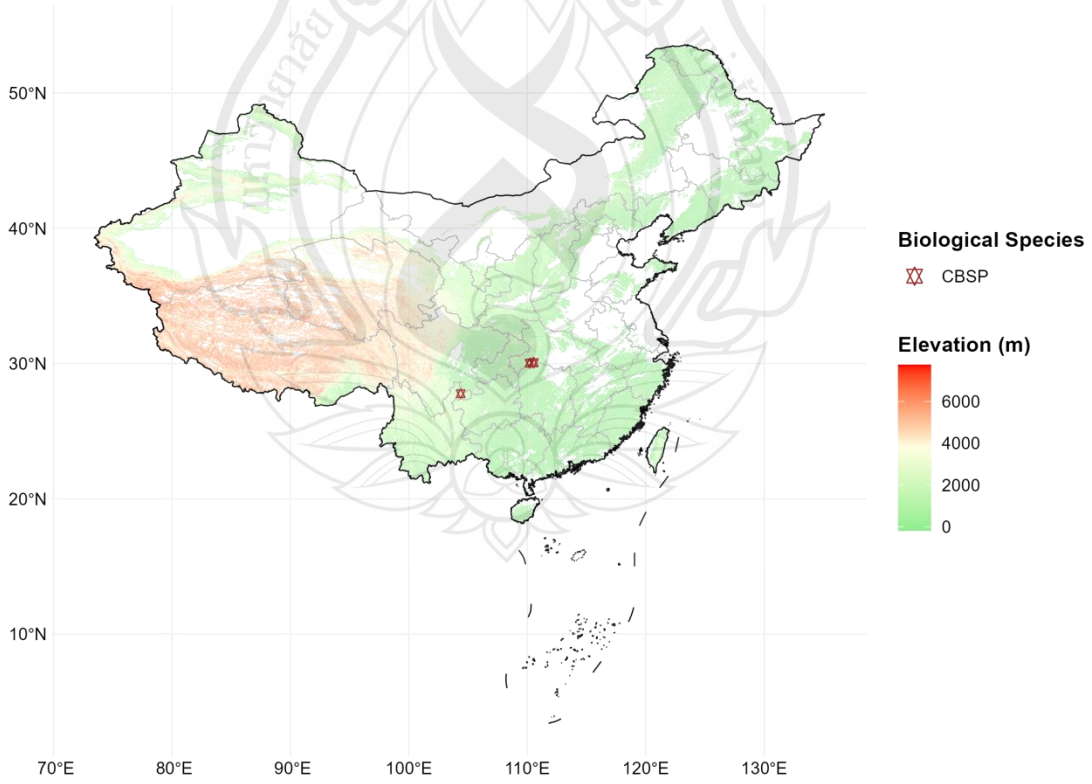


Figure 8.44 Distribution of samples of *Armillaria sinapina* subsp. *sinapina*

Average nuclear Weir & Cockerham's F_{ST} vs. the closest species (*A. algida*): 0.32.

Average mitochondrial dxy vs. the closest species (*A. linzhiensis*/*A. tibetica* (CBS J) lineage 2-mtDNA/*A. tibetica* (CBS J) lineage 3-mtDNA/*A. amygdalispora*/*A. violacea*): 0.04.

Average mitochondrial ΦST vs. the closest species (*A. amygdalispora*): 0.36.

Armillaria sinapina* subsp. *alpina G.F. Qin, J. Zhao, Y. Yuan & Y.C. Dai

MycoBank: MB 854558

Biological species: It belongs to Chinese Biological Species A (CBS A).

This species was described by Qin et al. (2025) from China, Asia, Northern Hemisphere.

Pileus is 3—10 cm in diameter, initially campanulate or hemispherical with a mammilla, later plano-convex or applanate, sometimes depressed or undulate with mammillae. **Pileus surface** is dry, colored pale yellow to brown, often darker at the center. Colors range from greyish yellow to brownish orange and brown; scales are hairy, greyish white to brown, more crowded and erect toward the center, and flattened toward the margin. **Margin** is entire, slightly incurved, often with radial striations and white veil remnants. **Lamellae** are decurrent to long decurrent, sometimes sinuate, white to yellowish grey or pale orange, subdistant with a smooth margin. **Stipe** is central, 4—10 cm long, 0.4—1.5 cm thick at the apex, cylindrical to clavate, and colored white to greyish brown depending on the region. Veil remnants often densely cover the stipe, occasionally forming zigzag markings. **Annulus** is arachnoid, thin and delicate, collapsing with maturity and usually appressed to the stipe. The inner veil is white to yellowish white, while the outer margin is greyish orange to brown.

Basidiospores are pale yellow in mass, ellipsoid to almond-shaped, (6)6.8—9(9.2) × (4)4.3—5.8(6) µm, Q = (1.32)1.33—1.85(2.09), Qm = 1.57 ± 0.13; smooth, cyanophilous, inamyloid, with prominent apiculus. **Basidia** are clavate, 30—49 × 6—10 µm, sometimes constricted near the apex, four-sterigmate, with clamp connections. **Cheilocystidia** are polymorphic, clavate to spherical, usually catenulate and forming chains, with clamp connections; pleurocystidia are absent. **Pileal squamules** are composed of cylindrical hyphae, thin- to slightly thick-walled, clampless, pale brown

to brownish yellow. **Rhizomorphs** are attached to the stipe base, monopodially branched.

Ecology/Substrate/Host: Fruiting bodies occur singly or in caespitose to imbricate caespitose clusters on stumps or fallen trunks. Found from late August to early September. Hosts include *Larix olgensis*, *Pinus koraiensis*, *Abies nephrolepis*, *Betula ermanii*, *Salix* spp., and decayed angiosperm wood debris.

Distribution: Now known to be distributed in Jilin, Heilongjiang, and eastern Inner Mongolia, China, Northern Hemisphere.

New study specimens: **CHINA**, **Heilongjiang**, Dailing area, Liangshui virgin forest, 129.5300°E, 47.1861°N (approx.), QZ99108 (strain); Dailing area, Liangshui virgin forest, 129.5300°E, 47.1861°N (approx.), QZ99116 (strain); Dailing area, Liangshui virgin forest, 129.5300°E, 47.1861°N (approx.), QZ99117 (strain); Dailing area, Liangshui virgin forest, 129.5300°E, 47.1861°N (approx.), QZ99118 (strain); Dailing area, Liangshui virgin forest, 129.5300°E, 47.1861°N (approx.), QZ99121 (strain). **Jilin,** Antu County, Changbai Mountain Nature Reserve, 128.0500°E, 42.0500°N, QZ96025 (strain; **holotype**); Antu County, Changbai Mountain Nature Reserve, 128.0500°E, 42.0500°N, QZ96007 (strain); Antu County, Changbai Mountain Nature Reserve, 128.0500°E, 42.0500°N, QZ96008 (strain); Antu County, Changbai Mountain Nature Reserve, 128.0500°E, 42.0500°N, QZ96015 (strain); Antu County, Changbai Mountain Nature Reserve, 128.0500°E, 42.0500°N, QZ96017 (strain); Antu County, Changbai Mountain Nature Reserve, 128.0500°E, 42.0500°N, QZ96023 (strain); Antu County, Changbai Mountain Nature Reserve, 128.0500°E, 42.0500°N, QZ96041 (strain).

Average nuclear Weir & Cockerham's F_{ST} vs. the closest species: No data available.

Average mitochondrial dxy vs. the closest species: No data available.

Average mitochondrial ΦST vs. the closest species: No data available.

Armillaria sinapina* subsp. *sinapina G.F. Qin, J. Zhao, Y. Yuan & Y.C. Dai, Figures 8.44—8.45

MycoBank: MB 854559

Biological species: It belongs to the North American biological species IX.

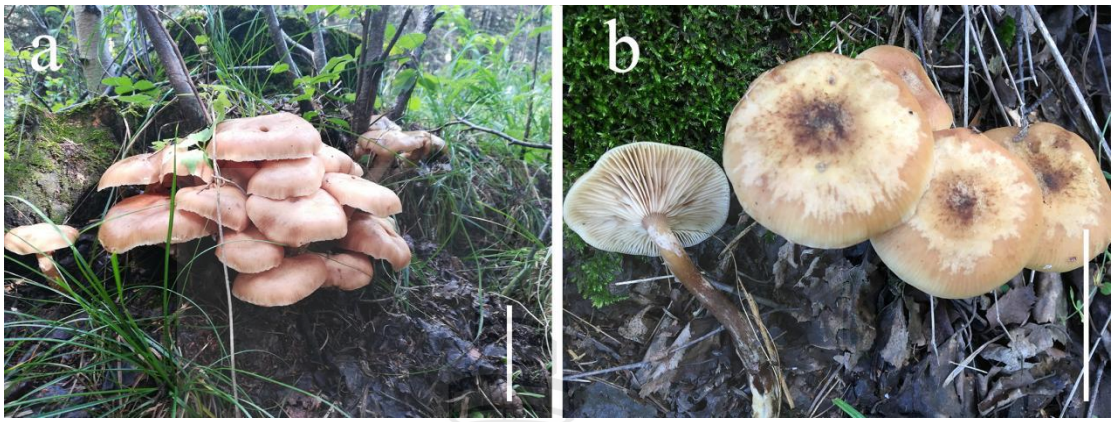
Described by Qin et al. (2025) from Canada, North America, the Northern Hemisphere.

Pileus is 2—6 cm in diameter, brown to umber, cinnamon, brick-red, or reddish-brown, covered with dark brown fibrils and scales, and initially convex before becoming plano-convex, occasionally mammilate. **Pileus surface** is fibrillous, rarely denuded, and typically covered with dark brown or brick-red tufts of hairs and fibrils, sometimes densely scaled. The universal veil is golden yellow to mustard yellow, covering young fruiting bodies and leaving small tufts of fibrils or wart-like structures on mature caps. **Margin** is straight, sometimes striate, concolorous with the cap or darker, with white membranous patches from the partial veil. **Lamellae** are cream to cinnamon, sinuate to subdecurrent, sometimes strongly decurrent, thick, and closely spaced. **Stipe** is central, 4—8 cm long, 0.5—1 cm thick at the apex, slightly striated, fibrous, and clavate. **Context** is cream to alabaster, covered with fine fibers, greyish-brown to brick-red, occasionally bruising. The base is darker, zoned with golden yellow ringlets of the universal veil, sometimes reduced to faint yellow fibers. **Annulus** is fibrous, sometimes membranous but very thin and delicate, later collapsing and usually appressed to the stipe, white to cream on the upper portion, and golden yellow to mustard yellow on the lower portion, sometimes entirely golden yellow or mustard yellow (Bérubé, 1988).

Basidiospores are ivory in mass, broadly elliptical to ovate, 5.9—8 × 8.2—10 µm, smooth, apiculate, and nonamyloid. **Basidia** are clavate, four-spored, and some have a clamp connection at the base. Pleurocystidia are absent. **Pileal squamules** consist of three layers: a suprapellis of parallel, loose, thin-walled, hyaline hyphae; a mediopellis of tightly packed, thick-walled, parallel hyphae; and a subpellis of loosely arranged, irregularly shaped, thick-walled hyphae. **Subhymenial hyphae** are filamentous, unclamped, and binucleate. **Lamella trama** is bilateral.

Ecology/Substrate/Host: Fruiting bodies are found from early September to early October, occurring singly or in small fasciculate groups of two to five on dead stumps, healthy roots, and trees. Hosts include *Acer saccharum* Marsh. *Acer saccharinum* L. (silver maple), and *Pinus strobus* L.

Distribution: Now known to be distributed in Canada, North America, Northern Hemisphere.



Note a–b Basidiomata. Scale bars: a–b = 5 cm.

Figure 8.45 Basidiomata of *Armillaria sinapina* subsp. *sinapina*

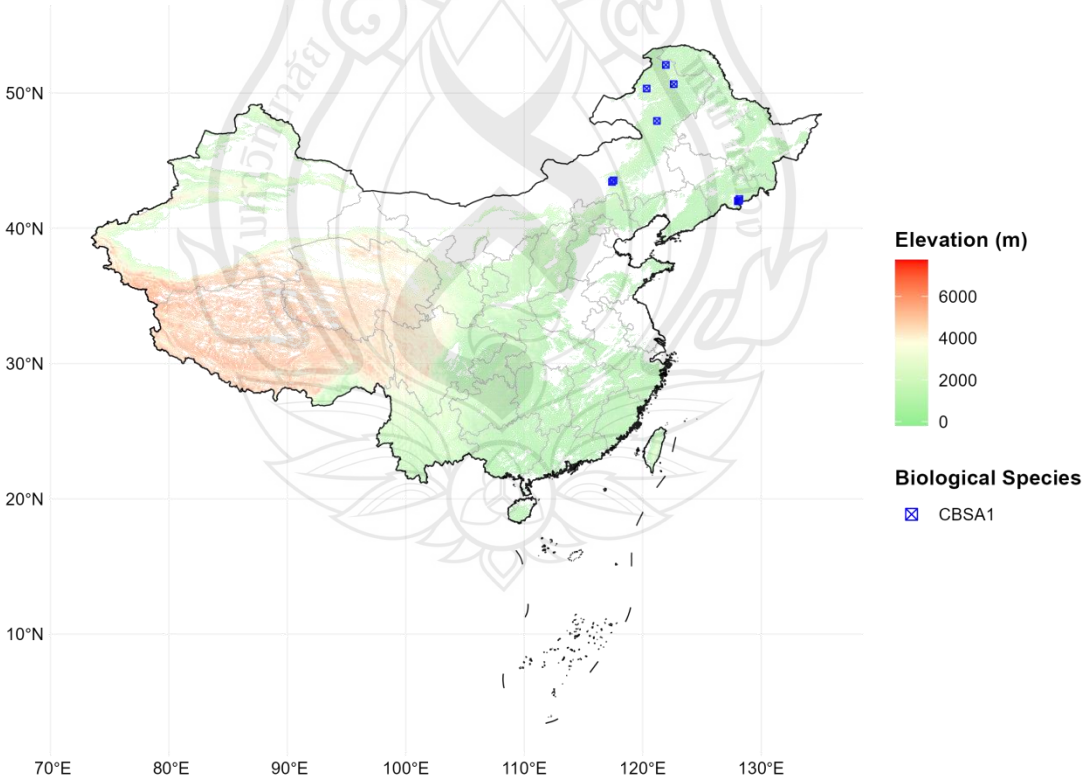


Figure 8.46 Distribution of samples of *Armillaria sinapina* subsp. *sinapina*

Additional material examined: **CHINA**, **Jilin**, Front Gate, Changbai Mountain, Fusong County, Baishan City, 128.1666°E, 42.1666°N, CBSA96008 (strain); Yuehualindai, Changbai Mountain, Fusong County, Baishan City, 128.0500°E, 42.0500°N, CBSA96016 (strain); Yuehualindai, Changbai Mountain, Fusong County, Baishan City, 128.0500°E, 42.0500°N, CBSA96025 (strain); Changbai Mountain, Antu County, Yanbian Korean Autonomous Prefecture, 128.1333°E, 42.0333°N, HMAS 96969; West Main Line, Changbai Mountain, Fusong County, Baishan City, 128.0216°E, 42.0030°N, HMJAU 22761. **Inner Mongolia Autonomous Region:** Taerqi Town, Yakeshi City, Hulunbeier City, 121.2004°E, 47.9381°N, CBSA96042 (strain); Huanggangliang, Hexigten Banner, 117.5368°E, 43.5456°N, HMAS 248128; Huanggangliang, Hexigten Banner, 117.5368°E, 43.5456°N, HMAS 255468; Huanggangliang, Hexigten Banner, 117.5368°E, 43.5456°N, HMAS 255489; Huanggangliang National Forest Park, Hexigten Banner, Chifeng City, 117.4036°E, 43.4325°N, HMAS 281266; Keyihe, Hulunbeier City, 122.6225°E, 50.6600°N, HMJAU 23501; Genhe City, Hulunbeier City, 120.3339°E, 50.3339°N, HMJAU 33876; Iksama National Forest Park, Hulunbeier City, 121.9517°E, 52.0823°N, HMJAU 60486.

Average nuclear Weir & Cockerham's F_{ST} vs. the closest species (*A. sinapina* subsp. *sinapina*): 0.12.

Average mitochondrial dxy vs. the closest species (*A. sinapina* subsp. *sinapina*): 0.04.

Average mitochondrial ΦST vs. the closest species (*A. sinapina* subsp. *sinapina*): 0.57.

Armillaria sinensis G.F. Qin, J. Zhao, H.C. Wang, Y. Yuan & Y.C. Dai, *Mycology* 16(2): 798, Figures 8.46－8.47

Index Fungorum number: IF 831856

Biological species: It belongs to the Chinese Biological Species F (CBSF).

This species was described by Qin et al. (2024) from northeast and central China, Asia, the Northern Hemisphere.

Pileus of this species range in size from small to medium and can be found either solitary, in clusters, or loosely grouped on decaying wood. **Pilei** measure 3－15

cm in diameter and 0.4—2.5 cm in thickness. Initially hemispherical or bell-shaped, they later become plano-convex to flattened, often with a depression. **Pileus surface** is typically dry and displays a variety of colors, including pale yellow to brown at the margin. The center is often yellowish orange to dark brown when young. As they mature, the colors shift to pale yellow, brownish yellow, and pale brown at the margin, while the center may exhibit pale yellow to dark brown, sometimes with an ocellate pattern. **Pileal surface** is covered with fibrillose squamules that are brownish orange to dark brown. **Squamules** are more concentrated and erect towards the center and more dispersed and flattened towards the margin. **Margin** is entire, often incurved, and striate. **Lamellae** are decurrent, with striped ridges extending downwards to the annulus. They are initially white to pale brown and are subdistant with smooth margins. **Lamellulae** are also present. **Stipe** is central, 4—11 cm in length and 0.3—2 cm in diameter at the apex. It is clavate to bulbous at the base, sometimes abruptly bulbous, and occasionally cylindrical. The surface is longitudinally striate and varies in color: white to pale brown above the annulus; pale yellow to brown in the middle; and greyish yellow to dark brown at the base. The stipe is densely covered with flocculose veil remnants that are greenish yellow to brown, resembling zigzag markings. Sometimes, the base is densely covered with white or greyish green mycelium. **Annulus** is submembranous, usually single and thick, but sometimes double and thin, and persistent. Rarely, it is cortinate and ephemeral. The inner veil is yellowish white, while the outer margin is pale yellow, greenish yellow, vivid yellow, greyish yellow, grey, brown, or dark brown. **Rhizomorphs** are black, thick, and exhibit monopodial branching in nature (Qin et al., 2024).

Basidiospores are ivory white in mass, ellipsoid, and lack a suprahilar depression, [332/20/14] (6.0)7.0—9.5(41.0) × (4.0)4.5—6.0(9.0) μm, with a Q value of (1.14)1.20—1.87(4.56) and Qm = 1.55 ± SD0.23. The walls are thin to thick (≤ 1.1 μm), nearly colorless to brownish yellow, smooth, cyanophilous, and inamyloid, with a prominent apiculus. **Basidia** are clavate, 10.0 — 60.0 × 4.0 — 12.5 μm, with a constricted or inconspicuously constricted upper portion. They have a clamp connection at the base and are typically four-sterigmate, though occasionally one or two-sterigmate. The walls are thin to slightly thick, and the color ranges from yellowish

green to brownish yellow. The pigments dissolve in KOH, and sometimes brownish-yellow crassobasidia (≤ 2 μm) form when the lamellae develop abnormally. Sterigmata measure 3—7 μm (5 ± SD1.06). **Cheilocystidia** measure 9—53 × 4—13.5 μm and are polymorphic, appearing fusiform, elliptical, ovoid, cylindrical, or clavate. **Clamp connection** present at the base and often feature irregular papillae at the apex. They are nearly hyaline, with thin to slightly thick walls (≤ 0.2 μm), and typically form a compact sterile lamella-edge that is fragile and easily disappears. Pleurocystidia are absent. **Pileal squamules** consist of more or less parallel, cylindrical hyphae with slightly thick to thick walls (≤ 1.1 μm). These hyphae are clampless, grey to brownish yellow, and measure 16—92 × 4.5—17 μm (Qin et al., 2024).

Ecology/Substrate/Host: They were found growing on a variety of substrates, primarily decaying wood or stumps of both coniferous and angiosperm trees. The specific hosts include *Pinus koraiensis*, *Ulmus*, *Acer*, *Betula platyphylla*, *Tilia* (including Tilia amurensis), *Fraxinus mandshurica*, *Fraxinus rhynchophylla*, *Quercus mongolica*, and unidentified angiosperm wood. The specimens were typically found on stumps, fallen trunks, or rotten wood debris in forested areas, indicating a saprotrophic or possibly weakly parasitic lifestyle. The collections span from late August to mid-September, suggesting fruiting occurs during late summer to early autumn in these regions.

Distribution: Now known to be distributed in Northeast China.



Note a–d Basidiomata. Scale bars: a–d = 5 cm.

Figure 8.47 Basidiomata of *Armillaria sinensis*

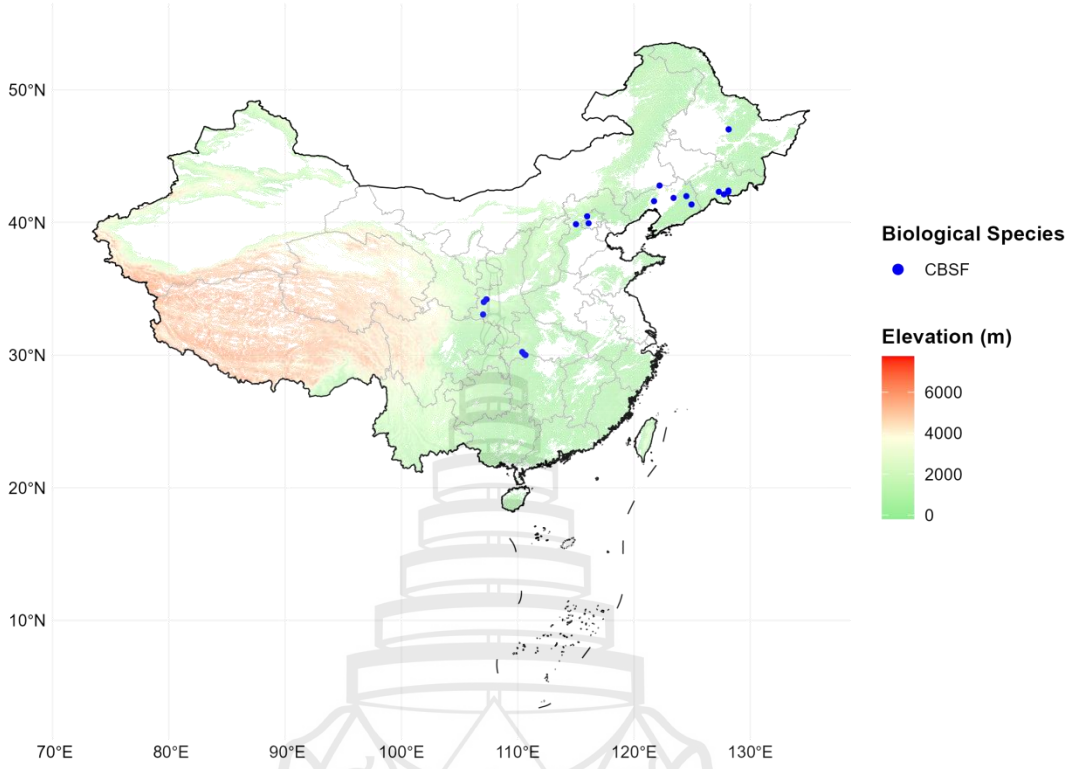


Figure 8.48 Distribution of samples of *Armillaria sinensis* used in this study

Additional material examined: **CHINA**, **Liaoning**, Longxi Residential Area, Shenyang City, 123.4000°E, 41.8500°N, 2104919020 (strain); Houtoushan Town Fair, Qingyuan Manchu Autonomous County, Fushun City, 124.5000°E, 41.9833°N, CBSF19020 (strain); Laotudingzi National Nature Reserve, Huanren Manchu Autonomous County, Benxi City, 124.9424°E, 41.3565°N, HKAS 86584; Yiwulv Mountain, Beizhen City, Jinzhou City, 121.7208°E, 41.6037°N, HMJAU 28935. **Hubei**, Wangjia Shapo, Houhe Nature Reserve, Wufeng Tujia Autonomous County, Yichang City, 110.5633°E, 30.0636°N, HKAS 135485; Niuzhuang Town, Wufeng Tujia Autonomous County, Yichang City, 110.3884°E, 30.2348°N, HKAS 135486. **Shaanxi**, Honghegu, Taibai Mountain, Fengxian County, Baoji City, 107.0833°E, 34.0000°N, CBSF05030 (strain); Hantai District, Hanzhong City, 107.0231°E, 33.0663°N, HMAS 61686; National Highway 244, Fengxi Town, Chencang District, Baoji City, 107.3063°E, 34.2052°N, HKAS 135547; National Highway 244, Fengxi Town, Chencang District, Baoji City, 107.3070°E, 34.2056°N, HKAS 135549. **Jilin**, Dianzhan Houshan, Changbai Mountain, Antu County, Yanbian Korean Autonomous

Prefecture, 128.1000°E, 42.3000°N, CBSF97033 (strain); Back Mountain of Changbaishan Academy of Sciences, Erdao Baihe Town, Yanbian Korean Autonomous Prefecture, 128.1148°E, 42.4052°N, HMJAU 23737; Changbai Mountain National Nature Reserve, Ring Mountain Line, Donggang Town, Fusong County, Baishan City, 127.7341°E, 42.1200°N, HKAS 135540; Fusong Town, Fusong County, Baishan City, 127.2939°E, 42.3119°N, HKAS 135526; Yangzishao Town, Huinan County, Tonghua City, 126.1628°E, 42.4452°N, HMJAU 22795. **Beijing**, Yudu Mountain, Yanqing District, 115.9690°E, 40.4634°N, HMAS 253828; Xiaolongmen, Mentougou District, 116.0962°E, 39.9366°N, HMAS 273636. **Inner Mongolia Autonomous Region**, Dachingu Nature Reserve, Horqin Zuoyi Houqi, Tongliao City, 122.1945°E, 42.7830°N, HMJAU 23629. **Hunan**, Hupingshan National Nature Reserve, Shimen County, Changde City, 110.6701°E, 30.0035°N, MHHNU 7577. **Hebei**, Xiaowutai Mountain, Yuxian County, Zhangjiakou City, 115.0076°E, 39.8677°N, HMAS 22782. **Yunnan**, Xiaocaoba Shennong Company, Yiliang County, Zhaotong City, Null, Null, HKAS 8654 7; Xiaocaoba Shennong Company, Yiliang County, Zhaotong City, Null, Null, guo12 (commercial strain); Yang Dayong's Fungi Materials, Xiaocaoba, Yiliang County, Zhaotong City, Null, Null, guo7 (commercial strain); Long An (Huangshi) "龙安（黄氏）", Null, Null, ZT-8 (commercial strain).

Average nuclear Weir & Cockerham's F_{ST} vs. the closest species (*Armillaria* sp. PXL): 0.08.

Average mitochondrial dxy vs. the closest species (*A. luteopileata*): 0.04.

Average mitochondrial ΦST vs. the closest species (*A. luteopileata*): 0.45.

Armillaria singula J.Y. Cha & Igarashi, in Cha, Sung & Igarashi, *Mycoscience* 35(1): 45 (1994)

Index Fungorum number: IF 362059

Biological species: It belongs to the intersterility group V.

This species was described by Cha et al. (1994) from Japan, Asia, the Northern Hemisphere.

Pileus are initially hemispherical when young, becoming plano-convex to nearly flat as they mature, often with an obtuse umbo. **Pileus surface** is dry, with a pale yellow to very pale brown coloration at the center, transitioning to yellow or brownish yellow toward the margin. It is covered with tufts of fine fibers that are dark reddish

brown to very dark gray, more densely concentrated toward the center and more dispersed toward the marginal zone, where yellow fibrils are present. **Margin** is initially inrolled, becoming acute with age, translucent-striate, and typically concolorous with the pileus or slightly paler. The flesh is firm, thin to thick at the stipe apex, and white in color. **Lamellae** are cream-colored when young, turning pale brown with age. They are closely spaced, subdecurrent, thick at the apex, and thinner toward the margin. **Stipe** is central, 4.2－6.0 cm in length and 0.4－0.6 cm in diameter, cylindrical to clavate, and fibrous. It is white at the apex, transitioning to very pale brown or reddish yellow toward the base, and bruises red. **Stipe** is fragile, solid when young, and becomes slightly hollow with age. The annulus is fibrous, membranous, very thin, appressed to the stipe or sometimes lost later, and white to cream in color (Cha et al., 1994).

Basidiospores are cream to white in mass, broadly elliptical to ovate, with an apiculus, 6.2－10.6 × 3.6－6.2 μm. They are smooth, hyaline, and nonamyloid. **Basidia** are clavate, 33－37.8 × 5.4－7.5 μm, with four sterigmata and a clamp connection at the base. Pleurocystidia are absent. **Pileal squamules:** the suprapellis consists of parallel, filamentous, thin-walled, hyaline hyphae with cells 32－65 × 10－20 μm, with the uppermost layer being brownish-pigmented. **Mediopellis** is composed of a tight mosaic of parallel, thick-walled hyphae with irregularly elliptical cells 22.5－70 × 12.5－18.8 μm. **Subpellis** is made up of loosely arranged, net-like filamentous hyphae with cells 50－100 × 10－50 μm, which stain in toluidine blue. **Subhymenial hyphae** are filamentous, sometimes with clamp connections, and binucleate. **Lamellar trama** is bilateral in structure (Cha et al., 1994).

Ecology/Substrate/Host: They were found on swampy land.

Distribution: Now known to be distributed in Japan.

Average nuclear Weir & Cockerham's F_{ST} vs. the closest species: No data available.

Average mitochondrial dxy vs. the closest species: No data available.

Average mitochondrial ΦST vs. the closest species: No data available.

Armillaria solidipes Peck, Bull. *Torrey bot. Club* 27(12): 611 (1900)

Index Fungorum number: IF 185839

Biological species: No biological species information available.

This species was described by Peck in 1900 from Colorado, Western United States, Southern Hemisphere.

Pileus measures 2.5－4.5 cm in diameter and appears planate, possibly due to the specimen having been pressed. There are slight indications of a surface tomentum, with a color ranging from tan to reddish brown, slightly darker toward the center. The margin is regular, even, and rolled under, concolorous or paler brown than the disc. **Lamellae** are well-formed, extending to the margin, and are concolorous with the pileus and stipe, 2.0－3.0 mm deep and decurrent by a thin line, giving a slight striped appearance to the apex of the stipe. **Stipe** is central, 9.5－10.5 cm in length and 0.6－1.2 cm in width. It is nearly cylindrical above, widening in the lower half to as much as 1.2 cm before tapering to a pointed base as the aggregated stipes are compacted. The surface is smooth and concolorous with other parts of the basidiome, with no evident surface fibrils. The stipe flesh is loose and fibrous, and the stipes appear to have been nearly hollow before pressing of the specimens. **Annulus** is not evident except for a small floccose area on the margin of one pileus. The pileus flesh is up to 3.0 mm thick over the disc, thinning toward the margin (Burdsall & Volk, 2008).

Basidiospores measure 7.5－9.5 × 5.0－6.5 μm, are smooth-walled, ellipsoid with slight adaxial flattening, hyaline, smooth, with slight wall thickening, and do not react with Melzer's reagent. **Basidia** are clavate, hyaline, 4-sterigmate, smooth, thin-walled, with some having clamp connections at the base. **Cystidia** are lacking. **Pileal squamules:** The pileus cutis is a compact layer about 100 μm thick, with hyphae 3.0－5.0(－7.5) μm in diameter, smooth, thin-walled, simple septate, and arranged parallel to the pileus surface. There are poorly preserved apparent aggregations of vertically arranged hyphae 2.5－4.0(－7.5) μm in diameter, possibly remnants of surface fibrils and tufts, of various lengths, smooth, nearly hyaline but with a pale yellow or yellow-brown tint, thin-walled, and simple septate. The cutis grades abruptly into the pileus trama, which is composed of interwoven hyphae 2.5－7.0(－12) μm in diameter. Narrow hyphae are cylindrical, while wider hyphae are broadly ovoid or short cylindrical, hyaline, smooth, mostly thin-walled, and simple septate (Burdsall & Volk, 2008).

Ecology/Substrate/Host: They were found on spruce stumps.

Distribution: Now known to be distributed in North America.

Average nuclear Weir & Cockerham's F_{ST} vs. the closest species: No data available.

Average mitochondrial dxy vs. the closest species: No data available.

Average mitochondrial ΦST vs. the closest species: No data available.

Armillaria sparrei (Singer) Herink, *Sympozium o Václavce Obecné Armillaria mellea (Vahl ex Fr.) Kumm.* (Brno): 43 (1973)

Index Fungorum number: IF 134996

Biological species: No biological species information available.

Average nuclear Weir & Cockerham's F_{ST} vs. the closest species: No data available.

Average mitochondrial dxy vs. the closest species: No data available.

Average mitochondrial ΦST vs. the closest species: No data available.

Armillaria tigrensis (Singer) T.J. Volk & Burds., *Syn. Fung.* (Oslo) 8: 115 (1995)

Index Fungorum number: IF 434355

Biological species: No biological species information available.

This species was described by Singer (1970) from the Southern Hemisphere. Currently is found in Buenos Aires Province, Argentina, particularly in marginal forests along the Paraná and Río de la Plata rivers.

Pileus broadly convex to subumbonate or umbonate, dry, ochraceous to pale yellowish, occasionally deeper brown in the center, subhygrophanous, smooth or with scattered fibrillose scales in youth, becoming subrugulose or smooth at maturity; margin pellucid-striate or short-sulcate when young, uplifted in age; 21—127(—175) mm broad. **Context** thin to moderately thick, pallid to reddish brown in the stipe base, white in the pileus, not reddening; odor none, taste mild or slightly astringent. **Lamellae** white to cinnamon-white, sometimes fulvous-brown, spotted when bruised, narrow to moderately broad, 2—12 mm, close to subclose, adnate to subdecurrent or sinuate-decurrent, occasionally splitting longitudinally or anastomosing in the upper part. **Stipe** 25—90(—170) mm long, 2—18 mm thick, equal with a bulbous base or later subequal

to slightly ventricose, solid or hollow, sometimes bifurcate or branched, apex ribbed or sulcate, surface pallid to fulvous-pallid or fuliginous from apex to base, black rhizomorphs occasionally present in substrate. **Annulus** membranous or thin-membranous, cortinoid, superior, often fragmented and forming flocculose patches on the upper stipe. **Basidiospores** measure 9.3 — 11 × 6.5 — 7.3 μm, ellipsoid to subelliptical, hyaline, smooth, amyloid, without suprahilar depression. **Basidia** measure 40—47 × 7.3—8.8 μm, 4-spored, clavate, thin- to slightly thick-walled, with or without a basal clamp. **Cheilocystidia** numerous, swollen-ventricose to vesiculose-fusoid, 17.5—18.5 × 10—12.5 μm. **Pleurocystidia** absent (Singer, 1970).

Ecology/Substrate/Host: Fasciculate to caespitose on trunks and logs of Salix humboldtiana, in marginal forests.

Distribution: Southern South America—Argentina, in the Paraná and Río de la Plata regions, including Buenos Aires Province (Punta Lara and San Fernando); fruiting in May and June.

Average nuclear Weir & Cockerham's F_{ST} vs. the closest species: No data available.

Average mitochondrial dxy vs. the closest species: No data available.

Average mitochondrial ΦST vs. the closest species: No data available.

Armillaria umbrinobrunnea (Singer) Pildain & Rajchenb., *Mycologia* 102(2): 399 (2010)

Index Fungorum number: IF 516941

Biological species: No biological species information available.

This species was described by Pildain et al. (2010) from southern South America, the Southern Hemisphere, and is currently known from Argentina (Chubut, Neuquén) and Chile (Valdivia), occurring in Andean—Patagonian forests dominated by Nothofagus species.

Pileus is broadly convex, densely covered with relatively large and homogeneous squamules, beige to light brown, often with a dark umbrinous center; margin striate; 15—50 mm broad. **Context** is not specifically described in color, but the basidiome flavor is strongly sharp and acidic. **Lamellae** subdecurrent, white to pallid, with lamellulae, and lines running down the apex of the stipe. **Stipe** is

cylindrical, subbulbose at the base, equal or slightly tapering upward, solid, with brown squamules beneath the annulus. **Annulus** is membranous, white, well formed when fresh, but becomes vestigial after drying.

Basidiospores measure (7 −)9 − 11(− 13) × (5 −)5 − 6.5(− 7) μm, subelliptical. **Basidia** measure 38 − 42(− 47) × 7.5 − 8(− 9) μm. **Cheilocystidia** is clavate, trama regular, with barrel-shaped (lacunar) cells centrally and a hyphal structure toward the subhymenium. **Squamules** are composed of hyphae up to 20 μm in diameter.

Ecology/Substrate/Host: On living or dead wood of Nothofagus pumilio and Nothofagus dombeyi; fruiting on soil or wood near lake shores and forests dominated by Nothofagus species.

Distribution: Southern South America—Argentina (Chubut: Futaleufú, Los Alerces National Park; Neuquén: Nahuel Huapi National Park) and Chile (Valdivia: Cordillera Pelada); temperate forests in Andean-Patagonian regions.

Average nuclear Weir & Cockerham's F_{ST} vs. the closest species: No data available.

Average mitochondrial dxy vs. the closest species: No data available.

Average mitochondrial ΦST vs. the closest species: No data available.

Armillaria vara (Berk.) Sacc., *Syll. fung. (Abellini)* 5: 83 (1887)

Index Fungorum number: IF 192839

Biological species: No biological species information available.

This species was first described by Saccardo (1887) in the Northern Hemisphere, specifically from the eastern Himalayas of India, and is currently reported from the Sinchul Himalaya at an elevation of 2600 m.

Pileus broadly convex to plane when dry, margin wavy (repando), pale umber, sometimes tinged reddish; 5 cm broad. **Context** is not explicitly described. **Lamellae** pallid, distant, linearly decurrent. **Stipe** is 10 cm long and 8 mm thick, curved and solid, flexuous, thickening downward (deorsum incrassatus), fuscous, becoming blackish toward the base, nearly glabrous. **Annulus** is ample, superior, erect, and white. **Basidiospores** not described.

Ecology/Substrate/Host: On decayed wood (in ligno emarcido), growing in dense clusters (cespitosa), odorless (inodora).

Distribution: India, Eastern Himalayas, recorded from Sinchul Himalaya at an elevation of 2600 meters.

Average nuclear Weir & Cockerham's F_{ST} vs. the closest species: No data available.

Average mitochondrial dxy vs. the closest species: No data available.

Average mitochondrial ΦST vs. the closest species: No data available.

Armillaria violacea H.C. Wang, W.M. Qin, G.F. Qin, J. Zhao & Y.C. Dai, *Mycology* 26(2)*:* 804 (2024), Figures 8.48—8.49

Index Fungorum number: IF 831859

Biological species: It belongs to the Chinese Biological Species N (CBSN).

Described by Qin et al. (2024) from southwestern and central China, the Northern Hemisphere, specifically, is currently found in Hubei, Shaanxi, and Sichuan Provinces.

Basidiomata range in size from small to large in size and can be found either solitary or in clusters, often fused at the base. **Pilei** 1.7—10 cm in diameter, initially hemispherical or convex, often with a mammillate shape, later becoming plano-convex to applanate or slightly depressed, sometimes with an umbo. The surface is typically dry, displaying colors such as greyish orange to reddish brown at the margin when young, while the center is brownish orange to dark brown. As they mature, the margin becomes greyish orange to brown, while the center shifts to greyish orange to dark purple. The pileal scales are fine-velvety or flocculose, abundant, white or nearly white, and more concentrated toward the center, often disappearing when mature or after rain. The margin is straight and entire, usually incurved when young and striate when mature. **Lamellae** are adnate or adnate with a decurrent tooth, with striped ridges extending downward to the annulus. They are white to dull red when mature. They are subdistant, with lamellulae present, and have smooth margins. **Stipe** is central, 3.5—12 cm in length and 0.3—1.5 cm in diameter at the apex, cylindrical or broadened at the base, sometimes slightly bulbous. When young, it is white to orange-white above the annulus, with the middle portion greyish orange to brownish orange and the base pale brown. As it matures, the upper part becomes greyish yellow to greyish red, while the middle portion shifts to greyish yellow to dull red, and the base becomes pale brown to dark

brown. Stipe is covered with white or nearly white fibrillose veil remnants, sometimes resembling snakeskin markings, which disappear when touched. **Annulus** is cortinate, single, thin, delicate, and ephemeral, white or nearly white (Qin et al., 2024).

Basidiospores are ivory white in mass, elongate, lacking a suprahilar depression, (7.0)7.5－9.8(10.0) × (4.3)4.7－6.0(6.0) μm. They are thin- to slightly thick-walled (≤ 0.8 μm), nearly hyaline, greenish blue to brownish yellow, smooth, cyanophilous, inamyloid, and have a prominent apiculus. **Basidia** are clavate, 26－50 × 7－10 μm, four-sterigmate, usually with a constricted upper portion or inconspicuous constriction, and have a clamp connection at the base. They are thin- to slightly thick-walled, yellowish green to brownish yellow, with pigments that gradually disappear in KOH. Occasionally, brownish-yellow crassobasidia (≤ 1.5 μm) are formed, and crassobasidia with septa appear when lamellae develop abnormally. **Cheilocystidia** 12 －44 × 6－11 μm and are polymorphic, including clavate, fusiform, cylindrical, elliptical, and ovoid forms, with a clamp connection at the base and sometimes with papillae or irregularly branched papillae at the apex. They are slightly thick-walled (≤ 1.0 μm), nearly hyaline, and usually form a compact sterile lamella edge that is easily broken and disappears. **Pleurocystidia** are absent. **Pileal squamules** are composed of cylindrical, slightly thick- to thick-walled (≤ 1.2 μm) hyphae, sometimes thickened in a wavy pattern, simple septate, pale brown to brown, and 15－145 × 4.5－20 μm (Qin et al., 2024).

Ecology/Substrate/Host: They were found growing on a variety of substrates, primarily decaying wood, fallen trunks, and living trees of both coniferous and angiosperm species. Specific hosts include *Cunninghamia lanceolata*, *Betula*, *Magnolia liliflora*, and *Castanopsis platyacantha*. The specimens were also found on living angiosperm roots and rotten angiosperm stumps. The collections span from mid-September to early November, indicating fruiting occurs during late summer to autumn in these regions.

Distribution: Now known to be distributed in Southwest and Central China.



Note a–d Basidiomata. Scale bars: a–f = 5 cm.

Figure 8.49 Basidiomata of *Armillaria violacea*

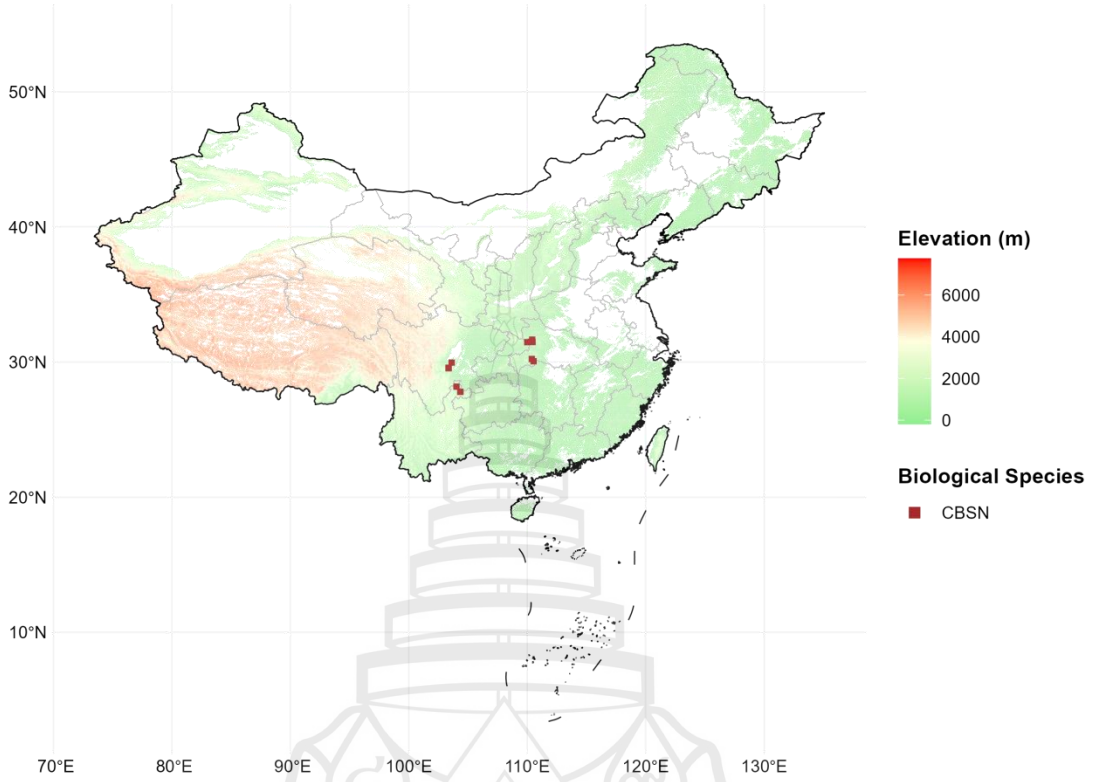


Figure 8.50 Distribution of samples of *Armillaria violacea* used in this study

CHINA, **Hubei**, Heishuihe, Yanjiawan, Muyu Town, Shennongjia, 110.4315°E, 31.4887°N, HKAS 135495; Heishuihe, Yanjiawan, Muyu Town, Shennongjia, 110.4317°E, 31.4893°N, HKAS 135491; Heishuihe, Yanjiawan, Muyu Town, Shennongjia, 110.4310°E, 31.4930°N, 21SNJ17 (strain); Dajiu Lake, Shennongjia, 109.9978°E, 31.4779°N, HKAS 135494; Near Shennong Hotel, Shennongjia, 110.3493°E, 31.5030°N, HKAS 135498; Near Shennong Hotel, Shennongjia, 110.3493°E, 31.5030°N, HKAS 135499; Lingyun Village, Niuzhuang Town, Wufeng Tujia Autonomous County, Yichang City, 110.3833°E, 30.2333°N, CBSN16022 (strain); Yangzixi, Houhe Nature Reserve, Wufeng Tujia Autonomous County, Yichang City, 110.5333°E, 30.0667°N, CBSN19098 (strain); Shennongjia International Skiing Park, Shennongjia Forest Region, 110.4166°E, 31.6666°N, CBSNW16024 (strain); Shennongjia Scenic Area, Muyu Town, Shennongjia Forest District, 110.3565°E, 31.4972°N, HKAS 135560 (specimen); Shennongjia Scenic Area, Muyu Town, Shennongjia Forest District, 110.3535°E, 31.4981°N, HKAS

135563 (specimen); Shennongjia Scenic Area, Muyu Town, Shennongjia Forest District, 110.3534°E, 31.4979°N, HKAS 135564 (specimen); Shennongjia Scenic Area, Muyu Town, Shennongjia Forest District, 110.3535°E, 31.4978°N, HKAS 135565. **Sichuan**, Emei Mountain, Emeishan City, Leshan City, 103.3500°E, 29.5666°N, CBSN02066 (strain); Emei Mountain, Meishan City, Leshan City, 103.3500°E, 29.5666°N, CBSN02067 (strain); Emei Mountain, Meishan City, Leshan City, 103.3500°E, 29.5666°N, CBSN02068 (strain); Emei Mountain, Meishan City, Leshan City, 103.3500°E, 29.5666°N, CBSN02069 (strain); Emei Mountain, Meishan City, Leshan City, 103.3500°E, 29.5666°N, CBSN02070 (strain); Zhanglaoping, Emei Mountain, Dongpo District, Meishan City, 103.6166°E, 29.9666°N, CBSN19107 (strain). **Yunnan**, Mugan Town, Daguan County, Zhaotong City, 104.0209°E, 28.1837°N, DG (strain); Chaotianma National Nature Reserve in Wumeng Mountain, 104.3481°E, 27.7996°N, YLCTM (strain); Xiaocaoba Town, Yiliang County, Zhaotong City, 104.3508°E, 27.7979°N, ZZZT01 (strain).

Average nuclear Weir & Cockerham's F_{ST} vs. the closest species (*A. violacea*): 0.11.

Average mitochondrial dxy vs. the closest species (*A. bruneocystidia*/*A. linzhiensis*/*A. tibetica* (CBS J) lineage 1-mtDNA/*A. tibetica* (CBS J) lineage 2-mtDNA/*A. tibetica* (CBS J) lineage 3-mtDNA/*A. amygdalispora*/*A. pungentisquamosa*): 0.04.

Average mitochondrial ΦST vs. the closest species (*A. amygdalispora*): 0.37.

Armillaria viridiflava (Singer) T.J. Volk & Burds., *Syn. Fung.* (Oslo) 8: 119 (1995)

Index Fungorum number: IF 434356

Biological species: No biological species information available.

This species was described by Singer (1989) from the Northern Hemisphere, and is currently found in Spain (Catalonia), Austria, and the western parts of North America, notably in temperate broadleaf forests.

Pileus broadly convex to campanulate-convex, dry, entirely covered with minute fibrillose olive scales, pale olive in color with a dark olive center; margin striate, often whitish at the edge, center often rugulose; 30－64 mm broad. **Context** is not explicitly described in color, but the odor is weak, and the flavor is slightly astringent

when chewed. **Lamellae** close to moderately spaced, white to yellowish, often with ferruginous edges, decurrent. **Stipe** is 80 — 125 mm long, 9 — 11.5 mm thick, cylindrical, solid, slightly attenuated toward base, white to pale yellowish white, sometimes tinged with reddish tones toward base. **Annulus** is membranous, superior, persistent, often large and subcoriaceous, white.

Basidiospores measure 6.2—8.5 × 4.5—5.5(—6) µm, ellipsoid, smooth, thin-walled, non-amyloid, subelliptical.

Ecology/Substrate/Host: Growing on decaying wood (ad lignum truncorum Dicotyledonearum e gr. Cistacearum et Rosacearum), often on well-decayed stumps and logs of broadleaf trees. The species is saprotrophic and fruiting in autumn. Rhizomorphs are black and found near the base of the stipe.

Distribution: Southern Europe— described from Spain (Catalonia, mountains near Tosa), and also recorded from Austria (Vienna) and the western Florida forest (United States). Associated with more southern habitats compared to other Armillaria species.

Average nuclear Weir & Cockerham's F_{ST} vs. the closest species: No data available

Average mitochondrial dxy vs. the closest species: No data available

Average mitochondrial ΦST vs. the closest species: No data available

Armillariella yungensis Singer, Fl. Neotrop., *Monogr.* 3: 12 (1970)

Index Fungorum number: IF 308944

Biological species: No biological species information available.

This species was described by Singer (1970) from the Southern Hemisphere, specifically the Yungas region of Bolivia.

Pileus broadly convex to subumbonate or subumbilicate when mature, dry, slightly fibrillose to dotted-squamulose in the center, smooth or subfibrillose at the margin, brownish to reddish-brown in color ("India Buff" to "Piccaninny"); 34—64 mm broad. **Context** is whitish, with brownish surface staining in places, fleshy in texture; odor none; taste mild. **Lamellae** close or subclose, arcuate-decurrent, salmon-colored ("Beige soirée" to "9-B-4", then "Toltec"), narrow. **Stipe** is 25—65 mm long and 3.5—12 mm thick, equal or tapering upward, solid, whitish, subfibrillose to subsquamulose.

Annulus is cinereous (ash-colored), cortinoid, subcorbeloid, and located near the upper part of the stipe.

Basidiospores 7.9 × 4.5—5.3 μm, ellipsoid to ovoid or short-cylindric, hyaline, smooth, amyloid.

Ecology/Substrate/Host: On dead dicotyledonous wood in tropical montane and marginal forests. The species grows saprotrophically on well-decayed wood, sometimes with black rhizomorphs.

Distribution: South America, known from Bolivia (Carmen Pampa, Nor Yungas, Andes Mountains, 2000 m a.s.l.) and Argentina (Buenos Aires Province, Punta Lara). Distributed in the Andes southward to the La Plata region.

Average nuclear Weir & Cockerham's F_{ST} vs. the closest species: No data available.

Average mitochondrial dxy vs. the closest species: No data available.

Average mitochondrial ΦST vs. the closest species: No data available.

8.3 Conclusion

To date, including the present study, a total of 21 *Armillaria* taxa have been recognized in China (Hou et al., 2025; Liu et al., 2024; Qin et al., 2007, 2024, 2025). Among them, six cryptic taxa representing all subgenera and sections of the genus are newly described here as formal species or subspecies, further enriching the species diversity of *Armillaria* in China. Besides, the *Armillaria* species previously considered to have intercontinental distributions in fact represent multiple lineages that have evolved independently through long-term geographic isolation (Qin et al., 2025: e.g., *A. gallica*, *A. mellea*, *A. ostoyae*, *A. sinapina*; this study: e.g., *A. borealis* and *A. tabescens*). This finding suggests that the cosmopolitanism of fungi has often been overestimated and that only by integrating evidence from reproductive isolation and genomic analyses can we accurately uncover their true species diversity and evolutionary patterns. Globally, the total number of recognized *Armillaria* species now stands at 78. In our analyses, *Armillaria xiaocaobaensis* and *A. pungentisquamosa* (CBS P) are conspecific (Figure D1). However, we did not synonymize

A. *pungentisquamosa*, as *A*. *xiaocaobaensis* was described solely based on tef1-α data without evidence of reproductive isolation (Peng & Zhao, 2020). Qin et al. (2024) discussed that the tef1-α gene offers limited phylogenetic resolution due to potential balancing selection, and only about 55% of Chinese *Armillaria* isolates can be reliably distinguished using this marker. Moreover, because incomplete lineage sorting (ILS) and introgressive hybridization are widespread in *Armillaria*, species delimitation based on single-gene phylogenies is often unreliable. Therefore, the species *A*. *desertorum*, which was also described solely on tef1-α data by Hou et al. (2025), requires further verification. Excessive reliance on the principle of nomenclatural priority may lead to endless taxonomic revisions, because many historically described species based on morphology or single-locus data did not account for biological factors such as incomplete lineage sorting and hybridization and may comprise mixed samples representing multiple biological species.

CHAPTER 9

OVERALL CONCLUSIONS AND FUTURE PERSPECTIVES

We conducted an integrated phylogenomic, taxonomic, and speciation investigation of the genus *Armillaria,* a genus of fungi with significant ecological and economic importance as pathogens, saprotrophs, and symbionts. By integrating nuclear and mitochondrial genome data from over 600 specimens, we established a robust phylogenetic framework, delineating 21 species in China—including six novel taxa—and resolving long-standing uncertainties in species boundaries. Population genetic analyses revealed that nuclear $F_{ST} \geq 0.09$ and mitochondrial $F_{ST} \geq 0.37$ serve as key thresholds for species delimitation in genus *Armillaria,* though biological mating trials remain essential for validation. We document widespread phylogenetic discordance—predominantly driven by incomplete lineage sorting, with hybridization and introgression playing secondary roles. And use network analyses to reveal hybrid origins in key lineages such as the *Gallicae* section and the *A. tibetica* (CBS J) complex, while phylogeographic patterns highlighted distinct maternal lineages shaped by historical biogeographic processes.

Beyond taxonomy, this study advances practical applications for *Armillaria* research and industry. We developed a multi-level identification framework combining genomic databases, deep learning-based visual barcodes, PCR-optimized markers, and SSR fingerprinting systems to enable rapid species and strain discrimination. Additionally, we reconstructed divergence times and ancestral distributions, linking speciation events to climatic fluctuations and plant biogeography. The findings also address the cultivation of *Gastrodia elata* (Tianma), providing strategic recommendations for strain selection and sustainable industry development.

By reconciling genomic divergence with reproductive biology and ecological roles, this work not only refines *Armillaria* systematics but also bridges fundamental research with applied needs in forestry, medicine, and biotechnology.

Despite significant advances in understanding the phylogeny, species delimitation, and speciation of *Armillaria*, several key challenges remain that warrant further investigation, including difficulties in ensuring data quality from historical specimens,

limited understanding of chromosomal structural variations, unresolved molecular mechanisms underlying homothallism and heterothallism, insufficient characterization of incomplete lineage sorting (ILS) at the gene level, and unclear evolutionary mechanisms of pathogenicity-related and symbiotic genes. Future research should prioritize constructing chromosome-level genomes using Hi-C and long-read sequencing to analyze structural variations' phylogenetic impacts, conducting pangenome analyses to identify core and accessory genes, employing comparative genomics to elucidate reproductive strategies, integrating population genomics to dissect ILS effects at the gene level, and systematically investigating the evolution of virulence and symbiosis-related genes. Additionally, developing machine learning-based classification tools and combining ecological modeling with paleoclimatic data will be crucial for reconstructing population dynamics, ultimately advancing both fundamental knowledge of *Armillaria* evolution and practical applications in forest disease management and medicinal fungus cultivation.

REFERENCES

Anderson, J. B., & Stasovski, E. (1992). Molecular phylogeny of northern hemisphere species of *Armillaria*. *Mycologia, 84*(4), 505–516.

Anderson, J. B., & Ullrich, R. C. (1979). Biological species of *Armillaria mellea* in North America. *Mycologia, 71,* 402–414.

Andrews, S. (2010). *FastQC: A quality control tool for high throughput sequence data*. https://www.bioinformatics.babraham.ac.uk/projects/fastqc/

Antonín, V., Tomšovský, M., Sedlák, P., Májek, T., & Jankovský, L. (2009). Morphological and molecular characterization of the *Armillaria cepistipes–A. gallica* complex in the Czech Republic and Slovakia. *Mycological Progress, 8,* 259–271.

Banik, M. T., & Burdsall, H. H., Jr. (1998). Assessment of compatibility among *Armillaria cepistipes*, *A. sinapina*, and North American biological species X and XI, using culture morphology and molecular biology. *Mycologia, 90*(5), 798–805.

Bankevich, A., Nurk, S., Antipov, D., Gurevich, A. A., Dvorkin, M., Kulikov, A. S., . . . Pevzner, P.A. (2012). SPAdes: A new genome assembly algorithm and its applications to single-cell sequencing. *Journal of Computational Biology, 19*, 455–477.

Bayman, P., & Collins, O. R. (1989). Homothallism in *Coprinus patouillardii*: distribution and variation. *Mycologia*, *81*(5), 728–734.

Beck, N., & Lang, B. F. (2010). MFannot, organelle genome annotation webserver.

Berkeley, M. J. (1850). Decades of fungi. Decades XXV. to XXX. Sikkim Himalaya fungi, collected by Dr. J.D. Hooker. *Hooker's Journal of Botany and Kew Garden Miscellany*, *2*, 42–51.

Bérubé, J. A., & Dessureault, M. (1988). Morphological characterization of *Armillaria ostoyae* and *Armillaria sinapina* sp. nov. *Canadian Journal of Botany*, *66*(10), 2027–2034.

Bérubé, J. A., & Dessureault, M. (1989). Morphological studies of the *Armillaria mellea* complex: two new species, *A. gemina* and *A. calvescens*. *Mycologia*, *81*, 216–225.

Bi, G., Luan, X., & Yan, J. (2024). ORPA: a fast and efficient phylogenetic analysis method for constructing genome-wide alignments of organelle genomes. *Journal of Genetics and Genomics*, *51*(3), 352–358.

Bleasby, A. J., & Wootton, J. C. (1990). Construction of validated, non-redundant composite protein sequence databases. *Protein Engineering, Design and Selection*, *3*(3), 153–159.

Boesewinkel, H. J. (1977). New plant disease records in New Zealand: records in the period 1969–76. *New Zealand Journal of Agricultural Research*, *20*: 583–589.

Bolger, A. M., Lohse, M., & Usadel, B. (2014). Trimmomatic: a flexible trimmer for Illumina sequence data. *Bioinformatics*, *30*(15), 2114–2120.

Brazee, N. J., Ortiz-Santana, B., Banik, M. T., & Lindner, D. L. (2012). *Armillaria altimontana*, a new species from the western interior of North America. *Mycologia*, *104*(5), 1200–1205.

Cervantes, C. R., Montes, J. R., Rosas, U., & Arias, S. (2023). Phylogenetic discordance and integrative species delimitation in the *Mammillaria haageana* species complex (Cactaceae). *Molecular Phylogenetics and Evolution*, *187*, 107891.

Cha, J. Y., Sung, J. M., & Igarashi, T. (1994). Biological species and morphological characteristics of *Armillaria mellea* complex in Hokkaido: *A. sinapina* and two new species, *A. jezoensis* and *A. singula*. *Mycoscience*, *35*, 39–47.

Cha, J. Y., & Igarashi, T. (1995). *Armillaria* species associated with *Gastrodia elata* in Japan. *European Journal of Plant Pathology*, *25*, 319–326.

Chandra, A., & Watling, R. (1982). Indian *Armillaria* Basidiomycotina. *Kavaka*, *10*, 63–84.

Coetzee, M. P., Wingfield, B. D., Bloomer, P., Ridley, G. S., Kile, G. A., & Wingfield, M. J. (2001). Phylogenetic relationships of Australian and New Zealand *Armillaria* species. *Mycologia*, *93*(5), 887–896.

Coetzee, M. P., Wingfield, B. D., Bloomer, P., Ridley, G. S., & Wingfield, M. J. (2003). Molecular identification and phylogeny of *Armillaria* isolates from South America and Indo-Malaysia. *Mycologia*, *95*(2), 285–293.

Coetzee, M. P., Wingfield, B. D., Zhao, J., van Coller, S. J., & Wingfield, M. J. (2015). Phylogenetic relationships among biological species of *Armillaria* from China. *Mycoscience*, *56*(5), 530–541.

Coissac, E., Hollingsworth, P. M., Lavergne, S., & Taberlet, P. (2016). From barcodes to genomes, extending the concept of DNA barcoding. *Molecular Ecology*, *25*(7), 1423–1428.

Collins, C., Keane, T. M., Turner, D. J., O'Keeffe, G., Fitzpatrick, D. A., & Doyle, S. (2013). Genomic and proteomic dissection of the ubiquitous plant pathogen, *Armillaria mellea*: Toward a new infection model system. *Journal of Proteome Research*, *12*(6), 2552–2570.

Coordinators, N. R. (2017). Database resources of the national center for biotechnology information. *Nucleic Acids Research*, *44*, D7–D19.

Corcoran, P., Jacobson, D. J., Bidartondo, M. I., & Taylor, J. W. (2012). Quantifying functional heterothallism in the pseudohomothallic ascomycete *Neurospora tetrasperma*. *Fungal Biology*, *116*(9), 962–975.

Courtecuisse, R. (1995). Taxonomy of some fungi used by the Songola people (Zaïre). *African Study Monographs*, *16*(1), 45–60.

Danecek, P., Auton, A., Abecasis, G., Albers, C. A., Banks, E., DePristo, M. A., . . . Durbin, R. (2011). The variant call format and VCFtools. *Bioinformatics*, *27*, 2156–2158.

Danecek, P., Bonfield, J. K., Liddle, J., Marshall, J., Ohan, V., Pollard, M. O., . . . Davies, R. M. (2021). Twelve years of SAMtools and BCFtools. *GigaScience*, *10*(2), 1–4.

de Medeiros, B. A., Cai, L., Flynn, P. J., Yan, Y., Duan, X., Marinho, L. C., ... & Davis, C. C. (2025). A composite universal DNA signature for the Tree of Life. *Nature Ecology & Evolution*, 1–15.

Duchesne, L. C., & Anderson, J. B. (1990). Location and direction of transcription of the 5S rRNA gene in *Armillaria*. *Mycological Research*, *94*(2), 266–269.

Edelman, N. B., Frandsen, P. B., Miyagi, M., Clavijo, B., Davey, J. W., Dikow, R. B., . . . Mallet, J. (2019). Genomic architecture and introgression shape a butterfly radiation. *Science*, *366*(6465), 594–599.

Elías-Román, R. D., Medel-Ortiz, R., Alvarado-Rosales, D., Hanna, J. W., Ross-Davis, A. L., Kim, M. S., . . . Klopfenstein, N. B. (2018). *Armillaria mexicana*, a newly described species from Mexico. *Mycologia*, *110*(2), 347–360.

Eliott, C. G. (1994). Reproduction in fungi. Chapman & Hall, London.

Emel, L. (1921). *Le Genre Armillaria, Fr., Sa Suppression de la Systématique Botanique* (Master's thesis) (in French). Faculté de Pharmacie, Université de Strasbourg.

Emms, D. M., & Kelly, S. (2015). OrthoFinder: Solving fundamental biases in whole genome comparisons dramatically improves orthogroup inference accuracy. *Genome Biology*, *16*, 157.

Fan, L., Guo, S. X., Cao, W. Q., Xiao, P. G., & Xu, J. T. (1996). Isolation, culture, identification and biological activity of *Mycena orchidicola* sp. nov. in *Cymbidium sinense* (Orchidaceae). *Acta Mycologica Sinica*, *15*, 251–255.

Fan, L., Guo, S. X., & Xiao, P. G. (1998). Basidiomycetous endophytes from the roots of nineteen orchids. *Chinese Journal of Tropical Crops*, *4*, 77–82.

Feng, S., Bai, M., Rivas-González, I., Li, C., Liu, S., Tong, Y., . . . Wu, D. D. (2022). Incomplete lineage sorting and phenotypic evolution in marsupials. *Cell*, *185*(10), 1646–1660.

Feurtey, A., Stevens, D. M., Stephan, W., & Stukenbrock, E. H. (2019). Interspecific gene exchange introduces high genetic variability in crop pathogen. *Genome Biology and Evolution*, *11*(11), 3095–3105.

Fries, E. M. (1821). *Systema mycologicum*. Lundae, Ex Officina Berlingiana.

Gabriel, L., Brůna, T., Hoff, K. J., & Stanke, M. (2024). BRAKER3: Fully automated genome annotation using RNA-seq and protein evidence with GeneMark-ETP, AUGUSTUS, and TSEBRA. *Genome Research*, *34*(5), 769–777.

Gregory, S. C., & Watling, R. (1985). Occurrence of *Armillaria borealis* in Britain. *Transactions of the British Mycological Society*, *84*(1), 47–55.

Guillaumin, J. J., Mohammed, C., & Berthelay, S. (1992). *Armillaria novae-zelandiae* in Papua New Guinea. *Mycological Research*, *96*(4), 278–280.

Guo, S. X., Fan, L., Cao, W. Q., & Chen, X. M. (1999). *Mycena dendrobii*, a new mycorrhizal fungus. *Mycosystema*, *18*, 141–144.

Guo, S. X., Fan, L., Cao, W. Q., Xu, J. T., & Xiao, P. G. (1997). *Mycena anoectochila* sp. nov. isolated from mycorrhizal roots of *Anoectochilus roxburghii* from Xishuangbanna, China. *Mycologia*, *89*, 952–954.

Guo, T., Wang, H. C., Xue, W. Q., Zhao, J., & Yang, Z. L. (2016). Phylogenetic analyses of *Armillaria* reveal at least 15 phylogenetic lineages in China, seven of which are associated with cultivated *Gastrodia elata*. *PLoS One*, *11*, e0154794.

Hanna, J. W., Warwell, M. V., Sitz, R. A., Guyon, J. C., Hebertson, E. G., Saavedra, A. L., . . . McDonald, G. I. (2020). Toward DNA-based and bioclimatic modeling tools to identify *Armillaria* pathogens, predict host/pathogen distributions, and manage *Armillaria* root disease in the Intermountain Region under changing environments. In G. J. Reynolds, N. P. Wilhelmi & P. Palacios (Eds.), Proceeding of the 66th Western International Forest Disease Work Conference (pp. 177–182). Estes Park, CO.

Harrington, T. C., & Wingfield, B. D. (1995). A PCR-based identification method for species of *Armillaria*. *Mycologia*, *87*(2), 280–288.

Hasegawa, E., Ota, Y., Hattori, T., & Kikuchi, T. (2010). Sequence-based identification of Japanese *Armillaria* species using the elongation factor-1 alpha gene. *Mycologia*, *102*(4), 898–910.

He, M. Q., Cao, B., Liu, F., Boekhout, T., Denchev, T. T., Schoutteten, N., . . . Zhao, R. L. (2024). Phylogenomics, divergence times and notes of orders in Basidiomycota. *Fungal diversity*, *126*(1), 127-406.

He, W., Qin, G. F., & Shen, R. X. (1996). Biological species of *Armillaria* in the Great Xing-An Mountains and the Changbai Mountains in China. *Acta Mycologica Sin*, *15*, 9–16.

He, W., Xu, L., Wang, J., Yue, Z., Jing, Y., Tai, S., . . . Fang, X. (2024). VCF2PCACluster: a simple, fast and memory-efficient tool for principal component analysis of tens of millions of SNPs. *BMC Bioinformatics*, *25*(1), 173.

Heim, R. (1963). *L'Armillariella elegans* Heim. *Revue de Mycologie*, *28*, 85–94.

Heinzelmann, R., Dutech, C., Tsykun, T., Labbé, F., Soularue, J. P., & Prospero, S. (2019). Latest advances and future perspectives in *Armillaria* research. *Canadian Journal of Plant Pathology*, *41*(1), 1–23.

Hennings, P. (1895). *Fungi camerunenses* I. *Botanische Jahrbücher für Systematik Pflanzengeschichte und Pflanzengeographie 22*, 72–111.

Herink, J. (1973). *Taxonomie václavky obecné – Armillaria mellea* (Vahl ex Fr.) Kumm. In J. Hasek (Ed.), *Sympozium o václavce obecné* (pp. 21–48). Lesnicka fakulta VSZ.

Hessenauer, P., Fijarczyk, A., Martin, H., Prunier, J., Charron, G., Chapuis, J., . . . Landry, C. R. (2020). Hybridization and introgression drive genome evolution of Dutch elm disease pathogens. *Nature Ecology & Evolution 4*(4),626–638.

Hongo, T. (1976). Agarics from Papua-New Guinea. III. *Report of the Tottori Mycological Institute (Japan)*, *14*, 95–104.

Hood, I. A., & Ramsfield, T. D. (2016). *Armillaria aotearoa* species nova. *New Zealand Journal of Forestry Science*, *46*, 1–11.

Huson, D. H., & Bryant, D. (2024). The SplitsTree App: Interactive analysis and visualization using phylogenetic trees and networks. *Nature Methods*, *21*(10), 1773–1774.

Jacob, L., Steenwyk, T. J., Buida, T. J., Labella, A. L., Li, Y., Shen, X. X., & Rokas, A. (2021). PhyKIT: a broadly applicable UNIX shell toolkit for processing and analyzing phylogenomic data. *Bioinformatics*, *37*(16), 2325–2331.

Jia, D. R., & Bartish, I. V. (2018). Climatic changes and orogeneses in the Late Miocene of Eurasia: The main triggers of an expansion at a continental scale?. *Frontiers in Plant Science*, *9*, 1400.

Jin, J. J., Yu, W. B., Yang, J. B., Song, Y., dePamphilis, C. W., Yi, T. S., . . . Li, D. Z. (2020). GetOrganelle: a fast and versatile toolkit for accurate de novo assembly of organelle genomes. *Genome Biology*, *21*, 41.

Katoh, K., & Standley, D. M. (2013). MAFFT multiple sequence alignment software version 7: Improvements in performance and usability. *Molecular Biology and Evolution*, *30*(4), 772–780.

Katoh, K., Kuma, K., Toh, H., & Miyata, T. (2005). MAFFT version 5: Improvement in accuracy of multiple sequence alignment. *Nucleic Acids Research*, *33*(2), 511–518.

Keča, N., Klopfenstein, N. B., Kim, M. S., Solheim, H., & Woodward, S. (2015). Initial characterization of an unidentified *Armillaria* isolate from Serbia using LSU-IGS 1 and TEF-1-α genes. *Forest Pathology*, *45*(2), 120–126.

Kile, G. A., & Watling, R. (1983). *Armillaria* species from south-eastern Australia. *Transactions of the British Mycological Society*, *81*(1), 129–140.

Kile, G. A., & Watling, R. (1988). Identification and occurrence of Australian *Armillaria* species, including *A. pallidula* sp. nov. and comparative studies between them and non-Australian tropical and Indian *Armillaria*. *Transactions of the British Mycological Society*, *91*(2), 305–315.

Kim, M. S., Hanna, J. W., McDonald, G. I., & Klopfenstein, N. B. (2023). *Armillaria altimontana* in North America: Biology and ecology. *Journal of Fungi*, *9*(9), 904.

Kim, M. S., Klopfenstein, N. B., Hanna, J. W., & McDonald, G. I. (2006). Characterization of North American *Armillaria* species: genetic relationships determined by ribosomal DNA sequences and AFLP markers. *Forest Pathology*, *36*(3),145–164.

Kim, M. S., Klopfenstein, N. B., McDonald, G. I., Arumuganathan, K., & Vidaver, A. K. (2000). Characterization of North American *Armillaria* species by nuclear DNA content and RFLP analysis. *Mycologia*, *92*(5),874–883.

Kitahara, M., Nagamune, K., Kinoshita, A., Yugeta, C., Ohara, N., Shimazaki, A., . . . Ogura-Tsujita, Y. (2022). In-vitro symbiotic germination of seeds of five mycoheterotrophic *Gastrodia* orchids with *Mycena* and *Marasmiaceae* fungi. *Mycoscience*, *63*, 88–95.

Koch, R. A., Wilson, A. W., Séné, O., Henkel, T. W., & Aime, M. C. (2017). Resolved phylogeny and biogeography of the root pathogen *Armillaria* and its gasteroid relative, *Guyanagaster*. *BMC Evolutionary Biology*, *17*, 1–6.

Korhonen, K. (1978). Interfertility and clonal size in the *Armillariella mellea* complex. *Karstenia, 18*(2), 31–42.

Kornerup, A., & Wanscher, J. H. (1981). Taschenlexikon der Farben (3rd ed.). Muster-Schmidt Verlag, Zürich & Göttingen.

Kummer, P. (1871). *Der Führer in die Pilzkunde: Anleitung zum methodischen, leichten und sichern Bestimmen der in Deutschland vorkommenden Pilze*. Luppe.

Lamoure, D. (1965). Charactères mycéliens et position taxinomique de *Clitocybe ectypa* (Fr.) F.Moreau. *Comptes Rendus Hebdomadaires des Séances de l'Académie des Sciences, 260*(4), 4561–63.

Li, H. (2013). Aligning sequence reads, clone sequences and assembly contigs with BWA-MEM. *arXiv*, 1303.3997.

Liang, J., Pecoraro, L., Cai, L., Yuan, Z., Zhao, P., Tsui, C. K., . . . Zhang, Z. (2021). Phylogenetic relationships, speciation, and origin of *Armillaria* in the northern hemisphere: A lesson based on rRNA and elongation factor 1-alpha. *Journal of Fungi*, *7*(12), 1088.

Libkind, D., Hittinger, C. T., Valério, E., Gonçalves, C., Dover, J., Johnston, M., . . . Sampaio, J. P. (2011). Microbe domestication and the identification of the wild genetic stock of lager-brewing yeast. *Proceedings of the National Academy of Sciences, 108*(35), 14539–14544.

Lima, M. L., Asai, T., & Capelari, M. (2008). *Armillaria paulensis*: a new South American species. *Mycological Research*, *112*(9), 1122–1128.

Liu, J., Qin, G., Chen, J., Song, J., Yan, Z., Yang, S., . . . Bhunjun, C. S. (2024). *Armillaria korhonenii*, the sixteenth biological species of *Armillaria* from China. *Phytotaxa*, *637*(2), 149–164.

Liu, K. J., & Muse, S. V. (2005). PowerMarker: An integrated analysis environment for genetic marker analysis. *Bioinformatics*, *21*(9), 2128–2129.

Liu, L. N., Sheng, A. R., Shen, B. M., Tan, Y., Li, S. N., & Tan, Z. M. (2025). Preliminary study on species diversity of symbiotic *Mycena sensu lato* promoting *Gastrodia elata* seed germination. *Acta Edulis Fungi*, *32*, 65–76.

Liu, L. N., Zhou, G., Shen, A., Shen, B., Tan, Y., & Tan, Z. (2022). *Mycena subpiligera* sp. nov., a symbiotic species from China associated with the seed germination of *Gastrodia elata*. *Mycobiology*, *50*, 294–301.

Liu, Y., Schröder, J., & Schmidt, B. (2013). Musket: a multistage k-mer spectrum-based error corrector for Illumina sequence data. *Bioinformatics*, *29*(3), 308–315.

Liu, Y., Xu, X., Dimitrov, D., Pellissier, L., Borregaard, M. K., Shrestha, N., . . . Wang, Z. (2023). An updated floristic map of the world. *Nature Communications*, *14*, 2990.

Lopes, F., Oliveira, L. R., Beux, Y., Kessler, A., Cárdenas-Alayza, S., Majluf, P., ... & Bonatto, S. L. (2023). Genomic evidence for homoploid hybrid speciation in a marine mammal apex predator. *Science Advances*, *9*(18), eadf6601.

Lowe, T. M., & Chan, P. P. (2016). tRNAscan-SE On-line: Integrating search and context for analysis of transfer RNA genes. *Nucleic Acids Research*, *44*(W1), W54–W57.

Malinsky, M., Matschiner, M., & Svardal, H. (2021). Dsuite - fast D-statistics and related admixture evidence from VCF files. *Molecular Ecology Resources*, *21*, 584–595.

Maphosa, L., Wingfield, B. D., Coetzee, M. P., Mwenje, E., & Wingfield, M. J. (2006). Phylogenetic relationships among *Armillaria* species inferred from partial elongation factor 1-alpha DNA sequence data. *Australasian Plant Pathology*, *35*, 513–520.

Marxmüller, H. (1982). Étude morphologique des *Armillaria* ss.str. à anneau. *Bulletin de la Société Mycologique de France*, *98*(1), 87–124.

Matheny, P. B., Curtis, J. M., Hofstetter, V., Aime, M. C., Moncalvo, J. M., Ge, Z. W., . . . Bougher, N. L. (2006). Major clades of *Agaricales*: a multilocus phylogenetic overview. *Mycologia*, *98*(6), 982–995.

Meleshko, O., Martin, M. D., Korneliussen, T. S., Schröck, C., Lamkowski, P., Schmutz, J., ... & Stenøien, H. K. (2021). Extensive genome-wide phylogenetic discordance is due to incomplete lineage sorting and not ongoing introgression in a rapidly radiated bryophyte genus. *Molecular Biology and Evolution*, *38*(7), 2750–2766.

Menardo, F., Praz, C. R., Wyder, S., Ben-David, R., Bourras, S., Matsumae, H., . . . Schaefer, L. K. (2016). Hybridization of powdery mildew strains gives rise to pathogens on novel agricultural crop species. *Nature Genetics*, *48*(2), 201–205.

Minh, B. Q., Schmidt, H. A., Chernomor, O., Schrempf, D., Woodhams, M. D., Von Haeseler, A., . . . Lanfear, R. (2020). IQ-TREE 2: New models and efficient methods for phylogenetic inference in the genomic era. *Molecular Biology and Evolution*, *37*(5), 1530–1534.

Mirarab, S., Reaz, R., Bayzid, M. S., Zimmermann, T., Swenson, M. S., & Warnow, T. (2014). ASTRAL: Genome-scale coalescent-based species tree estimation. *Bioinformatics*, *30*(17), i541–i548.

Mohammed, C., Guillaumin, J. J., & Berthelay, S. (1994). *Armillaria* species identified in China and Japan. *Mycological Research*, *98*, 607–613.

Morrison, D. J. (2004). Rhizomorph growth habit, saprophytic ability and virulence of 15 *Armillaria* species. *Forest Pathology*, *34*(1), 15–26.

Morrison, D. J., Chu, D., & Johnson, A. L. (1985). Species of *Armillaria* in British Columbia. *Canadian Journal of Plant Pathology*, *7*(3), 242–246.

Mulholland, V., MacAskill, G. A., Laue, B. E., Steele, H., Kenyon, D., & Green, S. (2012). Development and verification of a diagnostic assay based on EF-1 α for the identification of *Armillaria* species in Northern Europe. *Forest Pathology*, *42*(3), 229–238.

Newton, R. R., & Newton, I. L. G. (2013). Phybin: binning trees by topology. *PeerJ*, *1*, e187.

Ohenoja, E. (2006). *Armillaria ectypa*, a vulnerable indicator of mires. *Acta Mycologica*, *41*(2), 223–228.

Ota, Y., Kim, M. S., Neda, H., Klopfenstein, N. B., & Hasegawa, E. (2011). The phylogenetic position of an *Armillaria* species from Amami-Oshima, a subtropical island of Japan, based on elongation factor and ITS sequences. *Mycoscience*, *52*(1), 53–58.

Palcu, D. V., Patina, I. S., Șandric, I., Lazarev, S., Vasiliev, I., Stoica, M., & Krijgsman, W. (2021). Late Miocene megalake regressions in Eurasia. *Scientific Reports*, *11*(1), 11471.

Paradis, E., & Schliep, K. (2019). APE 5.0: an environment for modern phylogenetics and evolutionary analyses in R. *Bioinformatics*, *35*(3), 526–528.

Paradis, E. (2010). pegas: An R package for population genetics with an integrated–modular approach. *Bioinformatics*, *26*(3), 419–420.

Peck, C. H. (1897). New species of fungi. *Bulletin of the Torrey Botanical Club*, *24*, 137–147.

Peck, C. H. (1900). New species of fungi. *Bulletin of the Torrey Botanical Club*, *27*(12), 609–613.

Pegler, D. N. (1977). A preliminary Agaric flora of East Africa. *Kew Bulletin, Additional Series*, *6*, 92.

Peng, J. H., & Zhao, C. L. (2020). *Armillaria xiaocaobaensis* sp. nov. from China. *Mycotaxon 135*(2), 431–441.

Petch, T. (1909). New Ceylon fungi. *Annals of the Royal Botanic Gardens Peradeniya*, *4*, 299–330.

Petersen, J. H., & Vesterholt, J. (2008). Key to genera. In H. Knudsen & J. Vesterholt (Eds.), *Funga Nordica* (pp. 40–62). Nordsvamp.

Pildain, M. B., Coetzee, M. P., Wingfield, B. D., Wingfield, M. J., & Rajchenberg, M. (2010). Taxonomy of *Armillaria* in the Patagonian forests of Argentina. *Mycologia 102*(2), 392–403.

Podger, F. D., Kile, G. A., Watling, R., & Fryer, J. (1978). Spread and effects of *Armillaria luteobubalina* sp. nov. in an Australian *Eucalyptus regnans* plantation. *Transactions of the British Mycological Society 71*(1), 77–87.

Pound, M. J., & Salzmann, U. (2017). Heterogeneity in global vegetation and terrestrial climate change during the late Eocene to early Oligocene transition. *Scientific Reports*, *7*(1), 43386.

Poplin, R., Chang, P. C., Alexander, D., Schwartz, S., Colthurst, T., Ku, A., . . . DePristo, M. A. (2018). A universal SNP and small-indel variant caller using deep neural networks. *Nature Biotechnology 36*(10), 983–987.

Proffer, T. J., Jones, A. L., & Ehret, G. R. (1987). Biological species of *Armillaria* isolated from sour cherry orchards in Michigan. *Phytopathology 77*(6), 941–943.

Qin, G. F. (2002). Genetic and phylogenetic studies on Chinese *Armillaria* species. *Chinese Academy of Forestry*, 60–62.

Qin, G. F., Liu, J. W., Qin, W. M., Zhao, J., Ma, H. X., Chen, J., . . . Yuan, Y. (2025). Global phylogeny and taxonomy of *Armillaria* based on genealogical concordance phylogenetic species recognition. *Persoonia*. (in press)

Qin, G. F., Qin, W. M., Wang, H. C., Zhao, J., Korhonen, K., Chen, J., . . . Yuan, Y. (2024). Phylogeny and species diversity of *Armillaria* in China based on morphological, mating test, and GCPSR criteria. *Mycology, 15*, 1–35.

Qin, G. F., Zhao, J., & Korhonen, K. (2007). A study on intersterility groups of *Armillaria* in China. *Mycologia 99*(3), 430–441.

Qin, G. F., Zhao, J., Dai, Y. C., Tian, S. M., & Niemela, T. (1999). The identification of root rot pathogen *Armillaria* in northeast China. *Fungi Science, 14*, 53–62.

Rabiee, M., Sayyari, E., & Mirarab, S. (2019). Multi-allele species reconstruction using ASTRAL. *Molecular Phylogenetics and Evolution, 130*, 286–296.

Raper, C. A., & Raper, J. R. (1966). Mutations modifying sexual morphogenesis in Schizophyllum. *Genetics*, *54*(5), 1151.

Romagnesi, H. (1970). Observations sur les *Armillariella* (I). *Bulletin de la Société Mycologique de France*, *86*(1), 257–266.

Ronquist, F., & Huelsenbeck, J. P. (2003). MrBayes 3: Bayesian phylogenetic inference under mixed models. *Bioinformatics*, *19*, 1572–1574.

Ross-Davis, A. L., Hanna, J. W., Klopfenstein, N. B., & Kim, M. S. (2012). Advances toward DNA-based identification and phylogeny of North American *Armillaria* species using elongation factor-1 alpha gene. *Mycoscience, 53*(2), 161–165.

Saccardo, P. A. (1887). *Sylloge Hymenomycetum*, Vol. I. *Agaricineae*. *Sylloge Fungorum*, *5*, 83–84.

Samarasinghe, H., You, M., Jenkinson, T. S., Xu, J., & James, T. Y. (2020). Hybridization facilitates adaptive evolution in two major fungal pathogens. *Genes, 11*(1), 101.

Sarmashghi, S., Bohmann, K., Gilbert, M. T., Bafna, V., & Mirarab, S. (2019). Skmer: Assembly-free and alignment-free sample identification using genome skims. *Genome Biology, 20*, 34.

Simão, F. A., Waterhouse, R. M., Ioannidis, P., Kriventseva, E. V., & Zdobnov, E. M. (2015). BUSCO: assessing genome assembly and annotation completeness with single-copy orthologs. *Bioinformatics*, *31*(19), 3210–3212.

Singer, R. (1970). *Omphalinae* (*Clitocybeae–Tricholomataceae* Basidiomycetes). *Flora Neotropica*, *3*, 1–84.

Shaw, J., & Yu, Y. W. (2023). Fast and robust metagenomic sequence comparison through sparse chaining with skani. *Nature Methods, 20*(11), 1661–1665.

Shi, C. M., Ji, Y. J., Liu, L., Wang, L., & Zhang, D. X. (2013). Impact of climate changes from Middle Miocene onwards on evolutionary diversification in Eurasia: Insights from the mesobuthid scorpions. *Molecular Ecology*, *22*(6), 1700–1716.

Singer, R. (1956). The *Armillariella mellea* group. *Lloydia*, *19*, 176–187.

Singer, R. (1989). New taxa and new combinations of *Agaricales* (Diagnoses fungorum novorum Agaricalium IV). *Fieldiana: Botany New Series*, *21*, 1–33.

Smith, S. A., Moore, M. J., Brown, J. W., & Yang, Y. (2015). Analysis of phylogenomic datasets reveals conflict, concordance, and gene duplications with examples from animals and plants. *BMC Evolutionary Biology*, *15*, 1–15.

Spegazzini, C. (1889). Fungi Puiggariani. Pugillus 1. *Boletín, Academia Nacional de Ciencias, Córdoba*, *11*(4), 381–622.

Spegazzini, C. (1899). *Fungi Argentini* novi v. critici. *Anales del Museo Nacional de Buenos Aires, 3*, 81–365.

Stamatakis, A. (2014). RAxML version 8: a tool for phylogenetic analysis and post-analysis of large phylogenies. *Bioinformatics*, *30*(9), 1312–1313.

Stasinska, M. (2015). *Armillaria ectypa*, a rare fungus of mire in Poland. *Acta Mycologica*, *50*(1).

Steensels, J., Gallone, B., & Verstrepen, K.J. (2021). Interspecific hybridization as a driver of fungal evolution and adaptation. *Nature Reviews Microbiology, 19*, 485–500.

Steenwyk, J. L., Li, Y., Zhou, X., & Rokas, A. (2023). Incongruence in the phylogenomics era. *Nature Reviews Genetics*, *24*(12), 834–850.

Stevenson, G. (1964). The *Agaricales* of New Zealand: V. *Kew Bulletin 19*(1), 1–59.

Tang, M. J., & Tolgorb, B. (2020). Study on the germination fungi as *Mycena* and *Gastrodia elata* seeds in northeast of China. *Northern Horticulture*, *17*, 118–123.

Terashima, K., Cha, J. Y., Yajima, T., & Kawai, M. (1998). Phylogenetic analysis of Japanese Armillaria based on the intergenic spacer (IGS) sequences of their ribosomal DNA. E*uropean Journal of Forest Pathology*, *28*(1), 11–19.

Tsykun, T., Rigling, D., & Prospero, S. (2013). A new multilocus approach for a reliable DNA-based identification of *Armillaria* species. *Mycologia*, *105*(4), 1059–1076.

Utescher, T., & Mosbrugger, V. (2007). Eocene vegetation patterns reconstructed from plant diversity—a global perspective. *Palaeogeography, Palaeoclimatology, Palaeoecology*, *247*(3–4), 243–271.

Velenovský, J. (1920). *České Houby*, Vol. 2. České Botanické Společnosti.

Vellinga, E. C., & Noordeloos, M. E. (2001). Glossary. In Noordeloos, M. E., Kuyper, T. W., & Vellinga, E. C. (Eds.), Flora Agaricina Neerlandica, Volume 5. Balkema, Rotterdam.

Volk, T. J., & Burdsall, H. H., Jr. (1995). A nomenclatural study of *Armillaria* and *Armillariella* species (Basidiomycotina, Tricholomataceae). *Synopsis Fungorum*, *8*, 1–121.

Volk, T. J., Burdsall, H. H., Jr., & Banik, M. T. (1996). *Armillaria nabsnona*, a new species from western North America. *Mycologia*, *88*(3), 484–491.

Wang, R. J., & Hahn, M. W. (2018). Speciation genes are more likely to have discordant gene trees. *Evolution Letters*, *2*(4), 281–296.

Wang, J. Z., Wang, S. B., Liu, X. Q., Tan, D. F., & Fu, C. (2007). Cultivation condition affected to quality of seed stem of *Gastrodia* by no soil bag planted. *Chinese Archives of Traditional Chinese Medicine*, *25*, 724–726.

Wang, Y. Y., Tu, X., Wang, C. H., Lu, S., Deng, Q. Y., & Sun, X. B. (2020). Genetic diversity, growth and hydrolases of *Armillaria* spp. associated with cultivated *Gastrodia elata*. *Mycosystema*, *39*, 265–279.

Watling, R. (1992). *Armillaria staude* in the Cameroon Republic. *Persoonia*, *14*(4), 483–491.

Xia, E., Yao, Q., Zhang, H., Jiang, J., Zhang, L., & Gao, L. (2016). CandiSSR: an efficient pipeline used for identifying candidate polymorphic SSRs based on multiple assembled sequences. *Frontiers in Plant Science*, *6*.

Xie, J., Chen, Y., Cai, G., Cai, R., Hu, Z., & Wang, H. (2023). Tree Visualization By One Table (tvBOT): A web application for visualizing, modifying and annotating phylogenetic trees. *Nucleic Acids Research*, *51*(W1), W587–W592.

Xu, F., LoBuglio, K. F., & Pfister, D. H. (2019). On the co-occurrence of species of *Wynnea* (Ascomycota, Pezizales, Sarcoscyphaceae) and *Armillaria* (Basidiomycota, Agaricales, Physalacriaceae). *Fungal Systematics and Evolution*, *4*(1), 1–12.

Xu, H., Luo, X., Qian, J., Pang, X., Song, J., Qian, G., . . . Chen, S. (2012). FastUniq: A fast de novo duplicates removal tool for paired short reads. *PLoS One*, *7*(12), e52249.

Xu, J. T. (1993). *The Cultivation of Gastrodia elata Blume in China*. Peking Medical University and Peking Union Medical College Press.

Xu, J. T., & Guo, S. X. (1989). Fungus associated with nutrition of seed germination of *Gastrodia elata—Mycena osmundicola* Lange. *Acta Mycologica Sinica*, *8*, 221–226.

Yang, Z. (2007). PAML 4: Phylogenetic analysis by maximum likelihood. *Molecular Biology and Evolution*, *24*(8), 1586–1591.

Yu, Y., Harris, A. J., Blair, C., & He, X. (2015). RASP (Reconstruct Ancestral State in Phylogenies): A tool for historical biogeography. *Molecular Phylogenetics and Evolution*, *87*, 46–49.

Yun, T., Li, H., Chang, P. C., Lin, M. F., Carroll, A., & McLean, C.Y. (2020). Accurate, scalable cohort variant calls using DeepVariant and GLnexus. *Bioinformatics*, *36*(24), 5582–5589.

Zang, M., Li, B., & Xi, J. X. (1996). *Fungi of the Hengduan Mountains*. Science Press.

Zachos, J., Pagani, M., Sloan, L., Thomas, E., & Billups, K. (2001). Trends, rhythms, and aberrations in global climate 65 Ma to present. *Science*, *292*(5517), 686–693.

Zeller, S. M. (1933). New or noteworthy agarics from Oregon. *Mycologia*, *25*(5), 376–391.

Zeller, S. M. (1935). Some miscellaneous fungi of the Pacific Northwest. *Mycologia 27*(5), 449–466.

Zhang, B. L., Chen, W., Wang, Z., Pang, W., Luo, M. T., Wang, S., . . . Wu, D. D. (2023). Comparative genomics reveals the hybrid origin of a macaque group. *Science Advances*, *9*(22), eadd3580.

Zhang, C., Nielsen, R., & Mirarab, S. (2025). CASTER: Direct species tree inference from whole-genome alignments. *Science*, eadk9688.

Zhang, C., Rabiee, M., Sayyari, E., & Mirarab, S. (2018). ASTRAL-III: Polynomial time species tree reconstruction from partially resolved gene trees. *BMC Bioinformatics*, *19*, 15–30.

Zhao, J., Zhao, J., & Qin, G. F. (2007). Cross breeding of *Armillaria gallica* strains. *Acta Edulis Fungi*, *14*, 31–35.

Zhou, X., Yang, X. H., Liang, H. X., & Liu, C. Y. (1987). Morphology of *Gastrodia elata*. Beijing: *Science Press*, 1–122.

APPENDIX A

ABSTRACT OF PUBLICATIONS

Phytotaxa 637 (2): 149–164
https://www.mapress.com/pt/
Copyright © 2024 Magnolia Press

Article

ISSN 1179-3155 (print edition)
PHYTOTAXA
ISSN 1179-3163 (online edition)

https://doi.org/10.11646/phytotaxa.637.2.3

Armillaria korhonenii, the sixteenth biological species of *Armillaria* from China

JIANWEI LIU[1,2,3,4,9], GUOFU QIN[5,10], JIAN CHEN[6,11], JING SONG[1,2,12], ZHUYUE YAN[1,2,13], SHIMEI YANG[1,2,14], MENG-HUA TIAN[7,15], XIN XU[7,16], CHANGFEI ZHANG[7,17], THATSANEE LUANGHARN[3,18], CHITRABHANU S. BHUNJUN[3,4,19], FUQIANG YU[1,2,20,*] & ZHU L. YANG[1,8,21,*]

[1]*The Germplasm Bank of Wild Species, Kunming Institute of Botany, Chinese Academy of Sciences, 132 Lanhei Road, Kunming, Yunnan 650201, People's Republic of China.*
[2]*Yunnan Key Laboratory for Fungal Diversity and Green Development, Kunming 650201, Yunnan, China.*
[3]*Center of Excellence in Fungal Research, Mae Fah Luang University, Chiang Rai 57100, Thailand.*
[4]*School of Science, Mae Fah Luang University, Chiang Rai 57100, Thailand.*
[5]*Botanical Museum, University of Helsinki, P. O. box 7, FIN-00014 Helsinki, Finland.*
[6]*School of Ecology and Nature Conservation, Beijing Forestry University, Beijing 100083, China.*
[7]*Zhaotong Institute of Gastrodia, Zhaotong 657000, China.*
[8]*CAS Key Laboratory for Plant Diversity and Biogeography of East Asia, Kunming Institute of Botany, Chinese Academy of Sciences, Kunming 650201, Yunnan, China.*
[9] *liujianwei@mail.kib.ac.cn; https://orcid.org/0000-0001-5683-5152*
[10] *armillaria@sina.com; https://orcid.org/0009-0004-0404-2512*
[11] *xnchenjian@163.com; https://orcid.org/0000-0001-8409-7791*
[12] *songjing@mail.kib.ac.cn; https://orcid.org/0009-0004-8516-4107*
[13] *yanzhuyue@mail.kib.ac.cn; https://orcid.org/0009-0001-5954-6839*
[14] *yangshimei@mail.kib.ac.cn; https://orcid.org/0009-0008-3637-4182*
[15] *tianmenghua@126.com; https://orcid.org/0009-0005-9697-4321*
[16] *2934150808@qq.com; https://orcid.org/0000-0003-1551-5587*
[17] *zcfei001@163.com; https://orcid.org/0009-0000-4772-8718*
[18] *thatsanee.lua@mfu.ac.th; https://orcid.org/0000-0002-1684-6735*
[19] *chitrabhanu.bhu@mfu.ac.th; https://orcid.org/0000-0001-8098-3390*
[20] *fqyu@mail.kib.ac.cn; https://orcid.org/0000-0001-7931-050X*
[21] *fungi@mail.kib.ac.cn; https://orcid.org/0000-0001-9745-8453*
**Corresponding author; Jianwei Liu and Guofu Qin have equally contributed to this work.*

Abstract

Armillaria korhonenii, designated as Chinese biological species Q (CBSQ) here, is described as a new species based on phylogenetic and morphological evidence as well as the results of mating tests. This species is the sixteenth biological species of *Armillaria* reported from China following the discovery of 15 previously known biological species. Phylogenetically, *A. korhonenii* is the earliest divergent lineage of the genus *Armillaria* as inferred from the nucleotide sequences of the Elongation Factor 1-Alpha (*EF1a*). Morphologically, it is characterized by its ellipsoid to elongate basidiospores, yellowish orange to honey yellow pileus with fibrillose squamules. Mating tests indicated that *A. korhonenii* is a tetrapolar heterogeneous species and is inter-sterile with all the tested species except partial compatibility with CBSH.

Key words: phylogenetics, Physalacriaceae, one new taxon

Introduction

Armillaria (Fr.) Staude (1857:130) is a genus of the family Physalacriaceae, with the type species *A. mellea* (Vahl: Fr.) P. Kumm (1871:134) (Kirk *et al*. 2008). Species belonging to *Armillaria* hold significant economic and ecological importance, with both positive and negative aspects from an anthropocentric perspective (Wu *et al*. 2019, Yuan *et al*. 2023). As serious pathogens, they can kill living plants, with detrimental consequences of forest destruction and substantial economic losses (Dai *et al*. 2007). On the other hand, as saprotrophs, they play a crucial role in carbon and mineral cycling within forest ecosystems (Heinzelmann *et al*. 2019). Furthermore, species of *Armillaria* can serve as symbionts of orchid plants and other fungi (Cha *et al*. 1995, Cha *et al*. 1996, Guo & Xu 1992, Guo *et al*. 2016,

Accepted by Iqbal Hosen: 4 Feb. 2024; published: 20 Feb. 2024

MITOCHONDRIAL DNA PART B: RESOURCES
2024, VOL. 9, NO. 6, 716–719
https://doi.org/10.1080/23802359.2024.2356131

Taylor & Francis
Taylor & Francis Group

MITOGENOME REPORT

OPEN ACCESS Check for updates

The complete mitochondrial genome of enigmatic mycoparasitic fungus *Squamanita imbachii*

Jian-Wei Liu[a,b,c], Thatsanee Luangharn[b], Fu-Qiang Yu[a] and Chitrabhanu S. Bhunjun[b,c]

[a]Germplasm Bank of Wild Species & Yunnan Key Laboratory for Fungal Diversity and Green Development, Kunming Institute of Botany, Chinese Academy of Sciences, Kunming, China; [b]Center of Excellence in Fungal Research, Mae Fah Luang University, Mueang Chiang Rai, Thailand; [c]School of Science, Mae Fah Luang University, Mueang Chiang Rai, Thailand

ABSTRACT

The complete mitochondrial genome of *Squamanita imbachii* I. Saar, is unveiled in this research for the first time. It covers 76,643 base pairs (bp) and exhibits a guanine-cytosine (GC) content of 23%. The genome includes 14 conserved protein-coding genes, 1 DNA polymerase gene, 2 ribosomal RNA gene (RNS and RNL), 25 transfer RNA (tRNA) genes and 18 open reading frames (ORFs). Phylogenetic analysis, utilizing a mitochondrial gene dataset from 15 taxa across seven families within the Agaricales order, was conducted employing the maximum-likelihood (ML) approach. This analysis identified a close phylogenetic relationship between *S. imbachii* and *Floccularia luteovirens* (Alb. & Schwein.) Pouzar 1957, positioning both within the Squamanitaceae family.

ARTICLE HISTORY
Received 18 March 2024
Accepted 12 May 2024

KEYWORDS
Agaricales; fungicolous fungi; phylogeny; Squamanitaceae

Introduction

Squamanita is a genus in the family Squamanitaceae (Vizzini et al. 2019; Kalichman et al. 2020; Liu et al. 2021), which may represent one of the most unique basidiomycetes fungi in the world as nearly all the species are parasitic on other living fungi. Saar et al. (2022) split *Squamanita* into two monophyletic groups, viz. *Squamanita* and *Dissoderma* (A.H. Sm. & Singer) Singer 1973. Fourteen and nine species are accepted in *Squamanita* and *Dissoderma* worldwide, respectively (Species Fungorum 2024).

Squamanita imbachii has been documented in Europe and North America (Liu et al. 2021; Saar et al. 2022). Liu et al. (2021) sequenced a specimen (HKAS107325A) collected from Liguria, Italy, resulting in the generation of four genes (ITS: MW258856; LSU: MW258908; TEF1-α: MW324508; 18S: MW258935 & MW258886) and noted that this species acts as a parasite on *Amanita excelsa* species complex (Fr.) Bertill. 1866. Saar et al. (2022) confirmed the identity of HKAS107325A as *S. imbachii*. In this study, we used this dried specimen archived in the Herbarium of Cryptogams, Kunming Institute of Botany, Chinese Academy of Sciences (http://www.kib.ac.cn/) (Figure 1).



Figure 1. Image of *Squamanita imbachii* (HKAS107325A) sequenced in this work Liu et al. (2021).

CONTACT Fu-Qiang Yu fqyu@mail.kib.ac.cn Germplasm Bank of Wild Species & Yunnan Key Laboratory for Fungal Diversity and Green Development, Kunming Institute of Botany, Chinese Academy of Sciences, Kunming, Yunnan, China; Chitrabhanu S. Bhunjun chitrabhanu.bhu@mfu.ac.th Center of Excellence in Fungal Research, Mae Fah Luang University, Mueang Chiang Rai, Thailand.

Supplemental data for this article can be accessed online at https://doi.org/10.1080/23802359.2024.2356131.

© 2024 The Author(s). Published by Informa UK Limited, trading as Taylor & Francis Group.
This is an Open Access article distributed under the terms of the Creative Commons Attribution License (http://creativecommons.org/licenses/by/4.0/), which permits unrestricted use, distribution, and reproduction in any medium, provided the original work is properly cited. The terms on which this article has been published allow the posting of the Accepted Manuscript in a repository by the author(s) or with their consent.

Mycoscience VOL.63 (2022) MYC592

Mycoscience

AN OPEN ACCESS JOURNAL FOR GENERAL MYCOLOGY

The Mycological Society of Japan

Short communication

A new edible species of *Gomphus* (*Gomphaceae*) from southwestern China

Jian-Wei Liu[a,b,d], Thatsanee Luangharn[a*], Shan-ping Wan[c], Ran Wang[d], Fu-Qiang Yu[d*]

[a] *Center of Excellence in Fungal Research, Mae Fah Luang University, Chiang Rai 57100, Thailand*
[b] *School of Science, Mae Fah Luang University, Chiang Rai 57100, Thailand*
[c] *College of Resource and Environment, Yunnan Agricultural University, Kunming, Yunnan 650100, China*
[d] *The Germplasm Bank of Wild Species, Yunnan Key Laboratory for Fungal Diversity and Green Development, Kunming Institute of Botany, Chinese Academy of Sciences, Kunming 650201, Yunnan, China*

ABSTRACT

Gomphus matijun, a new edible species, is described from southwestern China based on phylogenetic and morphological evidence. Phylogenetic analyses of the nrLSU and ITS datasets indicated that *G. matijun* is related to *G. crassipes* and *G. ludovicianus* with weak statistical support in maximum likelihood but strong statistical support in Bayesian analyses. *Gomphus matijun* is characterized by its gray-blue to blue or blue-purple pileus with a round or irregular outline, relatively smaller basidiospores [9–11(–13) × 6–7(–8) µm], mostly 2-spored basidia, and occurs in subtropical fagaceous forests. A key to the known species of *Gomphus* is provided.

Keywords: Gomphales, *Gomphus crassipes*, *G. ludovicianus*, taxonomy, wild edible mushroom

Article history: Received 13 March 2022, Revised 9 September 2022, Accepted 10 September 2022, Available online 21 October 2022.

Gomphus Pers. was introduced by Persoon (1797) and has then undergone many taxonomic and nomenclatural modifications. Giachini (2004), Giachini, Hosaka, Nouhra, Spatafora, and Trappe (2010), and Giachini and Castellano (2011) revealed that *Gomphus* sensu lato was polyphyletic, and species of the genus were recombined into multiple genera, viz. *Gloeocantharellus* Singer., *Gomphus* sensu stricto, *Phaeoclavulina* Brinkmann, and *Turbinellus* Earle (Giachini & Castellano, 2011). The pileus of *Gomphus* is from fan-shaped to slightly funnel-shaped, bright violet, pale olivaceous or brown; its hymenium is wrinkled to almost poroid, violet, vinaceous brown to milky-coffee colored with verrucose basidiospores (Giachini & Castellano, 2011). *Gomphus* is generally distributed in terrestrial habitats (Giachini, 2004). Five species, *G. brunneus* (Heinem.) Corner, *G. clavatus* (Pers.) Gray, *G. crassipes* (Kuntze) Maire, *G. ludovicianus* R.H. Petersen, Justice & D.P. Lewis, and *G. orientalis* R.H. Petersen & M. Zang, are known for the genus, among them *G. orientalis* is an easily overlooked species described from China and similar to *G. clavatus* (Zang, 1996).

During a survey of mushroom markets in Guizhou Province, China, we have found a hoof-shaped *Gomphus* species that is commonly called "matijun" and consumed by local residents. The aim of the present study is to report this new edible *Gomphus* species and then describe its morphological characteristics and phylogenetic traits since it differs from all other known species.

Morphological characteristics of fresh materials were recorded. All specimens were then dried at 45 °C and deposited in the Herbarium of Cryptogams, Kunming Institute of Botany, Chinese Academy of Sciences (HKAS), Yunnan, China.

Macro-morphological characteristics were described following the methods described by Giachini, Camelini, Rossi, Soares, and Trappe (2012) and Petersen, Hughes, Justice, and Lewis (2014). The dried specimens were sectioned by hand and mounted in 5% of KOH, and observed using a compound microscope (Leica DM2500, Leica Microsystems, Wetzlar, Germany). Twenty basidiospores per collection were measured, and their sizes and shapes were recorded and photographed. The color codes were recorded following Kornerup and Wanscher (1981). Basidiospores were photographed using a Scanning Electron Microscopy (SEM). Basidiospores were taken from the dried hymenium edge with tweezers and pasted with double-sided tape, which was directly mounted on an SEM stub, coated with gold-palladium, and examined and photographed with a JSM-5600LV SEM (JEOL, Tokyo, Japan). The notations [n/m/p] indicated that the measurements were made "n" basidiospores from "m" basidiomata of "p" collections with a minimum of 20 basidiospores. The basidiospore quotient was followed by [Q = L/W], where Q, the quotient of basidiospore length to width (L/W) of a basidiospore in side view and Qm, the mean of Q-values ± SD, was calculated considering the mean value of the lengths and widths of basidiospores. The basidiospore size was measured with and without the myxosporium and given as (a–)b–c(–d) (Tulloss, 2005).

Dried specimens were used to extract DNA. Universal primer

* Corresponding author. Kunming Institute of Botany, Chinese Academy of Sciences, Kunming 650201, Yunnan, China
E-mail address: fqyu@mail.kib.ac.cn (Fu-Qiang Yu).
* Corresponding author. Center of Excellence in Fungal Research, Mae Fah Luang University, Chiang Rai 57100, Thailand
E-mail address: thatsanee.lua@mfu.ac.th (Thatsanee Luangharn).

This is an open-access paper distributed under the terms of the Creative Commons Attribution-NonCommercial-NoDerivative 4.0 international license (CC BY-NC-ND 4.0: https://creativecommons.org/licenses/by-nc-nd/4.0/).

doi: 10.47371/mycosci.2022.09.002

MITOCHONDRIAL DNA PART B
2022, VOL. 7, NO. 6, 1066–1068
https://doi.org/10.1080/23802359.2022.2086077

Taylor & Francis
Taylor & Francis Group

MITOGENOME ANNOUNCEMENT

OPEN ACCESS Check for updates

The complete mitochondrial genome of *Polyozellus multiplex* (Thelephorales)

Jian-Wei Liu[a,b,c], Thatsanee Luangharn[a], Shi-Mei Yang[c] and Fu-Qiang Yu[c]

[a]Center of Excellence in Fungal Research, Mae Fah Luang University, Chiang Rai, Thailand; [b]School of Science, Mae Fah Luang University, Chiang Rai, Thailand; [c]The Germplasm Bank of Wild Species, Yunnan Key Laboratory for Fungal Diversity and Green Development, Kunming Institute of Botany, Chinese Academy of Sciences, Kunming, China

ABSTRACT

The complete mitogenome of *Polyozellus multiplex* (Underw.) Murrill 1910, was first sequenced, assembled, and annotated in the present study. The mitogenome length was 47,054 bp with a GC content of 23.35%, including 14 conserved protein-coding genes, one ribosomal protein (RPS3), two DNA polymerases (DPO), two rRNA genes (RNS and RNL), and 24 transfer RNA (tRNA) genes. Phylogenetic analysis, based on a combined mitochondrial gene dataset from 17 taxa of four orders within the class Agaricomycetes, was conducted using maximum-likelihood (ML) and Bayesian inference (BI) methods. It is revealed that *P. multiplex* is closely related to *Thelephora aurantiotincta* Corner 1968, both of them have been clustered into Thelephorales.

ARTICLE HISTORY
Received 27 March 2022
Accepted 29 May 2022

KEYWORDS
Mitochondrial genome; phylogenetic relationships; wild edible mushroom

Polyozellus multiplex (Underw.) Murrill. was originally described from Mount Desert, Maine, USA and classified in the genus *Cantharellus* Adans. ex Fr. 1821 with *Cantharellus multiplex* Underw. 1899 (Underwood 1899). Then, Murrill (1910) classified this fungus to a new genus, *Polyozellus* Murrill. 1910, as its cespitose imbricate habit differed from that of other species of *Cantharellus*. Imazeki (1953) reclassified this genus to the *Thelephora* Ehrh. ex Wild. 1787 group according to its lobed nodulose basidiospores thelephoric acid content, which differed from other *Cantharellus* species. Since then, *Polyozellus* has remained a monotypic genus. Voitk et al. (2017) revealed that *P. multiplex* was a species complex including five phylogenetic species, viz. *P. multiplex*, *P. atrolazulinus* Trudell & Kõljalg 2018, *P. mariae* Voitk & Kõljalg 2018, *P. marymargaretae* Beug & I. Saar 2018 and *P. purpureoniger* Spirin & I. Saar 2018. Among them, *P. multiplex* is a good edible fungus distributing in eastern Asia and northeastern North America (Yang 1992). Here, the mitochondrial genome of *P. multiplex* is first reported to promote our understanding in *Polyozellus* taxonomy and genetics.

Two genes (ITS1-5.8S-ITS2: OL913875, LSU rDNA: OL913876) were combined to identify *P. multiplex*, which was from the Dashaba Agriculture Market (104°5′48″E; 26°13′17″N), Xuanwei City, Yunnan, China. In accordance with guidelines and regulations provided by Kunming Institute of Botany, Chinese Academy of Sciences and the local government agency, the fungus collection from this local market was performed without a required ethical approval or other relevant permissions from a national or local agency. The dried specimen (voucher # HKAS122651) was deposited in the Herbarium of Cryptogams, Kunming Institute of Botany, Chinese Academy of Sciences (http://www.kib.ac.cn/, the contact person and e-mail: Mr. Tao Deng, dengtao@mail.kib.ac.cn).

The total genomic DNA of this dried *P. multiplex* specimen was extracted using the CTAB method (Doyle 1987). The whole-genome sequencing was performed on an Illumina sequencing platform (HiSeq PE150) with standard procedures. The 150 bp paired-end libraries were prepared to generate approximately 8 GB of raw data. The mitochondrial genome was assembled by GetOrganelle v. 1.7.5 with the default parameters (Jin et al. 2020). The mitogenome was annotated by the MFannot tool (http://megasun.bch.umontreal.ca/cgi-bin/mfannot/mfannotInterface.pl) and was compared with the result annotated from the reference sequence *Thelephora aurantiotincta* with manual corrections in Geneious Prime 2020.0.3 (BioMatters, Ltd., Auckland, New Zealand).

The complete mitochondrial genome sequence of *Polyozellus multiplex* has been deposited in GenBank (GenBank accession no. OL790394). The circular genome (47,054 bp) comprised of 14 conserved protein-coding genes (PCGs), one ribosomal protein (RPS3), two DNA polymerases (DPO), two rRNA genes (RNS and RNL), and 24 transfer RNA (tRNA) genes. The 14 conserved PCGs respectively encoded the seven ubiquinone reductase subunits of NADH (NAD1, NAD2, NAD3, NAD4, NAD4L, NAD5, and NAD6), three cytochrome oxidase subunits (COX1, COX2, and COX3), three ATP synthase subunits (ATP6, ATP8, and ATP9), and the apocytochrome b (COB). The 24 tRNA genes ($tRNA^{Ala(UGC)}$, $tRNA^{Cys(GCA)}$, $tRNA^{Asp(GUC)}$, $tRNA^{Glu(UUC)}$, $tRNA^{Phe(GAA)}$, $tRNA^{Gly(UCC)}$, $tRNA^{His(GUG)}$, $tRNA^{Ile(GAU)}$, $tRNA^{Lys(UUU)}$, $tRNA^{Leu(UAA)}$,

CONTACT Fu-Qiang Yu fqyu@mail.kib.ac.cn Kunming Institute of Botany, Chinese Academy of Sciences, Kunming 650201, Yunnan, China; Thatsanee Luangharn thatsanee.lua@mfu.ac.th Center of Excellence in Fungal Research, Mae Fah Luang University, Chiang Rai 57100, Thailand

© 2022 The Author(s). Published by Informa UK Limited, trading as Taylor & Francis Group.
This is an Open Access article distributed under the terms of the Creative Commons Attribution License (http://creativecommons.org/licenses/by/4.0/), which permits unrestricted use, distribution, and reproduction in any medium, provided the original work is properly cited.

Asian Journal of Mycology 6(1): 77–85 (2023) ISSN 2651-1339
www.asianjournalofmycology.org **Article**
Doi 10.5943/ajom/6/1/7

Cystoderma lignicola, a new species from southwestern China

Liu JW[1,2,3], Luangharn T[2*] and Yu FQ[1*]

[1]The Germplasm Bank of Wild Species, Yunnan Key Laboratory for Fungal Diversity and Green Development, Kunming Institute of Botany, Chinese Academy of Sciences, Kunming 650201, Yunnan, China
[2]Center of Excellence in Fungal Research, Mae Fah Luang University, Chiang Rai 57100, Thailand
[3]School of Science, Mae Fah Luang University, Chiang Rai 57100, Thailand

Liu JW, Luangharn T, Yu FQ 2023 – *Cystoderma lignicola*, a new species from southwestern China. Asian Journal of Mycology 6(1),77–85, Doi 10.5943/ajom/6/1/7

Abstract

In this study, we describe a new species, *Cystoderma lignicola*, collected from rotten woods in the temperate region in Yunnan Province, southwestern China. Our new species was described based on macro- and micro-morphological characteristics and molecular data of combined internal transcribed spacers (ITS) and large subunit (nrLSU) of the nuclear ribosomal DNA (rDNA) sequences. *Cystoderma lignicola* is characterized by its light orange to brown cap, globose, subglobose, ellipsoid to broadly ellipsoid basidiospores, with 4–5 × 3–4 µm diam. Phylogenetically, *C. lignicola* showed a sister clade to *C. chocoanum* with statistical support of SH-aLRT/UFB = 90.9/90 in maximum likelihood analysis and statistical support of BPP = 0.99 in the Bayesian analysis.

Keywords – Amyloid basidiospore – phylogenetic analysis – saprotrophic – Squamanitaceae – taxonomy

Introduction

Cystoderma Fayod, a genus in the family Squamanitaceae (Vizzini et al. 2019, Kalichman et al. 2020, Liu et al. 2021), was established by Fayod in 1889 with *C. amianthinum* (Scop.) as the type species. Harmaja (2002) considered the results of the phylogenetic analysis of *Cystoderma*, which is not monophyletic in the study of Moncalvo et al. (2002), and divided *Cystoderma* into two genera, viz., *Cystoderma* and *Cystodermella* Harmaja, where *Cystoderma* contains species that possess amyloid basidiospores, and *Cystodermella* encompasses species with inamyloid basidiospores. *Cystoderma* members can be found in forest ecosystems in open areas, growing on soil, among mosses and litter, and some species grow on rotten wood (Saar 2012). Currently, 31 *Cystoderma* species have been reported worldwide (Li et al. 2021). In China, ten species have been recorded up to now, viz., *C. amianthinum*, *C. aureum* (Matt.) Kühner & Romagn., *C. carcharias* (Pers.) Fayod., *C. granosum*, *C. japonicum* Thoen & Hongo., *C. lilaceum* R.L. Zhao, M.Q. He & J.X. Li, *C. pseudoamianthinum* R.L. Zhao, M.Q. He & J.X. Li, *C. rugosolateritium* R.L. Zhao, M.Q. He & J.X. Li, *C. subglobisporum* R.L. Zhao, M.Q. He & J.X. Li, and *C. subvinaceum* A.H. Sm (Tai 1979, Li et al. 2015, 2021, Liu et al. 2021, Mao 2000).

In this study, we reported new knowledge of *Cystoderma* collected from the Ailao Mountains of Nanhua County in central Yunnan Province, China. Morphological comparison with all known species of the genus *Cystoderma* and phylogenetic analysis supported our collections as a new

Submitted 22 December 2022, Accepted 11 May 2022, Published 30 May 2023
Corresponding Author: Fu-Qiang Yu – e-mail – fqyu@mail.kib.ac.cn,
Thatsanee Luangharn – email – thatsanee.lua@mfu.ac.th

Phytotaxa 527 (4): 248–256
https://www.mapress.com/j/pt/
Copyright © 2021 Magnolia Press

Article

ISSN 1179-3155 (print edition)
PHYTOTAXA
ISSN 1179-3163 (online edition)

https://doi.org/10.11646/phytotaxa.527.4.2

Tuber qujingense and *T. songlu*, two new species from Yunnan, China

SHANPING WAN[1,2,3], JIANWEI LIU[2,4], LANLAN HUANG[1,2,5], XIAOMIN QIN[1,6], WEI LIU[1,7] & FUQIANG YU[2,8]*

[1] *College of Resource and Environment, Yunnan Agricultural University, Kunming, Yunnan 650100, People's Republic of China*
[2] *The Germplasm Bank of Wild Species, Yunnan Key Laboratory for Fungal Diversity and Green Development, Kunming Institute of Botany, Chinese Academy of Sciences, 132 Lanhei Road, Kunming, Yunnan 650201, People's Republic of China*
[3] *wsp871117@163.com; https://orcid.org/0000-0002-0794-3701*
[4] *liujianwei@mail.kib.ac.cn; https://orcid.org/0000-0001-5683-5152*
[5] *huanglanlan@mail.kib.ac.cn; https://orcid.org/0000-0003-2365-8027*
[6] *qinxiaomin89@163.com; https://orcid.org/0000-0002-3411-444X*
[7] *liuwei9712@163.com; https://orcid.org/0000-0002-0075-9434*
[8] *fqyu@mail.kib.ac.cn; https://orcid.org/0000-0001-7931-080X*
**Corresponding author*
Shanping Wan and Jianwei Liu have contributed equally to this work.

Abstract

Tuber qujingense and *T. songlu* are described as new species based on both phylogenetic and morphological analyses. Phylogenetically, these two species are clearly distinct from described species of *Tuber*. Morphologically, these two species have whitish smooth ascomata, pubescent and prosenchymatous peridium and 1–4 spored asci; however, *T. qujingense* is characterized by its fusiform ascospores and taller alveolar walls (4.5–11 µm) while *T. songlu* has larger ellipsoid ascospores and lower alveolar walls (1–7 µm).

Keywords: White truffles, phylogeny, taxonomy

Introduction

Tuber P. Micheli ex F.H. Wigg. (1780: 109) (Ascomycota, Pezizales) is one of the most quintessential genera of hypogeous fungi, which has important edible and economic values (Mello *et al*. 2006; Jeandroz *et al*. 2008; Trappe *et al*. 2009; Bonito *et al*. 2013). Furthermore, *Tuber* species play a key role in forest ecosystems, including disturbed forests, where they are often common ectomycorrhizal symbionts. *Tuber* speciation and function in ecosystems are tightly linked to their ectomycorrhizal (ECM) ecology and putative co-diversification with major plant families including Pinaceae (pines), Fagaceae (oak/beech), Myrtaceae (eucalypts), and Salicaceae (willows/poplar) and to adaptations for animal dispersal in the Northern and Southern Hemispheres (Kauserud *et al*. 2010; Zambonelli *et al*. 2016).

Recent taxonomic and molecular studies on *Tuber* in China have revealed several new species (García-Montero *et al*. 2010; Fan *et al*. 2016a, b; Wan *et al*. 2016, 2017a, b). During our survey of hypogeous fungi in Yunnan, China, two whitish truffles were found under pure coniferous forest in Huize County, Qujing City, Yunnan Province. According to observation and analysis, we found two specimens that showed clear differences compared with other *Tuber* species. The results of the molecular and morphological studies confirmed that the two collections are two undescribed species which we present in this paper with descriptions, illustrations and molecular work and name *T. qujingense* and *T. songlu*.

Materials and methods

Morphological studies

Fresh samples were collected from forests of *Pinus armandii* Franch. in Yunnan, China. Macromorphological description

 Accepted by Genevieve Gates: 10 Aug. 2021; published: 8 Dec. 2021

Phytotaxa 464 (1): 085–092
https://www.mapress.com/j/pt/
Copyright © 2020 Magnolia Press

Article

ISSN 1179-3155 (print edition)
PHYTOTAXA
ISSN 1179-3163 (online edition)

https://doi.org/10.11646/phytotaxa.464.1.7

Pachyphlodes atropurpurea and *P. excavata*, two new truffle species from Southwest China

JIAN-WEI LIU[1,4], SHANPING WAN[2,5], HEDE GONG[3,6,*] & FUQIANG YU[1,7,*]

[1] *The Germplasm Bank of Wild Species, Yunnan Key Laboratory for Fungal Diversity and Green Development, Kunming Institute of Botany, Chinese Academy of Sciences, 132 Lanhei Road, Kunming, Yunnan 650201, People's Republic of China*
[2] *College of Resource and Environment, Yunnan Agricultural University, Kunming, Yunnan 650100, People's Republic of China*
[3] *School of Geography and Ecotourism, Southwest Forestry University, Kunming, Yunnan 650224, People's Republic of China*
[4] *liujianwei@mail.kib.ac.cn; https://orcid.org/0000-0001-5683-5152*
[5] *wsp871117@163.com; https://orcid.org/0000-0002-0794-3701*
[6] *gonghede3@163.com; https://orcid.org/0000-0001-6033-6065*
[7] *fqyu@mail.kib.ac.cn; https://orcid.org/0000-0001-7931-080X*
**Corresponding author*
Jianwei Liu and Shanping Wan have equally contributed to this work

Abstract

Pachyphlodes atropurpurea and *P. excavata* are described as new species of truffles based on both phylogenetic and morphological analyses. Phylogenetically these two species are clearly distinct from described species of *Pachyphlodes*. Morphologically, *P. atropurpurea* is characterized by subglobose, purple black ascomata, and ascospores with acute-tipped spines. *P. excavata* is characterized by its ascomata with an obvious basal and internal cavity and slender fusiform asci (150–180 × 30–40 µm).

Keywords: Hypogeous fungi, Pezizales, Pezizaceae, Two new species, Taxonomy

Introduction

Truffle-like genus *Pachyphlodes* Zobel (1854:55) is a member of hypogeous fungi in the Pezizales and widely distributes across the northern hemisphere. Species of this genus can form ectomycorrhizae with dominant tree species of Fagaceae Dumort. (1829: 11), Pinaceae Spreng. ex F. Rudolphi (1830: 35), and Betulaceae Gray (1821: 222) (Frank *et al.* 2006, Erős-Honti & Jakucs 2009, Tedersoo *et al.* 2009, Healy *et al.* 2013, Healy *et al* 2015, Fan & Cai 2015, Healy *et al.* 2018). Macroscopically, *Pachyphlodes* ascomata are fleshy, displaying colors ranging from black, reddish, brown, yellowish, and orange (Healy *et al.* 2018). Microscopically, *Pachyphlodes* ascocarps have a thick peridium with pigmented cells in the outer layer, with asci in fertile glebal tissue that contain globose to narrowly cylindrical containing ascospores that are globose and ornamented with acute to capitate spines that may or may not be amyloid (Laessø & Hansen 2007, Healy *et al.* 2009, 2018).

Ascocarps of *Pachyphlodes* are hypogeous, meaning that they develop beneath the soil surface, and they are easily overlooked and rarely recorded (Hobart 2013). So far 18 *Pachyphlodes* species have been reported worldwide (Li *et al.* 2019, Index Fungorum 2020, Accessed date: 1 October 2020), only five described species have been recorded in China and include *P. citrina* (Berk. & Broome 1846: 79) Doweld (2013: 1), *P. thysellii* (W. Colgan & Trappe 2004:282) Doweld (2013: 1), *P. depressa* (L. Fan 2015: 615) L. Fan (2015: 1), and the newly described *P. cinnabarina* L. Fan, K. B. Hang & T. Li (2015: 111) and *P. wulushanensis* L. Fan, K. B. Hang & T. Li (2015: 112) (Chang & Tao 1989, Healy *et al.* 2013, Fan & Cai 2015, Li *et al.* 2019). Another two undescribed species are apparent in the phylogeny presented by Li *et al.* (2019).

While visiting edible mushroom markets in Yunnan province, China, we obtained samples of black truffles (e.g. *Tuber indicum* Cooke & Massee (1892: 67)) that had been collected in southwest Yunnan. Upon visual inspection, we found two specimens that showed clear morphological differences (in the color and size of the ascocarps) compared to the *Tuber* P. Micheli ex F. H. Wigg. (1780: 109) ascocarps. The results of the morphological and molecular studies confirmed that the two collections are undescribed species of *Pachyphlodes*: *P. atropurpurea.* and *P. excavata.*

Accepted by Ruvishika Jayawardena: 29 Sept. 2020; published: 14 Oct. 2020

Liu et al. IMA Fungus (2021) 12:4
https://doi.org/10.1186/s43008-021-00057-z

IMA Fungus

RESEARCH Open Access

Squamanitaceae and three new species of *Squamanita* parasitic on *Amanita* basidiomes

Jian-Wei Liu[1,2], Zai-Wei Ge[1,3], Egon Horak[4], Alfredo Vizzini[5], Roy E. Halling[6], Chun-Lei Pan[7] and Zhu L. Yang[1,3*]

Abstract

The systematic position of the enigmatically mycoparasitic genus *Squamanita* (*Agaricales*, *Basidiomycota*) together with *Cystoderma*, *Phaeolepiota*, *Floccularia*, and *Leucopholiota* is largely unknown. Recently they were recognized as *Squamanitaceae*, but previous studies used few DNA markers from a restricted sample of taxa from the family and lacked a formal taxonomic treatment. In this study, with newly generated sequences of the type of the genus *Squamanita*, *S. schreieri*, and several additional species of the family, the phylogeny is reinvestigated with a concatenated (18S-5.8S-nrLSU-RPB2-TEF1-α) dataset. This study reveals that *Cystoderma*, *Phaeolepiota*, *Squamanita*, *Floccularia*, and *Leucopholiota* are a monophyletic clade with strong statistical support in Bayesian analysis and form *Squamanitaceae*. *Phaeolepiota* nested within *Cystoderma*; *Squamanita*, *Leucopholiota*, and *Floccularia* clustered together as two monophyletic subclades; and *Squamanita* was present as a monophyletic clade with strong statistical support in both Maximum Likelihood and Bayesian analyses. The family name *Squamanitaceae* is formally emended and a detailed taxonomic treatment is presented to accommodate the five genera. Meanwhile, another concatenated (18S-ITS-nrLSU-RPB2-TEF1-α) dataset is used to investigate phylogenetic relationships and species delimitation in *Squamanita*. Our data indicates that "*S. umbonata*" from the Northern hemisphere forms two species complexes, one complex includes six specimens from North America, Europe, and East Asia, the other includes two specimens from Central America and North America respectively. Futhermore, species of *Squamanita* can parasitize species of *Amanita*, besides other fungal species: *Squamanita mira* parasitizes *A. kitamagotake* (*A.* sect. *Caesareae*), while *S. orientalis* and *S. sororcula* are parasites of species belonging to the *A. sepiacea* complex (*A.* sect. *Validae*). "*Squamanita umbonata*" from Italy occurs on *A. excelsa* (*A.* sect. *Validae*). Three new species of *Squamanita* from East Asia, viz. *S. mira*, *S. orientalis* and *S. sororcula* are documented with morphological, multi-gene phylogenetic, and ecological data, along with line drawings and photographs, and compared with similar species. A key for identification of the global *Squamanita* species is provided.

Keywords: *Amanita*, Mycoparasitic fungi, *Squamanita*, Host preference, Three new taxa

* Correspondence: fungi@mail.kib.ac.cn
[1]Yunnan Key Laboratory for Fungal Diversity and Green Development, Kunming Institute of Botany, Chinese Academy of Sciences, Kunming 650201, Yunnan, China
[2]CAS Key Laboratory for Plant Diversity and Biogeography of East Asia, Kunming Institute of Botany, Chinese Academy of Sciences, Kunming 650201, Yunnan, China
Full list of author information is available at the end of the article

© The Author(s). 2021 **Open Access** This article is licensed under a Creative Commons Attribution 4.0 International License, which permits use, sharing, adaptation, distribution and reproduction in any medium or format, as long as you give appropriate credit to the original author(s) and the source, provide a link to the Creative Commons licence, and indicate if changes were made. The images or other third party material in this article are included in the article's Creative Commons licence, unless indicated otherwise in a credit line to the material. If material is not included in the article's Creative Commons licence and your intended use is not permitted by statutory regulation or exceeds the permitted use, you will need to obtain permission directly from the copyright holder. To view a copy of this licence, visit http://creativecommons.org/licenses/by/4.0/.

APPENDIX B

PATENTS



证书号第6544702号

发明专利证书

发 明 名 称：高卢蜜环菌多态性微卫星分子标记及其引物与应用

发 明 人：刘建伟;于富强;杨祝良;田孟华;徐鑫

专 利 号：ZL 2023 1 0299314.5

专利申请日：2023年03月24日

专 利 权 人：中国科学院昆明植物研究所

地 址：650201 云南省昆明市盘龙区茨坝街道蓝黑路132号

授权公告日：2023年12月08日　　授权公告号：CN 116426677 B

国家知识产权局依照中华人民共和国专利法进行审查，决定授予专利权，颁发发明专利证书并在专利登记簿上予以登记。专利权自授权公告之日起生效。专利权期限为二十年，自申请日起算。

专利证书记载专利权登记时的法律状况。专利权的转移、质押、无效、终止、恢复和专利权人的姓名或名称、国籍、地址变更等事项记载在专利登记簿上。

局长
申长雨

国家知识产权局
2023年12月08日

第 1 页 (共 2 页)

其他事项参见续页

证书号第6561872号

发明专利证书

发 明 名 称：两种强寄生性蜜环菌通用多态性微卫星分子标记及其引物与应用

发 明 人：刘建伟;杨石美;杨祝良;于富强;徐鑫;张昌飞

专 利 号：ZL 2023 1 0299313.0

专利申请日：2023年03月24日

专 利 权 人：中国科学院昆明植物研究所

地 址：650201 云南省昆明市盘龙区茨坝街道蓝黑路132号

授权公告日：2023年12月15日　　授权公告号：CN 116790783 B

国家知识产权局依照中华人民共和国专利法进行审查，决定授予专利权，颁发发明专利证书并在专利登记簿上予以登记。专利权自授权公告之日起生效。专利权期限为二十年，自申请日起算。

专利证书记载专利权登记时的法律状况。专利权的转移、质押、无效、终止、恢复和专利权人的姓名或名称、国籍、地址变更等事项记载在专利登记簿上。

局长
申长雨

国家知识产权局
2023年12月15日

其他事项参见续页

证书号第6784824号

发明专利证书

发 明 名 称：十二种弱寄生蜜环菌通用多态性微卫星分子标记及其引物与应用

发 明 人：刘建伟;于富强;杨祝良;杨石美;王忠巧;丁培超;胡德分

专 利 号：ZL 2023 1 0299315.X

专利申请日：2023年03月24日

专 利 权 人：中国科学院昆明植物研究所

地 址：650201 云南省昆明市盘龙区茨坝街道蓝黑路132号

授权公告日：2024年03月15日　　授权公告号：CN 116377112 B

国家知识产权局依照中华人民共和国专利法进行审查，决定授予专利权，颁发发明专利证书并在专利登记簿上予以登记。专利权自授权公告之日起生效。专利权期限为二十年，自申请日起算。

专利证书记载专利权登记时的法律状况。专利权的转移、质押、无效、终止、恢复和专利权人的姓名或名称、国籍、地址变更等事项记载在专利登记簿上。

局长
申长雨

国家知识产权局
2024年03月15日

其他事项参见续页

APPENDIX C

SUPPLEMENTARY TABLES

Table C1 Information on the research materials used in this study

Phylogenetic/Biological species	Strain/specimen	Location	Longitude	Latitude
Armillaria altimontana (NABS X)	Strain: X1	Canada, British Columbia	Null	Null
A. altimontana (NABS X)	JGI: 83710	Colorado State University	Null	Null
A. calvescens (NABS III)	Strain: B621	Ampersand Mtn., NY, USA	Null	Null
A. cepistipes (EBS B)	Strain: 19041	Belarus	27.8000	53.1666
A. cepistipes (EBS B)	Strain: 19042	Belarus	27.8000	53.1666
A. cepistipes (EBS B)	JGI: B5	Italy	Null	Null
A. cepistipes (EBS B)	Strain: KK89066/1	Suonenjoki, Finland	Null	Null
A. ectypa	Strain: guo216	Europe	Null	Null
A. ectypa	Specimen: HKAS 86565	France	Null	Null
A. ectypa	Strain: KK70011/13	France, Auvergne	104.1661	27.8214
A. ectypa	NCBI: FPL8316v10	Daniel L. Lindner, Centre for Forest Mycology Research, Madison, Wisconsin, United States	Null	Null
A. fumosa	NCBI: CBS122221v10	Australia	Null	Null
A. fuscipes	JGI: CMW2740	Forestry and Agricultural Biotechnology Institute, University of Pretoria	Null	Null
A. gemina (NABS II)	Strain: II1	USA, Vermont	Null	Null
A. heimii	Strain: PFH87-45	Mityana, Uganda	Null	Null
A. luteobubalina	JGI: HWK02v1.0	Jonathan Plett, Western Sydney University, Sydney, Australia	Null	Null
A. mellea-1 (EBS D)	JGI: DSM3731	France	Null	Null
A. mellea-1 (EBS D)	Strain: KK89115/2	laminette, Luxembourg	Null	Null
A. mellea-2 (EBS D)	NCBI: ELDO17	University of Bristol, United Kingdom	Null	Null

Table C1 (continued)

Phylogenetic/Biological species	Strain/specimen	Location	Longitude	Latitude
A. melleoamericana (NABS VI)	Strain: VI_VIII1	Massachusetts, USA	Null	Null
A. melleoamericana (NABS VI)	Specimen: GDGM 70002	Massachusetts, USA	71.4000	42.4000
A. melleoamericana (NABS VI)	Specimen: GDGM 70010	Mycological Club, Boston, USA	71.0000	42.5000
A. melleoasiana subsp. *melleoasiana*	Strain: 22KM01	Shaoxia Village,Kunming, Yunnan Province	102.8153	25.1196
A. melleoasiana subsp. *melleoasiana*	Specimen: HKAS 135514	Shaoxia Village,Kunming, Yunnan Province	102.8162	25.1203
A. melleoasiana subsp. *melleoasiana*	Strain: 22KM02	Shaoxia Village,Kunming, Yunnan Province	102.8165	25.1212
A. melleoasiana subsp. *melleoasiana*	Strain: CBSK19083	Yangzixi, Houhe nature reserve, Wufeng Tujia Autonomous County, Yichang City, Hubei Province	110.9500	30.1333
A. melleoasiana subsp. *melleoasiana*	Specimen: HKAS 86589	Japan	Null	Null
A. melleoasiana subsp. *melleoasiana*	Specimen: HKAS 86600	Kenya	Null	Null
A. melleoasiana subsp. *melleoasiana*	Strain: guo256	USA, Moutampa	Null	Null
A. melleoasiana subsp. *melleoasiana*	Specimen: HKAS 49004	About 45km in the direction of Jiulong County to Mianning County, Ganzi Tibetan Autonomous Prefecture, Sichuan Province	101.5073	29.0003
A. melleoasiana subsp. *melleoasiana*	Specimen: HKAS 52389	Inside the Botanical Institute of Kunming City, Panlong District, Kunming City, Yunnan Province	102.7427	25.1379
A. melleoasiana subsp. *melleoasiana*	Specimen: HKAS 68003	Jade Dragon Snow Mountain, Yulong Naxi Autonomous County, Lijiang City, Yunnan Province	100.2106	27.1294

Table C1 (continued)

Phylogenetic/Biological species	Strain/specimen	Location	Longitude	Latitude
A. melleoasiana subsp. *melleoasiana*	Specimen: HKAS 82475	Sanjia Village, Shuanglong Township, Panlong District, Kunming City, Yunnan Province	102.8492	25.1100
A. melleoasiana subsp. *melleoasiana*	Strain: FM22-210	Motuo county, Linzhi City, Xizang Autonomous Region	95.4340	29.4733
A. melleoasiana subsp. *melleoasiana*	Strain: FM22-211	Motuo county, Linzhi City, Xizang Autonomous Region	95.4339	29.4730
A. melleoasiana subsp. *melleoasiana*	Strain: FM22-215	Motuo county, Linzhi City, Xizang Autonomous Region	95.4336	29.4732
A. melleoasiana subsp. *melleoasiana*	Strain: FM22-216	Motuo county, Linzhi City, Xizang Autonomous Region	95.4341	29.4733
A. melleoasiana subsp. *melleoasiana*	Specimen: HKAS 135500	Lijiang Alpine Botanical Garden, Lijiang, Yunnan Province	100.1788	27.0043
A. melleoasiana subsp. *melleoasiana*	Specimen: HKAS 135504	Lijiang Alpine Botanical Garden, Lijiang, Yunnan Province	100.2255	27.1386
A. melleoasiana subsp. *melleoasiana*	Specimen: HKAS 135505	Lijiang Alpine Botanical Garden, Lijiang, Yunnan Province	100.2230	27.1368
A. melleoasiana subsp. *melleoasiana*	Specimen: HKAS 135489	Zangluping，Muyu Town, Shennongjia, Hubei Province	110.4131	31.4853
A. melleoasiana subsp. *melleoasiana*	Specimen: HKAS 135490	Zangluping，Muyu Town, Shennongjia, Hubei Province	110.4148	31.4870
A. melleoasiana subsp. *melleoasiana*	Strain: 221003WSP	Donggu Town, Danba County, Ganzi Prefecture, Sichuan Province	101.7528	30.7865
A. melleoasiana subsp. *melleoasiana*	Strain: 22KM03	Mushroom Mountain, Shizong County, Qujing City, Yunnan Province	104.1572	24.6333
A. melleoasiana subsp. *melleoasiana*	Commercial Strain: A10	Taobao	Null	Null
A. melleoasiana subsp. *melleoasiana*	Strain: CBSG19037	Taiwan Province	120.8589	23.0930
A. melleoasiana subsp. *melleoasiana*	Strain: CBSK00111	Yunshanping, Yulong Naxi Autonomous County, Lijiang City, Yunnan Province	100.0333	27.1166

Table C1 (continued)

Phylogenetic/Biological species	Strain/specimen	Location	Longitude	Latitude
A. melleoasiana subsp. *melleoasiana*	Strain: CBSK19052	Yangzixi, Houhe nature reserve, Wufeng Tujia Autonomous County, Yichang City, Hubei Province	110.9500	30.1333
A. melleoasiana subsp. *melleoasiana*	Strain: FM21-172	Chentang Town, Dingjie County, Shigatse City, Tibet Autonomous Region	87.3643	27.9196
A. melleoasiana subsp. *melleoasiana*	Strain: FM21-173	Chentang Town, Dingjie County, Shigatse City, Tibet Autonomous Region	87.3641	27.9197
A. melleoasiana subsp. *melleoasiana*	Specimen: GDGM 76532	Nanling Xiaohuangshan, Ruyuan Yao Autonomous County, Shaoguan City, Guangdong Province	113.0465	24.9372
A. melleoasiana subsp. *melleoasiana*	Specimen: HKAS 86581	Huangnihe Central Market, Huangnihe County, Dunhua City, Yanbian Korean Autonomous Prefecture, Jilin Province	128.0227	43.5328
A. melleoasiana subsp. *melleoasiana*	Specimen: HKAS 86590	Dasuodao, Yulong Snow Mountain,Yulong Naxi Autonomous County, Lijiang City, Yunnan Province	100.2500	27.1500
A. melleoasiana subsp. *melleoasiana*	Specimen: HKAS 86592	Kuankuoshui Reservoir, Suiyang County, Zunyi City, Guizhou Province	107.1754	28.2050
A. melleoasiana subsp. *melleoasiana*	Specimen: HKAS 86593	Tianmushan Nature Reserve, Tianmushan Town, Lin 'an District, Hangzhou City, Zhejiang Province	119.4295	30.3475
A. melleoasiana subsp. *melleoasiana*	Specimen: HKAS 46275	Laojun Mountain, Yulong Naxi Autonomous County, Lijiang City, Yunnan Province	99.7761	26.6480
A. melleoasiana subsp. *melleoasiana*	Specimen: HKAS 57446	Astronomical Observatory, Yulong Naxi Autonomous County, Lijiang City, Yunnan Province	100.0324	26.6929

Table C1 (continued)

Phylogenetic/Biological species	Strain/specimen	Location	Longitude	Latitude
A. melleoasiana subsp. *melleoasiana*	Specimen: HKAS 58911	National Highway 320 at 3296km, Yongping County, Dali Bai Autonomous Prefecture, Yunnan Province	99.7759	25.5144
A. melleoasiana subsp. *melleoasiana*	Specimen: HKAS 68632	Hexi Township, Dayang Village, Lanping Bai Pumi Autonomous County, Nujiang Lisu Autonomous Prefecture, Yunnan Province	99.3825	26.8631
A. melleoasiana subsp. *melleoasiana*	Specimen: HKAS 68678	Dadong Township, Gucheng District, Lijiang City, Yunnan Province	100.3948	27.1461
A. melleoasiana subsp. *melleoasiana*	Specimen: HKAS 74997	Near X311-152, Lajing Township, Lanping Bai Pumi Autonomous County, Nujiang Lisu Autonomous Prefecture, Yunnan Province	99.2744	26.4907
A. melleoasiana subsp. *melleoasiana*	Specimen: HKAS 81274	Next to the horse road next to the ecological station of the Alpine Botanical Garden, Yulong Naxi Autonomous County, Lijiang City, Yunnan Province	100.2005	26.9968
A. melleoasiana subsp. *melleoasiana*	Specimen: HKAS 81827	Xishan Scenic Area, Kunming City, Yunnan Province	102.6285	24.9646
A. melleoasiana subsp. *melleoasiana*	Specimen: HKAS 81828	Xishan Scenic Area, Kunming City, Yunnan Province	102.6285	24.9646
A. melleoasiana subsp. *melleoasiana*	Specimen: HKAS 81829	Xishan Scenic Area, Kunming City, Yunnan Province	102.6285	24.9646
A. melleoasiana subsp. *melleoasiana*	Specimen: HKAS 81830	Xishan Scenic Area, Kunming City, Yunnan Province	102.6285	24.9646
A. melleoasiana subsp. *melleoasiana*	Specimen: HKAS 81831	Xishan Scenic Area, Kunming City, Yunnan Province	102.6285	24.9646

Table C1 (continued)

Phylogenetic/Biological species	Strain/specimen	Location	Longitude	Latitude
A. melleoasiana subsp. *melleoasiana*	Specimen: HKAS 81832	Xishan Scenic Area, Kunming City, Yunnan Province	102.6285	24.9646
A. melleoasiana subsp. *melleoasiana*	Specimen: HKAS 81834	Xishan Scenic Area, Kunming City, Yunnan Province	102.6285	24.9646
A. melleoasiana subsp. *melleoasiana*	Specimen: HKAS 82101	Yeya Lake, Panlong District, Kunming City, Yunnan Province	102.8635	25.1267
A. melleoasiana subsp. *melleoasiana*	Specimen: HKAS 87145	Alpine Botanical Garden, Yulong Naxi Autonomous County, Lijiang City, Yunnan Province	100.2005	26.9968
A. melleoasiana subsp. *melleoasiana*	Specimen: HMAS 23066	Longlin Autonomous County, Baise City, Guangxi Zhuang Autonomous Region	105.3438	24.7706
A. melleoasiana subsp. *melleoasiana*	Specimen: HMAS 253414	Ailaoshan Nature Reserve, Shuitang Town, Jingdong Yi Autonomous County, Pu 'er City, Yunnan Province	100.8374	24.4529
A. melleoasiana subsp. *melleoasiana*	Specimen: HMAS 272369	Lulang Sedila Mountain Area, Bayi District, Linzhi City, Xizang Autonomous Region	94.4845	29.5855
A. melleoasiana subsp. *melleoasiana*	Specimen: HMAS 33561	Taibai Mountain, Meixian County, Baoji City, Shaanxi Province	107.9024	34.1281
A. melleoasiana subsp. *melleoasiana*	Specimen: HMAS 50995	Jiuzhaigou County, Aba Tibetan and Qiang Autonomous Prefecture, Sichuan Province	103.9115	33.2821
A. melleoasiana subsp. *melleoasiana*	Specimen: JLK003	From Deqin to Gongshan Kongqueshan Pass in Nujiang Prefecture, Yunnan Province	98.7757	28.1061
A. melleoasiana subsp. *melleoasiana*	Specimen: HKAS 135480	Lijiang Alpine Botanical Garden, Lijiang, Yunnan Province	100.1824	26.9981

Table C1 (continued)

Phylogenetic/Biological species	Strain/specimen	Location	Longitude	Latitude
A. melleoasiana subsp. *melleoasiana*	Specimen: HKAS 135479	Lijiang Alpine Botanical Garden, Lijiang, Yunnan Province	100.1810	27.0043
A. melleoasiana subsp. *melleoasiana*	Specimen: HKAS 135477	Lijiang Alpine Botanical Garden, Lijiang, Yunnan Province	100.1833	27.0016
A. melleoasiana subsp. *melleoasiana*	Specimen: HKAS 126411	Lijiang Alpine Botanical Garden, Lijiang, Yunnan Province	100.1843	27.0017
A. melleoasiana subsp. *melleoasiana*	Specimen: HKAS 126412	Lijiang Alpine Botanical Garden, Lijiang, Yunnan Province	100.1809	27.0069
A. melleoasiana subsp. *melleoasiana*	Specimen: HKAS 135481	Lijiang Alpine Botanical Garden, Lijiang, Yunnan Province	100.1811	27.0066
A. melleoasiana subsp. *melleoasiana*	Specimen: HKAS 135475	Majie Town, Nanhua County, Chuxiong Yi Autonomous Prefecture, Yunnan Province	100.7995	22.9102
A. melleoasiana subsp. *melleoasiana*	Specimen: HKAS 135476	Mahuotang, Wudingshan Township, Nanhua County, Chuxiong Yi Autonomous Prefecture, Yunnan Province	100.7661	24.9067
A. melleoasiana subsp. *melleoasiana*	Specimen: MHHNU 31945	Badagong Mountain National Nature Reserve, Sangzhi County, Zhangjiajie City,Hunan Province	109.7400	29.6838
A. melleoasiana subsp. *melleoasiana*	Specimen: MHHNU 7419	Jiucailing, Dao County, Yongzhou City, Hunan Province	111.3357	25.5159
A. melleoasiana subsp. *melleoasiana*	Specimen: MHHNU 8577	Badagong Mountain National Nature Reserve, Sangzhi County, Zhangjiajie City, Hunan Province	110.0873	29.7882
A. melleoasiana subsp. *melleoasiana*	Specimen: HKAS 135554	Micangshan National Forest Park, Wuguang Town, Nanjiang County, Bazhong City, Sichuan Province	106.9192	32.6919

Table C1 (continued)

Phylogenetic/Biological species	Strain/specimen	Location	Longitude	Latitude
A. melleoasiana subsp. *melleoasiana*	Specimen: HKAS 135555	Micangshan National Forest Park, Wuguang Town, Nanjiang County, Bazhong City, Sichuan Province	106.9193	32.6919
A. melleoasiana subsp. *melleoasiana*	Specimen: HKAS 135556	Micangshan National Forest Park, Wuguang Town, Nanjiang County, Bazhong City, Sichuan Province	106.9206	32.6920
A. melleoasiana subsp. *melleoasiana*	Strain: WGS1051	Ailaoshan Subtropical Forest Ecosystem Research Station of the Chinese Academy of Sciences (the Ailaoshan Ecosystem Station) , Jingdong Yi Autonomous County, Pu 'er City, Yunnan Province	101.0300	24.5200
A. melleoasiana subsp. *melleoasiana*	Strain: XCB003	Lei Yunting "雷云霆"	Null	Null
A. melleoasiana subsp. *melleoasiana*	Specimen: HKAS 135515	Xu Xin "徐鑫"	Null	Null
A. melleoasiana subsp. *melleoasiana*	Specimen: HKAS 135509	Paimo Road, Motuo County, Linzhi City, Tibet Autonomous Region	95.1729	29.3224
A. melleoasiana subsp. *macrospora*	Strain: CBSK19105	Yangzixi, Houhe nature reserve, Wufeng Tujia Autonomous County, Yichang City, Hubei Province	110.9500	30.1333
A. melleoasiana subsp. *macrospora*	Specimen: HKAS 86591	Xujiazhuang, Shennongjia Forest Region, Hubei Province	110.5573	31.5599
A. melleoasiana subsp. *macrospora*	Specimen: HKAS 86588	Japan	Null	Null
A. melleoasiana subsp. *macrospora*	Specimen: HKAS 86598	Africa	Null	Null

Table C1 (continued)

Phylogenetic/Biological species	Strain/specimen	Location	Longitude	Latitude
A. melleoasiana subsp. *macrospora*	Specimen: HKAS 135553	Micangshan National Forest Park, Wuguang Town, Nanjiang County, Bazhong City, Sichuan Province	106.9156	32.6926
A. melleoasiana subsp. *macrospora*	Specimen: HMAS 51088	Jiuzhaigou County, Aba Tibetan and Qiang Autonomous Prefecture, Sichuan Province	104.2425	33.2520
A. melleoasiana subsp. *macrospora*	Strain: QZ000201-2	Maoniuiping Yulong Snow Mountain, Yulong Naxi Autonomous County, Lijiang City, Yunnan Province	100.2500	27.1500
A. nabsnona (NABS IX)	Strain: NAB	Null	Null	Null
A. nabsnona (NABS IX)	JGI: CMW6904v10	Martin Coetzee, University of Pretoria, Pretoria, South Africa	Null	Null
A. novaezelandiae	JGI: ICMP16352	New Zealand Forest Research Culture Collection (NZFS), Scion (New Zealand Forest Research Institute), New Zealand	Null	Null
A. ostoyae (EBS C)	Strain: CBSD19044	Belarus	27.8000	53.1666
A. ostoyae (EBS C)	NCBI:	Null	Null	Null
A. ostoyae (EBS C)	JGI: C189	Switzerland	Null	Null
A. pelmaspora	Specimen: HKAS 135507	Paimo Road, Motuo County, Linzhi City, Tibet Autonomous Region	95.1667	29.3000
A. pelmaspora	Specimen: HKAS 135508	Paimo Road, Motuo County, Linzhi City, Tibet Autonomous Region	95.1834	29.3414
A. puiggarii	Strain: PPg85-63	Petit-Bourg Guadeloupe	Null	Null
A. sinapina subsp. *sinapina*	JGI: MH282847	Genome Research and Education Center, Siberian Federal University, Akademgorodok, 50a/2, Krasnoyarsk 660036, Russia	Null	Null
A. sinapina subsp. *sinapina*	Strain: B618	Utawana Lake, NY	Null	Null
A. solidipes	NCBI: 284v10	Null	Null	Null
A. solidipes	JGI: ID001	USA: Idaho	Null	Null

Table C1 (continued)

Phylogenetic/Biological species	Strain/specimen	Location	Longitude	Latitude
A. algida (CBS O)	Strain: 19080	Yangzixi, Houhe nature reserve, Wufeng Tujia Autonomous County, Yichang City, Hubei Province	110.5333	30.0666
A. algida (CBS O)	Strain: BD4H	Mugan Town, Daguan County, Zhaotong City, Yunnan Province	102.0003	28.1687
A. algida (CBS O)	Commercial Strain: guo19	Yang Dayong's Fungi Materials, Xiaocaoba, Yiliang County, Zhaotong City, Yunnan Province	Null	Null
A. algida (CBS O)	Commercial Strain: guo37	Fungi of Laomengjia in Longan Village, Yiliang county, Zhaotong City, Yunnan Province	Null	Null
A. algida (CBS O)	Specimen: HMAS 253478	Go to the roadside of Bomi County from Medog County, Linzhi City, Xizang Autonomous Region	95.3189	29.3046
A. algida (CBS O)	Specimen: HMAS 272641	Motuo county, Linzhi City, Xizang Autonomous Region	95.3189	29.3046
A. algida (CBS O)	Specimen: HKAS 86554	Daqiao Village, Xiaocaoba Township, Zhaotong City, Yunnan Province	104.3307	27.7782
A. algida (CBS O)	Strain: LM-1	Xiaocaoba Tianma Trading Market, Xiaocaoba Town, Yiliang county, Zhaotong City, Yunnan Province	104.2608	27.7674
A. algida (CBS O)	Commercial Strain: LYT-F05	Yiliang County Tianma Industry Development Center, Yiliang county, Zhaotong City, Yunnan Province	Null	Null
A. algida (CBS O)	Commercial Strain: LYT-F19	Yiliang County Tianma Industry Development Center, Yiliang county, Zhaotong City, Yunnan Province	Null	Null

Table C1 (continued)

Phylogenetic/Biological species	Strain/specimen	Location	Longitude	Latitude
A. algida (CBS O)	Commercial Strain: LYT-F34	Yiliang County Tianma Industry Development Center, Yiliang county, Zhaotong City, Yunnan Province	Null	Null
A. algida (CBS O)	Commercial Strain: LYT-Y1	Xixia Occupy Fungi Industry Co., Ltd., Xixia County, Nanyang City, Henan Province	Null	Null
A. algida (CBS O)	Commercial Strain: MF-M6	Yiliang Maofeng Gastrodia elata Industry Development Co., Ltd., Yiliang County, Zhaotong City, Yunnan Province	Null	Null
A. algida (CBS O)	Specimen: MHHNU 8447	Badagong Mountain National Nature Reserve, Sangzhi County, Zhangjiajie City, Hunan Province	110.0879	29.7767
A. algida (CBS O)	Strain: O19095	Yangzixi, Houhe nature reserve, Wufeng Tujia Autonomous County, Yichang City, Hubei Province	110.5333	30.0666
A. algida (CBS O)	Commercial Strain: SM-1	Shaanxi Hanzhong Desheng Seed and Breeding Industry Association, Hanzhong City, Shaanxi Province	Null	Null
A. algida (CBS O)	Commercial Strain: ZT15	Baohujunzhong (Lianghe) "保护菌种（两河）"	Null	Null
A. algida (CBS O)	Commercial Strain: ZT-M6	Zhaotong Gastrodia Research Institute, Zhaotong City, Yunnan Province	Null	Null
A. algida (CBS O)	Commercial Strain: ZT-MF	Zhaotong Gastrodia Research Institute, Zhaotong City, Yunnan Province	Null	Null
A. algida (CBS O)	Commercial Strain: ztmh-1	Zhaotong Gastrodia Research Institute, Zhaotong City, Yunnan Province	Null	Null

Table C1 (continued)

Phylogenetic/Biological species	Strain/specimen	Location	Longitude	Latitude
A. algida (CBS O)	Commercial Strain: ztmh-13	Zhaotong Gastrodia Research Institute, Zhaotong City, Yunnan Province	Null	Null
A. amygdalispora (CBS L)	Strain: CBSL17017	Lushui town, Laifeng County, Enshi Tujia and Miao Autonomous Prefecture, Hubei Province	109.3000	29.3666
A. amygdalispora (CBS L)	Strain: CBSLW17003	Liziping town, Yiling District, Yichang City, Hubei Province	111.0666	31.1000
A. amygdalispora (CBS L)	Strain: CBSLW17016	Laifeng County, Enshi Tujia and Miao Autonomous Prefecture, Hubei Province	109.5000	29.6666
A. amygdalispora (CBS L)	Strain: CBSLW17039	Yuanbao town, Lichuan City, Enshi Tujia and Miao Autonomous Prefecture, Hubei Province	109.0000	30.2333
A. amygdalispora (CBS L)	Specimen: GDGM 71117	Xiaoxi, Yongshun County, Xiangxi Tujia and Miao Autonomous Prefecture, Hunan Province	109.6484	28.9614
A. amygdalispora (CBS L)	Specimen: HKAS 86613	Kuankuoshui Reservoir, Suiyang County, Zunyi City, Guizhou Province	107.1754	28.2050
A. amygdalispora (CBS L)	Specimen: HKAS 86615	Kuankuoshui Reservoir, Suiyang County, Zunyi City, Guizhou Province	107.1754	28.2050
A. amygdalispora (CBS L)	Strain: guo324	Haizi Town, Yiliang county, Zhaotong City, Yunnan Province	104.2598	27.5544
A. amygdalispora (CBS L)	Commercial Strain: guo82	Xiaocaoba Shennong Company, Yiliang County, Zhaotong City, Yunnan Province	Null	Null
A. amygdalispora (CBS L)	Specimen: HMAS 22781	Longlin Autonomous County, Baise City, Guangxi Zhuang Autonomous Region	105.3438	24.7706

Table C1 (continued)

Phylogenetic/Biological species	Strain/specimen	Location	Longitude	Latitude
A. amygdalispora (CBS L)	Specimen: HMIGD 71175	Xiaoxi, Yongshun County, Xiangxi Tujia and Miao Autonomous Prefecture, Hunan Province	109.6484	28.9614
A. amygdalispora (CBS L)	Strain: KIB5-guo90	Jiaokui Town, Yiliang county City, Zhaotong City, Yunnan Province	104.0508	27.6254
A. amygdalispora (CBS L)	Specimen: HKAS 86548	Lianghe Township, Yiliang county, Zhaotong City, Yunnan Province	Null	Null
A. amygdalispora (CBS L)	Strain: LH-22	Lianghe Village, Lianghe Township, Yiliang County, Zhaotong City, Yunnan Province	104.2081	27.8328
A. amygdalispora (CBS L)	Strain: LW17027	Wufeng Tujia Autonomous County, Yichang City, Hubei Province	110.6833	30.2000
A. amygdalispora (CBS L)	Commercial Strain: LYT-F01	Yiliang County Tianma Industry Development Center, Yiliang county, Zhaotong City, Yunnan Province	Null	Null
A. amygdalispora (CBS L)	Strain: LZP-11	Xiaocaoba Town, Yiliang County, Zhaotong City, Yunnan Province	104.2916	27.7388
A. amygdalispora (CBS L)	Strain: LZP-15	Xiaocaoba Town, Yiliang County, Zhaotong City, Yunnan Province	104.2916	27.7400
A. amygdalispora (CBS L)	Specimen: MHHNU 31060	Xiaoxi National Nature Reserve, Yongshun County, Xiangxi Tujia and Miao Autonomous Prefecture, Hunan Province	110.2693	28.8120
A. amygdalispora (CBS L)	Specimen: MHHNU 31772	Wulingyuan National Forest Park, Wulingyuan District, Zhangjiajie City, Hunan Province	110.4352	29.3469

Table C1 (continued)

Phylogenetic/Biological species	Strain/specimen	Location	Longitude	Latitude
A. amygdalispora (CBS L)	Strain: MW-27	Zhongming Township, Yiliang County, Zhaotong City, Yunnan Province	104.0858	27.8308
A. amygdalispora (CBS L)	Strain: TX	Null	Null	Null
A. amygdalispora (CBS L)	Commercial Strain: YSLF-1	Zhaotong Gastrodia Research Institute, Zhaotong City, Yunnan Province	Null	Null
A. amygdalispora (CBS L)	Strain: ZG-26	Shulin Yi and Miao Township, Yiliang County, Yunnan Province	104.2966	27.5075
A. amygdalispora (CBS L)	Commercial Strain: ZTMH-036	Zhaotong Gastrodia Research Institute, Zhaotong City, Yunnan Province	Null	Null
A. amygdalispora (CBS L)	Strain: guo278	Lianghe Town, Yiliang county, Zhaotong City, Yunnan Province	104.1648	27.8208
A. borealis subsp. *borealis* (EBS A)	Specimen: GDGM 77873	Finland	26.4000	64.1000
A. borealis subsp. *borealis* (EBS A)	Specimen: HKAS 86616	Helsinki, Finland	Null	Null
A. borealis subsp. *borealis* (EBS A)	Strain: KK90252/5	Punkaharju, Finland	Null	Null
A. borealis subsp. *borealis* (EBS A)	Strain: MH407470	Genome Research and Education Center, Siberian Federal University, Akademgorodok, 50a/2, Krasnoyarsk 660036, Russia	Null	Null
A. borealis subsp. *borealis* (EBS A)	JGI: AB13TR4IP16	USA: Idaho	Null	Null
A. borealis subsp. *borealis* (EBS A)	JGI: FPL8714v10	Daniel L. Lindner, Centre for Forest Mycology Research, Madison, Wisconsin, United States	Null	Null
A. borealis subsp. *sinoborealis* (CBS M)	Specimen: HKAS 135492	Dajiu lake, Shennongjia, Hubei Province	109.9935	31.4810
A. borealis subsp. *sinoborealis* (CBS M)	Specimen: HKAS 135493	Dajiu lake, Shennongjia, Hubei Province	109.9930	31.4809

Table C1 (continued)

Phylogenetic/Biological species	Strain/specimen	Location	Longitude	Latitude
A. borealis subsp. *sinoborealis* (CBS M)	Strain: CBSM01012	Jiuhuping, Shennongjia forest region, Hubei Province	110.3333	31.5000
A. borealis subsp. *sinoborealis* (CBS M)	Strain: CBSM01013	Jiuhuping, Shennongjia forest region, Hubei Province	110.3333	31.5000
A. borealis subsp. *sinoborealis* (CBS M)	Strain: CBSM01019	Jiuhuping, Shennongjia forest region, Hubei Province	110.3333	31.5000
A. borealis subsp. *sinoborealis* (CBS M)	Strain: CBSM04019	Taibai Mountain, Mei County, Baoji City, Shaanxi Province	107.8833	34.1166
A. borealis subsp. *sinoborealis* (CBS M)	Strain: CBSM05020	Honghegu, Taibai Mountain, Mei County, Baoji City, Shaanxi Province	107.7333	34.1000
A. borealis subsp. *sinoborealis* (CBS M)	Strain: CBSM05021	Honghegu, Taibai Mountain, Mei County, Baoji City, Shaanxi Province	107.7333	34.1000
A. borealis subsp. *sinoborealis* (CBS M)	Specimen: HKAS 86617	Jiuhuping in Shennongjia Forest Region, Hubei Province	110.3502	31.5062
A. borealis subsp. *sinoborealis* (CBS M)	Specimen: HMAS 131062	Laozhuang, Kang County, Longnan City, Gansu Province	105.6000	33.0333
A. borealis subsp. *sinoborealis* (CBS M)	Specimen: HMAS 63163	Wen County, Longnan City, Gansu Province	104.6834	32.9440
A. borealis subsp. *sinoborealis* (CBS M)	Strain: SNJ20	Shennongjia Dajiuhu Scenic Spot, Dajiuhu Town, Shennongjia Forest Region, Hubei Province	109.9936	31.4810
A. bruneocystidia (CBS H)	Specimen: HKAS 135501	Lijiang Alpine Botanical Garden, Lijiang, Yunnan Province	100.2327	27.1385
A. bruneocystidia (CBS H)	Specimen: HKAS 135506	Lijiang Alpine Botanical Garden, Lijiang, Yunnan Province	100.2234	27.1368
A. bruneocystidia (CBS H)	Strain: CBSH00019	Maoniuiping Yulong Snow Mountain, Yulong Naxi Autonomous County, Lijiang City, Yunnan Province	100.2500	27.1500

Table C1 (continued)

Phylogenetic/Biological species	Strain/specimen	Location	Longitude	Latitude
A. bruneocystidia (CBS H)	Strain: CBSH0006	Dasuodao, Yulong Snow Mountain, Yulong Naxi Autonomous County, Lijiang City, Yunnan Province	100.2500	27.1500
A. bruneocystidia (CBS H)	Strain: CBSH19074	Chudian, Emei Mountain, Emeishan City, Leshan City, Sichuan Province	103.3500	29.5500
A. bruneocystidia (CBS H)	Strain: CBSH99011	Yulong snow Mountain, Yulong Naxi Autonomous County, Lijiang City, Yunnan Province	100.2000	27.1000
A. bruneocystidia (CBS H)	Strain: CBSH99028	Yulong snow Mountain, Yulong Naxi Autonomous County, Lijiang City, Yunnan Province	100.2000	27.1000
A. bruneocystidia (CBS H)	Specimen: HKAS 86601	Lijiang Alpine Botanical Garden, Lijiang City, Yunnan Province	100.1788	27.0043
A. bruneocystidia (CBS H)	Specimen: HKAS 48804	Jade Dragon Snow Mountain, Yulong Naxi Autonomous County, Lijiang City, Yunnan Province	100.2106	27.1294
A. bruneocystidia (CBS H)	Specimen: HKAS 56216	Sandaowan, Jade Dragon Snow Mountain, Yulong Naxi Autonomous County, Lijiang City, Yunnan Province	100.2604	27.1646
A. bruneocystidia (CBS H)	Specimen: HMAS 253500	Guyu Township, Batang County, Ganzi Tibetan Autonomous Prefecture, Sichuan Province	99.1608	29.2046
A. bruneocystidia (CBS H)	Specimen: HKAS 135513	Luoji Township, Shangri-La City, Diqing Tibetan Autonomous Prefecture, Yunnan Province	100.0536	27.9596
A. bruneocystidia (CBS H)	Strain: CBSH0003	Dasuodao, Yulong Snow Mountain, Yulong Naxi Autonomous County, Lijiang City, Yunnan Province	100.2500	27.1500

Table C1 (continued)

Phylogenetic/Biological species	Strain/specimen	Location	Longitude	Latitude
A. bruneocystidia (CBS H)	Strain: CBSH00123	Tianshengqiao National Geothermal Park, Shangri-La, Diqing Tibetan Autonomous Prefecture, Yunnan Province	99.8130	27.7948
A. conifericola (CBS D)	Strain: 21043	Heping skiing park, Changbai Mountain, Jilin Province	128.1500	42.2667
A. conifericola (CBS D)	Strain: CBSD02171	Aihui District, Heihe city, Heilongjiang Province	127.0833	50.0333
A. conifericola (CBS D)	Strain: CBSD21030	Changbai Mountain Huangsongpu Forest Farm, Antu County, Yanbian Korean Autonomous Prefecture, Jilin Province	128.0699	42.1299
A. conifericola (CBS D)	Strain: CBSD5193	Emu forest farm, Dunhua city, Yanbian Korean Autonomous Prefecture, Jilin Province	128.1166	43.7500
A. conifericola (CBS D)	Strain: CBSD5295	Emu forest farm, Dunhua city, Yanbian Korean Autonomous Prefecture, Jilin Province	128.1166	43.7500
A. conifericola (CBS D)	Strain: CBSD93025	Baihe, Changbai Mountain, Antu County, Yanbian Korean Autonomous Prefecture, Jilin Province	128.1000	42.3000
A. conifericola (CBS D)	Strain: CBSD96043	Emu forest farm, Dunhua city, Yanbian Korean Autonomous Prefecture, Jilin Province	128.0500	43.1333
A. conifericola (CBS D)	Specimen: HMAS 145183	Taibai Mountain, Zhouzhi county, Xi 'an City, Shaanxi Province	107.7833	33.9500
A. conifericola (CBS D)	Specimen: HMJAU 25401	Qingling Town, Jiaohe City, Jilin City, Jilin Province	127.1790	44.0307
A. conifericola (CBS D)	Specimen: HMJAU 25404	Qingling Town, Jiaohe City, Jilin City, Jilin Province	127.1790	44.0307

Table C1 (continued)

Phylogenetic/Biological species	Strain/specimen	Location	Longitude	Latitude
A. conifericola (CBS D)	Specimen: HMJAU 25478	Qingling Town, Jiaohe City, Jilin City, Jilin Province	127.1790	44.0307
A. conifericola (CBS D)	Specimen: HMJAU 28932	Erdao Baihe Management Station, Yanbian Korean Autonomous Prefecture, Jilin Province	128.1439	42.4573
A. conifericola (CBS D)	Specimen: HMJAU 42023	Quanshuidong Forestry, Helong City, Yanbian Korean Autonomous Prefecture, Jilin Province	128.8870	42.6699
A. conifericola (CBS D)	Specimen: HMJAU 42034	Quanshuidong Forestry, Helong City, Yanbian Korean Autonomous Prefecture, Jilin Province	128.8870	42.6699
A. conifericola (CBS D)	Specimen: HMJAU 6143	Erdao Baihe Township, Yanbian Korean Autonomous Prefecture, Jilin Province	128.1439	42.4573
A. conifericola (CBS D)	Specimen: HMJAU 7339	Erdao Baihe Management Station, Yanbian Korean Autonomous Prefecture, Jilin Province	128.1439	42.4573
A. gallica subsp. *calidusa* (CBS B)	Strain: 6	Chenjiagou, Lueyang County, Hanzhong City, Shaanxi Province	106.0516	33.3190
A. gallica subsp. *calidusa* (CBS B)	Specimen: HKAS 135487	Niuzhuang Town, Wufeng Tujia Autonomous County, Yichang City, Hubei Province	110.3872	30.2350
A. gallica subsp. *calidusa* (CBS B)	Specimen: HKAS 135488	Niuzhuang Town, Wufeng Tujia Autonomous County, Yichang City, Hubei Province	110.3885	30.2360
A. gallica subsp. *calidusa* (CBS B)	Commercial Strain: 5H	Yiliang County Tianma Industry Development Center, Yiliang county, Zhaotong City, Yunnan Province	Null	Null

Table C1 (continued)

Phylogenetic/Biological species	Strain/specimen	Location	Longitude	Latitude
A. gallica subsp. *calidusa* (CBS B)	Commercial Strain: AHLD-A9	Anhui Landun Ecological Agriculture Technology Co., Ltd. Yueyang County, Anqing City, Anhui Province	Null	Null
A. gallica subsp. *calidusa* (CBS B)	Strain: BJ-M1	Yangchang Town, Longli County, Qiannan Buyi and Miao Autonomous Prefecture, Guizhou Province	107.0469	26.2784
A. gallica subsp. *calidusa* (CBS B)	Strain: CBSB03002	Qinggouzi forest farm, Huangnihe Forest Bureau, Dunhua City, Yanbian Korean Autonomous Prefecture, Jilin Province	128.3000	43.1333
A. gallica subsp. *calidusa* (CBS B)	Strain: CBSB19011	Dianzhan houshan, Changbai Mountain, Fusong County, Baishan City, Jilin Province	128.0166	42.0500
A. gallica subsp. *calidusa* (CBS B)	Strain: CBSB19014	Yingtaogou, Qipan Mountain, Hunnan District, Shenyang city, Liaoning Province	123.6666	41.9500
A. gallica subsp. *calidusa* (CBS B)	Strain: CBSB19036	Wuduhe, Yiling district, Yichang city, Hubei Province	111.2166	31.1000
A. gallica subsp. *calidusa* (CBS B)	Strain: CBSB96003	Qinggouzi forest farm, Huangnihe Forest Bureau, Dunhua City, Yanbian Korean Autonomous Prefecture, Jilin Province	128.3000	43.1333
A. gallica subsp. *calidusa* (CBS B)	Strain: CBSB96004	Jingou forest farm, Huangnihe Forest Bureau, Dunhua City, Yanbian Korean Autonomous Prefecture, Jilin Province	128.0166	43.1000
A. gallica subsp. *calidusa* (CBS B)	Strain: CBSB96011	Dianzhan houshan, Changbai Mountain, Dunhua City, Yanbian Korean Autonomous Prefecture, Jilin Province	128.0166	42.0500

Table C1 (continued)

Phylogenetic/Biological species	Strain/specimen	Location	Longitude	Latitude
A. gallica subsp. *calidusa* (CBS B)	Strain: CBSB96031	Huangsongpu, Changbai Mountain, Antu County, Yanbian Korean Autonomous Prefecture, Jilin Province	128.1500	42.2000
A. gallica subsp. *calidusa* (CBS B)	Strain: CBSB96032	Dianzhan houshan, Changbai Mountain, Fusong County, Baishan City, Jilin Province	128.0166	42.0500
A. gallica subsp. *calidusa* (CBS B)	Commercial Strain: CFY-1	Zhaotong Tianma Research Institute, Zhaotong City, Yunnan Province	Null	Null
A. gallica subsp. *calidusa* (CBS B)	Commercial Strain: CFY-2	Zhaotong Tianma Research Institute, Zhaotong City, Yunnan Province	Null	Null
A. gallica subsp. *calidusa* (CBS B)	Strain: DBRGZP	Dunhua City, Yanbian Korean Autonomous Prefecture, Jilin Province	128.5687	43.4237
A. gallica subsp. *calidusa* (CBS B)	Strain: guo349	Xinlin, Huma County, Daxinganling Prefecture, Heilongjiang Province	124.6919	52.2205
A. gallica subsp. *calidusa* (CBS B)	Commercial Strain: HB-1	Tianhe Fungi Factory, Wufeng Town, Wufeng County, Yichang City, Hubei Province	Null	Null
A. gallica subsp. *calidusa* (CBS B)	Commercial Strain: HB-2	Tianhe Fungi Factory, Wufeng Town, Wufeng County, Yichang City, Hubei Province	Null	Null
A. gallica subsp. *calidusa* (CBS B)	Commercial Strain: HB-3	Tianhe Fungi Factory, Wufeng Town, Wufeng County, Yichang City, Hubei Province	Null	Null
A. gallica subsp. *calidusa* (CBS B)	Commercial Strain: HB-4	Tianhe Fungi Factory, Wufeng Town, Wufeng County, Yichang City, Hubei Province	Null	Null
A. gallica subsp. *calidusa* (CBS B)	Commercial Strain: HB-5	Tianhe Fungi Factory, Wufeng Town, Wufeng County, Yichang City, Hubei Province	Null	Null
A. gallica subsp. *calidusa* (CBS B)	Commercial Strain: HB-6	Tianhe Fungi Factory, Wufeng Town, Wufeng County, Yichang City, Hubei Province	Null	Null

Table C1 (continued)

Phylogenetic/Biological species	Strain/specimen	Location	Longitude	Latitude
A. gallica subsp. *calidusa* (CBS B)	Commercial Strain: HDY	Nongxin Tianma Provenance Base, Yiling District, Yichang City, Hubei Province	Null	Null
A. gallica subsp. *calidusa* (CBS B)	Specimen: HKAS 45821	Inside the Botanical Institute of Kunming City, Panlong District, Kunming City, Yunnan Province	102.7427	25.1379
A. gallica subsp. *calidusa* (CBS B)	Specimen: HKAS 92018	Majia Village, Xiamatang Town, Benxi City, Liaoning Province	123.8649	40.9965
A. gallica subsp. *calidusa* (CBS B)	Specimen: HMAS 255521	Hashtus Mountain, Linxi county, Chifeng City, Inner Mongolia Autonomous Region	117.9661	44.1009
A. gallica subsp. *calidusa* (CBS B)	Specimen: HMAS 255525	Hashtus Mountain, Linxi county, Chifeng City, Inner Mongolia Autonomous Region	117.9661	44.1009
A. gallica subsp. *calidusa* (CBS B)	Specimen: HMAS 255529	Hashtus Mountain, Linxi county, Chifeng City, Inner Mongolia Autonomous Region	117.9661	44.1009
A. gallica subsp. *calidusa* (CBS B)	Specimen: HMAS 273634	Yunmeng Mountain, Miyun County, Beijing	116.8432	40.3733
A. gallica subsp. *calidusa* (CBS B)	Specimen: HMAS 276553	Huanghou Town, Huairou District, Beijing	116.5794	40.5334
A. gallica subsp. *calidusa* (CBS B)	Specimen: HMAS 33891	Baihuashan National Nature Reserve, Mentougou District, Beijing	115.5918	39.8377
A. gallica subsp. *calidusa* (CBS B)	Specimen: HMAS 37384	Kaiyuan city, Tieling City, Liaoning Province	124.0518	42.5776
A. gallica subsp. *calidusa* (CBS B)	Specimen: HMAS 61574	Tanchang County, Longnan City, Gansu Province	104.3933	34.0472
A. gallica subsp. *calidusa* (CBS B)	Specimen: HMAS 96967	Fuhe Village, Mingyue Township, Antu County, Yanbian Korean Autonomous Prefecture, Jilin Province	128.9000	43.1166

Table C1 (continued)

Phylogenetic/Biological species	Strain/specimen	Location	Longitude	Latitude
A. gallica subsp. *calidusa* (CBS B)	Specimen: HMAS 97093	Wangqing County, Yanbian Korean Autonomous Prefecture, Jilin Province	129.7851	43.3172
A. gallica subsp. *calidusa* (CBS B)	Specimen: HMJAU 55082	Heili River Nature Reserve, Harqin Banner, Chifeng City, Inner Mongolia Autonomous Region	118.3987	41.5746
A. gallica subsp. *calidusa* (CBS B)	Specimen: HMJAU 60448	Cuifeng Forestry Farm, Jiagedaqi Forestry Bureau, Daxinganling District, Heilongjiang Province	124.0531	50.7191
A. gallica subsp. *calidusa* (CBS B)	Commercial Strain: HS-01	Yichang Hongsheng Biotechnology Co., Ltd., Wufeng County, Yichang City, Hubei Province	Null	Null
A. gallica subsp. *calidusa* (CBS B)	Commercial Strain: HS-A25	Yichang Hongsheng Biotechnology Co., Ltd., Wufeng County, Yichang City, Hubei Province	Null	Null
A. gallica subsp. *calidusa* (CBS B)	Commercial Strain: HS-A9	Yichang Hongsheng Biotechnology Co., Ltd., Wufeng County, Yichang City, Hubei Province	Null	Null
A. gallica subsp. *calidusa* (CBS B)	Commercial Strain: J234	Shaanxi Chunsen Junye Co., Ltd., Xixiang County, Hanzhong City, Shaanxi Province	Null	Null
A. gallica subsp. *calidusa* (CBS B)	Specimen: HKAS 86558	Null	Null	Null
A. gallica subsp. *calidusa* (CBS B)	Commercial Strain: LD-M8	Anhui Landun Ecological Agriculture Technology Co., Ltd. Yueyang County, Anqing City, Anhui Province	Null	Null
A. gallica subsp. *calidusa* (CBS B)	Strain: LM-2	Xiaocaoba Tianma Trading Market, Xiaocaoba Town, Yiliang county, Zhaotong City, Yunnan Province	104.2608	27.7674

Table C1 (continued)

Phylogenetic/Biological species	Strain/specimen	Location	Longitude	Latitude
A. gallica subsp. *calidusa* (CBS B)	Commercial Strain: LYT-A9	Yiliang County Tianma Industry Development Center, Yiliang county, Zhaotong City, Yunnan Province	Null	Null
A. gallica subsp. *calidusa* (CBS B)	Commercial Strain: LZL-1	Xixia Occupy Fungi Industry Co., Ltd., Xixia County, Nanyang City, Henan Province	Null	Null
A. gallica subsp. *calidusa* (CBS B)	Commercial Strain: LZL-10	Xixia Occupy Fungi Industry Co., Ltd., Xixia County, Nanyang City, Henan Province	Null	Null
A. gallica subsp. *calidusa* (CBS B)	Commercial Strain: LZL-11	Xixia Occupy Fungi Industry Co., Ltd., Xixia County, Nanyang City, Henan Province	Null	Null
A. gallica subsp. *calidusa* (CBS B)	Commercial Strain: LZL-12	Xixia Occupy Fungi Industry Co., Ltd., Xixia County, Nanyang City, Henan Province	Null	Null
A. gallica subsp. *calidusa* (CBS B)	Commercial Strain: LZL-13	Xixia Occupy Fungi Industry Co., Ltd., Xixia County, Nanyang City, Henan Province	Null	Null
A. gallica subsp. *calidusa* (CBS B)	Commercial Strain: LZL-15	Xixia Occupy Fungi Industry Co., Ltd., Xixia County, Nanyang City, Henan Province	Null	Null
A. gallica subsp. *calidusa* (CBS B)	Commercial Strain: LZL-16	Xixia Occupy Fungi Industry Co., Ltd., Xixia County, Nanyang City, Henan Province	Null	Null
A. gallica subsp. *calidusa* (CBS B)	Commercial Strain: LZL-17	Xixia Occupy Fungi Industry Co., Ltd., Xixia County, Nanyang City, Henan Province	Null	Null

Table C1 (continued)

Phylogenetic/Biological species	Strain/specimen	Location	Longitude	Latitude
A. gallica subsp. *calidusa* (CBS B)	Commercial Strain: LZL-18	Xixia Occupy Fungi Industry Co., Ltd., Xixia County, Nanyang City, Henan Province	Null	Null
A. gallica subsp. *calidusa* (CBS B)	Commercial Strain: LZL-19	Xixia Occupy Fungi Industry Co., Ltd., Xixia County, Nanyang City, Henan Province	Null	Null
A. gallica subsp. *calidusa* (CBS B)	Commercial Strain: LZL2	Xixia Occupy Fungi Industry Co., Ltd., Xixia County, Nanyang City, Henan Province	Null	Null
A. gallica subsp. *calidusa* (CBS B)	Commercial Strain: LZL20	Xixia Occupy Fungi Industry Co., Ltd., Xixia County, Nanyang City, Henan Province	Null	Null
A. gallica subsp. *calidusa* (CBS B)	Commercial Strain: LZL-4	Xixia Occupy Fungi Industry Co., Ltd., Xixia County, Nanyang City, Henan Province	Null	Null
A. gallica subsp. *calidusa* (CBS B)	Commercial Strain: LZL-6	Xixia Occupy Fungi Industry Co., Ltd., Xixia County, Nanyang City, Henan Province	Null	Null
A. gallica subsp. *calidusa* (CBS B)	Commercial Strain: LZL-7	Xixia Occupy Fungi Industry Co., Ltd., Xixia County, Nanyang City, Henan Province	Null	Null
A. gallica subsp. *calidusa* (CBS B)	Commercial Strain: LZL-8	Xixia Occupy Fungi Industry Co., Ltd., Xixia County, Nanyang City, Henan Province	Null	Null
A. gallica subsp. *calidusa* (CBS B)	Commercial Strain: LZL-9	Xixia Occupy Fungi Industry Co., Ltd., Xixia County, Nanyang City, Henan Province	Null	Null

Table C1 (continued)

Phylogenetic/Biological species	Strain/specimen	Location	Longitude	Latitude
A. gallica subsp. *calidusa* (CBS B)	Commercial Strain: MF-M5	Yiliang Maofeng Gastrodia elata Industry Development Co., Ltd., Yiliang County, Zhaotong City, Yunnan Province	Null	Null
A. gallica subsp. *calidusa* (CBS B)	Commercial Strain: QA1	Shaanxi Hanzhong Qingruifeng Edible and Medicinal Fungi Technology Co., Ltd., Hanzhong City, Shaanxi Province	Null	Null
A. gallica subsp. *calidusa* (CBS B)	Commercial Strain: QF13	Shaanxi Hanzhong Qingruifeng Edible and Medicinal Fungi Technology Co., Ltd., Hanzhong City, Shaanxi Province	Null	Null
A. gallica subsp. *calidusa* (CBS B)	Commercial Strain: QM2	Shaanxi Hanzhong Qingruifeng Edible and Medicinal Fungi Technology Co., Ltd., Hanzhong City, Shaanxi Province	Null	Null
A. gallica subsp. *calidusa* (CBS B)	Commercial Strain: QM3	Shaanxi Hanzhong Qingruifeng Edible and Medicinal Fungi Technology Co., Ltd., Hanzhong City, Shaanxi Province	Null	Null
A. gallica subsp. *calidusa* (CBS B)	Commercial Strain: SA-19	Shaanxi Hanzhong Qingruifeng Edible and Medicinal Fungi Technology Co., Ltd., Hanzhong City, Shaanxi Province	Null	Null
A. gallica subsp. *calidusa* (CBS B)	Specimen: HKAS 135527	Z566, Xigangzi Town, Aihui District, Heihe City, Heilongjiang Province	127.1863	49.9785
A. gallica subsp. *calidusa* (CBS B)	Specimen: HKAS 135528	Z566, Xigangzi Town, Aihui District, Heihe City, Heilongjiang Province	127.1863	49.9787

Table C1 (continued)

Phylogenetic/Biological species	Strain/specimen	Location	Longitude	Latitude
A. gallica subsp. *calidusa* (CBS B)	Specimen: HKAS 135529	Z566, Xigangzi Town, Aihui District, Heihe City, Heilongjiang Province	127.1862	49.9788
A. gallica subsp. *calidusa* (CBS B)	Specimen: HKAS 135530	Aihui Town, Aihui District, Heihe City, Heilongjiang Province	127.3693	50.0922
A. gallica subsp. *calidusa* (CBS B)	Strain: SJ103	National Highway 244, Zuitou Town, Taibai County, Baoji City, Shaanxi Province	107.2239	33.9662
A. gallica subsp. *calidusa* (CBS B)	Specimen: HKAS 135551	National Highway 244, Zuitou Town, Taibai County, Baoji City, Shaanxi Province	107.2235	33.9664
A. gallica subsp. *calidusa* (CBS B)	Specimen: HKAS 135552	Micangshan National Forest Park, Wuguang Town, Nanjiang County, Bazhong City, Sichuan Province	106.9177	32.6906
A. gallica subsp. *calidusa* (CBS B)	Specimen: HKAS 135568	County Road 024, Mashiping Township, Nanzhao County, Nanyang City, Henan Province	112.3133	33.6699
A. gallica subsp. *calidusa* (CBS B)	Specimen: HKAS 135569	County Road 024, Mashiping Township, Nanzhao County, Nanyang City, Henan Province	112.3134	33.6699
A. gallica subsp. *calidusa* (CBS B)	Specimen: HKAS 135570	County Road 024, Mashiping Township, Nanzhao County, Nanyang City, Henan Province	112.3134	33.6699
A. gallica subsp. *calidusa* (CBS B)	Specimen: HKAS 135571	County Road 024, Mashiping Township, Nanzhao County, Nanyang City, Henan Province	112.3132	33.6699
A. gallica subsp. *calidusa* (CBS B)	Specimen: HKAS 135572	County Road 024, Mashiping Township, Nanzhao County, Nanyang City, Henan Province	112.3132	33.6700

Table C1 (continued)

Phylogenetic/Biological species	Strain/specimen	Location	Longitude	Latitude
A. gallica subsp. *calidusa* (CBS B)	Specimen: HKAS 135573	County Road 024, Mashiping Township, Nanzhao County, Nanyang City, Henan Province	112.3132	33.6700
A. gallica subsp. *calidusa* (CBS B)	Specimen: HKAS 135574	County Road 024, Mashiping Township, Nanzhao County, Nanyang City, Henan Province	112.3131	33.6699
A. gallica subsp. *calidusa* (CBS B)	Specimen: HKAS 135575	County Road 024, Mashiping Township, Nanzhao County, Nanyang City, Henan Province	112.3132	33.6695
A. gallica subsp. *calidusa* (CBS B)	Specimen: HKAS 135576	County Road 024, Mashiping Township, Nanzhao County, Nanyang City, Henan Province	112.3132	33.6696
A. gallica subsp. *calidusa* (CBS B)	Specimen: HKAS 135577	County Road 024, Mashiping Township, Nanzhao County, Nanyang City, Henan Province	112.3134	33.6693
A. gallica subsp. *calidusa* (CBS B)	Specimen: HKAS 135578	County Road 024, Mashiping Township, Nanzhao County, Nanyang City, Henan Province	112.3133	33.6691
A. gallica subsp. *calidusa* (CBS B)	Specimen: HKAS 135579	County Road 024, Mashiping Township, Nanzhao County, Nanyang City, Henan Province	112.3137	33.6683
A. gallica subsp. *calidusa* (CBS B)	Specimen: HKAS 135580	National Highway 241, Miaozi Town, Luanchuan County, Luoyang City, Henan Province	111.7071	33.7005
A. gallica subsp. *calidusa* (CBS B)	Specimen: HKAS 135581	National Highway 241, Miaozi Town, Luanchuan County, Luoyang City, Henan Province	111.7065	33.6636

Table C1 (continued)

Phylogenetic/Biological species	Strain/specimen	Location	Longitude	Latitude
A. gallica subsp. *calidusa* (CBS B)	Specimen: HKAS 135582	National Highway 241, Miaozi Town, Luanchuan County, Luoyang City, Henan Province	111.7065	33.6635
A. gallica subsp. *calidusa* (CBS B)	Specimen: HKAS 135583	National Highway 241, Miaozi Town, Luanchuan County, Luoyang City, Henan Province	111.7064	33.6634
A. gallica subsp. *calidusa* (CBS B)	Specimen: HKAS 135584	National Highway 241, Miaozi Town, Luanchuan County, Luoyang City, Henan Province	111.7063	33.6633
A. gallica subsp. *calidusa* (CBS B)	Specimen: HKAS 135585	National Highway 241, Miaozi Town, Luanchuan County, Luoyang City, Henan Province	111.7063	33.6632
A. gallica subsp. *calidusa* (CBS B)	Specimen: HKAS 135586	National Highway 241, Miaozi Town, Luanchuan County, Luoyang City, Henan Province	111.7063	33.6632
A. gallica subsp. *calidusa* (CBS B)	Specimen: HKAS 135531	Hengxing Road, Chaoyang Street, Yimei District, Yichun City, Heilongjiang Province	128.8547	47.7392
A. gallica subsp. *calidusa* (CBS B)	Specimen: HKAS 135532	Hengxing Road, Chaoyang Street, Yimei District, Yichun City, Heilongjiang Province	128.8546	47.7396
A. gallica subsp. *calidusa* (CBS B)	Specimen: HKAS 135533	Hengxing Road, Chaoyang Street, Yimei District, Yichun City, Heilongjiang Province	128.8546	47.7396
A. gallica subsp. *calidusa* (CBS B)	Specimen: HKAS 135534	Chaoyang Street, Yimei District, Yichun City, Heilongjiang Province	128.8904	47.7548
A. gallica subsp. *calidusa* (CBS B)	Specimen: HKAS 135535	Yilin Business Office, Yimei District, Yichun City, Heilongjiang Province	128.9597	47.8046

Table C1 (continued)

Phylogenetic/Biological species	Strain/specimen	Location	Longitude	Latitude
A. gallica subsp. *calidusa* (CBS B)	Specimen: HKAS 135536	Yilin Business Office, Yimei District, Yichun City, Heilongjiang Province	128.9592	47.8042
A. gallica subsp. *calidusa* (CBS B)	Specimen: HKAS 135537	Yilin Business Office, Yimei District, Yichun City, Heilongjiang Province	128.9592	47.8042
A. gallica subsp. *calidusa* (CBS B)	Specimen: HKAS 135538	Yilin Business Office, Yimei District, Yichun City, Heilongjiang Province	128.9592	47.8041
A. gallica subsp. *calidusa* (CBS B)	Specimen: HKAS 135539	Yilin Business Office, Yimei District, Yichun City, Heilongjiang Province	128.9599	47.8041
A. gallica subsp. *calidusa* (CBS B)	Specimen: HKAS 135543	Yuejin Village, Shuyuan Township, Dongshan District, Hegang City, Heilongjiang Province	130.2747	47.3741
A. gallica subsp. *calidusa* (CBS B)	Specimen: HKAS 135544	Songjianghe Town, Fusong County, Baishan City, Jilin Province	127.5115	42.1734
A. gallica subsp. *calidusa* (CBS B)	Specimen: HKAS 135541	Changbai Mountain National Nature Reserve, Ring Mountain Line, Donggang Town, Fusong County, Baishan City, Jilin Province	127.7341	42.1200
A. gallica subsp. *calidusa* (CBS B)	Specimen: HKAS 135542	Changbai Mountain National Nature Reserve, Ring Mountain Line, Donggang Town, Fusong County, Baishan City, Jilin Province	127.7866	42.2332
A. gallica subsp. *calidusa* (CBS B)	Specimen: HKAS 135545	Heihu Pass, Yingtou Town, Mei County, Baoji City, Shaanxi Province	107.7164	34.0896
A. gallica subsp. *calidusa* (CBS B)	Specimen: HKAS 135546	Heihu Pass, Yingtou Town, Mei County, Baoji City, Shaanxi Province	107.7160	34.0894

Table C1 (continued)

Phylogenetic/Biological species	Strain/specimen	Location	Longitude	Latitude
A. gallica subsp. *calidusa* (CBS B)	Specimen: HKAS 135548	National Highway 244, Fengxi Town, Chencang District, Baoji City, Shaanxi Province	107.3070	34.2055
A. gallica subsp. *calidusa* (CBS B)	Commercial Strain: SM18	Shaanxi Hanzhong Qingruifeng Edible and Medicinal Fungi Technology Co., Ltd., Hanzhong City, Shaanxi Province	Null	Null
A. gallica subsp. *calidusa* (CBS B)	Commercial Strain: SS-01	Shaanxi Sensheng Fungi Technology Co., Ltd., Hanzhong City, Shaanxi Province	Null	Null
A. gallica subsp. *calidusa* (CBS B)	Strain: SX_M2	Qixingguan District, Bijie City, Guizhou Province	105.3052	27.2982
A. gallica subsp. *calidusa* (CBS B)	Commercial Strain: T11	Taobao-Based Cultivation Company: Rongrong Jiayuan	Null	Null
A. gallica subsp. *calidusa* (CBS B)	Commercial Strain: T12	Taobao-Based Cultivation Company: Baike Chinese Medicinal Herb Cultivation Base	Null	Null
A. gallica subsp. *calidusa* (CBS B)	Commercial Strain: T14	Taobao-Based Cultivation Company: Baike Chinese Medicinal Herb Cultivation Base	Null	Null
A. gallica subsp. *calidusa* (CBS B)	Commercial Strain: T19	Individual Sellers via Taobao: Deng Xiaoqin-Wuhan City, Jiangxia District, Daqiao New Area	Null	Null
A. gallica subsp. *calidusa* (CBS B)	Commercial Strain: T20	Individual Sellers via Taobao: Hu Zhengjiang-Shibawan Village, Xiabaoping Town, Yiling District, Yichang City	Null	Null

Table C1 (continued)

Phylogenetic/Biological species	Strain/specimen	Location	Longitude	Latitude
A. gallica subsp. *calidusa* (CBS B)	Commercial Strain: T21	Individual Sellers via Taobao: Hu Zhengjiang-Shibawan Village, Xiabaoping Town, Yiling District, Yichang City	Null	Null
A. gallica subsp. *calidusa* (CBS B)	Commercial Strain: T25	Individual Sellers via Taobao: Farmer Gastrodia - Xiufeng Street, Xiabaoping Town, Yichang City, Hubei Province	Null	Null
A. gallica subsp. *calidusa* (CBS B)	Commercial Strain: T27	Null	Null	Null
A. gallica subsp. *calidusa* (CBS B)	Commercial Strain: T28	Personal Contacts: Du Jiulin-Xiabaoping Village, Yiling District, Yichang City	Null	Null
A. gallica subsp. *calidusa* (CBS B)	Commercial Strain: T3	Taobao-Based Cultivation Company: Wuhan Zhou Yulin Edible Fungi Research	Null	Null
A. gallica subsp. *calidusa* (CBS B)	Commercial Strain: T6	Taobao-Based Cultivation Company: Xiangnongcheng, Yichang	Null	Null
A. gallica subsp. *calidusa* (CBS B)	Commercial Strain: T9	Taobao-Based Cultivation Company: Mingyuan Mushroom Industry	Null	Null
A. gallica subsp. *calidusa* (CBS B)	Strain: WSB-M1	Wang Shaobai "王绍柏"	Null	Null
A. gallica subsp. *calidusa* (CBS B)	Strain: XY2	Kunming Institute of Botany, Chinese Academy of Sciences	Null	Null
A. gallica subsp. *calidusa* (CBS B)	Commercial Strain: Y3	Yiliang County Tianma Industry Development Center, Yiliang county, Zhaotong City, Yunnan Province	Null	Null
A. gallica subsp. *calidusa* (CBS B)	Specimen: HKAS 135525	Hengxing Road, Chaoyang Street, Yichun Yimei District, Heihe City, Heilongjiang Province	128.8543	47.7427

Table C1 (continued)

Phylogenetic/Biological species	Strain/specimen	Location	Longitude	Latitude
A. gallica subsp. *calidusa* (CBS B)	Specimen: HKAS 135524	Hengxing Road, Chaoyang Street, Yichun Yimei District, Heihe City, Heilongjiang Province	128.8543	47.7427
A. gallica subsp. *calidusa* (CBS B)	Specimen: HKAS 135522	Hengxing Road, Chaoyang Street, Yichun Yimei District, Heihe City, Heilongjiang Province	128.8543	47.7427
A. gallica subsp. *calidusa* (CBS B)	Specimen: HKAS 135523	Yuejin Village, Shuyuan Township, Dongshan District, Hegang City, Heilongjiang Province	130.2760	47.3755
A. gallica subsp. *calidusa* (CBS B)	Strain: ZM	Null	Null	Null
A. gallica subsp. *calidusa* (CBS B)	Strain: ZT-10	Tianhe 2 "天和 2"	Null	Null
A. gallica subsp. *calidusa* (CBS B)	Strain: ZT11	Yongqian 1 "涌前 1"	Null	Null
A. gallica subsp. *calidusa* (CBS B)	Strain: ZT-12	Yongqian 2 "涌前 2"	Null	Null
A. gallica subsp. *calidusa* (CBS B)	Commercial Strain: ZT-18	Xi Wang Hua Bao "硒旺华宝"	Null	Null
A. gallica subsp. *calidusa* (CBS B)	Commercial Strain: ZT-2	Qiligou Yangshi A9 Hao "七里沟杨氏 A9 号"	Null	Null
A. gallica subsp. *calidusa* (CBS B)	Commercial Strain: ZT20	Linfeng Jun "林丰菌"	Null	Null
A. gallica subsp. *calidusa* (CBS B)	Commercial Strain: ZT-21	Tianhe Jun "天合菌"	Null	Null
A. gallica subsp. *calidusa* (CBS B)	Commercial Strain: ZT22	Chu Fengyuan Jun "楚丰元菌"	Null	Null
A. gallica subsp. *calidusa* (CBS B)	Commercial Strain: ZT-23	Jiuhuan Jun "玖环菌"	Null	Null
A. gallica subsp. *calidusa* (CBS B)	Commercial Strain: ZT24	Zhou Zhonghe Jun in Xiaocaoba "小草坝周忠和菌"	Null	Null

Table C1 (continued)

Phylogenetic/Biological species	Strain/specimen	Location	Longitude	Latitude
A. gallica subsp. *calidusa* (CBS B)	Commercial Strain: ZT25	Shaanxi Changlong Agricultural Technology Development Co., Ltd., Hanzhong City, Shaanxi Province	Null	Null
A. gallica subsp. *calidusa* (CBS B)	Commercial Strain: ZT26	Shaanxi Changlong Agricultural Technology Development Co., Ltd., Hanzhong City, Shaanxi Province	Null	Null
A. gallica subsp. *calidusa* (CBS B)	Commercial Strain: ZT27	Ye Guniang Jun "野姑娘菌"	Null	Null
A. gallica subsp. *calidusa* (CBS B)	Commercial Strain: ZT28	Lin Zhong Guan “林忠冠”	Null	Null
A. gallica subsp. *calidusa* (CBS B)	Commercial Strain: ZT-3	Qiligou Huangshi (local) "七里沟黄氏"	Null	Null
A. gallica subsp. *calidusa* (CBS B)	Commercial Strain: ZT31	Qiming Jun "启鸣菌"	Null	Null
A. gallica subsp. *calidusa* (CBS B)	Commercial Strain: ZT-32	Tiankui "天葵"	Null	Null
A. gallica subsp. *calidusa* (CBS B)	Commercial Strain: ZT-33	Mangling "蟒岭"	Null	Null
A. gallica subsp. *calidusa* (CBS B)	Commercial Strain: ZT-34	Wumengteng Jun "乌蒙腾菌"	Null	Null
A. gallica subsp. *calidusa* (CBS B)	Commercial Strain: ZT-35	Nong Xin "农鑫"	Null	Null
A. gallica subsp. *calidusa* (CBS B)	Commercial Strain: ZT-36	Xing Da "兴达"	Null	Null
A. gallica subsp. *calidusa* (CBS B)	Commercial Strain: ZT37	Li Sen "立森"	Null	Null
A. gallica subsp. *calidusa* (CBS B)	Commercial Strain: ZT38	Ke Ruisen "科瑞森"	Null	Null
A. gallica subsp. *calidusa* (CBS B)	Commercial Strain: ZT-39	Hao Shanzhen "好山珍"	Null	Null
A. gallica subsp. *calidusa* (CBS B)	Commercial Strain: ZT-4	Qiligou Huangshi (Shaanxi) "七里沟黄氏（陕西）"	Null	Null
A. gallica subsp. *calidusa* (CBS B)	Commercial Strain: ZT-40	Dian Xun "滇蕈"	Null	Null

Table C1 (continued)

Phylogenetic/Biological species	Strain/specimen	Location	Longitude	Latitude
A. gallica subsp. *calidusa* (CBS B)	Commercial Strain: ZT-41	Xin Jue "鑫爵"	Null	Null
A. gallica subsp. *calidusa* (CBS B)	Commercial Strain: ZT-42	Sentai Jun "森泰菌"	Null	Null
A. gallica subsp. *calidusa* (CBS B)	Commercial Strain: ZT-43	Pengfei Jun "鹏飞菌"	Null	Null
A. gallica subsp. *calidusa* (CBS B)	Commercial Strain: ZT-44	Yuhe Jun "裕禾菌"	Null	Null
A. gallica subsp. *calidusa* (CBS B)	Commercial Strain: ZT-45	Lianfeng Jun (Shaanxi) "莲峰菌（陕西）"	Null	Null
A. gallica subsp. *calidusa* (CBS B)	Commercial Strain: ZT-46	Zhaotong Gastrodia Research Institute, Zhaotong City, Yunnan Province	Null	Null
A. gallica subsp. *calidusa* (CBS B)	Commercial Strain: ZT-6	De Sheng (Shaanxi) "德胜（陕西）"	Null	Null
A. gallica subsp. *calidusa* (CBS B)	Commercial Strain: ZT7	Bai Yanping Jun(Shaanxi) "陕西白彦平菌"	Null	Null
A. gallica subsp. *calidusa* (CBS B)	NCBI:	China	Null	Null
A. gallica subsp. *calidusa* (CBS B)	NCBI:	China	Null	Null
A. gallica subsp. *calidusa* (CBS B)	NCBI:	China	Null	Null
A. gallica subsp. *calidusa* (CBS B)	NCBI:	China	Null	Null
A. gallica subsp. *calidusa* (CBS B)	NCBI:	China	Null	Null
A. gallica subsp. *calidusa* (CBS B)	NCBI:	China	Null	Null
A. gallica subsp. *calidusa* (CBS B)	JGI: 012m	Yiliang county, Zhaotong City, Yunnan Province	104.0559	27.6242
A. gallica subsp. *calidusa* (CBS B)	JGI: Jzi34	China: Kunming, plantation field	Null	Null
A. gallica subsp. *calidusa* (CBS B)	Specimen: SJ04	Z566, Xigangzi Town, Aihui District, Heihe City, Heilongjiang Province	127.1864	49.9785

Table C1 (continued)

Phylogenetic/Biological species	Strain/specimen	Location	Longitude	Latitude
A. gallica subsp. *calidusa* (CBS B)	Specimen: SJ09	Aihui Town, Aihui District, Heihe City, Heilongjiang Province	127.3693	50.0922
A. gallica subsp. *gallica* 1 (EBS E)	JGI: 212v10	Null	Null	Null
A. gallica subsp. *gallica* 1 (EBS E)	JGI: MH878687	Genome Research and Education Center, Siberian Federal University, Akademgorodok, 50a/2, Krasnoyarsk 660036, Russia	Null	Null
A. gallica subsp. *gallica* 2 (NABS VII)	Specimen: HKAS 86569	EUROPE	Null	Null
A. griseocapilla	Specimen: HKAS 135519	Zhangmu Valley, Nyalam County, Shigatse City, Tibet Province	85.9856	27.9886
A. griseocapilla	Strain: WGS75	Pingbian Miao Autonomous County, Honghe Hani and Yi Autonomous Prefecture, Yunnan Province	103.6655	22.9553
A. korhonenii (CBS Q)	Specimen: HKAS 131999	Ailaoshan Subtropical Forest Ecosystem Research Station of the Chinese Academy of Sciences (the Ailaoshan Ecosystem Station), Jingdong Yi Autonomous County, Pu 'er City, Yunnan Province	101.0279	24.5315
A. korhonenii (CBS Q)	Specimen: HKAS 126473	Pingbian County, Daweishan Natural Reserve, Yunnan Province	103.6994	22.9119
A. korhonenii (CBS Q)	Specimen: HKAS 126466	Pingbian County, Daweishan Natural Reserve, Yunnan Province	103.6977	22.9204
A. korhonenii (CBS Q)	Specimen: HKAS 126467	Pingbian County, Daweishan Natural Reserve, Yunnan Province	103.7017	22.9640

Table C1 (continued)

Phylogenetic/Biological species	Strain/specimen	Location	Longitude	Latitude
A. korhonenii (CBS Q)	Specimen: HKAS 126468	Pingbian County, Daweishan Natural Reserve, Yunnan Province	103.6977	22.9061
A. korhonenii (CBS Q)	Specimen: HKAS 126469	Pingbian County, Daweishan Natural Reserve, Yunnan Province	103.6978	22.9076
A. korhonenii (CBS Q)	Specimen: HKAS 126470	Pingbian County, Daweishan Natural Reserve, Yunnan Province	103.7002	22.9111
A. korhonenii (CBS Q)	Specimen: HKAS 126471	Pingbian County, Daweishan Natural Reserve, Yunnan Province	103.6995	22.9127
A. korhonenii (CBS Q)	Specimen: HKAS 126472	Pingbian County, Daweishan Natural Reserve, Yunnan Province	103.6994	22.9134
A. korhonenii (CBS Q)	Specimen: HKAS 95344	Near Miaofang Pass, Tianyu Township, Zhen'an Township, Longling County, Baoshan City, Yunnan Province	98.9673	24.4981
A. linzhiensis (CBS N) lineage 2-mtDNA	Specimen: HMAS 272390	Xibu Road, Songzong Town, Bomi county, Linzhi City, Xizang Autonomous Region	95.7495	29.8704
A. linzhiensis (CBS N) lineage 2-mtDNA	Specimen: HMAS 272515	Layue Township, Bayi District, Linzhi City, Xizang Autonomous Region	94.4845	29.5855
A. luteopileata (CBS C)	Strain: 21024	Yuehualin conifers, Changbai Mountain, Jilin Province	128.0500	42.0500
A. luteopileata (CBS C)	Strain: C19004	Baihe fair, Changbai Mountain, Fusong County, Baishan City, Jilin Province	128.0166	42.0500
A. luteopileata (CBS C)	Strain: C21019	Dixiasnelin, Changbai Mountain, Fusong County, Baishan City, Jilin Province	128.0500	42.0500
A. luteopileata (CBS C)	Strain: CBSB19029	Lushuihe town, Changbai Mountain, Fusong County, Baishan City, Jilin Province	127.9833	42.5333

Table C1 (continued)

Phylogenetic/Biological species	Strain/specimen	Location	Longitude	Latitude
A. luteopileata (CBS C)	Strain: CBSC21009	Dixiasnelin, Changbai Mountain, Antu County, Yanbian Korean Autonomous Prefecture, Jilin Province	128.0666	42.0833
A. luteopileata (CBS C)	Strain: CBSC96027	Baihe, Changbai Mountain, Fusong County, Baishan City, Jilin Province	128.0166	42.0500
A. luteopileata (CBS C)	Strain: CBSC96029	Erdaobaihe, Changbai Mountain, Fusong County, Baishan City, Jilin Province	128.0166	42.0500
A. luteopileata (CBS C)	Strain: CBSC96038	Dixiasnelin, Changbai Mountain, Fusong County, Baishan City, Jilin Province	128.0166	42.0166
A. luteopileata (CBS C)	Specimen: HKAS 86578	Daqing Mountain Liangshui Nature Reserve, Yichun City, Heilongjiang Province	128.8923	47.1876
A. luteopileata (CBS C)	Specimen: HMJAU 24389	Fenglin National Nature Reserve, Fenglin County, Yichun City, Heilongjiang Province	129.1958	48.1332
A. luteopileata (CBS C)	Specimen: HMJAU 60487	Fenglin National Nature Reserve, Fenglin County, Yichun City, Heilongjiang Province	129.1958	48.1332
A. luteopileata (CBS C)	Commercial Strain: LZL-5	Xixia Occupy Fungi Industry Co., Ltd., Xixia County, Nanyang City, Henan Province	Null	Null
A. luteopileata (CBS C)	Specimen: MHHNU 7783	Delbul Forest Farm, Daxinganling, Inner Mongolia Autonomous Region	121.1070	50.9923
A. pseudoostoyae	Specimen: HKAS 50184	Miaogao Temple, Wuhua District, Kunming City, Yunnan Province	102.6314	25.0980

Table C1 (continued)

Phylogenetic/Biological species	Strain/specimen	Location	Longitude	Latitude
A. pseudoostoyae	Specimen: HKAS 56108	Yulong Naxi Autonomous County, Lijiang City, Yunnan Province	100.2355	26.8216
A. pseudoostoyae	Specimen: HKAS 58853	Shibao Mountain, Jianchuan County, Dali Bai Autonomous Prefecture, Yunnan Province	99.8417	26.3929
A. sinapina subsp. *alpina* (CBS A)	Strain: CBSA96008	Front gate, Changbai Mountain, Fusong County, Baishan City, Jilin Province	128.1666	42.1666
A. sinapina subsp. *alpina* (CBS A)	Strain: CBSA96016	Yuehualindai, Changbai Mountain, Fusong County, Baishan City, Jilin Province	128.0500	42.0500
A. sinapina subsp. *alpina* (CBS A)	Strain: CBSA96025	Yuehualindai, Changbai Mountain, Fusong County, Baishan City, Jilin Province	128.0500	42.0500
A. sinapina subsp. *alpina* (CBS A)	Strain: CBSA96042	Taerqi town, Yakeshi city, Hulunbeier City, Inner Mongolia autonomous region	121.2004	47.9381
A. sinapina subsp. *alpina* (CBS A)	Specimen: HMAS 248128	Huangganglіang, Hexigten Banner, Inner Mongolia Autonomous Region	117.5368	43.5456
A. sinapina subsp. *alpina* (CBS A)	Specimen: HMAS 255468	Huangganglіang, Hexigten Banner, Inner Mongolia Autonomous Region	117.5368	43.5456
A. sinapina subsp. *alpina* (CBS A)	Specimen: HMAS 255489	Huangganglіang, Hexigten Banner, Inner Mongolia Autonomous Region	117.5368	43.5456
A. sinapina subsp. *alpina* (CBS A)	Specimen: HMAS 281266	Huangganglіang National Forest Park, Hexigten Banner, Chifeng City, Inner Mongolia Autonomous Region	117.4036	43.4325
A. sinapina subsp. *alpina* (CBS A)	Specimen: HMAS 96969	Changbai Mountain, Antu County, Yanbian Korean Autonomous Prefecture, Jilin Province	128.1333	42.0333

Table C1 (continued)

Phylogenetic/Biological species	Strain/specimen	Location	Longitude	Latitude
A. sinapina subsp. *alpina* (CBS A)	Specimen: HMJAU 22761	West Main Line, Changbai Mountain, Fusong County, Baishan City, Jilin Province	128.0216	42.0030
A. sinapina subsp. *alpina* (CBS A)	Specimen: HMJAU 23501	Keyihe, Hulunbeier City, Inner Mongolia Autonomous Region	122.6225	50.6600
A. sinapina subsp. *alpina* (CBS A)	Specimen: HMJAU 33876	Genhe City, Hulunbeier City, Inner Mongolia Autonomous Region	120.3339	50.3339
A. sinapina subsp. *alpina* (CBS A)	Specimen: HMJAU 60486	Iksama National Forest Park, Hulunbeier City, Inner Mongolia Autonomous Region	121.9517	52.0823
A. sinensis (CBS F) lineage 1-mtDNA	Strain: 2104919020	Longxi residential area, Shenyang city, Liaoning Province	123.4000	41.8500
A. sinensis (CBS F) lineage 1-mtDNA	Specimen: HKAS 135485	Wangjia Shapo, Houhe nature reserve, Wufeng Tujia Autonomous County, Yichang City, Hubei Province	110.5633	30.0636
A. sinensis (CBS F) lineage 1-mtDNA	Specimen: HKAS 135486	Niuzhuang Town, Wufeng Tujia Autonomous County, Yichang City, Hubei Province	110.3884	30.2348
A. sinensis (CBS F) lineage 1-mtDNA	Strain: CBSF05030	Honghegu, Taibai Mountain, Fengxian County, Baoji City, Shaanxi Province	107.0833	34.0000
A. sinensis (CBS F) lineage 1-mtDNA	Strain: CBSF19020	Houtoushan town fair, Qingyuan Manchu Autonomous County, Fushun City, Liaoning Province	124.5000	41.9833
A. sinensis (CBS F) lineage 1-mtDNA	Strain: CBSF97033	Dianzhan houshan, Changbai Mountain, Antu County, Yanbian Korean Autonomous Prefecture, Jilin Province	128.1000	42.3000

Table C1 (continued)

Phylogenetic/Biological species	Strain/specimen	Location	Longitude	Latitude
A. sinensis (CBS F) lineage 1-mtDNA	Strain: CBSF99103	Yongcui forest farm, Dailing District, Tieli City, Yichun City, Heilongjiang Province	128.1333	47.0166
A. sinensis (CBS F) lineage 1-mtDNA	Strain: CBSF99107	Yongcui forest farm, Dailing District, Tieli City, Yichun City, Heilongjiang Province	128.1333	47.0166
A. sinensis (CBS F) lineage 1-mtDNA	Specimen: HKAS 86547	Xiaocaoba Shennong Company, Yiliang County, Zhaotong City, Yunnan Province	Null	Null
A. sinensis (CBS F) lineage 1-mtDNA	Specimen: HKAS 86584	Laotudingzi National Nature Reserve, Huanren Manchu Autonomous County, Benxi City, Liaoning Province	124.9424	41.3565
A. sinensis (CBS F) lineage 1-mtDNA	Commercial Strain: guo7	Yang Dayong's Fungi Materials, Xiaocaoba, Yiliang County, Zhaotong City, Yunnan Province	Null	Null
A. sinensis (CBS F) lineage 1-mtDNA	Specimen: HMAS 22782	Xiaowutai Mountain, Yuxian County, Zhangjiakou City, Hebei Province	115.0076	39.8677
A. sinensis (CBS F) lineage 1-mtDNA	Specimen: HMAS 253828	Yudu Mountain, Yanqing District, Beijing City, Beijing	115.9690	40.4634
A. sinensis (CBS F) lineage 1-mtDNA	Specimen: HMAS 273636	Xiaolongmen, Mentougou District, Beijing	116.0962	39.9366
A. sinensis (CBS F) lineage 1-mtDNA	Specimen: HMAS 61686	Hantai District, Hanzhong City, Shaanxi Province	107.0231	33.0663
A. sinensis (CBS F) lineage 1-mtDNA	Specimen: HMJAU 22795	Yangzishao Town, Huinan County, Tonghua City, Jilin Province	126.1628	42.4452
A. sinensis (CBS F) lineage 1-mtDNA	Specimen: HMJAU 23629	Dachingu Nature Reserve, Horqin Zuoyi Houqi, Tongliao City, Inner Mongolia Autonomous Region	122.1945	42.7830

Table C1 (continued)

Phylogenetic/Biological species	Strain/specimen	Location	Longitude	Latitude
A. sinensis (CBS F) lineage 1-mtDNA	Specimen: HMJAU 23737	Back Mountain of Changbaishan Academy of Sciences, Erdao Baihe Town, Yanbian Korean Autonomous Prefecture, Jilin Province	128.1148	42.4052
A. sinensis (CBS F) lineage 1-mtDNA	Specimen: HMJAU 28935	Yiwulv Mountain, Beizhen City, Jinzhou City, Liaoning Province	121.7208	41.6037
A. sinensis (CBS F) lineage 1-mtDNA	Specimen: MHHNU 7577	Hupingshan National Nature Reserve, Shimen County, Changde City, Hunan Province	110.6701	30.0035
A. sinensis (CBS F) lineage 1-mtDNA	Specimen: HKAS 135540	Changbai Mountain National Nature Reserve, Ring Mountain Line, Donggang Town, Fusong County, Baishan City, Jilin Province	127.7341	42.1200
A. sinensis (CBS F) lineage 1-mtDNA	Specimen: HKAS 135547	National Highway 244, Fengxi Town, Chencang District, Baoji City, Shaanxi Province	107.3063	34.2052
A. sinensis (CBS F) lineage 1-mtDNA	Specimen: HKAS 135549	National Highway 244, Fengxi Town, Chencang District, Baoji City, Shaanxi Province	107.3070	34.2056
A. sinensis (CBS F) lineage 1-mtDNA	Specimen: HKAS 135526	Fusong Town, Fusong County, Baishan City, Jilin Province	127.2939	42.3119
A. sinensis (CBS F) lineage 1-mtDNA	Commercial Strain: ZT-8	Long An (Huangshi) "龙安（黄氏）"	Null	Null
A. sinensis (CBS F) lineage 1-mtDNA	Commercial Strain: guo12	Xiaocaoba Shennong Company, Yiliang County, Zhaotong City, Yunnan Province	Null	Null
A. tabescens subsp. *orientala* CBS I	Strain: AT	Nuozhadu Dam, Puer State, Yunnan Province	100.4397	22.6230

Table C1 (continued)

Phylogenetic/Biological species	Strain/specimen	Location	Longitude	Latitude
A. tabescens subsp. *orientala* CBS I	Strain: CBSI99122	Beijing Zoon, Haidian district, Beijing	116.3166	39.9333
A. tabescens subsp. *orientala* CBS I	Specimen: HKAS 86603	Beijing Zoo, Xicheng District, Beijing	116.3366	3.9420
A. tabescens subsp. *orientala* CBS I	Specimen: HKAS 58683	Xiaowan Township, Fengqing County, Lincang City, Yunnan Province	100.0774	24.6761
A. tabescens subsp. *orientala* CBS I	Specimen: HKAS 58910	National Highway 320 at 3295km, Yongping County, Dali Bai Autonomous Prefecture, Yunnan Province	99.7759	25.5144
A. tabescens subsp. *orientala* CBS I	Specimen: HKAS 80228	Shuijingping Village, Niutoudian Town, Zhenping County, Ankang City, Shaanxi Province	109.5726	32.1054
A. tabescens subsp. *orientala* CBS I	Specimen: JLK921	Dadugang Township Nature Reserve, Jinghong City, Xishuangbanna Prefecture, Yunnan Province	100.9148	22.2854
A. tabescens subsp. *orientala* CBS I	Specimen: HKAS 126372	Longshan Reservoir, Nanhua County, Chuxiong Yi Autonomous Prefecture, Yunnan Province	101.2782	25.3278
A. tabescens subsp. *orientala* CBS I	Specimen: MHHNU 8836	Mangshan National Reserve, Tiantai Mountain Scenic Area, Yizhang County, Hunan	112.9490	24.9490
A. tabescens subsp. *orientala* CBS I	NCBI: NC_042769	Chungbuk National University (Cheongju, Chungcheongbuk-do, Korea; N36°37′43.64″, E127°27′04.87″).	127.4511	36.6286
A. tabescens subsp. *orientala* CBS I	Strain: SX_M1	Yangchang Town, Longli County, Qiannan Buyi and Miao Autonomous Prefecture, Guizhou Province	107.0469	26.2784

Table C1 (continued)

Phylogenetic/Biological species	Strain/specimen	Location	Longitude	Latitude
A. tabescens subsp. *orientala* CBS I	JGI: CCBAS213v10	Czech Republic	Null	Null
A. tabescens subsp. *orientala* CBS I	Specimen: HKAS 86604	Italy	Null	Null
A. tibetica (CBS J)	Specimen: HKAS 135503	Lijiang Alpine Botanical Garden, Lijiang, Yunnan Province	100.2306	27.1387
A. tibetica (CBS J)	Specimen: HKAS 46284	On the road from Nagela Village to Xiaomi Mountain, Shangri-La County, Diqing Tibetan Autonomous Prefecture, Yunnan Province	99.6277	28.3082
A. tibetica (CBS J)	Specimen: HKAS 97181	Yeren Sea, Mugecuo Scenic Spot, Yala Township, Kangding City, Ganzi Tibetan Autonomous Prefecture, Sichuan Province	101.8724	30.1702
A. tibetica (CBS J)	Specimen: HKAS 135496	Taiziya，Shennongjia, Hubei Province	110.1931	31.4472
A. tibetica (CBS J)	Specimen: HKAS 135497	Jinhouling, Shennongjia, Hubei Province	110.3085	31.4762
A. tibetica (CBS J)	Strain: CBSJ04043	Shennongjia Mountain, Shennongjia forest region, Hubei Province	110.3166	31.5166
A. tibetica (CBS J)	Strain: CBSJ05018	Taibai Mountain, Mei County, Baoji City, Shaanxi Province	107.8833	34.1166
A. tibetica (CBS J)	Specimen: HKAS 46283	Shangri-La Grand Canyon, Shangri-La County, Diqing Tibetan Autonomous Prefecture, Yunnan Province	99.4628	28.3318
A. tibetica (CBS J)	Specimen: HKAS 48936	Zhile Nature Reserve, Mianning County, Liangshan Yi Autonomous Prefecture, Sichuan Province	102.2294	28.9229

Table C1 (continued)

Phylogenetic/Biological species	Strain/specimen	Location	Longitude	Latitude
A. tibetica (CBS J)	Specimen: HKAS 49375	25km in the direction of Wenda, from Luhuo County, Ganzi Tibetan Autonomous Prefecture, Sichuan Province	100.6760	31.2906
A. tibetica (CBS J)	Specimen: HKAS 51007	Junba Village, Litang County, Ganzi Tibetan Autonomous Prefecture, Sichuan Province	100.2691	29.9942
A. tibetica (CBS J)	Specimen: HKAS 51692	Baiyu County, Ganzi Tibetan Autonomous Prefecture, Sichuan Province	98.8240	31.2096
A. tibetica (CBS J)	Specimen: HKAS 89531	Dalu Township, Jiuzhaigou County, Aba Tibetan and Qiang Autonomous Prefecture, Sichuan Province	103.6710	33.5617
A. tibetica (CBS J)	Specimen: HKAS 89629	Zhubalong Township, Mangkang County, Changdo City, Tibet Autonomous Region	99.0097	29.7757
A. tibetica (CBS J)	Specimen: HMAS 130389	Babao Township, Qilian County, Northern Tibetan Autonomous Prefecture, Qinghai Province	100.2000	38.0166
A. tibetica (CBS J)	Specimen: HMAS 130603	Forestry, Nanmenxia Township, Huzhu Tu Autonomous County, Haidong City, Qinghai Province	101.9666	36.8500
A. tibetica (CBS J)	Specimen: HMAS 132012	Xianmi Farm, Menyuan Hui Autonomous County, Northern Tibetan Autonomous Prefecture, Qinghai Province	101.6333	37.3666
A. tibetica (CBS J)	Specimen: HMAS 132015	Xigou state-owned forest farm, Xigou Township, Haidong Citizen and Hui and Tu Autonomous County, Qinghai Province	102.6591	36.1793

Table C1 (continued)

Phylogenetic/Biological species	Strain/specimen	Location	Longitude	Latitude
A. tibetica (CBS J)	Specimen: HMAS 254250	Lixian County, Aba Tibetan and Qiang Autonomous Prefecture, Sichuan Province	103.1632	31.4358
A. tibetica (CBS J)	Specimen: HMAS 26066	Halihe,Shiligou, Huangyuan County, Xining City, Qinghai Province	100.9690	36.7300
A. tibetica (CBS J)	Specimen: HMAS 26067	Ledu District, Haidong City, Qinghai Province	102.4016	36.4822
A. tibetica (CBS J)	Specimen: HMAS 274442	Tricholoma matsutake reserve in Heshang Village, Xiaojin County, Aba Tibetan and Qiang Autonomous Prefecture, Sichuan Province	102.9019	31.1104
A. tibetica (CBS J)	Specimen: HMAS 274553	Jiabigou, Miyaluo Township, Lixian County, Aba Tibetan and Qiang Autonomous Prefecture, Sichuan Province	102.8300	31.6286
A. tibetica (CBS J)	Specimen: HMAS 274644	Jiu Dao Guai, Shangsi Village, Jiuzhaigou County, Aba Tibetan and Qiang Autonomous Prefecture, Sichuan Province	104.2426	33.2520
A. tibetica (CBS J)	Specimen: HMAS 276211	Xiaqunsi Forest Park, Sitai Township, Ping 'an District, Haidong City, Qinghai Province	101.9084	36.3236
A. tibetica (CBS J)	Specimen: HMAS 276224	Cambra National Forest Park, Jianzha County, Huangnan Tibetan Autonomous Prefecture, Qinghai Province	101.7234	36.1168
A. tibetica (CBS J)	Specimen: HMAS 50996	Yajiang, Yucheng District, Ya'an City, Sichuan Province	103.0415	30.0099
A. tibetica (CBS J)	Specimen: HMAS 86328	Qilian County, Haibei Tibetan Autonomous Prefecture, Qinghai Province	100.2532	38.1771

Table C1 (continued)

Phylogenetic/Biological species	Strain/specimen	Location	Longitude	Latitude
A. tibetica (CBS J)	Specimen: HMAS 86329	Qilian County, Haibei Tibetan Autonomous Prefecture, Qinghai Province	100.2532	38.1771
A. tibetica (CBS J)	Specimen: HMAS 96843	Beishan National Forest Park, Huzhu Tu Autonomous County, Haidong City, Qinghai Province	101.9666	36.8500
A. tibetica (CBS J)	Specimen: HMAS 99098	Babao Township, Qilian County, Haibei Tibetan Autonomous Prefecture, Qinghai Province	100.2000	38.0166
A. tibetica (CBS J)	Commercial Strain: LYT-F31	Yiliang County Tianma Industry Development Center, Yiliang county, Zhaotong City, Yunnan Province	Null	Null
A. tibetica (CBS J)	Specimen: HKAS 135550	National Highway 244, Zuitou Town, Taibai County, Baoji City, Shaanxi Province	107.3145	34.1486
A. tibetica (CBS J)	Specimen: HKAS 135557	Shennongjia Scenic Area, Muyu Town, Shennongjia Forest District, Hubei Province	110.3587	31.4983
A. tibetica (CBS J)	Specimen: HKAS 135558	Shennongjia Scenic Area, Muyu Town, Shennongjia Forest District, Hubei Province	110.3595	31.4986
A. tibetica (CBS J)	Specimen: HKAS 135559	Shennongjia Scenic Area, Muyu Town, Shennongjia Forest District, Hubei Province	110.3595	31.4986
A. tibetica (CBS J)	Specimen: HKAS 135561	Shennongjia Scenic Area, Muyu Town, Shennongjia Forest District, Hubei Province	110.3552	31.4983

Table C1 (continued)

Phylogenetic/Biological species	Strain/specimen	Location	Longitude	Latitude
A. tibetica (CBS J)	Specimen: HKAS 135562	Shennongjia Scenic Area, Muyu Town, Shennongjia Forest District, Hubei Province	110.3541	31.4979
A. tibetica (CBS J)	Specimen: HKAS 135566	Shennongjia Scenic Area, Muyu Town, Shennongjia Forest District, Hubei Province	110.3540	31.4977
A. tibetica (CBS J)	Specimen: HKAS 135567	Shennongjia Scenic Area, Muyu Town, Shennongjia Forest District, Hubei Province	110.3543	31.4977
A. tibetica (CBS J)	Commercial Strain: YLSF-2	Zhaotong Gastrodia Research Institute, Zhaotong City, Yunnan Province	Null	Null
A. tibetica (CBS J)	Commercial Strain: YSLF-2	Zhaotong Gastrodia Research Institute, Zhaotong City, Yunnan Province	Null	Null
A. tibetica (CBS J)	Specimen: HKAS 45974	Near Qiongka Bridge, Karuo District, Changdu City, Tibet Autonomous Region	97.1682	31.1435
A. tibetica (CBS J)	Specimen: HMAS 48351	Batang County, Ganzi Tibetan Autonomous Prefecture, Sichuan Province	99.1105	30.0053
A. tibetica (CBS J)	Strain: 2105604028	Zhagonggou, Milin Town, Linzhi district, Xizang autonomous Region	95.6833	29.7833
A. tibetica (CBS J)	Specimen: HKAS 135502	Lijiang Alpine Botanical Garden, Lijiang, Yunnan Province	100.2323	27.1385
A. tibetica (CBS J)	Specimen: HKAS 135510	Xuejiping, Geza Township, Shangri-La City, Diqing Tibetan Autonomous Prefecture, Yunnan Province	99.8239	28.0069
A. tibetica (CBS J)	Specimen: HKAS 135511	Xuejiping, Geza Township, Shangri-La City, Diqing Tibetan Autonomous Prefecture, Yunnan Province	99.8239	28.0069

Table C1 (continued)

Phylogenetic/Biological species	Strain/specimen	Location	Longitude	Latitude
A. tibetica (CBS J)	Specimen: HKAS 135512	Xuejiping, Geza Township, Shangri-La City, Diqing Tibetan Autonomous Prefecture, Yunnan Province	99.8239	28.0069
A. tibetica (CBS J)	Strain: CBSJ04028	Bayi District, Linzhi City, Xizang Autonomous Region	94.3666	29.6333
A. tibetica (CBS J)	Strain: FM-X	Yadong county, Shigatse City，Xizang Autonomous Region	87.3643	27.9196
A. tibetica (CBS J)	Specimen: HKAS 86609	Shangri-La Shudu Lake Tourism Scenic Spot, Diqing Tibetan Autonomous Prefecture, Yunnan Province	99.9065	27.8025
A. tibetica (CBS J)	Specimen: HKAS 45609	Near Jangda County, Changdu City, Tibet Autonomous Region	98.2183	31.4991
A. tibetica (CBS J)	Specimen: HKAS 45688	Mountain near Zhuge Village, Karuo District, Changdu City, Tibet Autonomous Region	96.9998	31.0958
A. tibetica (CBS J)	Specimen: HKAS 45762	Near Bini Village, Binda Township, Leiwuqi County, Changdu City, Tibet Autonomous Region	96.8367	31.1104
A. tibetica (CBS J)	Specimen: HKAS 45773	In the mountains near Zhuge Village, Karuo District, Changdu City, Tibet Autonomous Region	96.9998	31.0958
A. tibetica (CBS J)	Specimen: HKAS 45807	On the way from Changdo to Tuoba, Karuo District, Changdu City, Tibet Autonomous Region	97.1704	31.1428
A. tibetica (CBS J)	Specimen: HKAS 45820	On the way from Maodu to Toba, Karuo District, Changdu City, Tibet Autonomous Region	97.5293	31.2812

Table C1 (continued)

Phylogenetic/Biological species	Strain/specimen	Location	Longitude	Latitude
A. tibetica (CBS J)	Specimen: HKAS 46314	Shangri-La Grand Canyon, Shangri-La County, Diqing Tibetan Autonomous Prefecture, Yunnan Province	99.4628	28.3318
A. tibetica (CBS J)	Specimen: HKAS 49197	About 15km from Luoxu to Shambuka Pass, Shiqu County, Ganzi Tibetan Autonomous Prefecture, Sichuan Province	97.9953	34.4662
A. tibetica (CBS J)	Specimen: HKAS 51046	Near Xinsan Village, Cangdui Township, Daocheng County, Ganzi Tibetan Autonomous Prefecture, Sichuan Province	100.0987	29.1843
A. tibetica (CBS J)	Specimen: HKAS 54932	Red Mountain, Gezan Township, Shangri-La County, Diqing Tibetan Autonomous Prefecture, Yunnan Province	99.7757	28.0545
A. tibetica (CBS J)	Specimen: HKAS 55489	Daxue Mountain, Shangri-La county, Diqing Tibetan Autonomous Prefecture, Yunnan Province	99.8270	28.5731
A. tibetica (CBS J)	Specimen: HKAS 82505	Hongla Pass, Mangkang County, Changdu City, Tibet Autonomous Region	98.6802	29.2599
A. tibetica (CBS J)	Specimen: HKAS 93952	Near Jiawa Township, Litang County, Ganzi Tibetan Autonomous Prefecture, Sichuan Province	100.3765	29.7569
A. tibetica (CBS J)	Specimen: HKAS 93966	Xuehai Village, Renda Township, luhuo County, Ganzi Tibetan Autonomous Prefecture, Sichuan Province	100.8213	31.2300
A. tibetica (CBS J)	Specimen: HMAS 272511	Motuo county, Linzhi City, Xizang Autonomous Region	95.3189	29.3046
A. tibetica (CBS J)	Specimen: HMAS 272651	Motuo county, Linzhi City, Xizang Autonomous Region	95.3189	29.3046

Table C1 (continued)

Phylogenetic/Biological species	Strain/specimen	Location	Longitude	Latitude
A. tibetica (CBS J)	Specimen: HMAS 51091	WuMing Mountain, Xiangcheng County, Ganzi Tibetan Autonomous Prefecture, Sichuan Province	100.0426	29.1314
A. tibetica (CBS J)	Specimen: HMAS 51095	Western slope of Gongga Mountain, Kangding city, Ganzi Tibetan Autonomous Prefecture, Sichuan Province	101.7179	29.5613
A. tibetica (CBS J)	Specimen: JLK213	Near 317 road from Qamdo, Tibet to Derge County, Sichuan	97.8966	31.4117
A. tibetica (CBS J)	Specimen: HKAS 135478	Geza Township, Shangri-La City, Diqing Tibetan Autonomous Prefecture, Yunnan Province	99.8437	28.0316
A. tibetica (CBS J)	Specimen: HKAS 135484	Xiaotianchi, Shangri-La City, Diqing Tibetan Autonomous Prefecture, Yunnan Province	99.6430	27.6354
A. tibetica (CBS J)	Specimen: HKAS 135482	Pudacuo National Park, Shangri-La City, Diqing Tibetan Autonomous Prefecture, Yunnan Province	99.9818	27.8282
A. tibetica (CBS J)	Specimen: HKAS 135483	Pudacuo National Park, Shangri-La City, Diqing Tibetan Autonomous Prefecture, Yunnan Province	99.9781	27.8289
A. tibetica (CBS J)	Strain: CBSJ04040	Cuona City, Shannan City, Xizang autonomous Region	91.9500	27.9833
A. tibetica (CBS J)	Specimen: HKAS 51258	Gongtso Lake, Bayi District, Linzhi County, Tibet Autonomous Region	94.7287	29.7419
A. tibetica (CBS J)	Specimen: HKAS 57133	About 10km from Lulang Township, Bayi District, Linzhi County, Tibet Autonomous Region	94.7339	29.7228

Table C1 (continued)

Phylogenetic/Biological species	Strain/specimen	Location	Longitude	Latitude
A. tibetica (CBS J)	Specimen: HKAS 89549	Bahe Township, Gongbujiangda County, Linzhi City, Tibet Autonomous Region	93.6652	29.8607
A. tibetica (CBS J)	Specimen: HKAS 90943	Bahe Township, Gongbujiangda County, Linzhi City, Tibet Autonomous Region	93.6652	29.8601
A. tibetica (CBS J)	Specimen: HKAS 94047	Mountain behind Lamaling Monastery, Bujiu Township, Bayi District, Linzhi City, Tibet Autonomous Region	94.3930	29.4566
A. tibetica (CBS J)	Specimen: HMAS 254378	Naidui La Shan Pass, Xiayadong Township, Yadong County, Shigatse City, Xizang Autonomous Region	88.8340	27.3941
A. tibetica (CBS J)	Specimen: HMAS 254476	Chentang Town, Dingjie County, Shigatse City, Xizang Autonomous Region	87.4233	27.8629
A. tibetica (CBS J)	Specimen: HMAS 264994	Dingjie County, Shigatse City, Xizang Autonomous Region	87.7658	28.3641
A. tibetica (CBS J)	Specimen: HMAS 272485	Bomi county, Linzhi City, Xizang Autonomous Region	95.7495	29.8704
A. tibetica (CBS J)	Specimen: HMAS 274066	Chentang Township, Dingjie County, Shigatse City, Xizang Autonomous Region	87.4233	27.8629
A. tibetica (CBS J)	Specimen: HMAS 274072	Nankou inspection station, Yadong County, Shigatse City, Xizang Autonomous Region	88.9071	27.4860
A. tibetica (CBS J)	Specimen: HMAS 274889	Xueshadong Township, Longzi County, Shannan City, Xizang Autonomous Region	92.4617	28.4074

Table C1 (continued)

Phylogenetic/Biological species	Strain/specimen	Location	Longitude	Latitude
A. tibetica (CBS J)	Specimen: HMAS 275000	Nanyigou, Yiluoba Nationality Township, Milin South, Linzhi City, Xizang Autonomous Region	94.2064	29.1598
A. tibetica (CBS J)	Specimen: HKAS 135521	Yadong County, Shigatse City, Xizang Autonomous Region	88.7986	27.4707
A. tibetica (CBS J)	Specimen: HKAS 135518	Yadong County, Shigatse City, Xizang Autonomous Region	88.9992	27.4307
A. tibetica (CBS J)	Specimen: HKAS 135520	Yadong County, Shigatse City, Xizang Autonomous Region	88.9673	27.3964
A. tibetica (CBS J)	Strain: MH	Null	Null	Null
A. tibetica (CBS J)	Specimen: LJW734	74th Legion, Zhaosu County, Zhaosu County, Ilikazak Autonomous Prefecture, Xinjiang Uygur Autonomous Region	80.2326	42.6487
A. tibetica (CBS J)	Strain: CBSJ02044	Nalati Yangshugou, Xinyuan County, Ilikazak Autonomous Prefecture, Xinjiang Uygur Autonomous Region	84.0166	43.2833
A. tibetica (CBS J)	Specimen: HMAS 270241	Jiangbulake Scenic Spot, Qitai County, Changji Hui Autonomous Prefecture, Xinjiang Uygur Autonomous Region	89.5879	44.0200
A. tibetica (CBS J)	Specimen: HMAS 38334	Tomur Peak in Wensu County, Aksu Prefecture, Xinjiang Uygur Autonomous Region	80.5763	41.7738
A. tibetica (CBS J)	Specimen: HMAS 99054	Tianchi, Fukang city, Changji Hui Autonomous Prefecture, Xinjiang Uygur Autonomous Region	88.0500	44.2000

Table C1 (continued)

Phylogenetic/Biological species	Strain/specimen	Location	Longitude	Latitude
A. tibetica (CBS J)	Specimen: HKAS 135474	Dongdatang, Shawan County, Tacheng, Xinjiang Uygur Autonomous Region	85.6716	43.8540
A. tibetica (CBS J)	Specimen: MHHNU 10251	Qiongkushtai Village, Tekes County, Ili Kazakh Autonomous Prefecture, Xinjiang Uygur Autonomous Region	82.2059	42.9122
A. tibetica (CBS J)	Specimen: HKAS 135516	Gongnaisi Forest Farm, Gongnaisi Town, Hejing County, Ili Kazakh Autonomous Prefecture, Xinjiang Uygur Autonomous Region	84.5449	43.3008
A. tibetica (CBS J)	Specimen: HKAS 135517	Nalati town, Xinyuan county, Ili Kazakh Autonomous Prefecture, Xinjiang Uygur Autonomous Region	84.2553	43.2780
A. tibetica (CBS J)	Specimen: GDGM 83473	Sidalong Forest Farm, Sunanyuguzu Autonomous County, Zhangye City, Gansu Province	99.8983	38.4459
A. tibetica (CBS J)	Specimen: HKAS 49177	About 18km from Luoxu to Shambuka Pass, Shiqu County, Ganzi Tibetan Autonomous Prefecture, Sichuan City	97.9953	34.4662
A. tibetica (CBS J)	Specimen: HKAS 53619	Daofu County, Ganzi Tibetan Autonomous Prefecture, Sichuan Province	101.1251	30.9734
A. tibetica (CBS J)	Specimen: HKAS 89519	Baixionggou, Wanglang National Nature Reserve, Pingwu County, Mianyang City, Sichuan Province	104.1580	32.9080

Table C1 (continued)

Phylogenetic/Biological species	Strain/specimen	Location	Longitude	Latitude
A. tibetica (CBS J)	Specimen: HKAS 89525	Zhugencha, Wanglang National Nature Reserve, Pingwu County, Mianyang City, Sichuan Province	104.0674	32.9386
A. tibetica (CBS J)	Specimen: HMAS 254774	Shuangqiao Goukou, Siguniang Mountain Town, Xiaojin County, Aba Tibetan and Qiang Autonomous Prefecture, Sichuan Province	102.7718	30.9790
A. tibetica (CBS J)	Specimen: HMAS 268710	Songpan County, Aba Tibetan and Qiang Autonomous Prefecture, Sichuan Province	103.5934	32.5275
A. tibetica (CBS J)	Specimen: HMAS 274349	Siguniang Mountain, Xiaojin County, Aba Tibetan and Qiang Autonomous Prefecture, Sichuan Province	102.9019	31.1104
A. tibetica (CBS J)	Specimen: HMAS 50997	Wolong Nature Reserve, Wenchuan County, Aba Tibetan and Qiang Autonomous Prefecture, Sichuan Province	103.1434	31.1403
A. tibetica (CBS J)	Specimen: HMAS 99623	Mengda National Nature Reserve, Xunhua Salar Autonomous County, Haidong City, Qinghai Province	102.6943	35.8094
A. violacea (CBS N) lineage 1-mtDNA	Specimen: HKAS 135495	Heishuihe, Yanjiawan, Muyu Town, Shennongjia, Hubei Province	110.4315	31.4887
A. violacea (CBS N) lineage 1-mtDNA	Specimen: HKAS 135491	Heishuihe, Yanjiawan, Muyu Town, Shennongjia, Hubei Province	110.4317	31.4893
A. violacea (CBS N) lineage 1-mtDNA	Strain: 21SNJ17	Heishuihe, Yanjiawan, Muyu Town, Shennongjia, Hubei Province	110.4310	31.4930
A. violacea (CBS N) lineage 1-mtDNA	Specimen: HKAS 135494	Dajiu lake, Shennongjia, Hubei Province	109.9978	31.4779

Table C1 (continued)

Phylogenetic/Biological species	Strain/specimen	Location	Longitude	Latitude
A. violacea (CBS N) lineage 1-mtDNA	Specimen: HKAS 135498	Near Shennong Hotel, Shennongjia, Hubei Province	110.3493	31.5030
A. violacea (CBS N) lineage 1-mtDNA	Specimen: HKAS 135499	Near Shennong Hotel, Shennongjia, Hubei Province	110.3493	31.5030
A. violacea (CBS N) lineage 1-mtDNA	Strain: CBSN02066	Emei Mountain, Emeishan City, Leshan City, Sichuan Province	103.3500	29.5666
A. violacea (CBS N) lineage 1-mtDNA	Strain: CBSN02067	Emei Mountain, Meishan city, Leshan City, Sichuan Province	103.3500	29.5666
A. violacea (CBS N) lineage 1-mtDNA	Strain: CBSN02068	Emei Mountain, Meishan city, Leshan City, Sichuan Province	103.3500	29.5666
A. violacea (CBS N) lineage 1-mtDNA	Strain: CBSN02069	Emei Mountain, Meishan city, Leshan City, Sichuan Province	103.3500	29.5666
A. violacea (CBS N) lineage 1-mtDNA	Strain: CBSN02070	Emei Mountain, Meishan city, Leshan City, Sichuan Province	103.3500	29.5666
A. violacea (CBS N) lineage 1-mtDNA	Strain: CBSN16022	Lingyun village, Niuzhuang town, Wufeng Tujia Autonomous County, Yichang City, Hubei Province	110.3833	30.2333
A. violacea (CBS N) lineage 1-mtDNA	Strain: CBSN19098	Yangzixi, Houhe nature reserve, Wufeng Tujia Autonomous County, Yichang City, Hubei Province	110.5333	30.0667
A. violacea (CBS N) lineage 1-mtDNA	Strain: CBSN19107	Zhanglaoping, Emei Mountain, Dongpo District, Meishan City, Sichuan Province	103.6166	29.9666
A. violacea (CBS N) lineage 1-mtDNA	Strain: CBSNW16024	Shennongjia International skiing park, Shennongjia forest region, Hubei Province	110.4166	31.6666

Table C1 (continued)

Phylogenetic/Biological species	Strain/specimen	Location	Longitude	Latitude
A. violacea (CBS N) lineage 1-mtDNA	Strain: DG	Mugan Town, Daguan County, Zhaotong City, Yunnan Province	104.0209	28.1837
A. violacea (CBS N) lineage 1-mtDNA	Specimen: HKAS 135560	Shennongjia Scenic Area, Muyu Town, Shennongjia Forest District, Hubei Province	110.3565	31.4972
A. violacea (CBS N) lineage 1-mtDNA	Specimen: HKAS 135563	Shennongjia Scenic Area, Muyu Town, Shennongjia Forest District, Hubei Province	110.3535	31.4981
A. violacea (CBS N) lineage 1-mtDNA	Specimen: HKAS 135564	Shennongjia Scenic Area, Muyu Town, Shennongjia Forest District, Hubei Province	110.3534	31.4979
A. violacea (CBS N) lineage 1-mtDNA	Specimen: HKAS 135565	Shennongjia Scenic Area, Muyu Town, Shennongjia Forest District, Hubei Province	110.3535	31.4978
A. violacea (CBS N) lineage 1-mtDNA	Strain: YLCTM	Chaotianma National Nature Reserve in Wumeng Mountain, Yunnan	104.3481	27.7996
A. violacea (CBS N) lineage 1-mtDNA	Strain: ZZZT01	Xiaocaoba Town, Yiliang County, Zhaotong City, Yunnan Province	104.3508	27.7979
A. xiaocaobaensis (CBS P)	Strain: 19060	Yangzixi, Houhe nature reserve, Wufeng Tujia Autonomous County, Yichang City, Hubei Province	110.5333	30.0666
A. xiaocaobaensis (CBS P)	Strain: 19062	Yangzixi, Houhe nature reserve, Wufeng Tujia Autonomous County, Yichang City, Hubei Province	110.5333	30.0666
A. xiaocaobaensis (CBS P)	Strain: SWFC 12638	Xiaocaoba Town, Yiliang County, Zhaotong City, Yunnan Province	104.3785	27.7743

Table C1 (continued)

Phylogenetic/Biological species	Strain/specimen	Location	Longitude	Latitude
A. xiaocaobaensis (CBS P)	Commercial Strain: LYT-F17	Yiliang County Tianma Industry Development Center, Yiliang county, Zhaotong City, Yunnan Province	Null	Null
A. xiaocaobaensis (CBS P)	Strain: QZ19053	Yangzixi, Houhe nature reserve, Wufeng County, Hubei Province	110.5333	30.0667
A. xiaocaobaensis (CBS P)	Strain: QZ19054	Yangzixi, Houhe nature reserve, Wufeng County, Hubei Province	110.5333	30.0665
A. xiaocaobaensis (CBS P)	Strain: QZ19055	Yangzixi, Houhe nature reserve, Wufeng County, Hubei Province	110.5345	30.0632
A. xiaocaobaensis (CBS P)	Strain: QZ19058	Yangzixi, Houhe nature reserve, Wufeng County, Hubei Province	110.5442	30.0689
A. xiaocaobaensis (CBS P)	Strain: QZ19059	Yangzixi, Houhe nature reserve, Wufeng County, Hubei Province	110.5366	30.0676
A. xiaocaobaensis (CBS P)	Strain: QZ19061	Heiwanya, Mulinzi Nature reserve, Hefeng County, Hubei Province	110.2000	30.0333
A. xiaocaobaensis (CBS P)	Commercial Strain: ZT-14	Hubei Jun Zhongshi "湖北菌钟氏"	Null	Null
A. xiaocaobaensis (CBS P)	Commercial Strain: ZT-29	Hong Sheng "鸿升"	Null	Null
A. xiaocaobaensis (CBS P)	Commercial Strain: ztmh-30	Zhaotong Gastrodia Research Institute, Zhaotong City, Yunnan Province	Null	Null
Armillaria sp. CMW 4456	JGI: CMW 4456	Zimbabwe	Null	Null
Armillaria sp. PXL (CBS F) lineage 2-mtDNA	Strain: PXL	Peng Shaolong "彭少龙"	Null	Null
Guyanagaster necrorhiza	NCBI: SRR4125583_1_4	Null	Null	Null

Table C2 BUSCO estimation results of all nuclear genomes

Samples	heterozygosity rate	Samples	heterozygosity rate	Samples	heterozygosity rate
21043	0.1121	HMAS248128	0.1186	MHHNU8836	0.0336
2104919020	0.1318	HMAS253414	0.3736	MW-27	0.117
2105604028	0.1548	HMAS253478	0.0674	NLT01	0.1009
21HH01	0.1666	HMAS253500	0.146	NLT05	0.0997
21HH02	0.1707	HMAS253828	0.1507	PXL	0.1456
21HH03	0.1523	HMAS254250	0.1434	QA1	0.1678
21HH04	0.1472	HMAS254378	0.134	QF13	0.1623
21LJ03	0.4727	HMAS254476	0.1451	QM2	0.1625
21LJ05	0.1579	HMAS254774	0.156	QM3	0.1633
21LJ06	0.1709	HMAS255468	0.1233	QZ000201-2	0.3282
21LJ07	0.1713	HMAS255489	0.1242	SA-19	0.1497
21LJ09	0.4397	HMAS255521	0.1437	SJ02	0.1405
21LJ10	0.1475	HMAS255525	0.1435	SJ06	0.1366
21LJ11	0.482	HMAS255529	0.1442	SJ07	0.138
21SNJ01	0.1525	HMAS26066	0.1242	SJ10	0.0822
21SNJ05	0.3644	HMAS26067	0.1227	SJ102	0.1518
21SNJ11	0.144	HMAS264994	0.1521	SJ103	0.1553
21SNJ13	0.1512	HMAS268710	0.1496	SJ104	0.1506
21SNJ17	0.1458	HMAS270241	0.0918	SJ105	0.0702
21SNJ18	0.0985	HMAS272369	0.4056	SJ106	0.3864
21SNJ19	0.1012	HMAS272390	0.0979	SJ113	0.3629
21SNJ21	0.152	HMAS272485	0.1402	SJ115	0.3719
21SNJ22	0.1459	HMAS272511	0.1549	SJ116	0.3644
21SNJ24	0.1508	HMAS272515	0.0953	SJ131	0.1476
21SNJ25	0.1474	HMAS272641	0.0647	SJ135	0.1494
21SNJ26	0.1471	HMAS272651	0.1527	SJ136	0.1503
221003WSP	0.5213	HMAS273634	0.1422	SJ139	0.1536
22DWS03	0.126	HMAS273636	0.1463	SJ141	0.1496
22DWS04	0.1409	HMAS274066	0.145	SJ142	0.1506
22KM01	0.4521	HMAS274072	0.1413	SJ143	0.1529
22KM02	0.4562	HMAS274349	0.1537	SJ144	0.152
22KM03	0.4864	HMAS274442	0.1565	SJ145	0.1534
22LL03	0.526	HMAS274553	0.1571	SJ146	0.1527
5H	0.1689	HMAS274644	0.1572	SJ147	0.1533
6	0.1694	HMAS274889	0.1448	SJ150	0.1494
87-45	0.1911	HMAS275000	0.1453	SJ151	0.1516
A10	0.4765	HMAS276211	0.1445	SJ152	0.1464
AHLD-A9	0.1622	HMAS276224	0.1319	SJ153	0.1508
Ar-3	0.1574	HMAS276553	0.1483	SJ154	0.1506

Table C2 (continued)

Samples	heterozygosity rate	Samples	heterozygosity rate	Samples	heterozygosity rate
Ar-8	0.1584	HMAS281266	0.1222	SJ155	0.1524
Ar-9	0.153	HMAS33561	0.4457	SJ156	0.1535
BD4H	0.1403	HMAS33891	0.1364	SJ158	0.1522
BJ-M1	0.1637	HMAS37384	0.1397	SJ159	0.1545
C21019	0.0832	HMAS38334	0.0863	SJ161	0.1516
CFY-1	0.1634	HMAS48351	0.1454	SJ162	0.1532
CFY-2	0.1663	HMAS50995	0.5235	SJ164	0.1467
CLZ12638	0.0769	HMAS50996	0.1561	SJ172	0.15
DBRGZP	0.1647	HMAS50997	0.1568	SJ175	0.1512
DG	0.156	HMAS51088	0.3322	SJ176	0.1507
FM21-172	0.4379	HMAS51091	0.1476	SJ177	0.15
FM21-173	0.4456	HMAS51095	0.1425	SJ180	0.1508
FM22-210	0.4673	HMAS61574	0.1484	SJ181	0.1476
FM22-211	0.4634	HMAS61686	0.1541	SJ182	0.1531
FM22-215	0.4691	HMAS63163	0.1115	SJ22	0.1366
FM22-216	0.4413	HMAS86328	0.1277	SJ27	0.1409
FM-X	0.1611	HMAS86329	0.1285	SJ28	0.1403
GDGM70002	0.2356	HMAS96843	0.1427	SJ31	0.1418
GDGM70010	0.2403	HMAS96967	0.1326	SJ35	0.1383
GDGM71117	0.1705	HMAS96969	0.1285	SJ38	0.1432
GDGM76532	0.5617	HMAS97093	0.1367	SJ39	0.1416
GDGM77873	0.1132	HMAS99054	0.1014	SJ40	0.1395
GDGM83473	0.1391	HMAS99098	0.1378	SJ42	0.1413
guo117	0.1621	HMAS99623	0.1294	SJ63	0.1397
guo19	0.1475	HMIGD71175	0.1677	SJ73	0.1389
guo230	0.315	HMJAU22761	0.1389	SJ75	0.1482
guo237-	0.3183	HMJAU22795	0.1542	SJ76	0.1459
guo238-	0.3432	HMJAU23501	0.1375	SJ79	0.1514
guo239-	0.3084	HMJAU23629	0.1626	SJ85	0.1561
guo242-	0.4085	HMJAU23737	0.1565	SJ93	0.1496
guo247	0.4278	HMJAU24389	0.1386	SJ94	0.1559
guo248-	0.4011	HMJAU25401	0.1688	SJ96	0.1399
guo249	0.4657	HMJAU25404	0.1663	SJ97	0.1584
guo252	0.5241	HMJAU25478	0.1725	SM-1	0.1423
guo256	0.46	HMJAU28932	0.1726	SM18	0.1633
guo349	0.1661	HMJAU28935	0.1534	SNJ20	0.0945
guo37-	0.1181	HMJAU33876	0.137	SS-01	0.1603
guo7	0.1633	HMJAU42023	0.1674	SX_M1	0.0665
guo82	0.1156	HMJAU42034	0.1634	SX_M2	0.1579

Table C2 (continued)

Samples	heterozygosity rate	Samples	heterozygosity rate	Samples	heterozygosity rate
HB-1	0.1509	HMJAU55082	0.1391	T11	0.1461
HB-2	0.1501	HMJAU60448	0.1527	T12	0.1665
HB-3	0.1602	HMJAU60486	0.1489	T14	0.1567
HB-4	0.1615	HMJAU60487	0.1402	T19	0.168
HB-5	0.1612	HMJAU6143	0.1662	T20	0.1201
HB-6	0.1451	HMJAU7339	0.1694	T21	0.168
HDY	0.1682	HS-01	0.1576	T25	0.1602
HKAS45609	0.1718	HS-A25	0.1497	T27	0.1304
HKAS45688	0.1398	HS-A9	0.168	T28	0.1423
HKAS45762	0.1359	J234	0.1447	T3	0.134
HKAS45773	0.1653	JLK003	0.4073	T6	0.1674
HKAS45807	0.1542	JLK213	0.154	T9	0.1524
HKAS45820	0.1254	JLK921	0.0437	TX	0.1666
HKAS45821	0.1687	KIB5-guo90	0.133	WGS1051	0.4151
HKAS45974	0.1492	KIB6-guo322	0.1331	WGS75	0.1077
HKAS46275	0.4126	KIB7-guo345	0.1422	WSB-M1	0.1117
HKAS46283	0.1227	KIB9-GUO278	0.0476	XCB003	0.3552
HKAS46284	0.1384	LDM-18	0.0429	Xu156	0.3496
HKAS46314	0.1454	LD-M8	0.1692	XY2	0.1408
HKAS48804	0.1238	LEI_439	0.0986	XZ151	0.0484
HKAS48936	0.1519	LEI_860	0.1416	XZ199	0.0504
HKAS49004	0.5678	LEI374	0.1467	XZ258	0.4733
HKAS49177	0.1627	LEI768	0.1433	Y3	0.1403
HKAS49197	0.1471	LH-22	0.071	YLCTM	0.056
HKAS49375	0.1503	LJW1577	0.1663	YLSF-2	0.1627
HKAS50184	0.1372	LJW1634	0.1539	YSLF-1	0.165
HKAS51007	0.1542	LJW1854	0.3882	YSLF-2	0.1634
HKAS51046	0.1542	LJW1870	0.4462	YSM_470	0.1347
HKAS51258	0.1318	LJW2225	0.3666	YSM_472	0.144
HKAS51692	0.1691	LJW2229	0.417	YSM_474	0.144
HKAS52389	0.3237	LJW2248	0.3902	YSM_481	0.1398
HKAS53619	0.1446	LJW2249	0.4189	ZG-26	0.0604
HKAS54932	0.1524	LJW2388	0.1582	ZM	0.1592
HKAS55489	0.1741	LJW2390	0.1582	ZT-10	0.1572
HKAS56108	0.1328	LJW668	0.1093	ZT11	0.1618
HKAS56216	0.1442	LJW779	0.4049	ZT-12	0.1625
HKAS57133	0.1416	LJW849	0.4478	ZT-14	0.0667
HKAS57446	0.3399	LM-1	0.1472	ZT15	0.1415
HKAS58683	0.0452	LM-2	0.1252	ZT-18	0.1537

Table C2 (continued)

Samples	heterozygosity rate	Samples	heterozygosity rate	Samples	heterozygosity rate
HKAS58853	0.1044	LYT-A9	0.1267	ZT-2	0.1665
HKAS58910	0.0519	LYT-F01	0.1468	ZT20	0.1602
HKAS58911	0.3758	LYT-F05	0.1267	ZT-21	0.1641
HKAS68003	0.4453	LYT-F17	0.0671	ZT22	0.1625
HKAS68632	0.3827	LYT-F19	0.1503	ZT-23	0.1602
HKAS68678	0.4232	LYT-F31	0.0471	ZT24	0.1637
HKAS74997	0.3864	LYT-F34	0.1241	ZT25	0.1633
HKAS80228	0.0588	LYT-Y1	0.1309	ZT26	0.1639
HKAS81274	0.407	LZL-1	0.1512	ZT27	0.153
HKAS81827	0.3549	LZL-10	0.1577	ZT28	0.1602
HKAS81828	0.445	LZL-11	0.1562	ZT-29	0.0667
HKAS81829	0.3211	LZL-12	0.1573	ZT-3	0.1608
HKAS81830	0.4441	LZL-13	0.1571	ZT31	0.1633
HKAS81831	0.3018	LZL-15	0.1561	ZT-32	0.1648
HKAS81832	0.434	LZL-16	0.1405	ZT-33	0.1632
HKAS81834	0.3333	LZL-17	0.1451	ZT-34	0.1398
HKAS82101	0.2985	LZL-18	0.135	ZT-35	0.1549
HKAS82475	0.3682	LZL-19	0.1513	ZT-36	0.1536
HKAS82505	0.1584	LZL2	0.1539	ZT37	0.1586
HKAS87145	0.437	LZL20	0.156	ZT38	0.1633
HKAS89519	0.1569	LZL-4	0.1523	ZT-39	0.1528
HKAS89525	0.1601	LZL-5	0.0864	ZT-4	0.1552
HKAS89531	0.1402	LZL-6	0.1561	ZT-40	0.1584
HKAS89549	0.1435	LZL-7	0.1537	ZT-41	0.1655
HKAS89629	0.1613	LZL-8	0.1672	ZT-42	0.1567
HKAS90943	0.1384	LZL-9	0.1488	ZT-43	0.1531
HKAS92018	0.1495	LZP-11	0.0668	ZT-44	0.1579
HKAS93952	0.1612	LZP-15	0.1375	ZT-45	0.1646
HKAS93966	0.153	MF266	0.1429	ZT-46	0.1624
HKAS94047	0.1411	MF-M5	0.1322	ZT-6	0.1619
HKAS95344	0.1485	MF-M6	0.144	ZT7	0.1589
HKAS97181	0.1733	MH	0.124	ZT-8	0.1522
HMAS130389	0.1458	MHHNU10251	0.0951	ZT-M6	0.1401
HMAS130603	0.1254	MHHNU31060	0.1571	ZT-MF	0.1313
HMAS131062	0.0956	MHHNU31772	0.1489	ZTMH-036	0.1677
HMAS132012	0.1381	MHHNU31945	0.4588	ztmh-1	0.1427
HMAS132015	0.131	MHHNU7419	0.2778	ztmh-13	0.1428
HMAS145183	0.1512	MHHNU7577	0.1582	ztmh-30	0.0711
HMAS22781-	0.1675	MHHNU7783	0.1021	ZZZT01	0.157

Table C2 (continued)

Samples	heterozygosity rate	Samples	heterozygosity rate	Samples	heterozygosity rate
HMAS22782	0.139	MHHNU8447	0.1384	CBSG19037	0.4563
HMAS23066	0.4736	MHHNU8577	0.3827		

Table C3 Mitochondrial assembly results, including genome length, structural type, and ambiguous configuration status

Taxa	sample	length	Mt genome type	Ambiguous configuration
A. algida	BD4H	112070	Circle	No
A. algida	CBSO19095	85699	Circle	No
A. algida	guo19	103632	Circle	No
A. algida	guo37	78132	Circle	No
A. algida	HMAS253478	79497	Circle	No
A. algida	HMAS272641	92822	Circle	No
A. algida	KIB6-guo322	80884	Circle	No
A. algida	LM-1	112074	Circle	No
A. algida	LYT-F05	86980	Circle	No
A. algida	LYT-F19	115093	Circle	No
A. algida	LYT-F34	112917	Circle	No
A. algida	LYT-Y1	112074	Circle	No
A. algida	MF-M6	112074	Circle	No
A. algida	MHHNU8447	100761	Circle	No
A. algida	SM-1	113988	Circle	No
A. algida	ZT-MF	112073	Circle	No
A. algida	ZT15	95592	Circle	No
A. algida	ZT-M6	112074	Circle	No
A. algida	ztmh-1	112074	Circle	No
A. algida	19080	102038	Circle	No
A. algida	ztmh-13	112074	Circle	No
A. altimontana	ALTI	120359	Circle	No
A. amygdaliformospora	CBSL17017_graph7	102622	Circle	Yes
A. amygdaliformospora	CBSLW17003	90869	Circle	No
A. amygdaliformospora	CBSLW17016_graph8	102622	Circle	Yes
A. amygdaliformospora	CBSLW17039	101658	Circle	No
A. amygdaliformospora	GDGM71117	96884	Circle	No
A. amygdaliformospora	guo271	105663	Circle	No

Table C3 (continued)

Taxa	sample	length	Mt genome type	Ambiguous configuration
A. amygdaliformospora	guo272	105662	Circle	No
A. amygdaliformospora	guo324	86156	Circle	No
A. amygdaliformospora	guo82	82866	Circle	No
A. amygdaliformospora	HMAS22781	101186	Circle	No
A. amygdaliformospora	HMIGD71175	114922	Circle	No
A. amygdaliformospora	KIB5-guo90	106629	Circle	No
A. amygdaliformospora	KIB9-GUO278	97144	Circle	No
A. amygdaliformospora	LH-22	98254	Circle	No
A. amygdaliformospora	LW17027	104619	Circle	No
A. amygdaliformospora	LYT-F01	85701	Circle	No
A. amygdaliformospora	LZP-11	81645	Circle	No
A. amygdaliformospora	LZP-15	81645	Circle	No
A. amygdaliformospora	MHHNU31060	114958	Circle	No
A. amygdaliformospora	MHHNU31772	114952	Circle	No
A. amygdaliformospora	MW-27	99714	Circle	No
A. amygdaliformospora	TX	96447	Circle	No
A. amygdaliformospora	YSLF-1	109118	Scaffolds	NA
A. amygdaliformospora	ZG-26	124817	Circle	No
A. amygdaliformospora	ZTMH-036	83448	Circle	No
A. borealis subsp. *borealis*	ARMILLARIA_BOREALIS	116433	Circle	No
A. borealis subsp. *borealis*	GDGM77873	118215	Circle	No
A. borealis subsp. *borealis*	guo338	116389	Circle	No
A. borealis subsp. *borealis*	KK902525	116389	Circle	No
A. borealis subsp. *borealis*	MH407470	116433	Circle	No
A. borealis subsp. *sinoborealis*	21SNJ18	105739	Scaffolds	NA
A. borealis subsp. *sinoborealis*	21SNJ19	105603	Scaffolds	NA
A. borealis subsp. *sinoborealis*	CBSM01012	105390	Circle	No
A. borealis subsp. *sinoborealis*	CBSM01013	105390	Circle	No
A. borealis subsp. *sinoborealis*	CBSM01019	105389	Circle	No

Table C3 (continued)

Taxa	sample	length	Mt genome type	Ambiguous configuration
A. borealis subsp. *sinoborealis*	CBSM04019	105386	Circle	No
A. borealis subsp. *sinoborealis*	CBSM05020	105367	Circle	No
A. borealis subsp. *sinoborealis*	CBSM05021	105392	Circle	No
A. borealis subsp. *sinoborealis*	guo336	105391	Circle	No
A. borealis subsp. *sinoborealis*	HMAS131062	105393	Circle	No
A. borealis subsp. *sinoborealis*	HMAS63163	105393	Circle	No
A. borealis subsp. *sinoborealis*	SNJ20	105385	Circle	No
A. bruneocystidia	21LJ05_graph2	96047	Circle	Yes
A. bruneocystidia	21LJ10_graph1	88395	Circle	Yes
A. bruneocystidia	CBSH00019	102491	Circle	No
A. bruneocystidia	CBSH0006	92469	Circle	No
A. bruneocystidia	CBSH19074_graph2	109098	Circle	Yes
A. bruneocystidia	CBSH99011_graph1	104662	Circle	Yes
A. bruneocystidia	CBSH99028_graph1	101434	Circle	Yes
A. bruneocystidia	guo260_graph2	104665	Circle	Yes
A. bruneocystidia	HKAS48804	103410	Circle	No
A. bruneocystidia	HKAS56216	99900	Circle	No
A. bruneocystidia	HMAS253500	104952	Circle	No
A. bruneocystidia	HMAS272390_graph1	84959	Circle	Yes
A. bruneocystidia	HMAS272515_graph2	89707	Circle	Yes
A. bruneocystidia	MF266_graph1	109556	Circle	Yes
A. calvescens	B621	133290	Scaffolds	NA
A. cepistipes	19041	105717	Circle	No
A. cepistipes	19042	108108	Circle	No
A. cepistipes	KK890661_1	103532	Circle	No
A. conifericola	21043	134999	Circle	No
A. conifericola	CBSD02171	139690	Circle	No
A. conifericola	CBSD21030	144618	Circle	No
A. conifericola	CBSD5193	138482	Circle	No

Table C3 (continued)

Taxa	sample	length	Mt genome type	Ambiguous configuration
A. conifericola	CBSD5295	138481	Circle	No
A. conifericola	CBSD93025	131461	Circle	No
A. conifericola	CBSD96043	117604	Circle	No
A. conifericola	HMAS145183	115822	Circle	No
A. conifericola	HMJAU25401	128295	Circle	No
A. conifericola	HMJAU25404	126426	Circle	No
A. conifericola	HMJAU25478	139925	Circle	No
A. conifericola	HMJAU28932	126428	Circle	No
A. conifericola	HMJAU42023	138995	Circle	No
A. conifericola	HMJAU42034	138995	Circle	No
A. conifericola	HMJAU6143	123716	Circle	No
A. conifericola	HMJAU7339	126425	Circle	No
A. ectypa	ectypa	86926	Scaffolds	NA
A. ectypa	guo216	86928	Circle	No
A. ectypa	guo246	86928	Circle	No
A. ectypa	KK700113	86928	Circle	No
A. fumosa	fumosa	128272	Scaffolds	NA
A. gallica subsp. *calidusa*	21HH03_graph2	96291	Circle	Yes
A. gallica subsp. *calidusa*	21HH04_graph2	96291	Circle	Yes
A. gallica subsp. *calidusa*	5H_graph2	96291	Circle	Yes
A. gallica subsp. *calidusa*	6_graph1	96291	Circle	No
A. gallica subsp. *calidusa*	AHLD-A9_graph2	96291	Circle	Yes
A. gallica subsp. *calidusa*	BJ-M1_graph1	120769	Circle	Yes
A. gallica subsp. *calidusa*	CBSB03002_graph1	116108	Circle	Yes
A. gallica subsp. *calidusa*	CBSB19011_graph1	100383	Circle	Yes
A. gallica subsp. *calidusa*	CBSB19014_graph2	88656	Circle	Yes
A. gallica subsp. *calidusa*	CBSB19036_graph2	96291	Circle	Yes
A. gallica subsp. *calidusa*	CBSB96003	90231	Scaffolds	NA
A. gallica subsp. *calidusa*	CBSB96004_graph2	124742	Circle	Yes
A. gallica subsp. *calidusa*	CBSB96011	118917	Scaffolds	NA
A. gallica subsp. *calidusa*	CBSB96031_graph2	119156	Circle	Yes
A. gallica subsp. *calidusa*	CBSB96032	107244	Circle	No
A. gallica subsp. *calidusa*	CFY-1_graph1	120769	Circle	Yes
A. gallica subsp. *calidusa*	CFY-2_graph1	120768	Circle	Yes
A. gallica subsp. *calidusa*	DBRGZP_graph1	96291	Circle	Yes

Table C3 (continued)

Taxa	sample	length	Mt genome type	Ambiguous configuration
A. gallica subsp. *calidusa*	GUO349_graph2	96291	Circle	Yes
A. gallica subsp. *calidusa*	HB-1_graph2	96290	Circle	Yes
A. gallica subsp. *calidusa*	HB-2_graph1	96290	Circle	Yes
A. gallica subsp. *calidusa*	HB-3_graph1	120769	Circle	Yes
A. gallica subsp. *calidusa*	HB-4_graph1	96290	Circle	Yes
A. gallica subsp. *calidusa*	HB-5_graph2	120769	Circle	Yes
A. gallica subsp. *calidusa*	HB-6_graph2	96291	Circle	Yes
A. gallica subsp. *calidusa*	HDY_graph1	96291	Circle	Yes
A. gallica subsp. *calidusa*	HKAS45821_graph2	122621	Circle	Yes
A. gallica subsp. *calidusa*	HKAS92018_graph1	108562	Circle	Yes
A. gallica subsp. *calidusa*	HMAS255521_graph1	88657	Circle	Yes
A. gallica subsp. *calidusa*	HMAS255525_graph2	88657	Circle	Yes
A. gallica subsp. *calidusa*	HMAS255529_graph1	112165	Circle	Yes
A. gallica subsp. *calidusa*	HMAS273634	112018	Scaffolds	NA
A. gallica subsp. *calidusa*	HMAS276553	95735	Circle	No
A. gallica subsp. *calidusa*	HMAS33891_graph2	110971	Circle	Yes
A. gallica subsp. *calidusa*	HMAS37384_graph1	101663	Circle	Yes
A. gallica subsp. *calidusa*	HMAS61574_graph2	104052	Circle	Yes
A. gallica subsp. *calidusa*	HMAS96967	117367	Scaffolds	NA
A. gallica subsp. *calidusa*	HMAS97093_graph2	116002	Circle	Yes
A. gallica subsp. *calidusa*	HMJAU55082_graph1	121027	Circle	Yes
A. gallica subsp. *calidusa*	HMJAU60448_graph1	110792	Circle	Yes
A. gallica subsp. *calidusa*	HS-01_graph1	120767	Circle	Yes
A. gallica subsp. *calidusa*	HS-A25_graph1	96291	Circle	Yes
A. gallica subsp. *calidusa*	HS-A9_graph1	96291	Circle	Yes
A. gallica subsp. *calidusa*	J234_graph2	96290	Circle	Yes
A. gallica subsp. *calidusa*	KIB7-GUO345_graph1	96291	Circle	Yes
A. gallica subsp. *calidusa*	LDM-18	93753	Circle	No
A. gallica subsp. *calidusa*	LM-2_graph1	96291	Circle	Yes
A. gallica subsp. *calidusa*	LYT-A9_graph1	96291	Circle	Yes
A. gallica subsp. *calidusa*	LZL-1_graph2	120768	Circle	Yes
A. gallica subsp. *calidusa*	LZL-10_graph2	96291	Circle	Yes
A. gallica subsp. *calidusa*	LZL-11_graph2	96291	Circle	Yes
A. gallica subsp. *calidusa*	LZL-12_graph1	96291	Circle	Yes
A. gallica subsp. *calidusa*	LZL-13_graph1	96269	Circle	Yes

Table C3 (continued)

Taxa	sample	length	Mt genome type	Ambiguous configuration
A. gallica subsp. *calidusa*	LZL-15_graph2	96291	Circle	Yes
A. gallica subsp. *calidusa*	LZL-16_graph1	120768	Circle	Yes
A. gallica subsp. *calidusa*	LZL-17_graph2	120769	Circle	Yes
A. gallica subsp. *calidusa*	LZL-18_graph2	120769	Circle	Yes
A. gallica subsp. *calidusa*	LZL-19_graph2	120744	Circle	Yes
A. gallica subsp. *calidusa*	LZL2_graph1	96290	Circle	Yes
A. gallica subsp. *calidusa*	LZL20_graph1	120768	Circle	Yes
A. gallica subsp. *calidusa*	LZL-4_graph2	94098	Circle	Yes
A. gallica subsp. *calidusa*	LZL-6_graph1	96290	Circle	Yes
A. gallica subsp. *calidusa*	LZL-7_graph1	120769	Circle	Yes
A. gallica subsp. *calidusa*	LZL-8_graph2	96291	Circle	Yes
A. gallica subsp. *calidusa*	LZL-9_graph1	120768	Circle	Yes
A. gallica subsp. *calidusa*	MF-M5_graph1	96291	Circle	Yes
A. gallica subsp. *calidusa*	OR783479	120789	unknown	NA
A. gallica subsp. *calidusa*	OR783479	120789	unknown	NA
A. gallica subsp. *calidusa*	OR885310	120775	unknown	NA
A. gallica subsp. *calidusa*	OR885311	120839	unknown	NA
A. gallica subsp. *calidusa*	OR885312	120785	unknown	NA
A. gallica subsp. *calidusa*	OR885313	120778	unknown	NA
A. gallica subsp. *calidusa*	QA1_graph1	96291	Circle	Yes
A. gallica subsp. *calidusa*	QF13_graph2	120769	Circle	Yes
A. gallica subsp. *calidusa*	QM2_graph2	120769	Circle	Yes
A. gallica subsp. *calidusa*	QM3_graph1	120768	Circle	Yes
A. gallica subsp. *calidusa*	SA-19_graph2	96291	Circle	Yes
A. gallica subsp. *calidusa*	SJ02_graph1	107640	Circle	Yes
A. gallica subsp. *calidusa*	SJ06_graph1	107640	Circle	Yes
A. gallica subsp. *calidusa*	SJ07_graph2	107640	Circle	Yes
A. gallica subsp. *calidusa*	SJ10_graph1	117049	Scaffolds	NA
A. gallica subsp. *calidusa*	SJ103_graph1	114784	Circle	Yes
A. gallica subsp. *calidusa*	SJ104_graph2	114784	Circle	Yes
A. gallica subsp. *calidusa*	SJ105_graph1	117349	Circle	Yes
A. gallica subsp. *calidusa*	SJ150_graph2	109866	Circle	Yes
A. gallica subsp. *calidusa*	SJ151_graph1	109866	Circle	Yes
A. gallica subsp. *calidusa*	SJ152_graph2	109866	Circle	Yes
A. gallica subsp. *calidusa*	SJ153_graph2	109866	Circle	Yes

Table C3 (continued)

Taxa	sample	length	Mt genome type	Ambiguous configuration
A. gallica subsp. *calidusa*	SJ154_graph2	109866	Circle	Yes
A. gallica subsp. *calidusa*	SJ155_graph2	109866	Circle	Yes
A. gallica subsp. *calidusa*	SJ156_graph2	109866	Circle	Yes
A. gallica subsp. *calidusa*	SJ158_graph1	109866	Circle	Yes
A. gallica subsp. *calidusa*	SJ159_graph2	109866	Circle	Yes
A. gallica subsp. *calidusa*	SJ161_graph2	109866	Circle	Yes
A. gallica subsp. *calidusa*	SJ162_graph2	109866	Circle	Yes
A. gallica subsp. *calidusa*	SJ164_graph1	107011	Circle	Yes
A. gallica subsp. *calidusa*	SJ172_graph2	113977	Circle	Yes
A. gallica subsp. *calidusa*	SJ175_graph1	113308	Circle	Yes
A. gallica subsp. *calidusa*	SJ176_graph1	113308	Circle	Yes
A. gallica subsp. *calidusa*	SJ177_graph1	113308	Circle	Yes
A. gallica subsp. *calidusa*	SJ180_graph2	113308	Circle	Yes
A. gallica subsp. *calidusa*	SJ181_graph1	117243	Circle	Yes
A. gallica subsp. *calidusa*	SJ182_graph1	117244	Circle	Yes
A. gallica subsp. *calidusa*	SJ22_graph2	107244	Circle	Yes
A. gallica subsp. *calidusa*	SJ27_graph2	107244	Circle	Yes
A. gallica subsp. *calidusa*	SJ28_graph1	107244	Circle	Yes
A. gallica subsp. *calidusa*	SJ31_graph1	92069	Circle	Yes
A. gallica subsp. *calidusa*	SJ35_graph2	116737	Circle	Yes
A. gallica subsp. *calidusa*	SJ38_graph1	116737	Circle	Yes
A. gallica subsp. *calidusa*	SJ39_graph1	116737	Circle	Yes
A. gallica subsp. *calidusa*	SJ40_graph2	116737	Circle	Yes
A. gallica subsp. *calidusa*	SJ42_graph2	116737	Circle	Yes
A. gallica subsp. *calidusa*	SJ63_graph2	118111	Circle	Yes
A. gallica subsp. *calidusa*	SJ73_graph2	118544	Circle	Yes
A. gallica subsp. *calidusa*	SJ76_graph1	103275	Circle	Yes
A. gallica subsp. *calidusa*	SJ79_graph1	112463	Circle	Yes
A. gallica subsp. *calidusa*	SJ85_graph1	112463	Circle	Yes
A. gallica subsp. *calidusa*	SJ93_graph2	112463	Circle	Yes
A. gallica subsp. *calidusa*	SJ96_graph2	109189	Circle	Yes
A. gallica subsp. *calidusa*	SM18_graph1	120767	Circle	Yes
A. gallica subsp. *calidusa*	SS-01_graph2	120768	Circle	Yes
A. gallica subsp. *calidusa*	SX_M2_graph1	94078	Circle	Yes
A. gallica subsp. *calidusa*	T11_graph1	96067	Circle	Yes

Table C3 (continued)

Taxa	sample	length	Mt genome type	Ambiguous configuration
A. gallica subsp. *calidusa*	T12_graph1	96291	Circle	Yes
A. gallica subsp. *calidusa*	T14_graph2	96291	Circle	Yes
A. gallica subsp. *calidusa*	T19_graph2	96291	Circle	Yes
A. gallica subsp. *calidusa*	T20	96305	Scaffolds	NA
A. gallica subsp. *calidusa*	T21_graph2	96291	Circle	Yes
A. gallica subsp. *calidusa*	T25_graph2	96271	Circle	Yes
A. gallica subsp. *calidusa*	T27_graph1	120765	Circle	Yes
A. gallica subsp. *calidusa*	T28_graph1	96291	Circle	Yes
A. gallica subsp. *calidusa*	T3	96403	Scaffolds	NA
A. gallica subsp. *calidusa*	T6_graph1	96291	Circle	Yes
A. gallica subsp. *calidusa*	T9_graph2	96291	Circle	Yes
A. gallica subsp. *calidusa*	WSB-M1_graph2	96291	Circle	Yes
A. gallica subsp. *calidusa*	XY2_graph1	119058	Circle	Yes
A. gallica subsp. *calidusa*	Y3_graph1	120768	Circle	Yes
A. gallica subsp. *calidusa*	YSM470_graph2	113977	Circle	Yes
A. gallica subsp. *calidusa*	YSM472_graph1	116737	Circle	Yes
A. gallica subsp. *calidusa*	YSM474_graph1	116737	Circle	Yes
A. gallica subsp. *calidusa*	YSM481_graph1	114923	Circle	Yes
A. gallica subsp. *calidusa*	ZM_graph1	120702	Circle	Yes
A. gallica subsp. *calidusa*	ZT-10	120788	Scaffolds	NA
A. gallica subsp. *calidusa*	ZT11_graph2	120767	Circle	Yes
A. gallica subsp. *calidusa*	ZT-12_graph2	96291	Circle	Yes
A. gallica subsp. *calidusa*	ZT-18_graph1	120769	Circle	Yes
A. gallica subsp. *calidusa*	ZT-2_graph1	120769	Circle	Yes
A. gallica subsp. *calidusa*	ZT20_graph1	120768	Circle	Yes
A. gallica subsp. *calidusa*	ZT-21_graph2	120768	Circle	Yes
A. gallica subsp. *calidusa*	ZT22_graph2	120766	Circle	Yes
A. gallica subsp. *calidusa*	ZT-23	120798	Scaffolds	NA
A. gallica subsp. *calidusa*	ZT24_graph1	120769	Circle	Yes
A. gallica subsp. *calidusa*	ZT25_graph2	120767	Circle	Yes
A. gallica subsp. *calidusa*	ZT26_graph1	120769	Circle	Yes
A. gallica subsp. *calidusa*	ZT27_graph1	120767	Circle	Yes
A. gallica subsp. *calidusa*	ZT28_graph2	120768	Circle	Yes
A. gallica subsp. *calidusa*	ZT-3_graph1	120769	Circle	Yes
A. gallica subsp. *calidusa*	ZT31_graph1	120768	Circle	Yes

Table C3 (continued)

Taxa	sample	length	Mt genome type	Ambiguous configuration
A. gallica subsp. *calidusa*	ZT-32_graph2	96291	Circle	Yes
A. gallica subsp. *calidusa*	ZT-33_graph1	96291	Circle	Yes
A. gallica subsp. *calidusa*	ZT-34_graph2	96290	Circle	Yes
A. gallica subsp. *calidusa*	ZT-35	76239	Scaffolds	NA
A. gallica subsp. *calidusa*	ZT-36_graph1	120769	Circle	Yes
A. gallica subsp. *calidusa*	ZT37_graph1	120768	Circle	Yes
A. gallica subsp. *calidusa*	ZT38_graph1	120769	Circle	Yes
A. gallica subsp. *calidusa*	ZT-39_graph2	120745	Circle	Yes
A. gallica subsp. *calidusa*	ZT-4_graph2	120765	Circle	Yes
A. gallica subsp. *calidusa*	ZT-40_graph1	96291	Circle	Yes
A. gallica subsp. *calidusa*	ZT-41_graph1	120769	Circle	Yes
A. gallica subsp. *calidusa*	ZT-42_graph1	96291	Circle	Yes
A. gallica subsp. *calidusa*	ZT-43_graph2	120769	Circle	Yes
A. gallica subsp. *calidusa*	ZT-44_graph1	96291	Circle	Yes
A. gallica subsp. *calidusa*	ZT-45_graph2	120767	Circle	Yes
A. gallica subsp. *calidusa*	ZT-46_graph1	120769	Circle	Yes
A. gallica subsp. *calidusa*	ZT-6_graph2	120768	Circle	Yes
A. gallica subsp. *calidusa*	ZT-7_graph2	120768	Circle	Yes
A. gallica subsp. *canadensis*	GUO222_graph1	130793	Circle	Yes
A. gallica subsp. *gallica*	ARMILLARIA_GALLICA	98896	Circle	No
A. gemina	GEMI	117223	Circle	No
A. griseocapilla	LEI439_graph1	167449	Circle	Yes
A. griseocapilla	WGS75_graph1	154216	Circle	Yes
A. heimii	87-45	130054	Circle	No
A. korhonenii	22DWS02_graph1	163427	Circle	Yes
A. korhonenii	22DWS03_graph2	163460	Circle	Yes
A. korhonenii	22DWS04	171939	Scaffolds	NA
A. korhonenii	22DWS05_graph2	169519	Circle	Yes
A. korhonenii	22DWS06	164878	Scaffolds	NA
A. korhonenii	22DWS07_graph1	182604	Circle	Yes
A. korhonenii	CBSQ22DWS01	171558	Circle	No
A. korhonenii	HKAS95344_graph1	127114	Circle	Yes
A. luteobubalina	Armillarialuteobubalina_6Scaffolds	205803	Scaffolds	NA
A. luteobubalina	21024	78882	Circle	No

Table C3 (continued)

Taxa	sample	length	Mt genome type	Ambiguous configuration
A. luteobubalina	C19004	87394	Circle	No
A. luteobubalina	C21019	76638	Circle	No
A. luteobubalina	CBSB19029	83554	Circle	No
A. luteobubalina	CBSC21009	76638	Circle	No
A. luteobubalina	CBSC96027	78213	Circle	No
A. luteobubalina	CBSC96029	83554	Circle	No
A. luteobubalina	CBSC96038	83141	Circle	No
A. luteobubalina	guo227	74631	Scaffolds	NA
A. luteobubalina	HMJAU24389	105723	Circle	No
A. luteobubalina	HMJAU60487	84075	Circle	No
A. luteobubalina	LZL-5	82940	Circle	No
A. luteobubalina	MHHNU7783_graph2	106450	Circle	Yes
A. mellea-1	KK891152_GRAPH1	146578	Scaffolds	NA
A. mellea-2	mellea	138074	Scaffolds	NA
A. melleoamericana	GDGM70002	130475	Scaffolds	NA
A. melleoamericana	GDGM70010	135337	Scaffolds	NA
A. melleoamericana	VI-VII	123424	Scaffolds	NA
A. nabsnona	Armillarianabsnona3Scaffolds	140831	Scaffolds	NA
A. nabsnona	NABS	137746	Circle	No
A. novae-zelandiae	novaezelandiae	265509	Scaffolds	NA
A. ostoyae	CBSD19044	119328	Circle	No
A. ostoyae	OZ035952	113369	unknown	NA
A. pelmaspora	XZ151	220880	Scaffolds	NA
A. pelmaspora	XZ199_graph1	227392	Circle	Yes
A. pseudoostoyae	HKAS50184	114061	Circle	No
A. pseudoostoyae	HKAS56108	102322	Circle	No
A. pseudoostoyae	HKAS58853	117834	Scaffolds	NA
A. puiggarii	85-63	201727	Scaffolds	NA
A. pungentisquamosa	19060	121413	Circle	No
A. pungentisquamosa	CBSP19062	85368	Circle	No
A. pungentisquamosa	CLZ12638	96765	Circle	No
A. pungentisquamosa	LYT-F17	109702	Circle	No
A. pungentisquamosa	QZ19053	88560	Circle	No
A. pungentisquamosa	QZ19054	92163	Circle	No

Table C3 (continued)

Taxa	sample	length	Mt genome type	Ambiguous configuration
A. pungentisquamosa	QZ19055	96775	Circle	No
A. pungentisquamosa	QZ19058	92163	Circle	No
A. pungentisquamosa	QZ19059	92163	Circle	No
A. pungentisquamosa	QZ19061	87748	Circle	No
A. pungentisquamosa	ZT-14	99169	Circle	No
A. pungentisquamosa	ZT29	99169	Circle	No
A. pungentisquamosa	ztmh-30	99168	Circle	No
A. sinapina subsp. *altilatituda*	ARMILLARIA_SINAPINA	103563	Circle	No
A. sinapina subsp. *altilatituda*	CBSA96008	85730	Circle	No
A. sinapina subsp. *altilatituda*	CBSA96016	94902	Circle	No
A. sinapina subsp. *altilatituda*	CBSA96025	94901	Circle	No
A. sinapina subsp. *altilatituda*	CBSA96042	100130	Circle	No
A. sinapina subsp. *altilatituda*	HMAS248128	106056	Circle	No
A. sinapina subsp. *altilatituda*	HMAS255468	85728	Circle	No
A. sinapina subsp. *altilatituda*	HMAS255489	111728	Circle	No
A. sinapina subsp. *altilatituda*	HMAS281266	107272	Circle	No
A. sinapina subsp. *altilatituda*	HMAS96969	94902	Circle	No
A. sinapina subsp. *altilatituda*	HMJAU22761	90841	Circle	No
A. sinapina subsp. *altilatituda*	HMJAU23501	103174	Circle	No
A. sinapina subsp. *altilatituda*	HMJAU33876	94788	Circle	No
A. sinapina subsp. *altilatituda*	HMJAU60486	95083	Circle	No
A. sinapina subsp. *sinapina*	B618	101466	Circle	No
A. sinensis	2104919020	73210	Scaffolds	NA
A. sinensis	21HH01	88027	Circle	No

Table C3 (continued)

Taxa	sample	length	Mt genome type	Ambiguous configuration
A. sinensis	21HH02	86587	Circle	No
A. sinensis	CBSF05030	92966	Circle	No
A. sinensis	CBSF19020	79937	Circle	No
A. sinensis	CBSF97033	99087	Circle	No
A. sinensis	CBSF99103	94062	Circle	No
A. sinensis	CBSF99107	97115	Circle	No
A. sinensis	GUO117	86482	Circle	No
A. sinensis	guo233	90648	Circle	No
A. sinensis	GUO7	86482	Circle	No
A. sinensis	HMAS22782	104548	Circle	No
A. sinensis	HMAS253828	86821	Circle	No
A. sinensis	HMAS273636	104548	Circle	No
A. sinensis	HMAS61686	89219	Circle	No
A. sinensis	HMJAU22795	110409	Circle	No
A. sinensis	HMJAU23629	86449	Circle	No
A. sinensis	HMJAU23737	95519	Circle	No
A. sinensis	HMJAU28935	87379	Circle	No
A. sinensis	MHHNU7577	87682	Circle	No
A. sinensis	SJ75	107737	Circle	No
A. sinensis	SJ94	90555	Circle	No
A. sinensis	SJ97	90555	Circle	No
A. sinensis	YSM656	105252	Circle	No
A. sinensis	ZT-8	86482	Circle	No
A. solidipes	SRR8393339	122787	Circle	No
A. tabescens subsp. *tabescens*	guo262	78194	Circle	No
A. tabescens subsp. *tabescens*	tabescens	81370	Scaffolds	NA
A. tabescens subsp. *orientala*	AT	92503	Circle	No
A. tabescens subsp. *orientala*	CBSI99122	92503	Circle	No
A. tabescens subsp. *orientala*	Desarmillaria_tabescens_NC_042769	93439	Circle	No
A. tabescens subsp. *orientala*	guo261	92503	Circle	No

Table C3 (continued)

Taxa	sample	length	Mt genome type	Ambiguous configuration
A. tabescens subsp. *orientala*	HKAS58683	51044	Scaffolds	NA
A. tabescens subsp. *orientala*	HKAS58910	84491	Scaffolds	NA
A. tabescens subsp. *orientala*	HKAS80228	92088	Scaffolds	NA
A. tabescens subsp. *orientala*	JLK921	93117	Circle	No
A. tabescens subsp. *orientala*	LD-M8_graph1	96290	Circle	Yes
A. tabescens subsp. *orientala*	MHHNU8836	24622	Scaffolds	NA
A. tabescens subsp. *orientala*	SX_M1	82257	Scaffolds	NA
A. tibetica (CBS J) lineage 1-mtDNA	21SNJ22	112778	Circle	No
A. tibetica (CBS J) lineage 1-mtDNA	21SNJ24	119772	Circle	No
A. tibetica (CBS J) lineage 1-mtDNA	CBSJ04043	116699	Circle	No
A. tibetica (CBS J) lineage 1-mtDNA	CBSJ05018_graph1	114743	Circle	Yes
A. tibetica (CBS J) lineage 1-mtDNA	HKAS48936	110500	Circle	No
A. tibetica (CBS J) lineage 1-mtDNA	HKAS49375	111820	Circle	No
A. tibetica (CBS J) lineage 1-mtDNA	HKAS51007	113719	Circle	No
A. tibetica (CBS J) lineage 1-mtDNA	HKAS51692	114942	Circle	No
A. tibetica (CBS J) lineage 1-mtDNA	HKAS89531	139550	Circle	No
A. tibetica (CBS J) lineage 1-mtDNA	HKAS89629	118536	Circle	No
A. tibetica (CBS J) lineage 1-mtDNA	HMAS130389	117510	Circle	No
A. tibetica (CBS J) lineage 1-mtDNA	HMAS130603	131053	Circle	No

Table C3 (continued)

Taxa	sample	length	Mt genome type	Ambiguous configuration
A. tibetica (CBS J) lineage 1-mtDNA	HMAS132012	123733	Circle	No
A. tibetica (CBS J) lineage 1-mtDNA	HMAS132015	121806	Circle	No
A. tibetica (CBS J) lineage 1-mtDNA	HMAS254250	90528	Circle	No
A. tibetica (CBS J) lineage 1-mtDNA	HMAS26066	113141	Circle	No
A. tibetica (CBS J) lineage 1-mtDNA	HMAS26067	126826	Circle	No
A. tibetica (CBS J) lineage 1-mtDNA	HMAS274442	107505	Circle	No
A. tibetica (CBS J) lineage 1-mtDNA	HMAS274553	137060	Circle	No
A. tibetica (CBS J) lineage 1-mtDNA	HMAS274644	125223	Circle	No
A. tibetica (CBS J) lineage 1-mtDNA	HMAS276211	120917	Circle	No
A. tibetica (CBS J) lineage 1-mtDNA	HMAS276224	125888	Circle	No
A. tibetica (CBS J) lineage 1-mtDNA	HMAS50996	113963	Circle	No
A. tibetica (CBS J) lineage 1-mtDNA	HMAS86328	104551	Circle	No
A. tibetica (CBS J) lineage 1-mtDNA	HMAS86329	118103	Circle	No
A. tibetica (CBS J) lineage 1-mtDNA	HMAS96843	132505	Scaffolds	NA
A. tibetica (CBS J) lineage 1-mtDNA	HMAS99098	117510	Circle	No
A. tibetica (CBS J) lineage 1-mtDNA	LYT-F31	115446	Circle	No
A. tibetica (CBS J) lineage 1-mtDNA	SJ131	126165	Circle	No
A. tibetica (CBS J) lineage 1-mtDNA	SJ135	109521	Circle	No
A. tibetica (CBS J) lineage 1-mtDNA	SJ136_graph1	115155	Scaffolds	NA

Table C3 (continued)

Taxa	sample	length	Mt genome type	Ambiguous configuration
A. tibetica (CBS J) lineage 1-mtDNA	SJ141	120060	Circle	No
A. tibetica (CBS J) lineage 1-mtDNA	SJ142	121691	Circle	No
A. tibetica (CBS J) lineage 1-mtDNA	SJ146	121691	Circle	No
A. tibetica (CBS J) lineage 1-mtDNA	SJ147	121691	Circle	No
A. tibetica (CBS J) lineage 1-mtDNA	YLSF-2	110757	Circle	No
A. tibetica (CBS J) lineage 1-mtDNA	YSLF-2	110757	Circle	No
A. tibetica (CBS J) lineage 2-mtDNA	FM-X	109382	Circle	No
A. tibetica (CBS J) lineage 2-mtDNA	guo335	107479	Circle	No
A. tibetica (CBS J) lineage 2-mtDNA	HKAS45609	100058	Circle	No
A. tibetica (CBS J) lineage 2-mtDNA	HKAS45688	100058	Circle	No
A. tibetica (CBS J) lineage 2-mtDNA	HKAS45762	100058	Circle	No
A. tibetica (CBS J) lineage 2-mtDNA	HKAS45773	77810	Circle	No
A. tibetica (CBS J) lineage 2-mtDNA	HKAS45807_graph2	122498	Circle	Yes
A. tibetica (CBS J) lineage 2-mtDNA	HKAS45820_graph2	122498	Circle	Yes
A. tibetica (CBS J) lineage 2-mtDNA	HKAS45974	87365	Circle	No
A. tibetica (CBS J) lineage 2-mtDNA	HKAS46283	98315	Circle	No
A. tibetica (CBS J) lineage 2-mtDNA	HKAS46284	97690	Circle	No
A. tibetica (CBS J) lineage 2-mtDNA	HKAS46314	99349	Scaffolds	NA
A. tibetica (CBS J) lineage 2-mtDNA	2105604028	113243	Circle	No

Table C3 (continued)

Taxa	sample	length	Mt genome type	Ambiguous configuration
A. tibetica (CBS J) lineage 2-mtDNA	21LJ06	86131	Circle	No
A. tibetica (CBS J) lineage 2-mtDNA	21LJ07	84825	Circle	No
A. tibetica (CBS J) lineage 2-mtDNA	Ar-3	100100	Circle	No
A. tibetica (CBS J) lineage 2-mtDNA	Ar-8	109202	Circle	No
A. tibetica (CBS J) lineage 2-mtDNA	Ar-9	106597	Circle	No
A. tibetica (CBS J) lineage 2-mtDNA	CBSJ04028	113243	Circle	No
A. tibetica (CBS J) lineage 2-mtDNA	HKAS49197_graph2	117433	Circle	Yes
A. tibetica (CBS J) lineage 2-mtDNA	HKAS51046	111341	Circle	No
A. tibetica (CBS J) lineage 2-mtDNA	HKAS54932	105501	Circle	No
A. tibetica (CBS J) lineage 2-mtDNA	HKAS55489	85696	Circle	No
A. tibetica (CBS J) lineage 2-mtDNA	HKAS82505	120451	Circle	No
A. tibetica (CBS J) lineage 2-mtDNA	HKAS93952	107210	Circle	No
A. tibetica (CBS J) lineage 2-mtDNA	HKAS93966	79804	Circle	No
A. tibetica (CBS J) lineage 2-mtDNA	HKAS97181	98667	Circle	No
A. tibetica (CBS J) lineage 2-mtDNA	HMAS272511	93556	Circle	No
A. tibetica (CBS J) lineage 2-mtDNA	HMAS272651	93556	Circle	No
A. tibetica (CBS J) lineage 2-mtDNA	HMAS48351	86417	Circle	No
A. tibetica (CBS J) lineage 2-mtDNA	HMAS51091	110981	Circle	No
A. tibetica (CBS J) lineage 2-mtDNA	HMAS51095	77822	Circle	No

Table C3 (continued)

Taxa	sample	length	Mt genome type	Ambiguous configuration
A. tibetica (CBS J) lineage 2-mtDNA	JLK213	100058	Circle	No
A. tibetica (CBS J) lineage 2-mtDNA	LJW1577	92276	Circle	No
A. tibetica (CBS J) lineage 2-mtDNA	LJW1634	97806	Circle	No
A. tibetica (CBS J) lineage 2-mtDNA	LJW2388	84748	Circle	No
A. tibetica (CBS J) lineage 2-mtDNA	LJW2390	107690	Circle	No
A. tibetica (CBS J) lineage 2-mtDNA	SJ102	121994	Circle	No
A. tibetica (CBS J) lineage 3-mtDNA	CBSJ04040_graph1	100151	Circle	Yes
A. tibetica (CBS J) lineage 3-mtDNA	HKAS51258_graph1	99822	Circle	Yes
A. tibetica (CBS J) lineage 3-mtDNA	HKAS57133_graph2	104507	Circle	Yes
A. tibetica (CBS J) lineage 3-mtDNA	HKAS89549_graph1	100992	Circle	Yes
A. tibetica (CBS J) lineage 3-mtDNA	HKAS90943_graph2	99823	Circle	Yes
A. tibetica (CBS J) lineage 3-mtDNA	HKAS94047_graph1	101431	Circle	Yes
A. tibetica (CBS J) lineage 3-mtDNA	HMAS254378_graph2	102364	Circle	Yes
A. tibetica (CBS J) lineage 3-mtDNA	HMAS254476_graph2	97501	Circle	Yes
A. tibetica (CBS J) lineage 3-mtDNA	HMAS264994_graph2	88266	Circle	Yes
A. tibetica (CBS J) lineage 3-mtDNA	HMAS272485_graph1	98145	Circle	Yes
A. tibetica (CBS J) lineage 3-mtDNA	HMAS274066_graph2	97501	Circle	Yes
A. tibetica (CBS J) lineage 3-mtDNA	HMAS274072_graph1	97370	Circle	Yes
A. tibetica (CBS J) lineage 3-mtDNA	HMAS274889_graph1	113453	Circle	Yes

Table C3 (continued)

Taxa	sample	length	Mt genome type	Ambiguous configuration
A. tibetica (CBS J) lineage 3-mtDNA	HMAS275000_graph2	95416	Circle	Yes
A. tibetica (CBS J) lineage 3-mtDNA	LEI860_graph2	99736	Circle	Yes
A. tibetica (CBS J) lineage 3-mtDNA	LEI374_graph1	95787	Circle	Yes
A. tibetica (CBS J) lineage 3-mtDNA	LEI768_graph1	94490	Circle	Yes
A. tibetica (CBS J) lineage 3-mtDNA	MH_graph1	95787	Circle	No
A. tibetica (CBS J) lineage 4-mtDNA	CBSJ02044	139177	Circle	No
A. tibetica (CBS J) lineage 4-mtDNA	HMAS270241	123005	Circle	No
A. tibetica (CBS J) lineage 4-mtDNA	HMAS38334	105282	Circle	No
A. tibetica (CBS J) lineage 4-mtDNA	HMAS99054	109597	Circle	No
A. tibetica (CBS J) lineage 4-mtDNA	LJW668	105322	Circle	No
A. tibetica (CBS J) lineage 4-mtDNA	MHHNU10251	133948	Circle	No
A. tibetica (CBS J) lineage 4-mtDNA	NLT01	119958	Scaffolds	NA
A. tibetica (CBS J) lineage 4-mtDNA	NLT05	105305	Circle	No
A. tibetica (CBS J) lineage 5-mtDNA	GDGM83473_graph2	149788	Circle	Yes
A. tibetica (CBS J) lineage 5-mtDNA	HKAS49177	100789	Circle	No
A. tibetica (CBS J) lineage 5-mtDNA	HKAS53619	112425	Circle	No
A. tibetica (CBS J) lineage 5-mtDNA	HKAS89519_graph1	135997	Circle	Yes
A. tibetica (CBS J) lineage 5-mtDNA	HKAS89525_graph2	118868	Circle	Yes
A. tibetica (CBS J) lineage 5-mtDNA	HMAS254774	115296	Circle	No

Table C3 (continued)

Taxa	sample	length	Mt genome type	Ambiguous configuration
A. tibetica (CBS J) lineage 5-mtDNA	HMAS268710	103323	Circle	No
A. tibetica (CBS J) lineage 5-mtDNA	HMAS274349_graph2	109775	Circle	Yes
A. tibetica (CBS J) lineage 5-mtDNA	HMAS50997_graph1	121203	Circle	Yes
A. tibetica (CBS J) lineage 5-mtDNA	HMAS99623_graph2	137434	Circle	Yes
A. violacea	21SNJ11	99490	Circle	No
A. violacea	21SNJ13	96508	Circle	No
A. violacea	21SNJ17	80828	Circle	No
A. violacea	21SNJ21	95025	Circle	No
A. violacea	21SNJ25	90664	Circle	No
A. violacea	21SNJ26	90664	Circle	No
A. violacea	CBSN02066	99330	Circle	No
A. violacea	CBSN02067	99087	Circle	No
A. violacea	CBSN02068	111494	Circle	No
A. violacea	CBSN02069	88456	Circle	No
A. violacea	CBSN02070	88458	Circle	No
A. violacea	CBSN16022	91731	Circle	No
A. violacea	CBSN19098	84007	Circle	No
A. violacea	CBSN19107	96047	Circle	No
A. violacea	CBSNW16024	81337	Circle	No
A. violacea	DG	83730	Circle	No
A. violacea	SJ139	101650	Circle	No
A. violacea	SJ143	92903	Circle	No
A. violacea	SJ144	82960	Circle	No
A. violacea	SJ145	82960	Circle	No
A. violacea	YLCTM	94851	Circle	No
A. violacea	ZZZT01	94851	Circle	No
Armillaria sp. PXL (CBS F) lineage 2-mtDNA	PXL	83104	Circle	No
CBS G+CBS K lineage 1-mtDNA	22KM01_graph2	125059	Circle	Yes
CBS G+CBS K lineage 1-mtDNA	22KM02_graph2	125057	Circle	Yes

Table C3 (continued)

Taxa	sample	length	Mt genome type	Ambiguous configuration
CBS G+CBS K lineage 1-mtDNA	22KM03_graph2	128941	Circle	Yes
CBS G+CBS K lineage 1-mtDNA	CBSK19083_graph2	134144	Circle	Yes
CBS G+CBS K lineage 1-mtDNA	CBSK19105_graph3	128943	Circle	Yes
CBS G+CBS K lineage 1-mtDNA	GUO238_graph4	125058	Circle	Yes
CBS G+CBS K lineage 1-mtDNA	GUO247_graph2	128940	Circle	Yes
CBS G+CBS K lineage 1-mtDNA	GUO248_graph4	128938	Circle	Yes
CBS G+CBS K lineage 1-mtDNA	GUO249_graph2	128941	Circle	Yes
CBS G+CBS K lineage 1-mtDNA	GUO252_graph4	128941	Circle	Yes
CBS G+CBS K lineage 1-mtDNA	guo256_graph2	125056	Circle	Yes
CBS G+CBS K lineage 1-mtDNA	HKAS49004_graph4	128933	Circle	Yes
CBS G+CBS K lineage 1-mtDNA	HKAS52389_graph4	128941	Circle	Yes
CBS G+CBS K lineage 1-mtDNA	HKAS68003_graph2	125058	Circle	Yes
CBS G+CBS K lineage 1-mtDNA	HKAS82475_graph2	128949	Circle	Yes
CBS G+CBS K lineage 1-mtDNA	SJ106_graph4	112872	Circle	Yes
CBS G+CBS K lineage 2-mtDNA	FM22-210	139575	Circle	No
CBS G+CBS K lineage 2-mtDNA	FM22-211	139575	Circle	No
CBS G+CBS K lineage 2-mtDNA	FM22-215	139575	Circle	No
CBS G+CBS K lineage 2-mtDNA	FM22-216	139575	Circle	No
CBS G+CBS K lineage 3-mtDNA	21LJ03	149026	Circle	No

Table C3 (continued)

Taxa	sample	length	Mt genome type	Ambiguous configuration
CBS G+CBS K lineage 3-mtDNA	21LJ09	135373	Circle	No
CBS G+CBS K lineage 3-mtDNA	21LJ11	131468	Circle	No
CBS G+CBS K lineage 3-mtDNA	21SNJ01	114601	Scaffolds	NA
CBS G+CBS K lineage 3-mtDNA	21SNJ05	117866	Circle	No
CBS G+CBS K lineage 3-mtDNA	221003WSP	127471	Circle	No
CBS G+CBS K lineage 3-mtDNA	22LL03	127471	Circle	No
CBS G+CBS K lineage 3-mtDNA	A10	127482	Circle	No
CBS G+CBS K lineage 3-mtDNA	CBSK00111	119039	Circle	No
CBS G+CBS K lineage 3-mtDNA	CBSK19052	137610	Circle	No
CBS G+CBS K lineage 3-mtDNA	FM21-172	123643	Circle	No
CBS G+CBS K lineage 3-mtDNA	FM21-173	123642	Circle	No
CBS G+CBS K lineage 3-mtDNA	GDGM76532	136267	Circle	No
CBS G+CBS K lineage 3-mtDNA	guo230	127482	Circle	No
CBS G+CBS K lineage 3-mtDNA	guo237	131483	Circle	No
CBS G+CBS K lineage 3-mtDNA	guo239	147364	Circle	No
CBS G+CBS K lineage 3-mtDNA	guo242	131123	Circle	No
CBS G+CBS K lineage 3-mtDNA	HKAS46275	125198	Circle	No
CBS G+CBS K lineage 3-mtDNA	HKAS57446	131669	Circle	No
CBS G+CBS K lineage 3-mtDNA	HKAS58911	146715	Circle	No

Table C3 (continued)

Taxa	sample	length	Mt genome type	Ambiguous configuration
CBS G+CBS K lineage 3-mtDNA	HKAS68632	120155	Circle	No
CBS G+CBS K lineage 3-mtDNA	HKAS68678	131659	Circle	No
CBS G+CBS K lineage 3-mtDNA	HKAS74997	117862	Circle	No
CBS G+CBS K lineage 3-mtDNA	HKAS81274	149026	Circle	No
CBS G+CBS K lineage 3-mtDNA	HKAS81827	133710	Circle	No
CBS G+CBS K lineage 3-mtDNA	HKAS81828	133710	Circle	No
CBS G+CBS K lineage 3-mtDNA	HKAS81829	133710	Circle	No
CBS G+CBS K lineage 3-mtDNA	HKAS81830	133710	Circle	No
CBS G+CBS K lineage 3-mtDNA	HKAS81831	133710	Circle	No
CBS G+CBS K lineage 3-mtDNA	HKAS81832	133710	Circle	No
CBS G+CBS K lineage 3-mtDNA	HKAS81834	133710	Circle	No
CBS G+CBS K lineage 3-mtDNA	HKAS82101_graph1	183789	Scaffolds	NA
CBS G+CBS K lineage 3-mtDNA	HKAS87145	149027	Circle	No
CBS G+CBS K lineage 3-mtDNA	HMAS23066	147364	Circle	No
CBS G+CBS K lineage 3-mtDNA	HMAS253414	127476	Circle	No
CBS G+CBS K lineage 3-mtDNA	HMAS272369	123614	Circle	No
CBS G+CBS K lineage 3-mtDNA	HMAS33561	129215	Circle	No
CBS G+CBS K lineage 3-mtDNA	HMAS50995	129212	Circle	No
CBS G+CBS K lineage 3-mtDNA	HMAS51088	129212	Circle	No

Table C3 (continued)

Taxa	sample	length	Mt genome type	Ambiguous configuration
CBS G+CBS K lineage 3-mtDNA	JLK003	125937	Circle	No
CBS G+CBS K lineage 3-mtDNA	LJW1854	140562	Circle	No
CBS G+CBS K lineage 3-mtDNA	LJW1870	131477	Circle	No
CBS G+CBS K lineage 3-mtDNA	LJW2225	149026	Circle	No
CBS G+CBS K lineage 3-mtDNA	LJW2229	131482	Circle	No
CBS G+CBS K lineage 3-mtDNA	LJW2248	149027	Circle	No
CBS G+CBS K lineage 3-mtDNA	LJW2249	149027	Circle	No
CBS G+CBS K lineage 3-mtDNA	LJW779	129224	Circle	No
CBS G+CBS K lineage 3-mtDNA	LJW849	151378	Circle	No
CBS G+CBS K lineage 3-mtDNA	MHHNU31945	139690	Circle	No
CBS G+CBS K lineage 3-mtDNA	MHHNU7419	117879	Circle	No
CBS G+CBS K lineage 3-mtDNA	MHHNU8577	127482	Circle	No
CBS G+CBS K lineage 3-mtDNA	SJ113	142484	Circle	No
CBS G+CBS K lineage 3-mtDNA	SJ115	142484	Circle	No
CBS G+CBS K lineage 3-mtDNA	SJ116	142484	Circle	No
CBS G+CBS K lineage 3-mtDNA	WGS1051	131022	Circle	No
CBS G+CBS K lineage 3-mtDNA	XCB003	132773	Circle	No
CBS G+CBS K lineage 3-mtDNA	Xu156	127475	Circle	No
CBS G+CBS K lineage 3-mtDNA	XZ258	123613	Circle	No

Table C3 (continued)

Taxa	sample	length	Mt genome type	Ambiguous configuration
CBS G+CBS K lineage 3-mtDNA	CBSG19037	146522	Circle	No
CBS G+CBS K lineage 3-mtDNA	QZ000201-2	131483	Circle	Yes
Guyanagaster necrorhiza	SRR4125583_1_4	327174	Scaffolds	NA

Table C4 Diploid samples confirmed by heterozygosity detection and sample information

Samples	Heterozygosity rate	Samples	Heterozygosity rate	Samples	Heterozygosity rate
21043	0.1121	HMAS248128	0.1186	MHHNU8836	0.0336
2104919020	0.1318	HMAS253414	0.3736	MW-27	0.117
2105604028	0.1548	HMAS253478	0.0674	NLT01	0.1009
21HH01	0.1666	HMAS253500	0.146	NLT05	0.0997
21HH02	0.1707	HMAS253828	0.1507	PXL	0.1456
21HH03	0.1523	HMAS254250	0.1434	QA1	0.1678
21HH04	0.1472	HMAS254378	0.134	QF13	0.1623
21LJ03	0.4727	HMAS254476	0.1451	QM2	0.1625
21LJ05	0.1579	HMAS254774	0.156	QM3	0.1633
21LJ06	0.1709	HMAS255468	0.1233	QZ000201-2	0.3282
21LJ07	0.1713	HMAS255489	0.1242	SA-19	0.1497
21LJ09	0.4397	HMAS255521	0.1437	SJ02	0.1405
21LJ10	0.1475	HMAS255525	0.1435	SJ06	0.1366
21LJ11	0.482	HMAS255529	0.1442	SJ07	0.138
21SNJ01	0.1525	HMAS26066	0.1242	SJ10	0.0822
21SNJ05	0.3644	HMAS26067	0.1227	SJ102	0.1518
21SNJ11	0.144	HMAS264994	0.1521	SJ103	0.1553
21SNJ13	0.1512	HMAS268710	0.1496	SJ104	0.1506
21SNJ17	0.1458	HMAS270241	0.0918	SJ105	0.0702
21SNJ18	0.0985	HMAS272369	0.4056	SJ106	0.3864
21SNJ19	0.1012	HMAS272390	0.0979	SJ113	0.3629
21043	0.1121	HMAS248128	0.1186	MHHNU8836	0.0336
2104919020	0.1318	HMAS253414	0.3736	MW-27	0.117
2105604028	0.1548	HMAS253478	0.0674	NLT01	0.1009
21HH01	0.1666	HMAS253500	0.146	NLT05	0.0997
21HH02	0.1707	HMAS253828	0.1507	PXL	0.1456

Table C4 (continued)

Samples	Heterozygosity rate	Samples	Heterozygosity rate	Samples	Heterozygosity rate
21HH03	0.1523	HMAS254250	0.1434	QA1	0.1678
21HH04	0.1472	HMAS254378	0.134	QF13	0.1623
21LJ03	0.4727	HMAS254476	0.1451	QM2	0.1625
21LJ05	0.1579	HMAS254774	0.156	QM3	0.1633
21LJ06	0.1709	HMAS255468	0.1233	QZ000201-2	0.3282
21LJ07	0.1713	HMAS255489	0.1242	SA-19	0.1497
21LJ09	0.4397	HMAS255521	0.1437	SJ02	0.1405
21LJ10	0.1475	HMAS255525	0.1435	SJ06	0.1366
21LJ11	0.482	HMAS255529	0.1442	SJ07	0.138
21SNJ01	0.1525	HMAS26066	0.1242	SJ10	0.0822
21SNJ05	0.3644	HMAS26067	0.1227	SJ102	0.1518
21SNJ11	0.144	HMAS264994	0.1521	SJ103	0.1553
21SNJ13	0.1512	HMAS268710	0.1496	SJ104	0.1506
21SNJ17	0.1458	HMAS270241	0.0918	SJ105	0.0702
21SNJ18	0.0985	HMAS272369	0.4056	SJ106	0.3864
21SNJ19	0.1012	HMAS272390	0.0979	SJ113	0.3629
21SNJ21	0.152	HMAS272485	0.1402	SJ115	0.3719
21SNJ22	0.1459	HMAS272511	0.1549	SJ116	0.3644
21SNJ24	0.1508	HMAS272515	0.0953	SJ131	0.1476
21SNJ25	0.1474	HMAS272641	0.0647	SJ135	0.1494
21SNJ26	0.1471	HMAS272651	0.1527	SJ136	0.1503
221003WSP	0.5213	HMAS273634	0.1422	SJ139	0.1536
22DWS03	0.126	HMAS273636	0.1463	SJ141	0.1496
22DWS04	0.1409	HMAS274066	0.145	SJ142	0.1506
22KM01	0.4521	HMAS274072	0.1413	SJ143	0.1529
22KM02	0.4562	HMAS274349	0.1537	SJ144	0.152
22KM03	0.4864	HMAS274442	0.1565	SJ145	0.1534
22LL03	0.526	HMAS274553	0.1571	SJ146	0.1527
5H	0.1689	HMAS274644	0.1572	SJ147	0.1533
6	0.1694	HMAS274889	0.1448	SJ150	0.1494
87-45	0.1911	HMAS275000	0.1453	SJ151	0.1516
A10	0.4765	HMAS276211	0.1445	SJ152	0.1464
AHLD-A9	0.1622	HMAS276224	0.1319	SJ153	0.1508
Ar-3	0.1574	HMAS276553	0.1483	SJ154	0.1506
Ar-8	0.1584	HMAS281266	0.1222	SJ155	0.1524

Table C4 (continued)

Samples	Heterozygosity rate	Samples	Heterozygosity rate	Samples	Heterozygosity rate
Ar-9	0.153	HMAS33561	0.4457	SJ156	0.1535
BD4H	0.1403	HMAS33891	0.1364	SJ158	0.1522
BJ-M1	0.1637	HMAS37384	0.1397	SJ159	0.1545
C21019	0.0832	HMAS38334	0.0863	SJ161	0.1516
CFY-1	0.1634	HMAS48351	0.1454	SJ162	0.1532
CFY-2	0.1663	HMAS50995	0.5235	SJ164	0.1467
CLZ12638	0.0769	HMAS50996	0.1561	SJ172	0.15
DBRGZP	0.1647	HMAS50997	0.1568	SJ175	0.1512
DG	0.156	HMAS51088	0.3322	SJ176	0.1507
FM21-172	0.4379	HMAS51091	0.1476	SJ177	0.15
FM21-173	0.4456	HMAS51095	0.1425	SJ180	0.1508
FM22-210	0.4673	HMAS61574	0.1484	SJ181	0.1476
FM22-211	0.4634	HMAS61686	0.1541	SJ182	0.1531
FM22-215	0.4691	HMAS63163	0.1115	SJ22	0.1366
FM22-216	0.4413	HMAS86328	0.1277	SJ27	0.1409
FM-X	0.1611	HMAS86329	0.1285	SJ28	0.1403
GDGM70002	0.2356	HMAS96843	0.1427	SJ31	0.1418
GDGM70010	0.2403	HMAS96967	0.1326	SJ35	0.1383
GDGM71117	0.1705	HMAS96969	0.1285	SJ38	0.1432
GDGM76532	0.5617	HMAS97093	0.1367	SJ39	0.1416
GDGM77873	0.1132	HMAS99054	0.1014	SJ40	0.1395
GDGM83473	0.1391	HMAS99098	0.1378	SJ42	0.1413
guo117	0.1621	HMAS99623	0.1294	SJ63	0.1397
guo19	0.1475	HMIGD71175	0.1677	SJ73	0.1389
guo230	0.315	HMJAU22761	0.1389	SJ75	0.1482
guo237-	0.3183	HMJAU22795	0.1542	SJ76	0.1459
guo238-	0.3432	HMJAU23501	0.1375	SJ79	0.1514
guo239-	0.3084	HMJAU23629	0.1626	SJ85	0.1561
guo242-	0.4085	HMJAU23737	0.1565	SJ93	0.1496
guo247	0.4278	HMJAU24389	0.1386	SJ94	0.1559
guo248-	0.4011	HMJAU25401	0.1688	SJ96	0.1399
guo249	0.4657	HMJAU25404	0.1663	SJ97	0.1584
guo252	0.5241	HMJAU25478	0.1725	SM-1	0.1423
guo256	0.46	HMJAU28932	0.1726	SM18	0.1633
guo349	0.1661	HMJAU28935	0.1534	SNJ20	0.0945

Table C4 (continued)

Samples	Heterozygosity rate	Samples	Heterozygosity rate	Samples	Heterozygosity rate
guo37-	0.1181	HMJAU33876	0.137	SS-01	0.1603
guo7	0.1633	HMJAU42023	0.1674	SX_M1	0.0665
guo82	0.1156	HMJAU42034	0.1634	SX_M2	0.1579
HB-1	0.1509	HMJAU55082	0.1391	T11	0.1461
HB-2	0.1501	HMJAU60448	0.1527	T12	0.1665
HB-3	0.1602	HMJAU60486	0.1489	T14	0.1567
HB-4	0.1615	HMJAU60487	0.1402	T19	0.168
HB-5	0.1612	HMJAU6143	0.1662	T20	0.1201
HB-6	0.1451	HMJAU7339	0.1694	T21	0.168
HDY	0.1682	HS-01	0.1576	T25	0.1602
HKAS45609	0.1718	HS-A25	0.1497	T27	0.1304
HKAS45688	0.1398	HS-A9	0.168	T28	0.1423
HKAS45762	0.1359	J234	0.1447	T3	0.134
HKAS45773	0.1653	JLK003	0.4073	T6	0.1674
HKAS45807	0.1542	JLK213	0.154	T9	0.1524
HKAS45820	0.1254	JLK921	0.0437	TX	0.1666
HKAS45821	0.1687	KIB5-guo90	0.133	WGS1051	0.4151
HKAS45974	0.1492	KIB6-guo322	0.1331	WGS75	0.1077
HKAS46275	0.4126	KIB7-guo345	0.1422	WSB-M1	0.1117
HKAS46283	0.1227	KIB9-GUO278	0.0476	XCB003	0.3552
HKAS46284	0.1384	LDM-18	0.0429	Xu156	0.3496
HKAS46314	0.1454	LD-M8	0.1692	XY2	0.1408
HKAS48804	0.1238	LEI_439	0.0986	XZ151	0.0484
HKAS48936	0.1519	LEI_860	0.1416	XZ199	0.0504
HKAS49004	0.5678	LEI374	0.1467	XZ258	0.4733
HKAS49177	0.1627	LEI768	0.1433	Y3	0.1403
HKAS49197	0.1471	LH-22	0.071	YLCTM	0.056
HKAS49375	0.1503	LJW1577	0.1663	YLSF-2	0.1627
HKAS50184	0.1372	LJW1634	0.1539	YSLF-1	0.165
HKAS51007	0.1542	LJW1854	0.3882	YSLF-2	0.1634
HKAS51046	0.1542	LJW1870	0.4462	YSM_470	0.1347
HKAS51258	0.1318	LJW2225	0.3666	YSM_472	0.144
HKAS51692	0.1691	LJW2229	0.417	YSM_474	0.144
HKAS52389	0.3237	LJW2248	0.3902	YSM_481	0.1398
HKAS53619	0.1446	LJW2249	0.4189	ZG-26	0.0604

Table C4 (continued)

Samples	Heterozygosity rate	Samples	Heterozygosity rate	Samples	Heterozygosity rate
HKAS54932	0.1524	LJW2388	0.1582	ZM	0.1592
HKAS55489	0.1741	LJW2390	0.1582	ZT-10	0.1572
HKAS56108	0.1328	LJW668	0.1093	ZT11	0.1618
HKAS56216	0.1442	LJW779	0.4049	ZT-12	0.1625
HKAS57133	0.1416	LJW849	0.4478	ZT-14	0.0667
HKAS57446	0.3399	LM-1	0.1472	ZT15	0.1415
HKAS58683	0.0452	LM-2	0.1252	ZT-18	0.1537
HKAS58853	0.1044	LYT-A9	0.1267	ZT-2	0.1665
HKAS58910	0.0519	LYT-F01	0.1468	ZT20	0.1602
HKAS58911	0.3758	LYT-F05	0.1267	ZT-21	0.1641
HKAS68003	0.4453	LYT-F17	0.0671	ZT22	0.1625
HKAS68632	0.3827	LYT-F19	0.1503	ZT-23	0.1602
HKAS68678	0.4232	LYT-F31	0.0471	ZT24	0.1637
HKAS74997	0.3864	LYT-F34	0.1241	ZT25	0.1633
HKAS80228	0.0588	LYT-Y1	0.1309	ZT26	0.1639
HKAS81274	0.407	LZL-1	0.1512	ZT27	0.153
HKAS81827	0.3549	LZL-10	0.1577	ZT28	0.1602
HKAS81828	0.445	LZL-11	0.1562	ZT-29	0.0667
HKAS81829	0.3211	LZL-12	0.1573	ZT-3	0.1608
HKAS81830	0.4441	LZL-13	0.1571	ZT31	0.1633
HKAS81831	0.3018	LZL-15	0.1561	ZT-32	0.1648
HKAS81832	0.434	LZL-16	0.1405	ZT-33	0.1632
HKAS81834	0.3333	LZL-17	0.1451	ZT-34	0.1398
HKAS82101	0.2985	LZL-18	0.135	ZT-35	0.1549
HKAS82475	0.3682	LZL-19	0.1513	ZT-36	0.1536
HKAS82505	0.1584	LZL2	0.1539	ZT37	0.1586
HKAS87145	0.437	LZL20	0.156	ZT38	0.1633
HKAS89519	0.1569	LZL-4	0.1523	ZT-39	0.1528
HKAS89525	0.1601	LZL-5	0.0864	ZT-4	0.1552
HKAS89531	0.1402	LZL-6	0.1561	ZT-40	0.1584
HKAS89549	0.1435	LZL-7	0.1537	ZT-41	0.1655
HKAS89629	0.1613	LZL-8	0.1672	ZT-42	0.1567
HKAS90943	0.1384	LZL-9	0.1488	ZT-43	0.1531
HKAS92018	0.1495	LZP-11	0.0668	ZT-44	0.1579
HKAS93952	0.1612	LZP-15	0.1375	ZT-45	0.1646

Table C4 (continued)

Samples	Heterozygosity rate	Samples	Heterozygosity rate	Samples	Heterozygosity rate
HKAS93966	0.153	MF266	0.1429	ZT-46	0.1624
HKAS94047	0.1411	MF-M5	0.1322	ZT-6	0.1619
HKAS95344	0.1485	MF-M6	0.144	ZT7	0.1589
HKAS97181	0.1733	MH	0.124	ZT-8	0.1522
HMAS130389	0.1458	MHHNU10251	0.0951	ZT-M6	0.1401
HMAS130603	0.1254	MHHNU31060	0.1571	ZT-MF	0.1313
HMAS131062	0.0956	MHHNU31772	0.1489	ZTMH-036	0.1677
HMAS132012	0.1381	MHHNU31945	0.4588	ztmh-1	0.1427
HMAS132015	0.131	MHHNU7419	0.2778	ztmh-13	0.1428
HMAS145183	0.1512	MHHNU7577	0.1582	ztmh-30	0.0711
HMAS22781-	0.1675	MHHNU7783	0.1021	ZZZT01	0.157
HMAS22782	0.139	MHHNU8447	0.1384	CBSG19037	0.4563
HMAS23066	0.4736	MHHNU8577	0.3827		

Table C5 species of Coalescent-Based Species Tree Inference

Species	BUSCO results				
	C	S	M	F	M
A. altimontana	97.80%	97.00%	0.80%	0.20%	2.00%
A. borealis	95.30%	94.70%	0.60%	0.60%	4.10%
A. calvescens	97.90%	97.10%	0.80%	0.20%	1.90%
A. cepistipe	97.50%	96.60%	0.90%	0.20%	2.30%
A. fumosa CBS122221	98.60%	97.30%	1.30%	0.70%	0.70%
A. gallica 21-2	98.80%	97.30%	1.50%	0.70%	0.50%
A. gallica subsp. *gallica*	97.70%	96.90%	0.80%	0.30%	2.00%
A. gemina	97.90%	97.30%	0.60%	0.30%	1.80%
A. luteobubalina	97.80%	93.10%	4.70%	1.00%	1.20%
A. mellea	97.90%	97.30%	0.60%	0.20%	1.90%
A. melleoamericana	98.00%	97.30%	0.70%	0.30%	1.70%
A. nabsnona CMW6904	98.90%	98.10%	0.80%	0.50%	0.60%
A. novae-zelandiae	97.10%	94.80%	2.30%	1.30%	1.60%
A. ostoyae	96.10%	95.40%	0.70%	1.90%	2.00%
A. puiggarii	94.40%	93.80%	0.60%	0.80%	4.80%
A. sinapina subsp. *sinapina*	98.00%	97.10%	0.90%	0.30%	1.70%
A. solidipes	98.70%	97.90%	0.80%	0.90%	0.40%

Table C5 (continued)

Species	BUSCO results				
	C	S	M	F	M
Armillaria CMW4456	97.90%	96.50%	1.40%	0.50%	1.60%
CBSA	97.80%	97.00%	0.80%	0.20%	2.00%
CBSB	97.60%	96.80%	0.80%	0.40%	2.00%
CBSC	97.80%	96.70%	1.10%	0.30%	1.90%
CBSD	96.80%	96.00%	0.80%	0.40%	2.80%
CBSF	97.60%	96.70%	0.90%	0.40%	2.00%
CBSH	96.70%	96.00%	0.70%	0.40%	2.90%
CBSH1	91.60%	90.90%	0.70%	0.90%	7.50%
CBSI	97.30%	96.50%	0.80%	0.30%	2.40%
CBSJ2	96.90%	96.10%	0.80%	0.50%	2.60%
CBSJ04043	96.60%	95.80%	0.80%	0.50%	2.90%
CBSJ3	97.10%	94.40%	2.70%	0.50%	2.40%
CBSK+G 3	97.10%	96.40%	0.70%	0.50%	2.40%
CBSK+G 2	95.70%	95.00%	0.70%	0.50%	3.80%
CBSL	98.00%	97.20%	0.80%	0.30%	1.70%
CBSN	97.80%	97.10%	0.70%	0.20%	2.00%
CBSO	96.40%	95.60%	0.80%	0.60%	3.00%
CBSP	97.60%	97.10%	0.50%	0.30%	2.10%
CBSQ2	98.00%	97.30%	0.70%	0.20%	1.80%

Table C6 Primer sequences and annealing temperatures used in Qin et al. (2025)

Gene name	Primers	Primer sequences (5'→3')	Annealing temperature (℃)	Reference sequence
actin	Fact1421	GAT GAA GCA CAA TCT AAG CGA GGT	60	Baumgartner et al., (2012)
	Ract2258	TCA CGA CGG ATA TCA AGA TC	60	Baumgartner et al., (2012)
h3h	H3hf1	ATG CAA CAA ATC GAC GAA G	60	Kotlobay et al., (2018)
	H3hr1	CTG AGA TAC AAG CCT CGC TTT	60	Kotlobay et al., (2018)
	H3hf3	TAG ATA CTT GAA TCT TCA A	49	Kotlobay et al., (2018)
	H3hr3	AGA CCC ATC CCG AAG CCT TG	60	Kotlobay et al., 2018

Table C6 (continued)

Gene name	Primers	Primer sequences (5'→3')	Annealing temperature (℃)	Reference sequence
hisps	HPf1655	CGA GGA AAG GCG ATG TGT T	58–60	Kotlobay et al., (2018)
	HPf1676	TCC GTA AGA AGA TTG AAG AT	50	Kotlobay et al., (2018)
	HPr3131	CCC TTG AGA ACG GCC GTT ATG	58–60	Kotlobay et al., (2018)
ITS	ITS4	TCC TCC GCT TAT TGA TAT GC	55	
	ITS5	GGA AGT AAA AGT CGT AAC AAG G	55	
LSU rDNA	ArmLRoR	ACC CGC TGA ACT TAA GCA TAT C	58–60	Vilgalys and Hester (1990)
	ArmLR7	GCT ACT ACC ACC AAG ATC TGC	58–60	Moncalvo et al., (2000)
pks	Fam4183	ACC GAT ATT CTT TCC TCA TC	61	JQ801748, Lackner et al., (2012)
	Ram5428	TCA TAC GCC GTT CGG GTC GTA A	61	JQ801748, Lackner et al., (2012)
*rpb*1	AF7786	CCC AAT TTT CTG GGG GCT CTC	58	LR732075
	R9448	CAC AAA ATG AGT ATG ATG AGT C	58	LR732075
	Rpbf1	GCG TTT TCG GTC GCT TGA TCG CCG	60–72	LR732075
	Rpbr1	TAC GAA CCA GTT CCT GCA GGT AAG C	60–72	LR732075
*tef*1α	EF595F	CGT GAC TTC ATC AAG AAC ATG	60	
	QtefR	GAT TTA CCC GTT CGG CGA TCA AT	60	Ross-Davis et al., (2012), Koch et al., (2017)

Table C7 Quality Assessment Results of varKoder Images

Samples	Species	Varkoder Low Quality Flag
Sample_HMJAU55082	Species_CBSB	FALSE
Sample_HMJAU60448	Species_CBSB	FALSE
Sample_HMJAU24389	Species_CBSC	FALSE
Sample_HMJAU60487	Species_CBSC	FALSE
Sample_alti	Species_ALTI	FALSE
Sample_CBSA96008	Species_CBSA1	FALSE
Sample_CBSA96016	Species_CBSA1	FALSE
Sample_CBSA96025	Species_CBSA1	FALSE
Sample_CBSA96042	Species_CBSA1	FALSE
Sample_HMAS248128	Species_CBSA1	FALSE
Sample_HMAS255468	Species_CBSA1	FALSE
Sample_HMAS255489	Species_CBSA1	FALSE
Sample_HMAS281266	Species_CBSA1	FALSE
Sample_HMAS96969	Species_CBSA1	FALSE
Sample_HMJAU22761	Species_CBSA1	FALSE
Sample_HMJAU23501	Species_CBSA1	FALSE
Sample_HMJAU33876	Species_CBSA1	FALSE
Sample_HMJAU60486	Species_CBSA1	FALSE
Sample_PXL	Species_CBSA2	FALSE
Sample_21HH03	Species_CBSB	FALSE
Sample_21HH04	Species_CBSB	FALSE
Sample_5H	Species_CBSB	FALSE
Sample_6	Species_CBSB	FALSE
Sample_AHLDA9	Species_CBSB	FALSE
Sample_BJM1	Species_CBSB	FALSE
Sample_CBSB03002	Species_CBSB	FALSE
Sample_CBSB19011	Species_CBSB	FALSE
Sample_CBSB19014	Species_CBSB	FALSE
Sample_CBSB19036	Species_CBSB	FALSE
Sample_CBSB96003	Species_CBSB	FALSE
Sample_CBSB96004	Species_CBSB	FALSE
Sample_CBSB96011	Species_CBSB	FALSE

Table C7 (continued)

Samples	Species	Varkoder Low Quality Flag
Sample_CBSB96031	Species_CBSB	FALSE
Sample_CBSB96032	Species_CBSB	FALSE
Sample_CFY1	Species_CBSB	FALSE
Sample_CFY2	Species_CBSB	FALSE
Sample_DBRGZP	Species_CBSB	FALSE
Sample_guo349	Species_CBSB	FALSE
Sample_HB1	Species_CBSB	FALSE
Sample_HB2	Species_CBSB	FALSE
Sample_HB3	Species_CBSB	FALSE
Sample_HB4	Species_CBSB	FALSE
Sample_HB5	Species_CBSB	FALSE
Sample_HB6	Species_CBSB	FALSE
Sample_HDY	Species_CBSB	FALSE
Sample_HKAS45821	Species_CBSB	FALSE
Sample_HKAS92018	Species_CBSB	FALSE
Sample_HMAS255521	Species_CBSB	FALSE
Sample_HMAS255525	Species_CBSB	FALSE
Sample_HMAS255529	Species_CBSB	FALSE
Sample_HMAS273634	Species_CBSB	FALSE
Sample_HMAS276553	Species_CBSB	FALSE
Sample_HMAS33891	Species_CBSB	FALSE
Sample_HMAS37384	Species_CBSB	FALSE
Sample_HMAS61574	Species_CBSB	FALSE
Sample_HMAS96967	Species_CBSB	FALSE
Sample_HMAS97093	Species_CBSB	FALSE
Sample_HS01	Species_CBSB	FALSE
Sample_HSA25	Species_CBSB	FALSE
Sample_HSA9	Species_CBSB	FALSE
Sample_J234	Species_CBSB	FALSE
Sample_KIB7guo345	Species_CBSB	FALSE
Sample_LDM8	Species_CBSB	FALSE
Sample_LM2	Species_CBSB	FALSE

Table C7 (continued)

Samples	Species	Varkoder Low Quality Flag
Sample_LYTA9	Species_CBSB	FALSE
Sample_LZL10	Species_CBSB	FALSE
Sample_LZL1	Species_CBSB	FALSE
Sample_LZL11	Species_CBSB	FALSE
Sample_LZL12	Species_CBSB	FALSE
Sample_LZL13	Species_CBSB	FALSE
Sample_LZL15	Species_CBSB	FALSE
Sample_LZL16	Species_CBSB	FALSE
Sample_LZL17	Species_CBSB	FALSE
Sample_LZL18	Species_CBSB	FALSE
Sample_LZL19	Species_CBSB	FALSE
Sample_LZL20	Species_CBSB	FALSE
Sample_LZL2	Species_CBSB	FALSE
Sample_LZL4	Species_CBSB	FALSE
Sample_LZL6	Species_CBSB	FALSE
Sample_LZL7	Species_CBSB	FALSE
Sample_LZL8	Species_CBSB	FALSE
Sample_LZL9	Species_CBSB	FALSE
Sample_MFM5	Species_CBSB	FALSE
Sample_QA1	Species_CBSB	FALSE
Sample_QF13	Species_CBSB	FALSE
Sample_QM2	Species_CBSB	FALSE
Sample_QM3	Species_CBSB	FALSE
Sample_SA19	Species_CBSB	FALSE
Sample_SJ02	Species_CBSB	FALSE
Sample_SJ06	Species_CBSB	FALSE
Sample_SJ07	Species_CBSB	FALSE
Sample_SJ10	Species_CBSB	FALSE
Sample_SJ103	Species_CBSB	FALSE
Sample_SJ104	Species_CBSB	FALSE
Sample_SJ105	Species_CBSB	FALSE
Sample_SJ150	Species_CBSB	FALSE

Table C7 (continued)

Samples	Species	Varkoder Low Quality Flag
Sample_SJ151	Species_CBSB	FALSE
Sample_SJ152	Species_CBSB	FALSE
Sample_SJ153	Species_CBSB	FALSE
Sample_SJ154	Species_CBSB	FALSE
Sample_SJ155	Species_CBSB	FALSE
Sample_SJ156	Species_CBSB	FALSE
Sample_SJ158	Species_CBSB	FALSE
Sample_SJ159	Species_CBSB	FALSE
Sample_SJ161	Species_CBSB	FALSE
Sample_SJ162	Species_CBSB	FALSE
Sample_SJ164	Species_CBSB	FALSE
Sample_SJ172	Species_CBSB	FALSE
Sample_SJ175	Species_CBSB	FALSE
Sample_SJ176	Species_CBSB	FALSE
Sample_SJ177	Species_CBSB	FALSE
Sample_SJ180	Species_CBSB	FALSE
Sample_SJ181	Species_CBSB	FALSE
Sample_SJ182	Species_CBSB	FALSE
Sample_SJ22	Species_CBSB	FALSE
Sample_SJ27	Species_CBSB	FALSE
Sample_SJ28	Species_CBSB	FALSE
Sample_SJ31	Species_CBSB	FALSE
Sample_SJ35	Species_CBSB	FALSE
Sample_SJ38	Species_CBSB	FALSE
Sample_SJ39	Species_CBSB	FALSE
Sample_SJ40	Species_CBSB	FALSE
Sample_SJ42	Species_CBSB	FALSE
Sample_SJ63	Species_CBSB	FALSE
Sample_SJ73	Species_CBSB	FALSE
Sample_SJ76	Species_CBSB	FALSE
Sample_SJ79	Species_CBSB	FALSE
Sample_SJ85	Species_CBSB	FALSE

Table C7 (continued)

Samples	Species	Varkoder Low Quality Flag
Sample_SJ93	Species_CBSB	FALSE
Sample_SJ96	Species_CBSB	FALSE
Sample_SM18	Species_CBSB	FALSE
Sample_SS01	Species_CBSB	FALSE
Sample_SX_M2	Species_CBSB	FALSE
Sample_T11	Species_CBSB	FALSE
Sample_T12	Species_CBSB	FALSE
Sample_T14	Species_CBSB	FALSE
Sample_T19	Species_CBSB	FALSE
Sample_T20	Species_CBSB	FALSE
Sample_T21	Species_CBSB	FALSE
Sample_T25	Species_CBSB	FALSE
Sample_T27	Species_CBSB	FALSE
Sample_T28	Species_CBSB	FALSE
Sample_T3	Species_CBSB	FALSE
Sample_T6	Species_CBSB	FALSE
Sample_T9	Species_CBSB	FALSE
Sample_WSBM1	Species_CBSB	FALSE
Sample_XY2	Species_CBSB	FALSE
Sample_Y3	Species_CBSB	FALSE
Sample_YSM_470	Species_CBSB	FALSE
Sample_YSM_472	Species_CBSB	FALSE
Sample_YSM_474	Species_CBSB	FALSE
Sample_YSM_481	Species_CBSB	FALSE
Sample_ZM	Species_CBSB	FALSE
Sample_ZT10	Species_CBSB	FALSE
Sample_ZT11	Species_CBSB	FALSE
Sample_ZT12	Species_CBSB	FALSE
Sample_ZT18	Species_CBSB	FALSE
Sample_ZT20	Species_CBSB	FALSE
Sample_ZT2	Species_CBSB	FALSE
Sample_ZT21	Species_CBSB	FALSE

Table C7 (continued)

Samples	Species	Varkoder Low Quality Flag
Sample_ZT22	Species_CBSB	FALSE
Sample_ZT23	Species_CBSB	FALSE
Sample_ZT24	Species_CBSB	FALSE
Sample_ZT25	Species_CBSB	FALSE
Sample_ZT26	Species_CBSB	FALSE
Sample_ZT27	Species_CBSB	FALSE
Sample_ZT28	Species_CBSB	FALSE
Sample_ZT3	Species_CBSB	FALSE
Sample_ZT31	Species_CBSB	FALSE
Sample_ZT32	Species_CBSB	FALSE
Sample_ZT33	Species_CBSB	FALSE
Sample_ZT34	Species_CBSB	FALSE
Sample_ZT35	Species_CBSB	FALSE
Sample_ZT36	Species_CBSB	FALSE
Sample_ZT37	Species_CBSB	FALSE
Sample_ZT38	Species_CBSB	FALSE
Sample_ZT39	Species_CBSB	FALSE
Sample_ZT40	Species_CBSB	FALSE
Sample_ZT4	Species_CBSB	FALSE
Sample_ZT41	Species_CBSB	FALSE
Sample_ZT42	Species_CBSB	FALSE
Sample_ZT43	Species_CBSB	FALSE
Sample_ZT44	Species_CBSB	FALSE
Sample_ZT45	Species_CBSB	FALSE
Sample_ZT46	Species_CBSB	FALSE
Sample_ZT6	Species_CBSB	FALSE
Sample_ZT7	Species_CBSB	FALSE
Sample_21024	Species_CBSC	FALSE
Sample_C19004	Species_CBSC	FALSE
Sample_C21019	Species_CBSC	FALSE
Sample_CBSB19029	Species_CBSC	FALSE
Sample_CBSC21009	Species_CBSC	FALSE

Table C7 (continued)

Samples	Species	Varkoder Low Quality Flag
Sample_CBSC96027	Species_CBSC	FALSE
Sample_CBSC96029	Species_CBSC	FALSE
Sample_CBSC96038	Species_CBSC	FALSE
Sample_guo227	Species_CBSC	FALSE
Sample_LZL5	Species_CBSC	FALSE
Sample_MHHNU7783	Species_CBSC	FALSE
Sample_21043	Species_CBSD1	FALSE
Sample_CBSD02171	Species_CBSD1	FALSE
Sample_CBSD21030	Species_CBSD1	FALSE
Sample_CBSD5193	Species_CBSD1	FALSE
Sample_CBSD5295	Species_CBSD1	FALSE
Sample_CBSD93025	Species_CBSD1	FALSE
Sample_CBSD96043	Species_CBSD1	FALSE
Sample_HMAS145183	Species_CBSD1	FALSE
Sample_HMJAU25401	Species_CBSD1	FALSE
Sample_HMJAU25404	Species_CBSD1	FALSE
Sample_HMJAU25478	Species_CBSD1	FALSE
Sample_HMJAU28932	Species_CBSD1	FALSE
Sample_HMJAU42023	Species_CBSD1	FALSE
Sample_HMJAU42034	Species_CBSD1	FALSE
Sample_HMJAU6143	Species_CBSD1	FALSE
Sample_HMJAU7339	Species_CBSD1	FALSE
Sample_HKAS50184	Species_CBSD2	FALSE
Sample_HKAS56108	Species_CBSD2	FALSE
Sample_HKAS58853	Species_CBSD2	FALSE
Sample_2104919020	Species_CBSF	FALSE
Sample_21HH01	Species_CBSF	FALSE
Sample_21HH02	Species_CBSF	FALSE
Sample_CBSF05030	Species_CBSF	FALSE
Sample_CBSF19020	Species_CBSF	FALSE
Sample_CBSF97033	Species_CBSF	FALSE
Sample_CBSF99103	Species_CBSF	FALSE

Table C7 (continued)

Samples	Species	Varkoder Low Quality Flag
Sample_CBSF99107	Species_CBSF	FALSE
Sample_guo117	Species_CBSF	FALSE
Sample_guo233	Species_CBSF	FALSE
Sample_guo7	Species_CBSF	FALSE
Sample_HMAS22782	Species_CBSF	FALSE
Sample_HMAS253828	Species_CBSF	FALSE
Sample_HMAS273636	Species_CBSF	FALSE
Sample_HMAS61686	Species_CBSF	FALSE
Sample_HMJAU22795	Species_CBSF	FALSE
Sample_HMJAU23629	Species_CBSF	FALSE
Sample_HMJAU23737	Species_CBSF	FALSE
Sample_HMJAU28935	Species_CBSF	FALSE
Sample_MHHNU7577	Species_CBSF	FALSE
Sample_SJ75	Species_CBSF	FALSE
Sample_SJ94	Species_CBSF	FALSE
Sample_SJ97	Species_CBSF	FALSE
Sample_YSM_656	Species_CBSF	FALSE
Sample_ZT8	Species_CBSF	FALSE
Sample_21LJ05	Species_CBSH1	FALSE
Sample_21LJ10	Species_CBSH1	FALSE
Sample_CBSH00019	Species_CBSH1	FALSE
Sample_CBSH0006	Species_CBSH1	FALSE
Sample_CBSH19074	Species_CBSH1	FALSE
Sample_CBSH99011	Species_CBSH1	FALSE
Sample_CBSH99028	Species_CBSH1	FALSE
Sample_guo260	Species_CBSH1	FALSE
Sample_HKAS48804	Species_CBSH1	FALSE
Sample_HKAS56216	Species_CBSH1	FALSE
Sample_HMAS253500	Species_CBSH1	FALSE
Sample_MF266	Species_CBSH1	FALSE
Sample_HMAS272390	Species_CBSH2	FALSE
Sample_HMAS272515	Species_CBSH2	FALSE

Table C7 (continued)

Samples	Species	Varkoder Low Quality Flag
Sample_AT	Species_CBSI	FALSE
Sample_CBSI99122	Species_CBSI	FALSE
Sample_guo261	Species_CBSI	FALSE
Sample_HKAS58683	Species_CBSI	FALSE
Sample_HKAS58910	Species_CBSI	FALSE
Sample_HKAS80228	Species_CBSI	FALSE
Sample_JLK921	Species_CBSI	FALSE
Sample_LDM18	Species_CBSI	FALSE
Sample_MHHNU8836	Species_CBSI	FALSE
Sample_SX_M1	Species_CBSI	FALSE
Sample_21SNJ22	Species_CBSJ1	FALSE
Sample_21SNJ24	Species_CBSJ1	FALSE
Sample_CBSJ04043	Species_CBSJ1	FALSE
Sample_CBSJ05018	Species_CBSJ1	FALSE
Sample_HKAS46283	Species_CBSJ1	FALSE
Sample_HKAS48936	Species_CBSJ1	FALSE
Sample_HKAS49375	Species_CBSJ1	FALSE
Sample_HKAS51007	Species_CBSJ1	FALSE
Sample_HKAS51692	Species_CBSJ1	FALSE
Sample_HKAS89531	Species_CBSJ1	FALSE
Sample_HKAS89629	Species_CBSJ1	FALSE
Sample_HMAS130389	Species_CBSJ1	FALSE
Sample_HMAS130603	Species_CBSJ1	FALSE
Sample_HMAS132012	Species_CBSJ1	FALSE
Sample_HMAS132015	Species_CBSJ1	FALSE
Sample_HMAS254250	Species_CBSJ1	FALSE
Sample_HMAS26066	Species_CBSJ1	FALSE
Sample_HMAS26067	Species_CBSJ1	FALSE
Sample_HMAS274442	Species_CBSJ1	FALSE
Sample_HMAS274553	Species_CBSJ1	FALSE
Sample_HMAS274644	Species_CBSJ1	FALSE
Sample_HMAS276211	Species_CBSJ1	FALSE

Table C7 (continued)

Samples	Species	Varkoder Low Quality Flag
Sample_HMAS276224	Species_CBSJ1	FALSE
Sample_HMAS50996	Species_CBSJ1	FALSE
Sample_HMAS86328	Species_CBSJ1	FALSE
Sample_HMAS86329	Species_CBSJ1	FALSE
Sample_HMAS96843	Species_CBSJ1	FALSE
Sample_HMAS99098	Species_CBSJ1	FALSE
Sample_LYTF31	Species_CBSJ1	FALSE
Sample_SJ102	Species_CBSJ1	FALSE
Sample_SJ131	Species_CBSJ1	FALSE
Sample_SJ135	Species_CBSJ1	FALSE
Sample_SJ136	Species_CBSJ1	FALSE
Sample_SJ141	Species_CBSJ1	FALSE
Sample_SJ142	Species_CBSJ1	FALSE
Sample_SJ146	Species_CBSJ1	FALSE
Sample_SJ147	Species_CBSJ1	FALSE
Sample_YLSF2	Species_CBSJ1	FALSE
Sample_YSLF2	Species_CBSJ1	FALSE
Sample_2105604028	Species_CBSJ2	FALSE
Sample_21LJ06	Species_CBSJ2	FALSE
Sample_Ar3	Species_CBSJ2	FALSE
Sample_Ar8	Species_CBSJ2	FALSE
Sample_Ar9	Species_CBSJ2	FALSE
Sample_CBSJ04028	Species_CBSJ2	FALSE
Sample_FMX	Species_CBSJ2	FALSE
Sample_guo335	Species_CBSJ2	FALSE
Sample_HKAS45609	Species_CBSJ2	FALSE
Sample_HKAS45688	Species_CBSJ2	FALSE
Sample_HKAS45762	Species_CBSJ2	FALSE
Sample_HKAS45773	Species_CBSJ2	FALSE
Sample_HKAS45807	Species_CBSJ2	FALSE
Sample_HKAS45820	Species_CBSJ2	FALSE
Sample_HKAS45974	Species_CBSJ2	FALSE

Table C7 (continued)

Samples	Species	Varkoder Low Quality Flag
Sample_HKAS46314	Species_CBSJ2	FALSE
Sample_HKAS49197	Species_CBSJ2	FALSE
Sample_HKAS51046	Species_CBSJ2	FALSE
Sample_HKAS54932	Species_CBSJ2	FALSE
Sample_HKAS55489	Species_CBSJ2	FALSE
Sample_HKAS82505	Species_CBSJ2	FALSE
Sample_HKAS93952	Species_CBSJ2	FALSE
Sample_HKAS93966	Species_CBSJ2	FALSE
Sample_HMAS272511	Species_CBSJ2	FALSE
Sample_HMAS272651	Species_CBSJ2	FALSE
Sample_HMAS48351	Species_CBSJ2	FALSE
Sample_HMAS51091	Species_CBSJ2	FALSE
Sample_HMAS51095	Species_CBSJ2	FALSE
Sample_JLK213	Species_CBSJ2	FALSE
Sample_LJW1577	Species_CBSJ2	FALSE
Sample_LJW1634	Species_CBSJ2	FALSE
Sample_LJW2388	Species_CBSJ2	FALSE
Sample_LJW2390	Species_CBSJ2	FALSE
Sample_CBSJ04040	Species_CBSJ3	FALSE
Sample_HKAS51258	Species_CBSJ3	FALSE
Sample_HKAS57133	Species_CBSJ3	FALSE
Sample_HKAS89549	Species_CBSJ3	FALSE
Sample_HKAS90943	Species_CBSJ3	FALSE
Sample_HKAS94047	Species_CBSJ3	FALSE
Sample_HMAS254378	Species_CBSJ3	FALSE
Sample_HMAS254476	Species_CBSJ3	FALSE
Sample_HMAS264994	Species_CBSJ3	FALSE
Sample_HMAS272485	Species_CBSJ3	FALSE
Sample_HMAS274066	Species_CBSJ3	FALSE
Sample_HMAS274072	Species_CBSJ3	FALSE
Sample_HMAS274889	Species_CBSJ3	FALSE
Sample_HMAS275000	Species_CBSJ3	FALSE

Table C7 (continued)

Samples	Species	Varkoder Low Quality Flag
Sample_LEI374	Species_CBSJ3	FALSE
Sample_LEI768	Species_CBSJ3	FALSE
Sample_LEI_860	Species_CBSJ3	FALSE
Sample_MH	Species_CBSJ3	FALSE
Sample_CBSJ02044	Species_CBSJ4	FALSE
Sample_HMAS270241	Species_CBSJ4	FALSE
Sample_HMAS38334	Species_CBSJ4	FALSE
Sample_HMAS99054	Species_CBSJ4	FALSE
Sample_LJW668	Species_CBSJ4	FALSE
Sample_MHHNU10251	Species_CBSJ4	FALSE
Sample_NLT01	Species_CBSJ4	FALSE
Sample_NLT05	Species_CBSJ4	FALSE
Sample_GDGM83473	Species_CBSJ5	FALSE
Sample_HKAS49177	Species_CBSJ5	FALSE
Sample_HKAS53619	Species_CBSJ5	FALSE
Sample_HKAS89519	Species_CBSJ5	FALSE
Sample_HKAS89525	Species_CBSJ5	FALSE
Sample_HMAS254774	Species_CBSJ5	FALSE
Sample_HMAS268710	Species_CBSJ5	FALSE
Sample_HMAS274349	Species_CBSJ5	FALSE
Sample_HMAS50997	Species_CBSJ5	FALSE
Sample_HMAS99623	Species_CBSJ5	FALSE
Sample_21LJ07	Species_CBSJunknown	FALSE
Sample_HKAS46284	Species_CBSJunknown	FALSE
Sample_HKAS97181	Species_CBSJunknown	FALSE
Sample_22KM01	Species_CBSKG1	FALSE
Sample_22KM02	Species_CBSKG1	FALSE
Sample_22KM03	Species_CBSKG1	FALSE
Sample_CBSK19083	Species_CBSKG1	FALSE
Sample_CBSK19105	Species_CBSKG1	FALSE
Sample_guo238	Species_CBSKG1	FALSE
Sample_guo247	Species_CBSKG1	FALSE

Table C7 (continued)

Samples	Species	Varkoder Low Quality Flag
Sample_guo248	Species_CBSKG1	FALSE
Sample_guo249	Species_CBSKG1	FALSE
Sample_guo252	Species_CBSKG1	FALSE
Sample_guo256	Species_CBSKG1	FALSE
Sample_HKAS49004	Species_CBSKG1	FALSE
Sample_HKAS52389	Species_CBSKG1	FALSE
Sample_HKAS68003	Species_CBSKG1	FALSE
Sample_HKAS82475	Species_CBSKG1	FALSE
Sample_SJ106	Species_CBSKG1	FALSE
Sample_FM22210	Species_CBSKG2	FALSE
Sample_FM22211	Species_CBSKG2	FALSE
Sample_FM22215	Species_CBSKG2	FALSE
Sample_FM22216	Species_CBSKG2	FALSE
Sample_21LJ03	Species_CBSKG3	FALSE
Sample_21LJ09	Species_CBSKG3	FALSE
Sample_21LJ11	Species_CBSKG3	FALSE
Sample_21SNJ01	Species_CBSKG3	FALSE
Sample_21SNJ05	Species_CBSKG3	FALSE
Sample_221003WSP	Species_CBSKG3	FALSE
Sample_22LL03	Species_CBSKG3	FALSE
Sample_A10	Species_CBSKG3	FALSE
Sample_CBSG19037	Species_CBSKG3	FALSE
Sample_CBSK00111	Species_CBSKG3	FALSE
Sample_CBSK19052	Species_CBSKG3	FALSE
Sample_FM21172	Species_CBSKG3	FALSE
Sample_FM21173	Species_CBSKG3	FALSE
Sample_GDGM76532	Species_CBSKG3	FALSE
Sample_guo230	Species_CBSKG3	FALSE
Sample_guo237	Species_CBSKG3	FALSE
Sample_guo239	Species_CBSKG3	FALSE
Sample_guo242	Species_CBSKG3	FALSE
Sample_HKAS46275	Species_CBSKG3	FALSE

Table C7 (continued)

Samples	Species	Varkoder Low Quality Flag
Sample_HKAS57446	Species_CBSKG3	FALSE
Sample_HKAS58911	Species_CBSKG3	FALSE
Sample_HKAS68632	Species_CBSKG3	FALSE
Sample_HKAS68678	Species_CBSKG3	FALSE
Sample_HKAS74997	Species_CBSKG3	FALSE
Sample_HKAS81274	Species_CBSKG3	FALSE
Sample_HKAS81827	Species_CBSKG3	FALSE
Sample_HKAS81828	Species_CBSKG3	FALSE
Sample_HKAS81829	Species_CBSKG3	FALSE
Sample_HKAS81830	Species_CBSKG3	FALSE
Sample_HKAS81831	Species_CBSKG3	FALSE
Sample_HKAS81832	Species_CBSKG3	FALSE
Sample_HKAS81834	Species_CBSKG3	FALSE
Sample_HKAS82101	Species_CBSKG3	FALSE
Sample_HKAS87145	Species_CBSKG3	FALSE
Sample_HMAS23066	Species_CBSKG3	FALSE
Sample_HMAS253414	Species_CBSKG3	FALSE
Sample_HMAS272369	Species_CBSKG3	FALSE
Sample_HMAS33561	Species_CBSKG3	FALSE
Sample_HMAS50995	Species_CBSKG3	FALSE
Sample_HMAS51088	Species_CBSKG3	FALSE
Sample_JLK003	Species_CBSKG3	FALSE
Sample_LJW1854	Species_CBSKG3	FALSE
Sample_LJW1870	Species_CBSKG3	FALSE
Sample_LJW2225	Species_CBSKG3	FALSE
Sample_LJW2229	Species_CBSKG3	FALSE
Sample_LJW2248	Species_CBSKG3	FALSE
Sample_LJW2249	Species_CBSKG3	FALSE
Sample_LJW779	Species_CBSKG3	FALSE
Sample_LJW849	Species_CBSKG3	FALSE
Sample_MHHNU31945	Species_CBSKG3	FALSE
Sample_MHHNU7419	Species_CBSKG3	FALSE

Table C7 (continued)

Samples	Species	Varkoder Low Quality Flag
Sample_MHHNU8577	Species_CBSKG3	FALSE
Sample_QZ0002012	Species_CBSKG3	FALSE
Sample_SJ113	Species_CBSKG3	FALSE
Sample_SJ115	Species_CBSKG3	FALSE
Sample_SJ116	Species_CBSKG3	FALSE
Sample_WGS1051	Species_CBSKG3	FALSE
Sample_XCB003	Species_CBSKG3	FALSE
Sample_Xu156	Species_CBSKG3	FALSE
Sample_XZ258	Species_CBSKG3	FALSE
Sample_CBSL17017	Species_CBSL	FALSE
Sample_CBSLW17003	Species_CBSL	FALSE
Sample_CBSLW17016	Species_CBSL	FALSE
Sample_CBSLW17039	Species_CBSL	FALSE
Sample_GDGM71117	Species_CBSL	FALSE
Sample_guo271	Species_CBSL	FALSE
Sample_guo272	Species_CBSL	FALSE
Sample_guo324	Species_CBSL	FALSE
Sample_guo82	Species_CBSL	FALSE
Sample_HMAS22781	Species_CBSL	FALSE
Sample_HMIGD71175	Species_CBSL	FALSE
Sample_KIB5guo90	Species_CBSL	FALSE
Sample_KIB9GUO278	Species_CBSL	FALSE
Sample_LH22	Species_CBSL	FALSE
Sample_LW17027	Species_CBSL	FALSE
Sample_LYTF01	Species_CBSL	FALSE
Sample_LZP11	Species_CBSL	FALSE
Sample_LZP15	Species_CBSL	FALSE
Sample_MHHNU31060	Species_CBSL	FALSE
Sample_MHHNU31772	Species_CBSL	FALSE
Sample_MW27	Species_CBSL	FALSE
Sample_TX	Species_CBSL	FALSE
Sample_YSLF1	Species_CBSL	FALSE

Table C7 (continued)

Samples	Species	Varkoder Low Quality Flag
Sample_ZG26	Species_CBSL	FALSE
Sample_ZTMH036	Species_CBSL	FALSE
Sample_21SNJ18	Species_CBSM	FALSE
Sample_21SNJ19	Species_CBSM	FALSE
Sample_CBSM01012	Species_CBSM	FALSE
Sample_CBSM01013	Species_CBSM	FALSE
Sample_CBSM01019	Species_CBSM	FALSE
Sample_CBSM04019	Species_CBSM	FALSE
Sample_CBSM05020	Species_CBSM	FALSE
Sample_CBSM05021	Species_CBSM	FALSE
Sample_guo336	Species_CBSM	FALSE
Sample_HMAS131062	Species_CBSM	FALSE
Sample_HMAS63163	Species_CBSM	FALSE
Sample_SNJ20	Species_CBSM	FALSE
Sample_21SNJ11	Species_CBSN	FALSE
Sample_21SNJ13	Species_CBSN	FALSE
Sample_21SNJ17	Species_CBSN	FALSE
Sample_21SNJ21	Species_CBSN	FALSE
Sample_21SNJ25	Species_CBSN	FALSE
Sample_21SNJ26	Species_CBSN	FALSE
Sample_CBSN02066	Species_CBSN	FALSE
Sample_CBSN02067	Species_CBSN	FALSE
Sample_CBSN02068	Species_CBSN	FALSE
Sample_CBSN02069	Species_CBSN	FALSE
Sample_CBSN02070	Species_CBSN	FALSE
Sample_CBSN16022	Species_CBSN	FALSE
Sample_CBSN19098	Species_CBSN	FALSE
Sample_CBSN19107	Species_CBSN	FALSE
Sample_CBSNW16024	Species_CBSN	FALSE
Sample_DG	Species_CBSN	FALSE
Sample_SJ139	Species_CBSN	FALSE
Sample_SJ143	Species_CBSN	FALSE

Table C7 (continued)

Samples	Species	Varkoder Low Quality Flag
Sample_SJ144	Species_CBSN	FALSE
Sample_SJ145	Species_CBSN	FALSE
Sample_YLCTM	Species_CBSN	FALSE
Sample_ZZZT01	Species_CBSN	FALSE
Sample_19080	Species_CBSO	FALSE
Sample_BD4H	Species_CBSO	FALSE
Sample_guo19	Species_CBSO	FALSE
Sample_guo37	Species_CBSO	FALSE
Sample_HMAS253478	Species_CBSO	FALSE
Sample_HMAS272641	Species_CBSO	FALSE
Sample_KIB6guo322	Species_CBSO	FALSE
Sample_LM1	Species_CBSO	FALSE
Sample_LYTF05	Species_CBSO	FALSE
Sample_LYTF19	Species_CBSO	FALSE
Sample_LYTF34	Species_CBSO	FALSE
Sample_LYTY1	Species_CBSO	FALSE
Sample_MFM6	Species_CBSO	FALSE
Sample_MHHNU8447	Species_CBSO	FALSE
Sample_O19095	Species_CBSO	FALSE
Sample_SM1	Species_CBSO	FALSE
Sample_ZT15	Species_CBSO	FALSE
Sample_ZTM6	Species_CBSO	FALSE
Sample_ZTMF	Species_CBSO	FALSE
Sample_ztmh1	Species_CBSO	FALSE
Sample_ztmh13	Species_CBSO	FALSE
Sample_19060	Species_CBSP	FALSE
Sample_19062	Species_CBSP	FALSE
Sample_CLZ12638	Species_CBSP	FALSE
Sample_LYTF17	Species_CBSP	FALSE
Sample_QZ19053	Species_CBSP	FALSE
Sample_QZ19054	Species_CBSP	FALSE
Sample_QZ19055	Species_CBSP	FALSE

Table C7 (continued)

Samples	Species	Varkoder Low Quality Flag
Sample_QZ19058	Species_CBSP	FALSE
Sample_QZ19059	Species_CBSP	FALSE
Sample_QZ19061	Species_CBSP	FALSE
Sample_ZT14	Species_CBSP	FALSE
Sample_ZT29	Species_CBSP	FALSE
Sample_ztmh30	Species_CBSP	FALSE
Sample_LEI_439	Species_CBSQ1	FALSE
Sample_WGS75	Species_CBSQ1	FALSE
Sample_22DWS01	Species_CBSQ2	FALSE
Sample_22DWS02	Species_CBSQ2	FALSE
Sample_22DWS03	Species_CBSQ2	FALSE
Sample_22DWS04	Species_CBSQ2	FALSE
Sample_22DWS05	Species_CBSQ2	FALSE
Sample_22DWS06	Species_CBSQ2	FALSE
Sample_22DWS07	Species_CBSQ2	FALSE
Sample_HKAS95344	Species_CBSQ2	FALSE
Sample_GDGM77873	Species_EBSA	FALSE
Sample_guo338	Species_EBSA	FALSE
Sample_KK902525	Species_EBSA	FALSE
Sample_19041	Species_EBSB	FALSE
Sample_19042	Species_EBSB	FALSE
Sample_KK890661	Species_EBSB	FALSE
Sample_CBSD19044	Species_EBSC	FALSE
Sample_KK891152	Species_EBSD	FALSE
Sample_gemi	Species_GIMI	FALSE
Sample_nabs	Species_NAB	FALSE
Sample_B621	Species_NABSIII	FALSE
Sample_B618	Species_NABSV	FALSE
Sample_GDGM70002	Species_NABSVI	FALSE
Sample_GDGM70010	Species_NABSVI	FALSE
Sample_VIVII	Species_NABSVI	FALSE
Sample_guo222	Species_NABSVII	FALSE

Table C7 (continued)

Samples	Species	Varkoder Low Quality Flag
Sample_XZ151	Species_NoBSN2	FALSE
Sample_XZ199	Species_NoBSN2	FALSE
Sample_8563	Species_NoBSN4	FALSE
Sample_8745	Species_NoBSN7	FALSE
Sample_guo216	Species_NoBSN8	FALSE
Sample_guo246	Species_NoBSN8	FALSE
Sample_KK700113	Species_NoBSN8	FALSE
Sample_guo262	Species_NoBSN9	FALSE

Table C8 The species identification results from the three validation sets. For each samples, a query set consisting of nine images generated from different post-cleaning base pairs (from 500K to 200000K) was used as input

Sample_id	Actual_labels	Correct Identification Rate	No Result	Incorrect Identification Rate
CBSA96008	Species_CBSA1	1/9	0/9	8/9
CBSA96025	Species_CBSA1	5/9	1/9	3/9
HMAS255489	Species_CBSA1	7/9	1/9	1/9
CBSA96042	Species_CBSA1	8/9	1/9	0/9
HMAS96969	Species_CBSA1	8/9	1/9	0/9
HMAS248128	Species_CBSA1	9/9	0/9	0/9
HMAS255468	Species_CBSA1	9/9	0/9	0/9
HMAS281266	Species_CBSA1	9/9	0/9	0/9
6	Species_CBSB	9/9	0/9	0/9
21HH03	Species_CBSB	9/9	0/9	0/9
21HH04	Species_CBSB	9/9	0/9	0/9
5H	Species_CBSB	9/9	0/9	0/9
AHLDA9	Species_CBSB	9/9	0/9	0/9
BJM1	Species_CBSB	9/9	0/9	0/9
CBSB03002	Species_CBSB	9/9	0/9	0/9
CBSB19011	Species_CBSB	9/9	0/9	0/9
CBSB19014	Species_CBSB	9/9	0/9	0/9

Table C8 (continued)

Sample_id	Actual_labels	Correct Identification Rate	No Result	Incorrect Identification Rate
CBSB19029	Species_CBSC	6/9	3/9	0/9
CBSC96027	Species_CBSC	6/9	3/9	0/9
CBSC21009	Species_CBSC	7/9	1/9	1/9
guo227	Species_CBSC	7/9	2/9	0/9
21024	Species_CBSC	8/9	1/9	0/9
C21019	Species_CBSC	8/9	1/9	0/9
CBSC96029	Species_CBSC	8/9	1/9	0/9
CBSC96038	Species_CBSC	8/9	0/9	1/9
C19004	Species_CBSC	9/9	0/9	0/9
CBSD93025	Species_CBSD1	0/9	7/9	2/9
HMAS145183	Species_CBSD1	7/9	2/9	0/9
CBSD21030	Species_CBSD1	8/9	0/9	1/9
21043	Species_CBSD1	9/9	0/9	0/9
CBSD02171	Species_CBSD1	9/9	0/9	0/9
CBSD5193	Species_CBSD1	9/9	0/9	0/9
CBSD5295	Species_CBSD1	9/9	0/9	0/9
CBSD96043	Species_CBSD1	9/9	0/9	0/9
HMJAU25401	Species_CBSD1	9/9	0/9	0/9
HKAS50184	Species_CBSD2	9/9	0/9	0/9
HKAS56108	Species_CBSD2	9/9	0/9	0/9
HKAS58853	Species_CBSD2	9/9	0/9	0/9
21HH01	Species_CBSF	6/9	2/9	1/9
2104919020	Species_CBSF	7/9	1/9	1/9
CBSF05030	Species_CBSF	7/9	2/9	0/9
CBSF97033	Species_CBSF	8/9	1/9	0/9
CBSF99103	Species_CBSF	8/9	1/9	0/9
CBSF99107	Species_CBSF	8/9	1/9	0/9
guo117	Species_CBSF	8/9	1/9	0/9
21HH02	Species_CBSF	9/9	0/9	0/9
CBSF19020	Species_CBSF	9/9	0/9	0/9

Table C8 (continued)

Sample_id	Actual_labels	Correct Identification Rate	No Result	Incorrect Identification Rate
CBSH99011	Species_CBSH1	5/9	2/9	2/9
CBSH00019	Species_CBSH1	6/9	3/9	0/9
HKAS48804	Species_CBSH1	6/9	3/9	0/9
21LJ05	Species_CBSH1	7/9	0/9	2/9
CBSH99028	Species_CBSH1	7/9	1/9	1/9
21LJ10	Species_CBSH1	8/9	0/9	1/9
CBSH19074	Species_CBSH1	8/9	1/9	0/9
guo260	Species_CBSH1	8/9	1/9	0/9
CBSH0006	Species_CBSH1	9/9	0/9	0/9
HMAS272390	Species_CBSH2	6/9	3/9	0/9
HMAS272515	Species_CBSH2	7/9	1/9	1/9
MHHNU8836	Species_CBSI	0/9	8/9	1/9
JLK921	Species_CBSI	7/9	0/9	2/9
CBSI99122	Species_CBSI	8/9	1/9	0/9
HKAS58683	Species_CBSI	8/9	0/9	1/9
LDM18	Species_CBSI	8/9	1/9	0/9
AT	Species_CBSI	9/9	0/9	0/9
guo261	Species_CBSI	9/9	0/9	0/9
HKAS58910	Species_CBSI	9/9	0/9	0/9
HKAS80228	Species_CBSI	9/9	0/9	0/9
HKAS46283	Species_CBSJ1	0/9	0/9	9/9
HKAS51692	Species_CBSJ1	2/9	3/9	4/9
CBSJ04043	Species_CBSJ1	6/9	2/9	1/9
21SNJ22	Species_CBSJ1	8/9	1/9	0/9
21SNJ24	Species_CBSJ1	8/9	0/9	1/9
CBSJ05018	Species_CBSJ1	8/9	1/9	0/9
HKAS51007	Species_CBSJ1	8/9	1/9	0/9
HKAS48936	Species_CBSJ1	9/9	0/9	0/9
HKAS49375	Species_CBSJ1	9/9	0/9	0/9
2105604028	Species_CBSJ2	4/9	2/9	3/9

Table C8 (continued)

Sample_id	Actual_labels	Correct Identification Rate	No Result	Incorrect Identification Rate
FMX	Species_CBSJ2	5/9	3/9	1/9
Ar3	Species_CBSJ2	7/9	0/9	2/9
Ar8	Species_CBSJ2	7/9	1/9	1/9
CBSJ04028	Species_CBSJ2	7/9	1/9	1/9
21LJ06	Species_CBSJ2	8/9	1/9	0/9
Ar9	Species_CBSJ2	8/9	1/9	0/9
guo335	Species_CBSJ2	9/9	0/9	0/9
HKAS45609	Species_CBSJ2	9/9	0/9	0/9
CBSJ04040	Species_CBSJ3	0/9	3/9	3/9
HMAS264994	Species_CBSJ3	0/9	9/9	0/9
HKAS89549	Species_CBSJ3	3/9	5/9	1/9
HKAS51258	Species_CBSJ3	8/9	1/9	0/9
HKAS57133	Species_CBSJ3	8/9	0/9	1/9
HKAS90943	Species_CBSJ3	8/9	0/9	1/9
HKAS94047	Species_CBSJ3	8/9	1/9	0/9
HMAS254378	Species_CBSJ3	8/9	0/9	1/9
HMAS254476	Species_CBSJ3	9/9	0/9	0/9
HMAS38334	Species_CBSJ4	2/9	6/9	1/9
HMAS99054	Species_CBSJ4	4/9	4/9	1/9
NLT01	Species_CBSJ4	6/9	1/9	2/9
NLT05	Species_CBSJ4	7/9	1/9	1/9
CBSJ02044	Species_CBSJ4	8/9	1/9	0/9
LJW668	Species_CBSJ4	8/9	0/9	1/9
HMAS270241	Species_CBSJ4	9/9	0/9	0/9
MHHNU10251	Species_CBSJ4	9/9	0/9	0/9
GDGM83473	Species_CBSJ5	0/9	4/9	5/9
HMAS254774	Species_CBSJ5	0/9	0/9	9/9
HMAS50997	Species_CBSJ5	0/9	1/9	8/9
HMAS268710	Species_CBSJ5	5/9	3/9	1/9
HKAS49177	Species_CBSJ5	9/9	0/9	0/9

Table C8 (continued)

Sample_id	Actual_labels	Correct Identification Rate	No Result	Incorrect Identification Rate
HKAS53619	Species_CBSJ5	9/9	0/9	0/9
HKAS89519	Species_CBSJ5	9/9	0/9	0/9
HKAS89525	Species_CBSJ5	9/9	0/9	0/9
HMAS274349	Species_CBSJ5	9/9	0/9	0/9
CBSK19105	Species_CBSKG1	1/9	7/9	1/9
guo238	Species_CBSKG1	7/9	0/9	2/9
guo247	Species_CBSKG1	7/9	1/9	1/9
22KM02	Species_CBSKG1	8/9	1/9	0/9
22KM03	Species_CBSKG1	8/9	1/9	0/9
22KM01	Species_CBSKG1	9/9	0/9	0/9
CBSK19083	Species_CBSKG1	9/9	0/9	0/9
guo248	Species_CBSKG1	9/9	0/9	0/9
guo249	Species_CBSKG1	9/9	0/9	0/9
FM22211	Species_CBSKG2	0/9	0/9	9/9
FM22215	Species_CBSKG2	5/9	0/9	4/9
FM22210	Species_CBSKG2	6/9	1/9	2/9
21SNJ01	Species_CBSKG3	0/9	0/9	9/9
CBSG19037	Species_CBSKG3	8/9	0/9	1/9
21LJ03	Species_CBSKG3	9/9	0/9	0/9
21LJ09	Species_CBSKG3	9/9	0/9	0/9
21LJ11	Species_CBSKG3	9/9	0/9	0/9
21SNJ05	Species_CBSKG3	9/9	0/9	0/9
221003WSP	Species_CBSKG3	9/9	0/9	0/9
22LL03	Species_CBSKG3	9/9	0/9	0/9
A10	Species_CBSKG3	9/9	0/9	0/9
CBSL17017	Species_CBSL	6/9	1/9	2/9
GDGM71117	Species_CBSL	7/9	1/9	1/9
CBSLW17003	Species_CBSL	8/9	0/9	1/9
CBSLW17016	Species_CBSL	8/9	0/9	1/9
CBSLW17039	Species_CBSL	8/9	0/9	1/9

Table C8 (continued)

Sample_id	Actual_labels	Correct Identification Rate	No Result	Incorrect Identification Rate
guo272	Species_CBSL	8/9	0/9	1/9
guo82	Species_CBSL	8/9	0/9	0/9
guo271	Species_CBSL	9/9	0/9	0/9
guo324	Species_CBSL	9/9	0/9	0/9
21SNJ19	Species_CBSM	1/9	8/9	0/9
CBSM05021	Species_CBSM	1/9	1/9	7/9
CBSM01019	Species_CBSM	6/9	3/9	0/9
CBSM05020	Species_CBSM	6/9	2/9	1/9
CBSM01013	Species_CBSM	8/9	1/9	0/9
guo336	Species_CBSM	8/9	1/9	0/9
21SNJ18	Species_CBSM	9/9	0/9	1/9
CBSM01012	Species_CBSM	9/9	0/9	1/9
CBSM04019	Species_CBSM	9/9	0/9	0/9
CBSN02067	Species_CBSN	6/9	2/9	1/9
CBSN02066	Species_CBSN	7/9	0/9	2/9
21SNJ13	Species_CBSN	8/9	1/9	1/9
21SNJ17	Species_CBSN	8/9	1/9	0/9
21SNJ21	Species_CBSN	8/9	0/9	1/9
21SNJ26	Species_CBSN	8/9	0/9	1/9
CBSN02068	Species_CBSN	8/9	1/9	0/9
21SNJ11	Species_CBSN	9/9	0/9	1/9
21SNJ25	Species_CBSN	9/9	0/9	0/9
HMAS253478	Species_CBSO	0/9	1/9	8/9
HMAS272641	Species_CBSO	0/9	1/9	8/9
19080	Species_CBSO	8/9	1/9	0/9
LYTF05	Species_CBSO	8/9	1/9	0/9
BD4H	Species_CBSO	9/9	0/9	0/9
guo19	Species_CBSO	9/9	0/9	0/9
guo37	Species_CBSO	9/9	0/9	0/9
KIB6guo322	Species_CBSO	9/9	0/9	0/9

Table C8 (continued)

Sample_id	Actual_labels	Correct Identification Rate	No Result	Incorrect Identification Rate
LM1	Species_CBSO	9/9	0/9	0/9
CLZ12638	Species_CBSP	0/9	6/9	3/9
QZ19053	Species_CBSP	8/9	0/9	1/9
QZ19055	Species_CBSP	8/9	1/9	0/9
QZ19059	Species_CBSP	8/9	1/9	0/9
19060	Species_CBSP	9/9	0/9	0/9
19062	Species_CBSP	9/9	0/9	0/9
LYTF17	Species_CBSP	9/9	0/9	0/9
QZ19054	Species_CBSP	9/9	0/9	0/9
QZ19058	Species_CBSP	9/9	0/9	0/9
LEI_439	Species_CBSQ1	0/9	0/9	9/9
WGS75	Species_CBSQ1	0/9	2/9	7/9
22DWS01	Species_CBSQ2	8/9	1/9	0/9
22DWS03	Species_CBSQ2	8/9	1/9	0/9
22DWS02	Species_CBSQ2	9/9	0/9	0/9
22DWS04	Species_CBSQ2	9/9	0/9	0/9
22DWS05	Species_CBSQ2	9/9	0/9	0/9
22DWS06	Species_CBSQ2	9/9	0/9	0/9
22DWS07	Species_CBSQ2	9/9	0/9	0/9
HKAS95344	Species_CBSQ2	9/9	0/9	0/9
KK902525	Species_EBSA	5/9	2/9	2/9
guo338	Species_EBSA	7/9	0/9	2/9
GDGM77873	Species_EBSA	8/9	1/9	0/9
19041	Species_EBSB	3/9	0/9	6/9
19042	Species_EBSB	7/9	1/9	1/9
KK890661	Species_EBSB	7/9	2/9	0/9
GDGM70002	Species_NABSVI	9/9	0/9	0/9
GDGM70010	Species_NABSVI	9/9	0/9	0/9
VIVII	Species_NABSVI	9/9	0/9	0/9
XZ151	Species_NoBSN2	8/9	1/9	0/9

Table C8 (continued)

Sample_id	Actual_labels	Correct Identification Rate	No Result	Incorrect Identification Rate
XZ199	Species_NoBSN2	9/9	0/9	0/9
guo216	Species_NoBSN8	8/9	1/9	0/9
guo246	Species_NoBSN8	9/9	0/9	0/9
KK700113	Species_NoBSN8	9/9	0/9	0/9

APPENDIX D

SUPPLEMENTARY FIGURES

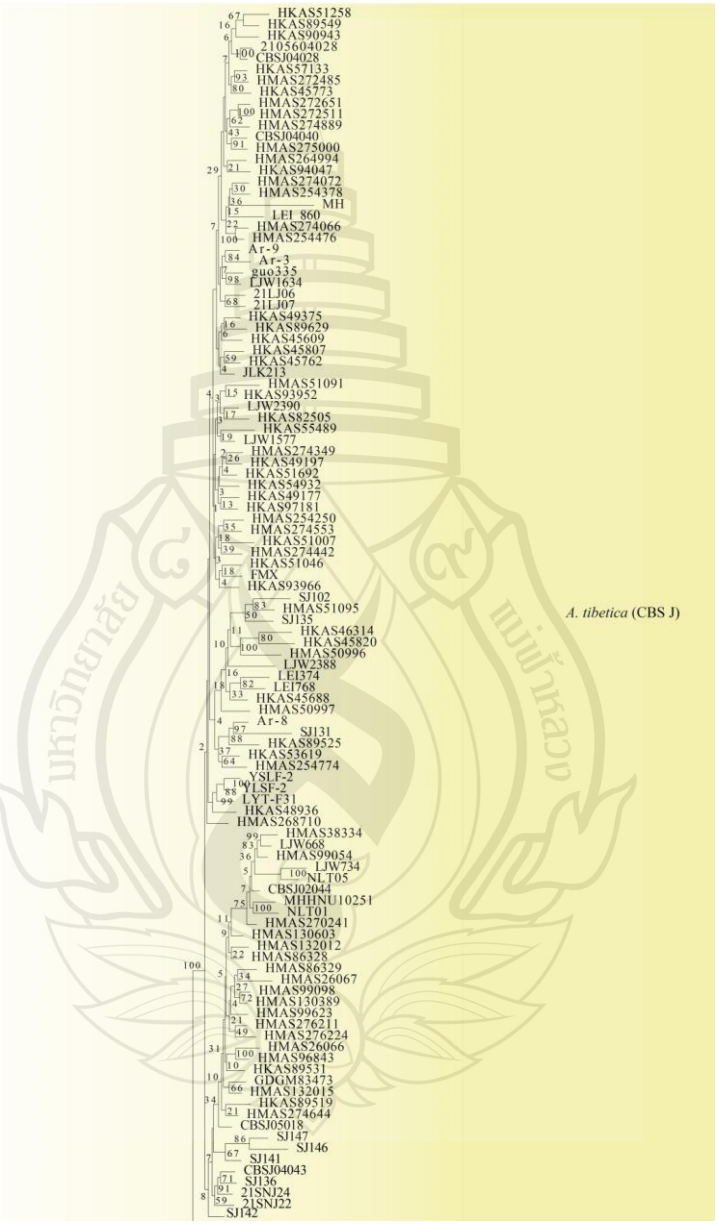


Figure D1 Maximum-likelihood (ML) phylogenetic tree of *Armillaria* inferred from 385 orthologues across 600 nuclear genomes

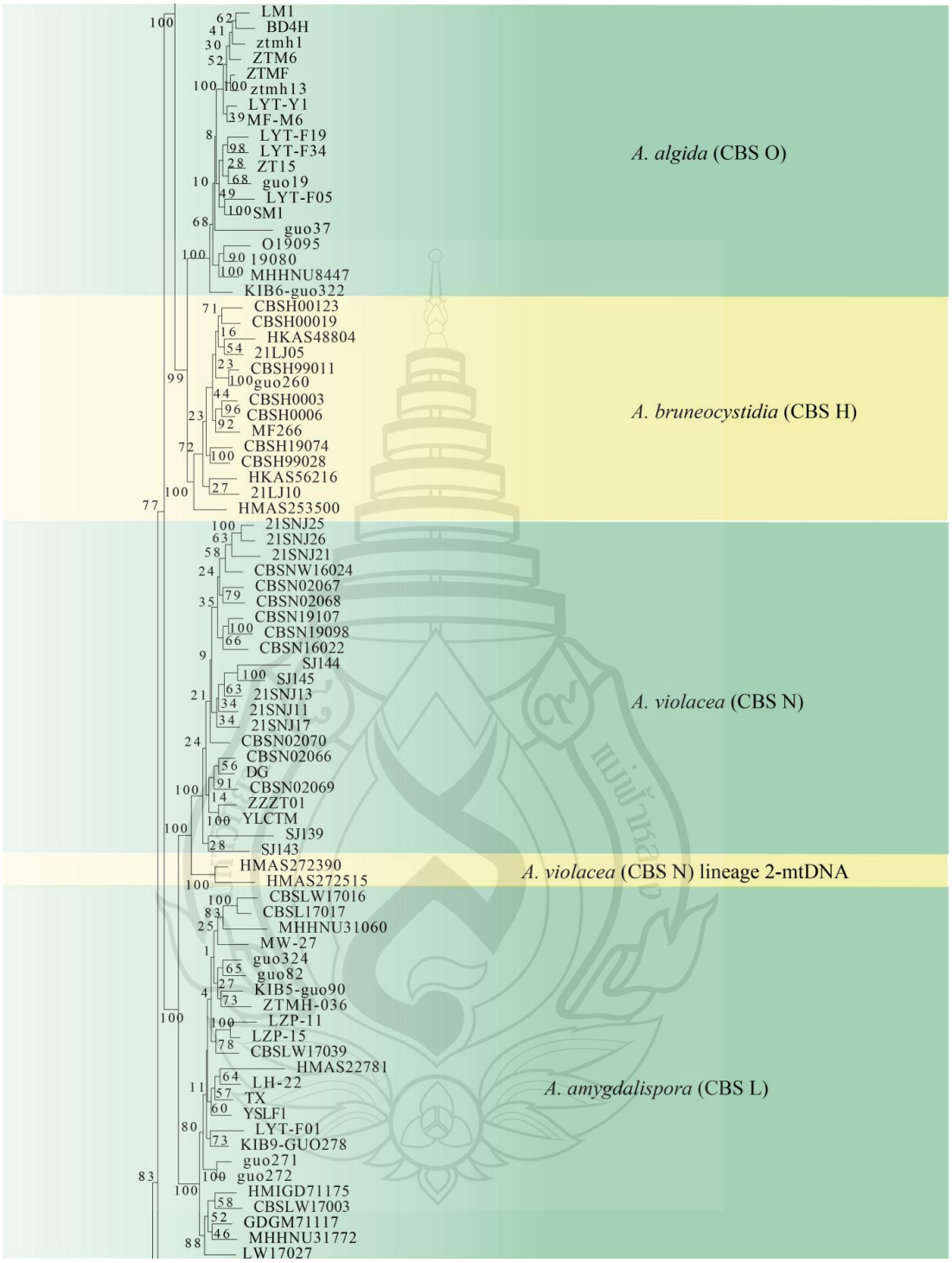


Figure D1 (continued)

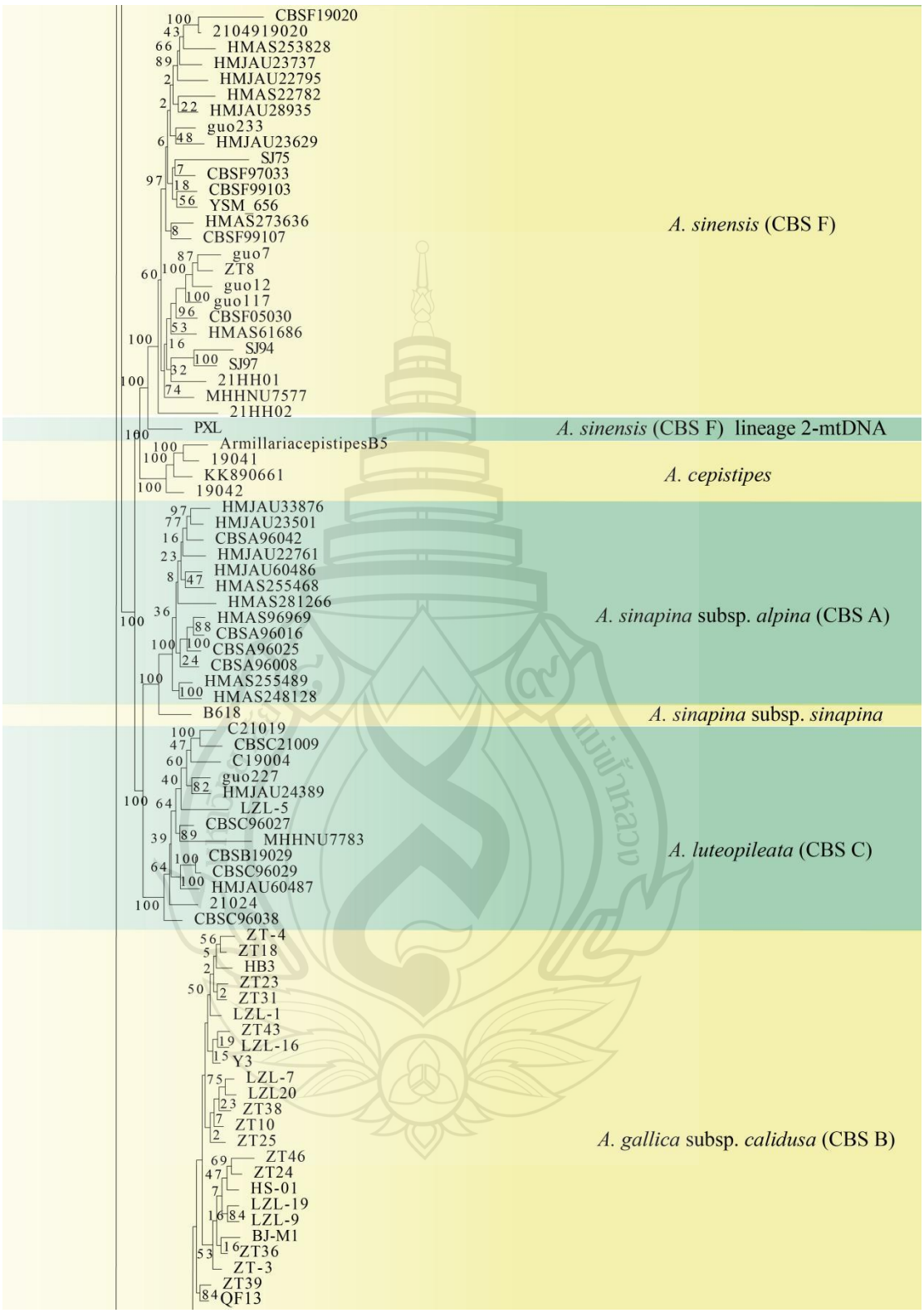


Figure D1 (continued)

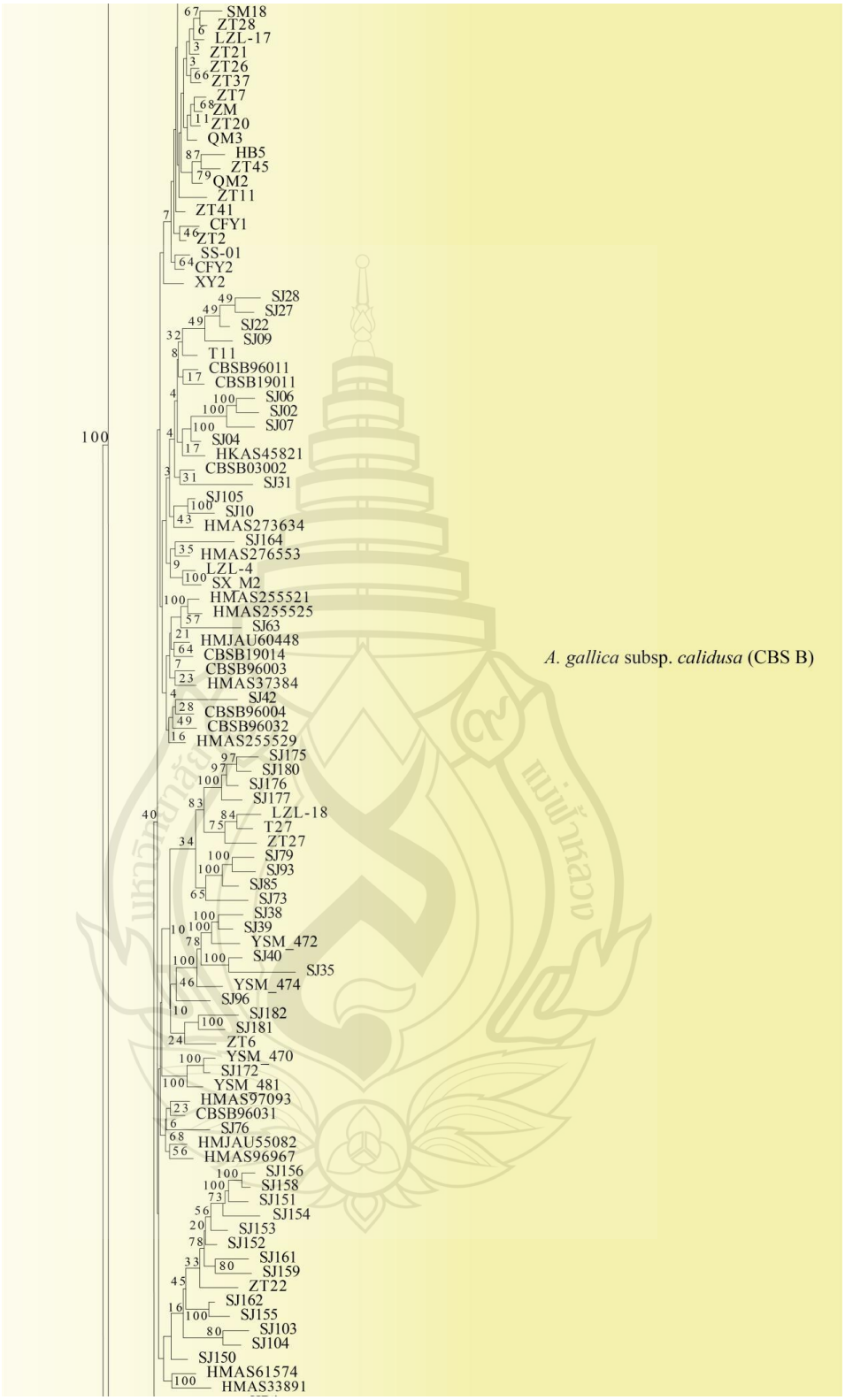


Figure D1 (continued)

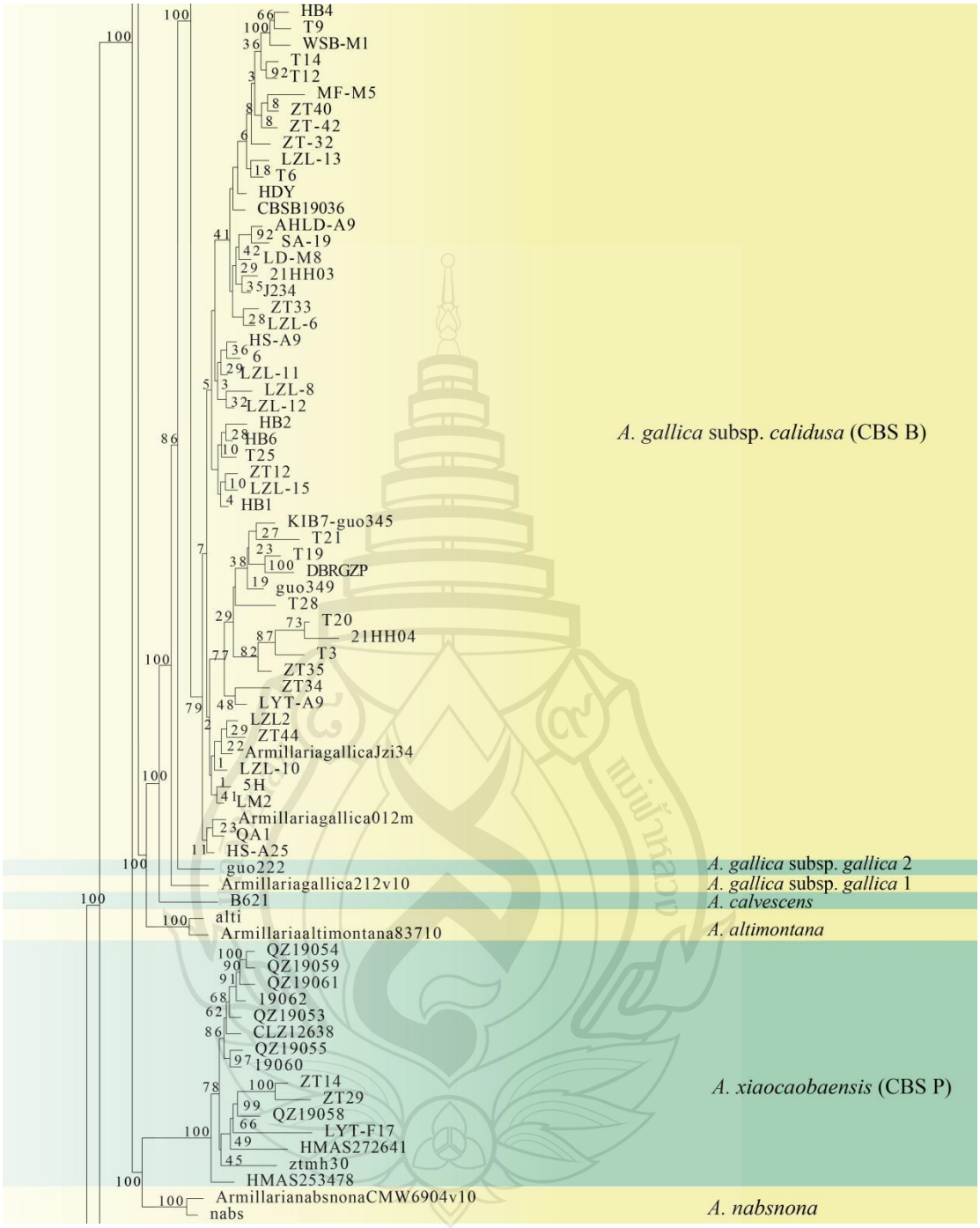


Figure D1 (continued)

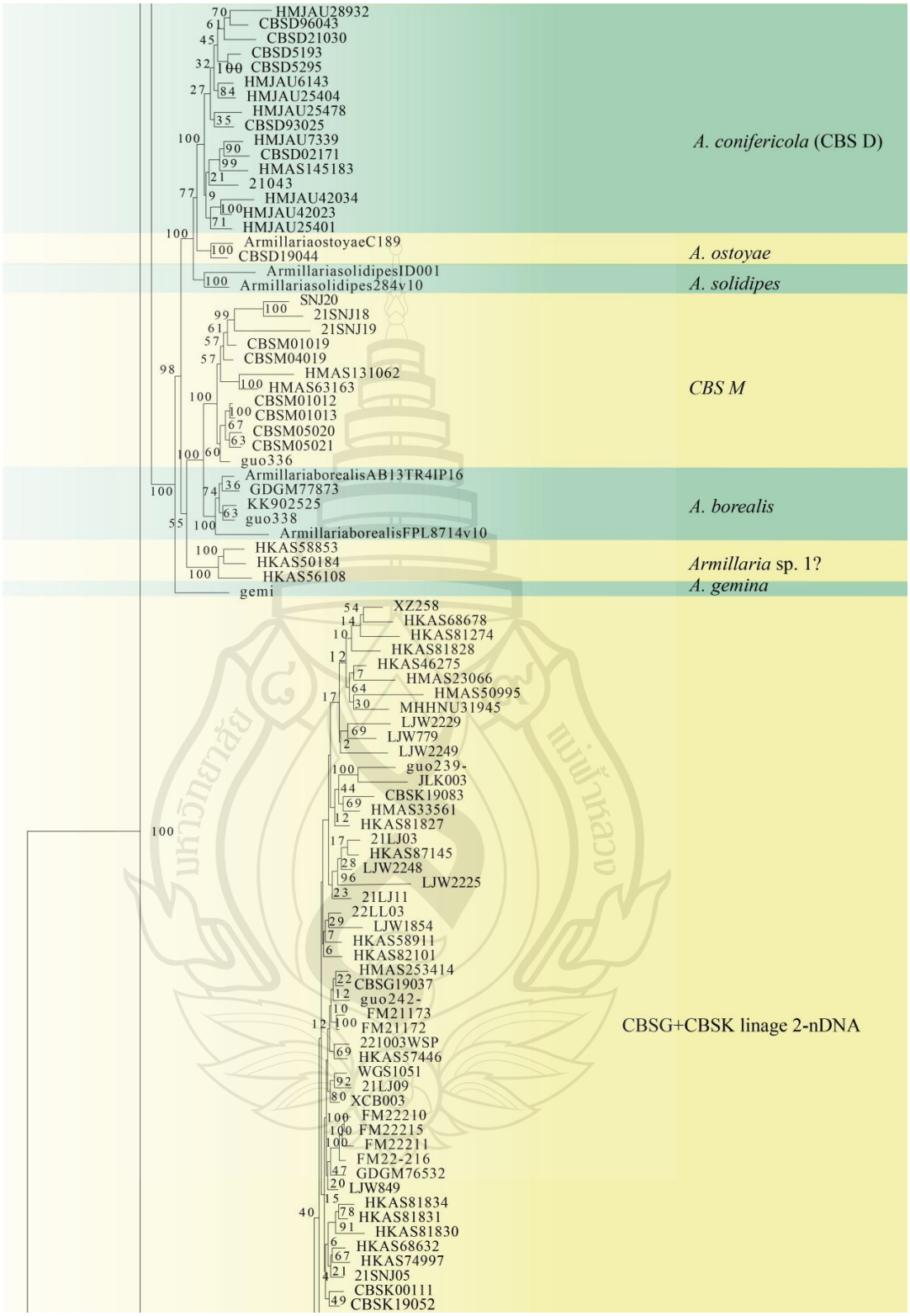
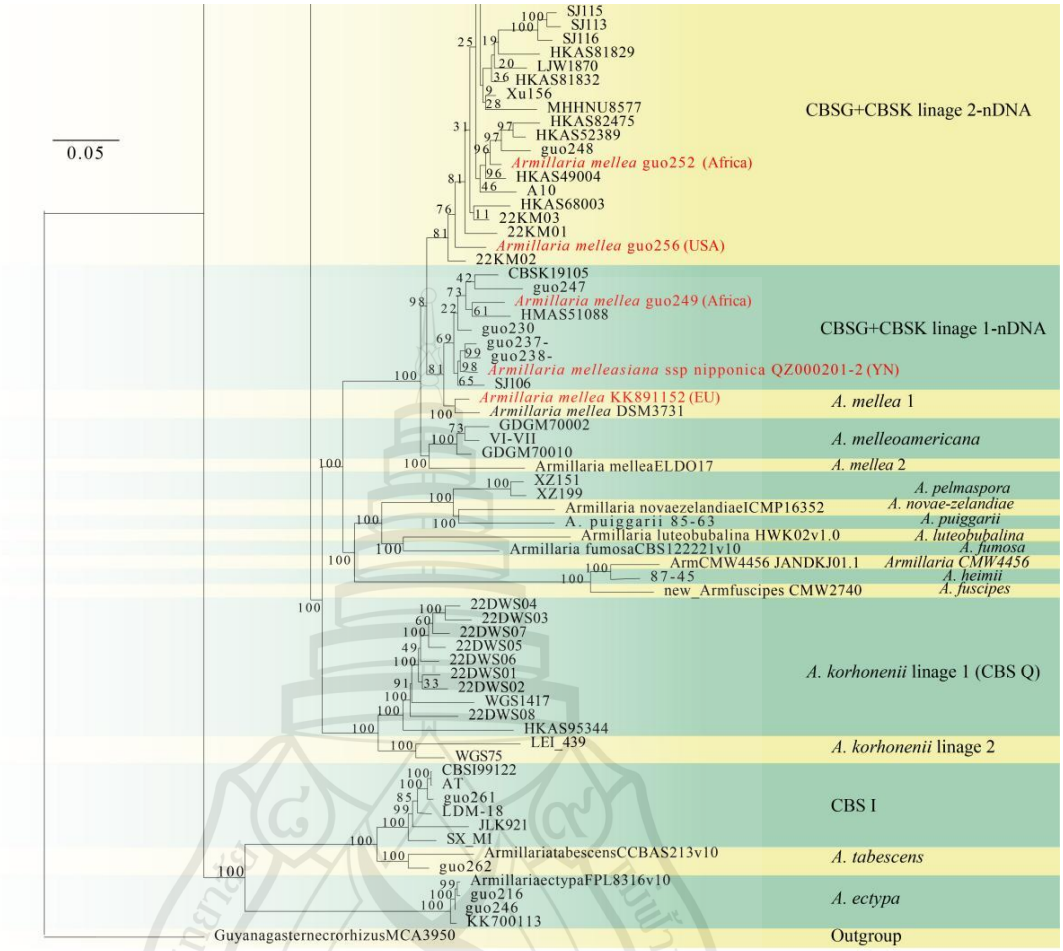


Figure D1 (continued)



Note Bootstrap (BS) values (≥ 70%) derived from the ML analysis are shown above the branches at the nodes. The tree is rooted with *Guyanagaster necrorhizus*.

Figure D1 (continued)

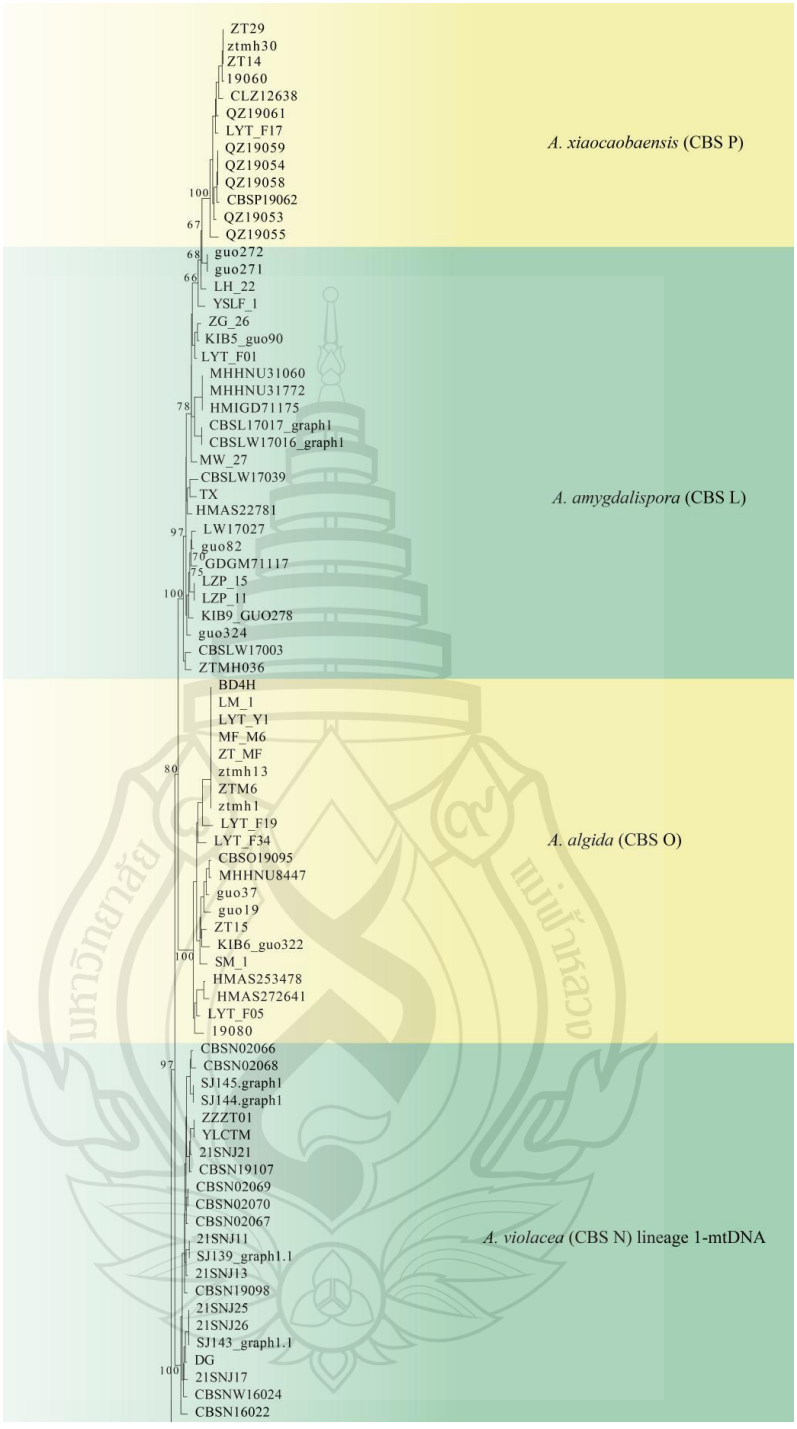


Figure D2 Maximum-Likelihood (ML) phylogenetic tree of genus *Armillaria* constructed from a concatenated dataset of 605 mitochondrial homeblocks

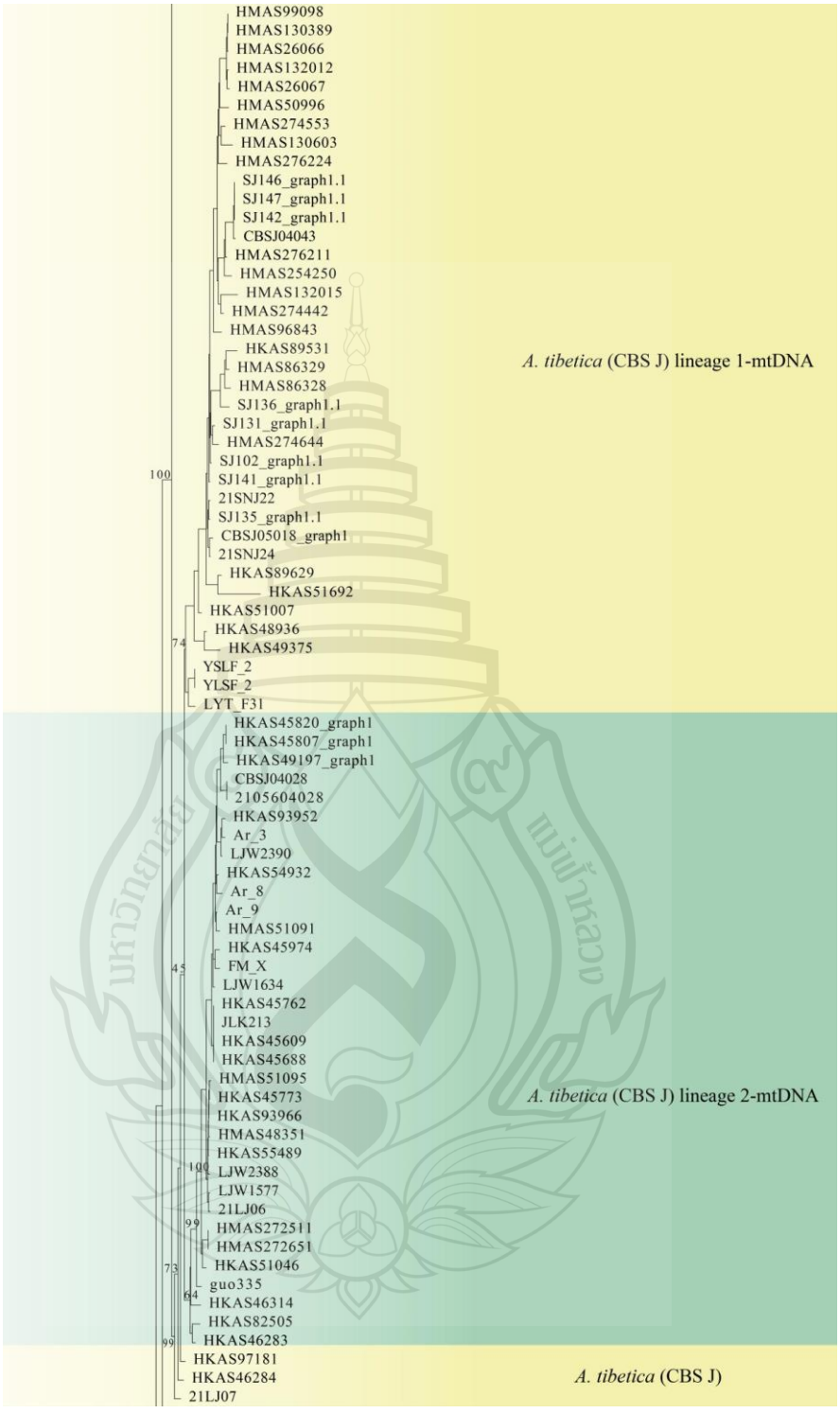


Figure D2 (continued)

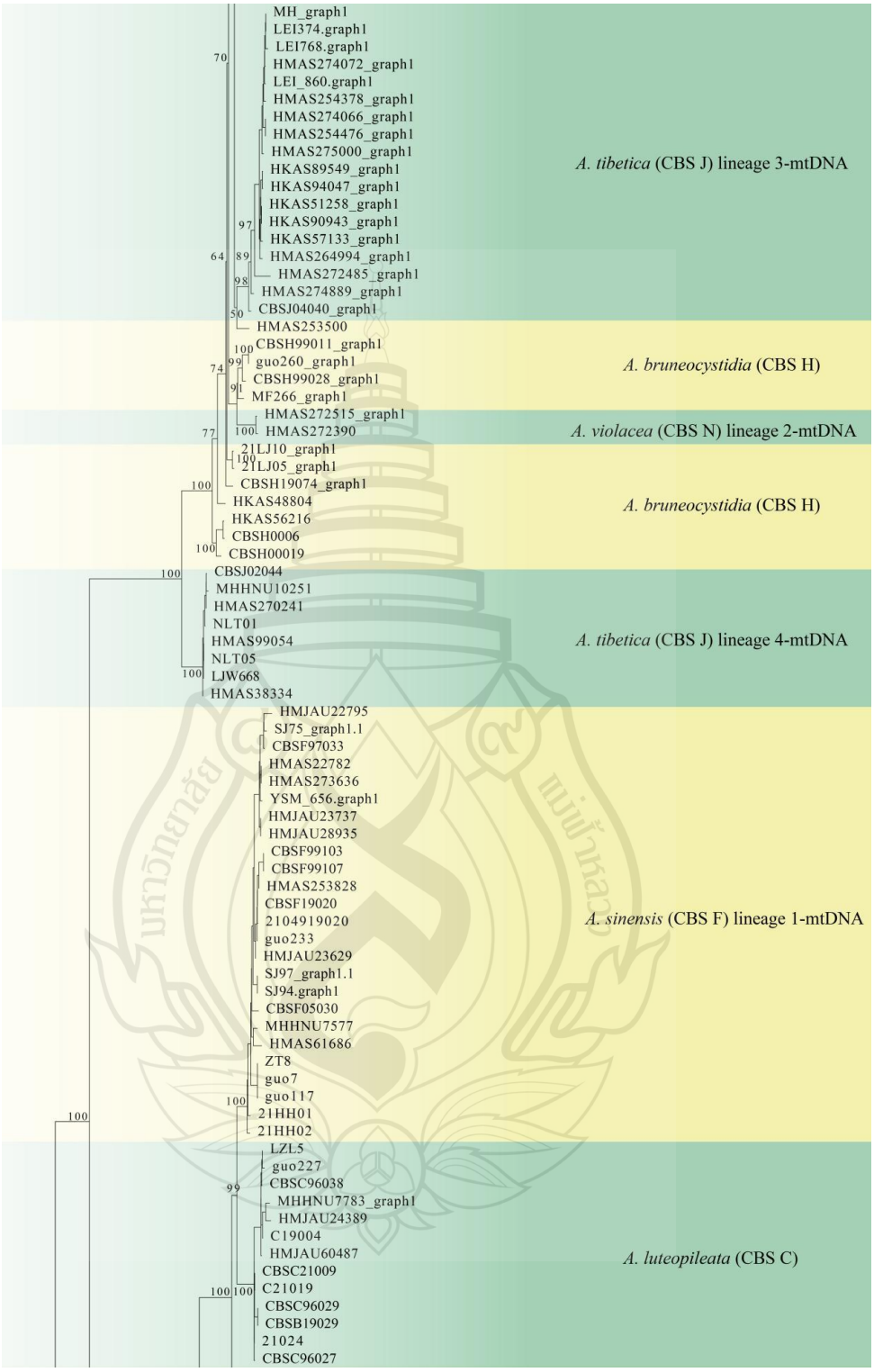


Figure D2 (continued)

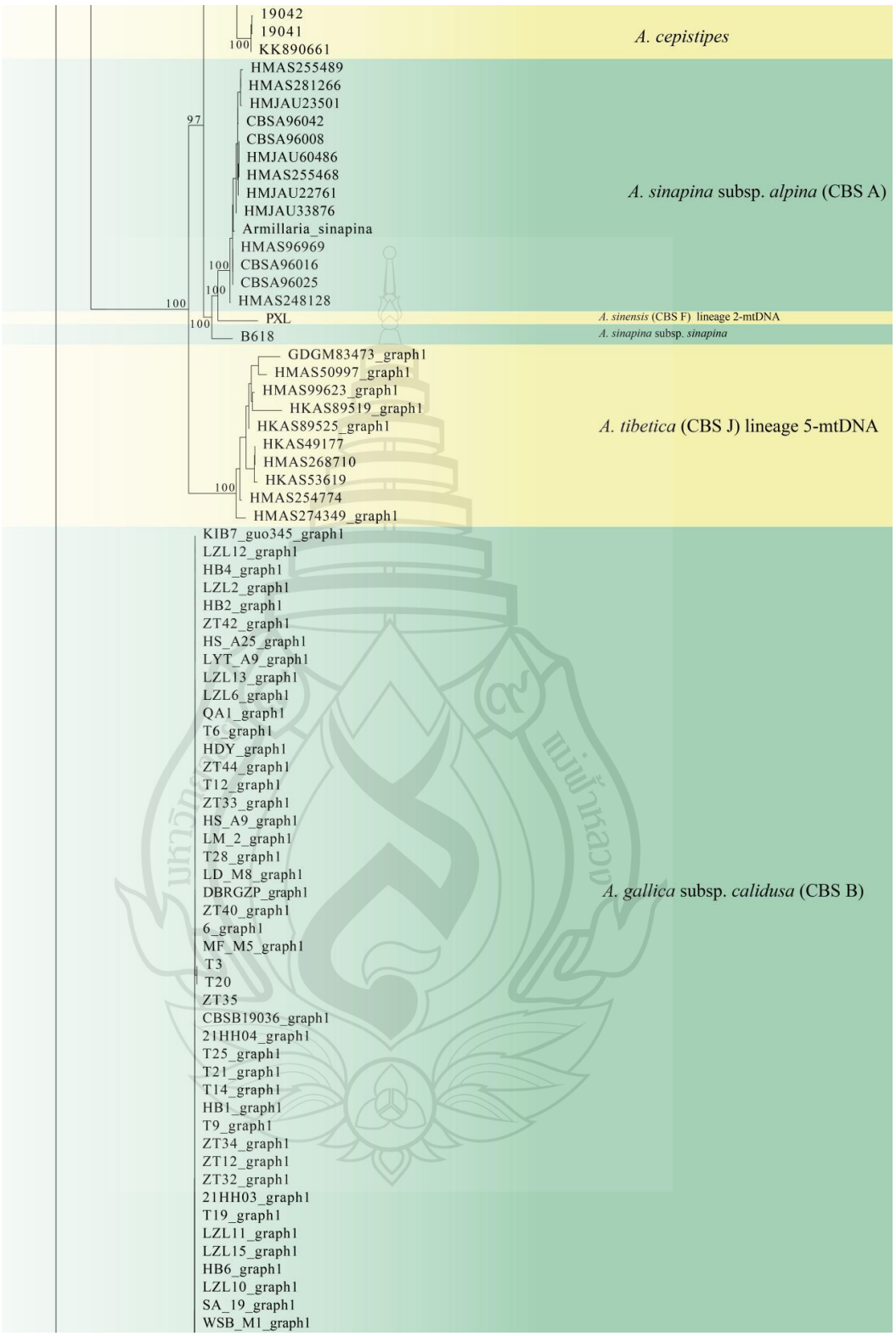


Figure D2 (continued)

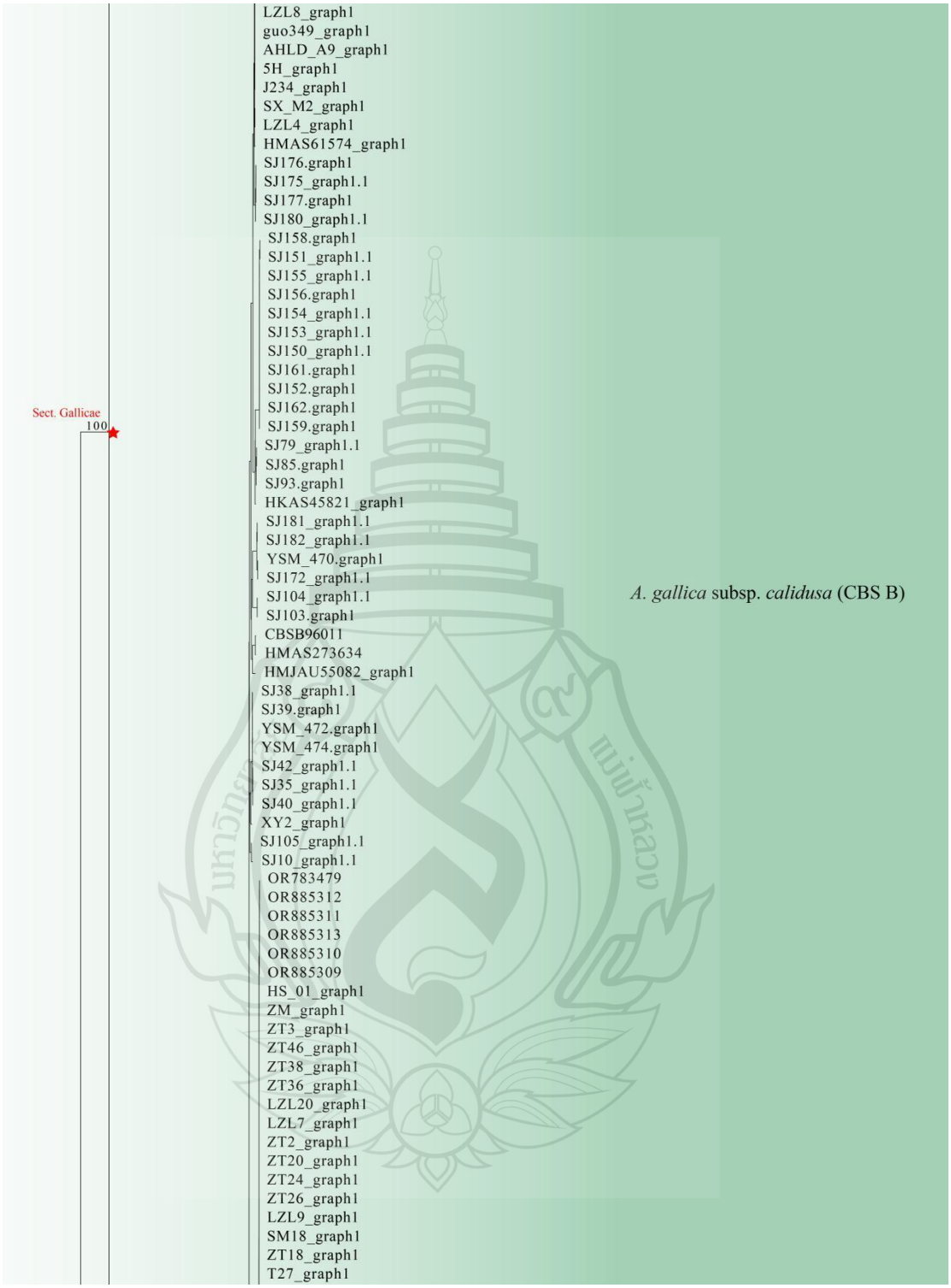


Figure D2 (continued)

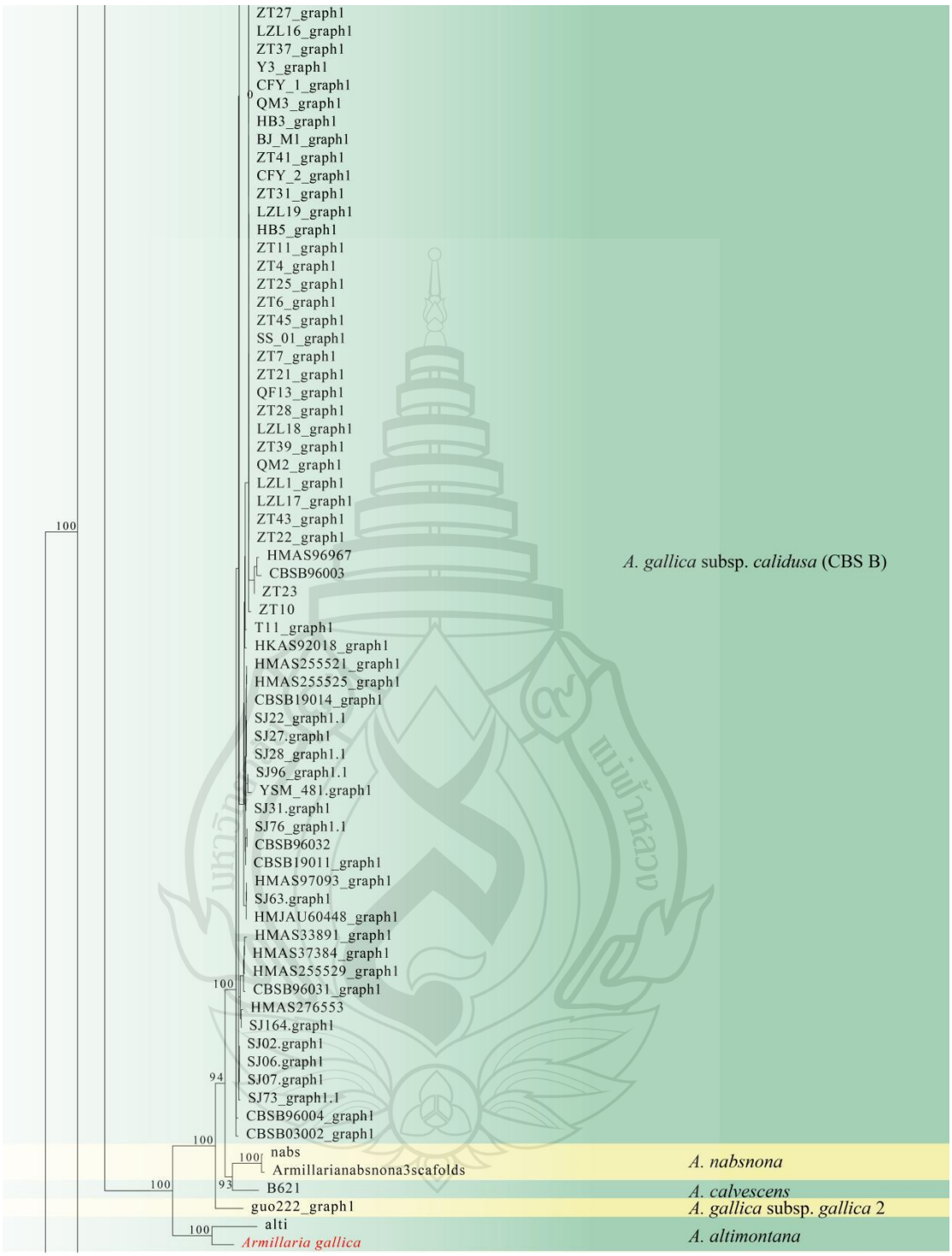


Figure D2 (continued)

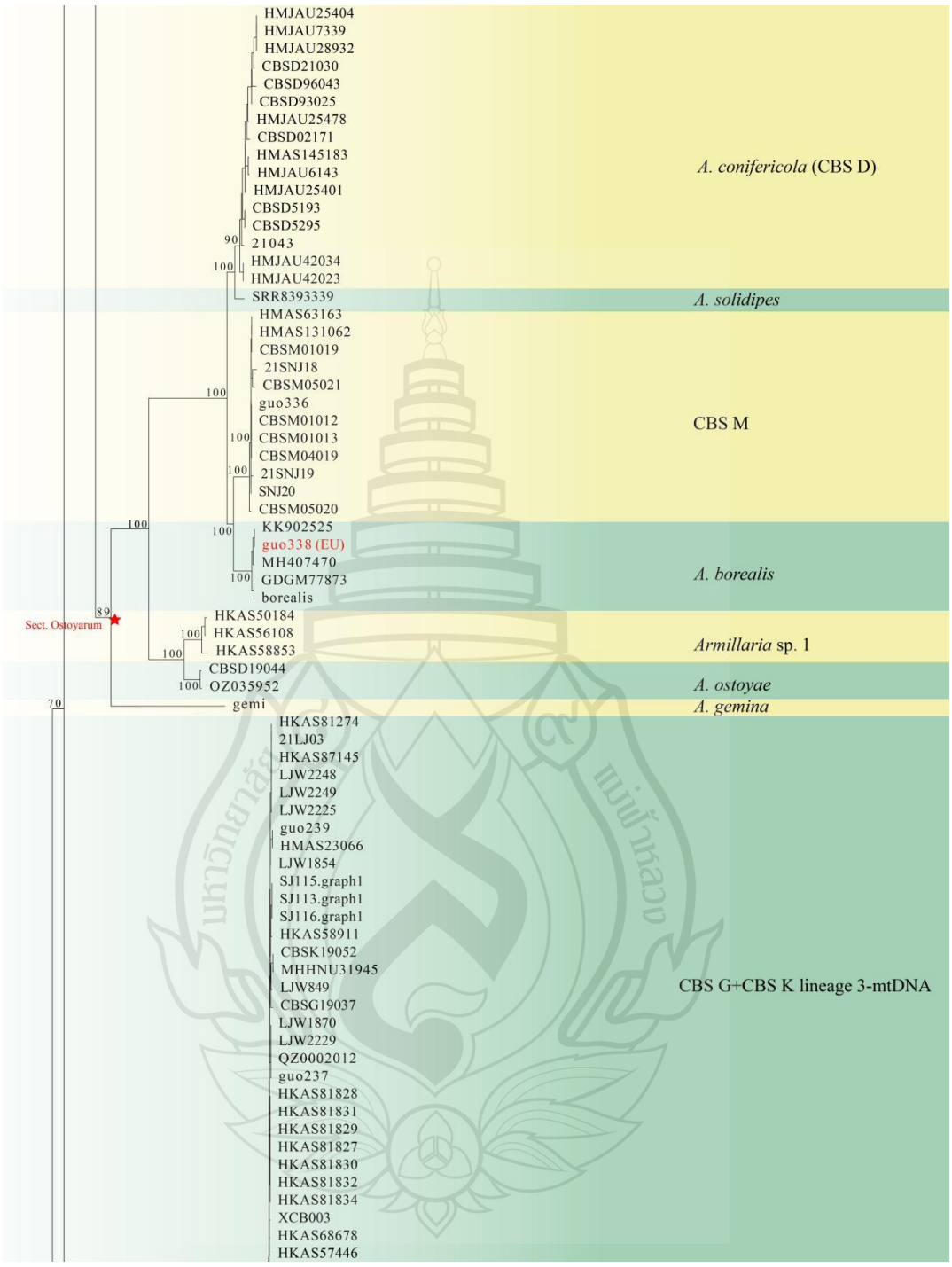
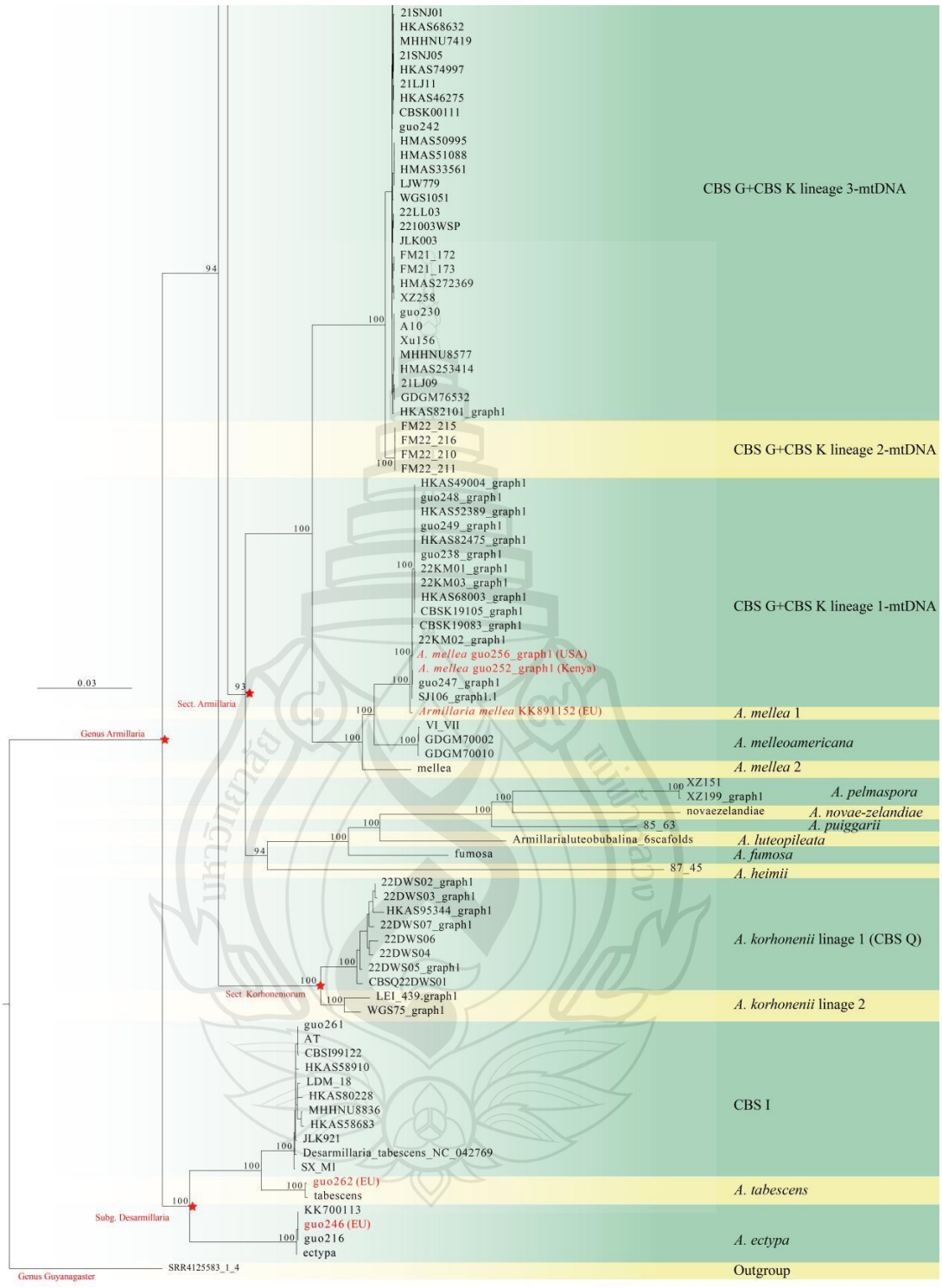


Figure D2 (continued)



Note Bootstrap support values (BS ≥ 70%) from the ML analysis are indicated above the branches at corresponding nodes. The tree is rooted with *Guyanagaster necrorhizus*.

Figure D2 (continued)

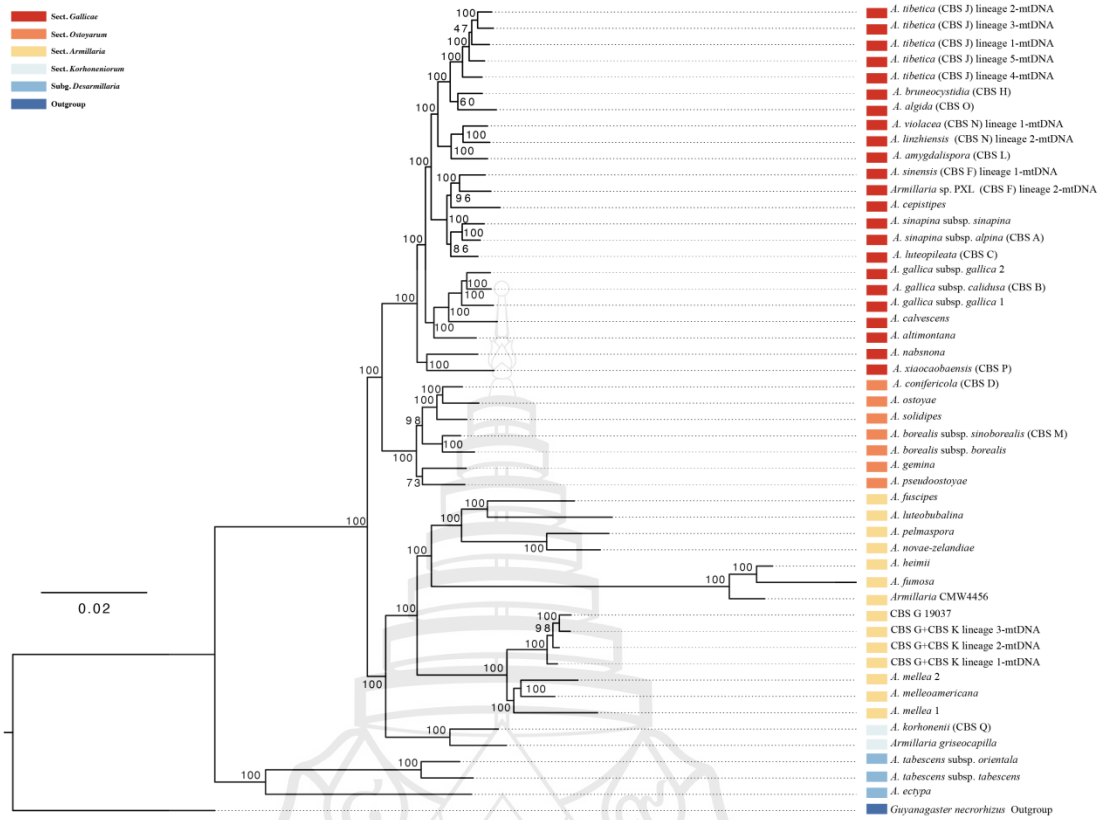
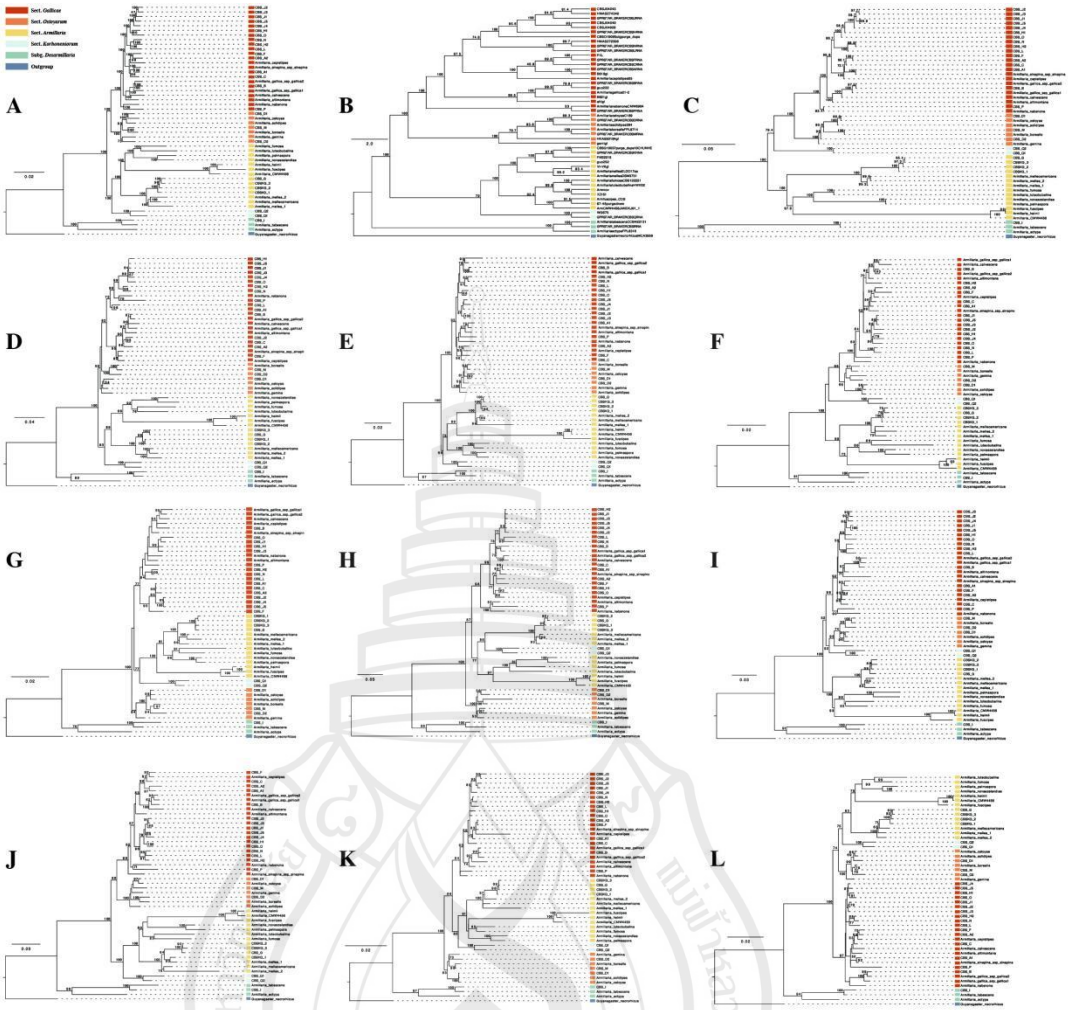


Figure D3 Species tree inferred by RAxML from the concatenated alignment of 629 single-copy genes under the PROTGAMMAWAG model



Note (A-C) Species trees generated using concatenation-based maximum likelihood (ML) and coalescent-based approaches under CASTER-site and CASTER-pair modes, respectively, based on the protein matrix. (D-L) A subset of the topological structures observed in the species-level phylogenetic trees of *Armillaria*.

Figure D4 Phylogenetic topology analysis at the species level within *Armillaria*

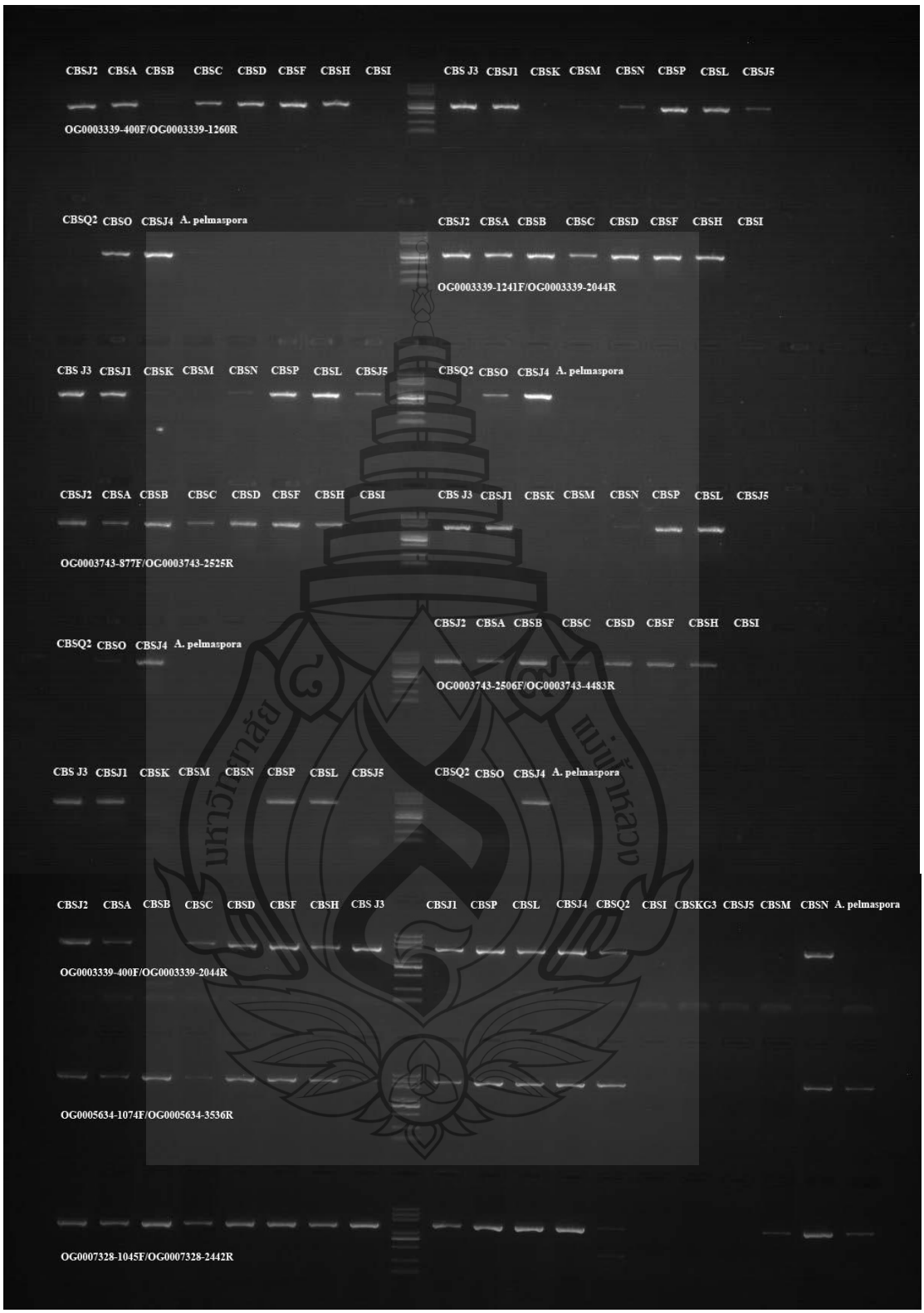


Figure D5 Amplification performance of candidate barcodes



Figure D5 (continued)



Figure D5 (continued)



Figure D5 (continued)

CURRICULUM VITAE

NAME Jianwei Liu

EDUCATIONAL BACKGROUND

2018	Master of Natural Science, Kunming Institute of Botany, Chinese Academy of Sciences, China
2014	Bachelor of Agriculture, College of Agriculture, Yunnan Agricultural University, China

PUBLICATIONS

First Author Publications

Liu, J. W., Wan, S., Gong, H., & Yu, F. (2020). *Pachyphlodes atropurpurea* and *P. excavata*, two new truffle species from Southwest China. *Phytotaxa*, *464*(1), 85–92. https://doi.org/10.11646/phytotaxa.464.1.7

Liu, J. W., Ge, Z. W., Horak, E., Vizzini, A., Halling, R. E., Pan, C. L., . . . Yang, Z. L. (2021). Squamanitaceae and three new species of *Squamanita* parasitic on *Amanita* basidiomes. *IMA fungus*, *12*, 1–24. https://doi.org/10.1186/s43008-021-00057-z

Wan, S. P., Liu, J. W., Huang, L. L., Qin, X. M., Liu, W., & Yu, F. Q. (2021). *Tuber qujingense* and *T. songlu*, two new species from Yunnan, China. *Phytotaxa*, *527*(4), 248–256. (†Co-first authors) https://doi.org/10.11646/phytotaxa.527.4.2

Liu, J. W., Luangharn, T., Yang, S. M., & Yu, F. Q. (2022). The complete mitochondrial genome of *Polyozellus multiplex* (Thelephorales). *Mitochondrial DNA Part B*, *7*(6), 1066–1068. https://doi.org/10.1080/23802359.2022.2086077

Liu, J. W., Luangharn, T., Wan, S. P., Wang, R., & Yu, F. Q. (2022). A new edible species of *Gomphus* (Gomphaceae) from southwestern China. *Mycoscience*, *63*(6), 293–297. https://doi.org/10.47371/mycosci.2022.09.002

Liu, J. W., Luangharn, T., & Yu, F. Q. (2023) *Cystoderma lignicola*, a new species from southwestern China. *Asian Journal of Mycology*, *6*(1), 77–85. https://doi.org/10.5943/ajom/6/1/7

Liu, J. W., Luangharn, T., Yu, F. Q., & Bhunjun, C. S. (2024). The complete mitochondrial genome of enigmatic mycoparasitic fungus *Squamanita imbachii*. *Mitochondrial DNA Part B*, *9*(6), 716–719. https://doi.org/10.1080/23802359.2024.2356131

Liu, J. W., Qin, G. F., Chen, J., Song, J., Yan, Z. Y., Yang, S. M., . . . Yang, Z. L. (2024). *Armillaria korhonenii*, the sixteenth biological species of *Armillaria* from China. *Phytotaxa*, *637*(2), 149–164. https://doi.org/10.1101/2023.12.04.569844

Co-author

He, Y., Liu, D., He, X., Wang, Y., Liu, J. W., Shi, X. F., . . . Yu, F. (2022). Characteristics of bacterial and fungal communities and their impact during cow manure and agroforestry biowaste co-composting. *Journal of Environmental Management*, *324*, 116377. https://doi.org/10.1016/j.jenvman.2022.116377

Fan, X. P., Liu, J. W., & Yang, Z. (2023). Phylogeny, taxonomy and evolutionary trade-offs in reproductive traits of gomphoid fungi (Gomphaceae, Gomphales). *Journal of Fungi*, *9*(6), 626. https://doi.org/10.3390/jof9060626

Cai, Q., Lin, W. F., Liu, J. W., Zhou, Y., & Yang, Z. L. (2023). Two new species of *Sarcomyxa* (Agaricales) from China. *Mycological Progress*, *22*(6), 38. https://doi.org/10.1007/s11557-023-01883-8

Xu, Y. D., Jiang, L., Yang, Z. L., Liu, J. W., Cai, Q., Xiao, Y. Q., . . . He, Z. M. (2024). *Lepista cremeoinvoluta* and *L. multiformis* (Clitocybaceae, Agaricales), a new species and a newly recorded species from Southwestern China. *Mycological Progress*, *23*(1), 47. https://doi.org/10.1007/s11557-024-01986-w

Senanayake, I. C., Rossi, W., Leonardi, M., & Song J. (2023). Fungal diversity notes 1611–1716: taxonomic and phylogenetic contributions on fungal genera and species emphasis in south China. *Fungal Diversity*, *122*, 161–403. https://doi.org/10.1007/s13225-023-00523-6

Wang, C. Q., Zhang, M., He, X. L., Liu, J. W., Wei, T. Z., Liu, T. Z., . . . Deng, W. Q. (2023). Species diversity of *Hygrophorus* in China and a phylogenetic study of the genus. *Mycosphere*, *14*(1), 1742–1834.

Zhan, J., Yuan, J., Liu, J., Zhang, F., Yu, F., & Wang, Y. (2023). Metabolomics analysis of mycelial exudates provides insights into fungal antagonists of *Armillaria*. *Mycology*, *14*(3), 264–274. https://doi.org/10.1080/21501203.2023.2238753